


Removal of Congo Red From Water By Adsorption Onto Chitosan-BN-Fe₂O₃: Kinetic and Isotherm Studies

Mehmet Semih BİNGÖL ^{1*}

¹ Eastern Anatolia High Technology Application and Research Center (DAYTAM), Atatürk Üniversitesi, Erzurum/Turkey

Received:26/09/2022, **Revised:** 26/11/2022, **Accepted:** 09/12/2022, **Published:** 30/12/2022

Abstract

In this study, an adsorbent for Congo red removal was made by combining Chitosan and Boron Nitride(BN)-Fe₂O₃. The chemical structures of this adsorbent (Ch-BN-Fe₂O₃) were confirmed by FT-IR analysis. In adsorption studies, the effects of adsorbent amount, pH and contact time on Congo red removal were investigated. Accordingly, the highest 99.58% removal was achieved under the conditions of 0.1 gram adsorbent mass, pH 7, 60 minutes. In addition, thermodynamic, isotherm and kinetic studies were performed in the study. In isotherm studies, the most suitable model was determined to be Langmuir and its q_{max} value was found to be 86.95 mg/g. However, the pseudo second order kinetic model was found to be suitable.

Keywords: Chitosan, boron nitride, iron oxide, adsorption

Kongo Kırmızısının Kitosan-BN-Fe₂O₃ Üzerine Adsorpsiyon Yoluyla Sudan Uzaklaştırılması: Kinetik ve İzoterm Çalışmaları

Öz

Bu çalışmada Kongo red giderimi için Kitosana Boron Nitride- Fe₂O₃ katkılanıp adsorbent hazırlanmıştır. Bu adsorbentin (Ch-BN-Fe₂O₃) kimyasal yapıları FT-IR analizi ile doğrulanmıştır. Adsorpsiyon çalışmalarında adsorbent kütleleri, pH, temas süresi congo red giderimi üzerine etkileri araştırılmıştır. Buna göre 0,1 gram adsorbent kütlesi, pH 7, 60 dk sürede en yüksek %99,58 giderim gerçekleşmiştir. Ayrıca çalışmada termodinamik, izoterm ve kinetik çalışmalar gerçekleştirilmiştir. İzoterm çalışmalarında en uygun modelin langmuir olduğu belirlenmiş ve q_{max} değeri de 86,95 mg/g bulunmuştur. Bununla birlikte pseudo second order kinetic modeli uygun olduğu tespit edilmiştir.

Anahtar Kelimeler: Kitosan, bor nitrit, demir oksit, adsorpsiyon.

1. Introduction

Growing industrial waste as a result of technology advancements has had detrimental effects on the environment [1]. The rising usage of dyes and their discharge into environmental waters, particularly in numerous industrial applications, causes significant environmental and human health hazards[2,3]. Therefore, it is of great importance to treat these dyes before they are disposed of directly[4]. When these dyes are mixed with the surrounding waters, they cause many problems such as the increase of bacteria with sunlight and the prevention of biodegradation[5]. Congo red is the sodium salt of an acid called benzidinediazo-bis-1-naphthylamine-4-sulfonic acid. It is a secondary diazo (R-N=N-R bond) dye[6]. Congo red is frequently used in the textile, paper, printing, and plastic sectors despite having cancer- and mutagenic-causing qualities [7].

The removal of dyes from wastewater can be accomplished using a variety of physical/chemical techniques, including flocculation/coagulation[8], ion exchange electrochemistry[9], photochemical decomposition[10], reverse osmosis [11], ultrafiltration adsorption [12], chemical oxidation[13], and biological treatment techniques[14]. It has been seen in many studies that the most effective and economically most convenient of these methods is adsorption[15]. However, the materials utilized or created as adsorbents must be natural, safe for the environment, and capable of being easily separated from water[16].

The use of natural resources such as chitin and the biopolymer derived from it, chitosan, is becoming more and more important. In adsorption studies, the most important parameter is that the adsorbent is natural and harmless to the environment/human health. Chitosan was employed in this investigation due to this reason [17]. A biological polymer known as chitosan (C₆H₁₁NO₄)_n is derived from several natural sources[18]. In our investigation, boron nitride, an additive that doesn't harm the environment, was also used[19]. It is well known that many contaminants can be removed using boron nitride[20]. Because of its high surface area and chemically inert structure, boron nitride has become an essential material in pollution adsorption. In addition, Fe₂O₃ was added due to the active role of oxidized compounds in adsorbents[21]. Until now, there is a study in the literature on dye removal using chitosan/BN composite adsorbent. However, in this study, congo red was not removed and Fe₂O₃ was not added. Therefore, this study is unique in the literature [22]. Investigated were the effects of this produced adsorbent on congo red removal in various parameters.

2. Material and Methods

2.1. Preparation of BN-Fe₂O₃ doped chitosan adsorbent

Boron Nitride (Purity :%99.7, Nanography/Turkey), Chitosan (>%99), Fe₂O₃ (>%96), and Acetic acid (>%99) Sigma(St. Louis, Missouri, ABD) were purchased commercially. BN was treated with sodium hydroxide (NaOH), Due to the limited number of functional groups on its surface and chemical resistance [23]. For 24 hours at 120°C, 1 gram of BN was mixed in the 5M NaOH. It was then washed and filtered numerous times with distilled water until the pH was restored. The resulting BNOH particles were dried at 60°C for 10 hours. Fe₂O₃ (2g) and

prepared BNOH (0.5g) were mixed at 90°C for 24 hours. The resulting particles were washed several times with distilled water and filtered. After that, it was dried for 10 hours at 60 °C.

In 100 mL of 2% acetic acid solution, chitosan was completely dissolved. This solution was mixed for 24 hours with BN-Fe₂O₃ particles. Afterwards, the solution was kept at -80°C for 24 hours and lyophilized. The resulting adsorbent was stored in a desiccator. Fourier Transform Infrared Spectroscopy (FTIR) analysis was carried out using a Bruker VERTEX 70v model instrument in the scanning range of 400-4000 cm⁻¹ in order to comprehend the chemical structures and bonding of adsorbents.

2.2. Adsorption Studies

Using various parameters conditions, a number of batch tests were conducted to look into the adsorption of Congo Red (CR) in produced adsorbents. These parameters are; dye concentration (50, 100, 150, 200 mg /L), pH levels (2–12) and mass of adsorbent (Ch-BN-Fe₂O₃) (0.01, 0.02, 0.03, 0.4, 0.05, 0.1, 0.15, 0.2 g/L) was determined. 1000 mg/L CR the stock solution was prepared to be diluted to the determined concentrations. Adsorption process was carried out by adding the determined amount of adsorbents into 50 ml of CR solution and running it at 150 rpm for the determined time in the IKA KS 3000i Control model shaker. The pH of the CR solution was adjusted using solutions of 0.1 M NaOH and 0.1 M HCl. After centrifugation, the adsorbents were removed from the solution. Using a colorimetric method, the remaining dye concentration in solution was determined using a UV spectrophotometer (Shimadzu UV-3600 Plus) (max wavelength 497.4 nm). An absorbance-concentration profile was constructed by drawing a calibration curve between dye solution absorbance and concentration. This graph is presented in Figure 1. The formulas below were used to calculate the % removal of CR and the adsorption capacity of the adsorbent.

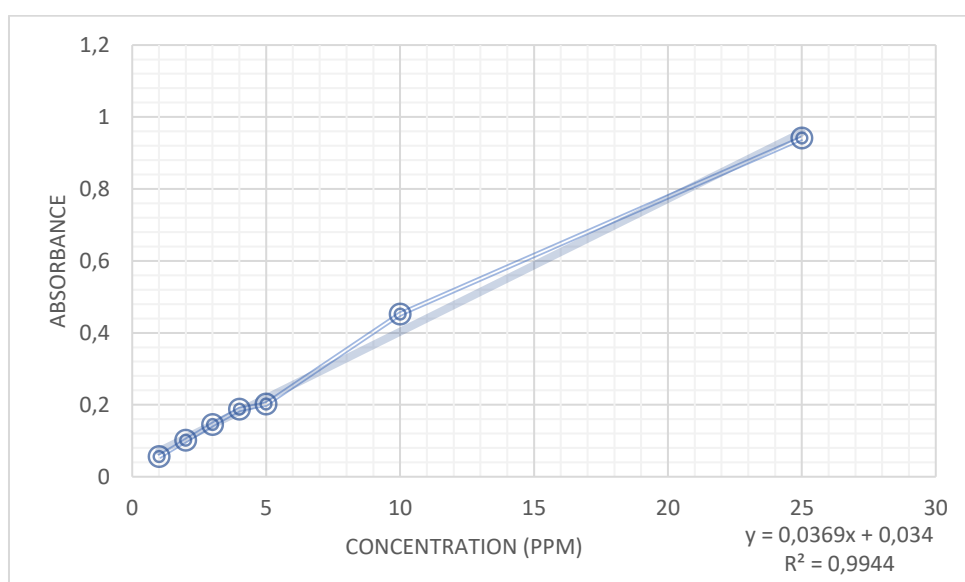


Figure 1. Congo red absorbance-concentration calibration curve

$$q_e = (c_0 - C_e) \times \frac{V}{W} \quad (1)$$

$$q_t = (c_0 - C_t) \times \frac{V}{W} \quad (2)$$

$$\text{Removal, \%} = \frac{(C_0 - C_e)}{C_0} \times 100 \quad (3)$$

Where C_0 is the initial concentration, C_e is equilibrium concentration and C_t is the concentration at time, q_e is equilibrium adsorption capacity and q_t adsorption capacity at time, V is the volume of CR solution, and W is the adsorbent mass [24].

2.3. Adsorption Thermodynamics, Isotherm and Kinetic Studies

Adsorption studies were carried out thermodynamically at 3 different temperatures (298, 308, 318 Kelvin). With the use of the findings from these investigations, the following equations were used to derive Gibbs, Enthalpy, and Entropy [25].

$$K_c = \frac{q_e}{C_e} \quad (4)$$

$$\ln K_c = \frac{\Delta S^0}{R} - \frac{\Delta H^0}{RT} \quad (5)$$

$$\Delta G^0 = \Delta H^0 - T\Delta S^0 \quad (6)$$

The adsorption isotherm is the most commonly used approach for representing an adsorption system's equilibrium state. The adsorption isotherm is the relationship between the amount of substance adsorbed by the adsorbent and the equilibrium concentration at constant temperature [26].

Equilibrium isotherm experiments were carried out at 25°C with 0.1 g adsorbent at pH 7 and different concentrations of CR (50-200 mg/L). The equilibrium adsorption values were analyzed using the Langmuir and Freundlich isotherm models.

The first adsorption isotherm to be formulated theoretically is the Langmuir isotherm equation. The majority of the later presented equations that successfully explain a variety of experimental findings are either based on this equation or were created utilizing the Langmuir method. As a result, both chemisorption and physical adsorption theories continue to benefit from the Langmuir isotherm model. The Langmuir isotherm can be expressed mathematically as follows [27].

$$\frac{C_e}{q_e} = \frac{1}{q_{max} K_c} + \frac{C_e}{q_{max}} \quad (7)$$

Where q_{max} , q_e and C_e are respectively; Maximum adsorption capacity (mg/g), adsorption capacity at equilibrium (mg/g), equilibrium concentration (mg/L)

The Freundlich isotherm, another popular experimental equation that uses two parameters and is consisted with a wide range of experimental data, is similar to the Langmuir isotherm. The following equation serves as a representation of the Freundlich isotherm [28].

$$\ln q_e = \ln K_F + \left(\frac{1}{n}\right) \ln C_e \quad (9)$$

K_F and n are the Freundlich constants.

The effect of adsorbate-adsorbent contact time can be calculated using adsorption kinetics. There are steps in the analysis of adsorption kinetics that impact the rate of the adsorption process. In order to investigate the CR adsorption mechanism on adsorbent surfaces, two distinct kinetic models were applied. These two models are, respectively, pseudo-first-order kinetic models (PFO-km) and pseudo-second-order kinetic models (PSO-km) [27,29].

Lagergren created the PFO-km (1898). Eqn. 11 shows the PFO-km.

$$\text{Log}(q_e - q_t) = \ln q_e - \frac{K_1 t}{2.303} \quad (11)$$

The PSO-km is given in Eqn. 12 [30].

$$\frac{t}{q_t} = \frac{1}{k_2 q_e^2} + \frac{t}{q_e} \quad (12)$$

K_1 (min⁻¹) and k_2 (g/mg min⁻¹) are the PFO-km constant and the PSO-km constant, respectively.

3. Results and Discussion

3.1. FT-IR analysis

The chemical structure of the adsorbent was confirmed by FT-IR analysis. The Figure 2 shows the FT-IR spectrums of BN, Fe₂O₃, BN-Fe₂O₃ and Ch-BN-Fe₂O₃. In BN spectrums, 1332 cm⁻¹ BN stretch vibration and 771 cm⁻¹ peak indicate B-N-B formation[31]. In the Fe₂O₃ FTIR analysis, the 698 and 546 peaks show the Fe₂O₃ tension, and 420 cm⁻¹ shows the Fe₂O₃ bending vibration[32]. Both BN and Fe₂O₃ have similar peaks in the BN-Fe₂O₃ analysis[33]. Ch-BN-Fe₂O₃ adsorbent originates from the Fe-O group at 611 cm⁻¹, the NH₂ absorption of chitosan at 1560 and 1654 cm⁻¹ and the C=O amide group. In addition, the 3268 and 2917 cm⁻¹ peaks originate from the OH- group[34,35]. In the FT-IR analysis of the adsorbent, the specific peaks of BN and Fe₂O₃ are seen similarly, although there are small shifts.

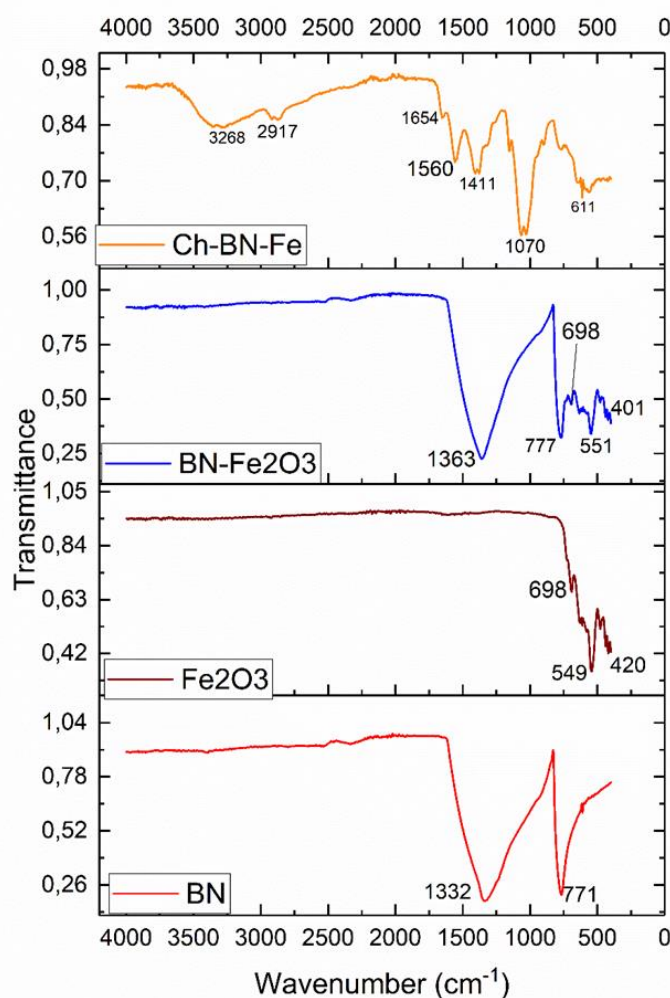


Figure 2. FT-IR spectra of the adsorbent

3.2. Effect of amount Ch-BN-Fe₂O₃

Firstly, the impact of adsorbent masses was assessed in the adsorption studies. The adsorption studies was performed in 120 min., at 25 °C, pH 7, and 100 mg/L CR concentration. According to Figure 3, the maximum CR adsorption removal was determined to be 99.06%. As the adsorbent amount is increased, the adsorption increased and remained constant after 0.1 gram.

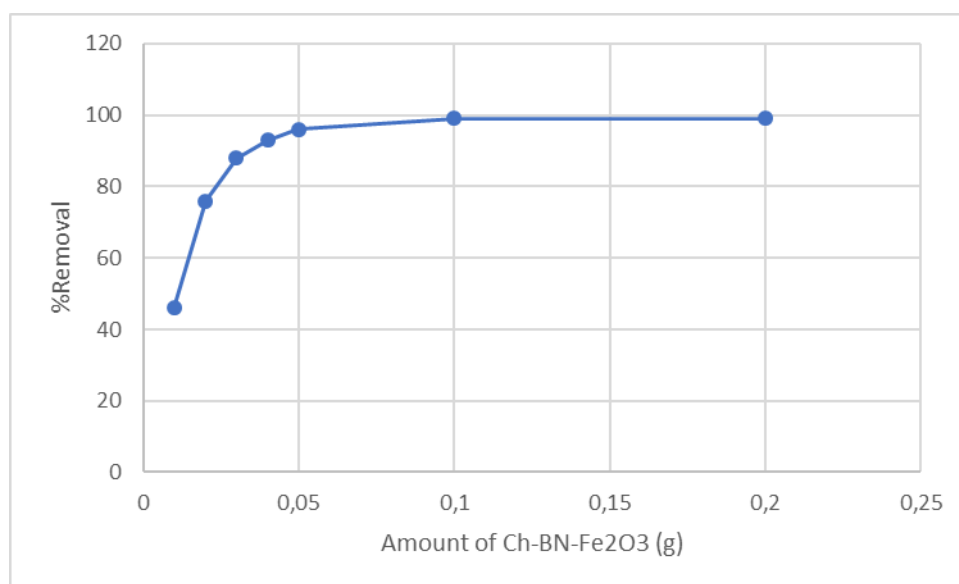


Figure 3. The effect of Ch-BN-Fe₂O₃ amount on adsorption.

3.3. Effect of pH on adsorption

The impact of pH on adsorption was investigated. The adsorption study was carried out for 120 min., at a temperature of 25 °C, using 0.1 grams of adsorbent and 100 mg/L of CR concentration. As shown in the Figure 4 that percentage of CR removal remained steady until pH 7, but then declined. According to the results, the highest CR removal was found to be 99.04% at pH 7[36].

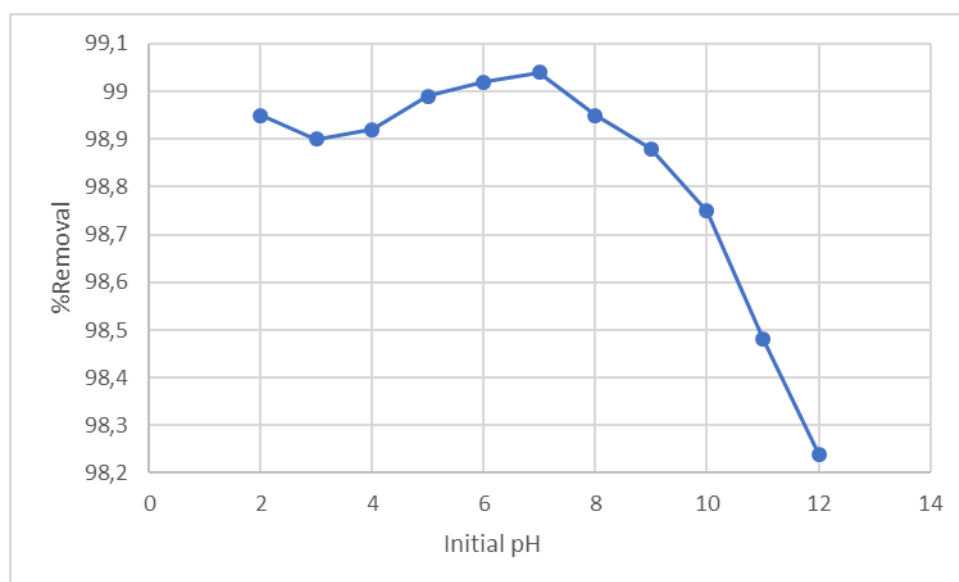


Figure 4. Effect of pH on CR removal

3.4. Effect of contact time and initial concentration

Figure 5 shows the effect of time and initial concentration on adsorption. These experiments were performed under conditions that a temperature of 25°C, using 0.1 grams of adsorbent and

pH 7. Accordingly, very fast adsorption took place up to 20 minutes and then remained stable. This results from the active sites on the adsorbent surface being filled. The highest CR removal was found to be 99.58% at 50 ppm initial concentration. The highest adsorption capacity was determined as 85 mg/g at an initial concentration of 200 ppm.

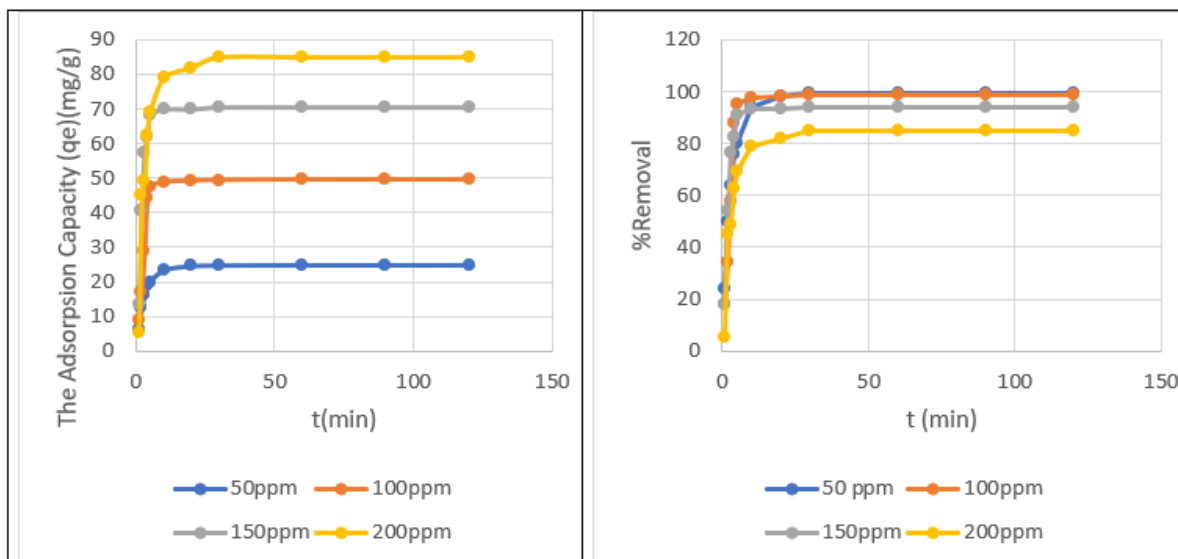


Figure 5. The effect of initial dye concentration and time on adsorption: (a) CR removal rate and (b) the amount of CR adsorbed at equilibrium

3.5. Results of Thermodynamic, Isotherm and Kinetic studies

Experiments were conducted at 100 ppm CR concentration, for 60 minutes, at pH 7, and under the circumstances of 0.1 gram adsorbent amount in order to study the effect of temperature and thermodynamic studies. It was observed that as the temperature increases, the adsorption increased slightly. Thermodynamic parameters were calculated with the help of Figure 6 and 7. Parameter results are presented in Table 1. At all temperatures, negative values of ΔG (-11.46, -11.68, and -12.1 kJ/mol) show that the reaction is spontaneous. In general, physisorption is represented by ΔG values of $-20 < \Delta G < 0$ (kJ/mol). Additionally, it was shown that ΔG fell as temperature rose, demonstrating the viability of adsorption at higher temperatures. Positive enthalpy ($\Delta H = 1.257$ kJ/mol) indicates endothermic adsorption. Positive entropy ($\Delta S = 0.042$ kJ/mol) indicates increased randomness during adsorption at the solid-solution interface[37].

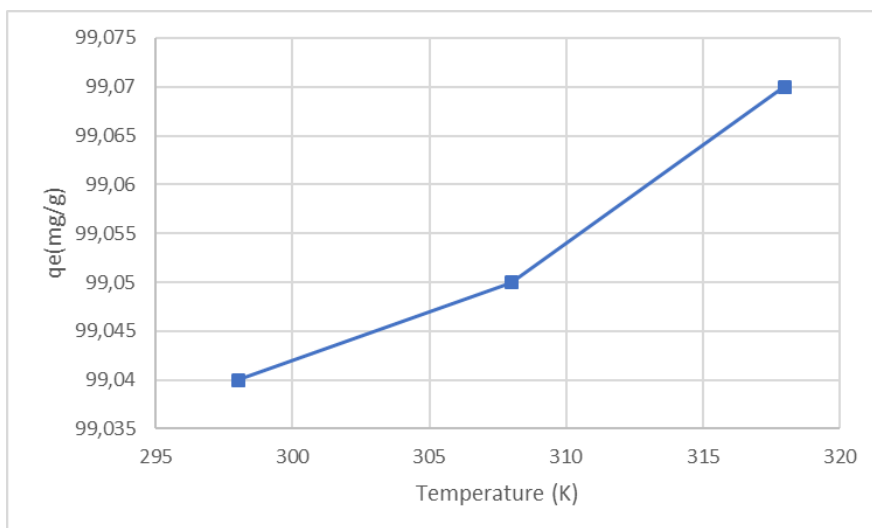


Figure 6. Effect of temperature on adsorption

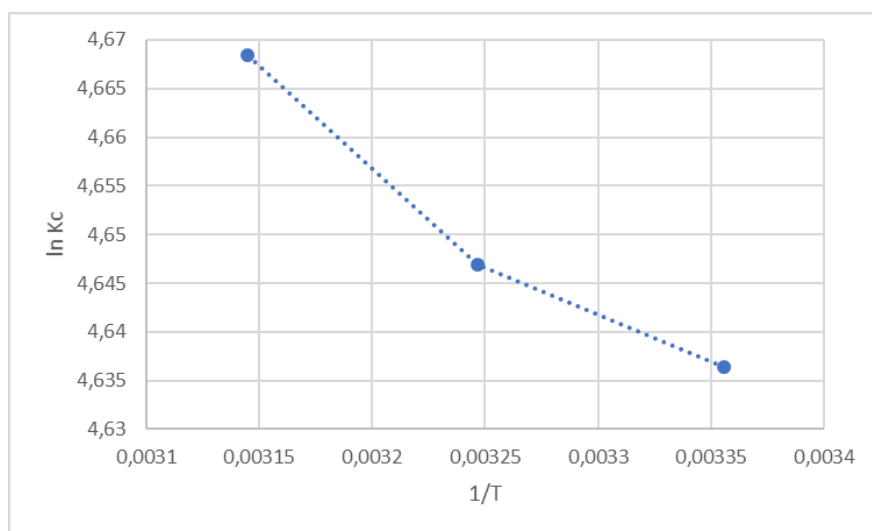


Figure 7. lnKc versus 1/T

Table 1. Thermodynamic parameters for CR adsorption

T (Kelvin)	ΔH (kJ/mol)	ΔS (kJ/mol)	ΔG (kJ/mol K)
298	1.257	0.042	-11.46
308	1.257	0.042	-11.68
318	1.257	0.042	-12.1

The values of the Langmuir and Freundlich model parameters for CR adsorption by the produced adsorbent are shown in Table 2 and Figure 8. Comparison of these two models showed that the Langmuir model with $R^2 > 0.99$ was a better match than the Freundlich model

($R^2=0.9289$). This showed that adsorption mechanism is compatible with the Langmuir isotherm. This demonstrates that CR is adsorbed as a single layer coating on the surface[38].

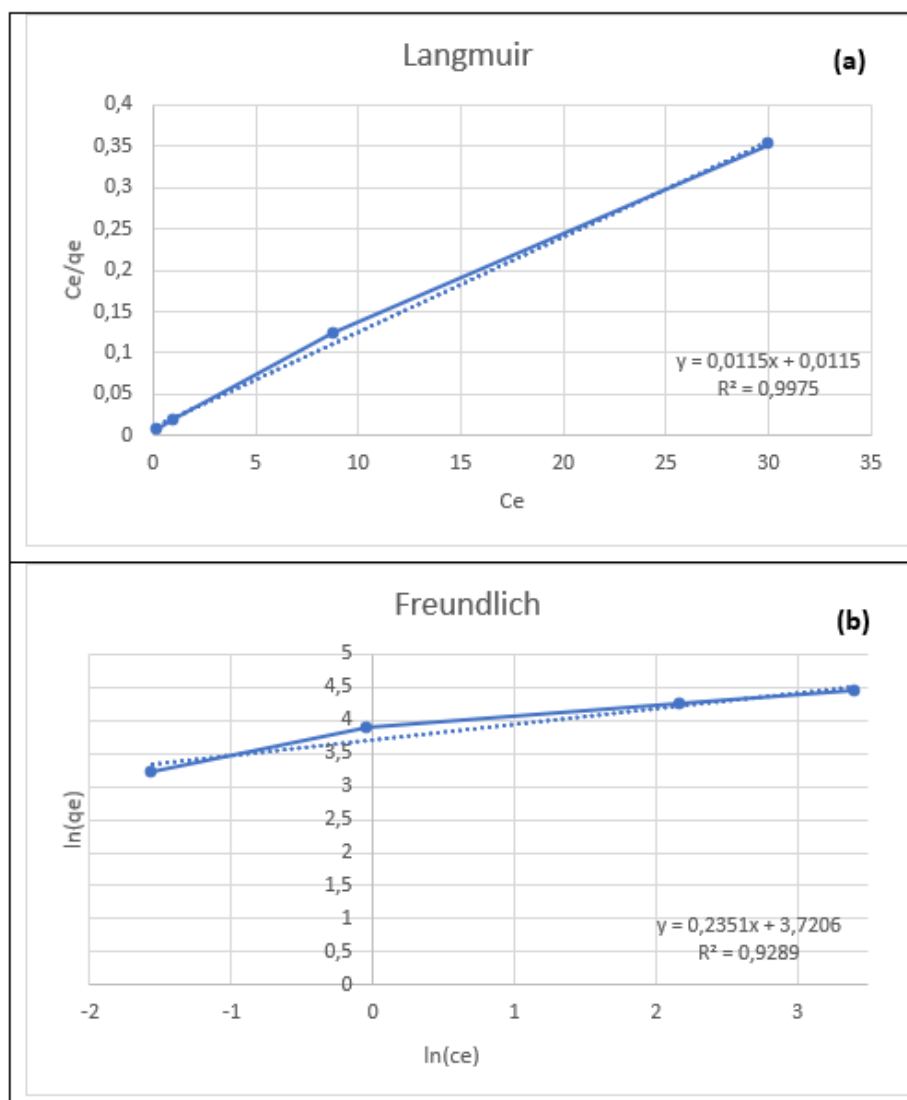


Figure 8. (a) Langmuir Isotherm Plot, (b) Freundlich Isotherm Plot

Table 2. Isotherm models parameters results.

Isotherm	Parameters	Value
Langmuir	R^2	0.9975
	$q_{max}(mg/g)$	86.95
	K_L	1.01
Freundlich	R^2	0.9289
	$K_F (L/mg)$	41.28
	n	0.25

The experimentally collected data were used to apply the linear forms of the PFO and PSO velocity models in order to examine the adsorption control mechanism. Table 3 and Figure 9

contain the data and graphs for the kinetic parameter results. Experimental findings are compatible with PSO. The PSO fit was further demonstrated by the R² value of 0.999. As seen in the Table 4, when the experimental results and the results in pso were compared, it was seen that they were very close to each other. This showed that adsorption study is suitable for the PSO model. Improved and experimental kinetic velocity profiles further supported this. As a result, the rate-controlling step for this adsorbent is probably chemical adsorption[39].

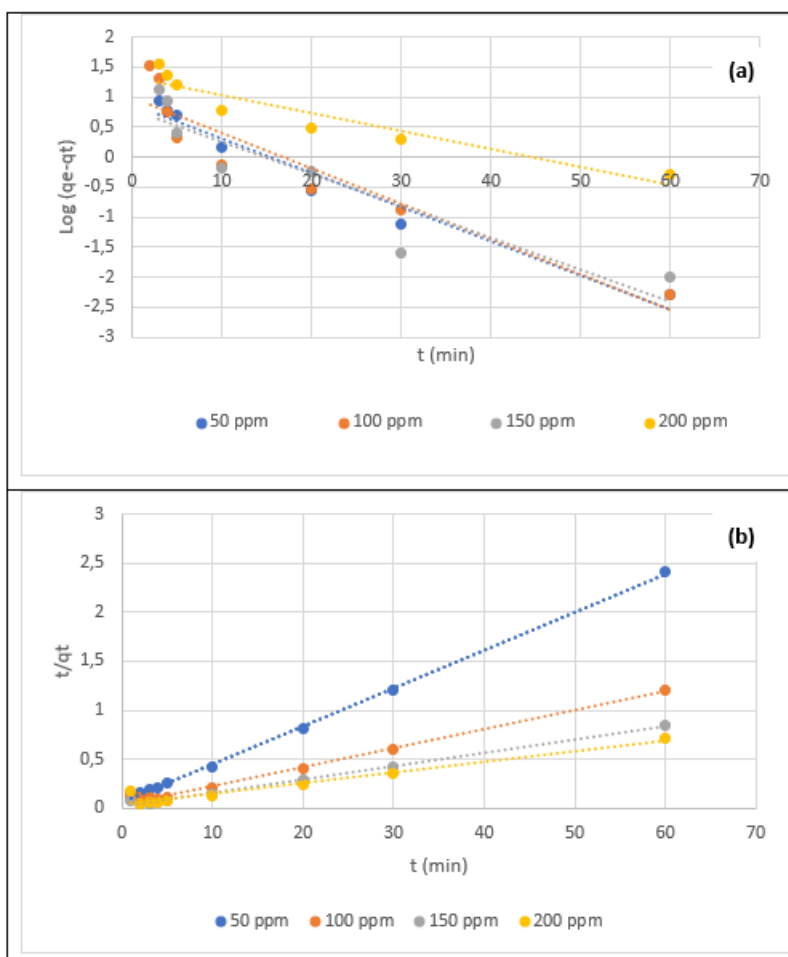


Figure 9. (a) PFO and (b) PSO kinetics plots of CR.

Table 4. The results of the kinetic parameters for CR adsorption

Co (mg/L)	q _{exp} (mg/g)	PFO-km			PSO-km		
		q _e (mg/g)	K ₁	R ²	q _e (mg/g)	K ₂	R ²
50	24,89	2,56	0,134	0.9584	25,9	0.0238	0.9985
100	49,52	3,08	0,142	0.8755	52,08	0.0091	0.9935
150	70,6	2,18	0,122	0,8305	72,99	0.0102	0.9958
200	85	3,79	0,069	0,8407	88,15	0.0073	0.9996

4. Conclusion

Chitosan doped with BN-Fe₂O₃ that was utilized to remove CR was created for the first time in the literature. By using FT-IR analysis, the produced adsorbent's chemical structures were verified. Adsorption studies have shown that 0.1 g of adsorbent, pH 7, and 60 minutes of adsorption time are the best conditions. It was discovered that the Langmuir isotherm model was appropriate for this adsorption. The q_{max} value was also discovered to be 85 mg/g. The kinetic studies led to the conclusion that the PSO-km was appropriate..

Ethics in Publishing

There are no ethical issues regarding the publication of this study.

References

- [1] Harja, M., Buema, G., & Bucur, D. (2022) Recent advances in removal of Congo Red dye by adsorption using an industrial waste. *Scientific Reports.*, *12*(1), 1–18
- [2] Zhang, H., Chen, H., Azat, S., Mansurov, Z. A., Liu, X., Wang, J., Su, X., et al. (2018) Super adsorption capability of rhombic dodecahedral Ca-Al layered double oxides for Congo red removal. *Journal of Alloys and Compounds.*, *768*, 572–581
- [3] Cheng, Y., Yan, F., Huang, F., Chu, W., Pan, D., Chen, Z., Zheng, J., et al. (2010) Bioremediation of Cr (VI) and immobilization as Cr (III) by *Ochrobactrum anthropi*. *Environmental science & technology.*, *44*(16), 6357–6363
- [4] You, J., Liu, C., Feng, X., Lu, B., Xia, L., & Zhuang, X. (2022) In situ synthesis of ZnS nanoparticles onto cellulose/chitosan sponge for adsorption–photocatalytic removal of Congo red. *Carbohydrate Polymers.*, *288*, 119332
- [5] Eltaweil, A. S., Elshishini, H. M., Ghatass, Z. F., & Elsubruiti, G. M. (2021) Ultra-high adsorption capacity and selective removal of Congo red over aminated graphene oxide modified Mn-doped UiO-66 MOF. *Powder technology.*, *379*, 407–416
- [6] Mandal, S., Calderon, J., Marpu, S. B., Omary, M. A., & Shi, S. Q. (2021) Mesoporous activated carbon as a green adsorbent for the removal of heavy metals and Congo red: Characterization, adsorption kinetics, and isotherm studies. *Journal of Contaminant Hydrology.*, *243*, 103869
- [7] Parvin, S., Biswas, B. K., Rahman, M. A., Rahman, M. H., Anik, M. S., & Uddin, M. R. (2019) Study on adsorption of Congo red onto chemically modified egg shell membrane. *Chemosphere.*, *236*, 124326
- [8] Lee, J.-W., Choi, S.-P., Thiruvengkatachari, R., Shim, W.-G., & Moon, H. (2006) Submerged microfiltration membrane coupled with alum coagulation/powdered activated carbon adsorption for complete decolorization of reactive dyes. *Water research.*, *40*(3), 435–444
- [9] Gu, J., Liu, H., Wang, S., Zhang, M., & Liu, Y. (2019) An innovative anaerobic MBR–reverse osmosis-ion exchange process for energy-efficient reclamation of municipal

- wastewater to NEWater-like product water. *Journal of Cleaner Production.*, 230, 1287–1293
- [10] Qi, L., Yu, J., & Jaroniec, M. (2013) Enhanced and suppressed effects of ionic liquid on the photocatalytic activity of TiO₂. *Adsorption.*, 19(2), 557–561
- [11] Atab, M. S., Smallbone, A. J., & Roskilly, A. P. (2018) A hybrid reverse osmosis/adsorption desalination plant for irrigation and drinking water. *Desalination.*, 444, 44–52
- [12] Naddeo, V., Secondes, M. F. N., Borea, L., Hasan, S. W., Ballesteros Jr, F., & Belgiorno, V. (2020) Removal of contaminants of emerging concern from real wastewater by an innovative hybrid membrane process—UltraSound, Adsorption, and Membrane ultrafiltration (USAMe®). *Ultrasonics Sonochemistry.*, 68, 105237
- [13] Michael-Kordatou, I., Karaolia, P., & Fatta-Kassinos, D. (2018) The role of operating parameters and oxidative damage mechanisms of advanced chemical oxidation processes in the combat against antibiotic-resistant bacteria and resistance genes present in urban wastewater. *Water research.*, 129, 208–230
- [14] Nancharaiah, Y. V., & Sarvajith, M. (2019) Aerobic granular sludge process: a fast growing biological treatment for sustainable wastewater treatment. *Current Opinion in Environmental Science & Health.*, 12, 57–65
- [15] Rashid, R., Shafiq, I., Akhter, P., Iqbal, M. J., & Hussain, M. (2021) A state-of-the-art review on wastewater treatment techniques: the effectiveness of adsorption method. *Environmental Science and Pollution Research.*, 28(8), 9050–9066
- [16] Velusamy, S., Roy, A., Sundaram, S., & Kumar Mallick, T. (2021) A review on heavy metal ions and containing dyes removal through graphene oxide-based adsorption strategies for textile wastewater treatment. *The Chemical Record.*, 21(7), 1570–1610
- [17] Saheed, I. O., Oh, W. Da, & Suah, F. B. M. (2021) Chitosan modifications for adsorption of pollutants—A review. *Journal of hazardous materials.*, 408, 124889
- [18] Qamar, S. A., Ashiq, M., Jahangeer, M., Riasat, A., & Bilal, M. (2020) Chitosan-based hybrid materials as adsorbents for textile dyes—A review. *Case Studies in Chemical and Environmental Engineering.*, 2, 100021
- [19] Yu, S., Wang, X., Pang, H., Zhang, R., Song, W., Fu, D., Hayat, T., et al. (2018) Boron nitride-based materials for the removal of pollutants from aqueous solutions: a review. *Chemical Engineering Journal.*, 333, 343–360
- [20] Li, J., Xiao, X., Xu, X., Lin, J., Huang, Y., Xue, Y., Jin, P., et al. (2013) Activated boron nitride as an effective adsorbent for metal ions and organic pollutants. *Scientific reports.*, 3(1), 1–7
- [21] Ouyang, J., Zhao, Z., Suib, S. L., & Yang, H. (2019) Degradation of Congo Red dye by a Fe₂O₃@ CeO₂-ZrO₂/Palygorskite composite catalyst: synergetic effects of Fe₂O₃. *Journal of colloid and interface science.*, 539, 135–145
- [22] Khose, R. V, Lokhande, K. D., Bhakare, M. A., Dhumal, P. S., Wadekar, P. H., & Some,

- S. (2021) Boron Nitride doped Chitosan Functionalized Graphene for an Efficient Dye Degradation. *ChemistrySelect.*, *6*(31), 7956–7963
- [23] Kim, K., Ju, H., & Kim, J. (2016) Surface modification of BN/Fe₃O₄ hybrid particle to enhance interfacial affinity for high thermal conductive material. *Polymer.*, *91*, 74–80
- [24] Kavci, E., Erkmén, J., & Bingöl, M. S. (2021) Removal of methylene blue dye from aqueous solution using citric acid modified apricot stone. *Chemical Engineering Communications.*, 1–16
- [25] Mondal, N. K., & Kar, S. (2018) Potentiality of banana peel for removal of Congo red dye from aqueous solution: isotherm, kinetics and thermodynamics studies. *Applied Water Science.*, *8*(6), 1–12
- [26] Wekoye, J. N., Wanyonyi, W. C., Wangila, P. T., & Tonui, M. K. (2020) Kinetic and equilibrium studies of Congo red dye adsorption on cabbage waste powder. *Environmental Chemistry and Ecotoxicology.*, *2*, 24–31
- [27] Lagergren, S. K. (1898) About the theory of so-called adsorption of soluble substances. *Sven. Vetenskapsakad. Handlingar.*, *24*, 1–39
- [28] Proctor, A., & Toro-Vazquez, J. F. (1996) The Freundlich isotherm in studying adsorption in oil processing. *Journal of the American Oil Chemists' Society.*, *73*(12), 1627–1633
- [29] Hubbe, M. A., Azizian, S., & Douven, S. (2019) Implications of apparent pseudo-second-order adsorption kinetics onto cellulosic materials: A review. *BioResources.*, *14*(3)
- [30] Ho, Y.-S., & McKay, G. (1999) Pseudo-second order model for sorption processes. *Process biochemistry.*, *34*(5), 451–465
- [31] Wei, R., Xiao, Q., Zhan, C., You, Y., Zhou, X., & Liu, X. (2019) Polyarylene ether nitrile and boron nitride composites: coating with sulfonated polyarylene ether nitrile. *e-Polymers.*, *19*(1), 70–78
- [32] Sobhanardakani, S., Jafari, A., Zandipak, R., & Meidanchi, A. (2018) Removal of heavy metal (Hg(II) and Cr(VI)) ions from aqueous solutions using Fe₂O₃@SiO₂ thin films as a novel adsorbent. *Process Safety and Environmental Protection.*, *120*, 348–357
- [33] Thangasamy, P., & Sathish, M. (2018) Dwindling the re-stacking by simultaneous exfoliation of boron nitride and decoration of α -Fe₂O₃ nanoparticles using a solvothermal route. *New Journal of Chemistry.*, *42*(7), 5090–5095
- [34] Zhu, H.-Y., Jiang, R., Xiao, L., & Li, W. (2010) A novel magnetically separable γ -Fe₂O₃/crosslinked chitosan adsorbent: Preparation, characterization and adsorption application for removal of hazardous azo dye. *Journal of Hazardous Materials.*, *179*(1), 251–257
- [35] Dhanavel, S., Sivaranjani, T., Sivakumar, K., Palani, P., Gupta, V. K., Narayanan, V., & Stephen, A. (2021) Cross-linked chitosan/hydroxylated boron nitride nanocomposites for co-delivery of curcumin and 5-fluorouracil towards human colon cancer cells. *Journal of the Iranian Chemical Society.*, *18*(2), 317–329

- [36] Kavci, E. (2021) Malachite green adsorption onto modified pine cone: Isotherms, kinetics and thermodynamics mechanism. *Chemical Engineering Communications.*, 208(3), 318–327
- [37] Wakkal, M., Khiari, B., & Zagrouba, F. (2019) Textile wastewater treatment by agro-industrial waste: Equilibrium modelling, thermodynamics and mass transfer mechanisms of cationic dyes adsorption onto low-cost lignocellulosic adsorbent. *Journal of the Taiwan Institute of Chemical Engineers.*, 96, 439–452
- [38] Mahmoud, M. S., & Mahmoud, A. S. (2021) Wastewater treatment using nano bimetallic iron/copper, adsorption isotherm, kinetic studies, and artificial intelligence neural networks. *Emergent Materials.*, 4(5), 1455–1463
- [39] Hasanzadeh, M., Simchi, A., & Far, H. S. (2020) Nanoporous composites of activated carbon-metal organic frameworks for organic dye adsorption: Synthesis, adsorption mechanism and kinetics studies. *Journal of Industrial and Engineering Chemistry.*, 81, 405–414

Design of RISC Processor with IEEE754 Standard Floating-Point Instruction Set in FPGA using VHDL for Digital Signal Processing Applications

Bahadır ÖZKILBAÇ ^{1*}, Tevhit KARACALI ¹

¹ Department of Electrical-Electronics Engineering, Faculty of Engineering, Ataturk University, Erzurum, Turkey

Received: 23/02/2022, **Revised:** 23/09/2022, **Accepted:** 19/06/2022, **Published:** 30/12/2022

Abstract

The design of RISC processors, which are the key of digital signal processing applications, are increasing in reconfigurable hardware. FPGAs are suitable reconfigurable hardware for RISC processor design, with advantages such as parallel processing and low power consumption. In this study, the design of the 32-bit RISC processor in a FPGA is presented. The designed RISC processor contains IEEE754 standard floating-point number processing unit, which is executed in one clock cycle. The verification of the processor is performed for the Zynq-7000 SoC Artix-7 FPGA chip in the Xilinx Vivado tool. Classification of an artificial neural network using the iris dataset is carried out in this designed RISC processor. In order to compare the performance, the same artificial neural network is executed in real time in the dual-core ARM Cortex-A9 processor in the operating system of the Zynq-7000 SoC. The results show that the RISC processor designed in the FPGA executes at 20x less clock cycles and 3x higher speed compared to the ARM processor.

Keywords: FPGA, ARM, RISC, reconfigurable hardware

VHDL Kullanarak, Dijital Sinyal İşleme Uygulamaları için IEEE754 Standart Kayan Noktalı Komut Kümesine Sahip RISC İşlemcinin FPGA'de Tasarımı

Öz

Dijital sinyal işleme uygulamalarının kalbi niteliğinde olan RISC işlemcilerin, yeniden yapılandırılabilir donanımlardaki tasarımları giderek artmaktadır. FPGA'ler, paralel çalışma, düşük güç tüketimi gibi avantajlara sahip, RISC işlemci tasarımı için ideal yeniden yapılandırılabilir donanımlardır. Bu çalışma 32-bit RISC işlemcinin FPGA'de tasarımını sunmaktadır. Tasarlanan RISC işlemci, tek saat darbesinde işlem yapabilecek paralellikte olan IEEE754 standartında kayan noktalı sayı işlem birimini içermektedir. İşlemcinin doğrulması, Xilinx Vivado aracında Zynq-7000 SoC Artix-7 FPGA çipi için yapılmıştır. Iris dataseti kullanılarak bir yapay sinir ağının sınıflandırma işlemleri, tasarlanan bu RISC işlemci içerisinde gerçekleştirilmiştir. Performans kıyaslaması yapabilmek için aynı yapay sinir ağı Zynq-7000 SoC'nin işletim sistemi kısmında bulunan çift çekirdekli ARM Cortex-A9 işlemcisinde de gerçek zamanlı olarak çalıştırılmıştır. Elde edilen sonuçlar, FPGA içerisinde tasarlanan RISC işlemcinin, ARM işlemciye kıyasla 20 kat daha az saat darbesinde 3 kat daha yüksek hızda bu işlemi gerçekleştirdiğini göstermektedir.

Anahtar Kelimeler: FPGA, ARM, RISC, yeniden yapılandırılabilir donanım

1. Introduction

With the development of technology, digital signal processing applications (DSP) are increasing significantly in space and defense industry, medicine and various commercial areas. The reduced instruction set computer (RISC) processor is at the heart of such DSP applications [1]. All processors have an instruction set architecture that perform operations according to instructions. Unlike other processors, the RISC processor architecture has a simple instruction set and each instruction is executed in one clock cycle. [2]. Through these advantages, the RISC processor offers a flexible and extensible architecture that provides maximum performance for any processing technology. RISC architectures are used today in phones, tablets and personal computers, as well as supercomputers such as Fugaku, Summit, Sierra, Sunway and TaihuLight [3]. The RISC processor has also been used in DSP applications, video decoding and image acquisition [4]-[5]. Such as applied mathematics and control systems, computations are other usage area of the RISC processor [6]-[7]. In artificial intelligence, speech recognition and motion estimation are examples of the use of the RISC processor [8]-[9].

Reconfigurable computing bridges the gap between software and hardware design using hardware like field programmable gate arrays (FPGAs) [10]. The role of reconfigurable processors in embedded system design has been increasing in recent years. Owing to reconfigurable hardware such as FPGA, processor architectures can be changed by programming [11]. Various RISC processor have been designed in the literature using FPGA. FPGA-based 64-bit RISC processor with self-test verifacated using VHDL was designed in the Xilinx ISE tool [12]. [13] describes a 16-bit RISC processor designed using VHDL, in which behavioral model is preferred to create components. The design is a four-stage pipelined processor. According to [14] presented the design of a pipeline microprocessor without interlocked pipeline stages (MIPS) RISC processor using VHDL. 32-bit RISC processor-based MIPS was designed using VHDL [15]. Unlike the previous paper given above, it presents five-stage, pipeline processor. A from top to down approach is preferred in the design. 16-bit RISC processor design is presented using the VHDL language [16]. The design is simulated and synthesized using Xilinx ISE 13.1. Pipelining is used to speed up to the processor. In pipelining, the instruction cycle is seperated so that multiple processes can be executed in parallel. Designs of subunits of processor are also among the studies in the literature. In the first of these studies, the fetch and decode units of the RISC processor was designed [17]. The design is successfully simulated in the Quartus II tool of Intel. In [18], it is aimed to design the fetch unit and ALU, which are subunits of the RISC processor. The Fetch unit is designed to read instructions stored in memory. The ALU that performs all the computations such as arithmetic and logical operations is at the execution stage of the pipeline. The Xilinx ISE 8.1 tool is used to simulate the design with the VHDL.

When designing real-time digital systems using the RISC processor, there is usually a need to operate with fractional or large numbers. To satisfy this need, various number representations are used according to the performance and accuracy of the design. The floating-point number representation is standardized by IEEE754 and used to represent real numbers in the binary number system. The design of floating point processing units is quite important for system

performance. In this study, RISC processor with IEEE754 standard floating-point unit (FPU) is designed in FPGA. Due to FPU, unlike other RISC processor designs in the literature, the designed processor can process with fractional numbers. Thus, it becomes suitable for real-time signal processing applications. In addition, taking advantage of the parallel processing of the FPGA, the FPU is designed to operate in one clock cycle. Thus, the processor reduces the execution time of any application. This design is verified in the Xilinx Zynq-7000 FPGA chip. Then, classification of iris flower is done by using artificial neural network in the designed processor. Finally, in order to compare the performance, the classification is executed in real time on the ARM processor in the Zynq-7000 chip in the same artificial neural network. The remainder of this article is organized as follows. In section 2, information about floating-point number arithmetic is given and the architecture of the designed RISC processor is presented. In section 3, simulation and synthesis studies of artificial neural network classifying iris flower species in RISC processor are given to verify the behavioral function of the RISC processor.

2. Material and Methods

This section presents the floating-point number representation, the floating-point arithmetic and the RISC processor designed in the FPGA, respectively.

2.1. IEEE754 Standard Floating-Point Number Representation

Floating-point number representation, which was made a standard by the IEEE in 1985, consists of three formats: single precision, double precision and extended precision [19]. A number represented as an IEEE754 floating point consists of sign, exponent and fraction bits. According to the format used, the bit lengths of the exponent and fraction changes. In Table 1, information about bit lengths for single precision, double precision and extended precision number formats is given.

Table 1. Floating-point number formats

Format	Sign Bits	Exponent Bits	Fraction Bits
Single	1	8	23
Double	1	11	52
Extended	1	15	112

2.2. Floating Point Arithmetic

Multiplication, division, addition, and subtraction are among floating-point number arithmetic operations. All operation are executed in specially designed units. Floating-point addition and subtraction is performed in only one unit given in Figure 1. This unit has the highest latency, the longest design time and the most complex among floating-point operations.

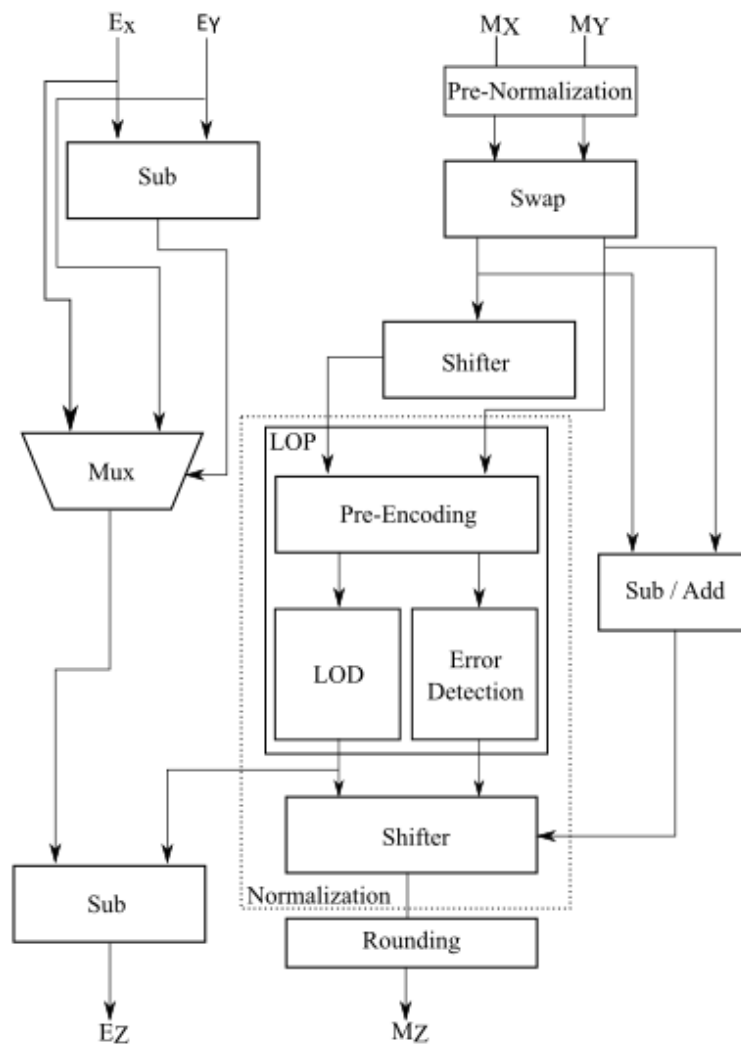


Figure 1. Adder/subtractor micro-architecture

Firstly, in the floating point addition/subtraction unit, first the exponents of the two numbers are subtracted to determine the large and small number. The '1' bit is placed to the left of the fraction bits for pre-normalization. The fraction of the smaller number is shifted to the right according to subtraction of exponents. The fraction from the shift operation and the fraction of the larger number are sent to the sub/add module. While the process is running in the sub/add module, the estimation of the position of the most significant '1' bit required for normalization is done by the leading one predictor module (LOP). Normalization is performed by shifting the numbers to the left by the estimated amount from LOP if the signs are different, or by shifting one bit to the left or right depending on the situation. The fraction obtained by normalization is rounded. To determine the exponent of the result, the exponent of the large number is set and the result is obtained.

Multiplication, another floating-point operation, is among the most used operations along with addition in digital signal processing applications. Floating-point multiplication is executed within the unit given in Figure 2.

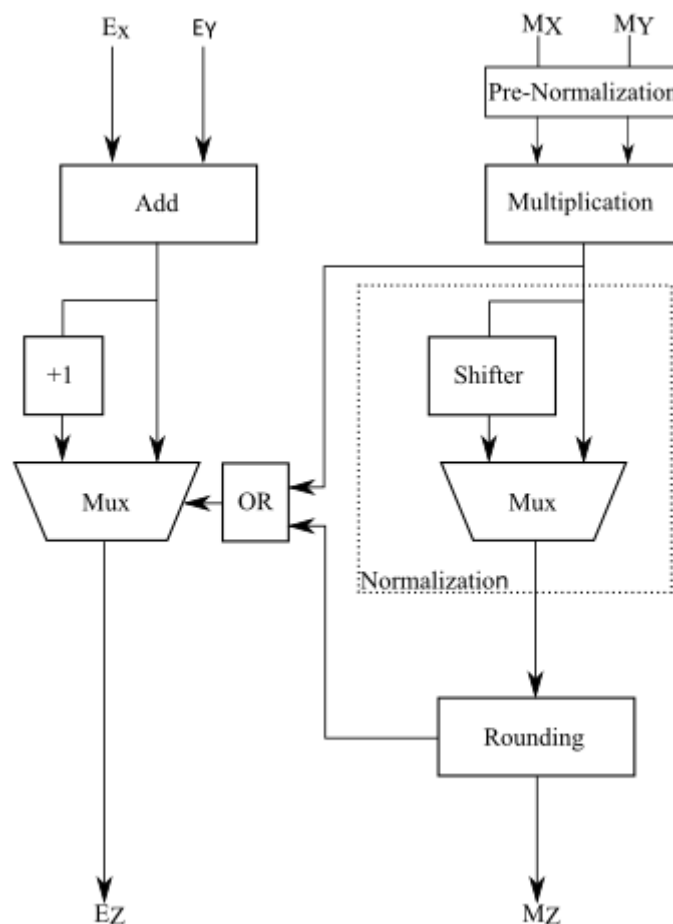


Figure 2. Multiplier micro architecture

Pre-normalization is performed by placing '1' to the left of the most significant bit of the fraction of two numbers in the floating point multiplication unit. After the pre-normalization, the fractions of the numbers are multiplied. As the multiplication continues, the exponents of the numbers are added to get the exponent of the result. The most significant bit of the multiplication result of the fractions is checked. If the corresponding bit is '1', the exponent resulting from the sum is increased by 1. The obtained fraction is rounded so that the result is found.

The floating-point division operation is similar to the multiplication. It is in the form of subtracting two numbers and dividing fractions. The micro-architecture of the floating point divider unit is given in Figure 3.

In the floating-point division operation, pre-normalization is performed by placing '1' to the left of the most significant bit of the fractions of two numbers. The fractions got by pre-normalization are divided. At this time, the exponents of the numbers are subtracted in parallel. The fraction from the division operation is rounded to form the fraction of the result, thus the result is obtained.

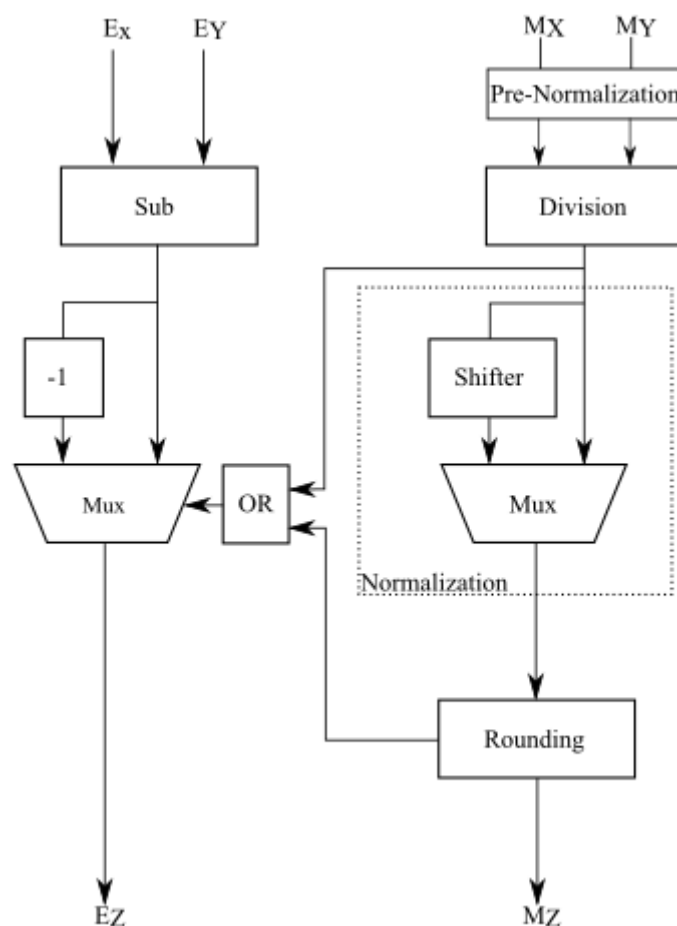


Figure 3. Floating-point divider micro architecture

2.3. 32-bit RISC Processor Design

In this section of the study, information is given about the designed RISC processor, FPU unit, CPU, registers, program counter, main memory and I / O ports.

Before any computer hardware can be designed, the instruction should be defined. Some computer hardware has very few instructions to reduce the physical size of the circuit required by the CPU. Such a design allows the CPU to execute instructions at a high frequency. This architectural approach used when designing computer hardware is called RISC [2].

In a RISC processor, one clock cycle is required to execute any instruction. It is easy to convert a RISC processor into a pipelined design, because all instructions are processed in the same time and the opcode and the operand take the same position in the number sequence. The RISC processor to be designed in this study consists of AN FPU operating in IEEE754 single precision floating-point number representation, a program memory, a data memory, a control unit and registers. The micro-architecture of the designed RISC processor is given in Figure 4.

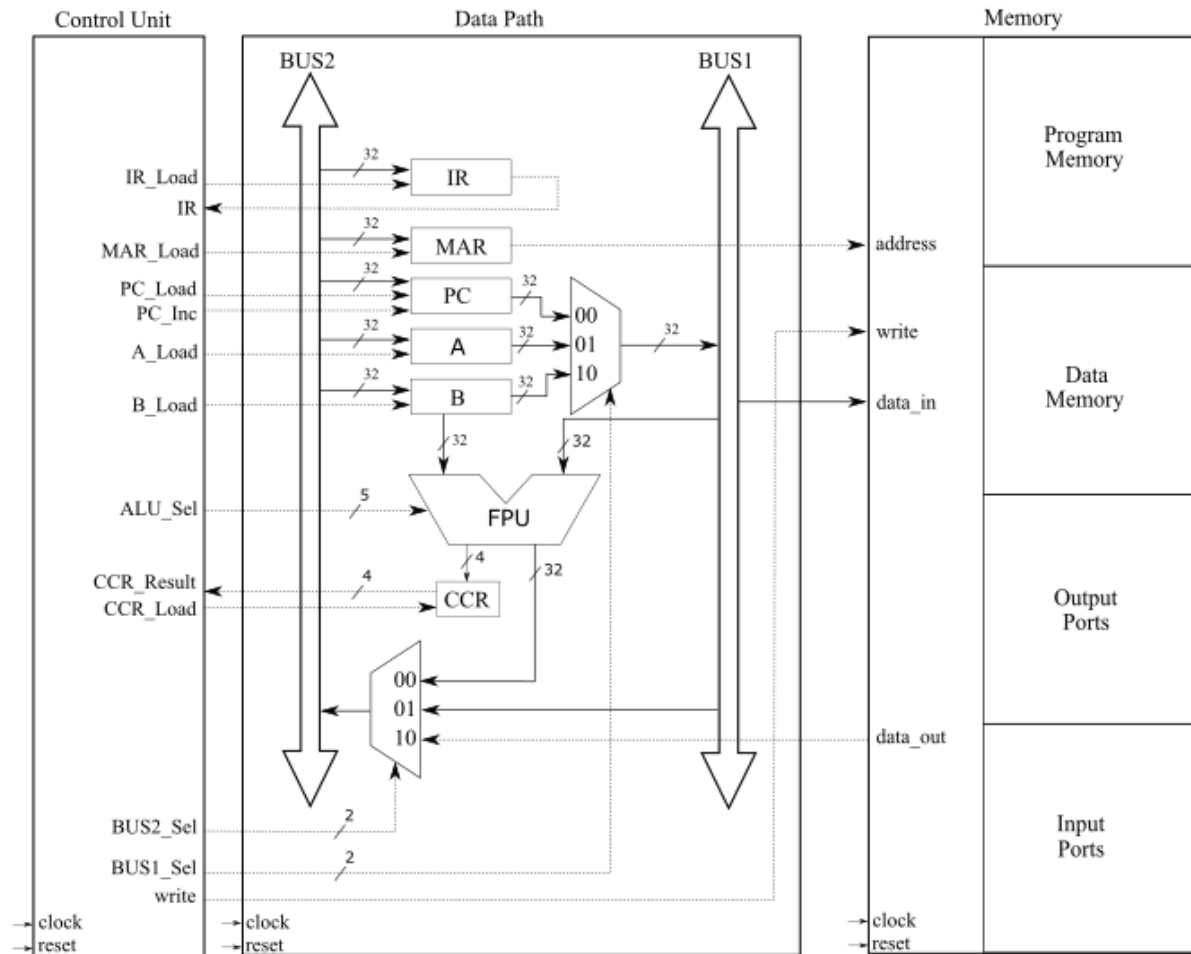


Figure 4. RISC processor micro architecture.

2.3.1. Control Unit

All operations performed within the RISC processor are managed by the control unit. Therefore, the design of the control unit is quite important so that the instruction to work properly in the right order. In this study, the control unit is designed as a finite state machine (FSM) that executes the Fetch, decode and execute stages. Two status signals, current state and next state, in the control unit are shown in Figure 5.

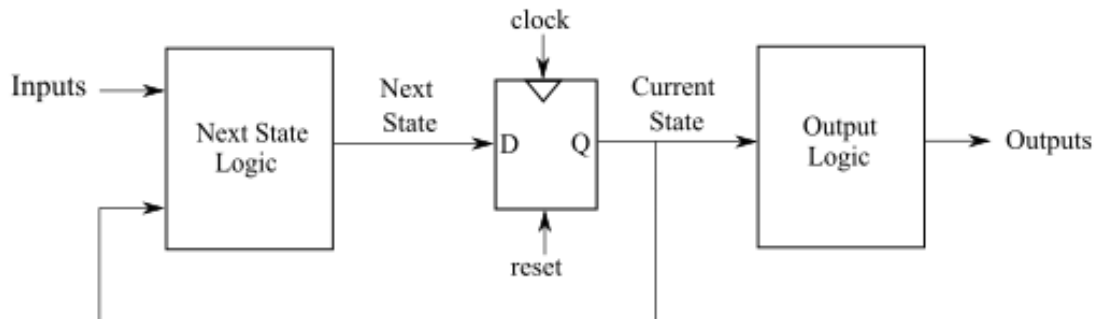


Figure 5. Control unit FSM

The current state is in a synchronous and sensitive to the clock and reset signal. Current state changes its state according to next state. Next state is a combinational structure that runs according to the current state and inputs. In addition, the output logic circuit, which is responsible for producing the relevant output in any situation, which changes depending on the current state, is also located in the control unit. The output logic circuit is only sensitive to the current state. Thus, the signals produced by the control unit can be sent to the memory or data bus asynchronously, without waiting for the next clock cycle. As can be seen in Figure 6, the current state and the next state in the control unit are three stages: Fetch, Decode and Execute.

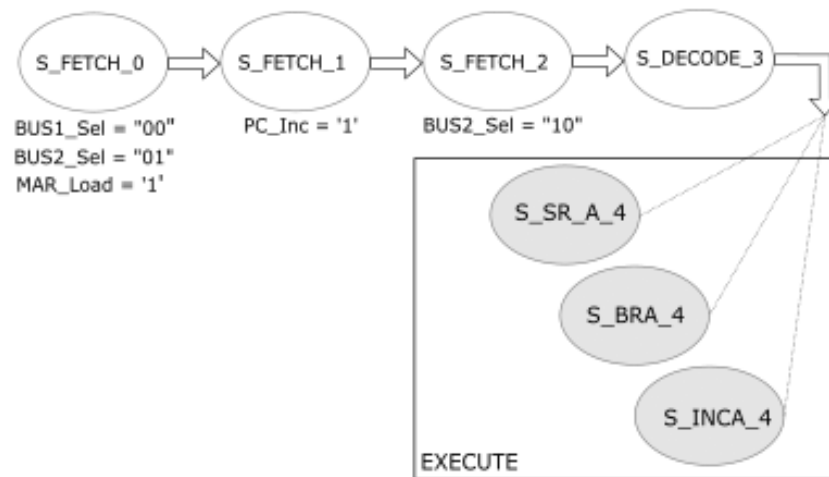


Figure 6. Fetch, Decode and Execute stages

In Fetch, the instruction in the program memory is read and written to the instruction register (IR). Fetch consists of three sub-branches. In S_FETCH_0, firstly BUS1_Sel signal is set to "00" value and PC register value is sent to BUS1. Then, the BUS2_Sel signal is set to "01" and the data in BUS1 is sent to BUS2. Finally, by making the MAR_Load signal '1', the address going to the memory is updated. Thus, the data at the corresponding address in the memory can be accessed.

The program counter is made ready by setting PC_Inc signal as '1' in S_FETCH_1 and increasing the value of PC register by 1. In S_FETCH_2, the BUS2_Sel signal is set to "10" and the value read at the relevant address in the memory is transferred to BUS2. Then, the IR_Load signal is set to '1' and the instruction in BUS2 is loaded into the IR register. In Decode, the identity of the instruction is detected. Finally, the instruction detected in the execute state is performed inside the processor. For this, the instructions given in Table 2 are used.

The instructions are executed sequentially in the program memory and the desired operation is performed by the processor. These instructions actually create a software. By correctly writing and sequencing the instructions, the software to be executed by the processor is built. Executing the software and converting it to machine code is carried out by the processor.

Table 2. Instruction Set of the Designed RISC Processor

Type	Instruction
Loads and Stores	<i>LDA_IMM, LDA_DIR LDB_IMM, LDB_DIR STA_DIR, STB_DIR</i>
Floating-Point Arithmetic	<i>FP_ADD_AB FP_SUB_AB FP_DIV_AB FP_MULT_AB</i>
Logical	<i>AND_AB, OR_AB, XOR_AB, NOT A, INCA, INCB DECA, DECB SR_A, SL_A SR_B, SL_B</i>
Branches	<i>BRA, BMI, BPL, BEQ, BNE, BVS, BVC, BCS, BCC</i>

The instructions for the software to be executed by the processor are written to the program memory in order. The sequential reading of these instructions in the program memory is realized by the PC register. In Figure 7, the PC register in the processor is given.

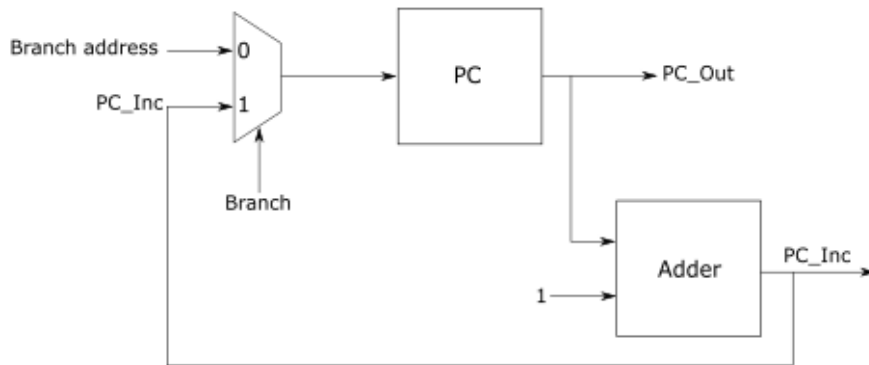


Figure 7. PC register structure

The PC register actually runs like a counter. The value of the PC register is zero in the first stage for any software to be implemented. Then the value of the PC register is incremented by 1 in each time a read is made from the memory. With the branches instructions listed in Table 2, the PC register jumps to the address value in the operand with or without negative, zero, overflow and carry flag conditions. This ensures that the instructions are executed correctly.

2.3.2. Program Memory

The program memory where the instructions are stored is located in the memory given in Figure 8 in the processor.

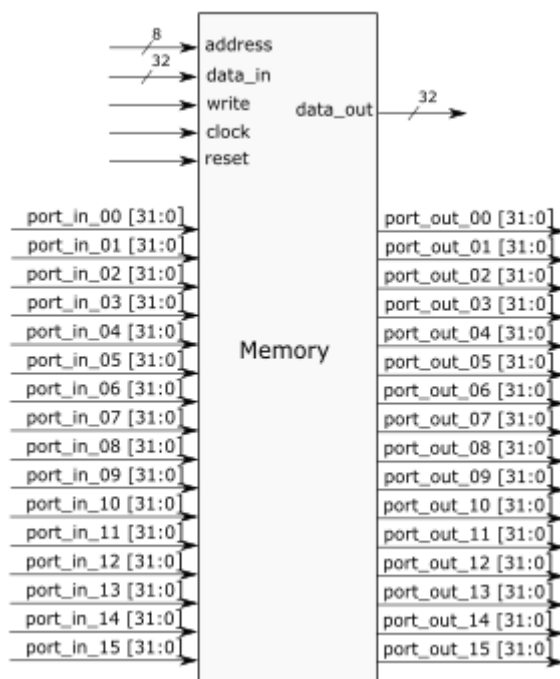


Figure 8. Processor memory

Memory consists of program memory, data memory and input and output ports. The program memory has a capacity of 512 bytes, and the data memory has a capacity of 384 bytes. Any instruction or data from the memory is read and written with the MAR register. The counter value in the PC register is sent to BUS2 in order to read or write. Then, the MAR_Load signal is set '1' and the address value in BUS2 is sent to the MAR output and thus to the memory.

2.3.3. Floating-Point Unit (FPU)

In the FPU, logical operations and shift operations are carried out as well as floating-point arithmetic operations. Figure 9 shows the FPU.

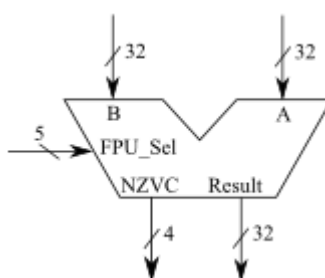


Figure 9. Floating-point unit

Which operation will be executed in the FPU is selected by FPU_Sel. The operations corresponding to FPU-Sel bits are listed in Table 3.

Table 3. FPU operations

FPU_Sel	Operation
00000	<i>A = A + B in floating-point</i>
00001	<i>A = A - B in floating-point</i>
00010	<i>A = A * B in floating-point</i>
00011	<i>A = A / B in floating-point</i>
00100	<i>A = A and B</i>
00101	<i>A = A or B</i>
00110	<i>A = A xor B</i>
00111	<i>A = not A</i>
01000	<i>B = not B</i>
01001	<i>A = A + 1 in floating-point</i>
01010	<i>B = B + 1 in floating-point</i>
01011	<i>A = A - 1 in floating-point</i>
01100	<i>B = B - 1 in floating-point</i>
01101	<i>Shifts A one bit to the right</i>
01110	<i>Shifts A one bit to the left</i>
01111	<i>Shifts B one bit to the right</i>
10000	<i>Shifts B one bit to the left</i>

The 4-bit NZVC number got from the FPU output is used to store negative, zero, overflow, carry exceptions. These exceptions are loaded into the CCR register and sent to the control unit. The corresponding NZVC values for the exceptions are listed in Table 4.

Table 4. NZVC exceptions

ALU_Sel	Operation
Negative Results	<i>1000</i>
Zero Result	<i>0100</i>
Overflow Result	<i>0010</i>
Carry Result	<i>0001</i>

3. Design Verification and Simulation Results

The processor is designed using the very high-speed integrated circuit hardware description language (VHDL). Behavioral verification of the designed processor is done on Xilinx Zynq-7000 using Vivado Design Suite. In order to perform the behavioral verification, the machine

code for the artificial neural network (ANN) given in Figure 10 is programmed and placed in the program memory.

ANN structure is quite simple. Inputs and weights are dot multiplication within the processor, and each product is summed. The result is calculated by adding bias to the summed value. The result obtained is passed through a decision mechanism. Also, the activation function used is a linear function.

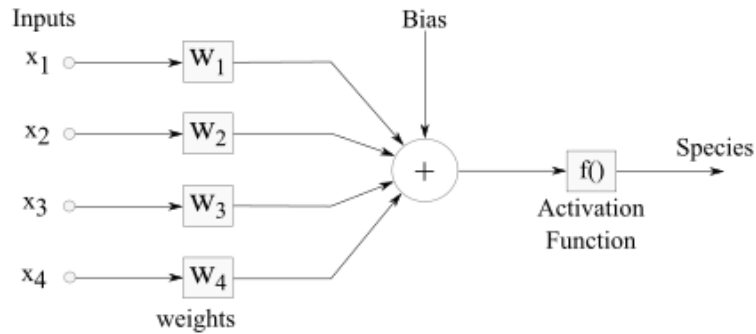


Figure 10. An artificial neural network architecture for Iris classification

100 data taken from the iris dataset, 67 are used for training the network and 33 are used for testing. Some test data used as input are given in Table 5 [20].

Table 5. Test data for iris flower

Sepal Length (x_1)	Sepal Width (x_2)	Petal Length (x_3)	Petal Width (x_4)	Species
6	2.7	5.1	1.6	<i>Versicolor</i>
4.8	3	1.4	0.3	<i>Setosa</i>
5.5	2.3	4	1.3	<i>Versicolor</i>
5.9	3.2	4.8	1.8	<i>Versicolor</i>
5.1	3.8	1.9	0.4	<i>Setosa</i>
5.1	3.4	1.5	0.2	<i>Setosa</i>
4.6	3.6	1	1.1	<i>Setosa</i>

These features are sent as input to the network and the species of iris flower is obtained at the output. ANN is simulated in Vivado Design Suite to verify the designed RISC processor. The simulation results for the features in the first four rows given in Table 5 are as in Figure 11.

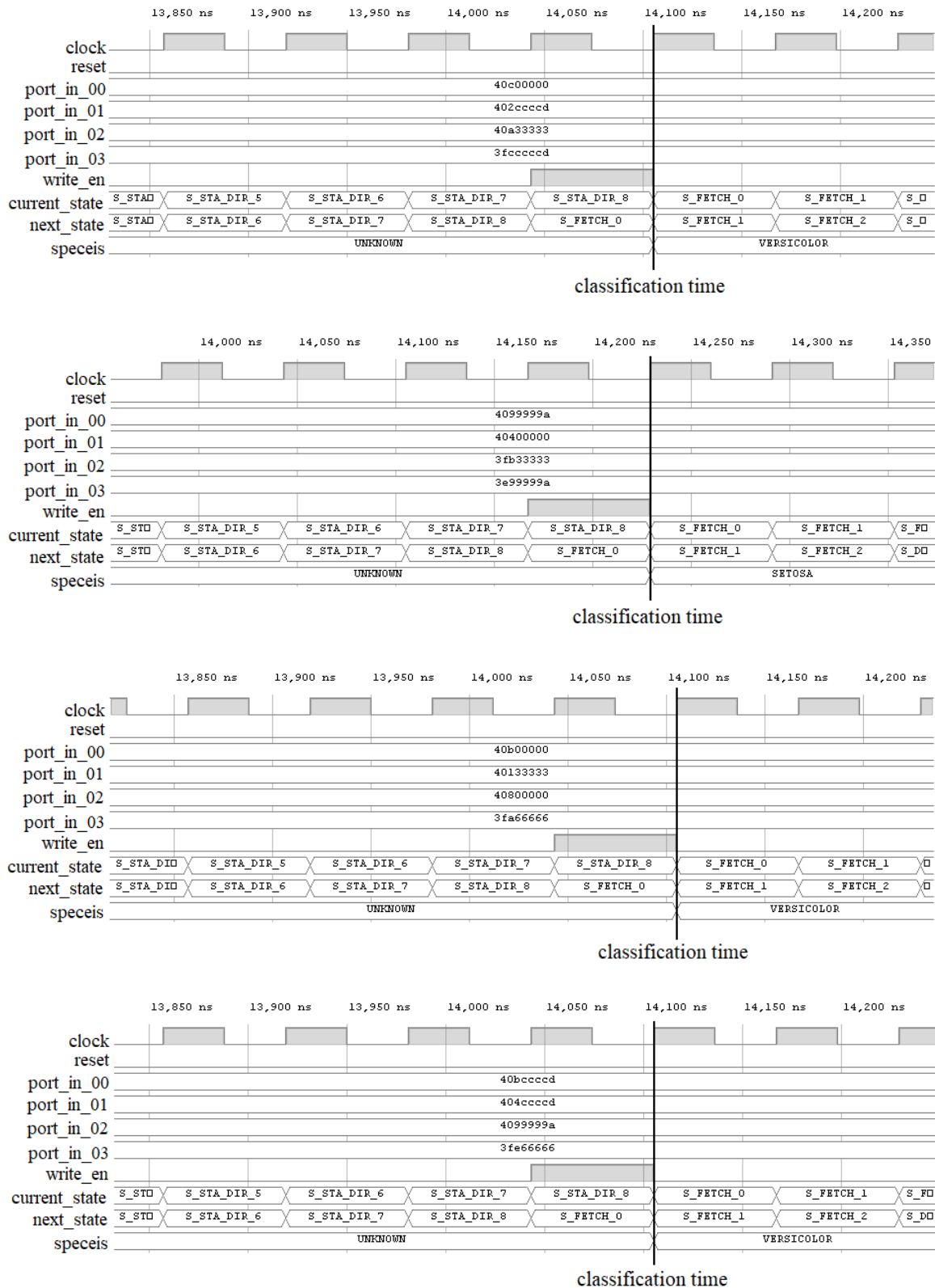


Figure 11. Simulation results for iris classification

In order to compare performance, the software of the same artificial neural network is carried out in real time in the dual-core ARM Cortex A9 processor in the same chip, the Zynq-7000, and the results given in Table 6. Results are obtained by Xilinx Vivado tool.

Table 6. Frequency, clock cycle and execution time for FPGA and ARM

	Frequency (MHz)	Clock Cycle	Execution Time (μ s)
RISC Processor Designed in FPGA	16	456	14.11
Software in ARM Processor	100	9140	45.7

4. Conclusion

FPGAs are widely used in processor design due to their advantages such as parallel processing, low power consumption and reconfiguration. This study focuses on the design of a RISC processor in a FPGA. Unlike other RISC designs, the RISC processor in this study includes an FPU. Through the FPU, various complex digital signal processing applications such as ANN, image processing, object recognition and video decoders can be implemented simply by software on this processor. Classification of Iris flower species is executed using ANN in the designed processor. In this way, both hardware design and software programming of the RISC processor in FPGA are included and its verification is also provided. The classification is implemented using the same ANN on the ARM processor to compare the performance. The results show that the processor designed in FPGA operates faster and with fewer clock cycles.

Ethics in Publishing

There are no ethical issues regarding the publication of this study.

Author Contributions

B.Ö: programming, design of the study, T.K: presented idea of the study. All authors discussed the results and contributed to the final manuscript.

References

- [1] Palekar, S., & Narkhede, N. (2016) 32-Bit RISC processor with floating point unit for DSP applications, Paper presented at the 2016 IEEE International Conference on Recent Trends in Electronics, Information & Communication Technology (RTEICT).
- [2] LaMeres, B. J. (2019) Introduction to logic circuits & logic design with VHDL. Springer.
- [3] Amit, S. (2006) Mac OS X internals: a systems approach, Addison-Wesley Professional.
- [4] Yamada, K., Kojima, M., Shimizu, T., Sato, F., & Mizuno, T. (2002) A new RISC processor architecture for MPEG-2 decoding, IEEE Transactions on Consumer Electronics, 48(1) 143-150.

- [5] Kumar, P. S., Shashidhar, B., & Bhargav, J. S. (2010) Image acquisition from CMOS Active Pixel Sensor using RISC processor. Paper presented at the 2010 International Conference on Signal and Image Processing.
- [6] Garbey, M. (2005) Acceleration of the Schwarz method for elliptic problems. *SIAM Journal on Scientific Computing*, 26(6) 1871-1893.
- [7] Bhakti, T. L., Susanto, A., Santosa, P. I., & Widayati, D. T. (2012) Design of Bovine Semen Temperature Controller Using PID. *Int. J. of Comp. Eng. Res*, 2(7) 52-58.
- [8] Chang, C.-T., Chang, C.-T., Yang, H.-L., & Chang, H.-T. (1996) Real-time implementation of speech recognition using RISC processor core. Paper presented at the Proceedings Ninth Annual IEEE International ASIC Conference and Exhibit.
- [9] Bilal, M., & Masud, S. (2007) Efficient color space conversion using custom instruction in a risc processor. Paper presented at the 2007 IEEE International Symposium on Circuits and Systems.
- [10] Hauck, S., & DeHon, A. (2010) *Reconfigurable computing: the theory and practice of FPGA-based computation*: Elsevier.
- [11] Ball, J. (2007) Designing soft-core processors for FPGAs. In *Processor Design* (pp. 229-256): Springer.
- [12] Mohammad, I., Ramananjaneyulu, K., & Veeraswamy, K. (2012) FPGA implementation of a 64-bit RISC processor using VHDL. *International Journal of Engineering Research and Applications (IJERA)*, 2(3) 2544-2549.
- [13] Thakor, K. P., & Pal, A. (2017) Design of a 16-bit RISC Processor Using VHDL. *Int. J. Eng. Res. Technol (IJERT)*, 6.
- [14] Valli, B., Kumar, A. U., & Bhaskar, B. V. (2012) FPGA Implementation and Functional Verification of a Pipelined MIPS Processor 1.
- [15] Mane, P. S., Gupta, I., & Vasantha, M. (2006) Implementation of RISC Processor on FPGA, Paper presented at the 2006 IEEE International Conference on Industrial Technology.
- [16] Kadam, S. U., & Mali, S. (2016) Design of risc processor using VHDL, 2016 *International Journal of Research Granthaalaya*, 4(6).
- [17] Luker, J. D., & Prasad, V. B. (2001) RISC system design in an FPGA. Paper presented at the Proceedings of the 44th IEEE 2001 Midwest Symposium on Circuits and Systems. MWSCAS 2001 (Cat. No. 01CH37257).
- [18] Ghaturlle, M. S., & Kadam, R. (2017) Review Paper on 32-Bit RISC Processor with Floating Point Arithmetic. *Int. Research Journal of Engineering and Technology (IRJET)*, 4.

- [19] Electrical, I. o., Committee, E. E. C. S. S., & Stevenson, D. (1985) IEEE standard for binary floating-point arithmetic: IEEE.
- [20] Fisher, R. A. and Marshall M. (1988) “UCI repository of machine learning databases”. University of California.

A Three-Stage Hybrid Multi-Criteria Model for Material Selection in Subsea Pipeline Design

Daniel O. AIKHUELE *

¹ Department of Mechanical Engineering, University of Port Harcourt, East-West Road, Port Harcourt, Rivers State, Nigeria

Received: 25/02/2022, Revised: 23/06/2022, Accepted: 07/07/2022, Published: 30/12/2022

Abstract

Subsea pipelines are such a crucial part of offshore oil and gas production, therefore their design and construction should be as efficient and cost-effective as possible. Proper material selection is critical for a successful operation and a longer pipeline lifespan. For the selection of a design material with the highest reliability under a dynamic environment as the one obtained in the oil and gas industry, a three-stage hybrid multi-criteria model has been proposed. The hybrid multi-criteria model, which is based on an integrated Analytical Hierarchy Process (AHP) model and the VlseKriterijumska Optimizacija I Kompromisno Resenje (VIKOR) model, is used for the evaluation and selection of a suitable and high reliability-based design material for the subsea pipeline design by considering several operational and environmental scenario the pipes might encounter in the field. With the vast amount of engineering materials available to the design engineer, selecting a suitable and high reliability-based material for the subsea pipeline design is a tedious and demanding task, especially in a dynamic environment and scenario. In this paper, ten subsea pipeline material alternatives of different types, with seven criteria, have been critically examined under a three-case scenario. Results from the evaluation show that for the first case study scenario -sour service hydrocarbon transport in deep waters-, 22% Cr stainless steel is found to be the best choice material, for the second case study scenario, Carbon Fiber Reinforced Polymer is selected as the best. While for the third case study scenario, carbons steel and polymers material is found to be the most reliable material choice.

Keywords: Three-stage hybrid multi-criteria model, AHP model, VIKOR model, subsea pipelines

Denizaltı Boru Hattı Tasarımında Malzeme Seçimi İçin Üç Aşamalı Hibrit Çok Kriterli Bir Model

Öz

Denizaltı boru hatları, açık deniz petrol ve gaz üretiminin çok önemli bir parçasıdır, bu nedenle tasarımları ve inşaatları mümkün olduğunca verimli ve uygun maliyetli olmalıdır. Doğru malzeme seçimi, başarılı bir operasyon ve daha uzun boru hattı ömrü için kritik öneme sahiptir. Petrol ve gaz endüstrisinde elde edilenden daha dinamik bir ortamda en yüksek güvenilirliğe sahip bir tasarım malzemesinin seçilmesi için, üç aşamalı hibrit çok kriterli bir model önerilmiştir. Entegre bir Analitik Hiyerarşi Süreci (AHP) modeline ve VlseKriterijumska Optimizacija I Kompromisno Resenje (VIKOR) modeline dayanan hibrit çok kriterli model, boruların sahada karşılaşılabileceği çeşitli operasyonel ve çevresel senaryolar göz önünde bulundurularak denizaltı boru hattı tasarımı için uygun ve yüksek güvenilirliğe dayalı bir tasarım malzemesinin değerlendirilmesi ve seçilmesi için kullanılmaktadır. Tasarım mühendisi için mevcut olan çok miktarda mühendislik malzemesi ile, denizaltı boru hattı tasarımı için uygun ve yüksek güvenilirliğe dayalı bir malzeme seçmek, özellikle dinamik bir ortamda ve senaryoda sıkıcı ve zorlu bir işittir. Bu yazıda, yedi kritere sahip farklı tipte on denizaltı boru hattı malzemesi alternatifi, üç vakalı bir senaryo altında eleştirel olarak incelenmiştir. Değerlendirmeden elde edilen sonuçlar, ilk vaka çalışması senaryosu için - derin sularda ekşi hizmet hidrokarbon taşımacılığı - için % 22 Cr paslanmaz çeliğin en iyi seçim malzemesi olarak bulunduğunu, ikinci vaka çalışması senaryosu için Karbon Fiber Takviyeli Polimerin en iyisi olarak seçildiğini göstermektedir.

Üçüncü vaka çalışması senaryosu için, karbonlar çelik ve polimer malzemesinin en güvenilir malzeme seçimi olduğu bulunmuştur.

Anahtar Kelimeler: Üç aşamalı hibrit çok kriterli model; AHP modeli; VIKOR modeli; denizaltı boru hatları.

1. Introduction

Subsea pipelines are one of the most important aspects of the offshore industry. Due to the rapid growth of the oil and gas industry, exploration and production are tending into deeper waters with harsher conditions. It is a well-known fact that corrosion is a common and costly issue in the oil and gas industry and even more costly in the offshore sector. The use of metals such as carbon steel has been the norm and the go-to for most offshore pipeline projects over the better part of the century, this is mainly because of its excellent mechanical properties and high pressure and thermal resistance. However, in harsher corrosion environments, carbon steel has proven to be inadequate and resulted in billions of dollars in repair costs. According to a study done by the National Association of Corrosion Engineers (NACE), the cost of corrosion had reached more than US\$ 600 billion in 2001, accounting for roughly 4%–6% of the country's gross national product [20].

In corrosive environments, intensive corrosion control methods, such as inhibitors, cathodic protection, and coating, are required to maintain the integrity of the pipes, insufficiency or inadequate measures can even result in the need for early replacement [18]. A more corrosion-resistant pipe technology, such as Corrosion-resistant alloys (CRA) and polymer composites, should be chosen to reduce pipeline corrosion. CRA such as duplex stainless steel, and nickel-based alloy have proven to be effective in harsher corrosion environments, however, they are significantly more costly than carbon steel and are mostly used to clad or line carbon steel pipes [9]. In the petroleum industry, the financial benefits from employing materials that are lighter, stiffer, stronger, and more corrosion resistant than carbon steel are significant. In this category, composite materials are a major contender. As exploration and production continue to extend globally into deeper waters and harsher environments, the spotlight is shifting to lightweight fiber-reinforced plastic (FRP) solutions as replacements for steel [10]. This is made possible with the approval of new industry standards DNV OS C501. Fiber-reinforced thermoplastics are ideal candidates for subsea applications across multiple sectors, including underwater vehicles, marine construction, and offshore oil and gas, due to several desirable characteristics including high specific strengths and moduli and excellent corrosion resistance [10].

Considering all these different materials, material selection is crucial to any engineering design. In the area of material selection where there are numerous choices and various influencing criteria, a more precise mathematical approach is required. It is observed that choosing the most appropriate material for a specific product from a finite set of alternatives is an example of multi-criteria decision-making (MCDM) problem [2, 14, 22]. To make the best decision on MCDM problems, the analytical hierarchy process (AHP) model, which has widely been used in literature is applied [1, 3, 8, 22]. This research addresses the problem of material selection of subsea pipelines. Material failure is the leading issue in offshore pipelines leading to billions of

dollars in loss. In the design and development of any structural elements, material selection is one of the most challenging issues and it is also critical for success and to meet the demands of cost reduction and better performance [5].

Designers should have a clear understanding of the functional requirements for each component and detailed knowledge of the considered criteria for a specific engineering design when choosing the most appropriate material from an ever-increasing array of viable alternatives, each with its characteristics, applications, advantages, and limitations. Improper selection of material may often lead to huge cost involvement and ultimately drive towards premature component failure [12]. Variations in national standards, legislative requirements, operator procedures, and risk tolerance also play a substantial role in the materials selection process. These challenges require different approaches to pipeline materials selection, which may vary strongly between different nations and operators. The most important factor to ensure the integrity of subsea pipelines is an excellent material selection process. Corrosion-resistant alloys, although known to be an excellent alternative to conventional carbon steel materials, carry a limitation when the factor of the cost is put into play. In this sense, non-metallics are gaining more and more appeal and attention, given their potential to minimize the cost of both corrosion management and material [16].

With the innovation of new non-metal materials that are well suited for subsea pipelines and the expensive limitations of current metal materials, the growing need for companies to re-evaluate their material choices is inherent. Although metals can undergo processes to combat the high requirements of corrosion environments, it is a costly and difficult process. Therefore, a more cost-effective solution is required which lies with materials with inherent corrosion resistance such as composite or polymers. Composite pipes are strong, durable, flexible, lightweight, and have low installation and maintenance costs but they have a higher material unit cost than carbon steel [17]. This is one of the reasons why it is attractive to use carbon steel, because of the high cost of operating the lay barge, the installation of a submarine pipeline accounts for the majority of the total cost. The faster the pipe can be welded, the faster it can be installed, and the lay barge may be used for a shorter period. This cost can be reduced in the case of Thermoplastic composite pipes (TCP), which are spool-able and are produced to be several kilometers in length.

As earlier stated, the problem of material selection arises in subsea pipelines due to the vast array of materials that can be used and the standards governing these materials. This research is aimed to develop a novel approach using numerical methods to guide the selection process based on the following criteria; corrosion resistance, thermal resistance, fatigue resistance, cost, ease of installation and manufacture, density, and hardness under a three case scenario that has been carefully examined for the material selection and evaluation [15, 23, 24]. These scenarios, which are related to the fluid passing through the pipe and the environmental conditions of the pipes, affect the weighting of the criteria used. The case study scenario includes sour service hydrocarbons transport in CO_2 environments, aggressive chemicals in deep waters, and non-corrosive fluids -industrial water lines- [7].

To address the aim of the study, a three-stage hybrid fuzzy multi-criteria decision model has been proposed for selecting suitable and reliable materials for the design of the subsea pipeline by considering cost, efficiency, and reliability with the view to meet the full requirements of the various international standards such as DNV-OS-F10, NORSOK M-001, ASME B36, and API codes.

The hybrid multi-criteria model is based on an integrated Analytical Hierarchy Process (AHP) model and the VlseKriterijumska Optimizacija I Kompromisno Resenje (VIKOR) model. The study contributes to material selection literature, by providing a new model that allows various material types such as metals, polymers, alloys, and composites to be selected depending on the operational and environmental scenario considered. This is completely novel, as previous researches and evaluation approaches presented in the literature are limited to the selection of a single type of material. The combination of the two models is based on the following advantages of the models. The AHP approach provides the weighting step of the criterion, as well as the consistency test to determine if the weight gained is consistent. The weighting process is only handed away by the experts without confirming the weighting consistency, which is a flaw in the VIKOR approach. The AHP approach, on the other hand, suffers from a flaw in the cracking process. If more and more options are added to the AHP cracking process, it becomes more difficult. The VIKOR approach, on the other hand, offers advantages in the cracking process due to its preference values for cracking and its ability to readily overcome many alternatives.

The remaining section is organized as follows, in Section 2, the methodology that comprises the three-stage hybrid multi-criteria model is introduced. This is followed by the application of the model for a real-life case study in Section 3. Finally, in Section 4, some concluding remarks are presented, as well as the limitations of the study.

2. Methodology

The proposed methodology consists of three basic stages; identification of criteria, AHP computations, and ranking of the alternative materials using the VIKOR model. Figure 1 shows the flow diagram of the proposed methodology. The proper criteria and materials are selected and analyzed in the first stage, and the decision hierarchy is framed, this hierarchy is then approved. After the approval, the criteria are assigned weight using the analytical hierarchy process (AHP) in the second stage. The third stage will consist of using the VIKOR method to rank the alternative materials. The result gives the best candidate material.

2.1. Criteria Definition

The following criteria are created to meet the objective for the material selection of subsea pipelines;

- I. Corrosion resistance (CR): the ability to withstand the destructive action of corrosive mediums.
- II. Thermal resistance (TR): the heat property and a measurement of a temperature difference by which an object or material resists heat flow.

- III. Fatigue resistance (FR): the highest stress that a material can withstand for a given number of cycles without breaking.
- IV. Cost (C): The value of money that has been used to purchase the material.
- V. Manufacture and installation (MI): The ease at which the material is manufactured and installed, including time, and cost.
- VI. Density (D): a measurement of how much mass is in a given volume.
- VII. Hardness (H): resistance to plastic deformation, penetration, indentation, and scratching.

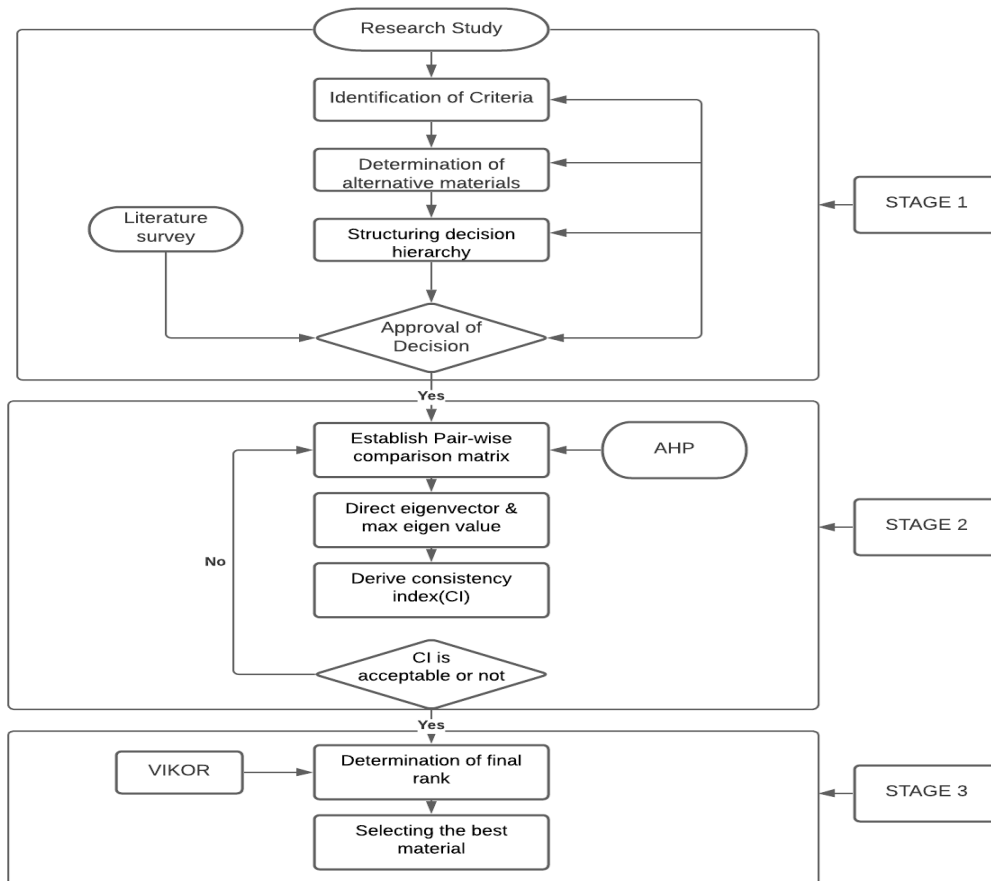


Figure 1. Schematic Diagram for Proposed Model for Material Selection

2.2. Alternative Materials

There is a wide range of engineering materials to choose from according to the certified codes and standards. Among these materials, the primary materials used for pipelines include metallic materials and non-metallic materials.

2.2.1. Metallic Materials

Traditionally, metals are the materials of choice in the offshore oil and gas sector because of the following advantages;

- I. Their performances have been well documented over the years in various design conditions.
- II. Can be used over a wide range of temperatures and pressures to meet a variety of design requirements.

III. Adequate standards governing the use of the materials.

The most common metallic materials used in subsea pipeline applications are steels and corrosion-resistant alloys (CRA). Amongst the steels, carbon steel has been used as the go-to material for pipelines, but one of the limitations of carbon steel is the lack of inherent corrosion resistance, which is vital in subsea pipelines. To combat the problem of corrosion, corrosion-resistant alloys have been found adequate, although not without their limitations. Examples of CRAs include stainless steels (e.g., austenitic, ferritic, martensitic, and duplex) and nickel-based alloys.

2.2.2. Non-Metallic Materials

Non-metallic materials offer the most appropriate choice for fluid services and process conditions that are very aggressive to commonly used metallic materials (such as steel), or as an economically attractive option between the use of steel and the relatively more expensive materials such as CRAs. Non-metallic materials used in offshore oil and gas applications are of two types, Polymers, and composites.

The use of polymers and composites in subsea pipelines is due to their high resistance to corrosion and also the economic advantages over CRAs. Polymers used in pipelines are of three types; Thermoplastic, thermosets, and Elastomers. The two common types of composites used in pipelines are Carbon fiber reinforced polymers (CFRP) and glass fiber reinforced polymers (GFRP).

2.2.3. Materials Selected

In this study, ten alternative materials will be evaluated and selected for the three different case study scenarios, the materials are as follows; Carbon steel (CS), 13% Cr martensitic stainless steel, 22% Cr Duplex stainless steel, 25% Cr Super Duplex stainless steel, 316L austenitic stainless steel, High-density Polyethylene (HDPE), ACETAL (Polyoxymethylene POM-C), Polyamide 12 (PA12), Glass fiber reinforced epoxy (GRE), and Carbon Fiber-reinforced polymer (CFRP). Table 1, highlights the materials, their type, capabilities, and limitations. From research and analysis, the material properties used for the different case scenarios were rated by a group of five (5) material engineering experts specially selected from the academia to evaluate and give their opinion on the materials considered by using the criteria rating (Likert) scale as presented in the Table. Finally, their evaluated results and opinions are then aggregated based on the scale, and the results are shown in Table 2.

Table 1. Material Capability

Material	Type	Capability	Limitations	
Carbon Steel	Steel	High ductility, toughness, machinability and weldability, low cost	Low corrosion resistance	
13% Cr Martensitic SS	CRA	good ductility and corrosion resistance, easily forged and machined	Costly, Requires PWHT	
22 % Cr Duplex SS	CRA	High corrosion resistance, temperature ranges from -50°C to 300°C	Expensive	
25%Cr Super Duplex	CRA	Higher Mechanical strength, corrosion resistance, good temperature range	Expensive	
316L	CRA	Good corrosion resistance is easily machined and welded.	Moderate cost to high cost	
HDPE	Thermoplastic	High impact resistance, resistance to CO ₂ and H ₂ S, low cost	Low strength, max temp of 90°C.	
Acetal	Thermoplastic	Good mechanical properties, good fatigue strength	Not resistant to Hydrocarbons over 80°C.	
PA12	Thermoplastic	Good chemical and corrosion resistance, flexibility, and durability.	Maximum temp of 80°C.	
GRE	Composite	Excellent corrosion resistance, good thermal resistance	High initial cost	
CFRP	Composite	Excellent chemical and corrosion resistance, low maintenance.	High initial cost	
Criteria rating (Likert) scale				
Very Good	Good	Moderate	Poor	Very Poor
5	4	3	2	1

Table 2. Material Properties with Respect to the Criteria

Materials	Criteria						
	CR	TR	FR	C	MI	D	H
Carbon Steel (CS)	1	5	4	5	3	3	4
13% Cr Martensitic SS	4	4	4	3	2	3	5
22 % Cr Duplex SS	5	5	5	2	3	3	5
25% Cr Super Duplex SS	5	5	4	1	3	3	5
316L	4	4	5	3	3	3	5
HDPE	4	3	3	5	5	5	2
Acetal	4	3	3	4	5	5	2
PA12	4	3	4	4	5	5	3
GRE	5	4	4	3	4	5	3
CFRP	5	3	4	3	5	5	3

2.3. Analytic Hierarchy Process (AHP)

The Analytic Hierarchy Process (AHP) is an MCDM method introduced by Thomas Saaty in 1980 [6]. This method is an Eigenvalue approach to pair-wise comparisons. The AHP method can be applied to analyze qualitative data quantitatively. It is used to transform complex and multi-criteria problems into a structural hierarchy [4].

Steps for implementing the AHP model

Step 1: Define the goal of the problem.

Step 2: Structure the problem in a hierarchy of different levels constituting goal, criteria, and alternative as shown in Figure 2.

Step 3: Perform a pair-wise comparison using the predefined Saaty's nine-point scale listed in Table 3. The pair-wise comparison generated say Matrix A

Step 4: Normalize matrix A and transform it into matrix B. Each element of matrix B is computed as,

$$b_{ik} = \frac{a_{ik}}{\sum_{i=1}^n a_{ik}} \quad (1)$$

Then calculate eigenvector = w_i , which is known as the criteria weight vector w , is built by averaging the entries on each row of matrix B, i.e.

$$w_i = \frac{\sum_{j=1}^n b_{ij}}{n} \quad (2)$$

Calculate the maximum eigenvalue according to the following equation on each row of matrix B, i.e.

$$\lambda_{max} = \frac{1}{n} \sum_{i=1}^n \frac{(Aw)_i}{w_i} \quad (3)$$

Where λ_{max} = maximum eigenvalue of the comparison matrix.

Step 5: Calculate consistency matrix CI

$$CI = \frac{\lambda_{max} - n}{n - 1} \quad (4)$$

Step 6: Find the Consistency ratio CR, which can be calculated as the ratio of the consistency index (CI) of the matrix to the consistency index of a random-like matrix (RI). The value of RI is taken from the Consistency indices for the randomly generated matrix in Table 4.

$$CR = \frac{CI}{RI} \quad (5)$$

Usually, a CR of 0.1 (10%) or less is considered acceptable.

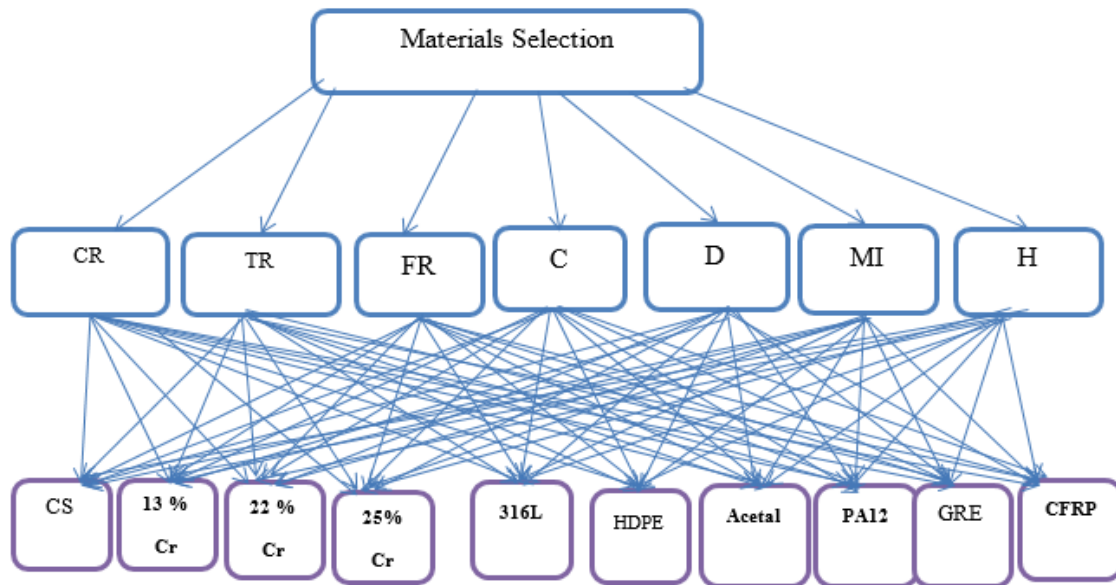


Figure 2. Decision Hierarchy for Material Selection for Subsea Pipelines.

Table 3. Saaty’s Nine-point Scale

Importance scale	Definition
1	Equally important
3	Moderately more important
5	Strongly more important
7	Very strongly more important
9	Extremely important
2,4,6,8	Intermediate values

Table 4. Consistency Indices for the Randomly Generated Matrix of the seven criteria N=7

Random Index RI							
Criteria Number (N)	1	2	3	4	5	6	7
RI	0	0	0.58	0.9	1.12	1.24	1.32

2.4. Vise Kriterijumska Optimizacija kompromisno Resenje (VIKOR)

Vise Kriterijumska Optimizacija kompromisno Resenje method was developed by Opricovic in 1998 to solve complex multi-criteria decision-making problems [13]. It assumes that compromise can be accepted for resolving the conflict and the feasible solution would be closest to the ideal solution and the alternatives are evaluated based on all the considered criteria [11].

Steps for implementing the VIKOR model are as follows:

Step 1: Identify the pivotal selection criteria and shortlist the alternatives depending on those criteria.

Step 2: In the decision matrix, determine the best, $(x_{ij})_{max}$ and the worst, $(x_{ij})_{min}$ values of all the criteria.

Step 3: Determine utility values (S_i) and regret values (R_i).

$$S_i = L_{1,i} = \sum_{j=1}^m \frac{w_j [(x_{ij})_{max} - x_{ij}]}{[(x_{ij})_{max} - (x_{ij})_{min}]} \quad (6)$$

$$R_i = L_{\infty,i} = \max^m \text{ of } \left\{ \frac{w_j [(x_{ij})_{max} - x_{ij}]}{[(x_{ij})_{max} - (x_{ij})_{min}]} \right\}, j = 1, 2, \dots, n \quad (7)$$

Step 4: Introduce v as the weight of the strategy for 'the maximum group utility'. The value of v ranges between 0 and 1, and usually, its value is taken as 0.5

Step 5: Calculate VIKOR index (Q_i)

$$Q_i = \frac{v(S_i - S_{i \min})}{(S_{i \max} - S_{i \min})} + \frac{(1 - v)(R_i - R_{i \min})}{(R_{i \max} - R_{i \min})} \quad (8)$$

Step 6: Arrange the alternatives in ascending order, according to Q_i values. The best alternative is the one having the minimum Q_i value.

3. Results and Discussion

In this paper, as previously stated, three different dynamic operating and environmental conditions in which the subsea pipeline designs are expected to operate in are examined and included in the evaluation model. The case study scenarios which include, sour service hydrocarbons transport in CO₂ environments, aggressive chemicals in deep waters, and non-corrosive fluids (industrial water lines) are studied in detail in the proceeding sub-sections.

3.1. Case Study Scenario 1

This case study describes the subsea pipeline material selection for sour service hydrocarbon transport in CO₂ environments. As stated earlier, the following criteria will be used for this study that is the corrosion resistance (CR), thermal resistance (TR), fatigue resistance (FR), cost (C), manufacture and installation (MI), density (D), and hardness (H). In applying the AHP model, a questionnaire was designed for collecting data of pairwise comparisons, which is used to determine the priority weight of each criterion. For each pair of criteria, the decision-maker (Expert) is asked to respond to a question like 'How important is criterion A in relation to criterion B?', and so on, then they rated using the Saaty's nine-point scale in Table 3. A pairwise comparison matrix for the seven criteria was formed according to step 3 of AHP as shown in Table 5.

Table 5. Pairwise Comparison Matrix for Criteria in Case Study Scenario 1

Criteria	CR	TR	FR	C	MI	D	H
CR	1.000	4.000	6.000	5.000	7.000	7.000	3.000
TR	0.250	1.000	3.000	2.000	6.000	5.000	0.500
FR	0.167	0.333	1.000	0.333	6.000	5.000	0.200
C	0.200	0.500	3.000	1.000	5.000	5.000	0.500
MI	0.143	0.167	0.167	0.200	1.000	0.333	0.143
D	0.143	0.200	0.200	0.200	3.000	1.000	0.167
H	0.333	2.000	5.000	2.000	7.000	6.000	1.000

The normalized matrix with criteria weights is solved using equation (1), then the criteria weight is calculated by using equation (2) as illustrated in Table 6. According to the results from Table 6, the most important criteria for sour service hydrocarbon transport (case study 1) is corrosion resistance (CR), with a value of 0.387, and the Hardness (H) has a value of 0.205. Hydrocarbons tend to be transported at high temperatures, so thermal resistance is also an important criterion, which ranked third in the criteria weight list.

Table 6. Normalized Matrix for Criteria in Case Study Scenario 1

Criteria	CR	TR	FR	C	MI	D	H	Criteria weights
CR	0.447	0.488	0.327	0.466	0.200	0.239	0.544	0.387
TR	0.112	0.122	0.163	0.186	0.171	0.170	0.091	0.145
FR	0.075	0.041	0.054	0.031	0.171	0.170	0.036	0.083
C	0.089	0.061	0.163	0.093	0.143	0.170	0.091	0.116
MI	0.064	0.020	0.009	0.019	0.029	0.011	0.026	0.025
D	0.064	0.024	0.011	0.019	0.086	0.034	0.030	0.038
H	0.149	0.244	0.272	0.186	0.200	0.205	0.181	0.205

The next step in AHP analysis is to find the maximum eigenvalue λ_{max} , using equation (3). Table 7 shows the consistency calculations which are obtained according to equation (4) and by using the random index (RI) value 1.32 as shown in Table 4 above. The consistency ratio calculated is given as 0.08999 which is less than 0.1, therefore it falls within the acceptable range. The consistency ratio result is presented in Table 8.

Table 7. Consistency Calculation for Case Study Scenario 1

Criteria	CR	TR	FR	C	MI	D	H	Weighted Sum
CR	0.387	0.580	0.498	0.580	0.175	0.266	0.615	3.101
TR	0.097	0.145	0.249	0.232	0.150	0.190	0.103	1.165
FR	0.065	0.048	0.083	0.039	0.150	0.190	0.041	0.615
C	0.077	0.073	0.249	0.116	0.125	0.190	0.103	0.932
MI	0.055	0.024	0.014	0.023	0.025	0.013	0.029	0.183
D	0.055	0.029	0.017	0.023	0.075	0.038	0.034	0.271
H	0.129	0.290	0.415	0.232	0.175	0.228	0.205	1.674

Table 8. Results obtained from AHP Analysis in Case Study Scenario 1

Criteria	Weights	λ_{max} , C.I, R.I	Consistency Ratio
CR	0.387	$\lambda_{max} = 7.713$ C.I = 0.11879 R.I = 1.32	0.08999
TR	0.145		
FR	0.083		
C	0.116		
MI	0.025		
D	0.038		
H	0.205		

Similarly, the VIKOR model is applied to evaluate the materials presented in Table 3 above. The values of the weights obtained from the AHP analysis are introduced into the matrix and normalized using step 2 of VIKOR as shown in Table 9. The S_i and R_i values were determined using equations (6) and (7) respectively. From the result, the value of Q_i was calculated using equation (8), and the obtained values are ranked and tabulated as shown in Table 10.

Table 9. Normalized Decision Matrix of VIKOR Analysis in Case Study Scenario 1

Material	Criteria and weights						
	CR	TR	FR	C	MI	D	H
Criteria weights	0.387	0.145	0.083	0.116	0.025	0.038	0.205
Carbon Steel	0.387	0.000	0.042	0.000	0.017	0.038	0.068
13% Cr Martensitic SS	0.097	0.073	0.042	0.058	0.025	0.038	0.000
22 % Cr Duplex SS	0.000	0.000	0.000	0.087	0.017	0.038	0.000
25% Cr Super Duplex SS	0.000	0.000	0.042	0.116	0.017	0.038	0.000
316L	0.097	0.073	0.000	0.058	0.017	0.038	0.000
HDPE	0.097	0.145	0.083	0.000	0.000	0.000	0.205
Acetal	0.097	0.145	0.083	0.029	0.000	0.000	0.205
PA12	0.097	0.145	0.042	0.029	0.000	0.000	0.137
GRE	0.000	0.073	0.042	0.058	0.008	0.000	0.137
CFRP	0.000	0.145	0.042	0.058	0.000	0.000	0.137

Table 10. Results Obtained from VIKOR Analysis in Case Study Scenario 1

Material	S_i	R_i	Q_i	Rank
Carbon Steel	0.552	0.387	0.991	10
13% Cr Martensitic SS	0.332	0.097	0.244	4
22 % Cr Duplex SS	0.142	0.087	0.000	1
25% Cr Super Duplex SS	0.212	0.116	0.133	2
316L	0.282	0.097	0.184	3
HDPE	0.530	0.205	0.662	8
Acetal	0.559	0.205	0.697	9
PA12	0.449	0.145	0.465	7
GRE	0.317	0.137	0.293	5
CFRP	0.381	0.145	0.384	6

In the sour service hydrocarbon transport pipe case scenario, the main criteria that affect the material selection process are found to be the corrosion resistance, hardness, and thermal resistance criteria as shown in the AHP results presented in Table 8. Similarly, with the VIKOR computed results as presented in Table 10, it is not hard to see that, out of ten materials evaluated, the 22 %Cr duplex stainless steel is selected as the most suitable material and with

the highest reliability-based potential to be used for the subsea pipeline design. In Figure 3 below, the overall ranking results of the ten materials for Case Study Scenario I are presented. Where the ranking order is given as; 22 %Cr duplex SS, 25 %Cr super duplex SS, 316L SS, 13 % Cr martensitic SS, Glass reinforced epoxy (GRE), Carbon fiber reinforced polymer (CFRP), PA12, HDPE, Acetal, and Carbon steel.

This result shows that corrosion-resistant alloys (CRAs) are the materials of choice for sour service hydrocarbon transport. Carbon steel is ranked last, although it can be lined or clad with CRAs for better performance. Composites also prove themselves as a contender for this application. The advantage of composites is that they can be designed specifically for a particular application. The results are consistent with the one presented by Sotoodeh (2018), whom they analyzed the improvement of the material selection process for piping systems in the offshore industry, the study concluded that 25% Cr super duplex SS is a good material of choice material for applications where high corrosion resistance and high strength is needed.

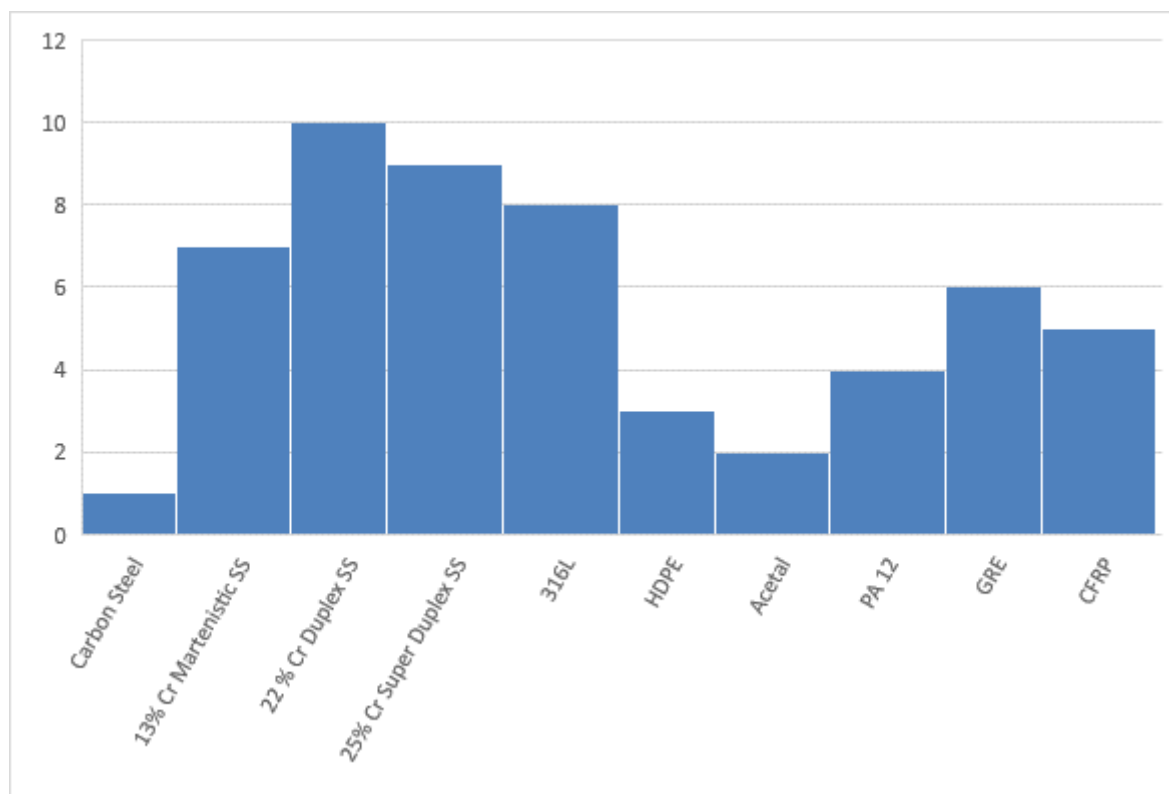


Figure 3. Material Rankings in Case Study Scenario 1

3.2. Case Study Scenario 2

This case study scenario describes the subsea pipeline design material selection for aggressive chemicals in deep waters. Since aggressive chemicals are highly corrosive, it is important that the materials used needs to have high corrosion and chemical resistance. In the following, the same steps are used in Case Study Scenario 1 above. The AHP results for the determination of the criteria weight have been presented in Table 11, where the corrosion resistance (CR) criterion is found to be the most important criteria for the aggressive chemical transport in deep

waters scenario with a weight value of 0.382, while the Cost (C) is found to be the closest most important criteria with a weight value of 0.247. Aggressive chemicals tend to be transported at normal temperatures, so thermal resistance isn't an important criterion, which ranked last in the criteria weight list. The consistency ratio was calculated to be 0.07882 which falls within the acceptable range.

Table 11. Results obtained from AHP analysis in Case Study Scenario 2

Criteria	Weights	λ_{max} , C.I, R.I	Consistency Ratio
CR	0.382	$\lambda_{max} = 7.624$ C.I = 0.10405 R.I = 1.32	0.07882
TR	0.031		
FR	0.078		
C	0.247		
MI	0.052		
D	0.055		
H	0.155		

Similarly, the VIKOR model is applied to evaluate the design materials just as in the Case Study Scenario 1. Here, the values of the weights obtained from the above AHP analysis in Table 11 are used for the matrix and normalization computation. The VIKOR model results for the S_i and R_i values as well as that of the Q_i value have been presented in Table 12. Ranking results for the evaluation shows that Carbon fiber reinforced polymer (CFRP) is the most suitable and highest reliability-based material for the subsea pipeline design when aggressive chemicals in deep waters are considered.

Table 12. Results from the VIKOR model for Case Study Scenario 2

Material	S_i	R_i	Q_i	Rank
Carbon Steel	0.562	0.382	1.000	10
13% Cr Martensitic SS	0.381	0.124	0.220	6
22 % Cr Duplex SS	0.275	0.185	0.147	5
25% Cr Super Duplex SS	0.376	0.247	0.433	9
316L	0.324	0.124	0.122	4
HDPE	0.360	0.155	0.240	7
Acetal	0.421	0.155	0.347	8
PA12	0.331	0.103	0.097	3
GRE	0.299	0.124	0.078	2
CFRP	0.297	0.124	0.074	1

In the subsea pipeline design for transporting aggressive chemicals in deep waters, the criteria evaluation from the AHP model shows that corrosion resistance is the most important criterion. This further confirms that the inherent corrosion resistance characteristic is of great value when designing subsea pipes. Some deep-water pipes also need to have a low specific weight that as in the case of risers. The results from the VIKOR computations also show that the ranking order for the most suitable and highest reliability-based materials are the Carbon fiber reinforced polymer (CFRP), Glass-reinforced epoxy (GRE), PA12, 316L SS, 22 %Cr duplex SS, 13 % Cr martensitic SS, HDPE, Acetal, 25 %Cr super duplex SS and Carbon steel. The study can therefore conclude that composite materials are the materials of choice for aggressive chemical transport for deepwater applications. Some polymers such as PA12 are also equipped to handle this condition. The overall ranking results of the ten materials evaluated for the Case Study Scenario 2 have been presented in Figure 4.

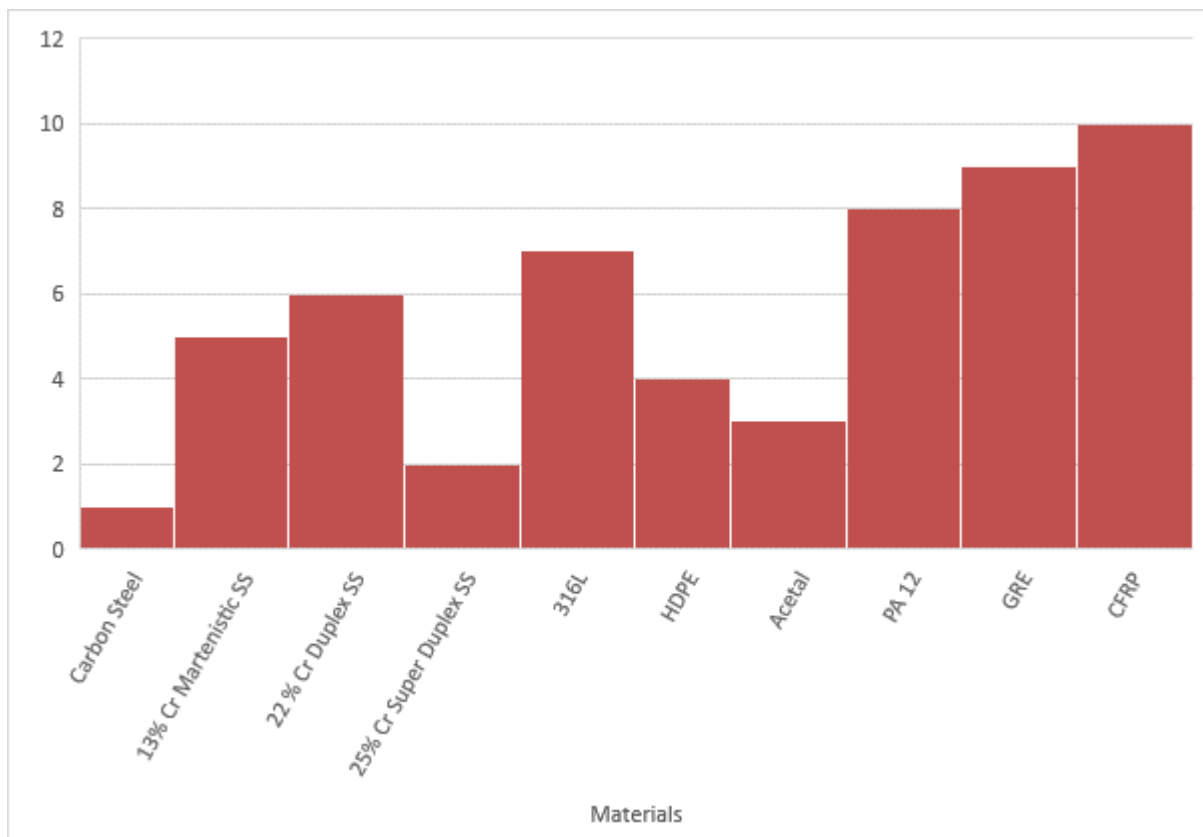


Figure 4. Material Rankings in Case Study Scenario 2

3.3. Case Study Scenario 3

In this case study scenario 3, subsea pipeline design materials are selected for non-corrosive fluid transport pipes such as those used in industrial water lines for transporting cooling water in environments of little to no H₂S content. Since corrosion wouldn't be a major problem in this case study scenario, the major concern here however is shifted to deal with the price and 'ease of use' criteria of the material. In the following, the same steps are used in the Case Study Scenarios above. The AHP results for the determination of the criteria weight have been presented in Table 13, where the cost (C) criteria with a weight value of 0.416 are found to be

the most important criteria for the non-corrosive fluid transport pipes scenario. While hardness (H), with a weight value of 0.181 is found to be the closest most important criterion. The consistency ratio was calculated to be 0.04411 which falls within the acceptable range.

Table 13. Results obtained from AHP Analysis in Case Study Scenario 3

Criteria	Weights	λ_{max} , C.I, R.I	Consistency Ratio
CR	0.036	$\lambda_{max} = 7.349$ C.I = 0.05822 R.I = 1.32	0.04411
TR	0.029		
FR	0.149		
C	0.416		
MI	0.096		
D	0.093		
H	0.181		

Similarly, the VIKOR model is applied to evaluate the design materials just as in the other Case Study Scenarios. Here, the values of the weights obtained from the above AHP analysis in Table 13 are used for the matrix and normalization computation. The VIKOR model results for the S_i and R_i values as well as that of the Q_i value have been presented in Table 14. The ranking results for the evaluation shows that Carbon steel is the most suitable and highest reliability-based material for the subsea pipeline design when non-corrosive fluid transport is considered.

Table 14. Results obtained from VIKOR Analysis in Case Study Scenario 3

Material	S_i	R_i	Q_i	Rank
Carbon Steel	0.328	0.093	0.000	1
13% Cr Martensitic SS	0.495	0.208	0.439	8
22 % Cr Duplex SS	0.469	0.312	0.560	9
25% Cr Super Duplex SS	0.648	0.416	1.000	10
316L	0.389	0.208	0.273	4
HDPE	0.368	0.181	0.199	3
Acetal	0.472	0.181	0.362	6
PA12	0.337	0.121	0.057	2
GRE	0.450	0.208	0.369	7
CFRP	0.432	0.208	0.341	5

The subsea pipeline is designed for transporting non-corrosive fluids and is very common in the oil and gas industry. The criteria evaluation approach using the AHP model shows that cost is the most important criterion. While the results from the VIKOR computations as presented in Table 14 shows the following ranking order; carbon steel, PA12, 316L, HDPE, CFRP, 13 % Cr martensitic SS, GRE, Acetal, 22 %Cr duplex SS and 25 %Cr super duplex SS.

It can be concluded from the results that, carbon steel is the most suitable and highest reliability-based design material for the subsea pipe design when non-corrosive fluids are considered. Similarly, polymer materials like the PA12 and HDPE are close alternatives that can be used for the design. If cost is a major factor in the material selection process, cheaper materials like carbon steel and polymers should be considered as they are cheaper than CRAs and Composites. The overall ranking results of the ten materials evaluated for the Case Study Scenario 3 have been presented in Figure 5.

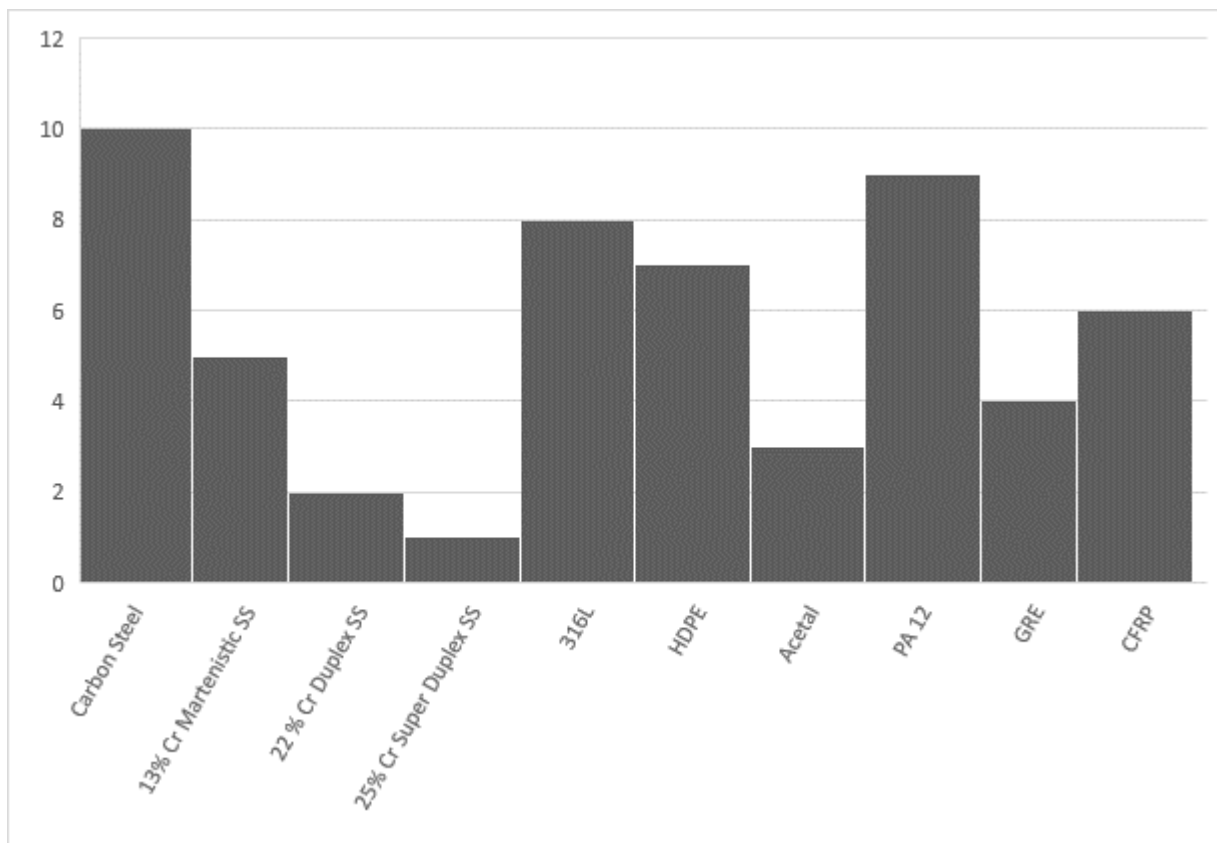


Figure 5. Material Rankings in Case Study Scenario 3

4. Conclusion

Subsea pipelines are a very important aspect of offshore oil and gas production, therefore their design and construction should be reliable and efficient as possible. Proper material selection plays a vital role in an efficient operation and a longer lifespan for the pipelines. This study presented a three-stage hybrid model that is based on an integrated Analytical Hierarchy Process (AHP) model and the ViseKriterijumskaOptimizacija I KompromisnoResenje (VIKOR) model for the evaluation and selection of a suitable and high reliability-based design

material for the subsea pipeline design by considering three operational and environmental scenario (three offshore application) that the pipes might encounter in the field.

Ten subsea pipeline design materials were examined critically with respect to seven criteria. The AHP model was applied in the different case study scenarios to determine the weight values of the different criteria. It was noticed for each case study scenario that the resulting weight values calculated were different and can affect the entire application. The results of the VIKOR analysis show that for sour service hydrocarbon transport in deep waters, 22% Cr Stainless steel is the best, most suitable, and highest reliability-based material for the subsea pipe design, for aggressive chemical transport, Carbon Fiber Reinforced Polymers are the best materials. While for the non-corrosive fluids, carbon steel and polymers are the material of choice.

Although Carbon steel may need to undergo some processes for protection against saltwater corrosion before use, the obtained results from the model, however, are in agreement with the previous research study of non-corrosive fluids. For a more efficient and cost-effective pipeline production, it is recommended that offshore oil-producing companies should adopt the use of the best fit and the highest reliability-based material for the design and construction of subsea pipes by considering the results obtained from a dedicated and a good research case study scenario. This research was limited in scope to just ten common materials, but with the variety of engineering materials that can be chosen, the research could be extended and further developed to suit other applications not examined.

Ethics in Publishing

There are no ethical issues regarding the publication of this study.

Author Contributions

All the authors were involved in designing the study, collecting data; evaluation of results and in the writing of the article.

References

- [1] Aikhuele D.O. Souleman F. S., & Azazi A. (2014). Application of Fuzzy AHP for Ranking Critical Success Factors for the Successful Implementation of Lean Production Technique. *Australian Journal of Basic and Applied Sciences*, 8(18), 399–407.
- [2] Aikhuele, D. O. (2019). A hybrid-fuzzy model with reliability-based criteria for selecting consumables used in welding dissimilar aluminum alloys joints. *Engineering and Applied Science Research*, 46(1), 79–85. <https://doi.org/10.14456/easr.2019.10>
- [3] Aikhuele, D. (2019). Evaluation of Adhesive Materials Used in Wind Turbine Blades. *Erzincan University Journal of Science and Technology*, 12(3), 1189-1200. DOI: 10.18185/erzifbed.456945
- [4] Aikhuele, D & Turan, F. (2017). A subjective and objective fuzzy-based analytical hierarchy process model for prioritization of lean product development practices. *Management Science Letters*, 7(6), 297-310.

- [5] Anojkumar, L., Ilangkumaran, M., & Sasirekha, V. (2014). Comparative analysis of MCDM methods for pipe material selection in sugar industry. *Expert Systems with Applications*, 41(6), 2964–2980. <https://doi.org/10.1016/j.eswa.2013.10.028>
- [6] Aliyev, R., Temizkan, H., Aliyev, R., (2020). Fuzzy Analytic Hierarchy Process-Based Multi-Criteria Decision Making for Universities Ranking. *Symmetry*, 12(8), 1351. <https://doi.org/10.3390/sym12081351>
- [7] Askari M., Aliofkhazraei M., Jafari R., Hamghalam P., & Hajizadeh A., (2021). Downhole corrosion inhibitors for oil and gas production – A review. *Applied Surface Science Advances*, 6(100128), <https://doi.org/10.1016/j.apsadv.2021.100128>.
- [8] Dweiri, F., & Oqla, F. M. A. (2006). Material selection using analytical hierarchy process. *International Journal of Computer Applications in Technology*, 26(4), 182. <https://doi.org/10.1504/ijcat.2006.010763>
- [9] Francis, R., & Byrne, G., (2021). Duplex Stainless Steels—Alloys for the 21st Century. *Metals* 11(5), 836 . <https://doi.org/10.3390/met1105083>
- [10] Hastie, J. C., Kashtalyan, M., & Guz, I. A. (2019). Failure analysis of thermoplastic composite pipe (TCP) under combined pressure, tension, and thermal gradient for an offshore riser application. *International Journal of Pressure Vessels and Piping*, 178, 103998. <https://doi.org/10.1016/j.ijpvp.2019.103998>
- [11] Ighravwe, D., Aikhuele, D., Fayomi, O & Basil, A. (2022). Adoption of a multi-criteria approach for the selection of operational measures in a maritime environment. *Journal of Project Management*, 7(1), 53-64.
- [12] Karande, P., & Chakraborty, S. (2012). Application of multi-objective optimization on the basis of ratio analysis (MOORA) method for materials selection. *Materials & Design*, 37, 317–324.
- [13] Liu, H. C., Liu, L., & Wu, J. (2013). Material selection using an interval 2-tuple linguistic VIKOR method considering subjective and objective weights. *Materials and Design*, 52, 158–167
- [14] Mathiyazhagan, K., Gnanavelbabu, A., & Lokesh Prabhuraj, B. (2019). A sustainable assessment model for material selection in construction industries perspective using hybrid MCDM approaches. *Journal of Advances in Management Research*, 16(2), 234–259.
- [15] Merayo, D., Rodriguez-Prieto, A., & Camacho, A. M. (2020). Prediction of Physical and Mechanical Properties for Metallic Materials Selection Using Big Data and Artificial Neural Networks. *IEEE Access*, 8, 13444–13456.
- [16] Pham, S., Truong, M. & Pham, B. (2017) Flow Assurance in Subsea Pipeline Design for Transportation of Petroleum Products. *Open Journal of Civil Engineering*, 7, 311-323. doi: [10.4236/ojce.2017.72021](https://doi.org/10.4236/ojce.2017.72021).
- [17] Razavi S. M., Mustafa, Z., Shafiq, N., & Syed, Z. I. (2014). A Review on Composite Materials for Offshore Structures. *Proceedings of the ASME 2014 33rd International Conference on Ocean, Offshore and Arctic Engineering. Volume 5: Materials Technology; Petroleum Technology*. San Francisco, California, USA. June 8–13, 2014. V005T03A016.

ASME. <https://doi.org/10.1115/OMAE2014-23542>

- [18] Rajabinezhad, M.; Bahrami, A.; Mousavinia, M.; Seyedi, S.J.; Taheri, P. (2020), Corrosion-Fatigue Failure of Gas-Turbine Blades in an Oil and Gas Production Plant. *Materials*, 13, 900. <https://doi.org/10.3390/ma13040900>
- [19] Renić, T., & Kišiček, T., (2021). Ductility of Concrete Beams Reinforced with FRP Rebars. *Buildings* 11(9), 424. <https://doi.org/10.3390/buildings11090424>
- [20] Sotoodeh, K. (2018). Analysis and Improvement of Material Selection for Process Piping System in Offshore Industry. *American Journal of Mechanical Engineering*, 6(1), 17–26.
- [21] Sofuoğlu M. A., & Orak, S., A (2017). Novel Hybrid Multi-Criteria Decision Making Model: Application to Turning Operations, *Int J Intell Syst Appl Eng*, 5(3), 124–131.
- [22] Sofuoğlu, M. A., Arapoğlu, R. A., & Orak, S. (2017). Multi-objective optimization of turning operation using hybrid decision-making analysis. *Anadolu University Journal of Science and Technology A - Applied Sciences and Engineering*, 18(3), 595-610. DOI: 10.18038/aubtda.287801
- [23] Yazdani, M., & Payam, A. F. (2015). A comparative study on material selection of microelectromechanical systems electrostatic actuators using Ashby, VIKOR, and TOPSIS. *Materials & Design*, 65, 328–334. doi.org/10.1016/j.matdes.2014.09.004
- [24] Zhang, H., Peng, Y., Tian, G., Wang, D., & Xie, P. (2017). Green material selection for sustainability: A hybrid MCDM approach. *PLOS ONE*, 12(5), e0177578.

In Vitro Cytotoxic Evaluation of a Silver(I) Complex Including Non-Steroidal Anti-Inflammatory Drug Niflumic Acid and 3-Picoline on Human-Derived Cancer Cell Lines

Sema CAGLAR ^{1*}, Ahmet ALTAY ¹, Bulent CAGLAR ¹, Esmâ YENİCERİ ²,
Betül HARURLUOĞLU ²

¹ Department of Chemistry, Faculty of Arts and Sciences, Erzincan Binali Yıldırım University, 24100
Erzincan, Turkey

² Department of Chemistry, Institute of Science and Technology, Erzincan Binali Yıldırım University, 24030,
Erzincan, Turkey

Received: 14/06/2022, **Revised:** 02/10/2022, **Accepted:** 02/10/2022, **Published:** 30/12/2022

Abstract

Here, a novel silver(I) complex including the non-steroidal anti-inflammatory drug niflumic acid and 3-picoline was synthesized and characterized by FT-IR, ¹H NMR, elemental and thermal analysis techniques. These techniques demonstrated that the formula of the synthesized complex is [Ag(nif)(3-pic)]. The cytotoxic ability of the complex, ligand (niflumic acid) and silver ions alone were tested against human breast adenocarcinoma (MDA-MB-453), lung adenocarcinoma (A-549), colorectal adenocarcinoma (HT-29), and mouse fibroblast (3T3-L1) cell lines. The XTT results indicated that although AgNO₃ and niflumic acid alone exhibited modest cytotoxicity on the cancer and healthy cell lines, the complex indicated strong cytotoxic activity on the cancer cells in dose-dependent manner. The strongest cytotoxicity and the highest selectivity by the complex were determined on HT-29 cells. These findings provide fundamental outputs for the evaluation of the novel silver(I) complex in advanced anticancer studies.

Keywords: Silver(I) complex, niflumic acid, cytotoxicity, cell culture

Steroid Olmayan Anti-İnflamatuvar İlaç Niflumik Asit ve 3-Pikolin İçeren Gümüş(I) Kompleksinin İnsan Kaynaklı Kanser Hücre Hatları Üzerinde İn Vitro Sitotoksik Değerlendirmesi

Öz

Burada, steroid olmayan anti-enflamatuvar ilaç niflumik asit ve 3-pikolin içeren yeni bir gümüş(I) kompleksi sentezlendi ve FT-IR, ¹H NMR, elemental ve termik analiz teknikleri ile karakterize edildi. Bu teknikler, sentezlenen kompleksin formülünün [Ag(nif)(3-pic)] olduğunu gösterdi. Kompleks, ligand (niflumik asit) ve gümüş iyonlarının tek başına sitotoksik yeteneği, insan meme adenokarsinomu (MDA-MB-453), akciğer adenokarsinomu (A-549), kolorektal adenokarsinom (HT-29) ve fare fibroblast hücre hatlarına (3T3-L1) karşı test edildi. XTT sonuçları, AgNO₃ ve niflumik asidin tek başına kanser ve sağlıklı hücre hatları üzerinde orta düzeyde sitotoksikite sergilemesine rağmen, kompleksin kanser hücreleri üzerinde doza bağlı bir şekilde güçlü sitotoksik aktivite sergiledi. Kompleksin en güçlü sitotoksikitesi ve en yüksek seçiciliği HT-29 hücrelerinde olduğu belirlendi. Bu bulgular, gelişmiş antikanser çalışmalarında yeni gümüş(I) kompleksinin değerlendirilmesi için temel oluşturmaktadır.

Anahtar Kelimeler: Gümüş(I) kompleksi, niflumik asit, sitotoksikite, hücre kültürü.

1. Introduction

Cancer is a very common type of disease that starts with the uncontrollable growth of abnormal cells and finally spreads to other parts of the body. World health organization (WHO) has declared that cancer is the second leading reason of death [1]. Therefore, scientists are making great efforts to develop new drugs and treatment methods to struggle with cancer. Especially, with the exploration of the anti-proliferative effect of cisplatin in cancer treatment in 1844, interest in medicinal inorganic chemistry has raised [2,3]. After that, a large number of metal-including complexes such as platinum, palladium, gold, copper and ruthenium have been designed and synthesized for using in preclinical and clinical trials [4–9]. Researches have also demonstrated that coordination complexes indicate high biological activity than the starting metal salts.

Silver compounds have been used in the treatment of burns, wounds infection, and especially antimicrobial diseases for thousands of years [10,11]. Despite silver compounds for the cure of infections have been utilized for a long time, the design of anticancer drugs on silver has been a comparatively new area of medicinal chemistry. The studies of silver compounds are increasing day by day due to their robust cytotoxic activity against cancer cells and low toxic effect towards healthy cells when compared to cisplatin [12–14].

Non-steroidal anti-inflammatory drugs (NSAIDs) are among the most widely used drugs in patient. They have been shown to display a variety of biological properties such as antipyretic, analgesic, anti-inflammatory agents. Additionally, NSAIDs display good anti-proliferative activity against various cancer cell lines [15–18]. NSAIDs compounds have been also utilized as ligand because they contain a nitrogen atom and oxygen atoms of carboxyl group that can form donor acceptor bonds with metal ions. Moreover, studies have demonstrated that coordination complexes including NSAIDs can improve the biological activity than free NSAIDs. The therapeutic effect of NSAIDs has encouraged researchers to synthesize new metal complexes and investigate their pharmacological applications [19–21].

Therefore, in the current study, a novel silver(I) complex of niflumic acid with auxiliary ligand 3-picoline was synthesized and characterized by Fourier transform infrared spectroscopy (FT-IR), proton nuclear magnetic resonance (^1H NMR), elemental and thermal analysis techniques. Afterwards, its potential cytotoxic ability and selectivity were determined over three different cancer cell lines and one normal cell line.

2. Material and Methods

2.1. Physical measurements

AgNO_3 , niflumic acid, 3-picoline, methanol and acetonitrile were purchased from Sigma Aldrich and used without further purification. The molecular structures of niflumic acid and 3-picoline are shown in Fig. 1. The LECO CHNS-932 device was used for elemental analysis. The FT-IR spectra were recorded with The Thermo Nicolet 6700 spectrophotometer (4000-400

cm^{-1}). The PRIS Diamond device was utilized for thermal analysis (TG/DTA/DTG) curves. The Agilent-VNMRS-400 spectrometer (400 MHz) was used for ^1H NMR spectra.

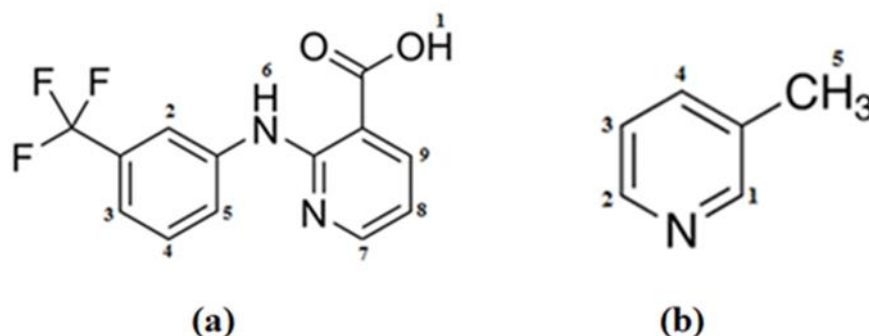


Figure 1. The molecular structures of (a) niflumic acid (b) 3-picoline

2.2. Synthesis of [Ag(nif)(3-pic)]

Niflumic acid (Hnif, 1 mmol) and KOH (1 mmol) were dissolved in 10 mL of methanol under stirring for 1 h at 50°C . Silver(I) nitrate (1 mmol) was dissolved in 10 mL of distilled water in the other beaker. After stirring 1 h, 3-picoline (3-pic, 1 mmol) and niflumic acid solution were added to silver(I) nitrate solution and white suspension occurred immediately. The addition of 10 mL of acetonitrile changed the suspension to colourless solution. The obtained clear solution was kept in the dark at room temperature. After two months, colourless microcrystals of complex were acquired. The molecular structure of [Ag(nif)(3-pic)] was given in Fig.2.

Colourless crystal product of [Ag(nif)(3-pic)] (81%): Analytical data for $[\text{C}_{19}\text{H}_{15}\text{N}_3\text{O}_2\text{F}_3\text{Ag}]$
Found: C, 47.29; H, 3.12; N, 8.70%; calcd: C, 47.28; H, 3.11; N, 8.71%.

^1H NMR (400 MHz, $\text{DMSO}-d_6$) (δ/ppm): 2.31 (3H, s, $\text{H}^5\text{-3-pic}$), 6.85 (1H, dd, $\text{H}^8\text{-nif}$), 7.21 (1H, d, $\text{H}^5\text{-nif}$), 7.34 (1H, dd, $\text{H}^3\text{-3-pic}$), 7.49 (1H, t, $\text{H}^4\text{-nif}$), 7.64 (1H, d, $\text{H}^4\text{-3-pic}$), 7.78 (1H, d, $\text{H}^3\text{-nif}$), 8.30-8.26 (2H, m, $\text{H}^2\text{-nif}$ and $\text{H}^9\text{-nif}$), 8.36 (1H, s, $\text{H}^7\text{-nif}$), 8.39 (1H, d, $\text{H}^2\text{-3-pic}$), 8.44 (1H, s, $\text{H}^1\text{-3-pic}$), 12.73 (1H, s, $\text{H}^6\text{-nif}$).

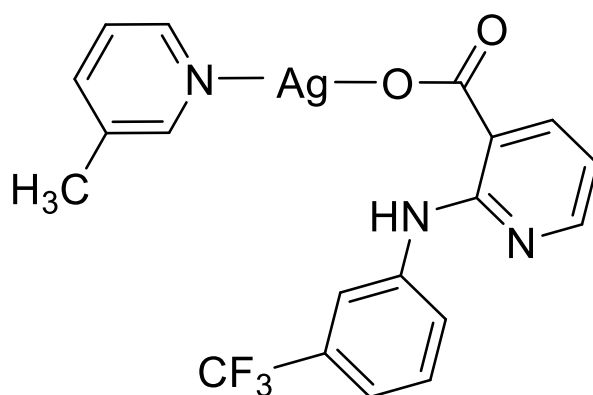


Figure 2. The molecular structure of [Ag(nif)(3-pic)]

2.3. Biological activity

2.3.1. Cell culture

Human breast adenocarcinoma (MDA-MB-453), lung carcinoma (A-549), colorectal adenocarcinoma (HT-29), and normal mouse fibroblast (3T3-L1) cell lines were purchased from the American Type Culture Collection (ATCC, USA). Passaging and culturing of the cells were performed according to the company's instructions. Accordingly, culturing of MDA-MB-453, A-549, HT-29, and 3T3-L1 cells were performed with the mediums of Leibovitz's L-15, F-12K, McCoy's 5a, and Eagle's Minimum Essential Medium, respectively. The studies were done using biosafety cabinet (Bilsen, Turkey) and incubations were performed using 5% CO₂ incubator at 37°C (Nuve, Turkey).

2.3.2. Cell proliferation assay

2,3-bis-(2-methoxy-4-nitro-5-sulfophenyl)-2H tetrazolium-5-carboxanilide (XTT) assay was carried out to investigate the potential anti-proliferative activity of the test compounds [22,23]. Accordingly, 7500 cells were planted into 96-well plate and incubated for 24 h to obtain their morphological shapes. After that, each cancer cell line was treated with varying concentrations of the Ag(I) complex (1-100 µM) and also ligand (niflumic acid) and silver(I) nitrate alone. The dose range applied for 3T3-L1 cells was from 1 to 250 µM. Following the exact incubation time, the absorbance of each well was measured spectrophotometrically at 490 nm (BioTek, USA). Carboplatin was evaluated as positive control. The IC₅₀ concentration of the compounds was calculated by plotting the graph between the different concentration of the compounds and the % inhibition of cell proliferation. Selectivity Index (SI) was calculated from the ratio of IC₅₀ concentration of the complex over the normal cell line (3T3-L1) to the IC₅₀ concentration over the cancer cell line tested. The percent cell proliferation inhibition was calculated using the following formula;

$$\% \text{ Cell proliferation inhibition} = 100 - [\text{Abs}(\text{drug})/\text{Abs}(\text{control})] \times 100.$$

2.3.3. Statistical analysis

Student's t-test was performed for statistical analysis using GraphPad Prism 6 (GraphPad, La Jolla, CA) Software 7.0) and $p < 0.05$ was considered significant.

3. Results and Discussion

3.1. FT-IR Spectra

The FT-IR spectra of niflumic acid and [Ag(nif)(3-pic)] complex are demonstrated in Figure 3 and Figure 4, respectively. Niflumic acid displayed band at 3315 cm⁻¹ which is attributed to stretching vibration of ν(NH) group and this peak is seen in almost the same region in the spectrum of [Ag(nif)(3-pic)] complex. This position showed that there is no interplay between the NH group and Ag(I) ion. This band at 1661 cm⁻¹ for niflumic acid is assigned to the carboxylate group. The spectrum of the complex indicated that this band turn into asymmetric

(COO⁻) and symmetric (COO⁻) stretching vibrations of carboxylate group of niflumato ligand at 1601 and 1389 cm⁻¹. $\Delta\nu$ value (difference between $\nu_{\text{asym}}(\text{COO}^-)$ and $\nu_{\text{sym}}(\text{COO}^-)$ stretching vibrations) is 212 cm⁻¹, representing a monodentate coordination mode between the silver(I) ion since the characteristic $\Delta\nu$ value for monodentate coordination mode is larger than for ionic compounds of the ligand ($\Delta\nu(\text{nifNa})$: 206 cm⁻¹). The bands between 3062 and 2936 cm⁻¹ are related to the aromatic and aliphatic $\nu(\text{C-H})$ stretching vibrations. The characteristic C=N and C=C stretching vibrations of benzene and pyridine rings are observed at 1605, 1597, 1514 and 1450 cm⁻¹. Also, the bands at 1330 and 775 cm⁻¹ probably correlate with CF₃ stretching vibration and CF₃ deformation, respectively.

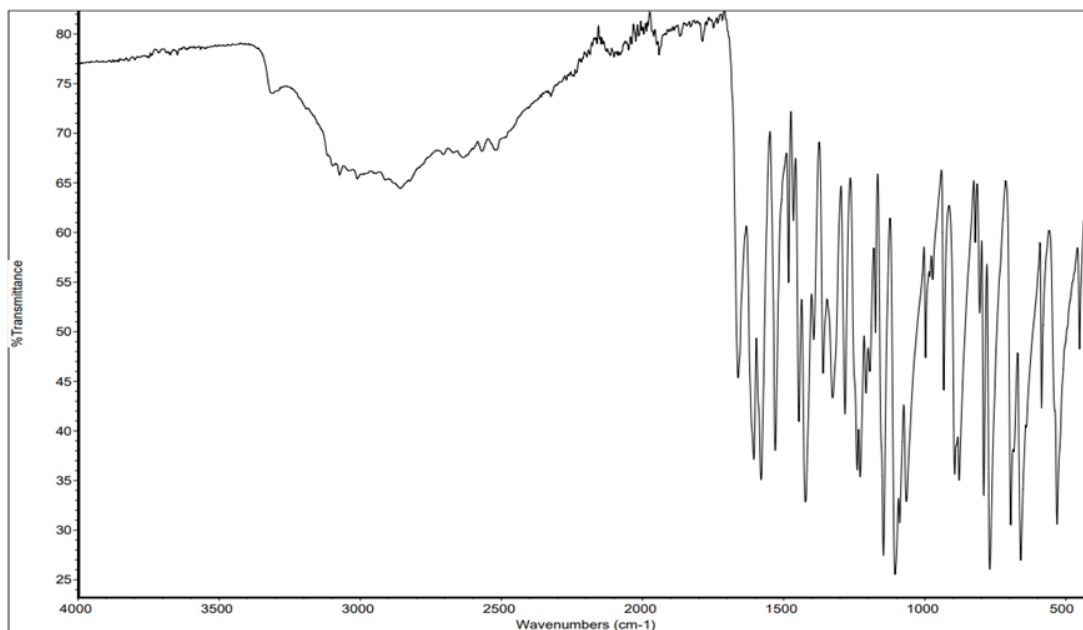


Figure 3. FT-IR spectrum of niflumic acid

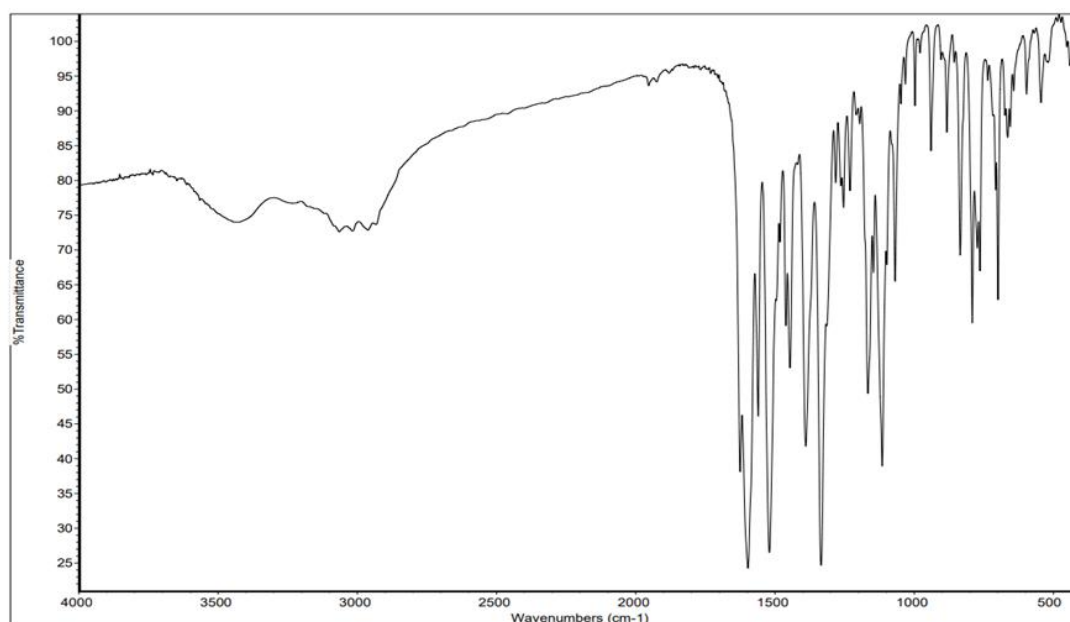


Figure 3. FT-IR spectrum of [Ag(nif)(3-pic)]

3.2. Thermal Analysis of [Ag(nif)(3-pic)]

[Ag(nif)(3-pic)] complex undergoes decomposition in two steps is showed in Fig. 5. The first decomposition step was occurred in the temperature range between 30 and 205 °C, showing the loss of 3-pic molecule. The percentage experimental mass loss (18.25%) is consistent with the calculated mass loss (19.28%) (DTA: 119(+), 178(-) °C, DTG: 114, 151, 178 °C). The second decomposition step was accompanied by weight loss (exper. mass loss of 60.22%; calc. mass loss 58.31%), appointed to the loss of nif ligand. This step was appeared to compose of three stages as indicated in DTG curve (at 213, 244 and 433 °C) whereas the DTA curve gave the peaks at 231(-), 259(-) and 414(-) °C. The residual thermal product was described as metallic silver according to experimental mass loss (21.53%) and calculated mass loss (22.36%).

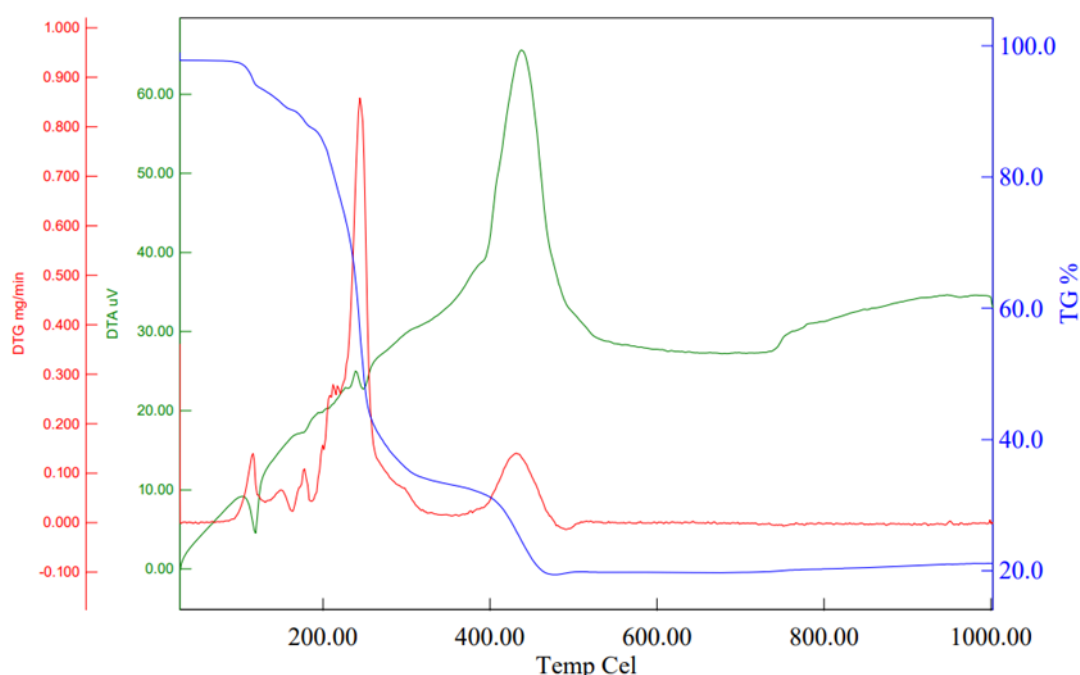


Figure 5. The TG/DTG/DTA curves of [Ag(nif)(3-pic)].

3.3. ¹H NMR studies

¹H NMR technique is used to determine the presence and ratio of ligands in complexes. ¹H NMR spectrum of [Ag(nif)(3-pic)] complex is demonstrated in Fig. 6. In the synthesized complex, all the expected signals of ligands were observed and also their multiplicities and integrals were shown to compatible with the structures. The number of protons showed that the ratio of nif: 3-pic is 1:1. All proton signals are observed to a little change binding to Ag(I) ion. The ¹H NMR spectrum of [Ag(nif)(3-pic)] complex showed a singlet signal at 2.31 ppm, which is ascribed to the methyl proton of 3-picoline ligands. The singlet peak at 12.73 ppm is attributed to NH proton of nif ligand. The spectrum was determined to be multiple resonance peaks for the aromatic protons at 6.85, 7.21, 7.49, 7.78, 8.26-8.30 and 8.36 ppm (niflumic acid) [24] and 7.34, 7.64, 8.39 and 8.44 ppm (3-picoline) [25]. The vanished of carboxylate hydrogen peak of the complex shows the connection of the nif ligand to Ag(I) ion via carboxylate group.

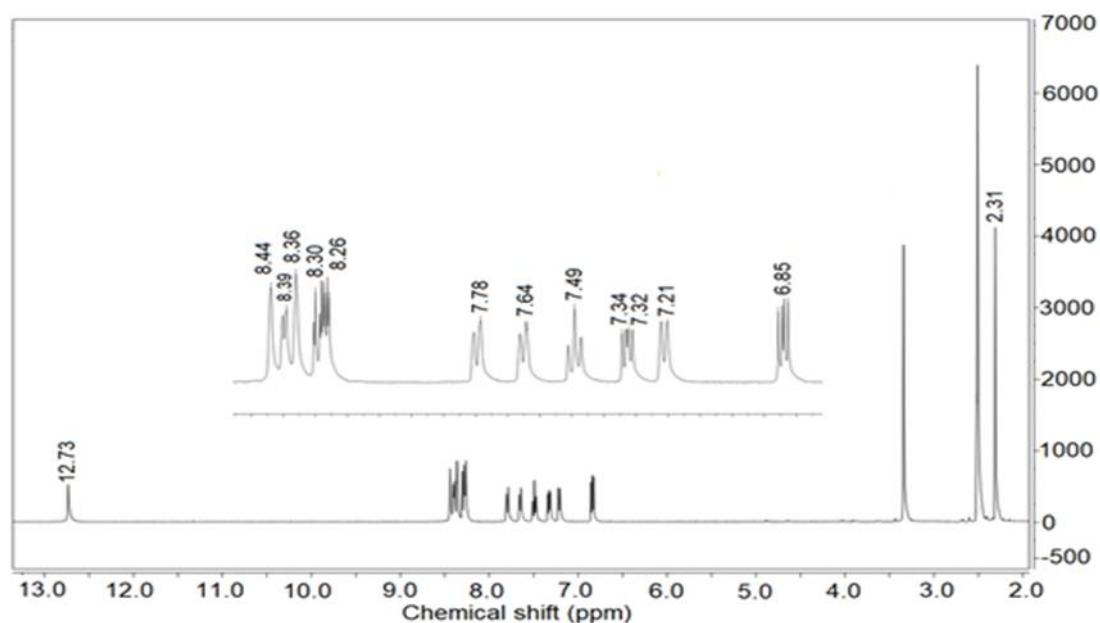


Figure 6. ¹H NMR spectrum of [Ag(nif)(3-pic)]

3.4. Cytotoxicity

The cytotoxic effects of the novel [Ag(nif)(3-pic)] complex and also ligand (niflumic acid) and silver(I) nitrate alone were tested on three different cancer and one healthy cell line. XTT results indicated that although niflumic acid and AgNO₃ alone showed very low cytotoxic activity against the human breast adenocarcinoma (MDA-MB-453), lung adenocarcinoma (A-549), colorectal adenocarcinoma (HT-29), and mouse fibroblast (3T3-L1) cell lines up to 100 μM, the complex exhibited dose-dependent cytotoxicity against three cancer cell lines (Fig. 7A-D). The half-maximum inhibitory concentrations (IC₅₀) of the complex, ligand, and silver salts were calculated from the standard curve using correlation–regression analysis and expressed with their mean ± standard deviations in Table 1. To investigate the anticancer feature of a new chemical agent isolated from a natural source or synthesized by organic and inorganic ways and also to determine its selectivity between normal and cancer cells is of a great importance. Therefore, we determined the IC₅₀ values of the agents on the tested cell lines.

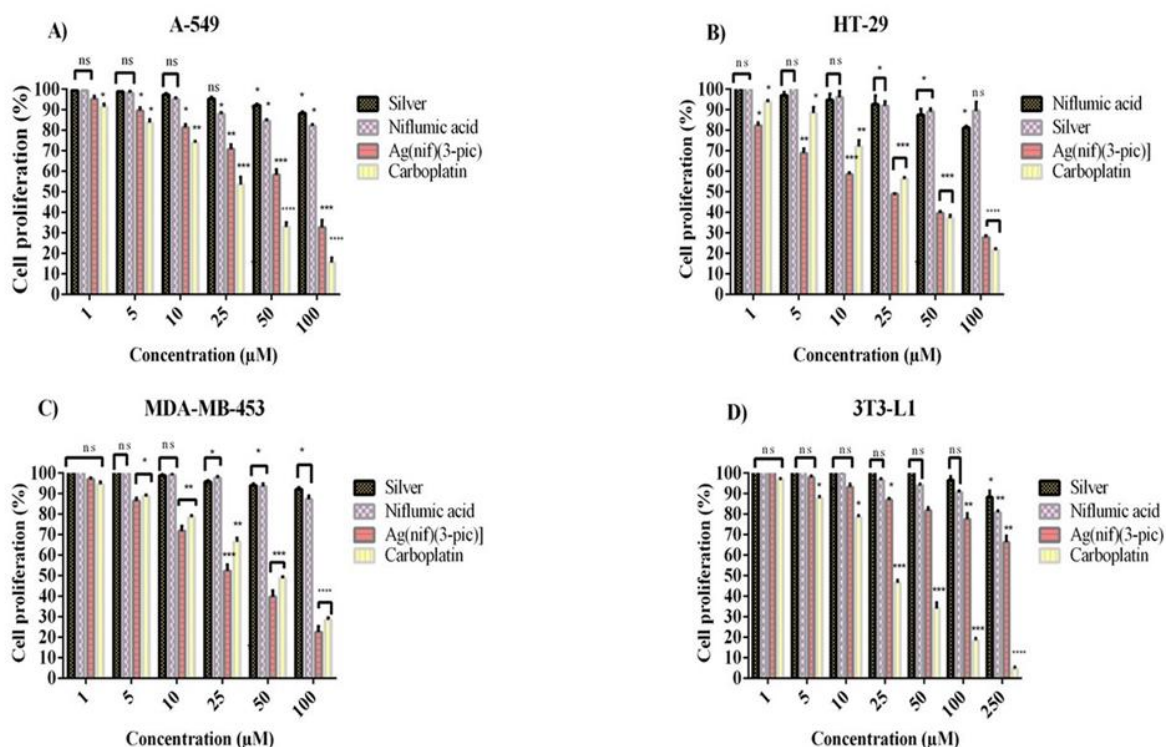


Figure 7. Dose-dependent anti-proliferative effects of [Ag(nif)(3-pic)], silver, niflumic acid, and carboplatin on human lung carcinoma (A-549), colorectal adenocarcinoma (HT-29) (B), breast adenocarcinoma (MDA-MB-453) (C), and normal mouse fibroblast (3T3-L1) (D) cell lines.

Table 1. The IC₅₀ values of the test compounds on cancer and fibroblast cells.

Test samples	Cell lines IC ₅₀ (µM) ^x			
	A-549	HT-29	MDA-MB-453	3T3-L1
[Ag(nif)(3-pic)]	66.45±1.52 ^b	39.05± 0.85 ^a	47.71±1.34 ^a	182.62 ± 2.40 ^b
SI(complex) ^y	2.74	4.67	3.82	
[Niflumic acid]	>100 ^c	>100 ^c	>100 ^c	>250 ^c
[Silver(I) nitrate]	>100 ^c	>100 ^c	>100 ^c	>250 ^c
[Carboplatin]	40.42±1.5 ^a	47.15±2.02 ^b	56,73±1.12 ^b	43.16±1.45 ^a
SI (carb) ^y	1.06	0.91	0.76	

^xIC₅₀ (µM): a-c superscripts in the same column displays the differences at $p < 0.05$.

^y(SI): Selectivity index

As given in Table 1, the IC₅₀ concentrations of the ligands and silver(I) nitrate alone on the cancer and normal cell lines were determined as greater than 100 µM and 250 µM, respectively. These results were consistent with the literature. For instance, the cytotoxic activity of niflumic acid against human osteosarcoma MG63 cells was reported to be between the range of 200 and 700 µM [26]. As for the silver salts, the IC₅₀ concentration of silver nanoparticles against human breast cancer (MCF-7) cells was reported to be 463 µM [27]. In another study, the IC₅₀ value

of AgNO_3 against human cervix adenocarcinoma (HeLa) was recorded as $158 \mu\text{M}$ [28]. These data confirm that niflumic acid and AgNO_3 alone exhibit a highly low cytotoxicity against cancer cell lines and also their IC_{50} concentration change depending on the cell line.

Considering the cytotoxic activity of the $[\text{Ag}(\text{nif})(3\text{-pic})]$ complex formed by niflumic acid belonging to NSAIDs, auxiliary ligand picolin, and silver salts against the cancer and normal cell line, the complex showed a good dose-dependent cytotoxicity on all of the cancer cell lines while exhibiting no considerable cytotoxicity on normal 3T3-L1 cells. As seen in Table 1, the Ag(I) complex exhibited the highest cytotoxic effect on HT-29 cells with the lowest IC_{50} value ($39.05 \mu\text{M}$), followed by MDA-MB-453 ($47.71 \mu\text{M}$) and A549 ($66.45 \mu\text{M}$) cells, respectively. Whereas, the complex showed a very low cytotoxicity against normal 3T3-L1 cells with a very high IC_{50} value ($182.62 \mu\text{M}$). Upon compared to carboplatin used as a chemotherapeutic drug, the complex was determined to show statistically higher cytotoxic activity against MDA-MB-453 and HT-29 cells, but comparable cytotoxicity on A-549 cells (Table 1). In the literature, the various cytotoxic activities of the metal complexes formed by niflumic acid with different metal ions against various cancer cells were examined. For instance, the cytotoxic activity of $[\text{Co}(\text{bcp})(\text{nif})_2]$ was scrutinized on various cancer cell types, namely HeLa, HT-29, PC-3 (human prostate cancer), and MCF-7 cells, and the IC_{50} values belonging these cell lines were reported to be 38.75 , 43.67 , 27.06 , and $41.53 \mu\text{M}$, respectively [29]. In another study, the IC_{50} value of the $[\text{Zn}(\text{neo})(\text{nif})_2]$ complex on two endometrial (hTERT and 12Z) cell lines was reported to be 4.2 and $0.9 \mu\text{M}$, respectively [30]. Moreover, in our previous study we tested the cytotoxicity of $\text{AgH}(\text{nif})_2$ complex against MCF-7, HT-29, and human hepatoma cells (HepG2) cancer cell lines, and the results indicated that the IC_{50} values of this complex on each cell line was 39.24 , 71.02 , and $58.38 \mu\text{M}$, respectively [31]. When HT-29 cells tested in both studies was considered, the cytotoxic activity was observed to be much stronger upon 3-picoline was introduced into the structure of the previous $[\text{AgH}(\text{nif})_2]$ complex. These data show that the type of NSAIDs, auxiliary ligand, and metal ion in the structure of the complex significantly affect the cytotoxicity, and also the cytotoxic effect varies significantly according to the cell type.

One of the necessary parameters to be considered in cytotoxicity studies is the selectivity of the test agents between cancer and healthy cells [32–34]. In this context, as seen in Table 1, the $[\text{Ag}(\text{nif})(3\text{-pic})]$ complex displayed much higher selectivity on cancer cells when compared to normal cells, and the highest selectivity was determined against HT-29 cells with an SI value of 4.67 , followed by MDA-MB-453 (SI: 3.82) and A-549 (SI: 2.74) cells, respectively. Besides, the complex exposed more selectivity against all the cancer cell lines compared to carboplatin. Many studies have shown that the synergistic effect contributes greatly to the stronger anticancer effect of various complexes of NSAIDs with transition metals compared to their individual effects [35]. In the synergistic action, both transition metals and NSAIDs contribute to cytotoxicity individually via exhibiting numerous characteristics including redox activity, variable coordination modes, stability, and reactivity towards the targeted-organic substrates involved in different anticancer mechanism pathways [36]. Herein, the findings in the present study indicated that $[\text{Ag}(\text{nif})(3\text{-pic})]$ formed by silver(I) nitrate with niflumic acid and picoline ligand showed much higher cytotoxicity and selectivity against the aforementioned cancer cell

lines with higher synergistic effect, which still needs to be clarified with further studies of anticancer mechanisms of action.

4. Conclusion

This study defined the synthesis, characterization, and anti-proliferative potency of a new Ag(I) complex of NSAIDs. The structure of the synthesized complex was identified by FT-IR, elemental, ¹H NMR, and thermal analysis techniques and subsequently subjected to the cytotoxicity treatments by XTT assay. Biological activity studies revealed that the novel Ag(I) complex exhibited the strongest cytotoxic activity against HT-29 cells with the lowest IC₅₀ value and the weakest activity against A-549 cells with the highest IC₅₀ value. The results also confirmed that the complex exhibited higher selectivity towards to the tested cancer cells compared to normal cells. To conclude, these findings provide an important basis for the evaluation of the [Ag(nif)(3-pic)] complex in *in vivo* anticancer activity studies.

Ethics in Publishing

There are no ethical issues regarding the publication of this study.

Acknowledgements

This work was financially supported by grants from Erzincan Binali Yıldırım University Scientific Research Projects Coordination Commission (EU-BAP) (Project No: FBA-2020-683).

Author Contributions

Conceived and designed the experiments: SC, AA. Performed the experiments: SC, AA, BC, EY, BH. Analysed the data: SC, AA, and BC. Contributed reagents/materials/analysis tools: AA, SC, and BC. Wrote the article: AA, SC, and BC. All authors read and approved the final manuscript.

References


- [1] Petersen, PE.(2009) Oral cancer prevention and control - The approach of the World Health Organization. *Oral Oncol*, 45(4–5): 454–60.
- [2] Rosenberg B.(1980) *Cisplatin: Its History and Possible Mechanisms of Action, Current Status and New Developments*. Academic Press.
- [3] Benedetti BT, Peterson EJ, Kabolizadeh P, Martínez A, Kipping R, Farrell NP.(2011) Effects of noncovalent platinum drug-protein interactions on drug efficacy: Use of fluorescent conjugates as probes for drug metabolism. *Mol. Pharm*, 8(3): 940–48.
- [4] Karlenius TC, Tonissen KF.(2010) Thioredoxin and cancer: A role for thioredoxin in all states of tumor oxygenation. *Cancers*, 2:209–232.
- [5] Bindoli A, Pia M, Scutari G, Gabbiani C, Casini A, Messori L.(2009) Thioredoxin

- reductase : A target for gold compounds acting as potential anticancer drugs. *Coord. Chem. Rev.*, 253: 1692–707.
- [6] Gupte A, Mumper RJ.(2009) Elevated copper and oxidative stress in cancer cells as a target for cancer treatment. *Cancer Treat. Rev*, 35(1): 32–46.
- [7] Monneret, C.(2011) Platinum anticancer drugs. From serendipity to rational design. *Ann. Pharm. Fr.*, 69(6): 286–295.
- [8] Johnstone TC, Suntharalingam K, Lippard SJ.(2016) The Next Generation of Platinum Drugs: Targeted Pt (II) Agents , Nanoparticle Delivery, and Pt (IV) Prodrugs. *Chem. Rev*, 116:3436–3486.
- [9] Mi Q, Ma Y, Gao X, Liu R, Liu P, Mi Y, Fu X, Gao Q.(2016) 2-Deoxyglucose conjugated platinum (II) complexes for targeted therapy: design, synthesis, and antitumor activity. *J. Biomol. Struct. Dyn*, 34(11): 2339–50.
- [10] Hindi KM, Panzner MJ, Tessier CA, Cannon CL, Youngs WJ.(2009) The Medicinal Applications of Imidazolium Carbene–Metal Complexes. *Chem. Rev*, 109(8): 3859–3884.
- [11] Gasser G, Ott I, Metzler-Nolte N.(2011) Organometallic anticancer compounds. *J. Med. Chem*, 54:3–25.
- [12] Pedro M, Mara M, Lidia C.(2014) Organometallic Compounds in Cancer Therapy: Past Lessons and Future Directions. *Bentham Sci. Publ*, 14:1199–1214.
- [13] Kunkely H, Vogler A.(2011) Absorption and luminescence spectra of cochineal. *Inorg. Chem. Commun*, 14:1153–1155.
- [14] Li S, Zhang S, Jin X, Tan X, Lou J, Zhang X, Zhao Y.(2014) Singly protonated dehydronorcantharidin silver coordination polymer induces apoptosis of lung cancer cells via reactive oxygen species-mediated mitochondrial pathway. *Eur. J. Med. Chem*, 86: 1–11.
- [15] Mahendiran D, Kumar RS, Rahiman AK.(2017) Heteroleptic silver(I) complexes with 2,2':6',2''-terpyridines and naproxen: DNA interaction, EGFR/VEGFR2 kinase, growth inhibition and cell cycle arrest studies. *Mater. Sci. Eng. C*, 76:601–615.
- [16] Johnsen, JI, Lindskog M, Ponthan F, Pettersen I.(2005) NSAIDs in neuroblastoma therapy. *Cancer Lett*, 228(1–2): 195–201.
- [17] Banti CN, Giannoulis AD, Kourkoumelis N, Owczarzak AM, Kubickic M, Hadjidakou SK.(2014) Novel metallo-therapeutics of the NSAID naproxen. Interaction with intracellular components that leads the cells to apoptosis. *Dalt. Trans*, 18: 6848–63.
- [18] Ho Woo D, Han IS, Jung G.(2004) Mefenamic acid-induced apoptosis in human liver

- cancer cell-lines through caspase-3 pathway. *Life Sci*, 75:2439–2449.
- [19] Kyros L, Banti CN, Kourkoumelis N, Kubicki M, Sainis I, Hadjikakou SK.(2014) Synthesis, characterization, and binding properties towards CT-DNA and lipoxygenase of mixed-ligand silver (I) complexes with 2-mercaptothiazole and its derivatives and triphenylphosphine. *J. Biol. Inorg. Chem*, 6: 449–464.
- [20] Núñez C, Fernández-Lodeiro A, Fernández-Lodeiro J, Carballo J, Capelo JL, Lodeiro C.(2014) Synthesis, spectroscopic studies and in vitro antibacterial activity of Ibuprofen and its derived metal complexes. *Inorg. Chem. Commun*, 45: 61–65.
- [21] Pereira IM, De Moraes Profirio D, De Paiva REF, Lancellotti M, Barboza Formiga AL, Corbi PP.(2013) A silver complex with ibuprofen: Synthesis, solid state characterization, DFT calculations and antibacterial assays. *J. Mol. Struct*, 1049: 1–6.
- [22] Altay A, Bozoğlu F.(2017) *Salvia fruticosa* Modulates mRNA Expressions and Activity Levels of Xenobiotic Metabolizing CYP1A2, CYP2E1, NQO1, GPx, and GST Enzymes in Human Colorectal Adenocarcinoma HT-29 Cells. *Nutr. Cancer*,0:1–12.
- [23] Harurluoglu B, Altay A, Caglar S, Kubra E, Yeniceri K, Caglar B, Sahin ZS.(2021) Binuclear silver (I) complexes with the non-steroidal anti-inflammatory drug tolfenamic acid: Synthesis, characterization, cytotoxic activity and evaluation of cellular mechanism of action. *Polyhedron*,202:115189.
- [24] Tarushi A, Raptopoulou CP, Psycharis V, Kessissoglou DP, Papadopoulos AN, Psomas G. (2017) Interaction of zinc(II) with the non-steroidal anti-inflammatory drug niflumic acid. *J Inorg Biochem*, 176:100-112.
- [25] Yu X, Ji D, Liu R, Yang F, Xie J, Zhou J, Li X, Yi P. (2010) NMR and theoretical study on the interaction between diperoxovanadate and 3-picoline derivatives. *J. Coord. Chem.*, 63:1555-1562.
- [26] Liao WC, Chou CT, Liang WZ, Hao LJ, Kuo CC, Lin KL, Wang JL, Jan, CR.(2018) Exploration of niflumic acid's action on Ca²⁺ movement and cell viability in human osteosarcoma cells. *Chin. J. Physiol*, 61(6): 341–48.
- [27] Ramar M, Manikandan B, Marimuthu PN, Raman T, Mahalingam A, Subramanian P, Karthick S, Munusamy A.(2015) Synthesis of silver nanoparticles using *Solanum trilobatum* fruits extract and its antibacterial, cytotoxic activity against human breast cancer cell line MCF 7. *Spectrochim. Acta - Part A Mol. Biomol. Spectrosc.*,140: 223–228.
- [28] Miura N, Shinohara Y.(2009) Cytotoxic effect and apoptosis induction by silver nanoparticles in HeLa cells. *Biochem. Biophys. Res. Commun* ,390:733–737.
- [29] Smolko L, Smolková R, Samol'ová E, Morgan I, Saoud M, Kaluđerović GN.(2020) Two

- isostructural Co (II) flufenamato and niflumato complexes with bathocuproine : Analogues with a different cytotoxic activity. *J. Inorg. Biochem*, 111:160.
- [30] Smolko L, Špaková I, Klepcová Z, Dubayová K, Samořová E, Rabajdová M, Mareková M.(2021) Zinc(II) niflumato complex with neocuproine: Synthesis, crystal structure, characterization and cytotoxic effects on human endometrial cell lines. *J. Mol. Struct*, 1237.
- [31] Altay A, Caglar S, Caglar B.(2022) Silver(I) complexes containing diclofenac and niflumic acid induce apoptosis in human-derived cancer cell lines. *Arch. Physiol. Biochem*,128:69-79.
- [32] Altay A, Caglar S, Caglar B, Sahin ZS.(2019) Novel silver(I) complexes bearing mefenamic acid and pyridine derivatives: Synthesis, chemical characterization and in vitro anticancer evaluation, *Inorganica Chim. Acta*, 493: 61–71.
- [33] Caglar S, Altay A, Harurluoğlu, B. and Caglar, B.(2021) Trinuclear silver(I) complex of non-steroidal anti-inflammatory drug naproxen: Synthesis, characterization, and in vitro cytotoxicity, *Maced. J. Chem. Chem. Eng*, 40(2): 171-80.
- [34] Caglar S, Altay A.(2021) In Vitro Anticancer Activity of Novel Co (II) and Ni (II) Complexes of Non-steroidal Anti-inflammatory Drug Niflumic Acid Against Human Breast Adenocarcinoma MCF-7 Cells, *Cell Biochem. Biophys*, 79(4): 729-46.
- [35] Adolfo R, Marta C, Pedro L, Otaciro N, Daniel D, Joaquín L, Ignacio L, Lucas B, Luis L, Diógenes I.(2021) Synergy of DNA intercalation and catalytic activity of a copper complex towards improved polymerase inhibition and cancer cell cytotoxicity. *Dalt. Trans*, 34.
- [36] Umar N, Ndumiso M, Mahmoud ES.(2017) Metal complexes in cancer therapy – an update from drug design perspective. *Drug Des Devel Ther*,11: 599–616.

On Prime Hyperideals of a Krasner Hyperring

Burcu Nişancı Türkmen ^{1*}

¹ Amasya University, Faculty of Science and Art, Department of Mathematics

Received:29/09/2022, **Revised:** 13/10/2022, **Accepted:** 25/10/2022, **Published:** 30/12/2022

Abstract

The basis of this study, which was put forth in order to appropriate a special area in the hyperring theory, which has recently been studied as a generalization of the ring theory, which uses the module theory as an application field, is based on integrally closed Krasner hyperrings and (almost) integral dependence applications in Krasner hyperrings.

Keywords: Krasner hyperring, hyperideal, integral dependence, almost integral dependence

Krasner Yüksek Halkaların Asal Yüksek İdealleri Üzerine

Öz

Modül teorisini uygulama alanı olarak kullanan, son zamanlarda halka teorisinin bir genellemesi olarak çalışılan yüksek halka teorisinde özel bir saha oluşturmak üzere ortaya konulan bu çalışmanın temelini, tam kapalı Krasner yüksek halkalar ve Krasner yüksek halkalarda (hemen hemen) tam bağımlılık uygulamaları oluşturmaktadır.

Anahtar Kelimeler: Krasner yüksek halka, yüksek halka, tam bağımlılık, hemen hemen tam bağımlılık.

1. Introduction

Hyperrings and hypermodules categories have significant roles in hyperstructure theory. We refer to the reader having some elementary features of these theory in [1],[6] and [8]. In addition, since our study is a generalization of [9]'s work, the integral dependence in rings can be accessed from this source. Recall that some definitions and theorems from the above references are necessary to improve this article.

For an arbitrary set $A \neq \emptyset$, let $P^*(A) = P(A) \setminus \emptyset$. The couple (A, \circ) is defined as *hypergroupoid* if there is $\circ: A \times A \rightarrow P^*(A)$ is a function, namey hyperoperation. As can be understood from this definition, hypergroupoids are a proper generalization of groupoids. For two nonempty subsets $X, Y \leq A$, let $X \circ Y = \bigcup_{x \in X, y \in Y} x \circ y$. We write $\{s\} \circ X := s \circ X$ and $X \circ \{s\} := X \circ s$ whenever

$s \in A$. If a hypergroupoid (A, \circ) satisfies the equality $a \circ (b \circ c) = (a \circ b) \circ c$ for every $a, b, c \in A$, then (A, \circ) is said to be a *semi-hypergroup*. A hypergroupoid (A, \circ) is called a *quasihypergroup* in case $s \circ A = A \circ s = A$ for every element s in A . If (A, \circ) is a quasihypergroup and a semi-hypergroup, then (A, \circ) is defined as a *hypergroup*. Let (A, \circ) be a hypergroup and $B (\neq \emptyset)$ be a subset of A . B is said to be a *subhypergroup* of A if

$b \circ B = B = B \circ b$ for every element b of B . In [5], a hypergroup (A, \circ) is called *canonical* (i) if for every $a, b \in A$, $a \circ b = b \circ a$, i.e. (A, \circ) is commutative; (ii) there is an element $e \in A$ such that $\{a\} = (a \circ e) \cap (e \circ a)$ for each $a \in A$; (iii) there is a unique $a^{-1} \in A$ such that $e \in a \circ a^{-1}$ for every $a \in A$; (iv) $s \in y \circ z$ provides that $y \in s \circ z^{-1}$ for every element s of A . In the second expression, the element e is said to be the *identity element* of the hypergroup (A, \circ) . In this paper, we consider some types of hyperrings and hypermodules. A triple $(S, +, \cdot)$ is named a *Krasner hyperring* provided

1. $(S, +)$ is hypergroup which is canonical;
2. (S, \cdot) is semi-hypergroup with zero element x providing $0 \cdot x = x \cdot 0 = 0$;
3. " \cdot " is distributive with respect to " $+$ ".

$(S, +, \cdot)$ is named a *hyperring* if

1. The canonical hypergroup $(S, +)$ has scalar identity 0_R ;
2. (S, \cdot) is a semi-group;
3. " \cdot " is distributive with respect to " $+$ ".

In this place " \cdot " is a hyperoperation on S . Each hyperring $(S, +, \cdot)$ holds following two statements: $u \cdot 0 = 0 \cdot u = \{0\}$ and $u \cdot (-v) = \{-z \mid z \in u \cdot v\} = (-u) \cdot v = -(u \cdot v)$ for each $u, v \in S$. We denote a hyperring $(S, +, \cdot)$ with S for short. If S is commutative with respect to its hyperoperation " \cdot ", then S is named *commutative*. If $1 \in S$ for every element $f \in S$, 1 is named *identity element of a hyperring* S . Assume that S is a hyperring including 1 . Following [11], a *hypermodule* M over the hyperring S means a triple $(M, +, \circ)$ in the fact that a canonical hypergroup $(M, +)$ have a scalar identity 0_M and the operation $\circ: S \times M \rightarrow P^*(M)$ satisfies the followings for every element $f, g \in S$ and $a, b \in M$;

1. $f \circ (a + b) = f \circ a + f \circ b$;
2. $(f + g) \circ a = f \circ a + g \circ a$;
3. $(f \cdot g) \circ a = f \circ (g \circ a)$; $a \in 1 \circ a$

For an S -hypermodule $(M, +, \circ)$ and every $u \in S$ and $a \in M$, we can write $u \circ 0_M = \{0_M\} = 0 \circ a$ and $u \circ (-a) = (-u) \circ a = -(u \circ a) = \{-b \mid b \in u \circ a\}$. We denote an S -hypermodule $(M, +, \circ)$ with M for short. In [5], this notion is generalized as hypermodule over a Krasner hyperring.

For a commutative hyperring S , let $J (\neq \emptyset)$ be a subset of S . J is named *hyperideal* if $x - y \in J$ and $a \cdot x \in J$ for any element $a \in S$ and $x, y \in J$. If J_1, J_2 are hyperideals of S , the sum $J_1 + J_2$ is also hyperideal of S . For Krasner hyperrings S and S' , a function $f: S \rightarrow S'$ is named a *strong hyperring homomorphism* if $f(x + y) = f(x) + f(y)$ and $f(x \cdot y) = f(x) \cdot f(y)$ for every element $x, y \in M$. Assume that $(S, +, \cdot)$ is an arbitrary ring and H is a subset of S . H is named a *multiplicative subgroup* of S if (H, \cdot) is a group. If $S = SH$ and $sH = Hs$ for every element s in S , then H is named a *normal subgroup* of S . We indicate that the rings including identity elements known as normal subgroups. A normal subgroup H of S contains an equivalence relation P in S and a part of S in equivalence classes, which inherits a hyperring structure from S . The hyperrings obtained with this structure are named *quotient hyperrings* are written by S/H . Let S be a hyperring. S is named *integral hyperdomain* if for each $f, g \in S$, $0 \in f \cdot g$ implies that $f = 0$ or $g = 0$. S is named a *hyperfield* in which every nonzero element has a inverse in S in [8]. A hyperring S including 1 is named a *principal hyperideal hyperdomain* if S doesn't contain zero divisors and every hyperideal of S is generated by a

single element ([4]). Assume that S is a hyperring. S is named *Noetherian* if S satisfies the condition (ACC) on hyperideals of S (see [3]).

Assume that M is an S -hypermodule and $N (\neq \emptyset)$ is a subset of M . N is named a *subhypermodule* of M , denoted by $N \leq M$, if N is an S -hypermodule under the same hyperoperations on M . It is shown in (Proposition 2.3, [10]) that if $x \circ a \leq N$ and $a - b \in N$ for every element $x \in S$ and $a, b \in N$, then by $N \leq M$. Let M be a canonical S -hypermodule. If " \cdot ": $S \times M \rightarrow M$ via $(s, m) \mapsto s \cdot m \in M$ and $s \cdot 0 = 0$ is an external operation, then M is named a *Krasner S -hypermodule*. Let T be a nonempty subset of a hypermodule M . $\langle T \rangle$ is defined as a *subhypermodule of M generated by T* if $\langle T \rangle$ is the smallest subhypermodule of M containing T .

2. Main Theorems

2.1. Integral Dependence in Krasner Hyperring

Let R be a subhyperring of a hyperring R' and $a_1, a_2, \dots, a_m \in R'$. We denote with $R[a_1, a_2, \dots, a_m]$ that is a set of polynomial expressions in a_1, a_2, \dots, a_m with coefficients in R . Therefore, if X_1, X_2, \dots, X_m are indeterminates, then

$$R[a_1, a_2, \dots, a_m] = \{f(a_1, a_2, \dots, a_m) \mid f(X_1, X_2, \dots, X_m) \in R[X_1, X_2, \dots, X_m]\}.$$

The mapping $f(X_1, X_2, \dots, X_m) \mapsto f(a_1, a_2, \dots, a_m)$ is a strong hyperring homomorphism from $R[X_1, X_2, \dots, X_m]$ into R' , so its image $R[a_1, a_2, \dots, a_m]$ is to be a subhyperring of R' . Here $R \subseteq R[a_1, a_2, \dots, a_m]$.

2.1.1. Lemma *Given a hyperring R , let be $d = \det[a_{ij}]$ where $a_{ij}, b_j \in R$ for $i, j = 1, 2, \dots, m$. If $\sum_{j=1}^m a_{ij} \cdot b_j = 0$ for all $i = 1, 2, \dots, m$, then $d \cdot b_j = 0$ where $j = 1, 2, \dots, m$.*

Proof. Let d_{ij} be the cofactor of a_{ij} in the matrix $[a_{ij}]$. Then $\sum_{i=1}^m d_{ij} \cdot a_{ih} = \begin{cases} d & \text{if } j = h \\ 0 & \text{if } j \neq h \end{cases}$

Hence

$$\begin{aligned} 0 &= \sum_{i=1}^m d_{ih} \cdot \left(\sum_{h=1}^m a_{ih} \cdot b_h \right) \\ &= \sum_{h=1}^m \left(\sum_{i=1}^m d_{ih} \cdot a_{ih} \right) \cdot b_h = d \cdot b_j \end{aligned}$$

for $j = 1, 2, \dots, m$. ■

Given an R -hypermodule M . M is named *finitely generated* provided that there is a finite subset $\{m_1, m_2, \dots, m_k\}$ of M generating M , that is,

$$M = \{x \mid \exists r_1, r_2, \dots, r_k \in R, k \in \mathbb{N} \text{ such that } x \in \sum_{i=1}^k r_i m_i\}$$

2.1.2. Proposition *Assume that R' is a hyperring and a is an element in R' . For a subhyperring R , the followings are equivalent:*

1. *There are elements $\mathbf{b}_0, \mathbf{b}_1, \dots, \mathbf{b}_{m-1} \in R$ ($m \geq 1$) provided that $\mathbf{b}_0 + \mathbf{b}_1 \cdot \mathbf{a} + \dots + \mathbf{b}_{m-1} \cdot \mathbf{a}^{m-1} + \mathbf{a}^m = \mathbf{0}$.*
2. *Hypermodule $R[\mathbf{a}]$ over R is finitely generated.*
3. *There exists a subhyperring R'' of R' provided that $\mathbf{a} \in R''$ and the hypermodule R'' over R is finitely generated.*

Proof. (1)⇒(2) Assume $f(X) = c_0 + c_1.X + \dots + c_d.X^d \in R[X]$ is polynomial with $\deg f(X) = d > m$. Therefore we can write

$$\begin{aligned} f(a) &= c_0 + c_1.a + \dots + c_{d-1}.a^{d-1} + c_d.a^{d-m}b \\ &= c'_0 + c'_1.a + \dots + c'_{d-1}.a^{d-1} \text{ for some element } b \in R \end{aligned}$$

It is continued similar procedures until R -hypermodule generated by $1, a, \dots, a^m$ for $f(a)$. Therefore, as a R -hypermodule $[a] = R1 + Ra + \dots + Ra^m$; hence $R[a]$ is finitely generated.

(2)⇒(3) If R'' is taken as $R[a]$, the proof is provided.

(3)⇒(1) Suppose that a_1, a_2, \dots, a_m generate R'' over R . For $i = 1, 2, \dots, m$, $a.a_i = \sum_{j=1}^m b_{ij}.a_j$, $b_{ij} \in R$, or $\sum_{j=1}^m (b_{ij} - \delta_{ij}).a_j = 0$. If $d = \det[b_{ij} - \delta_{ij}.a]$ then $d.a_j = 0$ for $j = 1, 2, \dots, m$ by Lemma 2.1.1. Thus $d.c = 0$ for every $c \in R''$. With $c = 1$ we get $d = 0$. Since d is a polynomial in a with coefficients in R such that the coefficient of a^n is ± 1 , this is also desired. ■

2.1.3. Definition Assume R' is a hyperring, R is a subhyperring of R' and a is an element in R' . a is named *integral on R* if the equal conditions in the above proposition are satisfied. Moreover, R' is named *integral on R* in case every element in R' is integral on R . If the elements of R are the only elements of R' that are integral on R , R is named *integral closed in R'* . If R is integral closed in its total quotient hyperring, R is named *integral closed*.

2.1.4. Proposition Assume R is a subhyperring of a hyperring R' and $R_0 = \{a | a \in R' \text{ and } a \text{ is integral on } R\}$. Then R_0 is a subhyperring of R' and $R \subseteq R_0$.

Proof. Clearly, $R \subseteq R_0$. Let $a, b \in R_0$. Then the R -hypermodule $R[a]$ is finitely generated and the $R[a]$ -hypermodule $R[a, b] = R[a][b]$ is finitely generated. Since $a - b, a, b \in R[a, b]$, we obtain that $a - b, a, b \in R_0$. It means that R_0 is a subhyperring of R' . ■

Mentioned in Proposition 2.1.4, R_0 is named *the integral closure of R in R'* . It follows from the next proposition that R_0 is integrally closed in R' .

2.1.5. Proposition Let $R \leq R' \leq R''$ be hyperrings. Suppose that R' is integral on R and $a \in R''$ is integral on R' . Then a is integral on R .

Proof. Suppose $b_0 + b_1.a + \dots + b_{m-1}.a^{m-1} + a^m = 0$ where $b_0, b_1, \dots, b_{m-1} \in R'$. Therefore a is integral on $R[b_1, b_2, \dots, b_{m-1}]$. It follows that the krasner R -hypermodule $R[b_1, b_2, \dots, b_{m-1}, a]$ is finitely generated. This means that a is integral on R . ■

For a Krasner hyperring R , let S be multiplicatively closed subset of R with $1 \in S$. Following [7], the construction of $S^{-1}R$ is named *hyperring of fractions* if a hyperring structure is defined as follows: $\frac{a}{s} + \frac{b}{t} = \frac{a.t+b.s}{s.t}$ and $\frac{a}{s} \cdot \frac{b}{t} = \frac{a.b}{s.t}$ for every element $\frac{a}{s}, \frac{b}{t}$ of $S^{-1}R$. Here a relation “ \equiv ” is on $R \times S$ defined by $(a, s) \equiv (b, t)$ if and only if $0 \in (a.t - b.s).u$ for, where $u \in S$. Then obtained equivalence class of (a, s) with $\frac{a}{s}$ and family of whole equivalence classes is denoted by $S^{-1}R$.

2.1.6. Proposition Assume that R' is a hyperring, R is a subhyperring of R' and S is a multiplicative system in R . Then $S^{-1}R$ is a subhyperring of $S^{-1}R'$. Moreover, if R' is integral on R , then $S^{-1}R'$ is integral on $S^{-1}R$.

Proof. Let 0_S and $0_{S'}$ be the S -components of 0 in R and R' , respectively. We certainly have $0_S \subseteq 0_{S'} \cap R$. If $a \in 0_{S'} \cap R$, then $s \cdot a = 0$ for some $s \in S$. Since $S \subseteq R$, we obtain that $a \in 0_S$. Thus $0_S = 0_{S'} \cap R$. Hence the mapping taking $\frac{a}{s} \in S^{-1}R$ onto $\frac{a}{s} \in S^{-1}R'$ is an injective strong hyperring homomorphism; if we identify $\frac{a}{s} \in S^{-1}R$ with its image $\frac{a}{s} \in S^{-1}R'$, then $S^{-1}R$ can be considered as a subhyperring of $S^{-1}R'$. Suppose that R' is integral on R , $\frac{a}{s} \in S^{-1}R'$, $a \in R'$ and $s \in S$. There exists elements $b_0, b_1, \dots, b_{m-1} \in R$ such that we have

$$b_0 + b_1 \cdot a + \dots + b_{m-1} \cdot a^{m-1} + a^m = 0. \text{ Then}$$

$$\frac{b_0}{s^m} + \frac{b_1}{s^{m-1}} \cdot \frac{a}{s} + \dots + \frac{b_{m-1}}{s} \cdot \left(\frac{a}{s}\right)^{m-1} + \left(\frac{a}{s}\right)^m = \frac{b_0 + b_1 \cdot a + \dots + b_{m-1} \cdot a^{m-1} + a^m}{s^m} = 0$$

So $\frac{a}{s}$ is integral on $S^{-1}R$ ■

Assume that R is a hyperring. In [2] or [11], a proper hyperideal P of R is named a *prime hyperideal* of R if whenever $AB \subseteq P$, either $A \subseteq P$ or $B \subseteq P$ where A and B are hyperideals of R . For a prime hyperideal P of R , we obtain that $S = R \setminus P$ is *multiplicatively closed* and denote by $S^{-1}R = R_P$. Let R' be a hyperring, A be a hyperideal of R and A' be a hyperideal of R' such that $A = A' \cap R$, then A' is named *lie over* A .

2.1.7. Theorem Assume R is a subhyperring of a hyperring R' , R' is integral over R and P is a prime hyperideal of R . Then there is a prime hyperideal P' of R' that lies over P . Moreover, if P' and P'' are prime hyperideals of R' that lie over P and if $P' \subseteq P''$, then $P' = P''$.

Proof. The family of hyperideals A' of R' such that $A' \cap R \subseteq P$ is nonempty, and it follows from Zorn's lemma that this family contains a maximal element P' . Then $P' \cap R \subseteq P$. Suppose $P' \cap R \subset P$ and $a \in P$, $a \notin P'$. Then $P' \subset P' + R'a$ and consequently, by our choice of P' , $(P' + R'a) \cap R \not\subseteq P$. Therefore there is an element $c \in P'$ and $r \in R'$ such that $c + ra = b \notin P$ but $b \in R$. For $d_0, d_1, \dots, d_{m-1} \in R$, $d_0 + d_1 \cdot r + \dots + d_{m-1} \cdot r^{m-1} + r^m = 0$. Then

$$\begin{aligned} b^m + d_{m-1} \cdot a \cdot b^{m-1} + \dots + d_1 \cdot a^{m-1} \cdot b + d_0 \cdot a^m \\ = (c + r \cdot a)^m + d_{m-1} \cdot a \cdot (c + r \cdot a)^{m-1} + \dots + d_1 \cdot a^{m-1} \cdot (c + r \cdot a) + d_0 \cdot a^m \\ = f(c) + a^m \cdot (r^m + d_{m-1} \cdot r^{m-1} + \dots + d_1 \cdot r + d_0) = f(c) \in P' \cap R \subseteq P; \end{aligned}$$

where $f(c)$ is a polynomial in c with coefficients in R' . Hence, since $a \in P$, we have $b^m \in P$, so $b \in P$, a contradiction. Thus $P' \cap R = P$. Let $S = R \setminus P$. Therefore S is a multiplicative system in R' . If $P = R$, then $P' = R'$ which is prime, so we may assume $P \neq R$. Let A' be a hyperideal of R' with $P' \subset A'$. Then $A' \cap R \not\subseteq P$ so $A' \cap R$ meets S ; hence $A' \cap S \neq \emptyset$. Hence P' is a maximal in the set of hyperideals of R' whose intersection with S is empty. Assume $P' \subset P''$ are prime hyperideals of R' that lie over P . Let $a \in P''$ with $a \notin P'$. Since a is integral on R there exists at least positive integer m such that there are elements $b_0, b_1, \dots, b_{m-1} \in R$ for which $a^m + b_{m-1} \cdot a^{m-1} + \dots + b_1 \cdot a + b_0 \in P'$. Therefore $b_0 \in P'' \cap R = P = P' \cap R$. It follows that $a(a^{m-1} + b_{m-1} \cdot a^{m-2} + \dots + b_1) \in P'$, but $a \notin P'$, so

$a^{m-1} + b_{m-1}a^{m-2} + \dots + b_1 \in P'$. This contradicts our choice of m . Thus, if $P' \subseteq P''$, we must have $P' = P''$. ■

2.1.8. Corollary For a hyperring R , let R' be as in the Theorem 2.1.7. Let $P_0 \subset P_1 \subset \dots \subset P_m$ be a chain of prime hyperideals of R . If the prime hyperideal P'_0 of R' lies over P_0 , then there is a chain $P'_0 \subset P'_1 \subset \dots \subset P'_m$ of prime hyperideals of R' such that P'_i lies over P_i for $i = 0, 1, \dots, m$. If, for a given i , there is no prime hyperideal of R strictly between P_i and P_{i+1} , then there is no prime hyperideal of R' strictly between P'_i and P'_{i+1} .

Proof. By the hypothesis, we have shown that there is $P'_0 \subset \dots \subset P'_m$ of prime hyperideals of R' such that P'_i lies over P_i for $i = 0, 1, \dots, m$. Then $\frac{R}{P_k}$ can be considered as a subhyperring of $\frac{R'}{P'_k}$ for $0 \leq k \leq m$. Thus, by Theorem 2.1.7. there is a prime hyperideal P'_{k+1} of R' such that $P'_k \subset P'_{k+1}$ and $\frac{P'_{k+1}}{P'_k}$ lies over $\frac{P_{k+1}}{P_k}$. So we have P'_{k+1} lying over P_{k+1} . Suppose that P' is a prime hyperideal of R' and that $P'_i \subset P' \subset P'_{i+1}$. Again by Theorem 2.1.7, P' cannot lie over either P_i or P_{i+1} . Therefore the prime hyperideal $P' \cap R$ of R is strictly between P_i and P_{i+1} . ■

2.2. Almost Integral Dependence in Krasner Hyperring

Now we shall define notions of almost integral over a hyperring and complete integral closure of a hyperring and give some properties of these subhyperrings.

2.2.1. Definition Assume that R is a subhyperring of a hyperring R' . An element $a \in R'$ is named *almost integral over R* if there is a finitely generated subhypermodule of the R -hypermodule R' which contains all powers of a .

It is clear seen that every element of R' which is integral over R is also almost integral over R . But the converse is not always true. Assume that R is an integrally closed hyperdomain with quotient hyperfield K . Let $T = R + XK[X]$. T is integrally closed and $K[X]$ is the complete integral closure of R in $K[X]$. If Krasner hyperring R is Noetherian, then the converse holds.

2.2.2. Definition Let R be a subhyperring of a hyperring R' . The set R_0 of all elements of R' which are almost integral over R is the *complete integral closure of R in R'* . If $R_0 = R$, the R is *completely integrally closed in R* .

It is immediately clear that the complete integral closure R_0 of R in R' is a subhyperring of R' . However, R_0 is not necessarily itself completely integrally closed; an example is given in the Example 2.2.3.

2.2.3. Example The complete integral closure need not be completely integrally closed. Assume that K is a hyperfield and X, Y are indeterminates. Let $R = K[\{X^{2n+1}Y^{n(2n+1)} \mid n \geq 0\}]$. Then the quotient hyperfield of the hyperfield R is $K(X, Y)$. If $R' = K[\{XY^n \mid n \geq 0\}]$, then $R \subset R' \subseteq R'' \subseteq R^* \subseteq K[X, Y]$, where R^* is the complete integral closure of R . Since for any element of R , the exponent of Y in any of the monomials of that element is less than or equal to

the square of the exponent of X in the same monomial, Y is almost integral on R' , and hence is almost integral on R^* , but that $Y \notin R^*$.

Furthermore, if R, T , and T' are rings with $R \subseteq T \subseteq T'$, then an element $a \in T$ may be almost integral over R as an element of T' , but not almost integral over R as an element of T ; it is given a counter example of this fact in Example 2.2.4.

2.2.4. Example Assume that $R \subseteq T_1 \subseteq T_2$ are hyperrings. For $i = 1, 2$, let R_i be the complete integral closure of R in T_i . It is clear that $R_1 \subseteq R_2 \cap T_1$. If T is a subhypermodule of some T_1 -hypermodule M such that T_1 is a direct summand of M , then $R_1 = R_2 \cap T_1$. In addition, the same conclusion holds if every finitely generated T_1 -module M with $T_1 \subseteq M \subseteq T_2$ is a subhypermodule of a T_1 -hypermodule of which T_1 is direct summand. If T is a principal hyperideal hyperdomain, then $R_1 = R_2 \cap T_1$. Assume that K is a hyperfield and X, Y are indeterminates over K . Let $R = K[\{XY^n | n \geq 1\}]$, $T_1 = R[Y]$ and $T_2 = T_1[\frac{1}{X}]$. It is continued similar procedures until R_1 , and R_2 are as above, we have $R_1 \subset R_2 \cap T_1$.

Even though the complete integral closure of one ring in another may not be completely integrally closed, we have the following:

2.2.5. Proposition *Let R be a subhyperring of a hyperring R' and R_0 the complete integral closure of R in R' . Then R_0 is integrally closed in R' .*

Proof. Let $x \in R'$ be integral over R_0 ; $x^k + a_{k-1} \cdot x^{k-1} + \dots + a_0 = 0$, where $a_0, \dots, a_{k-1} \in R_0$. It follows that x is integral over the hyperring $R[a_0, \dots, a_{k-1}]$. a_i is contained in some finitely generated subhypermodule of the R -hypermodule R' for $i = 0, \dots, k - 1$, say $M_i = Rx_{i1} + \dots + Rx_{ik_i}$, where each $x_{ij} \in R'$. Then $R[a_0, \dots, a_{k-1}] \subseteq M_0 \dots M_{k-1}$, which is the subhypermodule of the R -hypermodule R' generated by all products $x_{0j_0} x_{1j_1} \dots x_{k-1, j_{k-1}}$ where each j_i runs between 1 and m_i . Hence x is contained in

$$\begin{aligned} R[x] &\subseteq R[a_0, \dots, a_{k-1}, x] \\ &= \sum_{h=0}^{k-1} R[a_0, \dots, a_{k-1}] x^h \\ &\subseteq \sum_{h=0}^{k-1} \sum_{i=0}^{k-1} \sum_{j_i=1}^{m_i} R x_{0j_0} x_{1j_1} \dots x_{k-1, j_{k-1}} x^h, \end{aligned}$$

which is finitely generated subhypermodule of the R -hypermodule R' . Thus x is almost integral over R , and so $x \in R_0$. Therefore R_0 is integrally closed. ■

2.2.5. Corollary *Let R, R_1 , and R_2 be subhyperrings such that $R \subseteq R_1 \subseteq R_2$. If each element of R_1 is almost integral over R , and if R_2 is integral over R_1 , then each element of R_2 is almost integral over R .*

3. Conclusion

In this paper, it is obtained integral dependence on krasner hyperring by using prime hyperideals of the hyperring. In this way various properties is brought in theory of Krasner hyperring. In

the second section, prime hyperideals of the hyperrings are classified. In the third section, it is treated as a subject of almost integral dependence in the notion of hyperfields.

Ethics in Publishing

There are no ethical issues regarding the publication of this study.



Acknowledgements

The author thanks the referees for the corrections and comments.

References

- [1] Ameri, R., (2003) On categories of hypergroups and hypermodules, *Journal of Discrete Mathematical Sciences and Cryptography*, 6:2-3, 121-132.
- [2] Bordbar, H., Cristea, I., (2017) Height of prime hyperideals in Krasner hyperrings, *Filomat*, 31:19,6153-6163.
- [3] Bordbar, H., Cristea, I., Novak, M., (2017) Height of hyperideals in Noetherian Krasner hyperrings, *U.P.B. Sci. Bull.Series A*, 79,2, 31-42.
- [4] Bordbar, H., Cristea, I., (2021) Regular parameter elements and regular local hyperrings, *Mathematics*, 9, 243, 1-13.
- [5] Corsini, P., (1993). *Prolegomena of Hypergroup Theory*, 2nd ed. Tricesimo Italy, Aviani editore Italy.
- [6] Davvaz, B., Fotea, V.L., (2007). *Hyperring Theory and Applications*, Palm Harbor, FL, USA, International Academic Press.
- [7] Davvaz, B., Salasi, A., (2006) A realization of hyperrings, *Comm. Algebra*, 34, 4389-4400.
- [8] Krasner, M., (1983) A class of hyperring and hyperfields, *IJMMS*, 6:2,307-311.
- [9] Larsen, M.D., McCarthy, P.J. (1971). *Multiplicative Theory of Ideals*, Pure and Applied mathematics, A Series of Monographs and Textbooks, Volume 43, Academic Press, New York and London.
- [10] Mahjoob, R., Ghaffari, V., (2018), Zariski topology for second subhypermodules, *Italian Journal of Pure and Applied Mathematics*, 39, 554-568.
- [11] Siraworakun, A., Pianskool, S. (2012), Characterizations of prime and weakly prime subhypermodules, *International Mathematical Forum*, Vol. 7, no. 58, 2853 – 2870.

New Analytical Method For Solution of Second Order Ordinary Differential Equations With Variable Coefficients

Yaşar PALA ^{1*}, Çağlar KAHYA ¹

¹ Bursa Uludağ University, Engineering Faculty, Mechanical Engineering Dept., Görükle, 16059, Bursa-Turkey.

Received: 14/10/2021, Revised: 15/08/2022, Accepted: 15/08/2022, Published: 30/12/2022

Abstract

In this study, we propose four methods for the analytical solution of second order ordinary non-homogeneous differential equations with variable coefficients. In the first case, the method directly gives the solution in explicit or integral form. In the second method, the solution of the problem reduces to the solutions of adjoined second order ordinary differential equation of homogeneous type. As long as the analytical solution of two adjoined equations can be solved, the analytical solution can always be found. In the third method, the differential equation is transformed into Riccati equation. Riccati equation is solved by means of a method recently developed. In order to solve non-homogeneous differential equation, the fourth method is developed. The strategy is different but the solution is again based on the solution of Riccati equation.

Keywords: Second order differential equations, analytical method, Riccati equation.

İkinci Mertebeden Değişken Katsayılı Diferansiyel Denklemlerin Analitik Çözümü Üzerine Yeni Bir Yöntem

Öz

Bu çalışmada değişken katsayılı ikinci mertebe non-homojen diferansiyel denklemlerin analitik çözümü için dört yöntem geliştirilmektedir. İlk yöntem çözümü doğrudan açık ya da kapalı formda vermektedir. İkinci yöntemde problemin çözümü homojen tipte ek ikinci mertebe denklemlerin çözümüne indirgenmektedir. Ek denklemler çözüldüğü sürece analitik çözüm daima bulunabilmektedir. Üçüncü yöntemde diferansiyel denklem Riccati denklemine dönüştürülmektedir. Riccati denkleminin çözümünde en son geliştirilen bir yöntem kullanılmaktadır. Dördüncü yöntem de strateji farklı olup, yöntem yine Riccati denklemin çözümüne indirgenmektedir.

Anahtar Kelimeler: İkinci mertebe diferansiyel denklem, analitik yöntem, Riccati denklemi.

1. Introduction

The second order non-homogeneous differential equations of general type are commonly encountered in engineering, physics, biology, astrophysics, etc. Therefore, their analytical solutions are extremely important for researchers in applied sciences. There have been many studies on the analytical solution of second order ordinary differential equations with variable

coefficients [2 - 6, 10, 11, 13 – 16]. When the solution methods developed are carefully checked, it can be seen that most of the analytical methods can be classified into three groups. In the first group, the equation is transformed into Riccati equation which is a first order nonlinear ordinary differential equation. As long as the analytical solution of Riccati differential equation is known, this method can be valid and logical. However, in the most general case, Riccati equation cannot be solved. The methods available require one proper solution of the equation. However, for an equation of general type, the proper solution cannot be found or proposed very easily. Therefore, this approach mostly remains inconclusive [1, 8 - 10, 12]. Other methods are of limited usage since they involve restrictions on the functions involved. To that end, Pala and Ertaş have recently developed a general method for solving Riccati equations of general type [7]. However, in the second part of this work, Riccati equation is again transformed into a second order ordinary equation of the simplest form. This simplest form reveals whether Riccati equation leads to an analytical or an exact solution. In the second group, the differential equation given is transformed into a solvable form or a second order differential equation with constant coefficients. This approach is far away from being general since the method brings several limitations on the functions involved in the differential equations. In the third group, the method of operator factorization is used to solve the second order equations with variable coefficients. Although this method seems to be more general compared to the other conventional methods, this method also includes several limitations and depends on the availability of the solution of Riccati equations [10]. Consequently, new analytical methods for solving this type of equations are always welcome.

2. Material and Methods

2.1. First Method of Solution

As a first method, we start with a known relatively simple method. Let us consider the second order non-homogeneous differential equation with variable coefficients

$$y'' + P(x)y' + Q(x)y = R(x) \tag{1}$$

where $P(x)$, $Q(x)$ and $R(x)$ are arbitrary smooth functions of x . In order to solve Eq. (1), a linear transformation in the following form is introduced:

$$\bar{y} = y' + P(x)y \tag{2}$$

By differentiating Eq. (2), we have

$$\bar{y}' = y'' + Py' + P'y \tag{3}$$

The right hand side of Eq. (3) will be the same as the left hand side of Eq. (1) if we assume $P' = Q$. Thus, if we assume $\bar{y}' = R(x)$, then Eq. (3) becomes identical to Eq. (1). We take care that this already known method brings a restriction of the form $P' = Q$ on the analytical solution of Eq. (1). This restriction will be removed later. The solution procedure after this point is as follows. First, we solve the transformed equation $\bar{y}' = R(x)$. Second, we substitute the result obtained into Eq. (2) to obtain $y(x)$.

Example 1. Let us consider the equation

$$y'' - xy' - y = 1 \tag{4}$$

The condition $P' = Q$ is satisfied here. Thus, integrating the equation $\bar{y}' = 1$ yields $\bar{y} = x + c_1$, where c_1 is a constant. Inserting this result into Eq. (2), we have

$$y' - xy = x + c_1$$

This is a first order ordinary equation which can readily be solved. The solution has the form

$$y(x) = c_2 e^{\frac{x^2}{2}} - 1 + c_1 e^{\frac{x^2}{2}} \int e^{-\frac{x^2}{2}} dx \tag{5}$$

Here, c_2 is a constant. Eq. (5) is the general solution of Eq. (4). Recall here that the term $c_1 e^{\frac{x^2}{2}} \int e^{-\frac{x^2}{2}} dx$ and $c_2 e^{\frac{x^2}{2}}$ are two different solutions of the homogeneous part of Eq. (4).

Example 2. Let us consider the equation

$$y'' - (\cos x)y' + (\sin x)y = -\sin x \tag{6}$$

Solving the equation $\bar{y}' = -\sin x$ gives $\bar{y} = \cos x + c_1$, where c_1 is a constant. Eq. (2) reads

$$y' - (\cos x)y = \cos x + c_1 \tag{7}$$

The Solution of Eq. (7) is obtained in the form

$$y(x) = c_2 e^{\sin x} - 1 + c_1 e^{\sin x} \int e^{-\sin x} dx$$

Recall that the term $c_2 e^{\sin x} - 1$ satisfies Eq. (6).

Example 3. In order to show the effectiveness of the method, let us now consider a simple second order equation with constant coefficient in the form

$$y'' - 5y' = e^x \tag{8}$$

The solution of $\bar{y}' = e^x$ yields $\bar{y} = e^x + c_1$. Inserting this result into Eq. (2) gives

$$y' - 5y = e^x + c_1 \tag{9}$$

The solution of Eq. (9) is obtained as

$$y(x) = c_2 e^{5x} - \frac{1}{4} e^x - \frac{c_1}{5} \tag{10}$$

Eq. (10) is the analytical solution of Eq. (8).

2.2. A More General Method of Solution

In the first section, the method of solution was valid provided that the condition $P' = Q$ is satisfied. It is obvious that this condition is not satisfied every time. Therefore, we need to develop a more general method for the solution of Eq. (1).

Now, we propose a new transformation of the form

$$\bar{y} = Ny' + My \tag{11}$$

where $N(x)$ and $M(x)$ are unknown functions to be (hopefully) determined. We differentiate Eq. (11):

$$\bar{y}' = N'y' + Ny'' + M'y + My'$$

or, arranging

$$y'' + \left(\frac{N'}{N} + \frac{M'}{N}\right)y' + \frac{M'}{N}y = \frac{\bar{y}'}{N}$$

If we take

$$\frac{N'}{N} + \frac{M'}{N} = P(x) \tag{12a}$$

$$\frac{M'}{N} = Q(x) \tag{12b}$$

$$\frac{\bar{y}'}{N} = R(x) \tag{12c}$$

we then obtain Eq. (1). Thus, if we can solve Eqs. (12) for $N(x)$ and $M(x)$ by any means, then we can obtain $y(x)$ from Eq. (11). The first two equations in Eqs. (12) can be combined in the following way:

$$N'' - PN' + (Q - P')N = 0 \tag{13}$$

or

$$M'' - \left(P + \frac{Q'}{Q}\right)M' + QM = 0 \tag{14}$$

If Eq. (13) or Eq. (14) is a Euler-Cauchy type equation, they can readily be solved. However, in the most general case, the analytical solutions of Eqs. (13) and (14) are still not known. Therefore, we consider various cases for which we can obtain the analytical solutions of Eqs. (13) and (14) to determine $N(x)$ or $M(x)$.

Although, Eqs. (13) and (14) cannot be solved in the most general case, they can give analytical solutions in some cases. In order to show this, we consider the equation proposed by Urdaletova and Kydyraliev [14].

$$y'' - 4xy' + (4x^2 - 2)y = 6xe^{x^2}$$

Comparing this equation with Eq. (1), we find

$$P = -4x, \quad Q = 4x^2 - 2, \quad R = 6xe^{x^2}$$

If we take $N = e^{-x^2}$, then Eq. (13) is satisfied. Using Eq. (12a), we have $M = -2xe^{-x^2}$. Inserting these functions into Eq. (12c) yields

$$\frac{\bar{y}'}{e^{-x^2}} = 6xe^{x^2}$$

from which we obtain

$$\bar{y} = 3x^2 + c_1$$

Putting now this result into Eq. (11), we have

$$e^{-x^2}y' - 2xe^{-x^2}y = 3x^2 + c_1 \tag{15}$$

The solution of Eq. (15) yields

$$y(x) = e^{x^2}(x^3 + c_1x + c_2)$$

This result is the same as that given by Urdaletova and Kydyraliev [14].

For the solution of Eq. (13) or Eq. (14), we can consider the following cases for which we obtain the analytical solution of the problem.

Case 1: Let us assume that $P = (ax + b)$, $Q = cx + d$ in Eq. (13). Here a, b, c, d are constants. In this case, Eq. (13) reads

$$N'' - (ax + b)N' + (cx + d - a)N = 0 \tag{16}$$

In addition, we assume $N = e^{sx}$ where s is a constant to be determined. Inserting this form into Eq. (16) and equating mutual terms, we have

$$-as + c = 0 \tag{17a}$$

$$s^2 - bs + d - a = 0 \tag{17b}$$

We have five unknowns. However, we can choose a, b, c and s . The constant d can be found from Eq. (17b). As an example, we choose $a = 1, c = 3, b = 1, s = 3$. Eq. (17b) gives $d = -5$. Thus, Eq. (13) takes the form

$$N'' - (x + 1)N' + (3x - 6)N = 0$$

whose solution is given by $N = e^{sx} = e^{3x}$. From Eq. (12) we have

$$M' = NQ = (3x - 5)e^{3x} \rightarrow$$

$$M = (x - 2)e^{3x} + c_1 \tag{18}$$

After we determine M and N in this way, for example, we can solve the equation

$$y'' + (x + 1)y' + (3x - 5)y = 5$$

Using Eq. (12c) gives

$$\frac{\bar{y}'}{N} = R(x)$$

$$\bar{y}' = 5e^{3x} \rightarrow \bar{y} = \frac{5}{3}e^{3x} + c_2 \tag{19}$$

Now, inserting Eq. (19) into Eq. (11), we have

$$e^{3x}y' + (x - 2)e^{3x}y = \frac{5}{3}e^{3x} + c_2 \tag{20}$$

Here, without loss of generality, we have omitted c_1 in Eq. (18). We simplify Eq. (20) as

$$y' + (x - 2)y = \frac{5}{3} + c_2e^{-3x} \tag{21}$$

The solution of Eq. (21) can readily be written as

$$y = c_3e^{2x - \frac{x^2}{2}} + e^{2x - \frac{x^2}{2}} \int e^{\frac{x^2}{2} - 2x} \left(\frac{5}{3} + c_2e^{-3x} \right) dx$$

Case 2: We assume that $N = 1$. Then, Eq. (13) yields

$$Q = P'$$

This case is identical to that in Section 1.

Case 3: We assume that $N = e^{ax}$, where a is constant. Then, Eq. (13) yields

$$a^2 - Pa + (Q - P') = 0 \tag{22}$$

When P is arbitrarily chosen, then Q must be determined from Eq. (22).

Example 4: Let us take $a = 1$, $P = x^2$. Eq. (22) gives $Q = 2x + x^2 - 1$. This means that we can solve the equation

$$y'' + x^2y' + (2x + x^2 - 1)y = x \tag{23}$$

Taking $N = e^x$, we find from Eq. (12b) that

$$M' = NQ = e^x(2x + x^2 - 1) \rightarrow M = e^x(x^2 - 1) + c_0$$

Eq. (12c) gives

$$\bar{y}' = NR = xe^x \rightarrow \bar{y} = e^x(x - 1) + c_1$$

Thus, we can write Eq. (11) as

$$\bar{y} = Ny' + My = y' + (x^2 - 1)y = (x - 1) + \frac{c_1}{e^x} \quad (24)$$

The solution of Eq. (24) is in the form

$$y(x) = e^{\left(x - \frac{x^3}{3}\right)} \left(c_2 + \int e^{\left(\frac{x^3}{3} - x\right)} [(x - 1) + c_1 e^{-x}] dx \right)$$

Case 4 : This time, we assume that $M = e^{ax}$ and use it in Eq. (14):

$$a^2 - a \left(P + \frac{Q'}{Q} \right) + Q = 0 \quad (25)$$

where a is an arbitrary constant. If P is given, Q can be determined from this equation.

Example 5 : Let us assume $a = 1, P = 0$. Then, Eq. (25) gives

$$Q' - Q^2 = Q$$

whose solution is given by

$$Q = \frac{1}{c_1 e^{-x} - 1}$$

Thus, taking

$$M = e^x, \quad a = 1, \quad P = 0, \quad N = \frac{M'}{Q} = c_1 - e^x$$

we can solve the equation

$$y'' + \left(\frac{e^x}{c_1 - e^x} \right) y = R(x) = e^{-2x}$$

Here, $R(x) = e^{-2x}$ is arbitrarily chosen. Eq. (12c) gives

$$\frac{\bar{y}'}{N} = e^{-2x} \rightarrow \bar{y}' = e^{-2x}(c_1 - e^x)$$

$$\bar{y} = -\frac{c_1}{2} e^{-2x} + e^{-x} + c_2$$

Here, without loss of generality, we can assume $c_2 = 0$. Using Eq. (11), we have

$$\bar{y} = -\frac{c_1}{2} e^{-2x} + e^{-x} = (c_1 - e^x)y' + e^x y$$

or

$$y' + \left(\frac{e^x}{c_1 - e^x}\right)y = \frac{-\frac{c_1}{2}e^{-2x} + e^{-x}}{c_1 - e^x}$$

The solution for $y(x)$ is

$$y = (c_1 - e^x) \left[c_3 + \frac{c_1^2 e^{-2x} + \frac{2e^x}{(c_1 - e^x)} - 2\ln(1 - c_1 e^{-x})}{4c_1^3} \right]$$

Case 5 : Let us consider the case when $P(x) = 0$ in Eq. (1). In this case, Eq. (1) reads

$$y'' + Q(x)y = R(x)$$

On the other hand, Eq. (13) takes the form

$$N'' + QN = 0 \tag{26}$$

There are many situations for which we can obtain a proper solution of Eq. (26). In this case, by obtaining N and M , we can solve the original equation given. For the present case, we have prepared Table 1 so as to solve some problems readily.

Example 6. We try to solve the following non-homogeneous differential equation

$$y'' - (2a + 4a^2x^2)y = x \tag{27}$$

where a is a constant. The homogeneous part of Eq. (27) is Weber equation in the form

$$y'' - (2a + 4a^2x^2)y = 0 \quad \text{or} \quad y'' - Qy = 0$$

where $Q = 2a + 4a^2x^2$. A proper solution to Eq. (27) is $s = e^{ax^2}$ (See, Table 1). We assume a solution $y = su$ for Eq. (27). Here, u is a function to be determined. Recalling that $y' = s'u + su'$, $y'' = s''u + 2u's' + su''$ and inserting these results into Eq. (27), after arrangement, we have

$$u'' + \frac{2s'}{s}u' + \left(\frac{s''}{s} - Q\right)u = \frac{x}{s} \tag{28}$$

However, we can readily show that the last term $(s''/s - Q)$ is zero. Then, Eq. (28) reads

$$u'' + 4axu' = xe^{-ax^2} \tag{29}$$

Putting $u' = v$, the solution of Eq. (29) can be obtained as

$$v = c_1 e^{-2ax^2} + \frac{1}{2a} e^{-ax^2}$$

Reminding $u' = v$ and integrating this equation, we have

$$u = c_1 \int e^{-2ax^2} dx + \frac{1}{2a} \int e^{-ax^2} dx + c_2$$

Thus, the general solution to Eq. (27) is given by

$$y = su = e^{ax^2} \left[c_1 \int e^{-2ax^2} dx + \frac{1}{2a} \int e^{-ax^2} dx + c_2 \right] \quad (30)$$

It can be verified that Eq. (30) is the solution of Eq. (27). The form given by Eq. (30) is perhaps the most suitable form to be used in initial or boundary value problems.

Using this approach, the general solutions of the non-homogeneous second order differential equations, whose proper solutions of their homogeneous parts are given in Table 1, can readily be obtained.

2.3. Third method of Solution

In the previous method, except for some special cases, Eq. (13) or Eq. (14) cannot be solved for arbitrary forms of $P(x)$ and $Q(x)$. Therefore, different new methods that can solve the equation for which the second method doesn't become successful. However, it is already known that a second order ordinary homogeneous differential equation with variable coefficients can be transformed into a Riccati equation. This method was not quite meaningful since the general solution to Riccati equation could not be found in most cases. However, when we follow the recently published paper by Pala and Ertas [7], this method can now be applied to the analytical solution of second order homogeneous equations. In this way, many equations that cannot be solved by means of the second method can be solved.

Under the transformation $y = e^{\int v dx}$, the second order equation

$$y'' + P(x)y' + Q(x)y = 0 \quad (31)$$

is transformed into a non-linear Riccati equation of the form

$$v' + P(x)v + v^2 = -Q(x) \quad (32)$$

In [7], by utilizing the transformation $\bar{y} = f e^{\int gy dx}$, Riccati equation of the form

$$y' + P(x)y + Qy^2 = R(x) \quad (33)$$

is transformed into

$$y' + \left[\frac{2f'}{f} + \frac{g'}{g} \right] y + gy^2 + \frac{f''}{fg} = \frac{1}{fg} \bar{y}'' e^{-\int gy dx} \quad (34)$$

Here, f , g and \bar{y} are functions to be determined. We take care that the left hand side of Eq. (34) has the form of Riccati equation. Comparing Eq. (33) and Eq. (34), we have

$$\left[\frac{2f'}{f} + \frac{g'}{g}\right] = P(x), \tag{35a}$$

$$g(x) = Q(x), \tag{35b}$$

$$s(x) - \frac{f''}{fg} = R(x) \tag{35c}$$

Here, $s(x)$ is a function to be determined later. If we wish to solve an equation of the form

$$y' + \left[\frac{2f'}{f} + \frac{g'}{g}\right]y + gy^2 + \frac{f''}{fg} = 0,$$

then, by Eqs. (35), in the first place, we can assume

$$\bar{y}'' = 0 \rightarrow \bar{y} = ax + b$$

The functions f and g are to be found such that Eqs. (35) are satisfied. Using the inverse transform, we obtain

$$y = \frac{1}{g} \frac{d}{dx} \left[\ln \frac{\bar{y}}{f} \right] \tag{36}$$

as the solution of Eq. (33). As an illustration of the method, we consider the following example.

Example 7. We try to solve the equation

$$y'' + 5xy' + \left(\frac{25}{4}x^2 + \frac{5}{2}\right)y = 0 \tag{37}$$

The transformation $y = e^{\int v dx}$ reduces Eq. (37) into

$$v' + 5xv + v^2 + \left(\frac{25}{4}x^2 + \frac{5}{2}\right) = 0 \tag{38}$$

Eq. (38) is a Riccati equation that can be solved by the new general method presented in (Pala and Ertas, 2017). Eqs. (35) give

$$\left[\frac{2f'}{f} + \frac{g'}{g}\right] = 5x, \tag{39a}$$

$$g(x) = 1, \tag{39b}$$

$$\frac{f''}{fg} = \left(\frac{25}{4}x^2 + \frac{5}{2}\right) \tag{39c}$$

Simultaneous solution of Eqs. (39a) and (39b) gives $f = c_0 e^{\frac{5}{4}x^2}$, where c_0 is a constant. Now, using Eq. (36), we obtain

$$v = \left(\frac{1}{x+c} - \frac{5}{2}x\right), \quad c = \text{constant}$$

Remembering the transformation $y = e^{\int v dx}$, we finally obtain

$$y = c_2(x + c)e^{-\frac{5}{4}x^2}, \quad c, c_2 \text{ are constants}$$

Example 8. We try to solve the equation

$$y'' + 8xy' + (16x^2 + 4)y = 0 \tag{40}$$

The transformation $y = e^{\int v dx}$ reduces Eq. (40) into

$$v' + 8xv + v^2 + (16x^2 + 4) = 0 \tag{41}$$

Comparing Eq. (41) and Eqs. (35), we have

$$\left[\frac{2f'}{f} + \frac{g'}{g} \right] = 8x, \tag{42a}$$

$$g(x) = 1, \tag{42b}$$

$$\frac{f''}{fg} = (16x^2 + 4) \tag{42c}$$

The first one of Eqs. (42) gives $f = c_1 e^{2x^2}$, where c_1 is a constant. Eq. (42c) is also satisfied. Thus, Using Eq. (36), we have

$$v = \left(\frac{1}{x+c} - 4x \right), \quad c = \text{constant}$$

Remembering the transformation $y = e^{\int v dx}$, we finally obtain

$$y = c_2(x + c)e^{-2x^2}, \quad c, c_2 \text{ are constants} \tag{43}$$

Example 9. In the buckling theory of tapered beams, we encounter the second order equations. Let us consider a beam as in Fig. (1). The equilibrium equation for the beam is given by

$$x^2 \frac{d^2 y}{dx^2} + \frac{Fa^2}{EI} y = 0, \quad y(a) = y'(L + a) = 0$$

Here, E is the modulus of elasticity and I is the moment of inertia. Under the transformation $y = e^{\int v dx}$, Eq. (32) can be written as

$$v' + v^2 + \frac{k}{x^2} = 0, \quad k = \frac{Fa^2}{EI} \tag{44}$$

The solution of (44) can be shown to be

$$v(x) = 1 - \frac{\sqrt{1-4k} \left(\frac{2c_1}{c_1+x\sqrt{1-4k}} - 1 \right)}{2x}$$

Thus, we have for $y(x)$ that

$$y(x) = c_2 \sqrt{x} \left(1 + \frac{c_1}{x^{\frac{\sqrt{1-4k}}{2}}} \right)$$

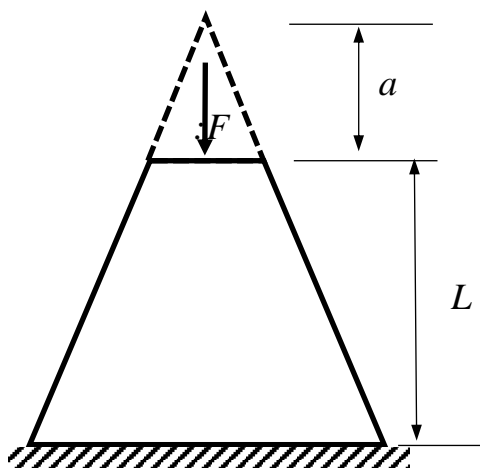


Figure 1 Buckling model of a tapered column.

Table 1. Proper solutions of some second order ordinary differential equations

Differential Equation	Proper Solution
$y'' - (2a + 4a^2x^2)y = 0$	$s = e^{ax^2}$, a is a constant
$y'' - (6a + 4a^2x^2)y = 0$	$s = xe^{ax^2}$
$y'' - (2x^{-2} + 10a + 4a^2x^2)y = 0$	$s = x^2e^{ax^2}$
$y'' - (12ax^2 + 16a^2x^6)y = 0$	$s = e^{ax^4}$
$y'' - (2a + (2ax + b)^2)y = 0$	$s = e^{ax^2+bx+c}$, a, b, c are constants
$y'' - [n(n-1)x^{-2} + 2an + 2a(n+1) + 4a^2x^2]y = 0$	$s = x^n e^{ax^2}$, a, n are constants
$y'' - \left[\frac{4adx}{dx+e} + 2a + 4a^2x^2 \right] y = 0$	$s = (dx + e)e^{ax^2}$, a, d, e are constants

Table 1. Continued

$y'' - \left[\frac{2(2ax + b)d}{dx + e} + 2a + (2ax + b)^2 \right] y = 0$	$s = (dx + e)e^{ax^2+bx+c},$ $a, b, c, d, e \text{ are constants}$
$y'' - [an(n - 1)x^{n-2} + a^2n^2x^{2(n-1)}]y = 0$	$s = e^{ax^n}$
$y'' - 2axy' - 2ay = 0$	$s = e^{ax^2}$
$y'' - (2ax + b)y' - 2ay = 0$	$s = e^{ax^2+bx+c} \text{ or } s = e^{ax^2+bx}$
$y'' - 3ax^2y' - 6axy = 0$	$s = e^{ax^3}$
$y'' - 4ax^3y' - 12ax^2y = 0$	$s = e^{ax^4}$
$y'' - anx^{n-1}y' - an(n - 1)x^{n-2}y = 0$	$s = e^{ax^n}$
$y'' - \left[\frac{dm(m - 1)x^{m-2} + es(s - 1)x^{s-2}}{dx^m + ex^s} + \frac{2dmx^{m-1} + esx^{s-1}}{dx^m + ex^s} (na)x^{n-1} + na(n - 1)x^{n-2} + n^2a^2x^{2(n-1)} \right] y = 0$	$s = (dx^m + ex^s)e^{ax^n}$ $d, e, a, m, n \text{ are constants}$
$y'' - ax^{n-2}(ax^n + n + 1)y = 0$	$s = xe^{ax^n/n}$
$y'' + ay' + b(-bx^2 + ax + 1)y = 0$	$s = e^{-\frac{b}{2}x^2}$
$y'' + (x^2 - b^2)y' - (x + b)y = 0$	$s = x - b$
$y'' + (ax^2 + bx)y' + c(ax^2 + bx - c)y = 0$	$s = e^{-cx}$
$y'' + (ax^n + bx^m)y' - (ax^{n-1} + x^{m-1})y = 0$	$s = x$
$y'' + (ax^2 + 2b)y' + (abx^2 - ax + b^2)y = 0$	$s = xe^{-bx}$

2.4. Alternative method of Solution

Now, as a new method, we propose the transformation $y = ae^{k \int b dx}$ where k is a constant while $a(x)$ and $b(x)$ are functions to be determined. Taking derivatives y', y'' , and substituting into Eq. (1), one obtains

$$a'' e^{k \int b dx} + (2kb + P)a' e^{k \int b dx} + (kab' + k^2 ab^2 + Pkab + Qa)e^{k \int b dx} = R(x) \quad (45)$$

Now, we choose $b(x)$ such that

$$b' + Pb + kb^2 + \frac{Q}{k} = 0 \quad (46)$$

Eq. (46) is a Riccati equation. Under this assumption, Eq. (45) can be written in the form of

$$a'' + Aa' = \bar{R} \quad (47)$$

where $\bar{R} = Re^{-k \int b dx}$ and $A = 2kb + P$. Putting $a' = u$ in Eq. (47) one obtains

$$u' + Au = \bar{R} \quad (48)$$

It is already known that the solution of Eq. (48) is given by

$$u = e^{-\int A dx} \left[c_4 + \int \bar{R}(x) e^{\int A dx} dx \right]$$

Example 10. The non-homogeneous equation of the form

$$y'' + 5xy' + \left(\frac{25}{4}x^2 + \frac{5}{2} \right) y = R(x) \quad (49)$$

Here, $R(x)$ is an arbitrary function. After taking $k = 1$, Eq. (46) takes the form of

$$b' + 5xb + b^2 + \left(\frac{25}{4}x^2 + \frac{5}{2} \right) = 0$$

The solution of the equation above is

$$b = \frac{1}{x+c} - \frac{5}{2}x$$

Inserting $b(x)$ into Eq. (48) yields

$$u' + \frac{2}{x+c}u = e^{\left[-\ln(x+c) + \frac{5}{4}x^2 \right]} R(x)$$

As an example, let us assume that $R(x) = e^{-5x^2/4}$. In this case, u is obtained as

$$u = \frac{c_2}{(x+c)^2} + \frac{1}{2}$$

Remembering that $a' = u$ and $y = ae^{\int b dx}$, we find

$$a = -\frac{c_2}{x+c} + \frac{x}{2} + c_3$$

and

$$y = \left[-c_2 + \frac{x(x+c)}{2} + c_3(x+c) \right] \left(e^{-\frac{5}{4}x^2} \right) \quad (50)$$

Eq. (50) can be written as follow

$$y = c_2 \left[-1 + \frac{x\left(\frac{x}{c_2} + \frac{c}{c_2}\right)}{2} + \frac{c_3}{c_2}(x+c) \right] \left(e^{-\frac{5}{4}x^2} \right)$$

Since Eq. (49) is linear, it can be taken $c_2 = 1$. Thus, the solution of Eq. (49) is obtained as

$$y = \left[-1 + \frac{x(x+c)}{2} + c_3(x+c) \right] \left(e^{-\frac{5}{4}x^2} \right)$$

Example 11. Let us consider the equation

$$y'' + 8xy' + (16x^2 - 12)y = R(x)$$

Here, $R(x)$ is a function that will be chosen arbitrarily later. Taking $k = 4$ and using the transformation equation $y = ae^{4 \int b dx}$, one finds

$$b' + 8xb + 4b^2 + 4x^2 - 3 = 0 \quad (51)$$

and

$$a'' + Aa' = \bar{R}$$

where $\bar{R} = Re^{-4 \int b dx}$ and $A = 2kb + P(x) = 8b + 8x$. To solve Eq. (51), the method proposed by Pala and Ertas [7] is used. Eqs. (35) are applied to this example as follows

$$g = 4 \quad (52a)$$

$$\left[\frac{2f'}{f} + \frac{g'}{g} \right] = 8x \quad (52b)$$

$$s(x) = \frac{f''}{fg} - (4x^2 - 3) \quad (52c)$$

Eq. (52a) and Eq. (52b) give $f(x) = ce^{2x^2}$. Substituting $f(x)$ into Eq. (52c) gives $s(x) = 4$. Then, the transformation equation $\bar{y}'' - gs(x)\bar{y} = 0$ yields

$$\bar{y}'' - 16\bar{y} = 0$$

whose solution is given by

$$\bar{y} = c_1 e^{4x} + c_2 e^{-4x}$$

Now, using Eq. (36), we obtain

$$b(x) = \frac{1}{g} \frac{d}{dx} \left(\ln \frac{\bar{y}}{f} \right) = \frac{c_1 e^{4x} - c_2 e^{-4x}}{c_1 e^{4x} + c_2 e^{-4x}} - x$$

or

$$b(x) = \frac{e^{8x-\bar{c}}}{e^{8x+\bar{c}}} - x$$

where $\bar{c} = c_2/c_1$. Putting $a' = u$ yields

$$u' + Au = \bar{R} \tag{53}$$

The solution of Eq. (53) is expressed as

$$u = e^{-\int A dx} [c_4 + \int e^{\int A dx} \bar{R} dx]$$

Remembering $A = 8b + 8x$ and putting into the equation above, we finally obtain

$$a' = u = \frac{e^{8x}}{(\bar{c} + e^{8x})^2} [c_4 + \int (\bar{c} + e^{8x})^2 e^{-8x} \bar{R}(x) dx]$$

$$a = \int \frac{e^{8x}}{(\bar{c} + e^{8x})^2} [c_4 + \int (\bar{c} + e^{8x})^2 e^{-8x} \bar{R}(x) dx] dx + c_5$$

and

$$y = \left(\int \frac{e^{8x}}{(\bar{c} + e^{8x})^2} [c_4 + \int (\bar{c} + e^{8x})^2 e^{-8x} \bar{R}(x) dx] dx \right) (\bar{c} + e^{8x}) e^{-2x(x+2)}$$

3. Conclusion

In this study, we have proposed new approaches for the analytical solution of second order ordinary differential equations of general type. Four methods have been given. The first one is limited in that it requires $P' = Q$ while the second method is general. However, the second method requires the solution of adjoined equations (13) or (14) of second order homogeneous type. Different cases have been considered for the solution of Eqs. (13) and (14). In order that the analytical solution of either Eq. (13) or (14) be obtained, we have included a table in which proper solutions of some important equations are given. The method of transforming into Riccati equation has also been studied and a different method has been proposed based on a new method developed in [7]. According to this method, the transformed equation takes the simplest form whatever the original equation is. The transformed equation reveals whether the problem is solved in terms of standard or special mathematical functions. In the fourth method, the approach is different, but the solution is also based on the solution of Riccati equation. Therefore, the last two methods utilize the recently developed method for Riccati equation.

Ethics in Publishing

There are no ethical issues regarding the publication of this study.



References

- [1] Allen, J.L and Stein, F.M. 1964. "On The Solution of Certain Riccati Equations", *The American Math. Montly*, U.S.A., 1113-1115.
- [2] Berkovic, L.M. 1966. "The Reduction of Linear Ordinary Differential Equations to Equations With Constant Coefficients", *Volz.Mat. Sb.5*, 38-44.
- [3] Boffa, V., Bollanti, S., Dattoli, G and Torre, A.1983. "Second-Order differential Equations With Variable Coefficients: Analytical Solutions", *IL NUOVO CIMENTO*, Vol:99B, No:1, 53-60.
- [4] Breuer, S and Gottlieb, D. 1970. "The Reduction of Linear Ordinary Differential Equations to Equations With Constant Coefficients", *Journal of Mathematical Analysis and Applications*, 32, 62-76.
- [5] Hwawcha, Laith K. and Abid, Namh, A.2008. "A New Approach for Solving Second Order Ordinary Differential Equations", *Journal of Mathematics and Statistics*,4(1), 58-59.
- [6] Munasinghe, R.2004. "Some Linear Differential Equations Forget That They Have Variable Coefficients", *The College Mathematics Journal*, Vol:35, pp:22-25.
- [7] Pala, Y and Ertas, Ö. 2017. "An Analytical Method for Solving General Riccati Equation", World Academy of Science, Engineering and Technology, *International Journal of Mathematical, Computational, Physical, Electrical and Computer Engineering*, 11(3), 11-16
- [8] Pala, Y.(2013). "Modern Uygulamalı Diferensiyel Denklemler (In Turkish)", *Nobel Publications*, Ankara, ISBN: 978-605-133-654-1, 63-69.
- [9] Rao,P.R.P and Ukidave, V.H.1968. "Separable forms of the Riccati Equation", *The American Mathematical Montly*, Vol.75, U.S.A.,38-39.
- [10] Robin, W. 2007. "Operator factorization Method and the Solution of Second Order Linear ordinary Differential Equations", *Int. Journal of Mathematical Education in Science and Technology*, ISSN:0020-739X, DOI: 10.1080/00207390601002815, 189-211.
- [11] Saravi, M.2012. "A Procedure for Solving Some Second Order Linear Ordinary Differential Equations", *Applied Mathematics Letters*, 25, 408-411.
- [12] Siller, H.1970. "On the Separability of the Riccati Differential Equation", *Mathematical Magazine*, Vol.43, No.4, U.S.A., pp.197-202, 1970.
- [13] Takayama, Ken.1986. "A Class of Solvable Second-Order Differential Equations With Variable Coefficients", *Journal of Mathematical Physics*, 27, DOI: 106371.527038, 1747-1749.
- [14] Urdeletova, A.B. and Kydyraliev. S.1996. "Solving Linear Differential Equations by Operator Factorization", *The College Mathematics Journal*, Vol:27, No:3, 199-203.
- [15] Wilmer, A and Costa, G.B.2008. "Solving Second Order Differential Equations With Variable Coefficients", *Int. Journal of Mathematical Education in Science and*

Technology, DOI: 10.1080/002073907014644709, 238-243.

- [16] Zroiqat, A and Al-Hwawcha, Laith K.2015. “On Exact Solutions of Second Order Nonlinear Ordinary Differential Equations”, *Applied mathematics*, 6, 953-957.

Stability, Neimark-Sacker Bifurcation Analysis of a Prey-Predator Model with Strong Allee Effect and Chaos Control

Deniz ELMACI^{1*} , Figen KANGALGİL¹ 

^{1*} Dokuz Eylül University, Bergama Vocational School, Izmir, Turkey.

Received: 20/11/2022, **Revised:** 16/12/2022, **Accepted:** 21/12/2022, **Published:** 30/12/2022

Abstract

In this study, the dynamical behaviors of a prey-predator model with strong Allee effect are investigated. Existence of the fixed points of the model are examined and topological classification of the coexistence fixed point is obtained. By selecting bifurcation parameter as a β , it is demonstrated that the model can experience a Neimark-Sacker bifurcation at the coexistence fixed point. Bifurcation theory is used to present the Neimark-Sacker bifurcation conditions of existence and the direction of the bifurcation. Additionally, some numerical simulations are provided to back up the analytical result. OGY feedback control method is implemented to control chaos in presented model due to emergence of Neimark-Sacker bifurcation. Following that, the model's bifurcation diagram, maximum Lyapunov exponents and the triangle-shaped stability zone are provided.

Keywords: Prey-predator model, strong Allee effect, Neimark-Sacker bifurcation analysis

Güçlü Allee Etkili Av-Avcı Modelinin Kararlılığı, Neimark-Sacker Çatallanma Analizi ve Kaos Kontrol

Öz

Bu çalışmada, güçlü Allee etkisi içeren bir av-avcı modelinin dinamik davranışları araştırılmıştır. Modelin sabit noktalarının varlığı incelenmiştir ve her iki türün bir arada olduğu denge noktasının topolojik sınıflandırması elde edilmiştir. β çatallanma parametresi olarak seçildiğinde, modelin her iki türün bir arada olduğu denge noktasında bir Neimark-Sacker çatallanması olacağı gösterilmiştir. Çatallanma teorisi, Neimark-Sacker çatallanma varoluş koşullarını ve çatallanmanın yönünü sunmak için kullanılır. Ek olarak, bazı sayısal simülasyonlar, analitik sonucu desteklemek için sunulmuştur. Sunulan modelde Neimark-Sacker çatallanmasının ortaya çıkması nedeniyle oluşan kaosu kontrol etmek için OGY geri besleme kontrol yöntemi uygulanmaktadır. Bunu takiben, modelin çatallanma diyagramı, maksimum Lyapunov üstelleri ve üçgen şeklindeki kararlılık bölgesi verilmiştir.

Anahtar Kelimeler: Av-avcı modeli, güçlü Allee etkisi, Neimark-Sacker çatallanma analizi.

1. Introduction

In the literature on bio-mathematics, the study of prey-predator systems that demonstrate interactions between two prey-predator species has been a significant topic. Many researchers have recently investigated the intricate dynamics of prey-predator systems [1, 2, 3, 4, 5, 6, 7]. The Lotka-Volterra model, created by Lotka and Volterra, is the original and most basic prey-predator model. Many researchers have altered this model because it ignored a number of real situations.

Ecological aspects like emigration and immigration, functional responses, diffusion, time delays, etc. have been introduced. Allee effect is one of the key ecological variables that can significantly alter the prey-predator system [7, 8]. When simulating the interactions between predators and prey, it is crucial to take into account the increase of the prey population to its carrying capacity in the absence of predators. Consider the development of logistics. The per capita growth rate of prey achieves its maximum while their population density is low and starts to decrease as prey density increases, according to this logistic growth. However, such growth rates are not always advantageous for lower densities [9, 10]. There are various biological causes for this.

The Allee term derives from an experimental research conducted by renowned ecologist Warder Clyde Allee. Allee discovered in the 1930s that many natural populations, including those of plants, birds, marine invertebrates, insects and mammals, frequently experience individual fitness losses at lower critical densities. It describes an association between any metric of species fitness and population size that is favorable. Allee effect can be split into two groups: strong effects and weak effects. For the strong Allee effect, there is a population threshold below which the species becomes extinct. On the other hand, the weak Allee effect appears when the growth rate slows down while still being positive at low population density [11, 12, 13, 14]. Many researchers have been interested in the dynamics of predator-prey models that incorporate the Allee effect in prey development rate [15, 16, 17, 18, 19, 20, 21, 22, 23].

It is not well recognized that two or more Allee effects can occur simultaneously in the same population. For the management of endangered or exploited populations, it is crucial to consider the presence and interplay of various Allee effects. This work presents a mathematical investigation of the stability of a prey-predator system with strong Allee effect.

The following discrete-time predator-prey model has been considered by the author in [24]:

$$\begin{aligned} N_{t+1} &= \beta N_t(1 - N_t) - N_t P_t \\ P_{t+1} &= \frac{1}{\alpha} N_t P_t \end{aligned} \tag{1}$$

where N_t and P_t represent the numbers of prey and predator, respectively. The α, β parameters are positive real numbers.

The current work looks at a discrete-time prey-predator model where the predator population outnumbered the prey population and the prey population is susceptible to a strong Allee effect. The stability and bifurcation analysis of the the prey-predator model with weak Allee effect will be examined in another study.

2. Preliminaries

The Model and Its Fixed Points

Modification of the model (1) is taken into consideration in this study,

$$\begin{aligned} N_{n+1} &= \beta N_n(1 - N_n) \left(\frac{N_n - \zeta}{N_n + \eta} \right) - N_n P_n \\ P_{n+1} &= \frac{1}{\alpha} N_n P_n \end{aligned} \quad (2)$$

where N_n and P_n represent the densities of prey and predator, respectively, α and β are the intrinsic growth rates of the predator and prey, η is the non-fertile prey population, ζ is the Allee coefficient.

By biological setting, we have $0 < \eta < 1$ and $-\eta < \zeta < 1$, so $\zeta + \eta > 0$. If $0 < \zeta < 1$, the Allee effect is called strong, while if $-\eta < \zeta < 0$, it is called weak Allee effect.

The $\frac{N_n - \zeta}{N_n + \eta}$ term represents the multiple Allee effect which means two or more Allee effects act simultaneously on the single population.

We now explore the discrete-time prey-predator model's stability and the existence of fixed points, including the Allee effect on prey.

If we write

$$N_n = N_{n+1} = N^*, \quad P_n = P_{n+1} = P^* \quad (3)$$

in system (2), the following system can be obtained as follows:

$$\begin{aligned} N^* &= \beta N^*(1 - N^*) \left(\frac{N^* - \zeta}{N^* + \eta} \right) - N^* P^* \\ P^* &= \frac{1}{\alpha} N^* P^* \end{aligned} \quad (4)$$

A simple calculation reveals that the system (2) has the following three fixed points:

$$\begin{aligned} D_1 &= (0, 0) \\ D_2 &= \left(\frac{\beta\zeta + \beta - 1 + \sqrt{\beta^2\zeta^2 - 2\beta^2\zeta + \beta^2 - 2\beta\zeta - 4\beta\eta - 2\beta + 1}}{2\beta}, 0 \right) \\ D_3 &= \left(\alpha, \beta(1 - \alpha) \left(\frac{\alpha - \zeta}{\alpha + \eta} \right) - 1 \right) \end{aligned}$$

3. Main Theorem and Proof

Lemma 3.1 For the system (2), the following statements hold true:

- i) The system (2) always has an axial fixed point $D_1 = (0, 0)$.
- ii) The system (2) has an axial fixed point $D_2 = \left(\frac{\beta\zeta + \beta - 1 + \sqrt{\beta^2\zeta^2 - 2\beta^2\zeta + \beta^2 - 2\beta\zeta - 4\beta\eta - 2\beta + 1}}{2\beta}, 0 \right)$ if

$$\eta \leq \frac{\beta^2(\zeta - 1)^2 - 2\beta(\zeta + 1) + 1}{4\beta}$$

- iii) The system (2) has an coexistence fixed point $D_3 = \left(\alpha, \beta(1 - \alpha) \left(\frac{\alpha - \zeta}{\alpha + \eta} \right) - 1 \right)$ if the following condition holds:

$$0 < \alpha < 1 \quad \beta > \left(\frac{\alpha + \eta}{(1 - \alpha)(\alpha - \zeta)} \right) \quad (5)$$

3.1. Local Stability Analysis

As D_3 is biologically significant, stability and bifurcation analysis has been studied for this fixed point only. The Jacobian matrix of the system (2) evaluated at the fixed point D_3 is as following:

$$J(D_3) = \begin{pmatrix} \frac{-\beta\alpha^3 + (-2\beta\eta + 1)\alpha^2 + ((2 + (\zeta + 1)\beta)\eta + \beta\zeta)\alpha + \eta^2}{(\alpha + \eta)^2} & -\alpha \\ -\frac{\beta\alpha^2 - \beta\alpha\zeta - \beta\alpha + \beta\zeta + \alpha + \eta}{(\alpha + \eta)\alpha} & 1 \end{pmatrix}$$

Moreover, the characteristic polynomial of $J(D_3)$ is given by:

$$F(\lambda) = \lambda^2 - \left(\frac{-\beta\alpha^3 + (-2\beta\eta + 2)\alpha^2 + ((4 + (\zeta + 1)\beta)\eta + \beta\zeta)\alpha + 2\eta^2}{(\alpha + \eta)^2} \right) \lambda + \frac{\beta(-2\alpha^3 + (\zeta - 3\eta + 1)\alpha^2 + 2\eta(\zeta + 1)\alpha - \zeta\eta)}{(\alpha + \eta)^2} \quad (6)$$

Then, by simple computations it follows that

$$F(1) = -\frac{\beta\alpha^2 - \beta\alpha\zeta - \beta\alpha + \beta\zeta + \alpha + \eta}{\alpha + \eta}, \quad (7)$$

$$F(-1) = \frac{-3\beta\alpha^3 + (3 + (\zeta - 5\eta + 1)\beta)\alpha^2 + (((3\zeta + 3)\eta + \zeta)\beta + 6\eta)\alpha - \beta\zeta\eta + 3\eta^2}{(\alpha + \eta)^2}, \quad (8)$$

and

$$F(0) = \frac{\beta(-2\alpha^3 + (\zeta - 3\eta + 1)\alpha^2 + 2\eta(\zeta + 1)\alpha - \zeta\eta)}{(\alpha + \eta)^2} \quad (9)$$

The following lemma will be used to discuss the dynamics of coexistence fixed point of system.

Lemma 3.2 $F(\lambda) = \lambda^2 + B\lambda + C$, where B and C are two real constants and let $F(1) > 0$. Suppose λ_1 and λ_2 are two roots of $F(\lambda) = 0$. Then the following statements hold.

- (i) $|\lambda_1| < 1$ and $|\lambda_2| < 1$ if and only if $F(-1) > 0$ and $F(0) < 1$.
- (ii) $|\lambda_1| > 1$ and $|\lambda_2| > 1$ if and only if $F(-1) > 0$ and $F(0) > 1$.
- (iii) $|\lambda_1| < 1$ and $|\lambda_2| > 1$, or $|\lambda_1| > 1$ and $|\lambda_2| < 1$, if and only if $F(-1) < 0$.
- (iv) λ_1 and λ_2 are a pair of conjugate complex roots and $|\lambda_1| = |\lambda_2| = 1$ if and only if $B^2 - 4C < 0$ and $F(0) = 1$.
- (v) $\lambda_1 = -1$ and $|\lambda_2| \neq 1$ if and only if $F(-1) = 0$ and $B \neq 0, 2$.

Assume that λ_1 and λ_2 are the roots of the characteristic polynomial at the coexistence fixed point (N, P) . Then, the point (N, P) is called sink if $|\lambda_1| < 1$ and $|\lambda_2| < 1$ and it is locally asymptotically stable. (N, P) is called source if $|\lambda_1| > 1$ and $|\lambda_2| > 1$ and it is locally unstable. The point (N, P) is called saddle if $|\lambda_1| < 1$ and $|\lambda_2| > 1$, or $|\lambda_1| > 1$ and $|\lambda_2| < 1$. And, (N, P) is called non-hyperbolic if either $|\lambda_1| = 1$ or $|\lambda_2| = 1$.

Theorem 3.3 For coexistence fixed point D_3 of system (2) the following holds true:

- (i) D_3 is a sink if and only if

$$3\beta\alpha^3 + 5\eta\beta\alpha^2 + \beta\zeta\eta < (3 + \zeta\beta + \beta)\alpha^2 + (3\zeta\eta\beta + 3\eta\beta + \zeta\beta + 6\eta)\alpha + 3\eta^2$$

and

$$\beta(\zeta + 1)\alpha(\alpha + 2\eta) < (\alpha + \eta)^2 + 2\beta\alpha^3 + 3\eta\beta\alpha^2 + \beta\zeta\eta$$

(ii) D_3 is a source if and only if

$$3\beta\alpha^3 + 5\eta\beta\alpha^2 + \beta\zeta\eta < (3 + \zeta\beta + \beta)\alpha^2 + (3\zeta\eta\beta + 3\eta\beta + \zeta\beta + 6\eta)\alpha + 3\eta^2$$

and

$$\beta(\zeta + 1)\alpha(\alpha + 2\eta) > (\alpha + \eta)^2 + 2\beta\alpha^3 + 3\eta\beta\alpha^2 + \beta\zeta\eta$$

(iii) D_3 is a saddle if and only if

$$3\beta\alpha^3 + 5\eta\beta\alpha^2 + \beta\zeta\eta > (3 + \zeta\beta + \beta)\alpha^2 + (3\zeta\eta\beta + 3\eta\beta + \zeta\beta + 6\eta)\alpha + 3\eta^2$$

(iv) The roots of Eq.(6) are complex with modulus one if and only if

$$\beta\alpha^3 + (2\beta\eta - 2)\alpha^2 + ((-4 + (-\zeta - 1)\beta)\eta - \beta\zeta)\alpha - 2\eta^2 < 4\beta(2\alpha^3 - \alpha^2\zeta + 3\alpha^2\eta - 2\alpha\zeta\eta - \alpha^2 - 2\alpha\eta + \zeta\eta)(\alpha + \eta)^2$$

and

$$\beta(\zeta + 1)\alpha(\alpha + 2\eta) = (\alpha + \eta)^2 + 2\beta\alpha^3 + 3\eta\beta\alpha^2 + \beta\zeta\eta$$

(v) Assume that λ_1 and λ_2 be roots of Eq.(6), then $\lambda_1 = -1$ and $|\lambda_2| \neq 1$ if and only if

$$3\beta\alpha^3 + 5\eta\beta\alpha^2 + \beta\zeta\eta = (3 + \zeta\beta + \beta)\alpha^2 + (3\zeta\eta\beta + 3\eta\beta + \zeta\beta + 6\eta)\alpha + 3\eta^2$$

$$\beta\alpha^3 + (2\beta\eta - 2)\alpha^2 + ((-4 + (-\zeta - 1)\beta)\eta - \beta\zeta)\alpha - 2\eta^2 \neq 0$$

and

$$\beta\alpha^3 + (2\beta\eta - 4)\alpha^2 + ((-8 + (-\zeta - 1)\beta)\eta - \beta\zeta)\alpha - 4\eta^2 \neq 0$$

3.2. Neimark–Sacker Bifurcation Analysis

We examine the Neimark-Sacker bifurcation conditions for the system (2) at coexistence fixed point $(\alpha, \beta(1 - \alpha)(\frac{\alpha - \zeta}{\alpha + \eta}) - 1)$ in this section. In addition, the direction of the Neimark-Sacker bifurcation is analyzed. From Eq.(6) it follows that $F(\lambda) = 0$ has two complex conjugate roots with modulus one, if the following conditions are satisfied:

$$\begin{aligned} \Delta &= (\beta\alpha^3 + (2\beta\eta - 2)\alpha^2 + ((-4 + (-\zeta - 1)\beta)\eta - \beta\zeta)\alpha - 2\eta^2)^2 \\ &\quad - 4\beta(\alpha + \eta)^2(2\alpha^3 + (-\zeta + 3\eta - 1)\alpha^2 + (-2\zeta\eta - 2\eta)\alpha + \zeta\eta) < 0 \\ \beta &= \frac{(\alpha + \eta)^2}{-2\alpha^3 + (\zeta - 3\eta + 1)\alpha^2 + 2\eta(\zeta + 1)\alpha - \eta\zeta}, \zeta \neq \frac{\alpha(2\alpha^2 + 3\alpha\eta - \alpha - 2\eta)}{\alpha^2 + 2\alpha\eta - \eta} \end{aligned} \quad (10)$$

Assume that

$$\Omega_{NS} = \left\{ (\beta, \alpha, \zeta, \eta) \in \mathbb{R}_+^4 : \Delta < 0, \quad \beta = \frac{(\alpha + \eta)^2}{-2\alpha^3 + (\zeta - 3\eta + 1)\alpha^2 + 2\eta(\zeta + 1)\alpha - \eta\zeta}, \quad \zeta \neq \frac{\alpha(2\alpha^2 + 3\alpha\eta - \alpha - 2\eta)}{\alpha^2 + 2\alpha\eta - \eta} \right\}$$

The coexistence fixed point of system (2) undergoes Neimark-Sacker bifurcation as a result of parameter change in the small neighborhood of the set Ω_{NS} . Set $\beta_2 = \frac{(\alpha + n)^2}{-2\alpha^3 + (\zeta - 3\eta + 1)\alpha^2 + 2\eta(\zeta + 1)\alpha - \eta\zeta}$

such that $\zeta \neq \frac{\alpha(2\alpha^2 + 3\alpha\eta - \alpha - 2\eta)}{\alpha^2 + 2\alpha\eta - \eta}$ and assume that $(\beta_2, \alpha, \zeta, \eta) \in \Omega_{NS}$, then system (2) can be expressed by following two-dimensional map:

$$\begin{pmatrix} N \\ P \end{pmatrix} \rightarrow \begin{pmatrix} \beta_2 N(1-N)\left(\frac{N-\zeta}{N+\eta}\right) - NP \\ \frac{1}{\alpha} NP \end{pmatrix} \quad (11)$$

Let $\bar{\beta}$ denotes the bifurcation parameter, then corresponding perturbed mapping of (11) is given as follows:

$$\begin{pmatrix} N \\ P \end{pmatrix} \rightarrow \begin{pmatrix} (\beta_2 + \bar{\beta})N(1-N)\left(\frac{N-\zeta}{N+\eta}\right) - NP \\ \frac{1}{\alpha} NP \end{pmatrix} \quad (12)$$

where $|\bar{\beta}| \ll 1$ denotes the small bifurcation parameter. Next, the transformations $t = N - \alpha$ and $s = P - \beta(1 - \alpha)\left(\frac{\alpha - \zeta}{\alpha + \eta}\right) - 1$ are considered, then from the map (12) we have

$$\begin{pmatrix} t \\ s \end{pmatrix} \rightarrow \begin{pmatrix} m_{11} & m_{12} \\ m_{21} & m_{22} \end{pmatrix} \begin{pmatrix} t \\ s \end{pmatrix} + \begin{pmatrix} f_1(t, s) \\ f_2(t, s) \end{pmatrix} \quad (13)$$

where

$$f_1(t, s) = m_{13}t^3 + m_{14}t^2 + m_{15}ts + O(|t| + |s|)^4$$

$$f_2(t, s) = m_{25}ts + O(|t| + |s|)^4$$

$$m_{11} = -\frac{\eta^2 + \alpha(-2\alpha(\beta_2 + \bar{\beta}) + (\zeta + 1)(\beta_2 + \bar{\beta}) + 2)\eta + \alpha(-(\beta_2 + \bar{\beta})\alpha^2 + \alpha + (\beta_2 + \bar{\beta})\zeta)}{(\alpha + \eta)^2}, \quad m_{12} = -\alpha$$

$$m_{21} = \frac{(\beta_2 + \bar{\beta})(1 - \alpha)(\alpha - \zeta) + (\alpha + \eta)}{\alpha(\alpha + \eta)} \quad m_{22} = 1$$

$$m_{13} = -\frac{\eta(\beta_2 + \bar{\beta})(\eta + 1)(m\zeta + \eta)}{(\alpha + \eta)^4}, \quad m_{14} = -\frac{(\alpha^3 + 3\alpha^2\eta + 3\alpha\eta^2 - \zeta\eta^2 - \zeta\eta - \eta^2)(\beta_2 + \bar{\beta})}{(\alpha + \eta)^3}$$

$$m_{15} = -1 \quad m_{25} = \frac{1}{\alpha}$$

The characteristic equation of Jacobian matrix of linearized system of (13) evaluated at the fixed (0, 0) can be written as follows:

$$\lambda^2 - A(\bar{\beta})\lambda + B(\bar{\beta}) = 0, \quad (14)$$

where

$$A(\bar{\beta}) = 2 - \frac{(\beta_2 + \bar{\beta})(\alpha^3 + 2\alpha^2\eta - \alpha\zeta\eta - \alpha\zeta - \alpha\eta)}{(\alpha + \eta)^2}$$

and

$$B(\bar{\beta}) = \frac{(\beta_2 + \bar{\beta})(-2\alpha^3 + (\zeta - 3\eta + 1)\alpha^2 + 2\eta(\zeta + 1)\alpha - \zeta\eta)}{(\alpha + \eta)^2}$$

Since $(\beta_2, \alpha, \zeta, \eta) \in \Omega_{NS}$, therefore the complex conjugate roots of Eq. (14) are given by:

$$\lambda_{1,2} = \frac{A(\bar{\beta}) \pm i\sqrt{4B(\bar{\beta}) - (A(\bar{\beta}))^2}}{2}$$

Then, we obtain that

$$|\lambda_1| = |\lambda_2| = \sqrt{\frac{(\beta_2 + \bar{\beta})(-2\alpha^3 + (\zeta - 3\eta + 1)\alpha^2 + 2\eta(\zeta + 1)\alpha - \zeta\eta)}{(\alpha + \eta)^2}}$$

Moreover, in order to obtain the non-degeneracy conditions, we assume that $\zeta \neq \frac{\alpha(2\alpha^2 + 3\alpha\eta - \alpha - 2\eta)}{\alpha^2 + 2\alpha\eta - \eta}$ then it follows that

$$\left(\frac{d|\lambda_1|}{d\bar{\beta}}\right)_{\bar{\beta}=0} = \left(\frac{d|\lambda_2|}{d\bar{\beta}}\right)_{\bar{\beta}=0} = -\frac{2\alpha^3 - (\zeta - 3\eta + 1)\alpha^2 - 2\eta(\zeta + 1)\alpha + \zeta\eta}{2(\alpha + \eta)^2} \neq 0$$

Moreover, we have $-2 < A(0) < 2$ because $(\beta_2, \alpha, \zeta, \eta) \in \Omega_{NS}$. On the other hand, we have $A(0) = 2 + \frac{\alpha(\alpha^2 + 2\alpha\eta - \zeta\eta - \zeta - \eta)}{2\alpha^3 + (-\zeta + 3\eta - 1)\alpha^2 + (-2\zeta\eta - 2\eta)\alpha + \zeta\eta}$. Assume that $\zeta \neq \frac{\alpha(2\alpha^2 + 3\alpha\eta - \alpha - 2\eta)}{\alpha^2 + 2\alpha\eta - \eta}$, $A(0) \neq 0$ and $A(0) \neq -1$, that is,

$$\frac{\alpha(\alpha^2 + 2\alpha\eta - \zeta\eta - \zeta - \eta)}{2\alpha^3 + (-\zeta + 3\eta - 1)\alpha^2 + (-2\zeta\eta - 2\eta)\alpha + \zeta\eta} \neq -2, -3 \tag{15}$$

Conditions in Eq.(15) and with $(\beta_2, \alpha, \zeta, \eta) \in \Omega_{NS}$ make sure that $A(0) \neq \pm 2, 0, -1$, and in a result we have $\lambda_1^m, \lambda_2^m \neq 1$ for all $m = 1, 2, 3, 4$ at $\bar{\beta} = 0$. Hence roots of Eq.(14) do not lie in the intersection of the unit circle with the coordinate axes when $\bar{\beta} = 0$. In order to obtain the normal form of Eq.(13) at $\bar{\beta} = 0$, assuming that $\xi = \frac{A(0)}{2}$ and $\tau = \frac{\sqrt{4B(0) - (A(0))^2}}{2}$. Furthermore, let us consider the following transformation:

$$\begin{pmatrix} t \\ s \end{pmatrix} \rightarrow \begin{pmatrix} m_{12} & 0 \\ \xi - m_{11} & -\tau \end{pmatrix} \begin{pmatrix} x \\ y \end{pmatrix} \tag{16}$$

Under transformation Eq.(16), the normal form of Eq.(13) can be written as:

$$\begin{pmatrix} x \\ y \end{pmatrix} \rightarrow \begin{pmatrix} \xi & -\tau \\ \tau & \xi \end{pmatrix} \begin{pmatrix} x \\ y \end{pmatrix} + \begin{pmatrix} \bar{f}(x, y) \\ \bar{g}(x, y) \end{pmatrix} \tag{17}$$

where

$$\begin{aligned} \bar{f}(x, y) &= \frac{m_{13}}{m_{12}}t^3 + \frac{m_{14}}{m_{12}}t^2 + \frac{m_{15}}{m_{12}}ts + O((|x| + |y|)^4), \\ \bar{g}(x, y) &= \left(\frac{(\xi - m_{11})m_{13}}{m_{12}\tau} - \frac{m_{23}}{\tau}\right)t^3 + \left(\frac{(\xi - m_{11})m_{14}}{m_{12}\tau} - \frac{m_{24}}{\tau}\right)t^2 + \left(\frac{(\xi - m_{11})m_{15}}{m_{12}\tau} - \frac{m_{25}}{\tau}\right)ts + O((|x| + |y|)^4), \\ t &= m_{12}x \text{ and } s = (\xi - m_{11})x - \tau y. \end{aligned}$$

$$L = \left(\left[-Re \left(\frac{(1 - 2\lambda_1)\lambda_2^2}{1 - \lambda_1} \kappa_{20}\kappa_{11} \right) - \frac{1}{2}|\kappa_{11}|^2 - |\kappa_{02}|^2 + Re(\lambda_2\kappa_{21}) \right] \right)_{\bar{\beta}=0}$$

where

$$\begin{aligned} \kappa_{20} &= \frac{1}{8} [\bar{f}_{xx} - \bar{f}_{yy} + 2\bar{g}_{xy} + i(\bar{g}_{xx} - \bar{g}_{yy} - 2\bar{f}_{xy})] \\ \kappa_{11} &= \frac{1}{4} [\bar{f}_{xx} + \bar{f}_{yy} + i(\bar{g}_{xx} + \bar{g}_{yy})] \\ \kappa_{02} &= \frac{1}{8} [\bar{f}_{xx} - \bar{f}_{yy} - 2\bar{g}_{xy} + i(\bar{g}_{xx} - \bar{g}_{yy} + 2\bar{f}_{xy})] \\ \kappa_{21} &= \frac{1}{16} [\bar{f}_{xxx} + \bar{f}_{xyy} + \bar{g}_{xxy} + \bar{g}_{yyx} + i(\bar{g}_{xxx} + \bar{g}_{xyy} - \bar{f}_{xxy} - \bar{f}_{yyx})] \end{aligned}$$

Moreover, the partial derivatives of \bar{f} and \bar{g} evaluated at $\bar{\beta} = 0$ are given by:

$$\begin{aligned} \bar{f}_{xx} &= 2m_{14}m_{12} + 2(\xi - m_{11})m_{15}, \quad \bar{f}_{yy} = \bar{g}_{yy} = 0, \quad \bar{g}_{xy} = -(\xi - m_{11})m_{15} + m_{25}m_{12} \\ \bar{g}_{xx} &= 2 \left(\frac{(\xi - m_{11})m_{12}(m_{14} - m_{25}) - m_{24}m_{12}^2 + (\xi - m_{11})^2m_{15}}{\tau} \right), \quad \bar{f}_{xy} = -\tau m_{15}, \quad \bar{f}_{xxx} = 6m_{12}^2m_{13}, \\ \bar{g}_{xxx} &= 6 \left(\frac{(\xi - m_{11})m_{13}m_{12}^2 - m_{23}m_{12}^3}{\tau} \right), \quad \bar{g}_{yyy} = \bar{g}_{xyy} = \bar{f}_{yyy} = \bar{f}_{xyx} = 0 \end{aligned}$$

Arguing as in [5, 6, 25, 26, 27] we have the following result which gives parametric conditions for existence and direction of Neimark-Sacker bifurcation for coexistence fixed point of system Eq.(2).

Theorem 3.4 Suppose that Eq. (15) holds true and $L \neq 0$, then system (2) endures Neimark-Sacker bifurcation at its unique positive steady-state $\left(\alpha, \beta(1 - \alpha)\left(\frac{\alpha - \zeta}{\alpha + \eta}\right) - 1\right)$ when the bifurcation parameter β varies in a small neighborhood of $\beta_2 = \frac{(\alpha + \eta)^2}{-2\alpha^3 + (\zeta - 3\eta + 1)\alpha^2 + 2\eta(\zeta + 1)\alpha - \eta\zeta}$ such that $\zeta \neq \frac{\alpha(2\alpha^2 + 3\alpha\eta - \alpha - 2\eta)}{\alpha^2 + 2\alpha\eta - \eta}$. Furthermore, if $L < 0$, then an attracting invariant closed curve bifurcates from the fixed point for $\beta > \beta_2$, and if $L > 0$, then a repelling invariant closed curve bifurcates from the fixed point for $\beta < \beta_2$.

3.3. Chaos Control

Population models, particularly those that deal with the biological reproduction of species, are thought to be critically dependent on the ability to control chaos and bifurcation. Discrete-time models often exhibit more complex behavior than continuous ones. To safeguard the public from unforeseen events, it is essential to put chaos control mechanisms into place. In this section, we will look at a feedback control strategy for reorienting the unstable trajectory toward the stable one. To accomplish this, we first use the OGY approach to run system (2) Ott et al.[28], proposed this strategy. See also [29] for further details on the OGY strategy. To apply the OGY method, we rewrite system (2) as follows:

$$\begin{aligned} N_{n+1} &= \beta N_n(1 - N_n)\left(\frac{N_n - \zeta}{N_n + \eta}\right) - N_n P_n = f(N_n, P_n, \beta) \\ P_{n+1} &= \frac{1}{\alpha} N_n P_n = g(N_n, P_n, \beta) \end{aligned} \quad (18)$$

where the necessary chaos control is achieved by using only very small disturbances and the regulating parameter β . To do this, the parameter β is restricted to lie inside the range $\beta \in (\beta_0 - \Psi, \beta_0 + \Psi)$, where $\Psi > 0$ and β_0 denote the nominal value associated with the chaotic region, respectively. We employ the stabilizing feedback control strategy to direct the trajectory toward the desired orbit. Assuming that the unstable fixed point of system (2) is $(N^*, P^*) = \left(\alpha, \beta(1 - \alpha)\left(\frac{\alpha - \zeta}{\alpha + \eta}\right) - 1\right)$. System (18) can be approximated concerning the unstable residual point in the chaotic zone brought on by the appearance of Neimark-Sacker bifurcation:

$$\begin{bmatrix} N_{n+1} - N^* \\ P_{n+1} - P^* \end{bmatrix} \approx J(x^*, y^*, \beta_0) \begin{bmatrix} N_n - N^* \\ P_n - P^* \end{bmatrix} + H[\beta - \beta_0], \quad (19)$$

where

$$J(N^*, P^*, \beta_0) = \begin{bmatrix} \frac{\partial f(N^*, P^*, \beta_0)}{\partial N} & \frac{\partial f(N^*, P^*, \beta_0)}{\partial P} \\ \frac{\partial g(N^*, P^*, \beta_0)}{\partial N} & \frac{\partial g(N^*, P^*, \beta_0)}{\partial P} \end{bmatrix} = \begin{bmatrix} \frac{-\beta_0\alpha^3 + (-2\beta_0\eta + 1)\alpha^2 + ((2 + (\zeta + 1)\beta_0)\eta + \beta_0\zeta)\alpha + \eta^2}{(\alpha + \eta)^2} & -\alpha \\ \frac{-\beta_0\alpha^2 + \beta_0\alpha\zeta + \beta_0\alpha - \beta_0\zeta - \alpha - \eta}{(\alpha + \eta)\alpha} & 1 \end{bmatrix}$$

and

$$B = \begin{bmatrix} \frac{\partial f(N^*, P^*, \beta_0)}{\partial \beta} \\ \frac{\partial g(N^*, P^*, \beta_0)}{\partial \beta} \end{bmatrix} = \begin{bmatrix} \frac{\alpha^2 - \alpha\zeta - \alpha^3 + \alpha^2\zeta}{\alpha + \eta} \\ 0 \end{bmatrix}$$

Moreover, system (18) is controllable provided that the following matrix

$$C = [B : JB] = \begin{bmatrix} \frac{\alpha^2 - \alpha\zeta - \alpha^3 + \alpha^2\zeta}{\alpha + \eta} & \frac{(-\alpha + \zeta)(-\beta_0\alpha^3 + (-2\beta_0\eta + 1)\alpha^2 + ((2 + (\zeta + 1)\beta_0)\eta + \beta_0\zeta)\alpha + \eta^2)(-1 + \alpha)\alpha}{(\alpha + \eta)^3} \\ 0 & \frac{(-1 + \alpha)(-\alpha + \zeta)(-\beta_0\alpha^2 + (-1 + (\zeta + 1)\beta_0)\alpha - \beta_0\zeta - \eta)}{(\alpha + \eta)^2} \end{bmatrix} \quad (20)$$

is of rank 2. Moreover, taking $[\beta - \beta_0] = -K \begin{bmatrix} N_n - N^* \\ P_n - P^* \end{bmatrix}$ where $K = [\rho_1 \quad \rho_2]$, then system (19) can be written as

$$\begin{bmatrix} N_{n+1} - N^* \\ P_{n+1} - P^* \end{bmatrix} \approx [J - BK] \begin{bmatrix} N_n - N^* \\ P_n - P^* \end{bmatrix} \quad (21)$$

Furthermore, the corresponding controlled system of Eq. (2) is given by

$$\begin{aligned} N_{n+1} &= (\beta_0 - \rho_1(N_n - N^*) - \rho_2(P_n - P^*))N_n(1 - N_n) \left(\frac{N_n - \zeta}{N_n + \eta} \right) - N_n P_n \\ P_{n+1} &= \frac{1}{\alpha} N_n P_n \end{aligned} \quad (22)$$

Furthermore, if and only if both of the eigenvalues of the matrix $J - BK$ are contained within an open unit disk, fixed point $(N^*, P^*) = \left(\alpha, \beta(1 - \alpha) \left(\frac{\alpha - \zeta}{\alpha + \eta} \right) - 1 \right)$ is locally asymptotically stable. The controlled system (22)'s Jacobian matrix $J - BK$ may be expressed as follows:

$$J - BK = \begin{bmatrix} \frac{-\beta_0 \alpha^3 + (-2\beta_0 \eta + 1)\alpha^2 + ((2 + (\zeta + 1)\beta_0)n + \beta_0 \zeta)\alpha + \eta^2}{(\alpha + \eta)^2} + \frac{\alpha(\alpha - 1)(\alpha - \zeta)\rho_1}{\alpha + \eta} & -\alpha + \frac{\alpha(\alpha - 1)(\alpha - \zeta)\rho_2}{\alpha + \eta} \\ \frac{-\beta_0 \alpha^2 + \beta_0 \alpha \zeta + \beta_0 \alpha - \beta_0 \zeta - \alpha - \eta}{(\alpha + \eta)\alpha} & 1 \end{bmatrix}.$$

Let λ_1 and λ_2 are the eigenvalues of the characteristic equation of Jacobian matrix $J - BK$, then we have

$$\lambda_1 + \lambda_2 = \frac{-\beta_0 \alpha^3 + (-2\beta_0 \eta + 1)\alpha^2 + ((2 + (\zeta + 1)\beta_0)\eta + \beta_0 \zeta)\alpha + \eta^2}{(\alpha + \eta)^2} + \frac{\alpha(\alpha - 1)(\alpha - \zeta)\rho_1}{\alpha + \eta}, \quad (23)$$

$$\begin{aligned} \lambda_1 \lambda_2 &= \frac{\alpha(\alpha - 1)(\alpha - \zeta)}{\alpha + \eta} \rho_1 + \frac{(-\alpha + \zeta)(\alpha - 1)(-\beta_0 \alpha^2 + (\beta_0 \zeta + \beta_0 - 1)\alpha - \beta_0 \zeta - \eta)}{(\alpha + \eta)^2} \rho_2 \\ &\quad + \frac{\beta_0(-2\alpha^3 + (\zeta - 3\eta + 1)\alpha^2 + 2\eta(\zeta + 1)\alpha - \zeta\eta)}{(\alpha + \eta)^2}. \end{aligned} \quad (24)$$

Next, in order to determine the lines of marginal stability for the corresponding controlled system, we choose $\lambda_1 = \pm 1$ and $\lambda_1 \lambda_2 = 1$. Additionally, these limitations guarantee that the open unit disk contains λ_1 and λ_2 . Inferring from Eq. (24) that $\lambda_1 \lambda_2 = 1$, it is implied that:

$$\begin{aligned} L_1 := & \frac{\alpha^4 + (-\zeta + \eta - 1)\alpha^3 + ((-\zeta - 1)\eta + \zeta)\alpha^2 + \alpha\zeta\eta}{(\alpha + \eta)^2} \rho_1 \\ & + \frac{\beta_0 \alpha^4 + (-2\beta_0 \zeta - 2\beta_0 + 1)\alpha^3 + (\beta_0 \zeta^2 + 4\beta_0 \zeta + \beta_0 - \zeta + \eta - 1)\alpha^2 + ((-\zeta - 1)\eta - 2\beta_0 \zeta + \zeta - 2\beta_0 \zeta^2)\alpha + \zeta\eta + \beta_0 \zeta^2}{(\alpha + \eta)^2} \rho_2 \\ & + \frac{-2\beta_0 \alpha^3 + (\beta_0 \zeta - 3\beta_0 \eta + \beta_0 - 1)\alpha^2 + (2\beta_0 \zeta + 2\beta_0 - 2)\eta\alpha - \beta_0 \zeta\eta - \eta^2}{(\alpha + \eta)^2} = 0 \end{aligned}$$

Moreover, we assume that $\lambda_1 = 1$, then Eq. (23) and Eq. (24) yield that:

$$\begin{aligned} L_2 := & \frac{\beta_0 \alpha^4 + (-2\beta_0 \zeta - 2\beta_0 + 1)\alpha^3 + (\beta_0 \zeta^2 + (4\beta_0 - 1)\zeta + \beta_0 + \eta - 1)\alpha^2 + (-2\beta_0 \zeta^2 + (1 - 2\beta_0 - \eta)\zeta - \eta)\alpha + \zeta\eta + \beta_0 \zeta^2}{(\alpha + \eta)^2} \rho_2 \\ & + \frac{-\beta_0 \alpha^3 + (\beta_0 \zeta - \beta_0 \eta + \beta_0 - 1)\alpha^2 + ((\beta_0 \eta - \beta_0)\zeta + \beta_0 \eta - 2\eta)\alpha - \beta_0 \zeta\eta - \eta^2}{(\alpha + \eta)^2} = 0 \end{aligned}$$

Finally taking $\lambda_1 = -1$, then from Eq. (23) and Eq. (24) we get

$$\begin{aligned} L_3 := & -\frac{2\alpha(\alpha - 1)\zeta - 2\alpha^3}{\alpha + \eta} \rho_1 + \frac{(-\alpha + \zeta)(\alpha - 1)(-\beta_0 \alpha^2 + (\beta_0 \zeta + \beta_0 - 1)\alpha - \beta_0 \zeta - \eta)}{(\alpha + \eta)^2} \rho_2 \\ & + \frac{-3\beta_0 \alpha^3 + (3 + (\zeta - 5\eta + 1)\beta_0)\alpha^2 + (((3\zeta + 3)\eta + \zeta)\beta_0 + 6\eta)\alpha - \beta_0 \zeta\eta + 3\eta^2}{(\alpha + \eta)^2} = 0 \end{aligned}$$

The triangular area in the $\rho_1 \rho_2$ -plane bounded by the straight lines L_1, L_2, L_3 then contains stable eigenvalues for a given parametric value.

3.4. Numerical Simulations

Using the Maple 2021 and Matlab R2022b programs, numerical simulations are utilized to demonstrate the correctness of the theoretical research included in this section. Different parameter values were utilized during these simulations, and unique graphs were created for each.

Example 3.4.1: For the parameter values $\alpha = 0.2, \zeta = 0.001, \eta = 0.05$ and with initial condition $(N_0, P_0) = (0.24, 0.08)$, the coexistence fixed point of the system (2) is obtained as $D_3 = (0.2, 0.04709287)$. The critical value of Neimark-Sacker bifurcation point is obtained as $\beta = 1.644304130$. The characteristic equation of the Jacobian matrix evaluated at $(0.2, 0.04709287)$ is given by:

$$\lambda^2 - 1.952907130\lambda + 1 = 0.$$

The roots of this characteristic equation are $\lambda_1 = 0.9764535650 + 0.2157276881i$ and $\lambda_2 = 0.9764535650 - 0.2157276881i$. And also, $|\lambda_1| = |\lambda_2| = 1$. Therefore $(\beta, \alpha, \zeta, \eta) = (1.644304130, 0.2, 0.001, 0.05) \in \Omega_{NS}$. The bifurcation diagrams and corresponding maximum Lyapunov exponents (MLE) are plotted in Figure 1.

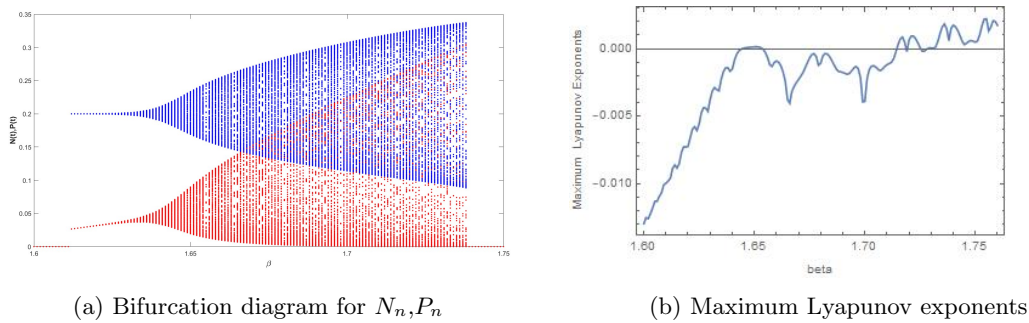


Figure 1: Bifurcation diagrams and MLE for system (2) with $\alpha = 0.2, \zeta = 0.001, \eta = 0.05$ and $(N_0, P_0) = (0.24, 0.08)$

Next, we implement OGY control strategy in order to control chaos due to emergence of Neimark-Sacker bifurcation. For this, we take $\beta_0 = 1.725, \alpha = 0.2, \zeta = 0.001, \eta = 0.05$ and $D_3 = (0.2, 0.09848)$, then corresponding controlled system is given by:

$$\begin{aligned} N_{n+1} &= (1.725 - \rho_1(N_n - 0.2) - \rho_2(P_n - 0.09848))N_n(1 - N_n) \left(\frac{N_n - 0.001}{N_n + 0.05} \right) - N_n P_n \quad (25) \\ P_{n+1} &= \frac{1}{0.2} N_n P_n \end{aligned}$$

Then, characteristic polynomial of the Jacobian matrix of the controlled system (25) evaluated at $(0.2, 0.09848)$ is given by:

$$F(\lambda) = \lambda^2 - (1.950596 - 0.12736\rho_1)\lambda + 1.049076 - 0.12736\rho_1 + 0.062712064\rho_2 \quad (26)$$

Additionally, the marginal stability lines are provided by for the controlled system (25)

$$\begin{aligned} L_1 &:= 0.049076 - 0.12736\rho_1 + 0.062712064\rho_2 = 0 \\ L_2 &:= 0.09848 + 0.062712064\rho_2 = 0 \\ L_3 &:= 3.999672 - 0.25472\rho_1 + 0.062712064\rho_2 = 0 \end{aligned}$$

Figure 2 depicts the triangle-shaped stability zone enclosed by these marginal stability lines L_1, L_2 , and L_3 .

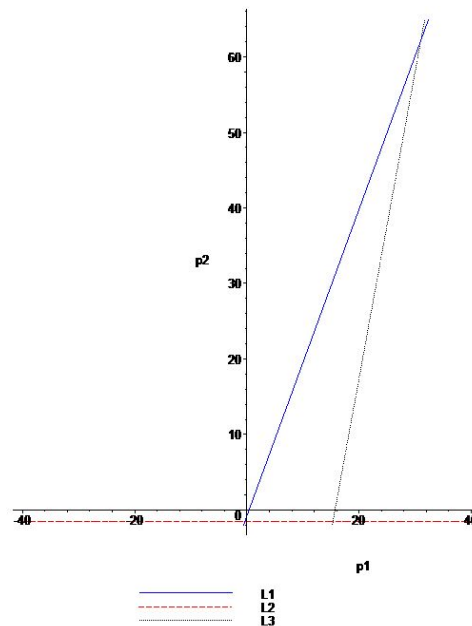


Figure 2: Triangular stability region bounded by L_1, L_2 and L_3 for the controlled system (25)

4. Conclusion

The stability and bifurcation analysis of a discrete-time predator-prey model with strong Allee effect are examined in this article. The system (2) has three fixed points, identified as D_1, D_2 and D_3 , as we proved. Topological classifications of these fixed locations were given. We showed using bifurcation theory that the system (2) will experience Neimark-Sacker bifurcation at a specific coexistence fixed point if a varies around the set Ω_{NS} . The parametric conditions for coexistence fixed point D_3 's direction Neimark-Sacker bifurcation were given. Finally, Neimark-Sacker bifurcation, chaos control and maximum Lyapunov exponent of the coexistence fixed point are verified with the help of numerical simulations. To support the theoretical conclusions, we also provided further numerical simulations using Maple 2021 and Matlab R2022b.

Ethics in Publishing

There are no ethical issues regarding the publication of this study.

Conflicts of Interest

No conflict of interest or common interest has been declared by the authors.

Acknowledgments

The authors would like to thank the reviewers for their constructive feedbacks towards improving our manuscript.

References

- [1] Arancibia-Ibarra, C., (2019), The basins of attraction in a modified May–Holling–Tanner predator–prey model with Allee affect, *Nonlinear Analysis*, 185, 15-28.

- [2] Kundu, S., Maitra, S., (2019), Asymptotic behaviors of a two prey one predator model with cooperation among the prey species in a stochastic environment, *Journal of Applied Mathematics and Computing*, 61(1), 505-531.
- [3] Martinez-Jeraldo, N., Aguirre, P., (2019), Allee effect acting on the prey species in a Leslie-Gower predation model, *Nonlinear Analysis: Real World Applications*, 45, 895-917.
- [4] Elaydi, S., (1996), *An introduction to difference equations*, Springer-Verlag, New York, 10, 978-1.
- [5] Kuznetsov, Y. A., Kuznetsov, I. A., Kuznetsov, Y., (1998), *Elements of applied bifurcation theory* (Vol. 112, pp. xx+-591), New York: Springer.
- [6] Wiggins, S., Wiggins, S., Golubitsky, M., (2003), *Introduction to applied nonlinear dynamical systems and chaos* (Vol. 2, No. 3), New York: Springer.
- [7] Zhou, S. R., Liu, Y. F., Wang, G., (2005), The stability of predator-prey systems subject to the Allee effects, *Theoretical Population Biology*, 67(1), 23-31.
- [8] Wang, S., Yu, H., (2021), Complexity Analysis of a Modified Predator-Prey System with Beddington-DeAngelis Functional Response and Allee-Like Effect on Predator, *Discrete Dynamics in Nature and Society*.
- [9] Allee, W. C., (1931), *Animal Aggregations: A study in General Sociology*, University of Chicago Press, USA.
- [10] Courchamp, F., Berec, L., Gascoigne, J., (2008), *Allee effects in ecology and conservation*, OUP Oxford.
- [11] Amarasekare, P., (1998), Interactions between local dynamics and dispersal: insights from single species models, *Theoretical Population Biology*, 53(1), 44-59.
- [12] Drake, J. M., (2004), Allee effects and the risk of biological invasion, *Risk Analysis: An International Journal*, 24(4), 795-802.
- [13] Shi, J., Shivaji, R., (2006), Persistence in reaction diffusion models with weak Allee effect, *Journal of Mathematical Biology*, 52(6), 807-829.
- [14] Taylor, C. M., Hastings, A., (2005), Allee effects in biological invasions, *Ecology Letters*, 8(8), 895-908.
- [15] Celik, C., Duman, O., (2009), Allee effect in a discrete-time predator-prey system, *Chaos, Solitons Fractals*, 40(4), 1956-1962.
- [16] Wang, W. X., Zhang, Y. B., Liu, C. Z., (2011), Analysis of a discrete-time predator-prey system with Allee effect, *Ecological Complexity*, 8(1), 81-85.
- [17] Pal, S., Sasmal, S. K., Pal, N., (2018), Chaos control in a discrete-time predator-prey model with weak Allee effect, *International Journal of Biomathematics*, 11(07), 1850089.

- [18] Kangalgil, F., İlhan, F., (2022), Period-doubling Bifurcation and Stability in a Two Dimensional Discrete Prey-predator Model with Allee Effect and Immigration Parameter on Prey, Cumhuriyet Science Journal, 43(1), 88-97.
- [19] Kangalgil, F., Topsakal, N., Öztürk, N., (2022), Analyzing bifurcation, stability, and chaos control for a discrete-time prey-predator model with Allee effect, Turkish Journal of Mathematics, 46(6), 2047-2068.
- [20] Kangalgil, F., Işık, S., (2022), Effect of immigration in a predator-prey system: Stability, bifurcation and chaos, AIMS Mathematics, 7(8), 14354-14375.
- [21] Işık, S., Kangalgil, F., (2022), On the analysis of stability, bifurcation, and chaos control of discrete-time predator-prey model with Allee effect on predator, Hacettepe Journal of Mathematics and Statistics, 1-21.
- [22] Kangalgil, F., Işık, S., (2020), Controlling chaos and Neimark-Sacker bifurcation in a discrete-time predator-prey system, Hacettepe Journal of Mathematics and Statistics, 49(5), 1761-1776.
- [23] Kangalgil, F., (2019), Neimark-Sacker bifurcation and stability analysis of a discrete-time prey-predator model with Allee effect in prey, Advances in Difference Equations, 2019(1), 1-12.
- [24] Khan, A. Q., (2016), Neimark-Sacker bifurcation of a two-dimensional discrete-time predator-prey model, SpringerPlus, 5(1), 1-10.
- [25] Guckenheimer, J., Holmes, P., (2013), Nonlinear oscillations, dynamical systems, and bifurcations of vector fields (Vol. 42), Springer Science Business Media.
- [26] Robinson, C., (1998), Dynamical systems: stability, symbolic dynamics, and chaos, CRC press.
- [27] Wan, Y. H., (1978), Computation of the Stability Condition for the Hopf Bifurcation of Diffeomorphisms on \mathbb{R}^2 . SIAM Journal on Applied Mathematics, 34(1), 167-175.
- [28] Ott, E., Grebogi, C., Yorke, J. A., (1990), Controlling chaos, Physical review letters, 64(11), 1196.
- [29] Din, Q., Donchev, T., Kolev, D., (2018), Stability, bifurcation analysis and chaos control in chlorine dioxide-iodine-malonic acid reaction, MATCH Commun. Math. Comput. Chem, 79(3), 577-606.

Zinc(II) and Cadmium(II) Salphen Catalyzed Alkylation Reactions to Form α -Alkylated Ketones

Salih GÜNNAZ *

Ege University, Chemistry Department, 35100 Bornova, Izmir, Turkey

Received:08/11/2022, **Revised:** 09/12/2022, **Accepted:** 22/12/2022, **Published:** 30/12/2022

Abstract

The catalytic α -alkylation reaction is one of the methods commonly used to form C-C bonds. In this study the zinc (II) and cadmium (II)-salphen catalyzed α -alkylation of ketones with primary alcohols is reported. Various α -alkylated ketones were obtained in good yields through a borrowing hydrogen strategy by using 1 % of catalysts and a catalytic amount of NaOH (10 mol%) as the base under air atmosphere. All synthesized compounds were characterized by ^1H and ^{13}C NMR. The highest conversion was obtained using the complex **1a**.

Keywords: Zinc, cadmium, salphen, alkylation, ketone

α -Alkillenmiş Ketonlar Oluşturmak için Çinko(II) ve Kadmiyum(II) Salfen Katalizli Alkilasyon Reaksiyonları

Öz

Katalitik α -alkilasyon reaksiyonu, C-C bağları oluşturmak için yaygın olarak kullanılan yöntemlerden biridir. Bu çalışmada, ketonların birincil alkollerle çinko (II) ve kadmiyum (II)-salfen katalizli α -alkilasyonu rapor edilmiştir. Hava atmosferi altında %1 katalizör ve baz olarak katalitik miktarda (%10 mol) NaOH kullanılarak bir ödünç hidrojen stratejisi yoluyla çeşitli α -alkillenmiş ketonlar iyi verimlerle elde edilmiştir. Sentezlenen tüm bileşikler, ^1H ve ^{13}C NMR ile karakterize edilmiştir. En yüksek dönüşüm kompleks **1a** kullanılarak elde edilmiştir.

Anahtar Kelimeler: Çinko, kadmiyum, salfen, alkilasyon, keton

1. Introduction

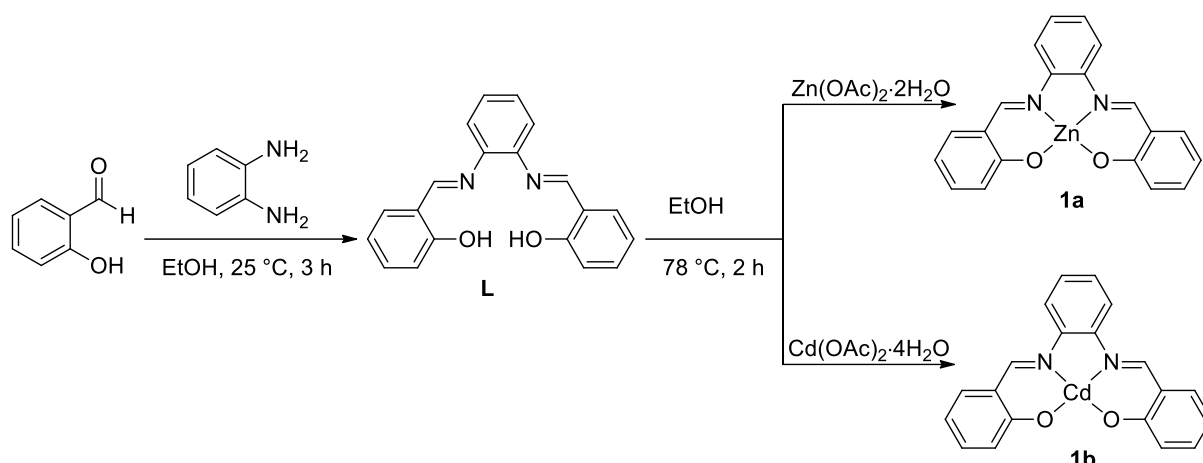
Condensation of salicylaldehyde derivatives with 1,2-diamines leads to the formation of an important class of ligand known as "Salens and Salphens". Many different salen ligands can be synthesized using of numerous differently substituted salicylic aldehydes or diamine derivatives. The variety of metal-salen complexes can be expressed by numerous references to these complexes available in chemical databases. The most prominent metals examined are cobalt [1], manganese[2], copper[3], nickel[4], iron[5] and chromium[6]. Metal-salen complexes of these elements are extensively used in catalysis. Due to the multifunctionality of the Salen complexes, they have been shown by Jacobsen as "privileged ligands for catalysis".[7]

Catalysts are highly important in the development of sustainable chemical processes. The catalytic α -alkylation reaction is one of the methods commonly used to form C-C bonds. Transition-metal catalysts based on ruthenium[8], rhodium[9], iridium[10] and gold[11] have confirmed to be highly efficient for this reaction. Although used in low catalyst loading, the attention in the use of more sustainable alternatives has increased as these metals bear inherent disadvantages such as limited availability, high price, and toxicity. In this regard, there has been increased interest in the use of earth-abundant first-row transition metals such as iron[12], manganese[13], cobalt[14], or nickel. [15]

The aim of the present work is to design an inexpensive catalyst that can be easily prepared for the α -alkylation reaction of ketones, utilizing the coordination between Schiff base. Herein, the synthesis and structure of Zn(II)- and Cd(II)-Salphen complexes (**1a-b**) incorporating N,N'-Bis(salicylidene)-1,2-phenylenediamine (**L**) ligand have been described. The complexes have been characterized via NMR spectroscopy techniques and screened to examine the catalytic activity for the α -alkylation of ketones. From the promising results, Zn(II)-salphen complex has been found to be potentially useful for this purpose. Zinc is a cheaper and more abundant metal, however, to the best of our knowledge, the activities of salphen ligands with zinc for the α -alkylation of ketones have not been reported in the literature.

2. Material and Methods

Scheme 1 describes the method used for the synthesis of the ligand (**L**) and complexes (**1a-b**). The four-coordinate Zn (II)- and Cd(II)-salphen complexes (**1a-b**) were synthesized by reaction of $M(\text{OAc})_2 \cdot x\text{H}_2\text{O}$ ($M = \text{Zn}, \text{Cd}$) with **L** at 78 °C in ethanol. The Zn (II) and Cd (II) complexes were synthesized according to a modified literature procedure in good yield. All complexes are stable in air, insoluble in H_2O and soluble in DMSO, DMF, moderately soluble in chlorinated solvents, partly soluble in ethanol. Synthesized compounds were characterized by NMR spectra. The physical properties and spectroscopic data of the obtained compounds are in accordance with previous reports. [16]



Scheme 1. Preparation of Zn(II)- and Cd(II)-Salphen Complexes **1a-b**.

Experimental Details. Unless otherwise specified, all reagents were obtained commercially and used without further purification. NMR spectra were recorded on Varian AS 400 Mercury NMR spectrometer and reported in units of parts per million (ppm) relative to tetramethyl silane ($\delta = 0$ ppm), CDCl₃ ($\delta = 7.26$ ppm for ¹H and $\delta = 77.0$ ppm for ¹³C NMR) or DMSO-*d*₆ ($\delta = 2.48$ ppm for ¹H and $\delta = 39.97$ ppm for ¹³C NMR).

Synthesis of ligand (L). A solution of salicylaldehyde (4.0 mmol) in ethanol (2 mL) was added dropwise to a solution of *o*-Phenylenediamine (2.0 mmol) in the same solvent (2 mL). The mixture was stirred at room temperature 3h, during which time a precipitate was formed. The product was filtered out, washed with ethanol (2x2 mL) and dried under reduced pressure.

Ligand L. Yield: 83%, yellow solid. ¹H NMR (400 MHz, DMSO-*d*₆): $\delta = 12.95$ (bs, 2 H, OH, [H19, H20]), 8.91 (s, 2 H, N=CH, [H5, H6]), 7.65 (dd, $J_1 = 8.0$ Hz, $J_2 = 1.6$ Hz, 2 H, [H9, H18]), 7.45-7.37 (m, 6H, [H11, H16, H21, H22, H23, H24]), 6.97-6.94 (m, 4H, [H10, H12, H15, H17]). ¹³C NMR (100.6 MHz, DMSO-*d*₆, TMS): $\delta = 164.5$ (C=N, [C5, C6]), 160.8 [C13, C14], 142.7 [C1, C2], 133.9 [C11, C16], 132.9 [C9, C18], 128.2 [C22, C23], 120.2 [C21, C24], 119.9 [C7, C8], 119.5 [C10, C17], 117.1 [C12, C15].

General procedures for the synthesis of complexes 1a-b. To hot 5 mL ethanol solution containing 1.0 mmol of the ligand, 5 mL of ethanol solution containing 1.0 mmol of M(OAc)₂·xH₂O (M = Zn, Cd) was added dropwise. After stirring for 2 h at 78°C the formed red complexes were filtered, collected, and then washed with ethanol. The complexes were dried under reduced pressure.

Complex 1a. Yield: 86%, yellow solid. ¹H NMR (400 MHz, DMSO-*d*₆, TMS, 25°C, ppm): 8.99 (s, 2H, N=CH, [H5, H6]), 7.88-7.85 (m, 2H, [H9, H18]), 7.41 (dd, 2H, $J_1 = 7.6$ Hz, $J_2 = 2.0$ Hz, [H11, H16]), 7.37-7.33 (m, 2H, [H22, H25]), 7.23 (td, 2H, $J_1 = 7.4$ Hz, $J_2 = 2.0$ Hz, [H23, H24]), 6.71 (d, 2H, $J = 8.4$ Hz, [H10, H17]), 6.50 (td, 2H, $J_1 = 7.4$ Hz, $J_2 = 2.0$ Hz, [H12, H15]). ¹³C NMR (100.6 MHz, DMSO-*d*₆, TMS): $\delta = 172.7$ (C=N, [C5, C6]), 163.3 [C13, C14], 139.8 [C1, C2], 136.7 [C11, C16], 134.8 [C9, C18], 127.7 [C23, C24], 123.5 [C22, C25], 119.9 [C7, C8], 116.9 [C10, C17], 113.5 [C12, C15].

Complex 1b. Yield: 84%, yellow solid. ^1H NMR (400 MHz, DMSO- d_6 , TMS, 25°C, ppm): 8.61 (s, 2H, N=CH, [H5, H6]), 7.55-7.53 (m, 2H, [H9, H18]), 7.33-7.28 (m, 4H, [H11, H16, H22, H25]), 7.14-7.10 (m, 2H, [H23, H24]), 6.62 (d, $J = 8.4$ Hz, 2 H, [H10, H17]), 6.40 (t, $J = 7.4$ Hz, 2H, [H12, H15]). ^{13}C NMR (100.6 MHz, DMSO- d_6 , TMS): $\delta = 173.5$ (C=N, [C5, C6]), 165.3 [C13, C14], 141.7 [C1, C2], 137.5 [C11, C16], 133.7 [C9, C18], 127.3 [C23, C24], 124.4 [C22, C25], 121.3 [C7, C8], 118.1 [C10, C17], 112.7 [C12, C15].

In ^1H -NMR spectra of the Schiff base, the -OH proton was observed at around δ 12.95 ppm. The proton of -N=CH ligand appear around δ 8.91 ppm. Upon coordination of Zn (II) (**1a**) and Cd (II) (**1b**), the ^1H -NMR spectra of complexes showed some differences from the ligand (**L**). The ^1H -NMR spectra of the metal complexes display lack of phenolic -OH, confirming involvement of the -OH proton in complexation. In ^{13}C -NMR spectra of the ligands, -N=CH carbons appeared at about 164.5 ppm. This azomethine carbon in the spectra of metal complexes shifted upfield compared to the free ligand. These results agree with the literature data¹⁻³. NMR spectral data for free ligand and the complexes (**1a**, **1b**) together with their assignments are presented in Table 1.

Table 1. NMR comparison between ligand and complexes.

^1H -NMR N=CH			^{13}C -NMR C=N		
L	1a	1b	L	1a	1b
8.91	8.99	8.61	164.5	172.7	173.5

Zinc(II) and Cadmium(II) Salphen Catalyzed Alkylation Reactions to Form α -Alkylated Ketones

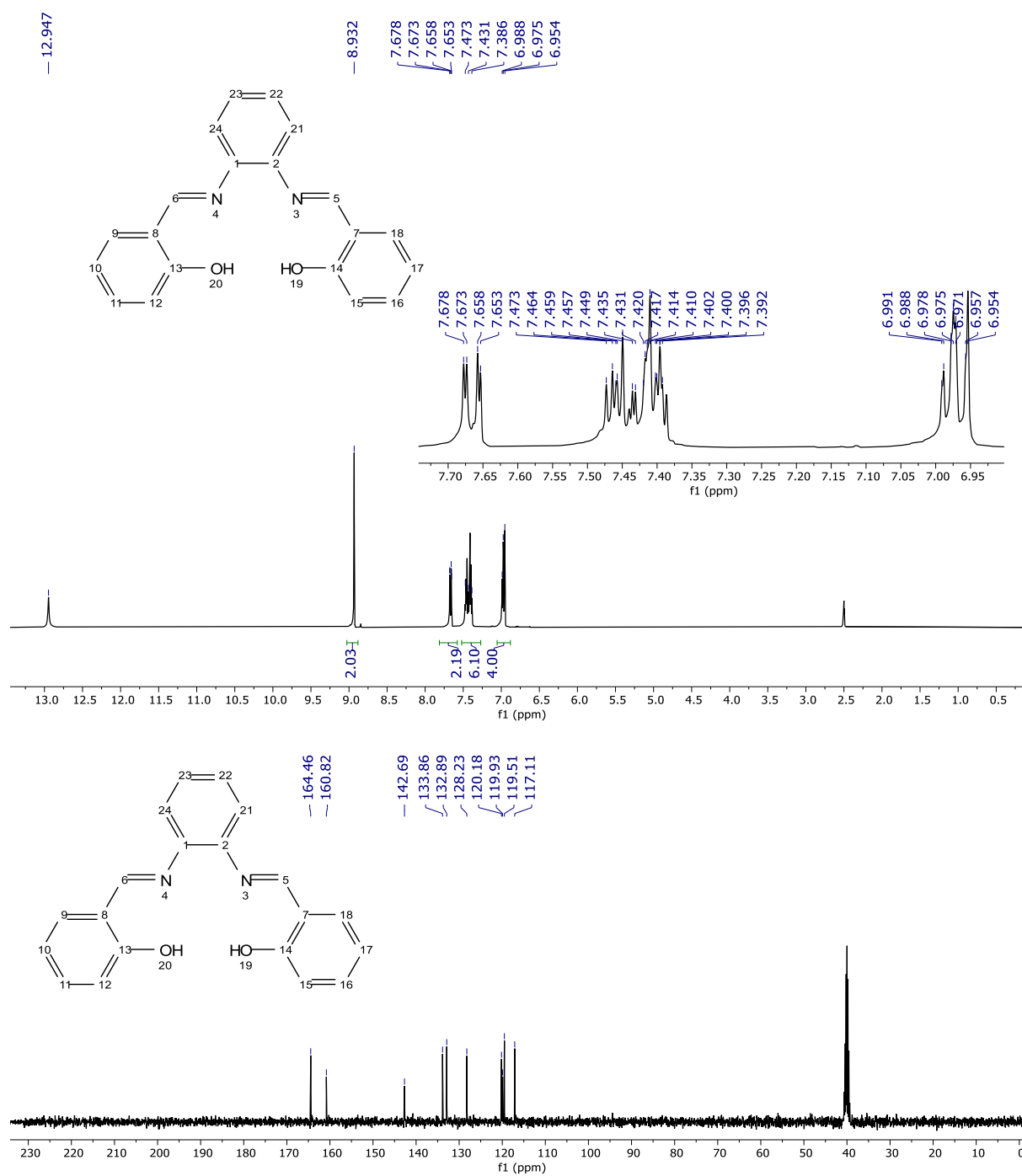


Figure 1. ¹H and ¹³C NMR (DMSO-*d*₆) of L.

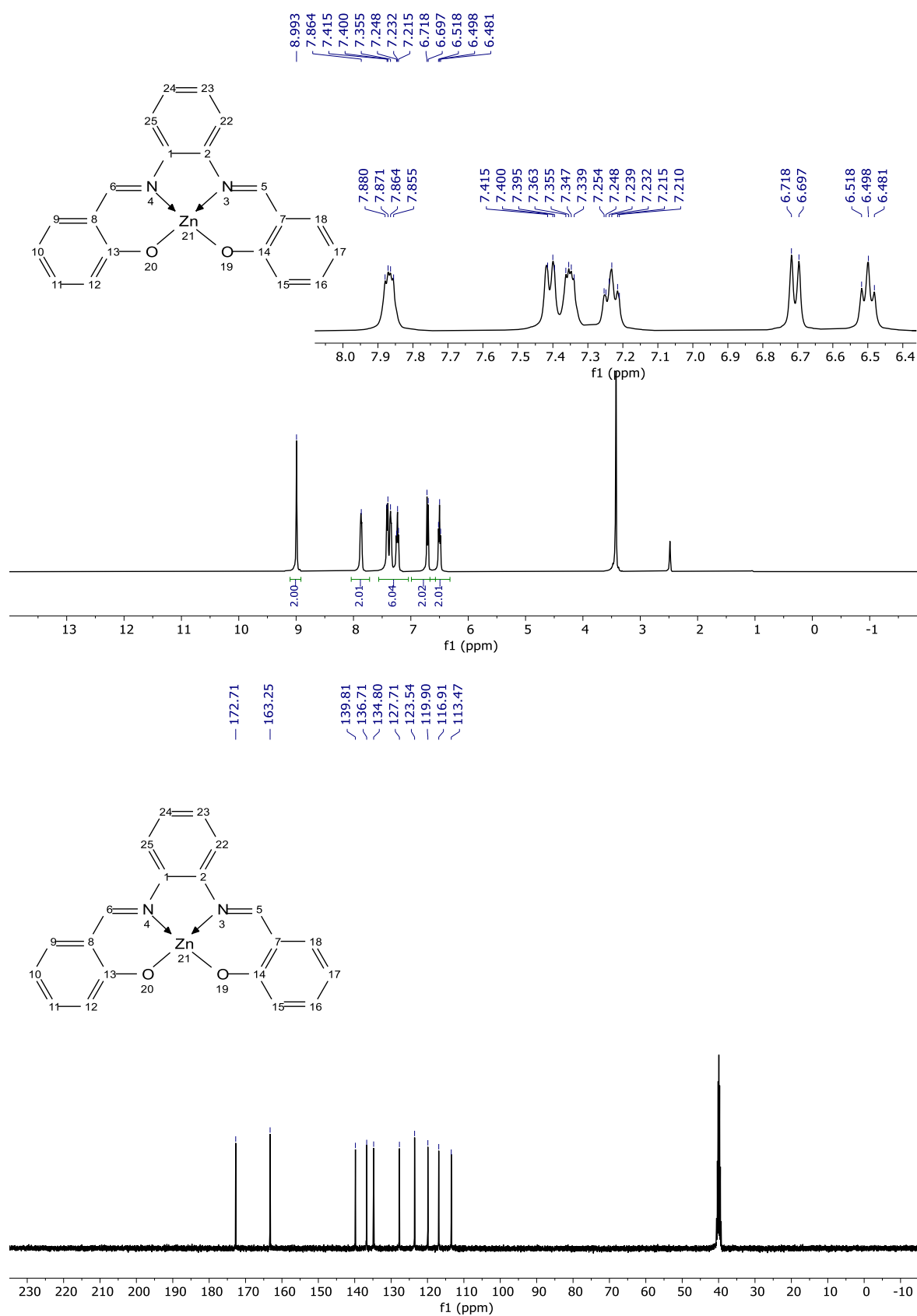


Figure 2. ¹H and ¹³C NMR (DMSO-*d*₆) of 1a.

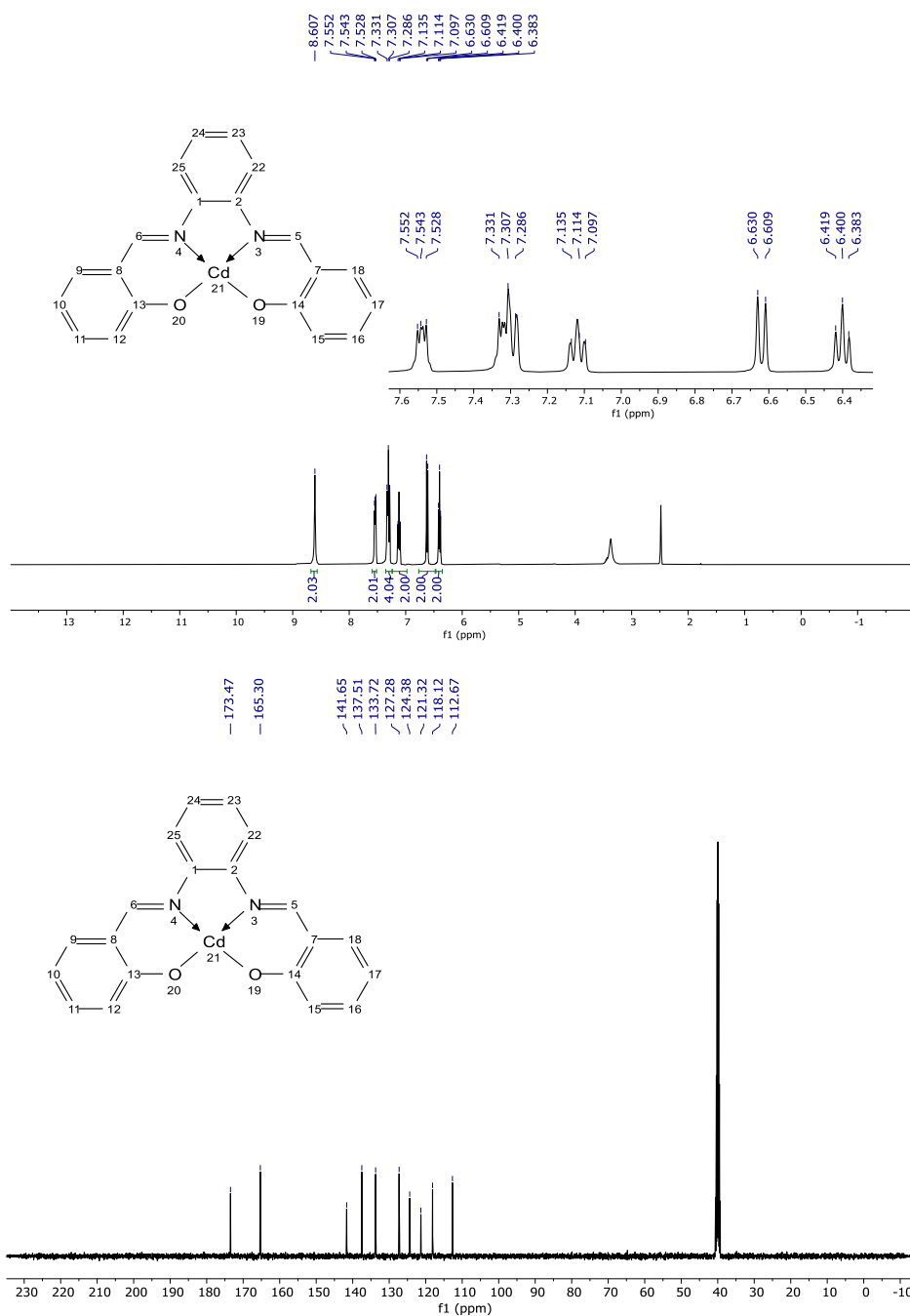
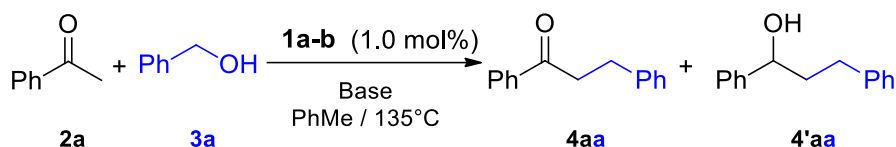


Figure 3. ^1H and ^{13}C NMR ($\text{DMSO-}d_6$) of **1b**.

3. Results and Discussion

To explore the effect of the catalysts on the α -alkylation of ketones with alcohols, the reaction of acetophenone (**2a**) with benzyl alcohol (**3a**) was chosen as a model reaction to evaluate the influence of catalysts (**1a-b**). The progress of the reaction was monitored by ^1H NMR spectroscopy, and the yields are based on 1,3,5-trimethoxybenzene as the internal standard (Table 2).

Table 2. Optimization of reaction conditions^a

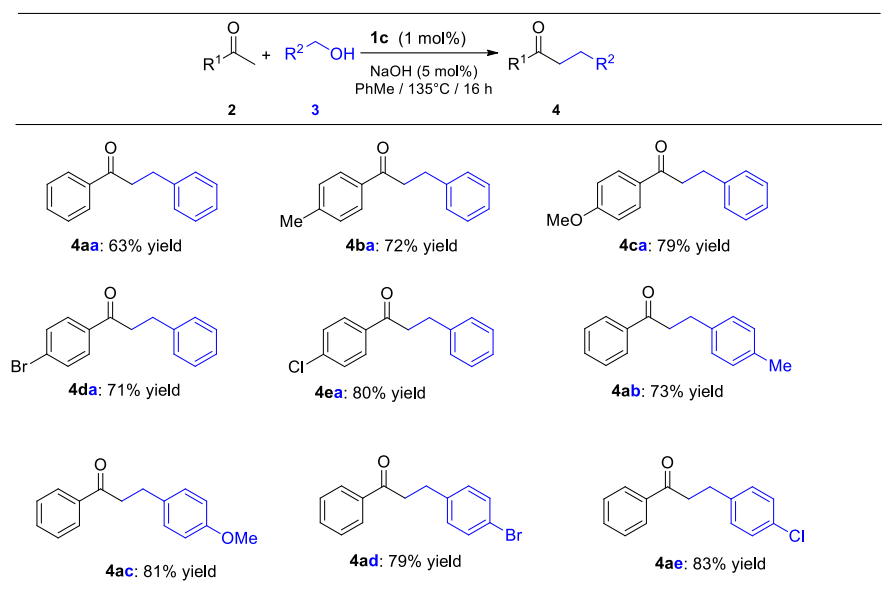
entry	cat.	base	solvent	T (°C)	time (h)	yield of 4aa ^b (%)	yield of 4'aa ^b (%)
1	1a	NaOH	Toluene	135	16	63	20
2	1b	NaOH	Toluene	135	16	54	16
3	1a	KOH	Toluene	135	16	41	18
4	1a	KO ^t Bu	Toluene	135	16	37	16
5	1a	NaO ^t Bu	Toluene	135	16	53	21
6	1a	Na ₂ CO ₃	Toluene	135	16	-	-
7	1a	NaHCO ₃	Toluene	135	16	-	-
8	1a	NaOH	DMSO	135	16	-	-
9	1a	NaOH	Toluene	100	16	18	06
10	1a	-	Toluene	135	16	-	-
11	-	NaOH	Toluene	135	16	38	12
12	Zn(OAc)₂	NaOH	Toluene	135	16	-	-
13 ^c	1a	NaOH	Toluene	135	16	61	21
14 ^d	1a	NaOH	Toluene	135	16	59	23

^aReaction Conditions: **2a** (1.0 mmol), **3a** (1.0 mmol), **1a-c** (1 mol%), base (10 mol%), toluene (2.0 mL), 135 °C, under air. ^bYields were determined by ¹H NMR analyses. ^cReaction was performed under an argon atmosphere. ^dReaction was performed under closed system.

The reaction was performed in the presence of catalysts (**1a-b**) (1 mol %) and NaOH (10 mol %) in toluene (2 ml) at 135 °C (bath temp.) under air atmosphere for 16h (entries 1-2). Among all catalysts tested, the best conversion was obtained with catalyst **1a** (entry 1). Replacing NaOH with KOH decreased the yield of the reaction to 41% (entry 3), Replacing NaOH with KO^tBu and NaO^tBu decreased the yield of the reaction to 37 and 53 % respectively (entry 4 and 5), Na₂CO₃ and NaHCO₃ were inactive under same conditions (entries 6 and 7). No conversion

was observed when DMSO was used as the solvent (entry 8). When the temperature was 100 degrees, the yield decreased to 18% (entry 9). Additional experiments were performed without NaOH, no product formation was observed (entry 10). In the experiment with NaOH without catalyst, 38% conversion was observed (entry 11). Moreover, no conversion was observed when Zn-acetate was used in the same reaction conditions instead of Zn (II)–salphen, which indicates the critical role of the salphen ligands (entry 12). Using the closed systems or inert reaction conditions did not improve the yield of the reaction significantly and the rest of the reactions were performed open to air (entries 13 and 14).

To study the scope of the reaction, various ketones and primary alcohols were reacted under optimized conditions (Scheme 2). All reactions resulted in conversion of starting materials affording selective formation of the corresponding ketone **4**.



Scheme 2. Scope of α -Alkylation of Ketones with Primary Alcohols Catalyzed by Complex **1a**^a

^aReaction Conditions: Ketone (1.0 mmol), primary alcohol (1.0 mmol), **1a** (1 mol%), base (10.0 mol%), toluene (2.0 mL), 135 °C, under air.

Various electron-rich or electron-deficient 1-arylketones (**2a–e**) were transformed into the corresponding ketones (**4aa–4ea**) in good yields by using **1c** (1 mol%) as the catalyst. The reaction of ketones bearing electron-donating -Me and -OMe substituents and electron-withdrawing -Br and -Cl substituents with benzyl alcohol gave desired products **4aa–4ea** with 72–80% isolated yields. Then the scope of the α -alkylation reaction compared to primary alcohols (**3**) were studied. For benzyl alcohol with electron-donating or electron-withdrawing groups the reactions produced α -alkylated ketones with good yields. The reactions of acetophenone with 4-Me, 4-OMe, 4-Br, and 4-Cl benzyl alcohols, were afforded the desired ketone products (**4ab–4ae**) in good yields (73–83%).

General procedure for the α -alkylation of ketones with primary alcohols to give α -alkylated ketones. In a 20 mL reaction tube (1 cm \times 20 cm) with a condenser were added NaOH (2.0 mg, 0.05 mmol) ketone (1.0 mmol), primary alcohol (1.0 mmol) and complex **1** (0.01 mmol, 1 mol%) in toluene (2.0 mL) under air atmosphere. The reaction mixture was vigorously stirred (1400 rpm) under reflux in a preheated oil bath at 135 °C for 3–24 h. Then the reaction mixture was cooled to ambient temperature and a 10 μ L solution was syringed out for GC analysis. The solvent was evaporated, and the crude product was submitted for NMR analysis to calculate the conversion. All the crude products were combined after analysis and purified by silica gel column chromatography using hexane and ethyl acetate (9:1) mixture as eluent to afford the desired ketone.

1,3-Diphenylpropan-1-one (4aa). Yield: 66%, white solid. ^1H NMR (CDCl_3 , 400 MHz) δ (ppm): 7.98 (d, $J = 7.6$ Hz, 2H), 7.57 (t, $J = 7.4$ Hz, 1H), 7.47 (t, $J = 7.6$ Hz, 2H), 7.34–7.21 (m, 5H), 3.32 (t, $J = 7.6$ Hz, 2H), 3.10 (t, $J = 7.6$ Hz, 2H); ^{13}C NMR (CDCl_3 , 100 MHz) δ (ppm): 199.1, 141.3, 136.9, 133.0, 128.6, 128.6, 128.5, 128.0, 126.1, 40.4, 30.2.

3-Phenyl-1-(p-tolyl)propan-1-one (4ba). Yield: 77%, white solid. ^1H NMR (CDCl_3 , 400 MHz) δ (ppm): 7.89 (d, $J = 8.0$ Hz, 2H), 7.34–7.23 (m, 7H), 3.29 (t, $J = 7.4$ Hz, 2H), 3.09 (t, $J = 7.6$ Hz, 2H), 2.42 (s, 3H); ^{13}C NMR (CDCl_3 , 100 MHz) δ (ppm): 198.8, 143.8, 141.4, 134.5, 129.3, 128.5, 128.4, 128.2, 126.1, 40.3, 30.3, 21.6.

1-(4-Methoxyphenyl)-3-phenylpropan-1-one (4ca). Yield: 81% white solid. ^1H NMR (CDCl_3 , 400 MHz) δ (ppm): 7.95 (d, $J = 8.8$ Hz, 2H), 7.32–7.19 (m, 5H), 6.93 (d, $J = 8.8$ Hz, 2H), 3.86 (s, 3H), 3.25 (t, $J = 7.8$ Hz, 2H), 3.07 (t, $J = 7.6$ Hz, 2H); ^{13}C NMR (CDCl_3 , 100 MHz) δ (ppm): 197.8, 163.4, 141.5, 130.3, 130.0, 128.5, 128.4, 126.1, 113.7, 55.4, 40.1, 30.3.

1-(4-Bromophenyl)-3-phenylpropan-1-one (4da). Yield: 74% white solid. ^1H NMR (CDCl_3 , 400 MHz) δ (ppm): 7.81 (d, $J = 8.8$ Hz, 2H), 7.59 (d, $J = 8.4$ Hz, 2H), 7.32–7.21 (m, 5H), 3.26 (t, $J = 7.6$ Hz, 2H), 3.06 (t, $J = 7.6$ Hz, 2H); ^{13}C NMR (CDCl_3 , 100 MHz) δ (ppm): 198.1, 141.0, 135.6, 131.9, 129.6, 128.6, 128.4, 128.2, 126.2, 40.4, 30.1.

1-(4-Chlorophenyl)-3-phenylpropan-1-one (4ea). Yield: 80%, white solid. ^1H NMR (CDCl_3 , 400 MHz) δ (ppm): 7.89 (d, $J = 8.8$ Hz, 2H), 7.42 (d, $J = 8.8$ Hz, 2H), 7.32–7.19 (m, 5H), 3.27 (t, $J = 7.4$ Hz, 2H), 3.06 (t, $J = 7.6$ Hz, 2H); ^{13}C NMR (CDCl_3 , 100 MHz) δ (ppm): 197.9, 141.1, 139.5, 135.2, 129.4, 129.0, 128.9, 128.6, 128.5, 128.4, 126.2, 40.4, 30.1.

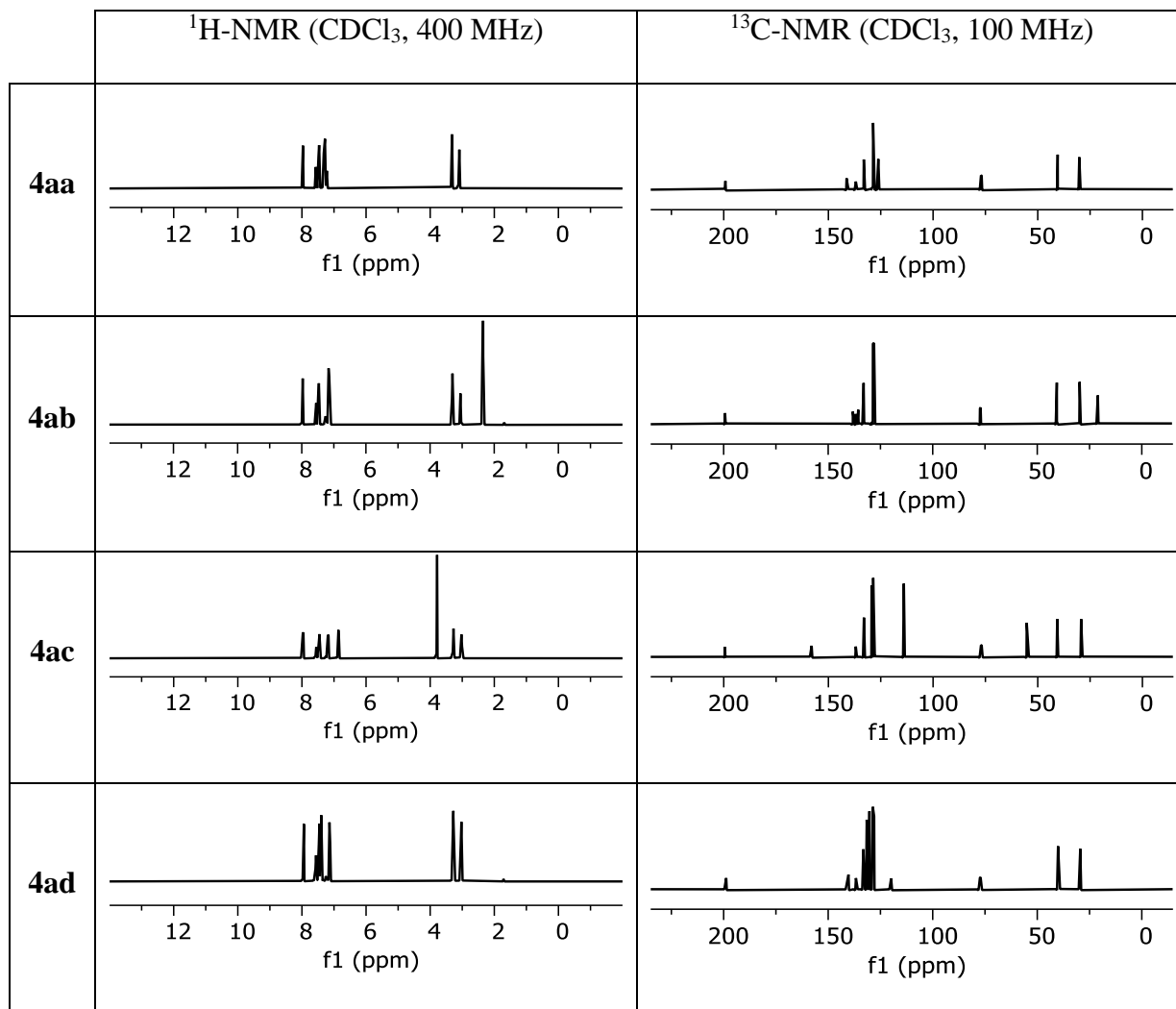
1-Phenyl-3-(p-tolyl)propan-1-one (4ab). Yield: 76%, white solid. ^1H NMR (CDCl_3 , 400 MHz) δ (ppm): 7.99 (d, $J = 8.0$ Hz, 2H), 7.56 (tt, $J_1 = 7.2$ Hz, $J_2 = 1.2$ Hz, 1H), 7.49–7.45 (m, 2H), 7.19–7.13 (m, 4H), 3.30 (t, $J = 7.6$ Hz, 2H), 3.07 (t, $J = 8.0$ Hz, 2H), 2.36 (s, 3H); ^{13}C NMR (CDCl_3 , 100 MHz) δ (ppm): 199.3, 138.2, 137.0, 135.6, 133.0, 129.2, 128.6, 128.3, 128.1, 40.6, 29.8, 21.0.

3-(4-Methoxyphenyl)-1-phenylpropan-1-one (4ac). Yield: 87%, white solid. ^1H NMR (CDCl_3 , 400 MHz) δ (ppm): 7.97 (d, $J = 8.0$ Hz, 2H), 7.56 (tt, $J_1 = 7.2$ Hz, $J_2 = 2.8$ Hz, 1H),

7.45 (t, $J = 7.6$ Hz, 2H), 7.18 (d, $J = 8.8$ Hz, 2H), 6.85 (d, $J = 9.2$ Hz, 2H), 3.79 (s, 3H), 3.28 (t, $J = 7.2$ Hz, 2H), 3.03 (t, $J = 8.0$ Hz, 2H); ^{13}C NMR (CDCl_3 , 100 MHz) δ (ppm): 199.3, 158.0, 136.9, 133.3, 132.9, 129.3, 128.6, 128.0, 113.9, 55.3, 40.7, 29.3.

3-(4-Bromophenyl)-1-phenylpropan-1-one (4ad). Yield: 79%, white solid. ^1H NMR (CDCl_3 , 400 MHz) δ (ppm): 7.95 (d, $J = 7.6$ Hz, 2H), 7.56 (t, $J = 7.0$ Hz, 1H), 7.45 (t, $J = 7.4$ Hz, 2H), 7.41 (d, $J = 8.4$ Hz, 2H), 7.13 (d, $J = 8.4$ Hz, 2H), 3.28 (t, $J = 7.4$ Hz, 2H), 3.03 (t, $J = 7.4$ Hz, 2H); ^{13}C NMR (CDCl_3 , 100 MHz) δ (ppm): 198.7, 140.2, 136.7, 133.1, 131.5, 130.2, 128.6, 127.9, 119.8, 40.0, 29.4.

3-(4-Chlorophenyl)-1-phenylpropan-1-one (4ae). Yield: 89%, white solid. ^1H NMR (CDCl_3 , 400 MHz) δ (ppm): 7.95 (d, $J = 7.6$ Hz, 2H), 7.56 (t, $J = 7.2$ Hz, 1H), 7.45 (t, $J = 8.0$ Hz, 2H), 7.26 (d, $J = 8.4$ Hz, 2H), 7.18 (d, $J = 8.4$ Hz, 2H), 3.28 (t, $J = 7.6$ Hz, 2H), 3.05 (t, $J = 7.4$ Hz, 2H); ^{13}C NMR (CDCl_3 , 100 MHz) δ (ppm): 198.7, 139.7, 136.7, 133.1, 131.8, 129.8, 128.6, 128.5, 127.9, 40.1, 29.4.



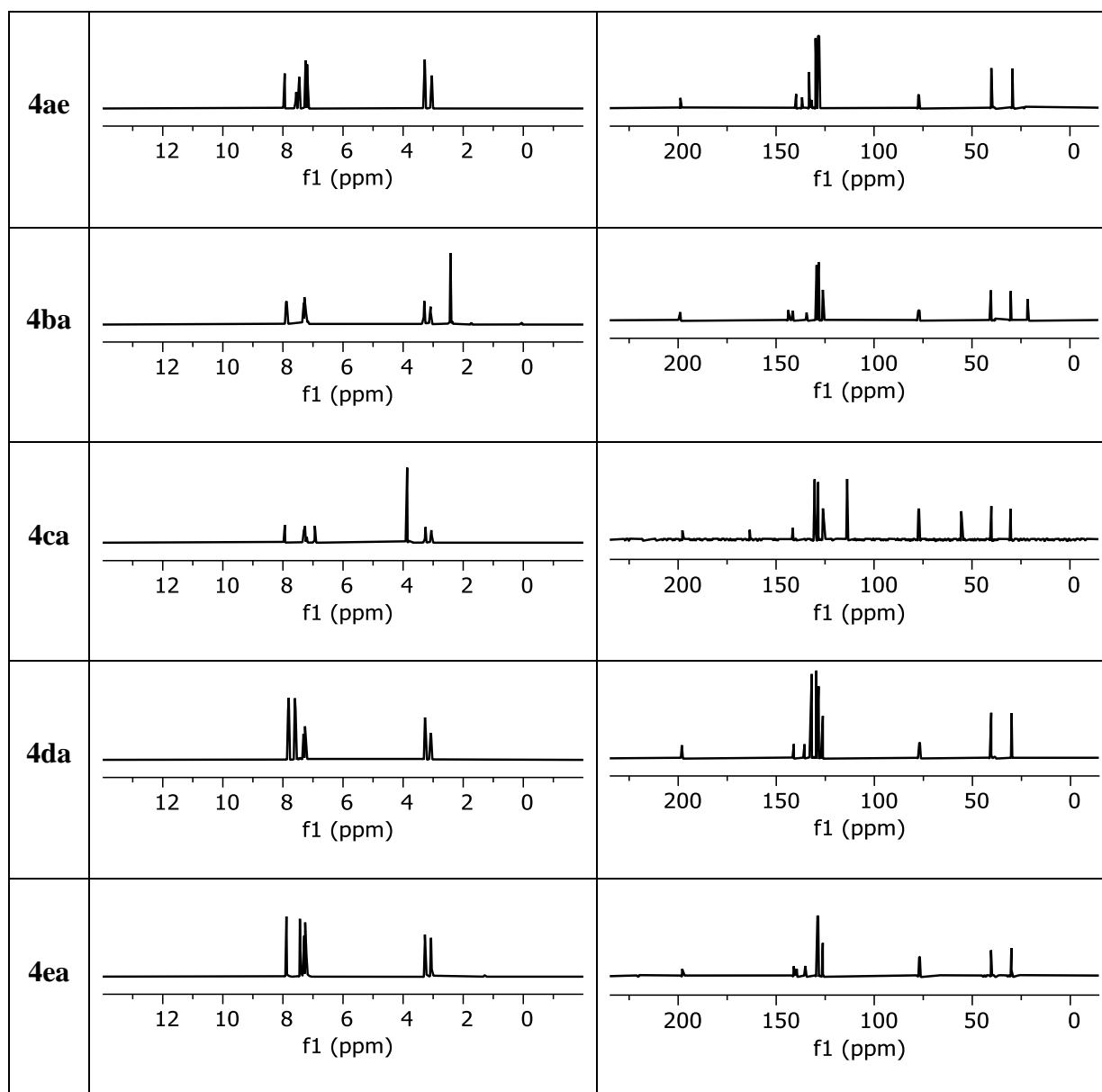


Figure 4. ^1H -NMR spectra of the catalytic products.

4. Conclusions

In this study, the preparation and characterization of Zn (II) and Cd (II) complexes (**1a-b**) were reported. Their catalytic activities were investigated for the α -alkylation of ketones. The zinc complex demonstrated higher catalytic activity compared to the cadmium complex under air atmosphere. Catalytic activity varies depending on the groups in the phenyl ring of acetophenone and benzyl alcohol. The best result was obtained using 4-chloro acetophenone and 4-chloro benzyl alcohol for 16 hours reaction time, and when **1a** was used as a catalyst, a yield of 83% was achieved. Based on these results, it is thought that the complexes obtained with Zn (II), which are quite cheap and abundant in nature, may be a good alternative to other metals frequently used in the α -alkylation reaction.

Ethics in Publishing

There are no ethical issues regarding the publication of this study.

References

- [1] (a) Narges, K., Abdolreza, R., Maasoumeh J. (2020). Silica Iminopyridine-Functionalized Nanomaghemite Enhances the Oxygenation Activity and Durability of Simple Co (II) Salophen Complex. *Appl. Organomet. Chem.*, *34*, e5535. (b) Hongyue, L., Dandan, X., Yan, N., Chao, W., Fengrong, X., Lei, L., Ping, X. (2019). Design, Synthesis and Biological Evaluation of Cobalt (II)-Schiff Base Complexes As ATP-Noncompetitive MEK1 Inhibitors. *J. Inorg. Biochem.*, *195*, 174-181.
- [2] Asraf, M. A., Ezugwu, C. I., Zakaria, C. M., Verpoort, F. (2019). Homogeneous Photochemical Water Oxidation with Metal Salophen Complexes in Neutral Media. *Photochem. Photobiol. Sci.*, *18*, 2782-2791.
- [3] Mehta, J. P., Parmar, D. K., Godhani, D. R., Nakum, H. D., Desai, N. C. (2016) Heterogeneous Catalysts Hold the Edge Over Homogeneous Systems: Zeolite-Y Encapsulated Complexes for Baeyer-Villiger Oxidation of Cyclohexanone. *J. Mol. Catal. A-Chem.*, *421*, 178-188.
- [4] (a) Yankin, A. N., Lukyanov, D. A., Beletskii, E. V., Bakulina, O. Y., Vlasov, P. S., Levin, O. V. (2019). Aryl-Aryl Coupling of Salicylic Aldehydes through Oxidative CH-activation in Nickel Salen Derivatives. *ChemistrySelect*, *4*, 8886-8890. (b) Choudhary, A., Das, B., Ray, S. (2016). Enhanced Catalytic Activity and Magnetization of Encapsulated Nickel Schiff-Base Complexes in Zeolite-Y: A Correlation with The Adopted Non-Planar Geometry. *Dalton Trans.*, *45*, 18967-18976.
- [5] Toniolo, D., Scopelliti, R., Zivkovic, I., Mazzanti, M. (2020). Assembly of High-Spin [Fe₃] Clusters by Ligand-Based Multielectron Reduction. *J. Am. Chem. Soc.*, *142*, 7301-7305.
- [6] (a) Ganesan, V., Yoon, S. (2020). Direct Heterogenization of Salphen Coordination Complexes to Porous Organic Polymers: Catalysts for Ring-Expansion Carbonylation of Epoxides. *Inorg. Chem.*, *59*, 2881-2889. (b) Elsebach, M., Sierda, E., Goedecke, J. J., Bignardi, L., Hermanowicz, M., Rohde, M., Wiesendanger, R., Bazarnik, M. (2020). In Situ Synthesis of Metal-Salophene Complexes on Intercalated Graphene. *J. Phys. Chem. C.*, *124*, 4279-4287.
- [7] Yoon, T. P., Jacobsen, E. N. (2003). Privileged Chiral Catalysts, *Science*, *299*, 1691-1693.
- [8] (a) Kavukcu, S. B., Günnaz, S., Şahin, O., Türkmen, H. (2019). Piano-Stool Ru (II) Arene Complexes That Contain Ethylenediamine and Application in Alpha-Alkylation Reaction of

Ketones with Alcohols. *Appl. Organometal. Chem.*, 33, e4888. (b) Chakrabarti, K., Maji, M., Panja, D., Paul, B., Shee, S., Das, G. K., Kundu, S. (2017). Utilization of MeOH as a C1 Building Block in Tandem Three-Component Coupling Reaction. *Org. Lett.*, 19, 4750-4753.

[9] Wang, R., Huang, L., Du, Z., Feng, H. (2017). RhCl(CO)(PPh₃)₂ Catalyzed α -alkylation of Ketones with Alcohols. *J. Organomet. Chem.*, 846, 40–43

[10] (a) Genç, S., Günnaz, S., Çetinkaya, B., Gülcemal, S., Gülcemal, D. (2018). Iridium(I)-Catalyzed Alkylation Reactions to Form α -Alkylated Ketones. *J. Org. Chem.*, 83, 2875-2881. (b) Genç, S., Arslan, B., Gülcemal, S., Günnaz, S., Çetinkaya, B., Gülcemal, D. (2019). Iridium(I)-Catalyzed C–C and C–N Bond Formation Reactions via the Borrowing Hydrogen Strategy. *J. Org. Chem.*, 84, 6286-6297.

[11] Yang, Y., Qin, A., Zhao, K., Wang D., Shi, X. (2016). Design and Synthesis of Alanine Triazole Ligands and Application in Promotion of Hydration, Allene Synthesis and Borrowing Hydrogen Reactions. *Adv. Synth. Catal.*, 358, 1433-1439.

[12] Alanthadka, A., Bera, S., Banerjee, D. (2019). Iron-Catalyzed Ligand Free α -Alkylation of Methylene Ketones and β -Alkylation of Secondary Alcohols Using Primary Alcohols. *J. Org. Chem.*, 84, 11676-11686.

[13] Peña-López, M., Piehl, P., Elangovan, S., Neumann, H., Beller, M. (2016). Manganese-Catalyzed Hydrogen-Autotransfer C-C Bond Formation: α -Alkylation of Ketones with Primary Alcohols. *Angew. Chem., Int. Ed.*, 55, 14967-14971.

[14] Zhang, G., Yin, Z., Zheng, S. (2016). Cobalt-Catalyzed N-Alkylation of Amines with Alcohols. *Org. Lett.*, 18, 300-303.

[15] (a) Bains, A. K., Kundu, A., Yadav, S., Adhikari, D. (2019). Borrowing Hydrogen-Mediated N-Alkylation Reactions by a Well-Defined Homogeneous Nickel Catalyst. *ACS Catal.*, 9, 9051-9059.

[16] (a) Pagadala, R., Ali, P., Meshram, J. S. (2009). Microwave Assisted Synthesis and Characterization of N,N'-Bis(salicylaldehyde)ethylenediamine Complexes of Mn(II), Co(II), Ni(II), and Zn(II). *J. Coord. Chem.*, 62, 4009–4017. (b) Hille, A., Ott, I., Kitanovic, A., Kitanovic, I., Alborzinia, H., Lederer, E., Wölf, S., Metzler-Nolte, N., Schäfer, S., Sheldrick, W. S., Bischof, C., Schatzschneider, U., Gust, R. (2009) [N,N'-Bis(salicylidene)-1,2-phenylenediamine]metal Complexes with Cell Death Promoting Properties. *J. Biol. Inorg. Chem.*, 14, 711–725. (c) Chong, J. H., Ardakani, S. J., Smith, K. J., MacLachlan, M. J. (2009). Triptycene-Based Metal Salphens-Exploiting Intrinsic Molecular Porosity for Gas Storage. *Chem.-Eur. J.*, 15, 11824–11828.

***In Vitro* Leishmanicidal Activity of Different Chalcone, Phthalonitrile and Their Peripheral Tetra Zinc Phthalocyanine Derivatives**

Ayşe AKTAŞ KAMILOĞLU^{1*}, Şahin DİREKEL², Gonca ÇELİK³

¹ Artvin Vocational School, Artvin Çoruh University, 08100, Artvin, Turkey

² Department of Medical Microbiology, Faculty of Medicine, Giresun University, 28100 Giresun, Turkey

³ Department of Chemistry, Faculty of Science, Karadeniz Technical University, 61080
Trabzon, Turkey

Received:28/07/2022, **Revised:** 29/09/2022, **Accepted:** 17/10/2022, **Published:** 30/12/2022

Abstract

In this study, *in vitro* leishmanicidal activities of different chalcone compounds (**5-8**), phthalonitrile derivatives (**5a-8a**), and zinc phthalocyanine (**5b-8b**) complexes bearing chalcone compound in peripheral positions were investigated. Phthalonitrile derivatives were obtained in the reaction of 4-nitrophthalonitrile with chalcone compound obtained by the reaction of acetophenone and various aldehydes. Zinc phthalocyanine complexes containing chalcone in the peripheral position were obtained as a result of the reaction of the synthesized phthalonitrile derivative with $Zn(CH_3COO)_2$ metal salt. The characterization of the synthesized original compounds (**8**, **8a** and **8b**) was performed by various spectroscopic methods (IR, 1H and ^{13}C NMR, MALDI-TOF-MS and UV-Vis). Leishmaniasis is a disease lead to by parasites of the genus *Leishmania*, which can result in death as well as various clinical syndromes, generally in developing countries. New drug studies are needed because the drugs used in the treatment are toxic and resistance develops against them. In this study, the leishmanicidal activities of synthesized chalcone, phthalonitrile and phthalocyanine series substances against *Leishmania infantum* and *Leishmania major* parasites were evaluated for the first time.

Keywords: Chalcone, phthalocyanine, *leishmania promastigotes*, anti-leishmania

Farklı Kalkon, Ftalonitril ve Periferik Tetra Çinko Ftalosiyenin Türevlerinin *In Vitro* Layşmanyasidal Aktivitesi

Öz

Bu çalışmada, farklı kalkon bileşikleri (5-8), ftalonitril türevleri (5a-8a) ve periferik pozisyonlarda kalkon bileşiği taşıyan çinko ftalosiyenin (5b-8b) komplekslerinin *in vitro* layşmanisidal aktiviteleri araştırıldı. Asetofenon ve çeşitli aldehitlerin reaksiyonu ile elde edilen kalkon bileşikleri ile 4-nitroftalonitrilin reaksiyonundan ftalonitril türevleri elde edilmiştir. Sentezlenen ftalonitril türevinin $Zn(CH_3COO)_2$ metal tuzu ile reaksiyonu sonucunda periferik pozisyonda kalkon içeren çinko ftalosiyenin kompleksleri elde edilmiştir. Sentezlenen orijinal bileşiklerin (8, 8a ve 8b) karakterizasyonu çeşitli spektroskopik yöntemlerle (IR, 1H ve ^{13}C NMR, MALDI-TOF-MS ve UV-Vis) gerçekleştirilmiştir. Layşmaniasis, genellikle gelişmekte olan ülkelerde, Layşmania cinsi parazitlerinin neden olduğu, ölüme ve çeşitli klinik sendromlara neden olabilen bir hastalıktır. Tedavide kullanılan ilaçların toksik olması ve bunlara karşı direnç gelişmesi nedeniyle yeni ilaç çalışmalarına ihtiyaç duyulmaktadır. Bu çalışmada, sentezlenen kalkon, ftalonitril ve ftalosiyenin serisi maddelerin *Layşmania infantum* ve *Layşmania major* parazitlerine karşı layşmaniasidal aktiviteleri ilk kez değerlendirilmiştir.

Anahtar Kelimeler: Kalkon, ftalosiyenin, *layşmanyaz promastigotları*, anti-layşmanyaz aktivite

1. Introduction

Leishmaniasis is an overlooked tropical parasitic disease found worldwide in tropical, subtropical and some countries of southern Europe. The disease still maintains its importance in developing countries. The disease is passed on humans by the bite of phlebotoma sand flies and has several different clinical forms [1]. The first form is visceral leishmaniasis (VL) can be fatal if left untreated. VL is diagnosed with weight loss, bouts of fever, anemia and spleen and liver enlargement. Most cases are detected in Brazil, India and East African countries. The most prevalent form of leishmaniasis is the cutaneous form, which causes skin lesions, primarily ulcers, on exposed parts of the body. The other form is mucocutaneous leishmaniasis, which usually affects the mucous membranes of the nose, mouth and throat in countries such as Bolivia, Brazil, Ethiopia and Peru (WHO). This disease is endemic in 98 countries and more than 350 million people are at risk of infection. It also causes 20000-40000 deaths worldwide each year [2]. There is no effective vaccine to prevent the disease. Pentavalent antimony compounds (SbV) are the first-choice drugs for the treatment of all types of leishmaniasis. In the treatment of the disease, drugs such as liposomal amphotericin B, azole groups, miltefosine and paromomycin are preferred as the second choice. Due to the high toxicity, cost and clinical resistance of existing drugs, new drug development against Leishmaniasis is needed [3]. In recent years, many studies have been carried out to develop drugs that are safe, inexpensive and have few side effects. For this purpose, antileishmanial tests were carried out on various synthetic and natural compounds [4,5]. In this work, it was aimed to researched the leishmanicidal activity of chalcone compounds against *Leishmania infantum* and *Leishmania major* promastigotes by microdilution broth method containing alamar blue.

Chalcone is an aromatic ketone possessing an α,β -unsaturated carbonyl group consisting of two aromatic rings. Chalcone derivative compounds have recently attracted the attention of researchers, especially in the departments of synthetic organic and pharmaceutical chemistry. Medicinal chemists interest in chalcone compounds because of their biological activity, which include anti-bacterial [6], antiobesity [7,8], anticancer [9], antioxidant [10,11], antileishmanial [12,13], anti-diabetic [14], antifungal [15], antiulcer [16], antitubercular [17], anti-inflammatory [18], antimalarial [19] and antiviral [20].

Phthalocyanines (Pcs), which have planar macrocyclic molecules and contain nitrogen atoms in the inner loop, contain a class of highly robust and versatile chemical compounds [21]. Phthalocyanines, which are still of great technological importance for the production of green and blue pigments, have applications such as such as DNA-binding and enzyme inhibition [22], catalysts [23,24], metal sensors [25], electrochemistry [26,27], solar cells [28], Langmuir-Blodgett films [29], fluorometric properties [25], liquid crystals [30], photodynamic therapy (PDT) [31], electrophotography [32], antimicrobial agent [33], optical disks [34], electrochromic displays [35], antioxidant [36] and modified supports in recent years. The leishmania activity studies of phthalocyanines, which have been studied in many application

areas, have not been found in the literature before. Since phthalocyanines (especially zinc phthalocyanines) show activity especially in the biological field [22, 33, 36, 31], this study was designed due to it is a question of how they will show activity against *Leishmania* parasites.

For the purpose of the study, first of all, we synthesized different chalcone compounds (5, 6, 7 and 8) by thinking that chalcone compounds may be an active in biological studies because of their medical applications in literature. In the second step, phthalonitrile derivatives (5a-8a), which are the starting compound for the synthesis of zinc phthalocyanine compounds were obtained the reaction of chalcone compounds with 4-nitrophthalonitrile. In the last part of the synthesis stage, the synthesis of peripheral tetra zinc phthalocyanine complexes (5b-8b) take place as a result of the reaction of the synthesized phthalonitrile derivatives with the zinc salt. The synthesized original compounds (8, 8a and 8b) were characterized by FT-IR, ¹H NMR, ¹³C NMR, UV-Vis (for zinc phthalocyanine 8b) and mass spectrometry. In the last part of the study, leishmanicidal activity of the synthesized chalcone (5, 6, 7 and 8), phthalonitrile (5a-8a) and zinc phthalocyanine (5b-8b) compounds were investigated.

2. Methods and Material

The used materials were supplied as Supplementary Information.

2.1. Synthesis

2.1.1. (2E)-3-(5-ethylthiophen-2-yl)-1-(3-hydroxyphenyl)prop-2-en-1-one (8)

The new chalcone compound (8) was synthesized using the method in the literature [37,38,39]. You can find detailed information in Supplementary Information. The obtained red product was cleansed by column chromatography (SiO₂) method using mobile phase CHCl₃ (chloroform) solvent. The structure of the pure compound was characterized by spectroscopic methods. Yield: 1.61 g (44 %). IR (ATR) (ν, cm⁻¹): 3333 (O–H), 3068 (Ar–H), 2969-2873 (Aliph.–H), 1643 (C=O), 1558-1446 (C=C). ¹H NMR (400 MHz, CDCl₃, ppm): δ = 7.94-7.90 (d, *J*=15Hz, 1H, =CH); δ = 7.65 (s, 1H, Ar–H); δ = 7.57-7.55 (d, *J*=8Hz, 1H, Ar–H); δ = 7.40-7.36 (t, *J*=15, 1H, =CH); δ = 7.23-7.19 (m, 2H, Ar–H); δ = 7.14-7.12 (d, *J*=6Hz, 1H, Ar–H); δ = 6.81-6.78 (m, 1H, Ar–H), δ = 6.57 (s, 1H, O–H), δ = 2.90-2.88 (k, 2H, –CH₂), δ = 1.35 (t, 3H, –CH₃). ¹³C NMR (400 MHz, CDCl₃, (δ) ppm): 190.20 (C=O), 156.46 (C–OH), 152.68, 139.67, 138.35, 137.94, 133.15, 129.83, 125.12, 120.76, 120.24, 119.36, 115.09, 23.99 (–CH₂), 15.56 (–CH₃). MALDI-TOF-MS (m/z) Found: 258.81 [M]⁺.

2.1.2. 5-{3-[(2E)-3-(5-ethyl-2-thienyl)prop-2-enoyl]phenoxy}phthalonitrile (8a)

The new chalcone bearing phthalonitrile compound (8a) was synthesized using the method in the literature [37,38,39]. You can find detailed information in Supplementary Information. The dried product was cleansed by column chromatography using alumina (Al₂O₃) as column material and a CHCl₃:EtOH (5:1) solvent system as mobile phase. An oily brown pure product was obtained. Yield: 0.72 g (30 %). IR (ATR) (ν, cm⁻¹): 3071 (Ar–H), 2965-2855 (Aliph.–H), 2232 (C≡N), 1664 (C=O), 1578-1436 (C=C), 1385-1246 (Ar–O–Ar). ¹H NMR (400 MHz, CDCl₃, ppm): δ= 8.03 (s, 1H, Ar–H); δ = 7.92 (d, *J*= 8Hz, 1H, Ar–H); δ= 7.78 (d, *J*= 8Hz, 2H, Ar–H); δ= 7.69 (s, 2H, Ar–H); δ= 7.63 (t, 2H, Ar–H); δ = 7.33 (m, 3H, =CH and CDCl₃); δ = 2.65 (s, 2H, –CH₂); δ = 1.27 (s, 3H, –CH₃). ¹³C NMR (400 MHz, CDCl₃, (δ)ppm): 196.52

(C=O), 162.55 (ArC–O), 161.20 157.14, 154.14, 139.71, 135.55, 131.04, 126.20, 125.17, 125.12, 121.74, 121.68, 121.64, 119.92, 117.86 (–C≡N), 115.20 (–C≡N), 114.78, 109.60, 108.93, 108.50, 31.44, 26.71. MALDI-TOF-MS (m/z) Found: 381.13 [M-3]⁺.

2.1.3. Zinc(II) phthalocyanine (8b)

The new chalcone substituted zinc phthalocyanine (8b) was synthesized using the method in the literature [37,38,39]. You can find detailed information in Supplementary Information. The resulting crude product was cleaned by column chromatography on alumina (Al₂O₃) by using CHCl₃:CH₃OH as the eluent system. Yield: 7 mg (14%). mp: >300 °C. IR (ATR) (ν, cm⁻¹): 3061 (Ar–H), 2.924-2854 (Aliph.–H), 1644 (C=O), 1599-1435 (C=C), 1359-1260 (Ar–O–Ar). ¹H NMR (400 MHz, DMSO-d₆ ppm) δ = 8.32 (s, 4H, Ar–H), 3.39 (s, 8H, –CH₂), 1.62 (m, 12H, –CH₃). UV-Vis (DMF): λ_{max}, nm (log ε): 681 (5.02), 613 (4.56), 352 (5.16).

2.2. Determination of in vitro Leishmanicidal Activities

The antiparasitic properties of chalcone, phthalonitrile and their zinc phthalocyanine derivatives were defined by testing their leishmanicidal activities against *Leishmania infantum* and *Leishmania major* promastigotes. The studies were achieved *in vitro* using microdilution broth method containing the alamar blue. The used method and materials were given as Supplementary Information.

3. Results and Discussion

3.1. Synthesis and Characterization

The compounds in the study and the original synthesized compounds were summarized in Figures 1 and 2. Chalcone derivatives bearing different groups (5, 6 and 7), phthalonitriles (5a, 6a and 7a) and their zinc phthalocyanine complexes (5b, 6b and 7b) were mentioned in our previous studies (Figure 3) [37-39].

The original chalcone compound bearing the thiophene group (8) was obtained by the Claisen-Schmidt reaction of 5-ethylthiophene-2-carbaldehyde (a) and 1-(3-hydroxyphenyl) ethanone (4) (aromatic ketone) (Figure 1).

The synthesis of the chalcone-based phthalonitrile derivative (8a) was accomplished by the nucleophilic substitution reaction between the chalcone compound (2*E*)-3-(5-ethylthiophen-2-yl)-1-(3-hydroxyphenyl)prop-2-en-1-one (8) and 4-nitrophthalonitrile (Figure 2). Synthesized phthalonitrile compound (8a) containing thiophene-chalcone group was used to synthesize zinc phthalocyanine compound (8b). The Zn(II)Pc (8b) was achieved from the reactions of 5-{3-[(2*E*)-3-(5-ethyl-2-thienyl)prop-2-enoyl]phenoxy}phthalonitrile (8a) with the metal salt Zn(CH₃COO)₂ in *n*-pentanol and DBU as the catalyst. After purification, spectroscopy techniques (IR, NMR and mass) were used to identify of the structure of chalcone (8), phthalonitrile (8a) and zinc phthalocyanine compound (8b) (Figures 4-7).

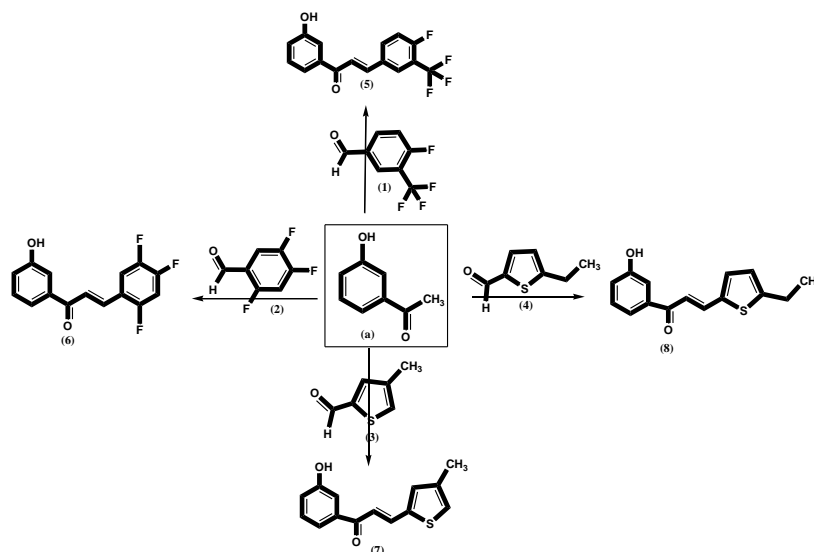


Figure 1. The synthetic route to the chalcone compounds (5) [37], (6) [39], (7) [38] and (8)

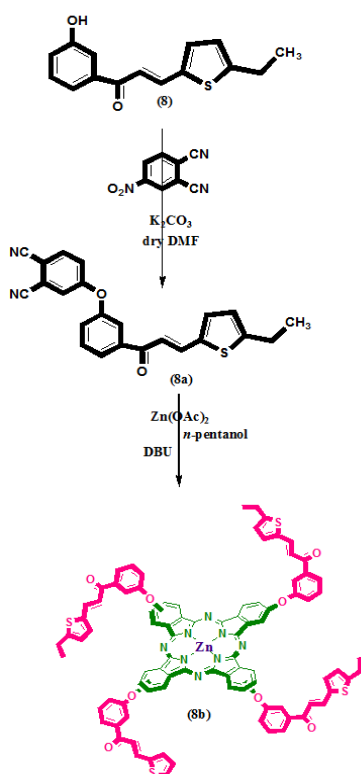


Figure 2. The synthetic route to the original phthalonitrile compound (8a) and zinc phthalocyanine (8b)

In the IR spectrum of chalcone compound (2*E*)-3-(5-ethylthiophen-2-yl)-1-(3-hydroxyphenyl)prop-2-en-1-one (8), the bands were observed at 3333 cm^{-1} (OH stretching), 3068 cm^{-1} (aromatic CH stretching vibration), $2969\text{--}2873\text{ cm}^{-1}$ (aliphatic CH stretching vibration), 1643 cm^{-1} (C=O stretching) and 1558 cm^{-1} (Ar=C=C stretching vibrations). In the IR spectrum of (8a), the expected after nucleophilic substitution reaction, the nitrile strong

characteristic stretching band at 2232 cm^{-1} ($\text{C}\equiv\text{N}$) was clearly observed. The band belonging to the OH group (hydroxyl) at 3333 cm^{-1} on the chalcone compound 8 was disappeared. Other characteristic vibration peaks for phthalonitrile derivative (8a) were observed aromatic C–H stretching at 3071 cm^{-1} , aliphatic C–H stretching at $2965\text{--}2855$; carbonyl groups ($\text{C}=\text{O}$) at 1664 cm^{-1} , Ar–C=C group stretching at $1578\text{--}1436\text{ cm}^{-1}$ and ether group (Ar–O–Ar) stretching at $1385\text{--}1246\text{ cm}^{-1}$.

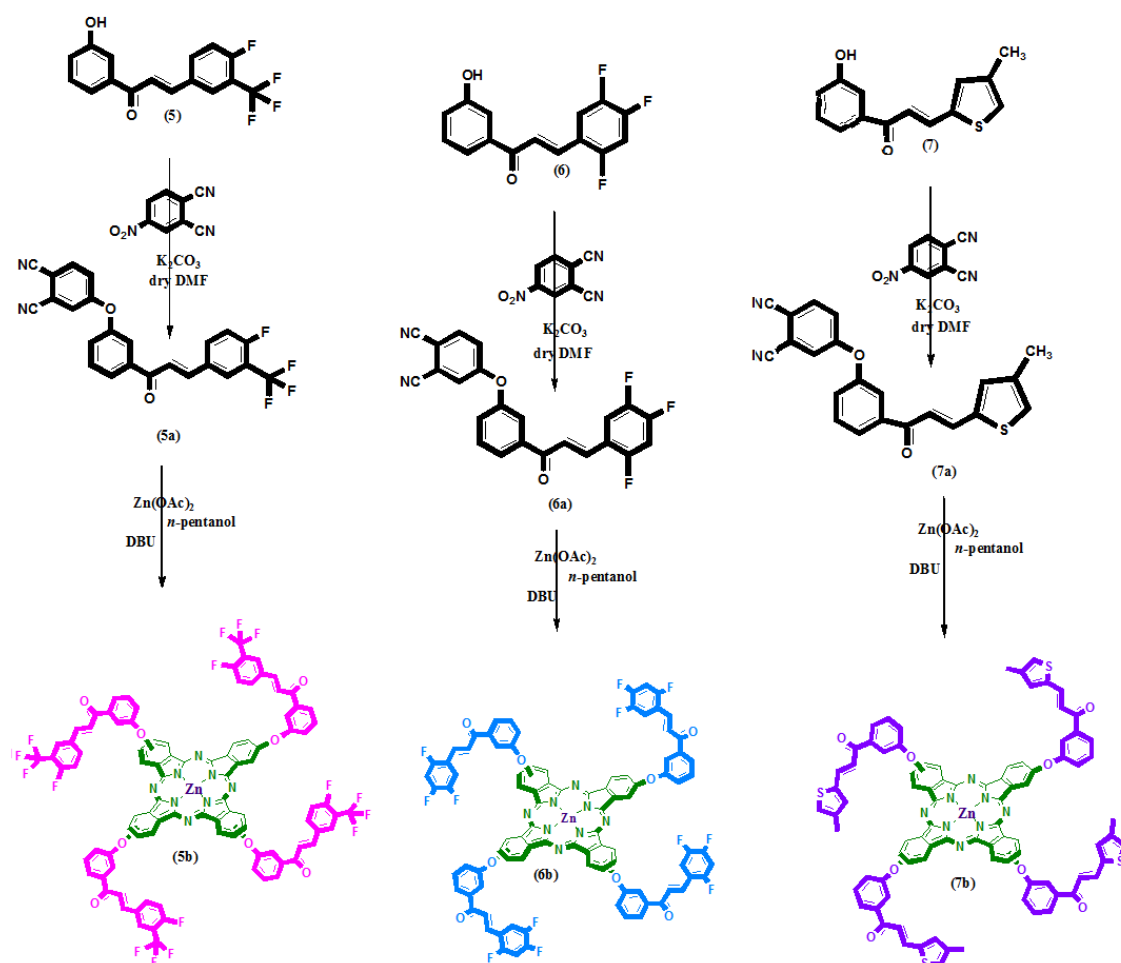


Figure 3. The synthetic route to the phthalonitrile compounds (5a [37], 6a [39], 7a [38]) and zinc phthalocyanine (5b [37], 6b [39], 7b [38])

In the IR spectrum of zinc phthalocyanine (ZnPc), no nitrile ($\text{C}\equiv\text{N}$) vibration band at 2232 cm^{-1} is considered as a clue of the formation of ZnPc (8b). The remaining IR stretching vibrations of (8b) were akin to the phthalonitrile compound (8a) (Figure 4).

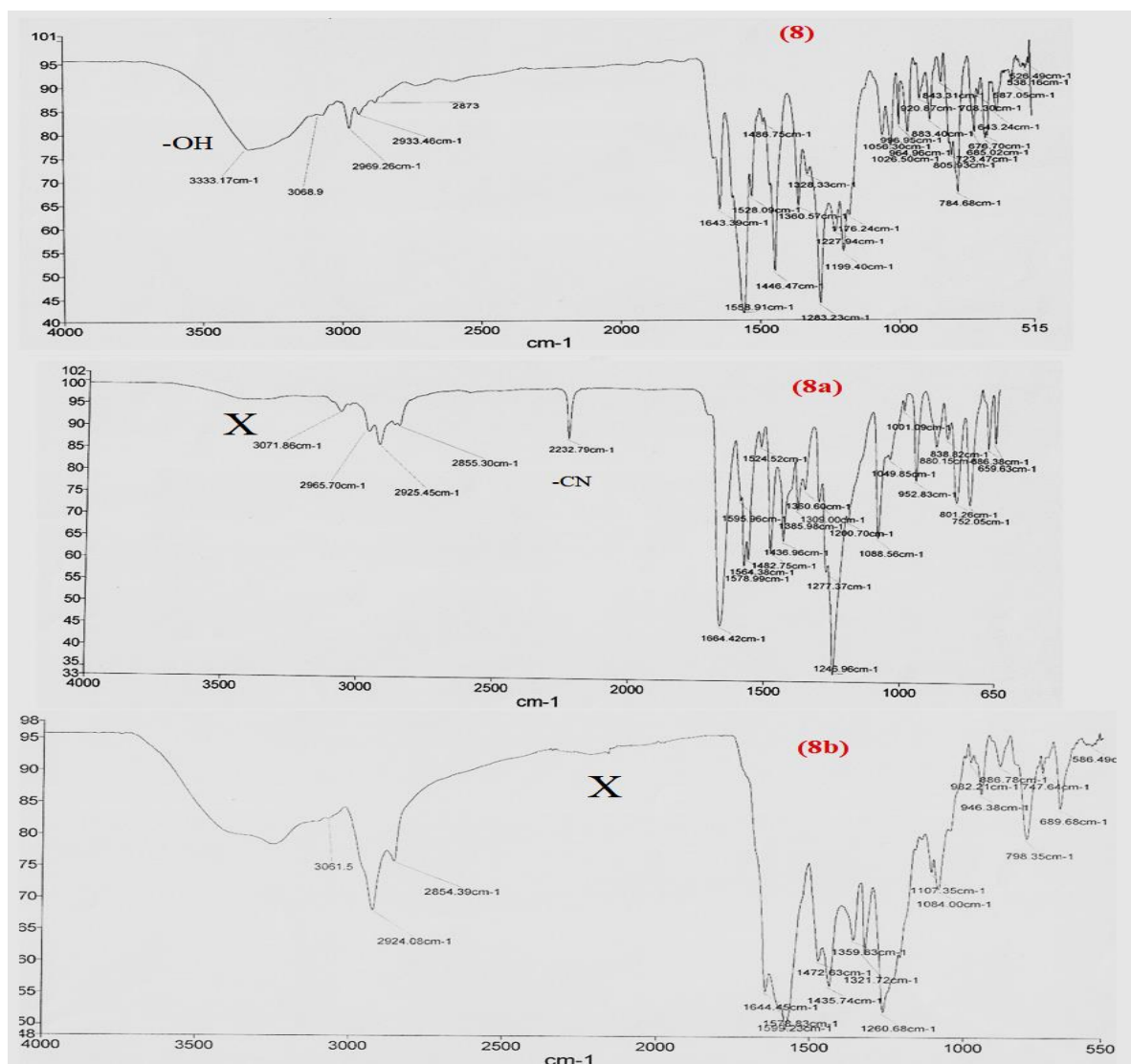


Figure 4. FT-IR spectra of original chalcone (8), phthalonitrile (8a) and zinc phthalocyanine (8b) compounds

In ^1H NMR spectrum of chalcone compound (8), phenolic OH signal was observed at 6.57 ppm together with the aromatic and aliphatic CH signals (Figure 5a). The C=O group was detected in the ^{13}C NMR spectrum, at 190.20 ppm, is evidence of the formation of the target structure (8) (Figure 5b). In the ^1H NMR spectrum of the phthalonitrile compound (8a), the peak for OH group at 6.57 ppm was disappeared and that for aromatic and aliphatic protons were observed at around 8.03-7.33 ppm and 2.65-1.27 ppm, respectively. ^{13}C NMR spectrum of 8a exhibited carbonyl carbon atom (C=O) at 196.52 ppm, nitrile carbon atoms (C \equiv N) at 117.86 and 115.20 ppm, aromatic carbon atoms between at 162.55 ppm and 108.50 ppm, and aliphatic carbon atoms (-CH₂ and -CH₃) 31.44 ppm and 26.71 ppm (SI Figure 1 in Supplementary Information). In the ^1H NMR spectrum of zinc(II) phthalocyanine complex (8b) exhibited aromatic protons at 8.32 (s, 44H, Ar-H) and aliphatic protons at 3.39 (s, 8H, -CH₂), 1.62 (m, 12H, -CH₃).

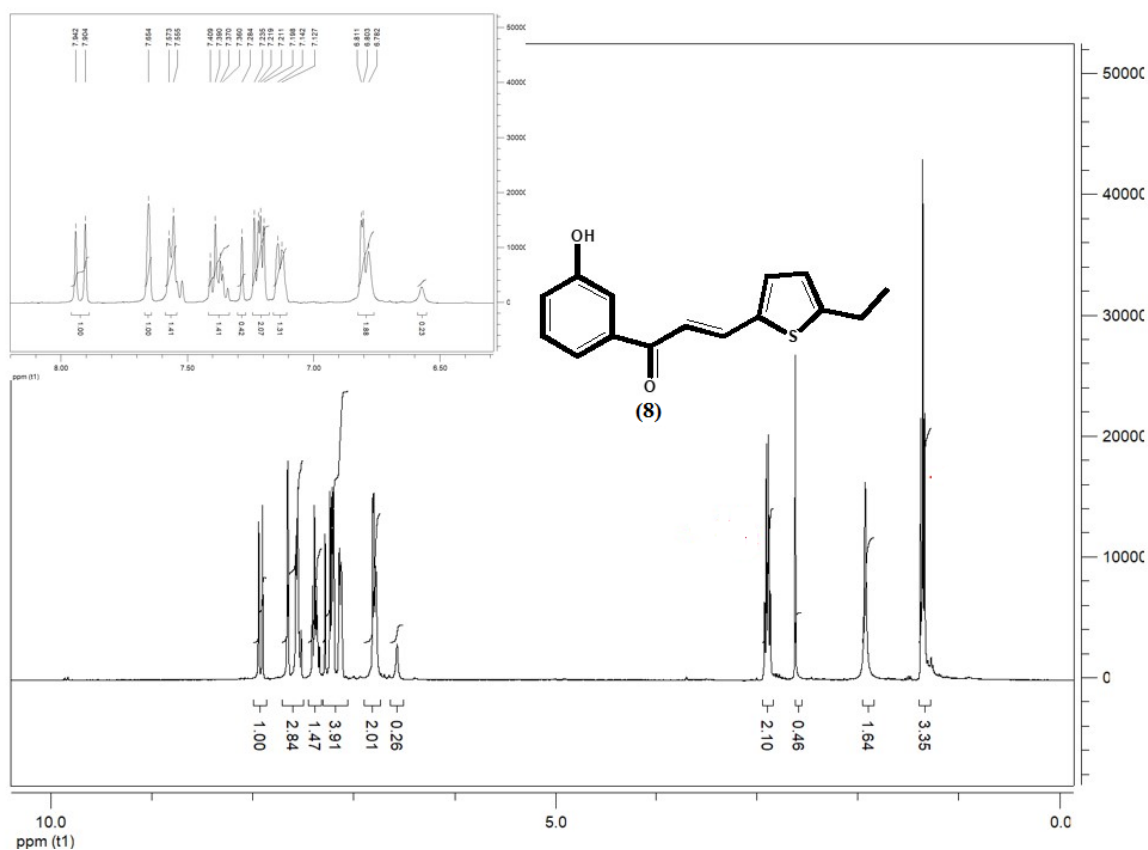


Figure 5a. ¹H NMR spectrum of original chalcone compound (8)

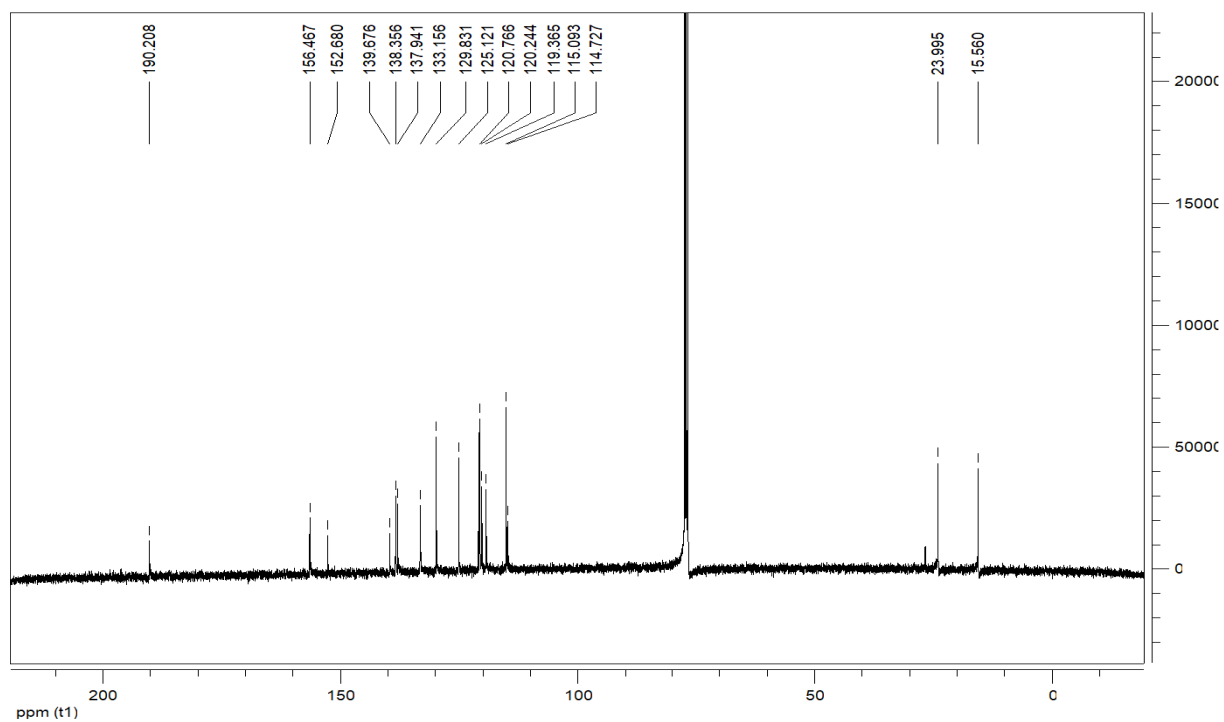


Figure 5b. ¹³C NMR spectrum of original chalcone compound (8).

In the MALDI-TOF-MS spectra (Figure 6a and 6b), the molecular ion peaks of chalcone (8) and phthalonitrile (8a) were observed at 258.81 $[M]^+$ and 381.13 $[M-3H]^+$, respectively. But the molecular ion peak of ZnPc (8b) was not detected due to non-ionisation.

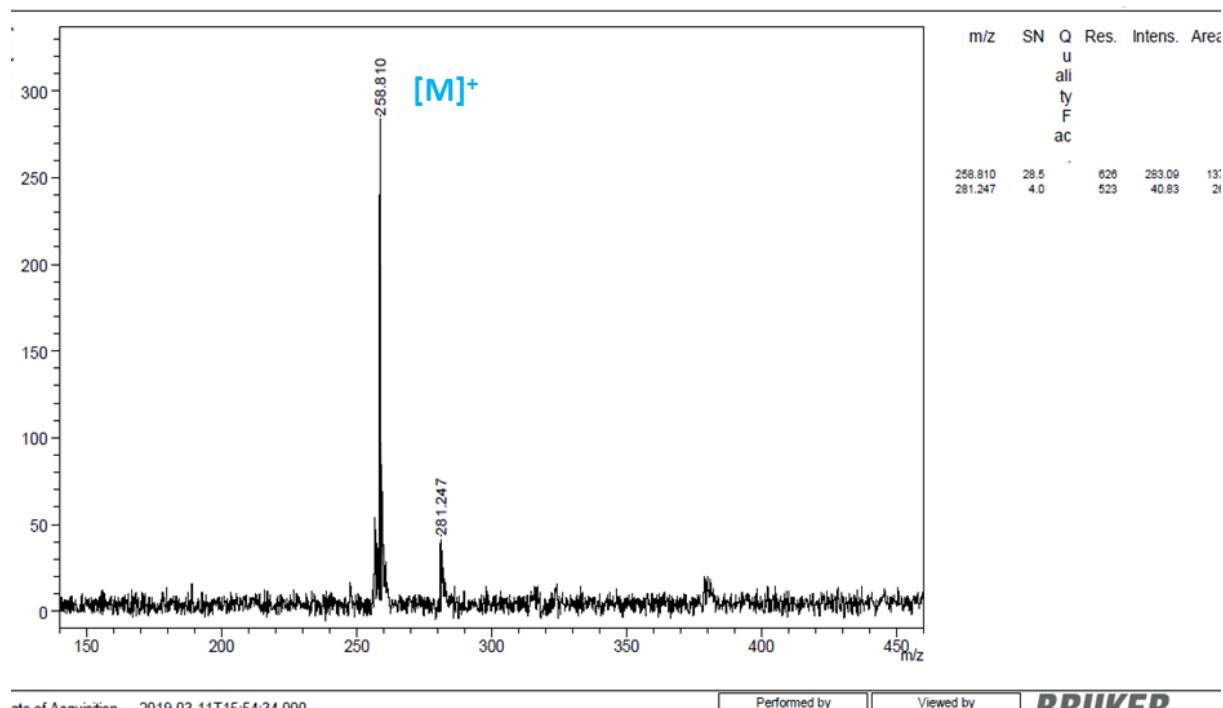


Figure 6a. MALDI-TOF-MS spectra of the chalcone compound (8)

As seen in our previous study [11,37,38,39], many fragmentation products peak are seen in the mass spectrum of phthalonitrile compounds containing chalcone (Figure 6b).

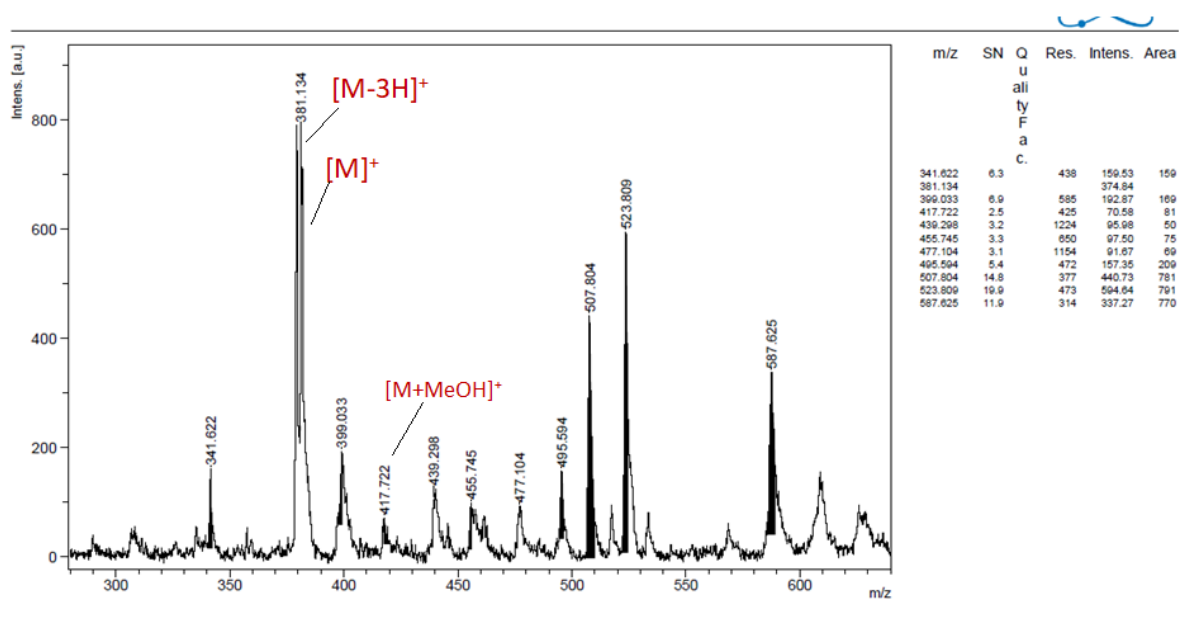


Figure 6b. MALDI-TOF-MS spectra of the phthalonitrile derivative bearing chalcone group (8a).

3.2. UV-Vis absorption spectra and aggregation properties of ZnPc (8b)

Since phthalocyanines are rich in π electrons, they give characteristic absorption bands corresponding to $n-\pi^*$ or $\pi-\pi^*$ electronic transitions in the ultraviolet and visible region [25]. The UV-vis spectra of phthalocyanines in solution display two strong characteristic absorption bands in the UV-visible (UV-Vis) region. The first is the Soret Band ($\pi-\pi^*$) at 300-500 nm in the near UV, while the second is the Q Band ($n-\pi^*$) at 600-700 nm in the red region of the spectrum [33]. It is important to investigate the absorption properties of phthalocyanines to determine their usability in many applications.

The aggregation depends on the type of solvent, metal ions in the core, pH of the solution, concentration, temperature and the structures of the substituents [25]. In this study, the aggregation behavior of ZnPc (8b) was investigated in different solvents in the UV-Vis spectroscopy (Figure 7) (Table 1).

Table 1. Electronic spectral data for the ZnPc (8b) in various solvents at 1×10^{-5} M.

Zinc Phthalocyanine (8b)		
Solvents	Q band, λ_{\max} (nm)	(log ϵ)
CHCl ₃	685 /616	(4.97) /(4.62)
DCM	683 /615	(5.02) /(4.61)
DMF	681 /613	(5.05) /(4.69)
DMSO	683 /615	(5.05) /(4.78)

The absorption intensities of Q band vary markedly by the solvent. Therefore, it is important to examine the aggregation behavior of the ZnPc (8b) in assorted solvents such as DMSO, DMF, chloroform (CHCl₃) and dichloromethane (DCM). The effects of these solvents on the aggregation of ZnPc (8b) were shown in Figure 7. ZnPc (8b) demonstrated the highest absorbance value in CHCl₃ and the lowest absorbance value in DMF.

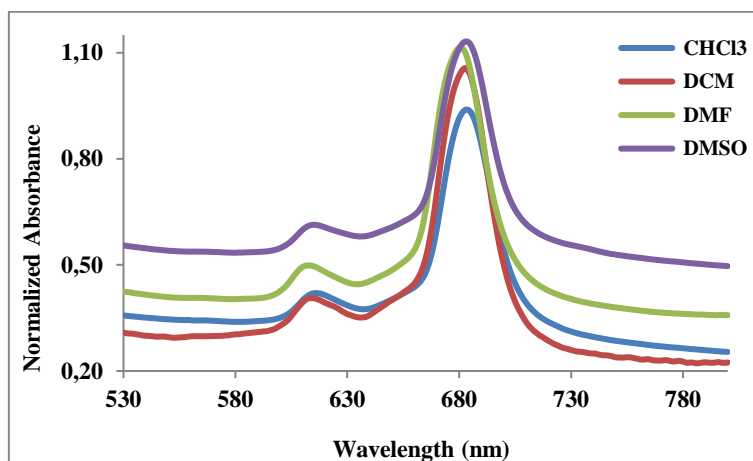


Figure 7. UV-Vis spectrum of zinc phthalocyanine compound (8b)

3.3. Leishmanicidal Activity Results

Leishmanicidal activities of compounds (5-8; 5a-8a; 5b-8b except 7b) against *Leishmania infantum* and *Leishmania major* promastigotes were ascertained *in vitro* by microdilution broth assay with alamar blue. Chalcone compounds (5-8) were found to be efficient at different concentrations (LC: 156-312 $\mu\text{g/ml}$). While the chalcone-derived phthalonitrile compounds except 7a and 8a showed activity at high concentrations, zinc phthalocyanine compounds (5b, 6b and 8b) bearing different chalcone group did show no activity at the concentrations studied (Figures 8- 9, and Table 2).

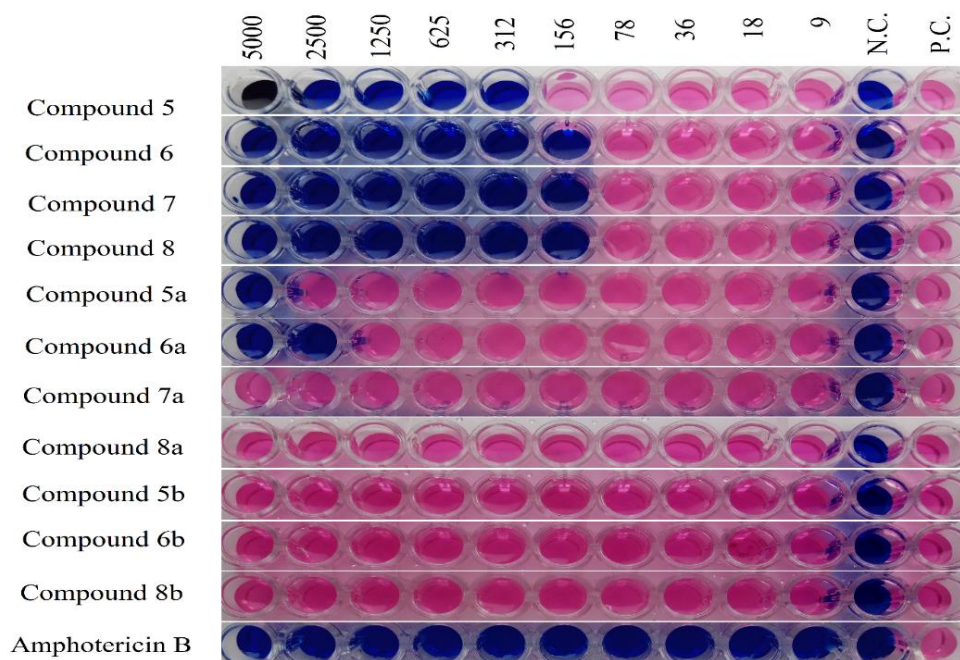


Figure 8. *In vitro* leishmanicidal activity results of compounds.

It is seen in the literature that chalcone compounds with different chemical structures have been studied at different concentrations and with different *Leishmania* species by different methods [40,41]. It would not be correct to compare the *Leishmania* activity results of this study with

literature. While IC₅₀ was studied in most articles [40,41], in our study the full leishmanicidal activity was studied (it can be called IC₁₀₀). There should be no living parasites. In addition, the concentrations of the compounds were calculated as microgram/milliliter (µg/mL) and dilution was made accordingly. Among the leishmania activity studies in the literature conducted with the same method, it was observed that the leishmania activities of the chalcone derivatives synthesized were active compared to other chemical structures [42,43].

Table 2. The Leishmanicidal Concentration (LC) values

Compounds	LC value for <i>Leishmania infantum</i> (µg/mL)	LC value for <i>Leishmania major</i> (µg/mL)
(5)	312	156
(6)	156	156
(7)	156	156
(8)	156	312
(5a)	5000	5000
(6a)	2500	2500
(7a)	>5000	>5000
(8a)	>5000	>5000
(5b)	>5000	>5000
(6b)	>5000	>5000
(8b)	>5000	>5000
Amphotericin B	<9	<9

It was found that amphotericin B drug used as a standard has leishmanicidal activity against *Leishmania infantum* and *Leishmania major* at all concentrations (LC: <9 µg/ml). It was determined that there was a perfect agreement between the color change of the indicator dye alamar blue in the wells and the microscopy results. In the evaluation of leishmanicidal activity, the color of alamar blue remained unchanged in the negative control. In the positive control, the blue color turned pink as the vitality continued. The LC values obtained from the tests were given in Table 2 (Figures 8 and 9).

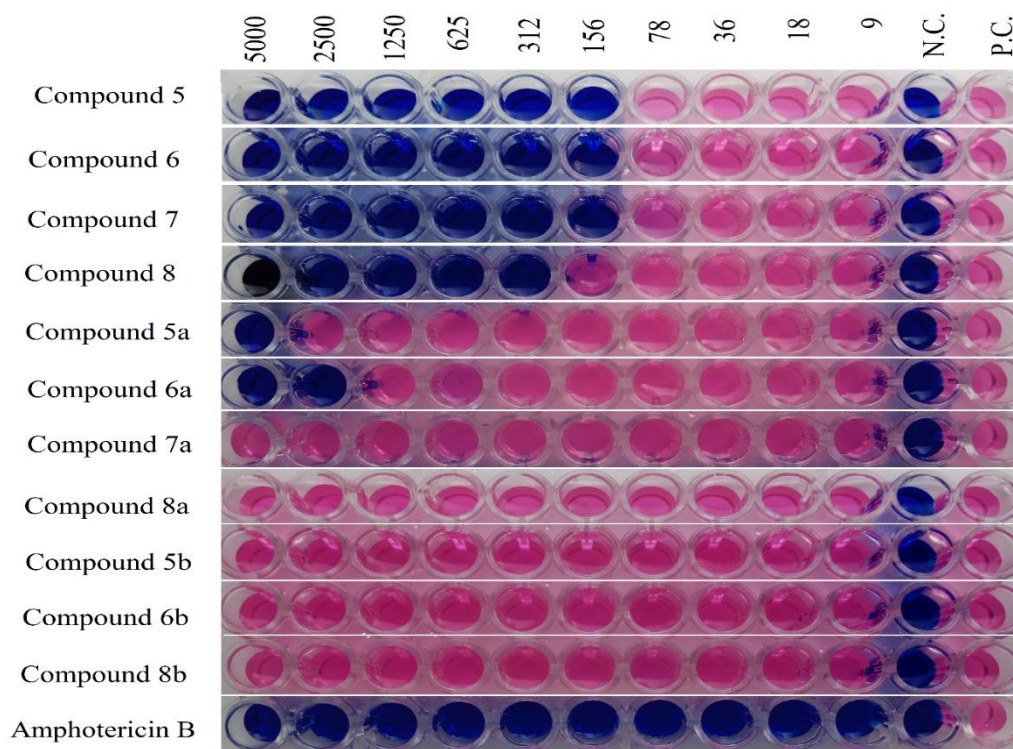


Figure 9. *In vitro* leishmanicidal activity results

In order for chalcone series compounds to be good drug nominee, *in vivo* toxicity tests and control studies should be performed in experimental animal models [44].

4. Conclusion

In this study, it was aimed to study the *in vitro* leishmanicidal activity of different chalcone derivatives and their phthalonitrile and phthalocyanine compounds. In accordance with this purpose, we synthesized different chalcone (5, 6, 7 and 8), phthalonitrile (5a, 6a, 7a and 8a) and zinc(II) (5b, 6b, 7b and 8b) phthalocyanine compounds substituted with chalcone compound. The synthesized novel chalcone compound (8), phthalonitrile (8a) and zinc phthalocyanine derivative (8b) were characterized by merger of the IR, ^1H and ^{13}C NMR, UV-Vis and MALDI-TOF-MS spectroscopies. Antiparasitic activities of the compounds (5-8, 5a-8a, 5b, 6b and 8b) were tested as *in vitro* against *Leishmania infantum* and *Leishmania major* promastigotes by Microdilution broth method. The leishmanicidal activities of the compounds were assessed by considering their LC values and the results obtained were contrasted with the results of the standard control drug Amphotericin B. In conclusion, the antiparasitic activity results of the chalcone compounds (5-8) synthesized in the study are promising, and due to their *in vitro* leishmanicidal activities, especially chalcone series compounds can be evaluated in pharmacological studies and the diversity of compounds may increase. In order for chalcone

series compounds to be good drug nominee, *in vivo* toxicity tests and control studies should be performed in experimental animal models. It is essential to multiply such studies in terms of combating this disease for which there is no effective vaccine.

Ethics in Publishing

There are no ethical issues regarding the publication of this study.

Author Contributions

- Ayşe AKTAŞ KAMILOĞLU: Designing the study, synthesis of organic and inorganic compounds, analysis, evaluation of results, writing the article
- Şahin DİREKEL: Performing leishmanicidal activity tests, evaluation of results, writing the article
- Gonca ÇELİK: Synthesis of organic compounds

Acknowledgements

The synthesized compounds in this study were supported by the Scientific&Technological Research Council of Turkey (TUBITAK), Project no:118Z578.

References

- [1] WHO, <https://www.who.int/news-room/fact-sheets/detail/leishmaniasis> (Date of access: 02.02.2022)
- [2] Cavalcante, G. M., Camara, C. A., Silva, E. M. S. D., Santos, M. S., Leite, A. B., Queiroz, A. C., Evelyn Da Silva, A., Araújo, M. V., Alexandre-Moreira, M. S., Silva, T. M. S. (2021). Leishmanicidal Activity of Propolis Collected in the Semiarid Region of Brazil., *Front. Pharmacol.*, 12, 702032.
- [3] Monzote, L. (2009). Current Treatment of Leishmaniasis: A Review. *The Open Antimicrobial Agents Journal*, 1, 9-19.
- [4] Burza, S., Croft, S. L., Boelaert, M. (2018). Leishmaniasis, *Lancet*, 392, 951–70.
- [5] Anversa, L., Tiburcio, M. G. S., Richini-Pereira, V. B., Ramirez, L. E. (2018). Human leishmaniasis in Brazil: A general review, *Rev. Assoc. Med. Bras.*, 64 (3), 281-289.
- [6] Gupta, K., Gaur, R., Sharma, A., Akther, J., Saini, M., Bhakuni, R. S., Pathania, R. (2019). A novel bi-functional chalcone inhibits multi-drug resistant *Staphylococcus aureus* and potentiates the activity of fluoroquinolones, *Bioorg. Chem.*, 83, 214.
- [7] Birari, B., Gupta, S., Mohan, C. G., Bhutani, K. K. (2011). Antiobesity and lipid lowering effects of Glycyrrhiza chalcones: experimental and computational studies, *Phytomedicine*, 18, 795.

- [8] Stellenboom, N. (2019). Comparison of the inhibitory potential towards carbonicanhydrase, acetylcholinesterase and butyrylcholinesterase of chalcone and chalcone epoxide, *J Biochem Mol Toxicol.*, 33, 22240.
- [9] Sharma, V., Kumar, V., Kumar, P. (2013). Heterocyclic chalcone analogues as potential anticancer agents, *Anti-Cancer Agents Med. Chem.*, 13, 422.
- [10] Eden, W. T., Alighiri, D., Wijayati, N., Mursiti, S. (2021). Synthesis of Chalcone Derivative from Clove Leaf Waste as a Natural Antioxidant, *Pharmaceutical Chemistry Journal*, 55, 3.
- [11] Aktas Kamiloglu, A., Can, Z., Celik, G. (2020). Antioxidant activity of phthalonitrile derivatives bearing different chalcone groups, *Turkish Journal of Analytical Chemistry*, 2 (2). 69-74.
- [12] Tajuddeen, N., Isah, M. B., Suleiman, M. A., Van Heerden, F. R., Ibrahim, M. A. (2018). The chemotherapeutic potential of chalcones against leishmaniasis: a review, *Int. J. Antimicrob. Agents*, 51, 311-318.
- [13] Boeck, P., Bandeira Falcao, C. A., De'sar Leal, P., Yunes, R. A., Filho, V. C., Torres-Santos, E. C., Rossi-Bergmann, B. (2006). Synthesis of chalcone analogues with increased antileishmanial activity, *Bioorganic & Medicinal Chemistry*, 14, 1538–1545.
- [14] Konidala, S. K., Kotra, V., Reddy Danduga, R. C. S., Kola, P. K. (2020). Coumarin-chalcone hybrids targeting insulin receptor: Design, synthesis, anti-diabetic activity, and molecular docking, *Bioorganic Chemistry*, 104, 104207.
- [15] Wang, Z. X., Gao, S., Ma, M., Ren, G., Liu, H., Chen, X. (2015). Synthesis and antifungal activity of chalcone derivatives, *Nat. Prod. Res.*, 29, 1804-10.
- [16] Mohan, S., Hobani, Y. H., Shaheen, E., Abou Elhamd, A. S., Abdelhaleem, A., Alhazmi, H. A., Abdelwahab, S. I. (2020). Ameliorative effect of Boesenbergin A, a chalcone isolated from Boesenbergia rotunda (Fingerroot) on oxidative stress and inflammation in ethanol-induced gastric ulcer in vivo, *Journal of Ethnopharmacology*, 261, 113104.
- [17] Ahmad, I., Thakur, J. P., Chanda, D., Saikia, D., Khan, F., Dixit, S., Kumar, A., Konwar, R., Negi, A. S., Gupta, A. (2013). Syntheses of lipophilic chalcones and their conformationally restricted analogues as antitubercular agents, *Bioorg. Med. Chem. Lett.*, 23, 1322.
- [18] Chen, Y.H., Wang, W.H., Wang, Y.H., Lin, Z.Y., Wen, C.C., Chern, C.Y. (2013). Evaluation of the Anti-Inflammatory Effect of Chalcone and Chalcone Analogues in a Zebrafish Model, *Molecules*, 18 (2), 2052-2060.
- [19] Zhuang, C., Zhang, W., Sheng, C., Zhang, W., Xing, C., Miao, Z. (2017). Chalcone: A Privileged Structure in Medicinal Chemistry, *Chem. Rev.*, 117, 7762-7810.
- [20] Tang, X., Su, S., Chen, M., He, J., Xia, R., Guo, T., Chen, Y., Zhang, C., Wang, J., Xue, W. (2019). Novel chalcone derivatives containing a 1,2,4-triazine moiety: design, synthesis, antibacterial and antiviral activities, *RSC Adv.*, 9, 6011.
- [21] Hanack, M., Schneider, T., Barthel, M., Shirk, J. S., Pong, R. G. S. (2001). Indium phthalocyanines and naphthalocyanines for optical limiting, *Coord. Chem. Rev.*, 219-221, 235-258.
- [22] Özenc, F., Günel, A., Barana, A. (2018). DNA-binding, enzyme inhibition, and photochemical properties of chalcone containing metallophthalocyanine compounds, *Bioorganic Chemistry*, 81, 71-78.

- [23] Riquelme, J., Neira, K., Marco, J. F., Hermosilla-Ibáñez, P., Orellana, W., Zagal, J. H., Tasca, F. (2018). Biomimicking vitamin B12. A Co phthalocyanine pyridine axial ligand coordinated catalyst for the oxygen reduction reaction, *Electrochim Acta*, 265, 547-555.
- [24] Azimi, F., Marjani, A. P., Keshipour, S. (2021). Fe(II)-phthalocyanine supported on chitosan aerogel as a catalyst for oxidation of alcohols and alkyl arenes, *Scientific Reports*, 11, 23769.
- [25] Aktas Kamiloglu, A., Karaca, H., Celik, G., Acar, I., Kantekin, H. (2020). New chalcone-substituted metallophthalocyanines: Synthesis, characterization, and investigation of their properties, *Journal of Chemical Research*, 44 (7,8), 367-375.
- [26] Orman, E. B., Pişkin, M., Odabaş, Z., Özkaya, A. R. (2021). Electrochemical, Spectroelectrochemical, and Electrocatalytic Dioxygen Reducing Properties of Peripheral Tetra-2,6-dimethoxyphenoxy Substituted Phthalocyanines, *Electroanalysis*, 33, 2310- 2322.
- [27] Bayrak, R., Kırlangıç Ata, S., Yılmaz, I., Yalçın, I., Erman, M., Ünver, Y., Degirmencioglu, I. (2021). Synthesis and Spectro-Electrochemical Properties of New Metallophthalocyanines Having High Electron Transfer Capability, *Journal of Molecular Structure*, 1231, 129677.
- [28] Shalini, S., Balasundara Prabhu, R., Prasanna, S., Mallick, T. K., Senthilarasu, S. (2015). Review on natural dye sensitized solar cells: operation, materials and methods, *Renew Sustain Energy Rev.*, 51, 1306-1325.
- [29] Palacin, S. (2000). Phthalocyanines in Langmuir and Langmuir-Blodgett films: from molecular design to supramolecular architecture, *Adv. Colloid Interface Sci.*, 87, 165-181.
- [30] Banasz, R., Wałęsa-Chora, M. (2019). Polymeric complexes of transition metal ions as electrochromic materials: Synthesis and properties, *Coord. Chem. Rev.*, 389, 1-18.
- [31] Sen, P., Managa, M., Nyokong, T. (2019). New type of metal-free and Zinc(II), In(III), Ga(III) phthalocyanines carrying biologically active substituents: Synthesis and photophysicochemical properties and photodynamic therapy activity, *Inorg Chim Acta*, 491, 1-8.
- [32] Koca, A., Kalkan, A., Bayır, Z. A. (2011). Electrocatalytic oxygen reduction and hydrogen evolution reactions on phthalocyanine modified electrodes: Electrochemical, in situ spectroelectrochemical, and in situ electrocolorimetric monitoring, *Electrochim Acta*, 56, 5513-5525.
- [33] Aktas Kamiloglu, A., Direkel, S., Yalazan, H., Kantekin, H., Acar, I. (2020). Octa- and tetra-substituted phthalocyanines with methoxyeugenol group: Synthesis, characterization and in vitro antimicrobial activity, *Journal of Coordination Chemistry*, 73 (7), 1177-1190.
- [34] Klyamer, D. D., Basova, T. V., Krasnov, P. O., Sukhikh, A. S. (2019). Effect of fluorosubstitution and central metals on the molecular structure and vibrational spectra of metal phthalocyanines, *J. Mol. Struct.*, 1189, 73-80.
- [35] Erbahar, D. D., Harbeck, M., Gümüş, G., Gürol, I., Ahsen, V. (2014). Self-assembly of phthalocyanines on quartz crystal microbalances for QCM liquid sensing applications, *Sensors Actuators B: Chem.*, 190, 651-656.
- [36] Ağırtaş, M. S., Cabir, B., Gonca, S., Ozdemir, S. (2022). Antioxidant, Antimicrobial, DNA Cleavage, Fluorescence Properties and Synthesis of 4- (3,4,5- Trimethoxybenzyloxy) Phenoxy) Substituted Zinc, *Phthalocyanine Polycyclic Aromatic Compounds*, 42(8), 5029-5043.

- [37] Aktaş Kamiloğlu, A., Yalazan, H., Durmuş, M., Çelik, G., Ömeroğlu, İ., Acar, İ., Kantekin, H. (2021). Synthesis, spectroscopic, and photophysical behavior of Zn(II) and Mg(II) phthalocyanine– chalcone conjugates, *Journal of Coordination Chemistry*, 74(15), 2491-2507.
- [38] Aktas Kamiloğlu, A., Ömeroğlu, İ., Yalazan, H., Durmuş, M., Çelik, G., Kantekin, H. (2022). Photophysical, Photochemical Properties of Chalcone Substituted Zinc(II) and Magnesium(II) Metallophthalocyanines Bearing Thiophene Units, *Journal of Inclusion Phenomena and Macrocyclic Chemistry*, 102 (10), 1-11.
- [39] Aktaş Kamiloğlu, A. (2021). Photochemical properties of fluoro-chalcone substituted peripherally tetra Zn(II)Pc and Mg(II)Pc, *Journal of Inclusion Phenomena and Macrocyclic Chemistry*, 99(3), 185-196.
- [40] Mello, T. F.P., Bitencourt, H. R., Pedroso, R.B., Aristides, S. M.A., Lonardon, M.V.C., Silveir, T. G.V. (2014). Leishmanicidal activity of synthetic chalcones in *Leishmania (Viannia) braziliensis*, *Experimental Parasitology*, 136, 27–34.
- [41] Aponte, J. C., Castillo, D., Estevez, Y., Gonzalez, G., Arevalo, J., Hammond, G.B., Sauvain, M. (2010). In vitro and in vivo anti-*Leishmania* activity of polysubstituted synthetic chalcones, *Bioorganic & Medicinal Chemistry Letters*, 20, 100–103.
- [42] Er, M., Ozer, A., Direkel, S., Karakurt, T., Tahtaci, H. (2019). Novel substituted benzothiazole and Imidazo[2,1-b][1,3,4]Thiadiazole derivatives: Synthesis, characterization, molecular docking study, and investigation of their in vitro antileishmanial and antibacterial activities, *Journal of Molecular Structure*, 1194, 284-296.
- [43] Ünver, Y., Bektaş, E., Direkel, Ş. (2018). Synthesis, Antioxidant, and Antileishmanial Activities of New Bis-*N*-amino Triazole Derivatives, *Russian Journal of General Chemistry*, 88, 2616–2620.
- [44] Souza, J.M., de Carvalho, É. A. A., Candido A. C. B. B., de Mendonça, R.P., da Silva, M. F., Parreira, R. L. T., Dias, F.G. G., Ambrósio, S. R., Arantes, A. T., da Silva Filho, A. A., Nascimento, A.N., Costa, M.R., Sairre, M. I., Veneziani, R. C. S., Magalhães, L.G. (2020). Licochalcone a Exhibits Leishmanicidal Activity *in vitro* and in Experimental Model of *Leishmania (Leishmania) Infantum*, *Frontiers in Veterinary Science*, 7, 527.

Genotoxic And Antigenotoxic Effects Of Corilagin In *In Vitro* Human Lymphocyte Cultures

Elif TURAN¹, Gökçe TANER^{2*}

¹ Bursa Technical University, Graduate Education Institute, Department of Biotechnology, Bursa, Türkiye
² Bursa Technical University, Faculty of Engineering and Natural Sciences, Department of Bioengineering, Bursa, Türkiye

Received: 25/07/2022, Revised: 01/09/2022, Accepted: 13/09/2022, Published: 30/12/2022

Abstract

It has been reported in many researches that natural compounds synthesized by plants as secondary metabolites has protective effects against oxidative stress caused by free radicals and genetic damage mediated by them. Among these natural compounds, polyphenols are known to have particularly strong antioxidant activities. Corilagin, a tannin found in many plant species such as *Euphorbiaceae*, *Geraniaceae* and *Lythracea* families has various pharmacological effects. In this study, the geno/antigenotoxic effects of corilagin was investigated in *in vitro* human peripheral blood lymphocyte cultures using micronucleus (MN) and chromosomal aberrations (CA) tests to determine the safe concentrations of corilagin. 10-100 µg/ml corilagin were applied to the cells alone and simultaneously with 0.2 µg/ml MMC and all analyzes were performed in 3 repetitions. According to the results of the analyzes, it was assessed that corilagin did not cause a statistically significant increase in the formation of MN and CA at 10, 25, 50 µg/ml concentrations, and it even provided a statistically significant decrease in the increased MN frequency and CA caused by MMC. On the other hand, it was determined that this effect was concentration dependent and increased DNA damage at the highest concentration of 100 µg/ml. This is thought to be due to the concentration-dependent prooxidant activity seen in many potent antioxidants. As a review of the study low concentrations of corilagin have an antigenotoxic effect against genetic damage caused by genotoxic agents such as MMC and shows that it can be used against the side effects of chemotherapy.

Keywords: Corilagin, Antioxidant, Antigenotoxicity, Micronucleus, Chromosome Aberration

Korilaginın *In Vitro* İnsan Lenfosit Kültürlerindeki Genotoksik ve Antigenotoksik Etkileri

Öz

Bitkiler tarafından ikincil metabolitler olarak sentezlenen doğal bileşiklerin, serbest radikallerin neden olduğu oksidatif strese ve bunların aracılık ettiği genetik hasara karşı koruyucu etkilerinin olduğu birçok araştırmada bildirilmiştir. *Euphorbiaceae*, *Geraniaceae* ve *Lythracea* familyaları gibi birçok bitki türünde bulunan bir tanen olan korilagin, çok çeşitli farmakolojik etkilere sahiptir. Bu çalışmada, korilaginın güvenli konsantrasyonlarını belirlemek için *in vitro* insan periferik kan lenfosit kültürlerinde mikroçekirdek (MÇ) ve kromozom anormallikleri (KA) testleri kullanılarak genotoksik/antigenotoksik etkileri araştırıldı. 10-100 µg/ml korilagin hücrelere tek başına ve 0.2 µg/ml MMC ile eş zamanlı olarak uygulandı ve tüm analizler 3 tekrarlı olarak gerçekleştirildi. Analizlerin sonuçlarına göre korilaginın 10, 25, 50 µg/ml uygulama konsantrasyonlarında MÇ ve KA oluşumunda istatistiksel olarak anlamlı bir artışa neden olmadığı hatta MMC uygulaması ile artan MÇ frekansında ve kromozom anormalliklerde istatistiksel olarak önemli oranda azalma sağladığı belirlenmiştir. Diğer yandan bu etkinin konsantrasyona bağlı olduğu ve 100 µg/ml'de DNA hasarını artırıcı etki gösterdiği belirlenmiştir. Bu durumun birçok güçlü antioksidanda görülen konsantrasyona bağlı prooksidan aktivite nedeniyle olduğu düşünülmektedir. Çalışma sonuçları korilaginın düşük konsantrasyonlarının MMC gibi genotoksik ajanlar tarafından oluşan genetik hasara karşı antigenotoksik etkisinin olduğunu, kemoterapinin yan etkilerine karşı kullanılabileceğini göstermektedir.

Anahtar Kelimeler: Korilagin, Antioksidan, Antigenotoksikite, Mikroçekirdek, Kromozom Anormallikleri

*Corresponding Author: gokce.taner@btu.edu.tr
Elif TURAN, <https://orcid.org/0000-0003-1836-6636>
Gökçe TANER, <https://orcid.org/0000-0002-0290-1166>

1. Introduction

Many studies have been conducted for many years to identify compounds that can protect humans from DNA damage and its consequences. In order to find the most effective antigenotoxic substances, especially natural products, medicinal plants and edible plants are studied. Phenolic compounds isolated from plants are mostly used in studies to determine the antigenotoxic effects of antioxidants. An important group of these compounds is tannins, which are an important part of the human diet and are widely found in nature, especially in herbal products. Tannins are phenolic compounds that can be found in various organs of plants such as fruits, seeds, leaves and roots and have a role in plant development. Tannins have anti-inflammatory, anticarcinogen, antiviral, antibacterial and antiparasitic effects based on their antioxidant and anti-radical activities [1, 2, 3]. Ellagitannins are hydrolyzable tannins with numerous biological properties that can be found in berries, muscadine grapes, walnuts, pomegranates, and tea. Ellagitannins have significant effects on human health and nutrition [3, 4]. Corilagin, a member of the ellagitannin family, is a natural product containing glucose and has been found in various medicinal plants such as *Phyllanthus urinaria* L., *Lumnitzera racemosa*, *Canarium album* L., *Phyllanthus reticulatus* [5]. Studies have shown that corilagin has many biological effects such as antioxidative, anti-inflammatory, antitumor, antimicrobial, and antiviral [5-8]. Studies have shown that corilagin inhibits the formation of proinflammatory cytokines, also reduces ROS production, free radical formation and lipid peroxidation *in vitro*. The first bioactivity of corilagin to be found is its inhibitory effect on reverse transcriptase activity of RNA tumor viruses. In later studies, it was observed that corilagin has various pharmacological properties including antihypertensive, antiatherogenic, antiviral, hepatoprotective, neuroprotective effects and it is effective in controlling type II diabetes mellitus [9, 10]. *In vivo* drug metabolism of corilagin leads to poor pharmacokinetic models, greatly contributes to the effectiveness and safety of the compounds. In addition, the metabolite profile is important in explaining the effectiveness, safety and further development of drugs [11,12].

Mitomycin-C (MMC) is a natural product of an Actinobacteria species, *Streptomyces caespitosus*, which is found in soil. MMC shows strong bioreductive alkylation and inhibits DNA synthesis under hypoxic conditions. Therefore it is highly activated in oxygen-poor cells. MMC has shown efficacy in a wide variety of cancers as an antitumor agent but it has a large side effect profile so its widespread use is prohibited. MMC has a large variety of genotoxic effects including the inhibition of DNA synthesis, clastogenesis and mutagenesis [13-15].

Although there are studies on the biological activity of corilagin in the literature, there are no studies on its genotoxic and/or antigenotoxic activity to our knowledge. In line with all these data, in this study the potential genotoxic effects of corilagin and also its antigenotoxic effects against genetic damage induced by mitomycin-C (MMC), a crosslinking chemotherapeutic agent, were investigated. Both genotoxic and antigenotoxic effects of corilagin were tested in human peripheral blood lymphocytes using cytokinesis-blocked micronucleus (CBMN) assay and chromosome aberration tests as widely used genotoxicity tests to determine clastogenic and aneugenic activities.

2. Materials and Methods

2.1 Chemical Substances

As the chemicals used in the experiments, corilagin (CAS number: 23094-69-1), mitomycin-C (CAS number 50-07-7), disodium hydrogen phosphate dihydrate ($\text{Na}_2\text{HPO}_4 \cdot 2\text{H}_2\text{O}$), acetic acid (Glacial, 99%), potassium dihydrogen phosphate (KH_2PO_4), ethyl alcohol (ethanol), methyl alcohol (methanol) (99%), cytochalasin B, and colchicine were purchased from Sigma, formaldehyde from Tekkim, dimethyl sulfoxide (DMSO), giemsa, chromosome medium from Merck, nitric acid (HNO_3) from VWR and potassium chloride (KCl) from Isolab.

Corilagin

Corilagin (β -1-O-galoyl-3,6-(R)-hexahydroxydiphenoyl-D-glucose) is a gallotannin, an off-white crystalline powder which is easily soluble in water, methanol, acetone, ethanol, and dimethyl sulfoxide (DMSO) [10]. It was isolated for the first time from the plant *Caesalpinia coriaria* in 1951 by Schmidt et al [16]. The chemical formula of corilagin is $\text{C}_{27}\text{H}_{22}\text{O}_{18}$ and its molecular weight is 634.45 g/mol. The structure of corilagin is given in Figure 1.

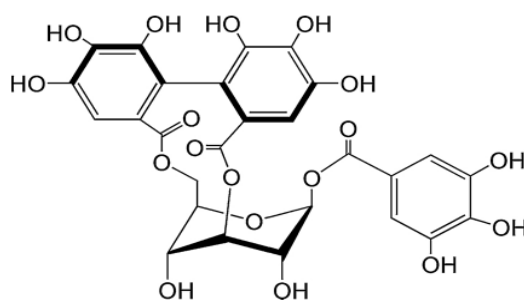


Figure1. Structure of corilagin [10]

Corilagin has been found in 16 plant families and a total of 50 species. There are 20 species in the *Euphorbiaceae* family, 10 species in the *Geraniaceae* family and 7 species in the *Combretaceae* family. Apart from these, studies have shown that corilagin is also present in *Phyllanthus niruri* L., *Phyllanthus emblica* L., *Phyllanthus urinaria* L., *Geranium sibiricum* L. and *Terminalia catappa* L. species. It has been observed that it is easier to isolate plants from above-ground parts, including leaves, flowers, fruits, and seeds [10].

In this study, we purchased and used 99% pure commercial form of corilagin as active ingredient. Test concentrations of corilagin were chosen on the basis of literature data [17-19] and preliminary tests. In line with the data in the literature, it has been determined that it is appropriate to use corilagin at increasing concentrations up to 100 $\mu\text{g}/\text{ml}$ in cell culture in terms of cell viability and biological activity. MN test and CA test protocols were followed to examine both genotoxic and antigenotoxic effects against MMC by applying 10, 25, 50, 100 $\mu\text{g}/\text{ml}$ corilagin concentrations to human lymphocyte cultures prepared in ethanol-sterile distilled water (1:4) mixture.

2.2 Cell cultures and treatments

Human peripheral blood lymphocyte cultures were prepared for both micronucleus (MN) and chromosome aberration (CA) methods. Blood samples were obtained from 3 healthy female donors (aged 20-25 years) who do not smoke, do not use alcohol or drugs, and did not have any health problems and no history of exposure to genotoxic agents. Blood samples were used to obtain biological material from healthy volunteers and there is no interventional clinical practice. While the study project was being prepared for this stage, an approval from the Uludağ University Faculty of Medicine Ethics Committee (2019-11/17) was obtained. Blood samples were taken into heparin tubes then 0.25 ml of heparinized peripheral blood was added into tubes with 2.5 ml of chromosome medium including fetal bovine serum, heparin, antibiotics and phytohaemagglutinin (PHA) under sterile conditions. Then, the total incubation time of the cells in the culture was followed for 72 hours (3 cell divisions). Corilagin concentrations (10, 25, 50, 100 µg/ml) and MMC (0,2 µg/ml) were added to the medium 24 hours after the beginning of the culture, allowing it to remain in the culture medium for 48 hours. During the culture, the tubes were gently inverted and shaken 2-3 times a day.

2.3 Cytokinesis-blocked micronucleus (CBMN) Assay

For CBMN assay, at the 44th hour of culture, cytochalasin-B (6 µg/ml) was added to all tubes to block cytokinesis. Then, the tubes were wrapped with foil to prevent light exposure. At the end of 72 hours, the culture was terminated and the tubes were centrifuged at 1000 rpm for 10 minutes, and the supernatant was discarded with a pasteur pipette, being careful not to remove the cells at the bottom. The 0.5-0.7 ml remaining in the tubes was homogenized by using vortex and then 5 ml of the cold 0.075 M KCl hypotonic solution, was appended slowly, drop by drop, then kept at 4°C for 5 minutes. The tubes were centrifuged at 1000 rpm for 10 minutes, and after the supernatant was discarded, 5 ml of cold fixative prepared from 3:1 methanol: acetic acid was added to the tubes and kept at 4°C for 15 minutes. The fixation process was applied 3 times. After the first fixative, the same procedure was applied two more times and the tubes were kept in the refrigerator for 5 minutes after each fixative. 1% formaldehyde was included into the third fixative. After the last centrifugation, the supernatant in the tubes was removed, and the remaining cell solution was slowly homogenized with a pipette. The prepared slides were left in a dust-free place at room temperature for 24 hours to dry. Air-dried slides were stained for 15 minutes with 5% Giemsa (pH=6.8) prepared with Sorensen buffer. Micronuclei were scored in 1,000 binucleated cells per donor (totally 3,000 binucleated cells per concentration). Only binuclear cells are counted during MN examination because these cells are the cells that divide after adding the chemical substances whose effects are examined. The micronuclei observed in mononuclear cells were micronuclei that were originally present in those cells, not due to the addition of test substance. In each treatment group, 1000 binuclear cells (total 3000 cells from 3 donors) are examined for the presence or absence of micronuclei (Figure 1). MN frequency was determined as MN number per cell (MN/cell) using the formula $1x(1MN)+2x(2MN)+3x(3MN+4MN)/N$ (N total number of cells examined).

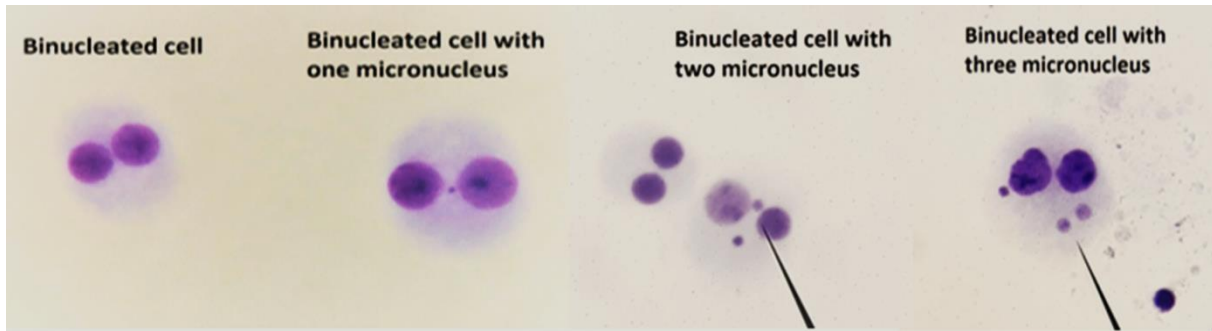


Figure 1 Micrographs of giemsa stained binucleated cells without and with different number of micronuclei

2.4 Chromosome aberrations (CA) test

For CA test, at the 70th hour of the culture, colchicine (0.06 µg/ml) was added to the tubes. The cells were then kept in an incubator at 37°C for 2 hours. At the end of the culture period, the tubes were centrifuged at 1200 rpm for 10 minutes and the supernatant was discarded. The 0.5-0.7 ml portion at the bottom of the tube was mixed in a vortex, and the remaining liquid was homogenized. Afterwards, 5 ml of 0.075M KCl hypotonic solution at 37°C was added to tubes drop by drop using a vortex. The tubes were kept at 37°C for 30 minutes. Then, the tubes were centrifuged at 1200 rpm for 10 minutes and after the supernatant was removed, 5 ml of cold fixative (3:1 methanol:acetic acid) was slowly added to the tubes in a vortex. After adding the first fixative, the tubes were kept at +4°C for 1 hour. The fixative process was repeated two more times to ensure complete clarification of the remaining contents in the tube. After each fixative process, the tubes were centrifuged, and the supernatant was removed, leaving 0.5-0.7 ml at the bottom after the last fixative application. After discarding the supernatant, the remaining content in the tube was homogenized by pipetting. Then, the cell suspension was dropped from a height of 15-20 cm on cold glass slides that were previously cleaned in 1N HNO₃ and taken into 70% alcohol. Then air-dried slides were stained with 5% Giemsa dye prepared in Sorensen buffer (pH 6.8) for 15-20 min. For each treatment group at least 100 metaphases were analyzed per donor (totally 300 metaphases per concentration).

2.5 Statistical analysis

z test was performed for statistical analysis of the results of the percentage of MN, abnormal cells, CA/cell. All data was expressed as mean±SE.

3. Results and Discussion

The total number of micronuclei (MN) and MN frequency values obtained from 3 replicate studies in human lymphocyte cultures in which corilagin was administered alone or in combination with MMC are shown in Table 1. When the groups treated with corilagin concentrations were compared with the untreated negative control group, it was determined that corilagin (10-100 µg/ml) did not cause a statistically significant increase in the formation of MN. On the other hand in all groups treated with 0.2 µg/ml MMC, the MN% frequency increased significantly ($p < 0.05$) compared to the control. When the groups in which corilagin was administered simultaneously with MMC were examined, a statistically significant decrease in MN frequency was observed in the groups in which 10, 25, 50 µg/ml concentrations of corilagin were applied compared to the group in which MMC was administered alone. In the group in which the highest concentration of corilagin (100 µg/ml) was applied with MMC, it was observed that the MN frequency did not decrease, even increased, compared to the MMC group.

Table 1. Micronucleus frequencies in human lymphocyte cultures treated with corilagin and MMC with corilagin.

Treatment groups	Cells scored	Distrubition of BN			Total MN	MN% ±SE
		Cells according to the number of MN				
		(1)	(2)	(3)		
Negative Control	3000	11	-	-	11	0,37 ± 0,11
MMC (0,2 µg/ml)	3000	201	7	-	215	7,17 ± 0,47 a
10 µg/ml Corilagin	3000	7	1	-	9	0,30 ± 0,10 b
25 µg/ml Corilagin	3000	12	-	-	12	0,40 ± 0,11 b
50 µg/ml Corilagin	3000	14	-	-	14	0,47 ± 0,12 b
100 µg/ml Corilagin	3000	17	-	-	17	0,57 ± 0,14 b
10 µg/ml Corilagin+ 0,2 µg/ml MMC	3000	127	6	-	139	4,63 ± 0,38 a,b
25 µg/ml Corilagin+ 0,2 µg/ml MMC	3000	150	6	-	162	5,40 ± 0,41 a,b
50 µg/ml Corilagin+ 0,2 µg/ml MMC	3000	163	2	2	173	5,77 ± 0,43 a,b
100 µg/ml Corilagin+ 0,2 µg/ml MMC	3000	186	21	1	231	7,70 ± 0,49 a

a Significantly different at $p \leq 0.05$ when compared with negative control (z test), b Significantly different at $p \leq 0.05$ when compared with MMC group (z test). MMC Mitomycin-C, BN Binucleat, MN micronucleus, SE standard error

It is thought that this may be due to the prooxidant activities and additive effects at high concentrations observed in many of the potent antioxidant substances. Many studies have shown that corilagin is more effective at lower concentrations. However, in the literature, it is seen that most of the studies on corilagin are based on *in vivo* experiments carried out in experimental animals. The results of the CA test indicated as structural and numerical abnormalities, total abnormality number and total abnormal cells in human lymphocyte cultures in which 10, 25, 50, 100 µg/ml corilagin alone and in combination with 0.2 µg/ml MMC are

applied, are shown in Table 2 and 3. When the corilagin treated groups were compared with the negative control group, it was determined that it did not cause a statistically significant increase in the formation of chromosomal abnormalities at the concentrations (10-100 µg/ml) applied alone, that shows it did not have a clastogenic effect at studied concentrations. When the groups in which corilagin was administered simultaneously with MMC were examined, a statistically significant decrease in abnormal cell frequency and CA/cell values was observed at 10, 25, 50 µg/ml corilagin concentrations compared to the group in which MMC was administered alone. In the group in which the highest concentration of corilagin (100 µg/ml) was applied with MMC, it was observed that there was no decrease in DNA damage compared to the MMC group, even increased. It is seen that the results of micronuclei and chromosomal abnormality test applied at the same time are compatible with each other and cause similar results.

Table 2. Chromosomal abnormality types and abnormal cell numbers in human peripheral lymphocytes treated with corilagin and MMC

Treatment Groups	Total Cells Scored	Chromosomal abnormalities							Total	Abnormal cells
		ctb	csb	f	scu	dic	cte	p		
Negative control	300	8	-	1	-	-	-	-	9	9
MMC (0,2 µg/ml)	300	45	9	4	4	3	20	-	85	81
10 µg/ml Corilagin	300	7	-	-	-	-	-	1	8	8
25 µg/ml Corilagin	300	9	-	-	-	-	-	-	9	9
50 µg/ml Corilagin	300	8	2	1	-	-	-	-	11	11
100 µg/ml Corilagin	300	9	3	-	-	-	-	1	13	13
10 µg/ml Corilagin+ MMC	300	42	7	2	1	1	18	-	71	69
25 µg/ml Corilagin+ MMC	300	38	9	1	-	-	12	-	60	58
50 µg/ml Corilagin+ MMC	300	33	11	1	1	-	9	1	56	56
100 µg/ml Corilagin+ MMC	300	55	13	2	-	1	22	-	93	89

MMC Mitomycin-C, ctb chromatid break, csb chromosome break, f fragment, scu sister chromatid union, dic dicentric, cte chromatid exchange, p polyploidy, CA/cell Chromosome aberrations/cell, SE Standard Error

The ellagitannins found in pomegranate fruit are very potent antioxidants, and pomegranate juice has a stronger *in vitro* antioxidant effect than other common commercial juices [20]. Corilagin is an elajitanen found in different organs and tissues in many plant species, including pomegranate, and numerous studies have been conducted on its antigenotoxic and anticarcinogen activity. Prakash et al. [21] conducted *in vitro* and *in vivo* studies using the extract they isolated from the leaves of the *Punica granatum* L. plant and examined the effects of its components on oxidative stress and genomic damage. As a result of their studies, they reported that *Punica granatum* L. plant is an important chemoprotective agent thanks to the antioxidant effects of apigenin, luteolin, gallitanins and ellagitannins such as punicalin, punikalagin, corilagin and punicafolin.

Table 3. Frequency of abnormal cells and number of abnormalities per cell in human peripheral lymphocytes treated with corilagin and MMC.

Treatment Group	Cells Scored	Abnormal cells ± SE (%)	CA/ cells ± SE
Negative control	300	3,00 ± 0,985 b	0,030 ± 0,010 b
MMC (0,2 µg/ml)	300	27,00 ± 2,563 a	0,283 ± 0,026 a
10 µg/ml Corilagin	300	2,67 ± 0,93 b	0,027 ± 0,009 b
25 µg/ml Corilagin	300	3,00 ± 0,985 b	0,030 ± 0,010 b
50 µg/ml Corilagin	300	3,67 ± 1,086 b	0,037 ± 0,011 b
100 µg/ml Corilagin	300	4,33 ± 1,175 b	0,043 ± 0,012 b
10 µg/ml Corilagin+ MMC	300	23,00 ± 2,429 a,b	0,237 ± 0,025 a,b
25 µg/ml Corilagin+ MMC	300	19,33 ± 2,279 a,b	0,200 ± 0,023 a, b
50 µg/ml Corilagin+ MMC	300	18,67 ± 2,250 a,b	0,187 ± 0,023 a, b
100 µg/ml Corilagin+ MMC	300	29,67 ± 2,637 a	0,310 ± 0,027 a

a Significantly different at $p \leq 0.05$ when compared with negative control (z test), b Significantly different at $p \leq 0.05$ when compared with positive control (z test). MMC Mitomycin-C, CA Chromosome Aberrations SE standard error

Tong et al. [22] used tumor-free breast epithelium and breast cancer cell lines (MCF-7, SK-BR 3 and MDA-MB-231) and applied 40, 60, 80 µmol/L corilagin. They observed that corilagin inhibited breast cancer growth through reactive oxygen species-dependent apoptosis and autophagy. Rencüzoğulları et al. (2019) reported that 5, 10, 25 and 50 µM corilagin had an antitumoral effect on A549 lung cancer cells [23]. In a study, 30 male Balb/c mice, 6-8 weeks old and 19-25 g, and the RAW264.7 cell line, they determined that corilagin exerts anti-inflammatory effects by regulating TLR4 signaling molecules to ameliorate the excessive inflammatory state in sepsis [24]. When corilagin isolated from the plant *Phyllanthus emblica L.* was applied to esophageal cancer cell lines (ECA109, KYSE150) and normal esophageal epidermis cell line (HEEPIC) at doses of 0, 5, 10, 20, 40 and 60 µM, it was observed that it exerted an antitumor effect by activating mitochondrial apoptosis and endoplasmic reticulum stress signaling pathways [25]. Tong et al. (2018) showed that corilagin inhibited cancer growth in breast cancer cell lines via reactive oxygen species-dependent apoptosis and autophagy [26]. Guo et al. (2017) reported that corilagin reduced lung injury by suppressing oxidative stress and anti-apoptotic activity in their *in vivo* study [27]. Tan et al. (2022) reported that corilagin inhibited intracellular oxidative stress and decreased the inflammatory bone defect caused by LPS [28]. It was reported by Zhang et al. (2022) that corilagin induced apoptosis and inhibited HMBG1/PI3K/AKT signaling pathways in gastric cancer *in vivo* [29]. Huang et al. (2022) reported that corilagin improved doxorubicin induced cardiac function by reducing injury, inflammation and promoting apoptosis in rats [30]. Liu et al. (2021) reported that corilagin reduced NRF2 expression and induced apoptosis and autophagy [4]. In the literature, there are many *in vivo* and *in vitro* studies to examine the biological effects of corilagin on genotoxic molecules and cancer cells. Up to date, Yang et al. (2021) showed that corilagin could be a safe antiviral agent against COVID-19 and could be used in anti-virus hygienic products [9].

4. Conclusion

Studies with natural compounds to prevent or eliminate the genotoxic effect give positive results to a large extent. For this purpose, researches are carried out on secondary metabolites found in different organs of plants and especially polyphenolic compounds. Various antioxidant and anticarcinogenic effects of polyphenols found in plants have been investigated in studies carried out to date. In this study, the possible genotoxic and antigenotoxic effects of corilagin, which is one of the phenolic compounds of many plant species including pomegranate and accepted as a natural antioxidant, were investigated on human peripheral lymphocyte cells. As a result it was determined that corilagin had a reducing effect on the damage caused by MMC, when used at low concentrations, similar with the *in vitro* and *in vivo* studies in the literature. Treatment concentrations of corilagin showed no genotoxic effects on healthy human peripheral lymphocyte cells even showed antigenotoxic effects against damage caused by MMC. These results suggest that it has the potential to be used as a therapeutic agent in reversing the damage caused by mutagens and chemotherapy drugs.

In this study, MN and CA tests were carried out in cell culture under *in vitro* conditions for the detection of DNA damage. Compared to *in vivo* studies, *in vitro* methods that both eliminate ethical problems and also provide cheap, easy, fast evaluation present important data as preliminary indicator studies. However, according to many researchers, data obtained from cell cultures and animal models may not fully reveal the effect in humans. For this purpose, it is recommended to carry out *in vivo* studies and epidemiological studies as a continuation of these studies, which are considered as the first step. In this respect, the genomic approach, which reveals the effects of different components, can be presented as a powerful tool to describe and predict the pharmaco-toxicological activities of medicinal plants.

Ethics in Publishing

In this study ethics committee approval (2019-11/17) was obtained from Uludag University Faculty of Medicine Ethics Committee for the use of human peripheral blood lymphocyte cultures.

Author Contributions

This study was completed by Elif Turan as a master's thesis. Study experiments, data evaluations, and manuscript writing were done jointly by both authors. Conceptualization, funding acquisition, project administration, methodology, writing - original draft was done by Gökçe Taner.

Acknowledgements

This study was supported by Bursa Technical University Scientific Research Projects Coordinatorship postgraduate thesis project numbered 190Y013

References

- [1] Aydın, S., Üstün, F. (2007) Tanenler: Kimyasal Yapıları, Farmakolojik Etkileri, Analiz Yöntemleri, İstanbul Üniversitesi Veteriner Fakültesi Dergisi, 33(1), 21-31.
- [2] Pinto, T., Aires, A., Cosme, F., Bacelar, E., Morais, M. C., Oliveira, I., Gonçalves, B. (2021) Bioactive (Poly) phenols, volatile compounds from vegetables, medicinal and aromatic plants, *Foods*, 10(1), 106.
- [3] Hasheminezhad, S. H., Boozari, M., Iranshahi, M., Yazarlu, O., Sahebkar, A., Hasanpour, M., & Iranshahy, M. (2022) A mechanistic insight into the biological activities of urolithins as gut microbial metabolites of ellagitannins., *Phytotherapy Research*, 36(1), 112-146.
- [4] Liu, J., Qin, X., Ma, W., Jia, S., Zhang, X., Yang, X., ... & Jin, F. (2021) Corilagin induces apoptosis and autophagy in NRF2-addicted U251 glioma cell line, *Molecular medicine reports*, 23(5), 1-10.
- [5] Yamada, H., Nagao, K., Dokei, K., Kasai, Y., Michihata, N. (2008) Total synthesis of Corilagin, *Journal of the American Chemical Society*, 130(24), 7566-7567.
- [6] Ding, Y., Ren, D., Xu, H., Liu, W., Liu, T., Li, L., Li, J., Li, Y., Wen, A. (2017) Antioxidant and pro-angiogenic effects of corilagin in rat cerebral ischemia via Nrf2 activation, *Oncotarget*, 8(70), 114816.
- [7] Wang, Z., Guo, Q. Y., Zhang, X. J., Li, X., Li, W. T., Ma, X. T., Ma, L. J. (2014) Corilagin attenuates aerosol bleomycin-induced experimental lung injury, *International Journal of Molecular Sciences*, 15(6), 9762-9779.
- [8] Liu, F. C., Chaudry, I. H., & Yu, H. P. (2017) Hepatoprotective effects of corilagin following hemorrhagic shock are through akt-dependent pathway, *Shock*, 47(3), 346.
- [9] Yang, L. J., Chen, R. H., Hamdoun, S., Coghi, P., Ng, J. P., Zhang, D. W., ... & Wong, V. K. W. (2021) Corilagin prevents SARS-CoV-2 infection by targeting RBD-ACE2 binding, *Phytomedicine*, 87, 153591.
- [10] Li, X., Deng, Y., Zheng, Z., Huang, W., Chen, L., Tong, Q., Ming, Y. (2018) Corilagin, a promising medicinal herbal agent, *Biomedicine & Pharmacotherapy*, 99, 43-50.
- [11] Lv, H., Hong, L., Tian, Y., Yin, C., Zhu, C., & Feng, H. (2019) Corilagin alleviates acetaminophen-induced hepatotoxicity via enhancing the AMPK/GSK3 β -Nrf2 signaling pathway, *Cell Communication and Signaling*, 17(1), 1-15.
- [12] Yisimayili, Z., Guo, X., Liu, H., Xu, Z., Abdulla, R., Aisa, H. A., & Huang, C. (2019) Metabolic profiling analysis of corilagin *in vivo* and *in vitro* using high-performance

- liquid chromatography quadrupole time-of-flight mass spectrometry, *Journal of pharmaceutical and biomedical analysis*, 165, 251-260.
- [13] Senobari, Z., Karimi, G., & Jamialahmadi, K. (2022) Ellagitannins, promising pharmacological agents for the treatment of cancer stem cells, *Phytotherapy Research*, 36(1), 231-242.
- [14] Labbé, A., & Baudouin, C. (2015) Modulation of Wound Healing: Choice of Antifibrosis Therapies. In *Glaucoma* (pp. 894-905). WB Saunders.
- [15] Gad, S. E. (2014). Mitomycin C. 354-356.
- [16] Schmidt, O. T., & Lademann, R. (1951) Natural tannins. X. Corilagin, another crystalline tannin from dividivi. *Liebigs Ann. Chem*, 571, 232-237.
- [17] Yang, W. T., Li, G. H., Li, Z. Y., Feng, S., Liu, X. Q., Han, G. K., ... & Jin, F. (2016) Effect of corilagin on the proliferation and NF- κ B in U251 glioblastoma cells and U251 glioblastoma stem-like cells. *Evidence-Based Complementary and Alternative Medicine*
- [18] Yang, F., Wang, Y., Li, G., Xue, J., Chen, Z. L., Jin, F., ... & Zhao, L. (2018) Effects of corilagin on alleviating cholestasis via farnesoid X receptor-associated pathways *in vitro* and *in vivo*. *British journal of pharmacology*, 175(5), 810-829.
- [19] Li, Y., Wang, Y., Chen, Y., Wang, Y., Zhang, S., Liu, P., ... & Zhao, L. (2020) Corilagin ameliorates atherosclerosis in peripheral artery disease via the toll-like receptor-4 signaling pathway *in vitro* and *in vivo*. *Frontiers in immunology*, 11, 1611.
- [20] Heber, D. (2011) *Herbal Medicine: Biomolecular and Clinical Aspects*. Benzie IFF, Wachtel-Galor S (Ed.), Chapter 10: Pomegranate ellagitannins. CRC Press/Taylor & Francis, England.
- [21] Prakash, C. V. S., & Prakash, I. (2011) Bioactive chemical constituents from pomegranate (*Punica granatum*) juice, seed and peel-a review, *International Journal of Research in Chemistry and Environment*, 1(1), 1-18.
- [22] Tong, Y., Zhang, G., Li, Y., Xu, J., Yuan, J., Zhang, B., Hu, T., & Song, G. (2018). Corilagin inhibits breast cancer growth via reactive oxygen species-dependent apoptosis and autophagy, *Journal of cellular and molecular medicine*, 22(8), 3795-3807.
- [23] Rencuzogullari, C., Cincin, Z. B., Iplik, E. S., Baran, Y., & Cakmakoglu, B. (2019) Investigation of Potential Anticarcinogenic Effects of Corilagin in Lung Cancer Cells, *Clinical and Experimental Health Sciences*, 9(3), 228-231.

- [24] Liu, F. C., Chaudry, I. H., & Yu, H. P. (2017) Hepatoprotective effects of corilagin following hemorrhagic shock are through akt-dependent pathway, *Shock* (Augusta, Ga.), 47(3), 346.
- [25] Wu, C., Huang, H., Choi, H. Y., Ma, Y., Zhou, T., Peng, Y., Pang, K., Shu, G., Yang, X. (2021) Anti-esophageal Cancer Effect of Corilagin Extracted from *Phyllanthus fructus* via the Mitochondrial and Endoplasmic Reticulum Stress Pathways, *Journal of Ethnopharmacology*, 269, 113700.
- [26] Tong, Y., Zhang, G., Li, Y., Xu, J., Yuan, J., Zhang, B., Hu, T., & Song, G. (2018) Corilagin inhibits breast cancer growth via reactive oxygen species-dependent apoptosis and autophagy, *Journal of cellular and molecular medicine*, 22(8), 3795-3807.
- [27] Guo, S., Fu, Y., Xiong, S., & Lv, J. (2017) Corilagin protects the acute lung injury by ameliorating the apoptosis pathway, *Biomedicine & Pharmacotherapy*, 95, 1743-1748.
- [28] Tan, S., Su, Y., Huang, L., Deng, S., Yan, G., Yang, X., ... & Cheng, J. (2022) Corilagin attenuates osteoclastic osteolysis by enhancing HO-1 and inhibiting ROS, *Journal of Biochemical and Molecular Toxicology*, e23049.
- [29] Zhang, L., Jia, B., Velu, P., & Wu, H. (2022) Corilagin induces apoptosis and inhibits HMBG1/PI3K/AKT signaling pathways in a rat model of gastric carcinogenesis induced by methylnitrosoguanidine, *Environmental Toxicology*, 37(5), 1222-1230.
- [30] Huang, J., Lei, Y., Lei, S., & Gong, X. (2022) Cardioprotective effects of corilagin on doxorubicin induced cardiotoxicity via P13K/Akt and NF- κ B signaling pathways in a rat model. *Toxicology Mechanisms and Methods*, 32(2), 79-86.

Magnetization of a Quantum Dot Superlattice System in the Presence of a Rashba Spin-Orbit Coupling Term

Arif M. Babanlı^{1*}

¹Department of Physics, Süleyman Demirel University, 32260 Isparta, Turkey

Received: 20/10/2022, **Revised:** 06/12/2022, **Accepted:** 16/12/2022, **Published:** 30/12/2022

Abstract

In this paper, we have investigated the magnetization and the magnetic susceptibility of a quantum dot superlattice system in the presence of a magnetic field parallel to the superlattice axis and confined in a lateral parabolic quantum well. We took the effect of the Rashba spin-orbit interaction and Zeeman term on the specific heat into account. We have calculated the energy spectrum of the electron in the quantum dot superlattice system. Moreover, we have calculated the magnetization and the magnetic susceptibility dependence on the magnetic field and temperature of a quantum dot superlattice system.

Keywords: Superlattice, Rashba spin-orbit interaction, Quantum dot.

Rashba Spin-Yörünge Etkileşimli Kuantum Nokta Süper Örgü Sisteminin Manyetizasyonu

Öz

Bu makalede, süper örgü eksenine paralel manyetik alan varlığında ve parabolik kuantum kuyusunda sınırlandırılmış kuantum nokta süper örgü sisteminin manyetizasyonunu ve manyetik duyarlılığını araştırdık. Rashba spin-yörünge etkileşiminin ve Zeeman teriminin özgül ısı üzerindeki etkisini dikkate aldık. Kuantum nokta süper örgü sistemindeki elektronun enerji spektrumunu hesapladık. Ayrıca, kuantum nokta süper örgü sisteminin manyetizasyon ve manyetik duyarlılığının manyetik alana ve sıcaklığa bağlılığını hesapladık.

Anahtar Kelimeler: Süperörgü, Rashba spin-yörünge etkileşimi, Kuantum Nokta

1. Introduction

Low-dimensional systems based on semiconductors have been the object of great interest for many years since then there have been numerous applications based on these systems. Recently, a great deal of attention is being given to the study of transport phenomena in low-dimensional systems. In such systems, transport phenomena are sharply different from transport phenomena in macrosystems. The Landau diamagnetism of an electron gas in superlattices was presented in the paper [1], and it was found that the magnetization of a strongly degenerate electron gas changes its sign depending on the degree of band filling and magnetic field magnitude. In Ref.[2] the influence of interband and intraband transitions on vertical conductance oscillations in superlattices in a strong longitudinal magnetic field is considered. The thermal properties of a system, comprising spinless noninteracting charged particles in the presence of a constant external magnetic field and confined in a parabolic quantum well were studied in Ref.[3].

*Corresponding Author: arifbabanlı@sdu.edu.tr
A. M. Babanlı: <https://orcid.org/0000-0003-4468-999X>

The thermodynamic properties of an InSb quantum dot have been investigated in paper [4] in the presence of Rashba spin-orbit interaction and a static magnetic field.

In Ref. [5] the heat capacity used for the electronic system in the quantum dot superlattices, including the Zeeman effect of GaAs, InAs, and InSb was investigated, respectively, by using an isotropic parabolic potential under a magnetic field based on canonical ensemble statistics.

Voskoboynikov et. al. [6] presented a theoretical study of the effect of spin-orbit interaction on the electron magnetization and magnetic susceptibility of quantum dots at the weak magnetic field for degenerate electron gas.

B. Boyacioglu et. al [7] studied the heat capacity and entropy in GaAs quantum wire taking Gaussian potential as confinement in the presence of a magnetic field using the canonical ensemble approach. They found that at high temperatures, entropy is a monotonic increasing function of temperature but decreases with an increase in the magnetic field at a sufficiently low temperature.

In this paper, we have investigated the magnetization of a quantum dot superlattice system in the presence of external magnetic fields and Rashba spin-orbit interaction in the case non-degenerate electron gas.

We consider the thermal properties of an electron system in a quantum dot superlattice structure with a periodic potential of a period along the z-direction by using a cosine shape under the tight-binding approximation $V(z)=\varepsilon_0(1-\cos ak_z)$. Here ε_0 is the miniband half-width of the superlattice, k_z is the wave vector.

2. Material and Methods

The electron gas in the quantum dot superlattice structure is assumed to be confined in parabolic lateral potential [6]:

$$V_c(\rho) = \frac{1}{2} m \omega_0^2 \rho^2 \quad (1)$$

Where $\hbar\omega_0$ is the characteristic confinement energy, and ρ is the radius vector. A static magnetic field B is applied parallel to the superlattice z-axis.

In an axial magnetic field of the symmetric gauge for the vector potential $\vec{A} = \frac{B\rho}{2} \vec{e}_\phi$ (where ϕ is the azimuthal angle) the Rashba spin-orbital term in the cylindrical coordinates is given by

$$V_{SO}^R(\rho, \phi) = \sigma_z \alpha \frac{dV_c(\rho)}{d\rho} \left(-i \frac{1}{\rho} \frac{\partial}{\partial \phi} + \frac{e}{2\hbar} B \rho \right) \quad (2)$$

α is the Rashba spin-orbit coupling parameter, σ_z -is the Pauli z matrix. By including the Zeeman term Hamiltonian can be written as:

$$H = -\frac{\hbar^2}{2m} \left(\frac{1}{\rho} \frac{\partial}{\partial \rho} \rho \frac{\partial}{\partial \rho} + \frac{1}{\rho^2} \frac{\partial^2}{\partial \phi^2} \right) - i \frac{\hbar \omega_c}{2} \frac{\partial}{\partial \phi} + \frac{1}{8} m \omega_c^2 \rho^2 + \frac{\sigma_z}{2} g \mu_B B + V_c(\rho) + V(z) + V_{SO}^R(\rho, \phi) \quad (3)$$

where B-is the applied magnetic field, $\omega_c = \frac{eB}{m}$ is the cyclotron frequency, μ_B -is the Bohr magneton, m-is the electron effective mass, and g -is the spin decoupling. The eigenfunctions and eigenenergies of the Hamiltonian are given by

$$\Psi(\rho, \phi, k_z) = \frac{1}{\sqrt{2\pi L}} e^{ik_z \phi + il\phi} R(\rho) \chi_\sigma \quad (4)$$

where

$$R(\rho) = \frac{\sqrt{2}}{\rho_\sigma} \sqrt{\left(\frac{n!}{n+|l|} \right)} \exp\left(-\frac{\rho^2}{2\rho_\sigma^2} \right) \left(\frac{\rho^2}{\rho_\sigma^2} \right)^{\frac{|l|}{2}} L_n^{|l|} \left(\frac{\rho^2}{\rho_\sigma^2} \right) \quad (5)$$

Where $\rho_\sigma = \frac{\hbar}{m\Omega_\sigma}$, and $L_n^{|l|} \left(\frac{\rho^2}{\rho_\sigma^2} \right)$ the generalized Laguerre polynomial and χ_σ is the spin wave function, L is the z directional normalization lengths

$$\varepsilon_{nl\sigma k_z} = \hbar \Omega_\sigma (2n + |l| + 1) + \frac{l}{2} \hbar \omega_c + \sigma \left(\frac{1}{2} g \mu_B B + l m \alpha \omega_0^2 \right) + \varepsilon_0 (1 - \cos ak_z) \quad (6)$$

It is convenient to reparametrize these quantum numbers in terms of a pair of integers n_+, n_- , defined as

$$n_+ = \frac{2n + |l| + l}{2}; n_- = \frac{2n + |l| - l}{2}; n_+ - n_- = l \quad (7)$$

With $n_\pm = 0, 1, 2, \dots \infty$. The energy spectrum can be rewritten as

$$\varepsilon_{n_+n_-\sigma k_z} = \hbar\omega_-^\sigma \left(n_- + \frac{1}{2} \right) + \hbar\omega_+^\sigma \left(n_+ + \frac{1}{2} \right) + \frac{\sigma}{2} g\mu_B B + \varepsilon_0 (1 - \cos ak_z) \quad (8)$$

where

$$\omega_+^\sigma = \Omega_\sigma + \frac{\omega_c}{2} + \frac{m\alpha\omega_0^2}{\hbar}; \omega_-^\sigma = \Omega_\sigma - \frac{\omega_c}{2} - \frac{m\alpha\omega_0^2}{\hbar}; \quad (9)$$

where $\sigma = \pm 1$ refers to the electron-spin polarization along the z-axis.

$$\Omega_\sigma = \sqrt{\omega_0^2 + \frac{\omega_c^2}{4} + \sigma\alpha\omega_c \frac{m\omega_0^2}{\hbar}} \quad (10)$$

The grand thermodynamic potential of a nondegenerate electron system is given as:

$$\Omega = -\frac{1}{\beta} \sum_{n_+n_-\sigma k_z} e^{-\beta(\mu - \varepsilon_{n_+n_-\sigma k_z})} \quad (11)$$

where $\varepsilon_{n_+n_-\sigma k_z}$ is the energy spectrum of the considered system, $\beta = \frac{1}{k_B T}$ with k_B being the Boltzmann constant, and μ is the chemical potential of the electron gas. We pass from the summation concerning k_z to the integration over k_z and after summation for n_+ , n_- equation (11) takes the form

$$\Omega = -\frac{LI(0, \beta\varepsilon_0) e^{\beta(\mu - \varepsilon_0)}}{\beta a} \left(\frac{e^{\frac{\beta\mu_B}{2} gB}}{4 \sinh\left(\beta \frac{\hbar\omega_+^+}{2}\right) \sinh\left(\beta \frac{\hbar\omega_-^+}{2}\right)} + \frac{e^{-\frac{\beta\mu_B}{2} gB}}{4 \sinh\left(\beta \frac{\hbar\omega_+^-}{2}\right) \sinh\left(\beta \frac{\hbar\omega_-^-}{2}\right)} \right) \quad (12)$$

where $I(0, \beta\varepsilon_0)$ is the modified Bessel function zero-order, and L is the length along the z-direction. We can find the total number of particles N of the system as

$$N = -\left(\frac{\partial \Omega}{\partial \mu}\right)_{V,T} = -\frac{LI(0, \beta\varepsilon_0) e^{\beta(\mu - \varepsilon_0)}}{a} \left(\frac{e^{\frac{\beta\mu_B}{2} gB}}{4 \sinh\left(\beta \frac{\hbar\omega_+^+}{2}\right) \sinh\left(\beta \frac{\hbar\omega_-^+}{2}\right)} + \frac{e^{-\frac{\beta\mu_B}{2} gB}}{4 \sinh\left(\beta \frac{\hbar\omega_+^-}{2}\right) \sinh\left(\beta \frac{\hbar\omega_-^-}{2}\right)} \right) \quad (13)$$

The chemical potential of a non-degenerate electron gas in a magnetic field from (13), we obtain

$$\mu = \frac{1}{\beta} \ln \left[\frac{Na}{L} \frac{e^{\beta \varepsilon_0}}{I(0, \beta \varepsilon_0)} \left(\frac{e^{\frac{\beta \mu_B}{2} g B}}{4 \sinh\left(\beta \frac{\hbar \omega_+}{2}\right) \sinh\left(\beta \frac{\hbar \omega_-}{2}\right)} + \frac{e^{-\frac{\beta \mu_B}{2} g B}}{4 \sinh\left(\beta \frac{\hbar \omega_+}{2}\right) \sinh\left(\beta \frac{\hbar \omega_-}{2}\right)} \right) \right]^{-1} \quad (14)$$

The magnetization of an electron gas M can be found in the form of the grand thermodynamic potential as follows [9]:

$$M = -\frac{1}{V} \left(\frac{\partial \Omega}{\partial B} \right)_{\mu, T} \quad (15)$$

The magnetic susceptibility

$$\chi = \frac{\partial M}{\partial B} \quad (16)$$

3. Results and Discussion

We introduce dimensionless parameters $x = \frac{\omega_c}{\omega_0}$ the quantity of the magnetic field strength,

which $\xi = \frac{2}{\beta \hbar \omega_0}$ represents the temperature measured, $z = \frac{2 \varepsilon_0}{\hbar \omega_0}$ to represent the miniband

half-width, and $\lambda = \alpha \frac{m \omega_0}{\hbar}$ to represent the Rashba spin-orbit coupling. For our calculation we consider the parameter corresponding to InSb materials: $m = 0.014 m_0$, where m_0 is the free electron mass, and $\varepsilon_0 = 1 \text{ meV}$ [8], $g = 3.2$, $\alpha = 500 \text{ \AA}^2$, $\hbar \omega_0 = 0.025 \text{ eV}$ are taken from the literature [8].

In Fig.1 we plot the reduced magnetization and the reduced magnetic susceptibility as a function of the reduced magnetic field x for the fixed value of the dimensionless parameter $\xi=0.5$, and the dimensionless Rashba parameter $\lambda=0;0.022$. As seen from Fig. 1 in InSb type quantum dot superlattice, the magnetization and the magnetic susceptibility change from a negative value (diamagnetic) to a positive value (paramagnetic) with magnetic field value $\lambda=0.022$. For parameter $\lambda=0$ the magnetic susceptibility and magnetization take a negative value. These results are consistent with the results in the literature [1].

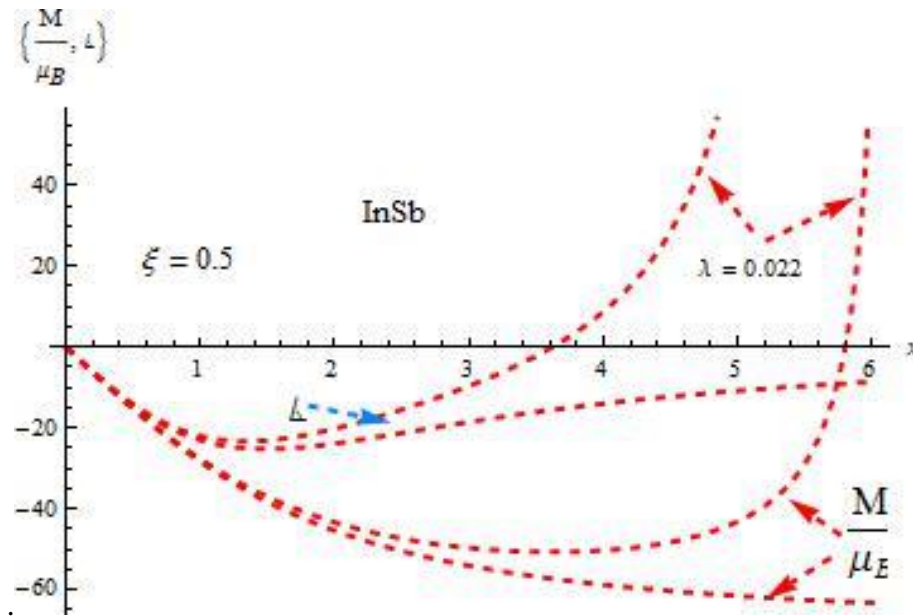


Fig.1. The reduced magnetization and the reduced magnetic susceptibility as a function of the reduced magnetic field x for a fixed value of the dimensionless parameter $\xi=0.5$, and the dimensionless Rashba parameter $\lambda=0;0.022$. $L = \frac{x}{\chi_0}$, $\chi_0 = \frac{N\mu_B}{B}$.

Fig.2 shows the behavior of reduced magnetic susceptibility and reduced magnetization versus the temperature for two values of Rashba parameters, at fixed reduced magnetic field $x=0.5$. It is seen from the figure that the system has diamagnetic behavior at the dimensionless Rashba parameter $\lambda=0$. For the dimensionless Rashba parameter $\lambda=0.022$, but with increasing the temperature the susceptibility shows a transition from a negative value (diamagnetic) to a positive value (paramagnetic) at a fixed magnetic field.

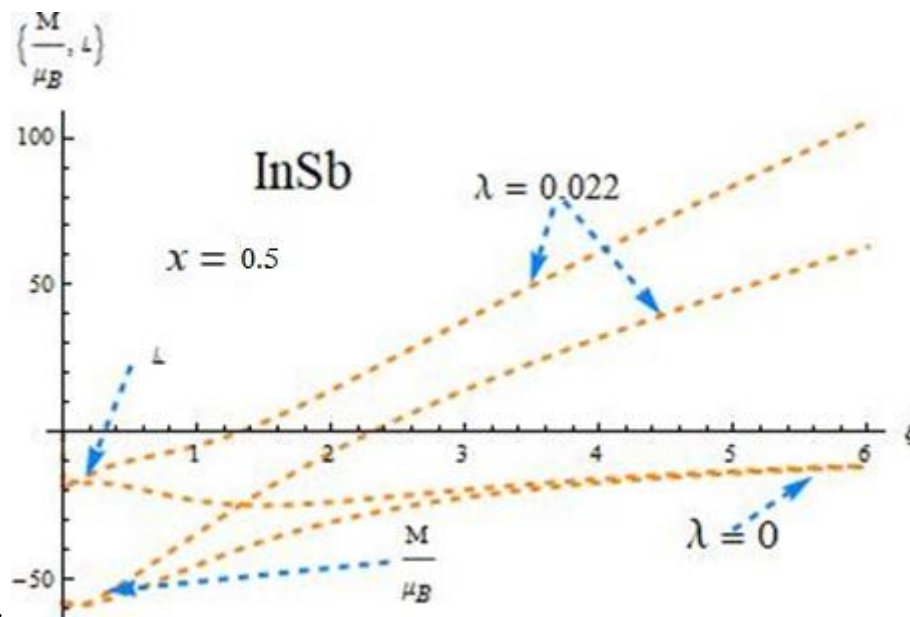


Fig.2. The reduced magnetic susceptibility and reduced magnetization versus the temperature for two values of Rashba parameters $\lambda=0;0.022$, at fixed reduced magnetic field $x=0.5$. $L = \frac{\chi}{\chi_0}$, $\chi_0 = \frac{N\mu_B}{VB}$.

4. Conclusions

We have calculated the magnetic susceptibility and magnetization of the quantum dot superlattice with Rashba spin-orbit coupling in the magnetic field for non-degenerate electron gas. Canonical formalism is used to calculate magnetization. We have investigated the dependence of the magnetic susceptibility and magnetization on the magnetic field and the temperature in quantum dots superlattice. As a function of temperature, magnetic susceptibility, and magnetization change signs.

Ethics in Publishing

There are no ethical issues regarding the publication of this study.

References

- [1] Askerov, B.M., Figarova, S.R., Mahmudov, M.M., (2008) Diamagnetism of an electron gas in superlattices, Proc. R. Soc. A 464(2100) 3213-3218.
- [2] Figarova, S.R., and Figarov, V.R., (2021) Vertical Conductance in Superlattice in Strong Magnetic Field during Inter- and Intraband Transitions, Russ Phys J 64, 949–955.
- [3] Tridev Mishra, Tapomoy Guba Sarkar, and Jayendra N.Bandyopadhyay, (2014) Thermal properties of a particle confined to a parabolic quantum well in two-dimensional space with conical disclination, Phys.Rev E 89 (1), 012103.

- [4] Sukirti Gumber, Manoj Kumar, Pradip Kumar Jha, and Man Mohan (2016) Thermodynamic behavior of Rashba quantum dot in the presence of the magnetic field, *Chin.Phys. B* 25,5,056502.
- [5] Sang Chil Lee, Suck Whan Kim, (2012) Heat capacity in a quantum-dot superlattice with the Zeeman effect, *Journal of the Korean Physical Society*,61, No.1,162-167.
- [6] Voskoboynikov O.,Bauga O. Lee, C.P., and Tretyak, O, (2003) Magnetic properties of parabolic quantum dots in the presence of the spin-orbit interaction,*Journal of Applied Physics*, 94 (9), 5891.
- [7] Boyacioglu, B. Chatterjee, A. (2012). Heat capacity and entropy of a GaAs quantum dot with Gaussian confinement, *Journal of Applied Physics*, 112(8), 083514.
- [8] Askerov B.M., Figarova S.R., Mahmudov M.M., (2006), Longitudinal magnetoresistance of layered crystals in a quantizing magnetic field taking into account the spin splitting, *Physica E*, 33(2), 303–307.
- [9] Askerov Bahram M.; Figarova, Sophia (2010), *Thermodynamics, Gibbs Method and Statistical Physics of Electron Gases*, Volume 57, Springer Series on Atomic, Optical, and Plasma Physics.
- [10].Figarova S.R., Mahmudov M.M , Magnetization of electron gas with a cosinoidal dispersion law in strong magnetic field, *News of Baku University*,4,115,20018

Design of Digital Low Pass FIR Filter Using Hybrid Particle Swarm – Grey Wolf Optimization Algorithm

Çağrı ALTINTAŞI^{1*}

¹Dept. of Electrical and Electronics Engineering, Erzincan Binali Yildirim University, Erzincan, Turkey

Received:01/04/2022, **Revised:** 28/04/2022, **Accepted:** 07/05/2022, **Published:** 30/12/2022

Abstract

In this study, digital low-pass Finite Pulse Response (FIR) filter is designed using Hybrid Particle Swarm – Grey Wolf Optimization Algorithm (HPSGWO). The purpose of digital FIR filter design with HPSGWO is to optimized filter coefficients that are closest to the characteristics of the ideal filter. The obtained results are compared with PSO, and GWO algorithms which were previously used for FIR filters design in the literature. According to the obtained results, HPSGWO has better filter response and less stop band ripple than other methods.

Keywords: finite impulse response (FIR), particle swarm optimization (PSO), grey wolf optimizer(GWO), hybrid particle swarm – grey wolf optimization (HPSGWO).

Hibrit Parçacık Sürü Gri Kurt Optimizasyon Algoritması Kullanılarak Dijital Alçak Geçiren FIR Filtresinin Tasarımı

Öz

Bu çalışmada, Hibrit Parçacık Sürü – Gri Kurt Optimizasyon Algoritması (HPSGKO) kullanılarak sayısal alçak geçiren sonlu dürtü yanıtı filtre (FIR) tasarlanmıştır. HPSGKO ile dijital FIR filtre tasarımının amacı, ideal filtrenin özelliklerine en yakın filtre katsayılarını optimize etmektir. Elde edilen sonuçlar, literatürde daha önce FIR filtre tasarımı için kullanılan PSO ve GKO ile karşılaştırılmıştır. Elde edilen sonuçlara göre, HPSGKO diğer yöntemlere göre daha iyi filtre yanıtına ve daha az maksimum durdurma bandı dalgalanmasına sahiptir.

Anahtar Kelimeler: sonlu dürtü yanıtı (FIR), parçacık sürüsü optimizasyonu (PSO), gri kurt optimizasyonu (GKO), hibrit parçacık sürüsü – gri kurt optimizasyonu (HPSGKO)..

1. Introduction

Filtering is widely used in signal processing to convert the frequency spectrum of the input signal to the desired characteristic. Digital filters have an important role in the communication systems, image processing, and processing of biomedical signals [1]. Two types of digital filter design are possible, Infinite Pulse Response (IIR) and Finite Pulse Response (FIR) [1]. Although IIR filters have less memory and less filter coefficient than FIR filters, FIR filters are linear and stable [2]. The characteristic of a designed digital filter is expected to be closest to the ideal filter characteristic. That is, it is expected to converge rapidly to the cutoff frequency, with the minimal ripple in the pass-band and the maximum stop-band attenuation. Stop-band attenuation gives information about the maximum ripple amount in decibel in the stop-band region and it is infinite for the ideal filter. Windowing types such as rectangular, Kaiser, Hamming, Hanning, Blackman are used as classical methods in filter design [1], [3]. Although the rectangular windowing method converges to the cutoff frequency faster than other classical methods, the ripples in the pass and stop bands are higher. In windowing methods such as Kaiser, Hamming, Hanning, and Blackman, the ripple in the pass and stop bands are low, but convergence to the cutoff frequency is too slow. Avci design exponential -hamming FIR filter to increase stop-band attenuation [4]. Although this filter has more stop-band attenuation than the hamming, kaiser, and hamming filter, has less stop-band attenuation than the Equiripple FIR filter.

In recent years, FIR filters have been designed with optimization algorithms in order to reduce both the rapid convergence and the ripples in the pass and stop bands in the literature. Gravitational Search Algorithm (GSA) [5], Cat Swarm Optimization (CSO) [6], Particle Swarm Optimization (PSO) [7-8], Genetic Algorithm (GA) [9-10], Cuckoo Search Algorithm (CSA) [11], Artificial Bee Colony (ABC) [12-13], Grey Wolf Optimizer (GWO) [3], and Moth Flame Optimization (MFO) [2] are implemented to design digital FIR filters.

When the magnitude characteristics of the digital FIR filter made with the above-mentioned optimization algorithm are examined, it is seen that there is high ripple in the pass and stop band. In this study, digital low-pass FIR filter design is carried out using the hybrid Particle Swarm – Grey Wolf Optimization Algorithm (HPSGWO) to minimize the ripples in the pass and stop bands. The obtained results are compared with PSO and GWO algorithms, and it is shown that the HPSGWO algorithm has less ripple in the stop band and better suppresses the frequency components above the cutoff frequency.

2. Low Pass FIR Filter Problem Statement

The mathematical representation of the FIR filter is shown in equation 1.

$$H(z) = \sum_{n=0}^{N-1} h[n]z^{-n} \quad (1)$$

In Equation 1, $N-1$ represents the order of the filter, and $h[n]$ represents the impulse response of N filter coefficients.

In the literature, the filter is classified into four types according to its length and property of symmetry. In this study, the filter design is carried out by considering the odd length and even symmetric defined as Type 1. With the advantage of the symmetry feature, $1+(N-1)/2$ filter coefficients of filter are estimated, then all the filter coefficients of $h[n]$ are obtained. The mathematical expression of magnitude response of the filter for the Type 1 is shown in Equation 2.

$$H_d(\omega) = h\left[\frac{N-1}{2}\right] + 2 \sum_{n=0}^{\left(\frac{N-1}{2}\right)-1} h[n] \cos\left(\left(\frac{N-1}{2} - n\right)\omega\right) \quad (2)$$

The magnitude response of the ideal low-pass FIR filter is shown in Equation 3.

$$H_i(\omega) = \begin{cases} 1, & 0 \leq \omega \leq \omega_c \\ 0, & \text{otherwise} \end{cases} \quad (3)$$

where, ω_c represents the cut off frequency.

In this study, the objective function defined in the literature as the absolute magnitude response error between the ideal and the designed filter shown in Equation 4 is minimized using the HPSGWO algorithm. In the equation 4, δ_p and δ_s are the passband and stopband ripples, respectively.

$$e(\omega) = \sum_{\omega=0}^{\omega_c} \left| |H_d(\omega)| - H_i(\omega) - \delta_p \right| + \sum_{\omega_c+1}^{\pi} \left| |H_d(\omega)| - H_i(\omega) - \delta_s \right| \quad (4)$$

3. Hybrid PSO–GWO (HPSGWO)

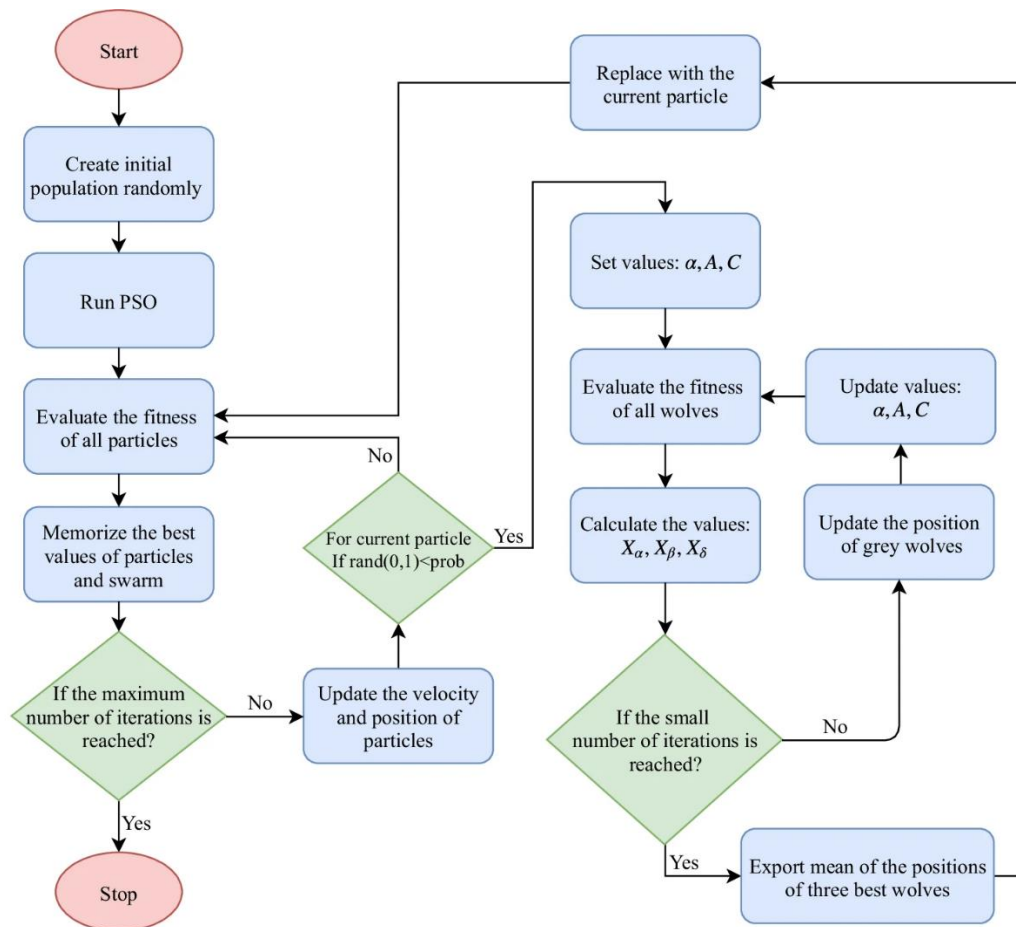
PSO and GWO are popular meta-heuristic algorithms preferred for many problems in the literature. Şenel developed the hybrid PSGWO algorithm by combining the GWO algorithm with the PSO algorithm in order to reduce the probability of the PSO algorithm catching a local minimum [14]. Thus, instead of randomly assigning the particles in the solution space in PSO, it is aimed to obtain more optimum results by directing them to the positions determined by the GWO algorithm. The flow diagram and the pseudocode of the HPSGWO algorithm is shown in Figure 1 [14].

In Figure 1, X_α, X_β and X_δ represent the best three wolves in each iteration. In addition, A and C in Figure 1 are the coefficient vectors of the GWO, and their mathematical expressions are shown in Equations 5 and 6.

$$A = a(2r_1 - 1) \quad (5)$$

$$C = 2r_2 \quad (6)$$

where a is the coefficient that decreases linearly from 2 to 0 as the number of iterations increases, and r_1 and r_2 are random numbers that change between 0 and 1.



Pseudocode of HPSGWO Algorithm
<pre> Initialize particles for i = 1 :1: 1000 for j = 1 :1:200 do Run PSO Update the velocity and the position of current particle if rand(0, 1) < prob Set a, A, C parameters for k = 1 :1: 10 do for m = 1 :1:10 do Run GWO Update the α, β and δ wolves and a, A, C parameters end for end for position of current particle = mean of the positions of three best wolves end if end for end for </pre>

Figure 1. Flow chart of HPSGWO algorithm [14].

4. Simulation Results

The simulation results are performed with the help of MATLAB based on the values given in Table 1 which are frequently used in the literature. The order of the low-pass FIR filter is chosen as 20 and because of the symmetry, 11 coefficients are estimated by the HPSGWO algorithm. In order to obtain the best filter coefficients, the algorithm is run 50 times and the obtained best filter coefficients are shown in Table 2.

Table 1. FIR filter design parameters

Parameters	Value
Particular Size	200
Iteration Number	1000
Filter Order	20
Number of Frequency Samples	128
Pass-band Ripples (δ_p)	0.01
Stop-band Ripples (δ_s)	0.01
w_c	0.5π

Table 2. HPSOGWO low pass FIR filter coefficients of order 20

h(N)	HPSGWO
h(1)=h(21)	0.0024
h(2)=h(20)	0.0176
h(3)=h(19)	-0.0009
h(4)=h(18)	-0.0324
h(5)=h(17)	0.0033
h(6)=h(16)	0.0523
h(7)=h(15)	-0.0032
h(8)=h(14)	-0.1008
h(9)=h(13)	0.0040
h(10)=h(12)	0.3152
h(11)	0.4971

Figure 2 shows the magnitude responses of low-pass FIR filters performed with HPSWGO, PSO and GWO algorithms. As seen in Figure 2, filter response of HPSGWO algorithm is better than PSO and GWO algorithms. Also, the FIR filter obtained with the HPSGWO algorithm has less ripple in the stopband. Table 3 shows the stop-band attenuation of the filters obtained by HPSGWO, PSO and GWO algorithms. When Table 3 is examined, it is clearly seen that the designed filter obtained with the HPSGWO algorithm has a higher stop-band attenuation. Thus, the characteristic of the low-pass FIR filter designed with the HPSGWO algorithm is closer to the characteristic of the ideal low-pass filter.

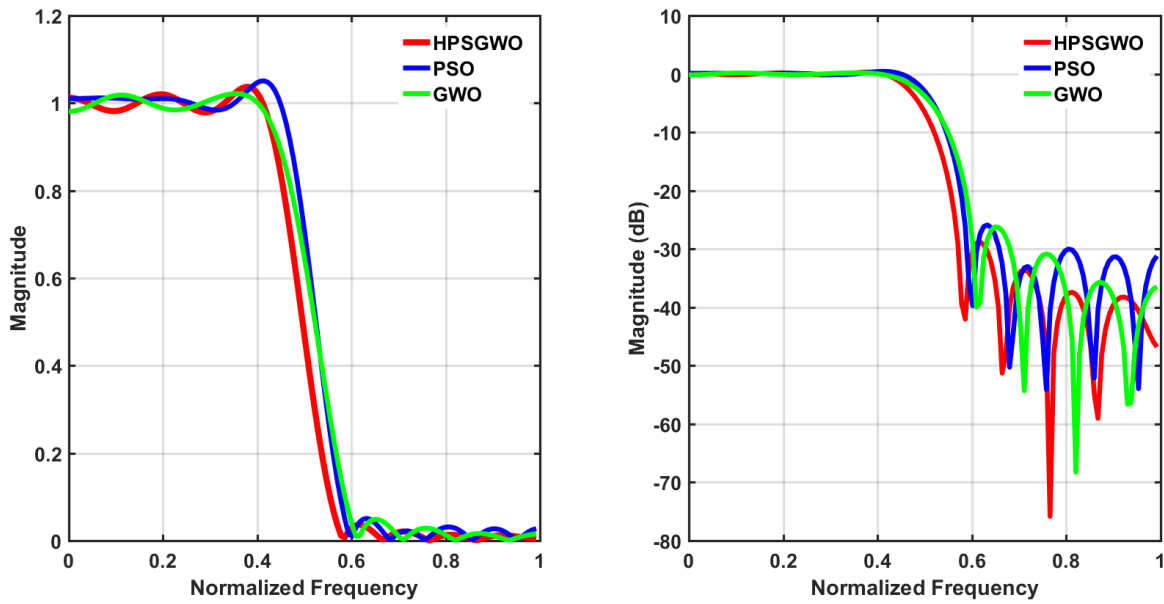


Figure 2. Magnitude response of low pass FIR filter of order 20

Table 3. Stop-band attenuation of HPSGWO, GWO and PSO algorithms

Algorithm	HPSGWO	GWO	PSO
Stop-Band Attenuation	28.8	26.2	25.8

5. Conclusion

The purpose of the digital FIR filter design is to obtain the filter coefficients of the filter response that are closest to the ideal filter response. In this study, a digital low-pass filter is designed with the HPSGWO algorithm, and it is shown that the filter response has less oscillation and is closer to the ideal real filter response than the filters realized with PSO and GWO algorithms. As a further study, it is planned to use the FIR filter designed with the HPSGWO algorithm in real system applications.

Ethics in Publishing

There are no ethical issues regarding the publication of this study.

References

[1] Winder, S. (2002). Analog and digital filter design. Elsevier.

[2] Adamu, Z. M., Dada, E. G., & Joseph, S. B. (2021). Moth Flame Optimization Algorithm for Optimal FIR Filter Design. *International Journal of Intelligent Systems & Applications*, 13(5).

[3] Sidhu, N. K., & Dhillon, J. S. (2017). Design of Digital FIR Filter Using Grey Wolf Optimizer Algorithm. *International Journal of Advanced Research in Computer Science*, 8(7).

- [4] Avci, K. (2016). Design of FIR filters using exponential--Hamming window family. *Turkish Journal of Electrical Engineering and Computer Sciences*, 24(4), 2513-2524.
- [5] Saha, S. K., Kar, R., Mandal, D., & Ghoshal, S. P. (2013). Design and simulation of FIR band pass and band stop filters using gravitational search algorithm. *Memetic Computing*, 5(4), 311-321.
- [6] Saha, S. K., Ghoshal, S. P., Kar, R., & Mandal, D. (2013). Cat swarm optimization algorithm for optimal linear phase FIR filter design. *ISA transactions*, 52(6), 781-794.
- [7] Kumari, N., & Jaglan, P. (2017). Design Of FIR Low Pass Filter Using Particle Swarm Optimization Algorithm. *International Journal of Advanced Research And Publications*, 1(3), 31-35.
- [8] Praneeth, A., & Shah, P. K. (2016, May). Design of FIR filter using particle swarm optimization. In *international conference on Advance in computing, communication and informatics (ICACCI)*, Jaipur in (pp. 2658-2661).
- [9] Suckley, D. (1991). Genetic algorithm in the design of FIR filters. *IEE Proceedings (Circuits, Devices and Systems)*, 138(2), 234-238.
- [10] GARIP, Z. B., & BOZ, A. F. (2018). The FIR Filter Design based on Genetic Algorithm. *Balkan Journal of Electrical and Computer Engineering*, 6, 33-36.
- [11] Kwan, H. K., & Liang, J. (2016, October). Minimax design of linear phase FIR filters using cuckoo search algorithm. In *2016 8th International Conference on Wireless Communications & Signal Processing (WCSP)* (pp. 1-4). IEEE.
- [12] Dwivedi, A. K., Ghosh, S., & Londhe, N. D. (2016). Low power FIR filter design using modified multi-objective artificial bee colony algorithm. *Engineering Applications of Artificial Intelligence*, 55, 58-69.
- [13] Ji, D. (2016, August). The application of artificial bee colony (ABC) algorithm in FIR filter design. In *2016 12th International Conference on Natural Computation, Fuzzy Systems and Knowledge Discovery (ICNC-FSKD)* (pp. 663-667). IEEE.
- [14] Şenel, F. A., Gökçe, F., Yüksel, A. S., & Yiğit, T. (2019). A novel hybrid PSO–GWO algorithm for optimization problems. *Engineering with Computers*, 35(4), 1359-1373.

An Electronically Tunable Low Power Low Pass Filter Employing Capacitor Multiplier for Biomedical Applications

Deniz Özenli^{1,3}, Ersin Alaybeyoğlu^{2,3*}

¹Department of Electronics Engineering, Turkish Air Force Academy, National Defence University, Istanbul, 34149, Turkey

²Electrical and Electronics Engineering, Bartın University, Bartın, Turkey

³Electrical and Communication Engineering, Istanbul Technical University, Istanbul, Turkey

Received: 07/06/2022, **Revised:** 03/07/2022, **Accepted:** 14/07/2022, **Published:** 30/12/2022

Abstract

In this work, a novel 0.9nW low pass filter is proposed using 0.18 μ m TSMC technology in Cadence environment to reject unwanted signals of biomedical applications. Active RC filter is designed with a new capacitor multiplier implementation providing high multiplication factor along with low power consumption. The designed circuit operates with ± 0.3 V supply voltages with DTMOS technique. At the same time, the power consumption of the proposed circuit is very low that can be implemented in implantable devices. The bandwidth of the designed filter is adjustable between 500mHz and 65Hz. In terms of Figure of Merit, the proposed filter outperforms the recommended circuits in the literature.

Keywords: Biomedical Applications, Low Pass Filter, Operational Transconductance Amplifier (OTA), Dynamic Threshold MOS (DTMOS)

Biyomedikal Uygulamalar için Kapasite Çarpıcı Kullanan Elektronik Olarak Ayarlanabilen Düşük Güçlü Alçak Geçiren Süzgeç

Öz

Bu çalışmada, biyomedikal uygulamaların istenmeyen işaretleri süzmek için Cadence ortamında 0.18 μ m TSMC teknolojisi kullanılarak yeni bir 0.9nW düşük geçiş filtresi önerilmiştir. Aktif RC filtresi, düşük güç tüketimi ile birlikte yüksek çarpma faktörü sağlayan ve üç katmalı OTA yapısından oluşan yeni bir kapasite çarpıcı devresi ile tasarlanmıştır. Tasarlanan filtrenin bant genişliği 500mHz ile 65Hz arasında ayarlanabilmektedir. Aynı zamanda önerilen devrenin güç tüketimi taşınabilir cihazlarda uygulanabilecek kadar düşüktür. Önerilen kapasite çarpıcı devresi özellikle güç tüketimi ve çalışma gerilimi açısından literatürde önerilen devrelerden daha yüksek performans göstermektedir.

Anahtar Kelimeler: Biyomedikal Uygulamalar, Alçak Geçiren Süzgeç, OTA, DTMOS

*Corresponding Author: ealaybeyoglu@bartin.edu.tr

Deniz ÖZENLİ, <https://orcid.org/0000-0002-6381-3629>

Ersin ALAYBEYOĞLU, <https://orcid.org/0000-0002-8318-4081>

1. Introduction

Today, the demand for wireless devices such as portable biomedical devices, smartphones, laptops, tablet computers, and various wireless devices is constantly increasing. Integration of system plays a role as important as power dissipation for portable devices. Industry 4.0 applications will further expand the use of mobile devices [1]. The portability of digital circuits is increased by the CMOS technology produced in small dimensions. However, the fact that CMOS transistors produced in small sizes cannot be used effectively in analog circuit design has led to the search for new methods to design analog circuits [1,2].

CMOS technology is ideal in terms of the circuit, which needs to be designed with low power consumption. The minimized supply voltage is functional to reduce the power consumption of the circuits. The threshold voltage cannot be downscaled by the same extent as the supply voltage in modern small size CMOS technologies gets smaller. The high V_{TH} is required to obtain a low current when the transistor is switched off. The current injection of MOSFETs is generally in several nano amper ranges in the weak inversion region that will be functional due to a minimized supply voltage [3,4]. Also, the circuit topology must be suitable for the minimized supply voltage. The above requirements encourage the innovative design strategies in CMOS analog circuit design [5-8]. For example, the Dynamic Threshold MOS (DTMOS) technique is an example of new design strategies proposed for CMOS technology [9,10]. Particularly, low power consumption has increased the importance for the circuits used in the Internet of Things applications that are becoming widespread in our lives [11,12].

In biomedical signal acquisition systems, low frequency filters are used to reject unwanted signals and extract low frequency bio-potential signals. The rejection of out-of-band noise and interference suppression is realized by using these low frequency filters [13,14]. Bio-potential signals are weak analog signals. The amplitude of bio-potential signals extends between $1\mu V$ to $10mV$ while the frequency of bio-potential signals ranges from less than $1Hz$ to $10kHz$ [15]. In the integration of low pass filters operated at low frequencies, the filter topology of RLC and RC are not practical due to the high costs [16]. Switched capacitor filters are not preferred to collect bio-potential signals because they are affected by leakage currents in the switching [17]. In biomedical systems, to catch the low frequency operation, $G_m - C$ filters are widely used [18]. In $G_m - C$ filters, the cut-off frequency is determined by the G_m / C ratio, where G_m is defined as the transconductance of the operational trans-conductance amplifier (OTA) and C is integrated capacitor. To implement the filter at low cut-off frequencies, large valued C and pretty small G_m are preferred. In this respect, various design techniques have been proposed in the literature to obtain low G_m to OTAs [19,20].

However, capacitance multiplier circuits are commonly used for applications described in the literature as sub-hertz [21-23]. In an RC network, circuits operating at low frequencies are designed by increasing the time constant with a huge value of resistance or capacitance. To improve the time constant of RC network, the multiplied capacitance can be implemented instead of conventional capacitor.

In this study, a low pass filter is designed to meet the wireless features of biomedical applications, with a wide range of settings based on capacitor multiplier. The design consumes very low power, suitable for bio-potential signal acquisition systems used in the applications of Internet of Things. The presented circuit is implemented with DTMOS transistors in sub-threshold region. Meanwhile, supply voltages of the design are $\pm 0.3V$. Overall simulations are realized in Cadence environment. Also, the performance of the circuit is verified using $0.18\mu m$ TSMC technology.

This paper is organized as follows. In the second section, circuit design of the capacitance multiplier is given. In the third section, the CMOS realization of capacitor multiplier is given

while second order Butterworth filter structure and its layout are given in forth section. Transient and AC analysis of the designed filter are given in forth section with noise analysis. Additionally, the performance of the designed filter is justified by comparing conventional designs in terms of Figure of Merit. Section V gives some conclusions.

2. Circuit Design of Proposed Capacitance Multiplier

One of the most limiting problems in the design of integrated circuits is the large area occupation on the integration of passive circuit elements such as resistance, inductance and capacitance. Continuous time applications in which the use of component (R, L and C) multipliers is inevitable have to deal with the problem of integration of high-value passive circuit elements. There is widespread research in the literature on this critical issue. In this respect, the design of capacitance multiplier circuits is of greater importance than others. Although it is used in RF designs with the general acceptance of inductance, capacitor is an indispensable circuit element in most of circuits such as capacitive low frequency filters, analog to digital converters, and digital to analog converter. In particular, $G_m - C$ filters including multiplier structures have been widely used in the literature. Such capacitance multiplier circuits have attractive properties of temperature insensitive C-values with good stability [24–27].

The categorization of capacitor multipliers designed in the literature can be divided to two parts as voltage and current-mode. The voltage-mode capacitor multiplier circuits are generally used for frequency compensation. In this regard, capacitor multipliers designed with operational amplifiers can be given as an example of voltage mode multipliers. The current mode multipliers can be designed with CCII, OTA and etc. The second generation current conveyor (CCII) has also been used to realize C-multiplier circuits due to its attractive characteristics [22,28]. Even though CCII are suitable for the multiplier design with high multiplication factor, OTAs are more attractive building blocks for the reconfigurable design of multiplication factor. A large number of OTA-based C-multiplier circuits using bias adjustment have been reported in literature [27,29].

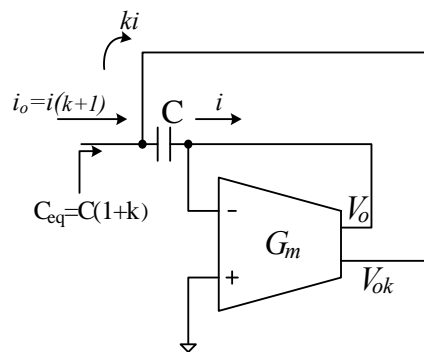


Figure 1. OTA based capacitor multiplier.

The simplest OTA based capacitor multiplier reported as current mode is shown in Figure1, while the proposed circuit is given in Figure 2. The first and second OTAs used in the implementation of the multiplier have multiple current outputs. In this topology, “ i ” on C is sensed with the low value of G_{m1} . Multiplication of the sensed current by multiplication factor denoted as k , is obtained with higher gain of $G_{m1} \cdot G_{m2} \cdot G_{m3} \cdot R_{o1} \cdot R_{o2}$ where R_o denotes the output impedances of the each OTA. In this respect, i_o is equal to “ i ” times $(1 + k)$, while C_{eq} is equal to the $C \cdot (1 + k)$. As a result, output current shown as i_o in the Figure 2, gives k times higher value of the current in (1) approximately. It should be noted that this simple scheme based on traditional topology provides good accuracy in spite of limited multiplication factor

and allows only single-ended applications, whereas the current multiplication inside single OTA with current mirror or other methods increases the consumption of power and the occupation area on the silicon [30].

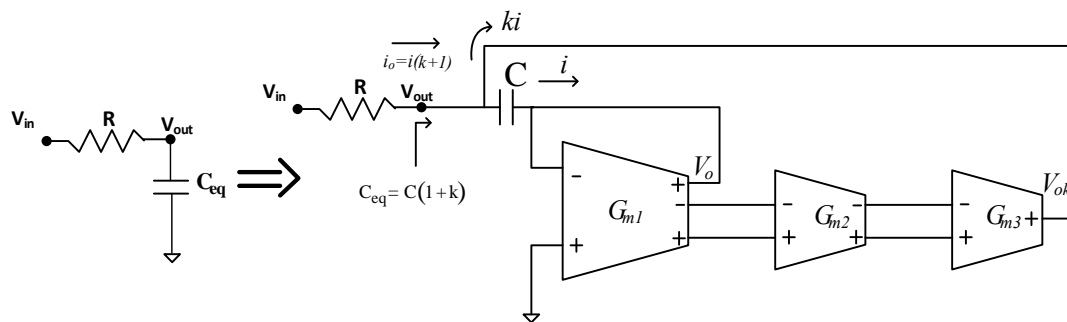


Figure 2. Proposed filter with capacitor multiplier.

This proposed topology is developed version of OTA based multipliers reported in literature [27], [31]. In this topology, the multiplied current $k \cdot i$ is obtained with three cascaded OTA. The non-inverting output of the first cell gives V_o , while V_{ok} is the non-inverting output of third cell. The third OTA is driven with the fully differential output of second OTA, while the fully differential output of first OTA drives the second OTA. The multiplication factor of k is maximized by selecting the conductivity of the second and third cell as high as possible. The equation of i is given in (1). G_m defines the transconductance of OTA, where V_P is non-inverting input of OTA and V_N is inverting input of OTA as well.

$$i = G_{m1}(V_P - V_N) \quad (1)$$

In this respect, taking into consideration output impedances of the OTAs, impedance seen from V_{out} node can be given in the following form:

$$Z = \frac{sC + G_{m1}}{sC(G_{m1} + 4R_{o1}R_{o2}G_{m1}G_{m2}G_{m3})} // R_{o3} \quad (2)$$

In the subthreshold operation, very high output impedances of OTAs can be obtained. Hence, for the simplicity of calculations, third OTA's output impedance can be ignored. Furthermore, in the low operating currents with the help of DTMOS technique, G_{m1} can be easily tuned from a few nS up to a couple of 10 nS. For the base capacitance (C) values in the range of a couple of 10pFs, (2) can be easily simplified as follows for the biomedical applications with the operating frequency up to around 100Hz:

$$Z \cong \frac{G_{m1}}{sC(G_{m1} + 4R_{o1}R_{o2}G_{m1}G_{m2}G_{m3})} \quad (3)$$

Moreover, if G_{m1} is increased up to 10nS, (3) keeps capacitance multiplier behavior up to 10kHz approximately. In this point of view, "k" multiplication factor can be approximated as follows:

$$k \cong 4R_{o1}R_{o2}G_{m2}G_{m3} \quad (4)$$

$$\omega_{cut-off} \cong \frac{1}{kRC} \quad (5)$$

In this view, (4) brings a large amount of capacitance value at the V_{out} node to attain very low operating frequency region in the biomedical applications. According to (4) and (5), cut-off frequency of the proposed first order low pass filter can be safely adjusted by output impedances and transconductance values of the three cascaded OTA stages. Hence, bias currents of the OTAs play an important role in determining the cut-off frequency of the proposed filter with capacitance multiplier. In the next sections, DTMOS technique is given with the CMOS implementation of the OTAs, whereas the operating mechanism of the filter is justified with the post layout simulations with regard to different bias currents of each OTAs.

3. CMOS Implementation of Low Pass Filter

Biomedical applications such as implantable and portable devices must be provided with low power operation. MOS transistors operating in deep sub-threshold region consume very low power. Generally, the designed circuits in sub-threshold region designed with MOS transistors have low supply voltage. For example, when the supply voltage of designed circuit with saturated MOS transistors for the 0.18 μm technology is 1.8V, the supply voltage of this circuit with MOS transistors in weak inversion region for the 0.18 μm technology can be lower than 0.7V.

Moreover, to improve the performance of the MOS transistors with the same power dissipation, different techniques such as Dynamic Threshold Metal Oxide Semiconductor (DTMOS) are investigated in literature [9], [32]–[36]. DTMOS can support high current gain and with low threshold characteristics and its leakage current is minimized. Because of its ultra-low voltage capability, DTMOS is very practical to design ultra-low voltage analog circuits [37], [38]. The idea of DTMOS is established by connecting the transistor gate and body to each other. This connection changes the threshold voltage. The threshold voltage of DTMOS is given in (6). The proposed CMOS circuit is implemented with DTMOS transistors as given in Figure 4, whereas DTMOS realization symbol is illustrated in Figure 3.

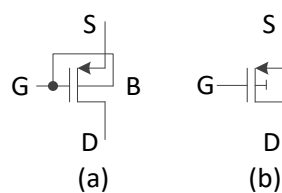


Figure 3. (a) The realization of DTMOS with standard MOS (b) The representation of DTMOS

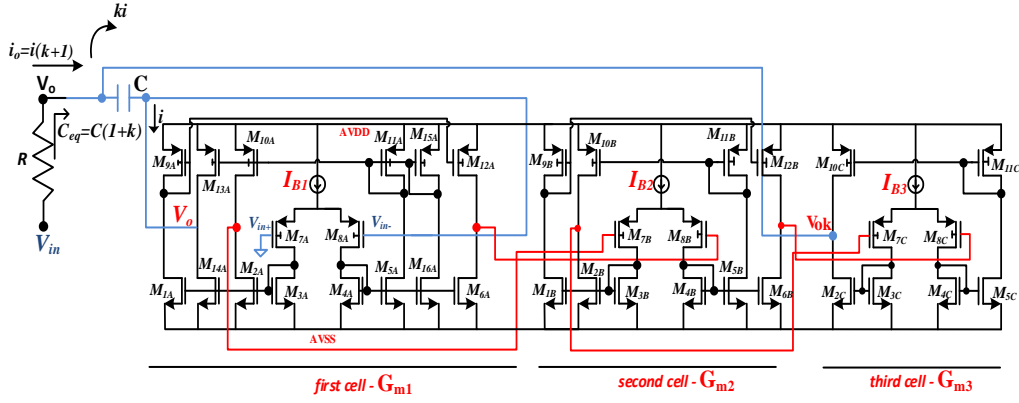


Figure 4. CMOS implementation of proposed filter.

$$|V_{th,p}| = |V_{th0,p}| + \gamma_p \left(\sqrt{|2\Phi_F| + V_{SB}} - \sqrt{|2\Phi_F|} \right) \quad (6)$$

The implementation of the proposed circuit is suitable to obtain high multiplication factor. The implementation of designed structure is advanced version of recently recommended cell-based variable transconductance amplifier [39], [40]. Three cascaded symmetric OTAs compose the structure. The first OTA is called “first cell” while the second OTA is “second cell” and the third one is “third cell”. Table 1 gives the size of the transistors. In the proposed structure, the fully differential output is easily implemented by symmetrical OTA to drive the second and the third cells. In this respect, (7) gives the gain of each OTA in the sub-threshold region.

Table 1. The size of transistors.

Transistors	First Cell	Transistors	Second Cell	Transistors	Third Cell
	W/L		W/L		W/L
M _{1A} , M _{2A} , M _{5A} , M _{6A} ,	2μm/360nm	M _{1B} , M _{2B} , M _{5B} , M _{6B} ,	6μm/360nm	M _{2C} , M _{5C}	6μm/360nm
M _{9A} , M _{10A} , M _{11A} , M _{12A}	2μm/360nm	M _{9B} , M _{10B} , M _{11B} , M _{12B}	6μm/360nm	M _{10C} , M _{11C}	6μm/360nm
M _{7A} , M _{8A}	360nm/360nm	M _{7B} , M _{8B}	5μm/360nm	M _{7C} , M _{8C}	5μm/360nm
M _{3A} , M _{4A}	4μm/220nm	M _{3B} , M _{4B}	2μm/220nm	M _{3C} , M _{4C}	2μm/220nm
M _{13A} , M _{14A} , M _{15A} , M _{16A}	2μm/360nm	-	-	-	-

$$K_{VO} = \frac{g_{m8} \cdot \left[\frac{W}{L} \right]_5}{g_{ds5} + g_{ds11}} \quad (7)$$

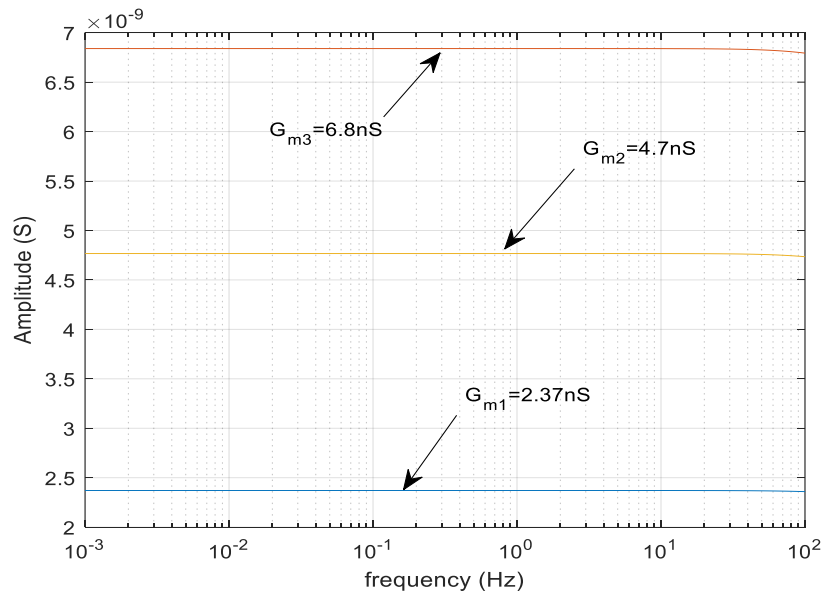
g_m and r_o of MOS transistor are shown in (8) for the sub-threshold region. g_m defines the transconductance of transistor, while r_o is the output impedance of transistor. κ denotes the subthreshold gate efficiency, whereas λ is the parameter of channel length modulation. $V_T = k \cdot T / q$ is the thermal voltage (k - Boltzmann constant, T - absolute temperature, q - elementary charge).

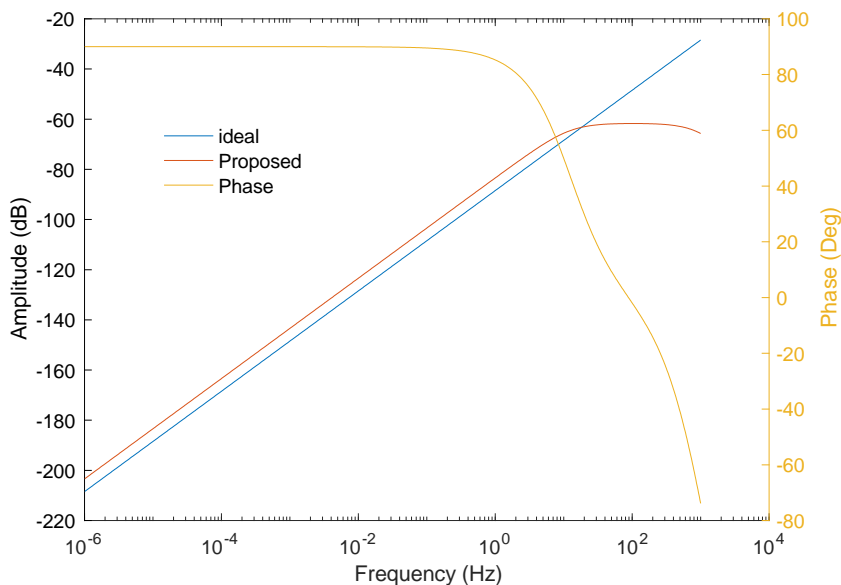
$$g_m \cong \frac{\kappa \cdot q \cdot I_D}{kT}, \quad r_o = \frac{1}{\lambda I_D} \quad (8)$$

In the proposed circuit, V_o is obtained from the first cell with the transistors of M_{13A} , M_{14A} , M_{15A} , M_{16A} , M_{2A} , M_{5A} , M_{10A} , M_{11A} , whereas V_{ok} comes from the third cell to increase the multiplication factor by passing through the first and second cells. The gain of $(k + 1)$ is maximized to be as large as possible by this way. (6), (7) and (8) are used to determine the dimensions of the transistors in Figure 4.

4. Layout and Post-Layout Simulations

Minimum power consumption of the designed circuit is 0.98nW under the minimum biasing current. The simulated results for the transconductance of the cells in the proposed topology are illustrated in Figure 5 (a). In this respect, transconductance of the first cell can be observed around 2.37nS for $I_{B1}=0.1nA$ current. Also, transconductance of the second cell is given as 4.7nS for $I_{B2}=0.1nA$, while transconductance of the third cell is found as 6.8nS for $I_{B3}=0.1nA$. Furthermore, multiplication factor for 10pF base capacitance is simulated as shown in Figure 5 (b). Multiplied capacitance is around 60nF, while the multiplication factor is 6000 with 90° phase response. According to Figure 5 (a) and (b), there is a good agreement between simulation results and equations of (2), (3), and (4) presented in the previous section.





(b)

Figure 5. (a) Transconductance of first, second and third cell, (b) multiplication factor for 10pF base capacitance.

Figure 6 gives the layout of the designed filter. The occupied area on chip without electrostatic discharge (ESD) protection of the designed circuit is $71.99\mu\text{m} \times 115.05\mu\text{m}$; 0.0083mm^2 . The post-layout simulation of the second-order low pass filter is shown in Figure 7. The cut-off frequency of the designed filter is 500mHz for $100\text{k}\Omega$ resistance with 10pF base capacitance.

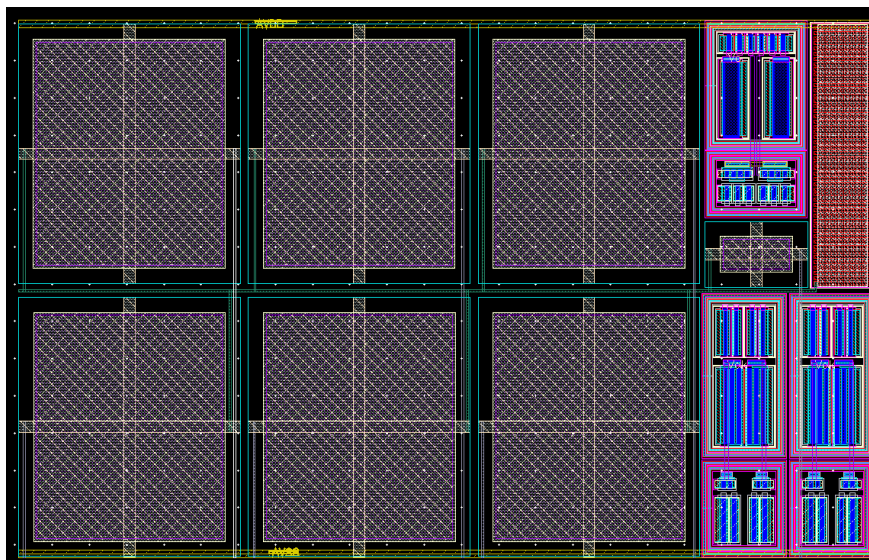


Figure 6. Layout of the proposed circuit (occupies 0.0083mm^2 area).

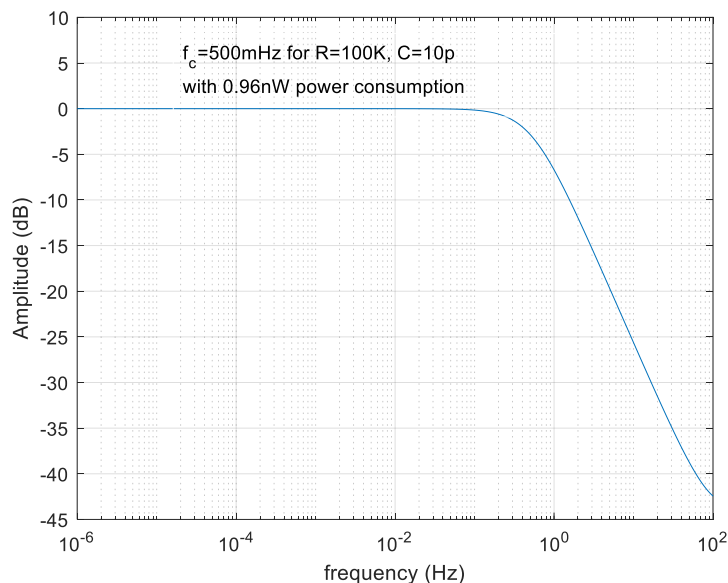


Figure 7. Post-layout simulation of designed filter for $R=100k\Omega$ and $C=10pF$ (base capacitor).

THD performance of the filter for peak-to-peak input signal at 1mHz frequency is given in Figure 8. The total harmonic distortion is 0.12% for 100mV peak-to-peak input signal at 1mHz, while output signal of the proposed filter is given in Figure 9 for the same input voltage signal. Furthermore, input referred noise is $9.09\mu V/\sqrt{\text{Hz}}$ as given in Figure 10. Spurious Free Dynamic Range (SFDR) of the designed filter is around -78.2dBc. The analysis of SFDR is given in Figure 11 at 1mHz input frequency for 100mV peak to peak input signal.

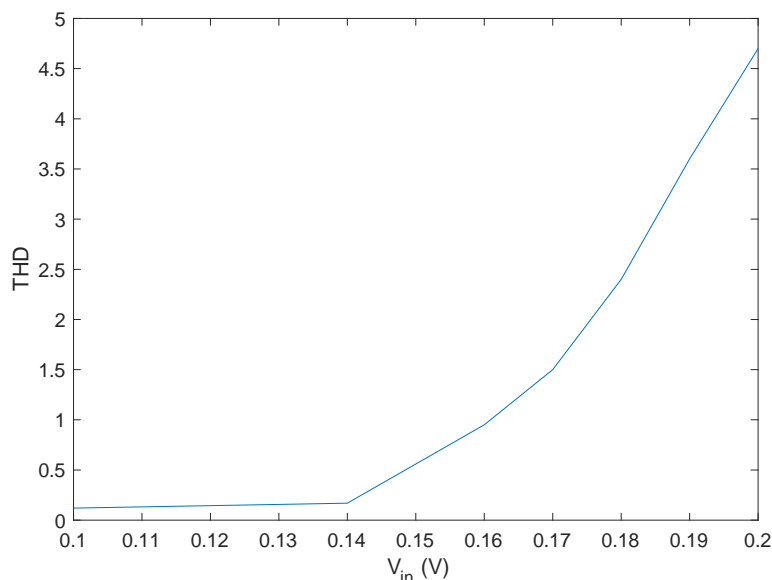


Figure 8. Linearity check of the designed filter (THD = 0.12% for 100mV of peak input signal at 1mHz).

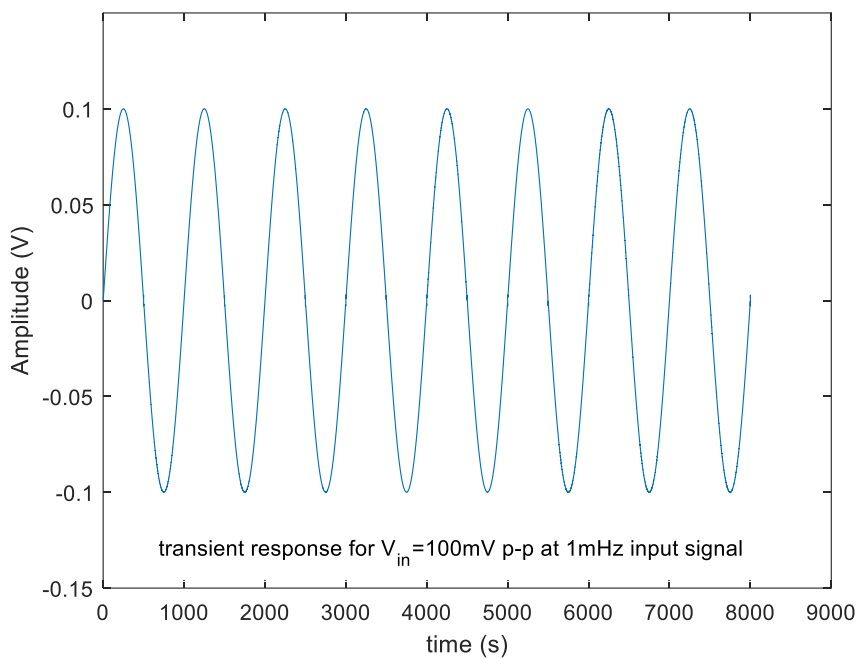


Figure 9. Transient response of the designed filter (THD = 0.12%).

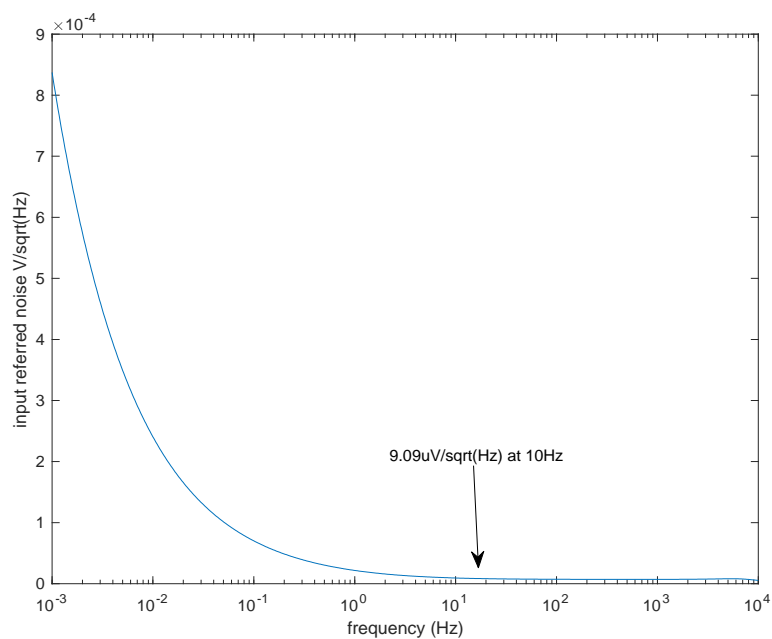


Figure 10. Input referred noise of the designed filter.

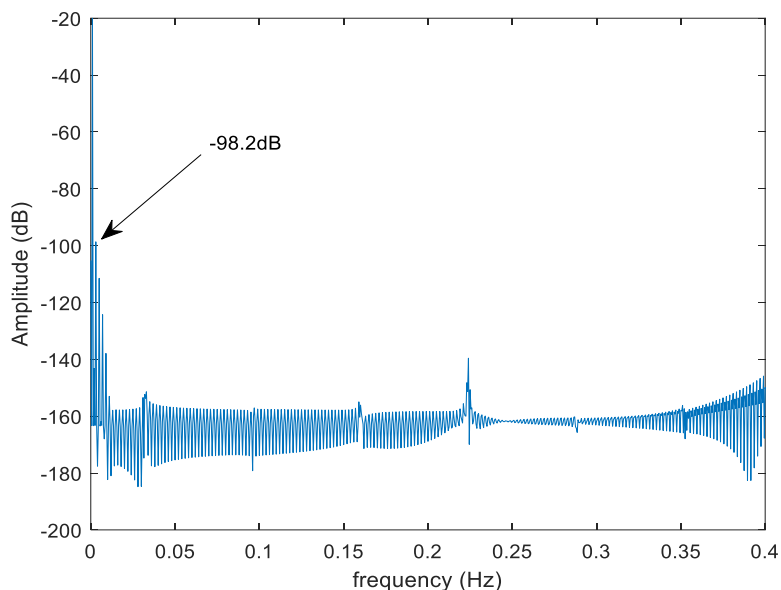


Figure 11. Spurious Free Dynamic Range.

The cut-off frequency of the designed filter can be adjustable with the biasing current as given in Figure 12. Table 2 gives the biasing current of each cell versus $f(-3\text{dB})$ as well. The configurability of the designed filter can be realized by changing G_{m2} and G_{m3} with different I_{B2} and I_{B3} , respectively. Also, output impedances of the first and second OTAs in the proposed filter structure in Figure 2 play an important role for the cut-off frequency. In this point of view, Figure 12 and Table 2 are in good agreement with equations of (3), (4), (5), (7) and (8) presented in the previous sections. Corner analysis of the designed filter including variations of process (ss, tt, ff, sf, fs), temperature (-40°C , 85°C), and power supplies of AVDD and AVSS (0.33V, 0.27, -0.33V and -0.27V) is realized to check resilience of the performance. It can be said that the filter performance remains in acceptable limits. The low pass function of the designed filter is preserved under the worst cases. In addition, Figure 13 gives the Monte Carlo analysis. To investigate resilience of proposed filter, cut-off frequency of the filter is analyzed under the Monte-Carlo seeds. The Monte-Carlo simulation runs including distinct process corners (ss, sf, fs, ff) also transistor mismatches by changing transistors' channel lengths and/or width independently. In the end of this process, it should be noted that standard deviation of the cut-off frequency is lower than 10%, where cut-off frequency of the designed filter is around 24Hz while standard deviation is 1.47Hz. In the Monte Carlo analysis, all process variations and mismatches are taken into consideration for 100 independent runs. Standard deviation of the designed filter for 1.47Hz while cut-off frequency is 24Hz. Table 3 gives the detailed comparison of the proposed circuit with other studies in the literature. The design is considered to give promising results when compared to the defined Figure of Merit given in (9).

$$FoM = \frac{\text{power}}{\text{dynamic range} \times \text{order}} \quad (9)$$

Table 2. Biasing current versus f_{-3dB}

I_{B1}	I_{B2}	I_{B3}	f_{-3dB}
0.1nA	0.1nA	0.1nA	500mHz
0.1nA	0.1nA	1nA	3Hz
0.1nA	1nA	0.1nA	9Hz
1nA	1nA	1nA	24Hz
1nA	1nA	10nA	65Hz

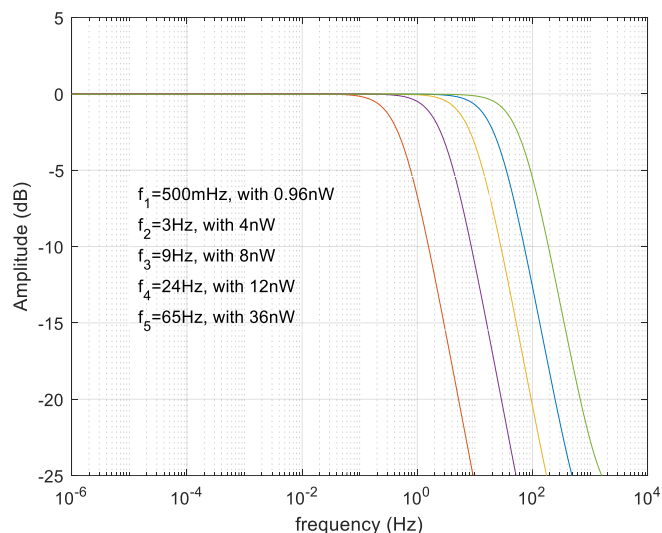


Figure 12. The reconfigurable output of the designed filter for different bias currents of three cascaded cells.

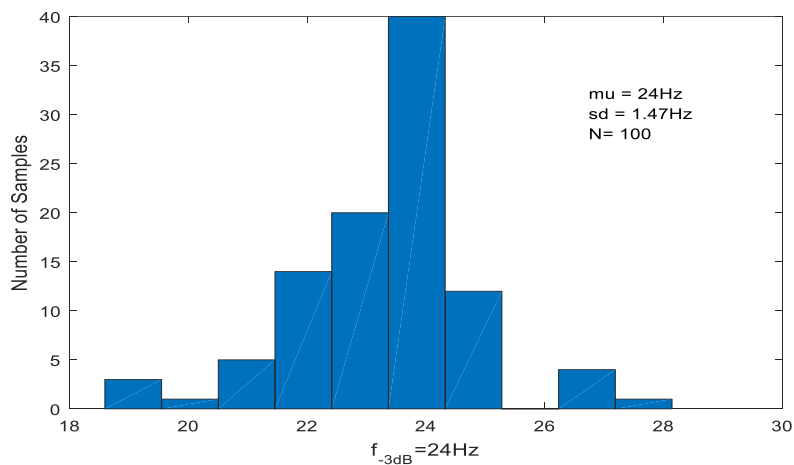


Figure 13. Monte Carlo analysis for $f_{-3dB} = 24\text{Hz}$.

Table 3. Comparison between conventional designs and the proposed work.

Parameters	[5]	[16]	[41]	[42]	[43]	[44]	[45]	This Work
V_{DD}, V	1	1.8	1.8	1	3	± 0.8	0.9	± 0.3
Technology, μm	0.18	0.18	0.18	0.18	0.35	0.25	0.13	0.18
Power, μW	0.35	0.57	200	0.453	0.75	30	2.8	0.9nW
DC gain, dB	-8	0	-6	-9.5	-6	-5	5.9	0
Filter order	5	4	5	5	4	5	4	2
THD, dB	-49.9	-40	-44	-48.6	-59	-40	-40	-43

Dynamic range, dB	49.8	56.06	52	50	54	65	43.22	78.2
Bandwidth, Hz	50	50	250	250	40	253	52	50
IRN, μV_{rms}	97	109	266	340	500	36	24.4	9.09
<i>FoM</i>	0.226	0.224	100	0.286	0.374	3.3	4.83	0.00575

5. Conclusions

In this work, a new implementation for low-pass filter of biomedical data acquisition system developed with DTMOS technique is proposed. The active RC filter is designed with OTA based capacitor multiplier. The cascaded cell-based implementation is performed with the design of capacitor multiplier, which is very appropriate for the low power and low frequency applications where high multiplication factor is required. The proposed structure works with a supply voltage of $\pm 0.3\text{V}$ and dissipates 0.98nW , whilst the occupation area of core circuit on chip is 0.0083mm^2 . The input referred noise of the designed filter is presented around $9.09\mu\text{V}/\sqrt{\text{Hz}}$. All simulations are performed in Cadence environment with $0.18\mu\text{m}$ TSMC technology.

Acknowledgments

There is no funding to support this work.

Authors' contributions

First Author performs the mathematical calculations. Second author simulates the circuit in Cadence environment.

Both authors read and approved the final manuscript.

Competing interests

The authors declare that they have no competing interests.

Ethics in Publishing

There are no ethical issues regarding the publication of this study.

References

- [1] Aazam M., Zeadally S., and Harras K. A., (2018) Deploying fog computing in industrial internet of things and industry 4.0, IEEE Transactions on Industrial Informatics, vol. 14, no. 10, pp. 4674–4682.
- [2] Wan J., Tang S., Shu Z., Li D., Wang S., Imran M., and Vasilakos A., (2016) Software-defined industrial internet of things in the context of industry 4.0, IEEE Sensors Journal, vol. 16, no. 20, pp. 1–1.
- [3] Vittoz E. and Fellrath J., (1977) CMOS analog integrated circuits based on weak inversion

operations, *IEEE Journal of Solid-State Circuits*, vol. 12, no. 3, pp. 224–231.

[4] Kim H. S. and Cha H.-K., (2018) A low-noise biopotential CMOS amplifier IC using low-power two-stage Ota for Neural Recording Applications, *Journal of Circuits, Systems and Computers*, vol. 27, no. 05, p. 1850068.

[5] Sun C.-Y., and Lee S.-Y., (2018) A fifth-order Butterworth Ota-C LPF with multiple-output differential-input OTA for ECG applications, *IEEE Transactions on Circuits and Systems II: Express Briefs*, vol. 65, no. 4, pp. 421–425.

[6] Li Y., Poon C. C., and Zhang Y.-T., (2010) Analog integrated circuits design for processing physiological signals,” *IEEE Reviews in Biomedical Engineering*, vol. 3, pp. 93–105.

[7] Bano S., Narejo G. B., and Usman Ali Shah S. M., (2018) Low voltage low power single ended operational transconductance amplifier for low frequency applications, *Wireless Personal Communications*, vol. 106, no. 4, pp. 1875–1884.

[8] Behrouj A. R., Ghorbani A. R., Ghaznavi-Ghouschi M. B., and Jalali M., (2019) A low-power CMOS transceiver in 130nm for wireless sensor network applications, *Wireless Personal Communications*, vol. 106, no. 3, pp. 1015–1039.

[9] Rout S. S., Acharya S., and Sethi K., (2018) A low phase noise gm -boosted DTMOS VCO design in 180nm CMOS technology, *Karbala International Journal of Modern Science*, vol. 4, no. 2, pp. 228–236.

[10] Alaybeyoglu E., (2019) Implementation of capacitor multiplier with cell-based variable transconductance amplifier, *IET Circuits, Devices & Systems*, vol. 13, no. 3, pp. 267–272.

[11] Sawigun C. and Thanapitak S., (2018) A 0.9-nW, 101-Hz, and 46.3-Vrms IRN Low-Pass Filter for ECG Acquisition Using FVF Biquads, *IEEE Transactions on Very Large Scale Integration (VLSI) Systems*, vol. 26, no. 11, pp. 2290–2298.

[12] Hou Y., Yousef K., Atef M., Wang G., and Lian Y., (2018) A 1-to-1-khz, 4.2-to-544-NW, multi-level comparator based level-crossing ADC for IoT applications, *IEEE Transactions on Circuits and Systems II: Express Briefs*, vol. 65, no. 10, pp. 1390–1394.

[13] Kaur A., Agarwal A., Agarwal R., and Kumar S., (2018) A novel approach to ECG R-peak detection,” *Arabian Journal for Science and Engineering*, vol. 44, no. 8, pp. 6679–6691.

[14] Ozenli D., Alaybeyoglu E., and Kuntman H., (2021)“A grounded capacitance multiplier circuit employing VDTA, 2021 13th International Conference on Electrical and Electronics Engineering (ELECO), pp. 38–41.

[15] Harrison R. R., (2007) A versatile integrated circuit for the acquisition of Biopotentials, *IEEE Custom Integrated Circuits Conference*, pp. 115–122.

[16] Machha Krishna J. R. and Laxminidhi T., (2019) Widely tunable low-pass gm–C filter for

biomedical applications., IET Circuits, Devices & Systems, vol. 13, no. 2, pp. 239–244.

[17] Nagaraj K., (1989) A parasitic-insensitive area-efficient approach to realizing very large time constants in switched-capacitor circuits, IEEE Transactions on Circuits and Systems, vol. 36, no. 9, pp. 1210–1216.

[18] Solis-Bustos S., Silva-Martinez J., Maloberti F., and Sanchez-Sinencio E., (2000) A 60-DB dynamic-range CMOS sixth-order 2.4-Hz low-pass filter for medical applications, IEEE Transactions on Circuits and Systems II: Analog and Digital Signal Processing, vol. 47, no. 12, pp. 1391–1398.

[19] Veeravalli A., Sanchez-Sinencio E., and Silva-Martinez J., (2002) Transconductance amplifier structures with very small transconductances: A comparative design approach, IEEE Journal of Solid-State Circuits, vol. 37, no. 6, pp. 770–775.

[20] Zhou L. and Chakrabartty S., (2015) Design of low-Gm transconductors using Varactor-based degeneration and linearization technique, IEEE Biomedical Circuits and Systems Conference (BioCAS), pp. 1-4.

[21] Tanzawa T., (2010) On two-phase switched-capacitor multipliers with minimum circuit area, IEEE Transactions on Circuits and Systems I: Regular Papers, vol. 57, no. 10, pp. 2602–2608.

[22] Yesil A., Yuce E., and Minaei S., (2017) Grounded capacitance multipliers based on active elements, AEU - International Journal of Electronics and Communications, vol. 79, pp. 243–249.

[23] Abuelma'atti M. T. and Tasadduq N. A., (1999) Electronically tunable capacitance multiplier and frequency-dependent negative-resistance simulator using the current-controlled current conveyor, Microelectronics Journal, vol. 30, no. 9, pp. 869–873.

[24] Prommee P. and Somdunayakanok M., (2011) CMOS-based current-controlled DDCC and its applications to capacitance multiplier and Universal Filter, AEU - International Journal of Electronics and Communications, vol. 65, no. 1, pp. 1–8.

[25] Khan A. A., Bimal S., Dey K. K., and Roy S. S., (2002) Current conveyor based R- and C- multiplier circuits, AEU - International Journal of Electronics and Communications, vol. 56, no. 5, pp. 312–316.

[26] Das B. P., Watson N. and Liu Y., (2010) Wide tunable all pass filter using OTA as active component". IEEE International Conference on Signals and Electronic Circuits, pp. 379-382.

[27] Liu P.-J., Hsu C.-Y., and Chang Y.-H., (2015) Techniques of dual-path error amplifier and capacitor multiplier for on-chip compensation and soft-start function, IEEE Transactions on Power Electronics, vol. 30, no. 3, pp. 1403–1410.

[28] Sagbas M., Ayten U. E., Sedef H., and Koksals M., (2009) Electronically tunable floating

inductance simulator,” *AEU - International Journal of Electronics and Communications*, vol. 63, no. 5, pp. 423–427.

[29] Shin S.-H., Kweon S.-J., Jo S.-H., Choi Y.-C., Lee S., and Yoo H.-J., (2015) A 0.7-MHz–10-MHz CT+ DT hybrid baseband chain with improved passband flatness for LTE application, *IEEE Transactions on Circuits and Systems I: Regular Papers*, vol. 62, no. 1, pp. 244–253.

[30] Rincon-Mora G. A., (2000) Active capacitor multiplier in Miller-compensated circuits, *IEEE Journal of Solid-State Circuits*, vol. 35, no. 1, pp. 26–32.

[31] Shukla P. and Gupta A., (2017) Current-mode PMOS capacitance multiplier, *IEEE International Conference on Inventive Systems and Control (ICISC)*, pp. 1–4.

[32] Achigui H. F., Fayomi C. J. B., and Sawan M., (2006) 1-V DTMOS-based class-AB operational amplifier: Implementation and experimental results, *IEEE Journal of Solid-State Circuits*, vol. 41, no. 11, pp. 2440–2448.

[33] Uygur A. and Kuntman H., (2013) DTMOS-based 0.4 V ultra low-voltage low-power VDTA design and its application to EEG data processing, *Radioengineering*, vol. 22, no. 2, pp. 458-466.

[34] Kalekar P., Vernekar P., Vasantha M. H., Kumar Y. B. N., and Bonizzoni E., (2018) A 0.5 V low power DTMOS OTA-C filter for ECG sensing applications, *IEEE SENSORS*, pp. 1-4.

[35] Srivastava P., Gupta R. K., Sharma R. K. and Ranjan R. K., (2020) MOS-only Memristor emulator, *Circuits, Systems, and Signal Processing*, vol. 39, no. 11, 5848-5861.

[36] Lorenzo R. and Chaudhury S., (2017) Dynamic threshold sleep transistor technique for high speed and low leakage in CMOS circuits, *Circuits, Systems, and Signal Processing*, 36(7), 2654-2671.

[37] Tsividis Y. and McAndrew C., (2011) *Operation and Modeling of the MOS Transistor*, Oxford Univ. Press.

[38] Parke S. A., Hu C., and Ko P. K., (1993) Bipolar-fet hybrid-mode operation of quarter-micrometer SOI mosfets (MESFETs read MOSFETs), *IEEE Electron Device Letters*, vol. 14, no. 5, pp. 234–236.

[39] Alaybeyoğlu E. and Kuntman H., (2019) Capacitor multiplier with high multiplication factor for integrated low pass filter of biomedical applications using DTMOS technique, *AEU-International Journal of Electronics and Communications*, vol. 107, pp. 291-297.

[40] Alaybeyoğlu E. and Kuntman H., (2018) A new implementation of the reconfigurable analog baseband low pass filter with cell-based variable transconductance amplifier, *Analog Integrated Circuits and Signal Processing*, vol. 97, no. 1, pp. 87-96.

[41] Lo T.-Y. and Hung C.-C., (2007) A wide tuning range Gm-C continuous-time analog filter,

IEEE Transactions on Circuits and Systems I: Regular Papers, vol. 54, no. 4, pp. 713–722.

[42] Lee S.-Y. and Cheng C.-J., (2009) Systematic design and modeling of a OTA-C filter for portable ECG detection,” IEEE Transactions on Biomedical Circuits and Systems, vol. 3, no. 1, pp. 53–64.

[43] Liu Y.-T., Lie D. Y. C., Hu W., and Nguyen T., (2012) An ultralow-power CMOS transconductor design with wide input linear range for biomedical applications, IEEE International Symposium on Circuits and Systems, pp. 2211–2214.

[44] Mahmoud S. A., Bamakhramah A., and Al-Tunaiji S. A., (2013) Low-noise low-pass filter for ECG portable detection systems with digitally programmable range, Circuits, Systems, and Signal Processing, vol. 32, no. 5, pp. 2029–2045.

[45] Arya R. and Oliveira J. P., (2016) Gm-C biquad filter for low signal sensor applications, 23rd International Conference Mixed Design of Integrated Circuits and Systems, pp. 207–210.

Mathematical Success with Fuzzy Logic Modeling

Ramazan UYHAN¹, Zülfiye GÖK²

¹Süleyman Demirel Üniversitesi, Fen Edebiyat Fakültesi, Matematik Bölümü, 32260, Isparta, Türkiye

²Süleyman Demirel Üniversitesi, Fen Bilimleri Enstitüsü, Matematik Bölümü, 32260, Isparta, Türkiye

Received: 16/06/2022, **Revised:** 29/08/2022, **Accepted:** 29/08/2022, **Published:** 30/12/2022

Abstract

In this paper, the effect of high school students on mathematics achievement by taking active participation and absent of high school students was investigated by using fuzzy logic modeling. The questionnaire prepared by the researcher is applied to the students to determine the active participation of the students. These written exam scores are used in order to evaluate the absences and achievements of the students until the end of the 1st semester written exam. In this study, inputs are active participation and absent, and output is mathematics achievement. These data were tabulated, graded and transferred to Matlab and the model is obtained by using fuzzy logic toolbox. The actual results obtained from this model with the output values R^2 review by making the similarity rate is found to be 80%.

Keywords: Mathematics Achievement, Fuzzy Logic, Education

Bulanık Mantık Modellemesi ile Matematik Başarısı

Öz

Lise öğrencilerinin derse aktif katılımları ve yapmış oldukları devamsızlıklar ele alınarak matematik başarısına olan etkisi modern optimizasyon tekniklerinden bulanık mantık modellemesi kullanılarak incelenmiştir. Öğrencilerin derse aktif katılımlarını saptamak için araştırmacı tarafından hazırlanan anket öğrencilere uygulanmıştır. Öğrencilerin 2018-2019 öğretim yılı 1. dönem 1. matematik yazılı sınav tarihine kadar olan devamsızlıkları ve başarılarının değerlendirilebilmesi için bu yazılı sınav puanları kullanılmıştır. Bu çalışmada girdiler aktif katılım ve devamsızlık, çıktı ise matematik başarısıdır. Elde edilen değerler ile veriler oluşturulmuştur. Bu veriler tabloleştirilip derecelendirilmiştir ve matlab programına aktararak fuzzy logic araç kutusu kullanılarak model elde edilmiştir. Bu modelden elde edilen çıktı değerleriyle var olan gerçek sonuç değerleri R^2 incelemesi yapılarak benzerlik oranı %80 olarak bulunmuştur.

Anahtar Kelimeler: Matematik Başarısı, Bulanık Mantık, Eğitim.

1. Introduction

Mathematical modeling is the process of considering and interpreting a real-life problem mathematically. The problem is defined, the data is collected and analyzed, then mathematically formulated and a mathematical model is created. The found result is adapted to real life and interpreted [1]. In this study, using the fuzzy toolbox in the Matlab program on the computer, one of the mathematical models, the input variables are the active participation and absent of the students, and the output variable is the mathematical success, then fuzzy logic modeling method is applied. The concept of fuzzy logic was introduced by Zadeh [2]. In fuzzy logic, it is desired to measure the degree of accuracy by determining how much the expressions are realized by creating membership degrees to the expressions used in daily life [3]. Today, fuzzy logic is used in economics, health, engineering, education, etc. It is preferred in many fields such as In the fuzzy logic system, the input variables are blurred and the data obtained within the rules are defuzzified and converted into numerical output values [4-7]. In this study, a surface is obtained depending on the input and output variables in the fuzzy logic system and the correlation percentages are calculated by comparing the system output data with the existing data.

2. Material and Methods

The importance active participation of students in the lesson and the effects of their absence from school on their mathematics achievement are discussed. The 'Active Participation Questionnaire in Mathematics Lesson' was created by the researcher to determine the active participation of the students. Absent was determined by evaluating the attendance documents of student until the 1st Term 1st Mathematics written exam date. The study was carried out by considering the scores they received in the 1st Term 1st Mathematics written exam applied to the students with mathematics achieve obtained from the data, It was transferred to the excel program, tabulated and evaluated.

The membership degree, $\mu(x)$, is specified for each value in the range of the variable X , which has lower and upper bounds such as X_a and X_b . Membership rating is between 0 and 1. As seen in the graph, this curve, which changes with the values of the cluster members, is called the membership function [8].

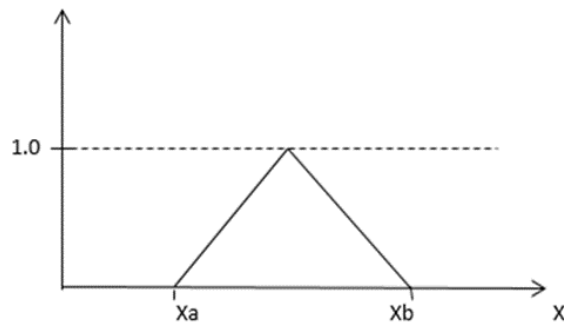


Figure 1. Fuzzy Set

Fuzzy systems are systems in which fuzzy set principles are used in order to reach output variables thanks to existing data and input variables. In the fuzzy model, the logical relations between input and output take place by applying if-then rules.

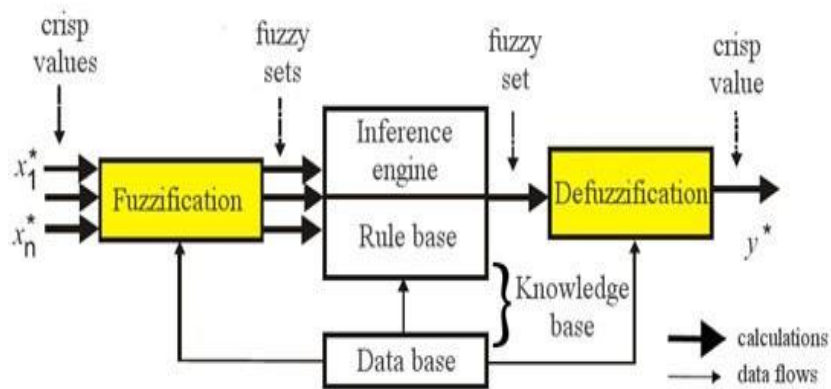


Figure 2. General Fuzzy System

Fuzzifier: It is the processor that enables to obtain fuzzy data by converting numerical input values into linguistic variables, that is, verbal expressions.

Fuzzy Rule Base Unit: It contains rules with if-then commands that enable to examine the logical relationships between input and output variables in the database.

Fuzzy Inference Engine Unit: It provides the inferences of the rules between the input and output fuzzy sets to determine what kind of output the system will give depending on its inputs.

Clarifier: It transforms the fuzzy results found as a result of fuzzy processes into clear digital output values [9-11].

3. Results and Discussion

The data obtained for the research are as follows.

Active Participation	Discontinuity	Success
89	5,5	46
100	2,5	77
100	1	91
88	1	92
55	1,5	66
93	2	92
26	1	73
54	3	47
92	2	85
74	8,5	10
61	5	27
38	0.5	52
71	2	30
96	4	42
68	2.5	10
74	8,5	15
69	2	14
58	7,5	20
76	4,5	36
66	1	70
87	1,5	62
80	4,5	68
67	1	81
72	3,5	50

72	3,5	64
84	1,5	78
86	2,5	84
63	6,5	24
85	3,5	52
80	5,5	64
90	1,5	97
53	1,5	55
94	3	77
72	3,5	50
72	1,5	58
88	5	50
71	2	22
98	1,5	100
86	0,5	86
86	0,5	100
78	0,5	85
75	1	81
57	2,5	28
82	0,5	92
81	8	26
69	6,5	50
67	12	43
95	1,5	100
80	1	91

84	1,5	100
94	2	90
80	0	90
89	0,5	85
96	0	90
85	1	87

82	0	98
85	3	82
82	3	44

Obtained values are modeled by fuzzy logic method. In this study, while active participation and absent constitute the input variables of the study, success also constitutes the output variable. Thus, a two-input and output model was obtained.

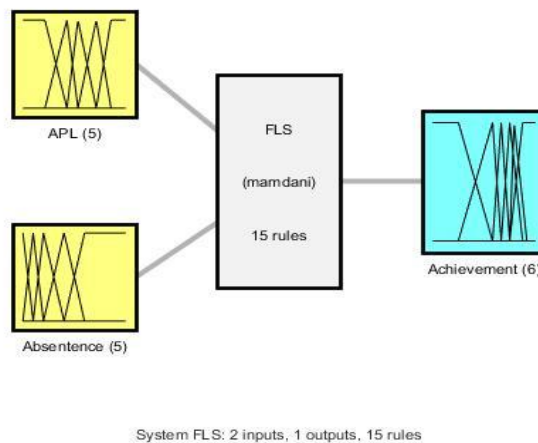


Figure 3. Main Diagram of Fuzzy Logic System

Thus, in the fuzzy logic model, a surface was obtained that determines the relationship between active participation of students in the lesson and their absent from school and their mathematics achievement.

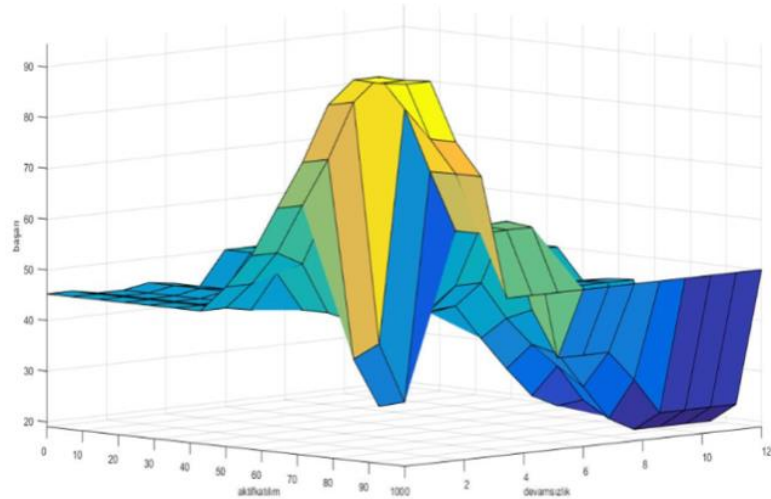


Figure 4. Surface obtained from the model

In the model obtained, output values were found in the fuzzy logic system for each input variables. In the table below, the success values obtained by the fuzzy logic method are compared with the success values available.

Current Values	Fuzzy Logic System Values
46	52,1
77	74,6
91	92
92	91,1
66	55,2
92	78,3
73	45,2
47	44,7
85	78,5
10	21,6
27	43,6
52	45,2

30	29,4
42	50
10	29
15	21,6
14	33
20	44,8
36	47,8
70	62,5
62	86,6
68	51,9
81	63,4
50	45,2
64	45,2

78	85,9
84	74,4
24	44,2
52	62,2
64	48,5
97	84,3
55	53,6
77	74,4
50	45,2
58	41,7
50	62,8
22	29,4
100	84,4
86	94,2
100	94,2
85	88,2
81	69,6

28	44,1
92	92
26	27,6
50	33,1
43	36,2
100	84,4
91	74
100	85,9
90	78,3
90	90
85	93,6
90	94,5
87	92,1
98	92
82	74,4
44	31,4

The correlation coefficient R^2 was calculated by comparing the existing success values with the success values obtained from the model. When these values were compared in the study, it is determined that the similarity rate was 80%.

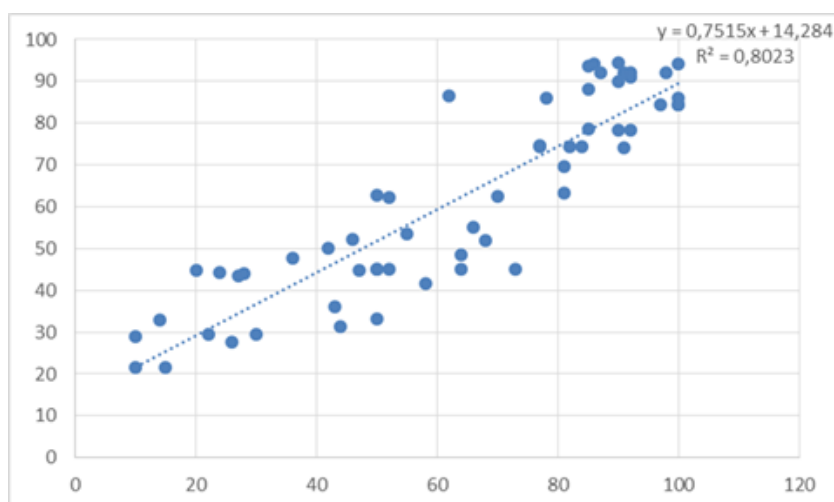


Figure 5. Comparison of Values

4. Conclusion

In this study, the effect of active participation of students in the lesson and their absence from school on their mathematics achievement is examined by fuzzy logic method. The active participation scores of the students are obtained by adding the scores of the marked situations in the survey study applied to the students. Student's absent from school is determined for the period until the 1st semester 1st mathematics written exam date, and their mathematics achievement is considered as the scores they got from the 1st semester 1st mathematics exam. In this study, while active participation and absent constitute the input variables, mathematics achievement constitutes the output variable. After determining the rules for the relationships between the inputs and the output, the model is obtained. On the surface obtained from the model created with the fuzzy logic method, while active participation has a positive effect on success, absent has a negative effect. High success is achieved in cases where active participation is high and absent is low. It has been determined that there is low success in cases where active participation is low and absent is high. In the study, the values obtained from the fuzzy logic system are compared with the actual values, and the similarity rate is found to be 80%.

If this study is to be investigated later by another researcher to investigate the active participation of the students in the lesson and their absent at school, which affects the mathematics achievement, thanks to the model we have obtained with the fuzzy logic method, we can enter our own data and obtain the results of mathematics achievement. In addition,

research can be conducted by adding other factors that affect the success besides the active participation of the students in the lesson and their absent from the school.

Ethics in Publishing

Ethical approval for this study was obtained from Suleyman Demirel University Ethics Committee (2022, 67(1)).

Author Contributions

The authors contributed equally. The first author performed all theorem's proof and calculating the examples. The second author put forward the first idea and making computer programme for the examples.

References

- [1] Ural, A., 2014, Investigation of Mathematical Modeling Skills of Pre-service Mathematics Teachers, Journal of Dicle University Ziya Gökalp Faculty of Education, 23,110-141.
- [2] Zadeh, L.A.,1965, FuzzySets. Information and Control, 8, 338-353.
- [3] Paksoy,T., Yapıcı Pehlivan, N., Özceylan, E., 2013. Fuzzy Set Theory. Nobel Publication, Ankara, 214s.
- [4] Özdemir, A., Alaybeyoğlu, A., Balbal, K.F., 2019. Applications of Fuzzy Logic in Education. Journal of Science, Education, Art and Technology, 3(1), 45-50.
- [5] Akbay, R., Sahiner, A., Yılmaz, N. (2016). Determining of the achievement of students by using classical and modern optimization techniques. Eurasian Journal of Physics & Chemistry Education, 8, 3–13.
- [6] Şener, K., (2001). İlköğretim öğrencilerinin çalışma alışkanlıklarının matematikteki başarılarına etkisi, Fırat Üniversitesi Sosyal Bilimler Enstitüsü, Yayınlanmamış Yüksek Lisans Tezi.
- [7] Yılmaz, M., Arslan, E., 2005. Using Fuzzy Logic in Solving Geodetic Problems. Chamber of Surveying and Cadastre Engineers Engineering Surveys STB Commission 2nd Engineering Surveys Symposium, 23-25 November, Istanbul, 512-522.
- [8] Sen, Z., 2009. Fuzzy Logic Principles and Modeling. Water Foundation Publications, Istanbul, 361s.
- [9] Takagi, T., Sugeno, M., (1985). Fuzzy identification of systems and its applications to modeling and control, IEEE Trans. Syst., Man and Cybernetics 15, 116-132

[10] Mamdani E. H.,(1974).Application of fuzzy algorithms for control of simple dynamic plant, Proc. IEEE 121(12), 1585-1588.

[11] Mamdani E. H., Assilian S., (1975), An experiment in linguistic synthesis with a fuzzy logic controller, International Journal of Man-Machine Studies 7(1) ,1-13.

Appendices

App. A. Active Participation Questionnaire in Mathematics Lesson

	I strongly disagree (1)	I do not agree (2)	I am undecided (3)	I agree (4)	Absolutely I agree (5)					
						lesson makes it easier for me to learn.				
						7. I get up on the board and tell the solution to my friends without hesitation.				
1. I like to have a say in the mathematics lesson and participate in the lesson.						8.The participation of my friends in the mathematics lesson in the class allows me to be more active in the lesson.				
2.My math teacher encourages me to ask questions in the lesson.						9.The use of different teaching methods in the mathematics lesson increases my interest and active participation in the lesson.				
3.My teacher's feedback and hints in the mathematics lesson allow me to participate in the lesson.						10 Feeling comfortable in the classroom environment increases my participation in the lesson.				
4.Getting a high grade in the math exam increases active participation in the lesson.						11. When I actively participate in the mathematics lesson, my belief that I can succeed in the lesson increases.				
5.When I understand the purpose and contribution of the mathematics course, my desire to participate in the course increases.						12.My active participation in the mathematics lesson is				
6.The use of materials (visual tools, videos, etc.) in the mathematics										

effective in my self-confidence.						not understand in the math class.					
13. When I speak, my math teacher's careful listening to me increases my participation in the lesson.						17. I hesitate to stand up at the blackboard in math class.					
						18. Even though I know the answer to the question my teacher asks in the math class, I don't want to take the floor.					
14. My math teacher's good communication with the class increases my participation in the lesson.						19. Getting a low grade on the math test reduces active participation in the lesson.					
						20. The fact that my classmates do not attend the mathematics lesson reduces my participation in the lesson.					
15. Using mathematics in daily life increases my interest and participation in the lesson.											
16. I do not hesitate to ask about the things I do											

Tribocorrosion Properties of Borided and Al_2O_3 -Coated NiTi Material

Yakup UZUN^{1*}

¹Ataturk University, Faculty of Engineering, Department of Mechanical Engineering, Erzurum, Turkey

Received:29/09/2022, **Revised:** 07/11/2022, **Accepted:** 16/11/2022, **Published:** 30/12/2022

Abstract

The purpose of this study was to investigate the tribological properties of NiTi shape-memory alloy that was borided and coated with Al_2O_3 using the electrophoretic deposition (EPD) method. For the study, the sample surface was borided for 1 and 4 h at 800°C with the method of pack boriding, and the surface of the sample that was borided was coated with Al_2O_3 using the EPD method. The tribocorrosion properties of the untreated samples, borided samples, and borided and (duplex) Al_2O_3 -coated samples were investigated and characterized using XRD and SEM devices. Accordingly, following the boriding treatment on the NiTi material, Al_2O_3 coating was successfully carried out with the EPD method. In comparison to the untreated samples, the tribocorrosion resistance of the surface-treated samples under a load of 3 N in a 3.5% NaCl solution increased. Additionally, among all samples, those that were subjected to the duplex surface treatment had the best tribocorrosion properties.

Keywords: NiTi, Boriding, EPD, Tribocorrosion

Borlanmış ve Al_2O_3 Kaplı NiTi Malzemenin Tribokorozyon Özellikleri

Özet

Bu çalışmanın amacı, borlanmış ve Elektroforetik biriktirme yöntemi (EPD) ile Al_2O_3 kaplanmış şekil hafızalı NiTi alaşımın tribolojik özelliklerini araştırmaktır. Araştırma için numune yüzeyi kutu borlama yöntemi ile 800 °C sıcaklıkta 1 ve 4 h borlama yapılmış ardından borlanmış numunelerin yüzeyi EPD yöntemi ile Al_2O_3 kaplanmıştır. Daha sonra işlemsiz, borlanmış ve borlanarak ardından Al_2O_3 (duplex) kaplanmış numunelerin tribokorozyon özellikleri araştırılmış, XRD ve SEM cihazı ile karakterize edilmiştir. NiTi malzeme üzerine yapılan borlama işleminden sonra EPD yöntemi ile Al_2O_3 kaplama başarılı bir şekilde gerçekleştirilmiştir. İşlemsiz numuneye göre yüzey işlemi uygulanmış numunelerin %3,5 NaCl çözeltisi içerisinde 3 N yük altında Tribokorozyon direnci artmıştır. Ayrıca duplex yüzey işlemi uygulanmış numunenin diğer numunelere göre en iyi Tribokorozyon özellikler gösterdiği sonucuna varılmıştır.

Anahtar kelimeler: NiTi, Borlama, EPD, Tribokorozyon

1. Introduction

NiTi shape-memory alloys (SMAs) are preferred in various industrial fields thanks to their shape-memory effects, excellent elasticity, and mechanical properties [1]. SMAs are a group of multifunctional metals that have shape memory and superelasticity properties. These properties come from the solid-state phase transition between the phases without diffusion [2]. Due to their properties such as biocompatibility and good compatibility with computed tomography and magnetic resonance applications, NiTi alloys are preferred in biomedical processes. These alloys are also used in several fields from aviation to communication and from automotive to microelectromechanical systems [3-6]. Despite their favorable elasticity properties, NiTi alloys suffer from wear occurring during their usage, as well as their inadequate bending and fatigue strength. To eliminate these shortcomings, surface treatments are applied to the material. While boriding can provide many advantages for the surfaces of materials such as resistance to wear, oxidation, and corrosion, it can also allow the preservation of hardness at high temperatures. The procedure of boriding, which can be applied to iron and non-iron metals, is based on the diffusion of boron atoms on the material's surface. Boriding is a thermochemical surface hardening method. While it can be applied to the material's surface using non-thermochemical methods including ion implantation, DVD, CVD, or plasma spraying, it can also be applied using thermochemical methods such as solid, liquid, gas, and plasma boriding [7-8].

In the colloidal process known as electrophoretic deposition (EPD), charged particles in a suspension are electrophoresed on a working electrode that is negatively charged. EPD has two steps. The first step involves the migration of charged particles suspended in a liquid towards the oppositely charged electrode (electrophoresis). The second step involves the formation of coating by the particles accumulating on the counter electrode (deposition). This method is fast and very cost-effective. Additionally, it is scalable, and intensive coating can be achieved with high purity at room temperature and on objects with complicated geometries. In this method, aqueous or organic suspensions can be used [9-13]. In this study, to improve the tribological properties of a NiTi shape-memory alloy, boriding was applied for 1 and 4 h at a temperature of 800°C using the pack boriding method, and the samples were then coated with Al₂O₃ using the EPD method. Next, the tribocorrosion properties of the untreated samples, borided samples, and borided and (duplex) Al₂O₃-coated samples were investigated and characterized using XRD and SEM devices.

2. Material and Methods

The material of this study consisted of NiTi alloy samples containing 50.6% Ni whose physical and mechanical properties are shown in Table 1. The samples were cut in dimensions of 15 × 15 × 5 mm. After that, they were progressively polished using sandpaper of 80–1200 grit. They were then polished even more using alumina powders having 0.3 to 0.5 μm particle diameters. To eliminate debris, ethanol was used to clean the produced samples.

Table 1. Comparison between physical and mechanical properties of NiTi alloy and stainless steel

Material	Density (g cm⁻³)	Modulus of elasticity (GPa)	Hardness (GPa)	Ultimate tensile stress (MPa)	Recovered elongation (a.u.)
NiTi alloy	6.45	65±3	4.15±0.5	1240	8%

2.1. Boriding Procedure

The samples that were created were placed into ceramic containers loaded with commercial EKABOR II (Bortech) powders and spaced equally from the walls and other objects in the container. Ekrit powder (Bortech) was applied to the tops of the containers to avoid oxidation at high temperatures, and the lid of the programmable box furnace was tightly closed. The samples were borided in the furnace at a temperature of 800 °C for 1 and 4 hours. As soon as the boriding procedure was over, the furnace was opened, and the samples were allowed to cool down to room temperature. To get rid of any powder residue that may have been collected, the sample surfaces were cleaned mechanically.

2.2. Electrophoretic deposition

Dilute solutions containing 1% acetic acid and 99% water were prepared by magnetic stirring at room temperature for 24 h. The suspension containing Al_2O_3 powder at a concentration of 0.6 g/L was prepared by dispersion using a sonicator. Before each deposition process, the suspension was magnetically stirred to prevent particle precipitation and flocculation. The EPD coating was deposited onto the borided NiTi surfaces. This process was carried out using a container and sheet steel electrodes at thicknesses of 0.2 mm. The spacing between the electrodes was kept constant at 10 mm. The potential difference was set at 20 V, and the time was set at 20 min. After the deposition process, the samples were removed from the suspension, rinsed under distilled water, and dried at room temperature for 24 h before characterization.

By using the necessary instruments simultaneously, corrosion and wear tests were performed on the materials to ascertain their tribocorrosion capabilities. Figure 3 depicts the tribocorrosion test apparatus, and Table 2 lists the values of the parameters that were employed throughout the test. Tribocorrosion tests were conducted using a sample holder, using samples with already known surface areas. This area measured 2.54 cm² in this holder and in contact with the solution. First, the samples were put through 3600 seconds of Open Circuit Potential (OCP) testing while being loaded. Alumina (Al_2O_3) balls with a 6 mm diameter were employed for the wear tests. The worn track length was changed to 8 mm, and the cycle frequency was set to 1 Hz. A ball-on-disk tribometer (UMT-2, Bruker) instrument linked to a chemical cell with three electrodes submerged in a saltwater solution was used to conduct the tribocorrosion tests at ambient temperature. The tests were carried out using the experimental parameters shown in Table 2 and based on the ASTM G119-09 procedure. The wear and potentiodynamic polarization tests were started simultaneously, and a scan was performed between -1 and 1.5 V. The scanning procedure and the wear testing procedure were ended at the same time.

The data were examined using the Gamry Echem Analyst software package following tribocorrosion testing. At least three more instances of each test and measurement were performed.

Table 2. Tribocorrosion parameters.

Normal load	3 N
Relative wear distance	40 m
Stroke length	8 mm
Sliding velocity	16 mm/s
Alumina ball diameter	6 mm
Electrolyte	3.5% NaCl solution
Temperature	22°C
Reference electrode	Ag/AgCl
Counter electrode	Graphite

Utilizing XRD-GNR-Explorer X-Ray diffractometer with a Co-K α ($\lambda = 1.7903 \text{ \AA}$) source and a 2θ scale between 10° and 100° , the samples' phases were determined at 40 kV and 30 mA. Using a scanning electron microscope (SEM FEI-Quanta 250), the samples' cross-sections and wear surfaces were examined. For the SEM photos of the surface, the surface was cleaned with methanol in a magnetic stirrer for 15 min and subsequently dried to remove contaminations that developed after coating. The samples' roughness and their wear track morphology (width and depth of tracks) after the tribocorrosion tests were examined with the 3-dimensional surface profilometry method (Bruker Contour GT-K1).

3. Results and Discussion

3.1. Characterization of samples

Figure 1 shows the XRD plots of the untreated samples and the samples that were borided for 4 h at 800°C and then coated with Al_2O_3 (duplex). The SEM images of the a) 800°C 4 h, b) 800°C 4 h + Al_2O_3 , c) untreated samples are given in Figure 2. According to the XRD plots, on the surface of the material that was borided at 800°C for 4 h and then coated with Al_2O_3 , NiB_2 , TiB_2 , and Al_2O_3 phases were formed. This result meant that the phases that are likely to occur in the structure could be dispersed homogeneously. This way, stable conditions could be

achieved with the phases that were homogeneously distributed in the microstructure. Moreover, Al_2O_3 coating was successfully achieved with the boriding procedure and the EPD method.

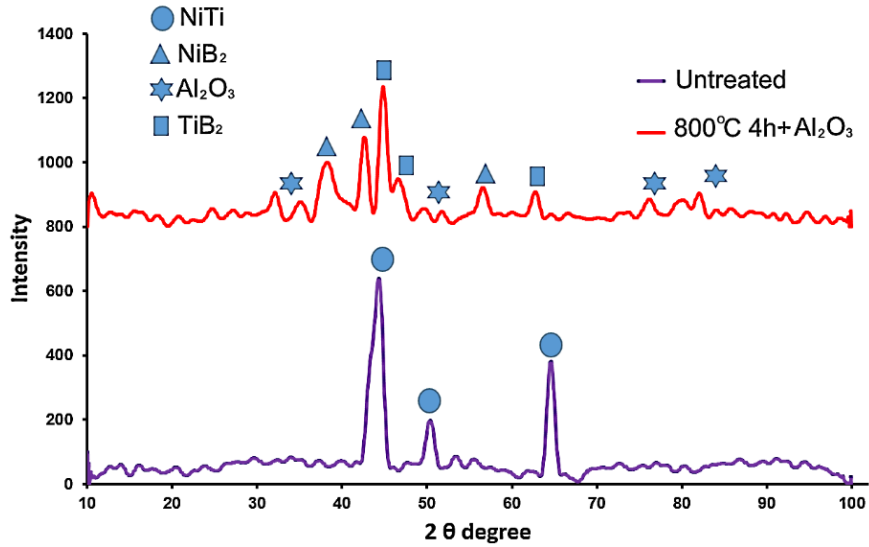


Figure 1. XRD plots of untreated NiTi samples and NiTi samples borided at 800°C for 4 h and coated with Al_2O_3

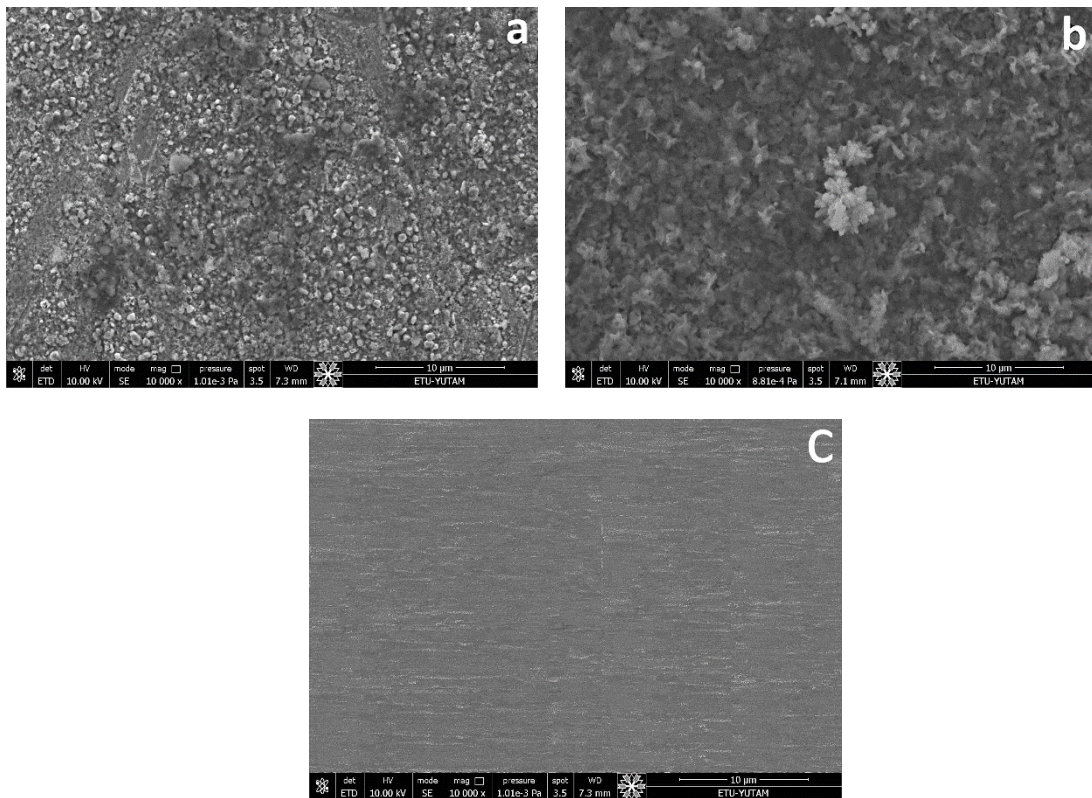


Figure 2. SEM images of a) 800°C 4 h, b) duplex (800°C 4 h + Al_2O_3), c) untreated

3.2. Tribocorrosion properties

Figure 3 presents The SEM images of the untreated samples' worn surfaces and the samples that were borided for 4 h at 800°C and then coated with Al_2O_3 (duplex) after the tribocorrosion tests. Because the structure of the base material contains Ni, and boron has a higher affinity

than Ni in borided samples, B atoms force Ni atoms to move inwards, and this results in a thin boride layer on the surface [14]. The boride layer increases the surface hardness of the NiTi alloy. Additionally, another cause of this increased hardness on the surface is the boride phases created on the surface by the boron with Ni and Ti found in the base metal. The compressive stress that is created with the help of these phases that are likely to be formed plays an effective role in the improvement of the mechanical and wear characteristics of the material [8]. Therefore, the mechanical and tribological properties of the material are enhanced with the help of this layer.

At the start of the wear process in the untreated NiTi sample, a two-body mechanism brings the sample surface and the Al₂O₃ ball into direct contact. The Ti and Ni that form as a result of friction adhere firmly to the ball. As the wear process continues, this adhesion leads to the formation of new wear products, and the surface of the untreated NiTi material transfers material to the surface of the hard abrasive ball. Consequently, the untreated sample's wear behavior persists across the testing period as a mix of the abrasion and plastic deformation mechanisms together with significant adhesive wear.

Treated samples can provide many advantages with the boriding process such as higher wear, oxidation, and corrosion resistance on the surface and the preservation of hardness at high temperatures [15]. Therefore, the Al₂O₃ that is deposited onto the surface with the coating process carried out after boriding leads to an increase in microhardness by increasing the cathodic duty cycle [16-17]. In their study on SiC particles, Luo et al. reported that increasing the concentration of Al₂O₃ initially provides superior mechanical properties including bending strength, fracture toughness, and Vickers hardness [18]. Additionally, uniform Al₂O₃ coating improves mechanical properties and prevents grain growth. However, the hardness and Young's modulus of the coating are strongly affected by the thickness of the coating, its composition, porosity, and microcracks [17]. As seen in the images of the wear surfaces, in this study, it was observed that the untreated samples and the duplex-coated samples showed different wear behaviors due to the aforementioned effects of the surface treatments. Throughout this analysis, wear mechanism damage was far more significant than corrosive damage.

The tribocorrosion behaviors of the untreated samples, the samples that were borided for 1-4 h at 800°C, and the samples that were coated with Al₂O₃ after boriding (duplex) during the sliding test were examined. For this purpose, open circuit potential (OCP) and potentiodynamic polarization tests were conducted. OCP provides information about the state of surface electrochemistry. The polarization curve shows changes in the specimens' ability to withstand corrosion while sliding [19].

Figure 4 presents the friction coefficients of different samples under 3 N load in a 3.5% wt. NaCl solution. As seen in Figure 4, the mean coefficients of friction (COF) for the untreated samples, 800°C 1 h borided samples, 800°C 4 h borided samples, 800°C 1 h borided + Al₂O₃-coated samples, and 800°C 4 h borided + Al₂O₃-coated samples were 0.2, 0.3, 0.4, 0.5, and 0.65, respectively. The fluctuation of COF under a load of 3 N indicates the displacement of the opposing ball along the coating interface [20]. Therefore, this situation shows that the sample has experienced wear. Additionally, as seen in the plot of the 800°C 4 h borided + Al₂O₃-coated

samples, these samples did not show noticeable fluctuations, especially compared to the untreated samples. Hence, the duplex-treated samples did not show much wear under a load of 3 N. This situation is related to the higher density and hardness of the sample surface. Wear on such a sample surface results in minimal loss of volume. High surface hardness values usually go through the phases of high resistance to adhesion, oxidation, and fatigue [21]. As seen in this study, during the sliding test against the Al_2O_3 ball inside the 3.5% NaCl solution, due to the high tendency of the surfaces of the untreated samples to wear, COF values with substantial fluctuations were observed on the surface of this alloy. This indicated the weak tribological behavior of the untreated samples. Among all samples, the course of fluctuations showed a relatively decreasing trend with the thickness of the boriding layer and the coating, and the lowest degree of fluctuations was observed on the duplex-treated surfaces. As seen here, the 800°C 4 h borided + Al_2O_3 -coated surface not only significantly increased the wear resistance of the samples but also affected the COF values during the two-body tribocorrosion test.

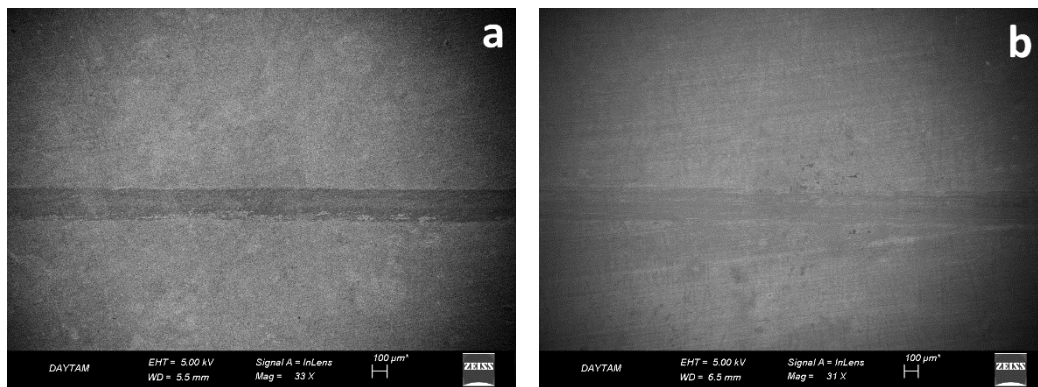


Figure 3. SEM images of wear analysis during tribocorrosion of **a)** Untreated **b)** 800°C 4h + Al_2O_3

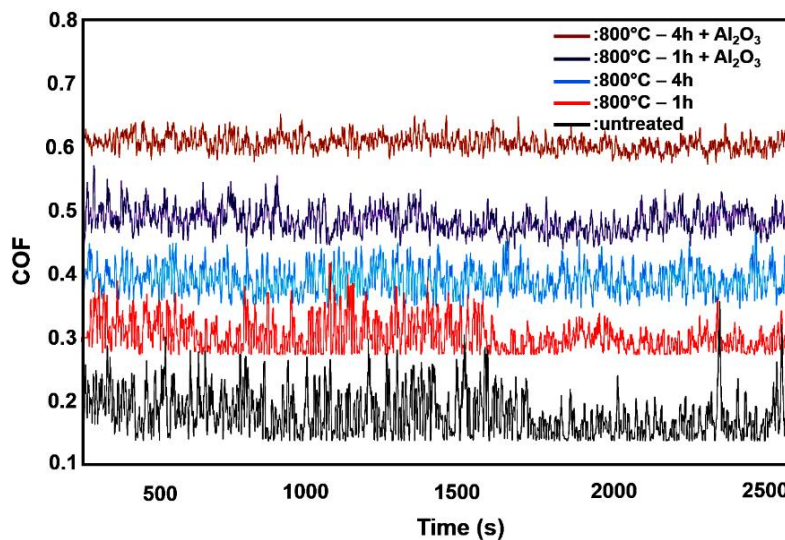


Figure 4. Variation of OCP with time recorded during sliding with the COF values of untreated, 800°C 1 h borided, 800°C 4 h borided, 800°C 1 h borided + Al_2O_3 , and 800°C 4 h borided + Al_2O_3 samples

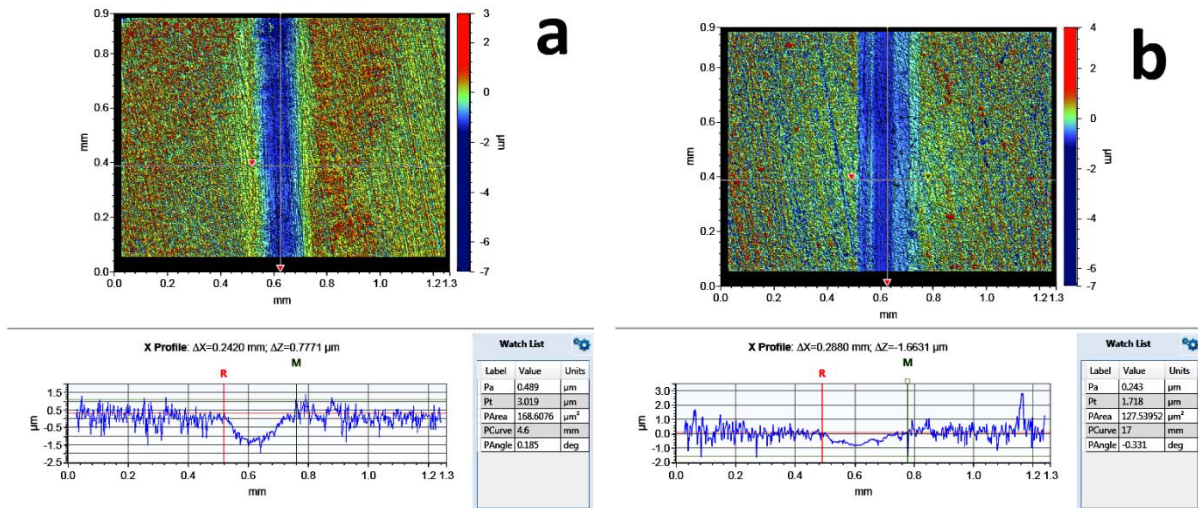


Figure 5. Wear analysis during tribocorrosion of a) Untreated, b) 800°C 4 h + Al_2O_3

Figure 5 displays the cross-sections of the untreated (Figure 5a) and the 800°C 4 h + Al_2O_3 samples, as well as the wear tracks' three-dimensional surface profiles (Figure 5b), respectively (the best and worst experimental conditions are given). It can be observed that the wear depth of the untreated sample was much higher than that of the 800°C 4 h + Al_2O_3 sample due to the lower tribocorrosion resistance of the former. A substantial improvement was seen in the wear behavior of the NiTi alloy during sliding under a load of 3 N in room conditions with the duplex coating treatment. The wear process that started in an adhesive form in the untreated samples gained a micro-abrasive characteristic with the effects of the particles that were released from the material. In the duplex-treated samples, the form of wear was usually adhesive. The surface hardness that increased with the duplex surface treatment led to a decrease in wear by making plastic deformation more difficult. The thicker boron layer that is formed with the prolongation of the boriding time increases the wear rate, although the wear does not reach the base material. For all samples that were examined in terms of COF, Figure 6 shows the potentiodynamic polarization curves during the 3 N sliding test, and Figure 7 displays the voltage-current density curves during the same test. Tribocorrosion causes a mixed potential in OCP. As a result, it demonstrates that the active wear areas and passive wear regions are in a rather steady state [22]. The mechanically passivated portions (anode) and the surrounding passive areas create a galvanic bond as a result of sliding (cathode). As a result, OCP undergoes a severe negative change. After then, the wear track's depassivation and repassivation rates are in balance with one another. This equilibrium brings OCP to a new stable state [19]. In this study, the sliding procedure may have accelerated the corrosion rate of the untreated layer of the NiTi alloy subjected to the corrosive medium inside the 3.5% wt. NaCl solution. This, in turn, may have resulted in a higher i_{corr} value under the 3 N load in the duplex-treated samples compared to the specimens that are untreated.

The OCP data that were obtained in this study showed that the duplex-coated samples had a more positive potential trend compared to the untreated samples. Respectively from the untreated samples to the borided samples, and finally, to the duplex-coated samples, it was seen that the corrosion rates decreased, and accordingly, the corrosion resistance values increased.

As the thickness of the coating on the surface decreased, due to mechanical wear, the potential changes in the negative direction. Additionally, potential is associated with the passive film on the surface [23]. A passive film can be formed during corrosion, it breaks very easily from the worn surface with the effect of mechanical wear, and it separates, which leads to a negative shift in the corrosion potential. As seen in Figure 6, considering that the duplex-treated samples had more positive values and less wear compared to the others, it may be stated that it showed better tribocorrosion properties. As a result, in comparison to the untreated samples, the tribocorrosion resistance values of the surface-treated samples inside the 3.5% NaCl solution under the load of 3 N increased. Furthermore, the samples to which duplex surface treatment was applied showed the best tribocorrosion-related properties among all samples.

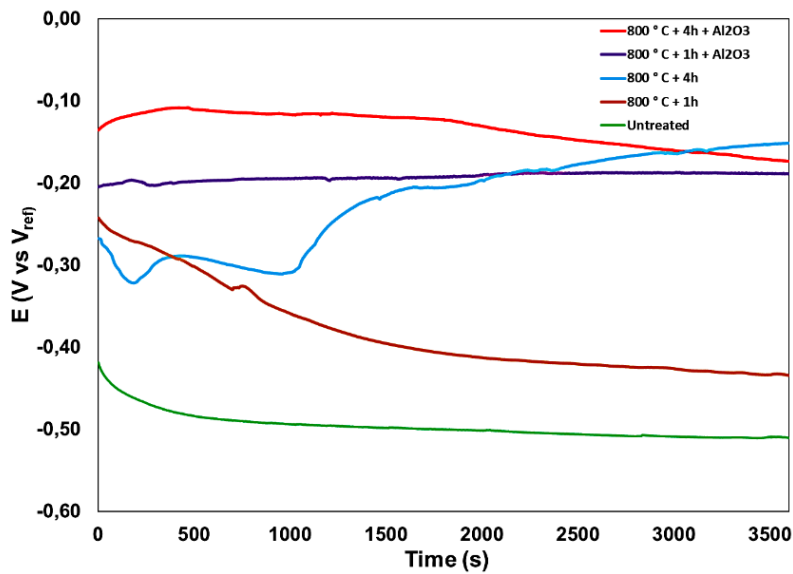


Figure 6. OCP curves of the samples inside the solution.

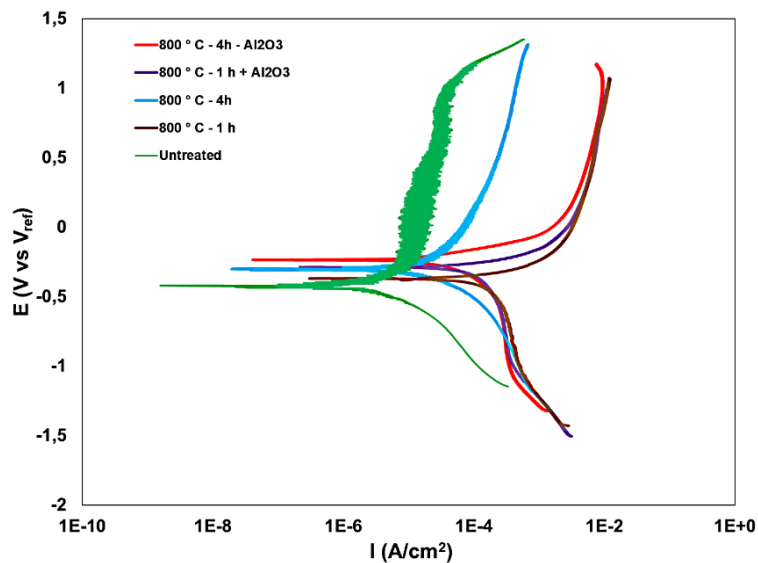


Figure 7. Voltage-current density curves

4. Conclusions

In this study, the tribocorrosion properties of a borided and Al₂O₃-coated NiTi material were investigated, and the results were as follows.

On the surface of the material that was borided at 800°C for 4 h and then coated with Al₂O₃, NiB₂, TiB₂, and Al₂O₃ phases were formed. With the boriding treatment and the EPD method, the Al₂O₃ coating process was successfully implemented. For all samples, the degree of COF fluctuations relatively decreased depending on the increased thickness of the boriding layer and the coating on it, and the lowest degree of fluctuations was found in the duplex-treated samples. In comparison to the untreated samples, the tribocorrosion resistance of the surface-treated samples under the load of 3 N in the 3.5% NaCl solution increased. The duplex-treated samples showed the best tribocorrosion-related characteristics among all samples.

Ethics in Publishing

There are no ethical issues regarding the publication of this study

Acknowledgement

For their cooperation in the use of the analysis and measurement systems employed in this work, we would like to thank Atatürk University Eastern Anatolia High Technology Application and Research Center (DAYTAM) and Erzurum Technical University High Technology Application and Research Center (ETU-YÜTAM).

References

- [1] Kaya, E., Kaya, İ., (2020) Tool wear progression of PCD and PCBN cutting tools in high speed machining of NiTi shape memory alloy under various cutting speeds, *Diamond and Related Materials*, 105 107810.
- [2] Ramaiah, K., Saikrishna, C., Bhaumik, S., (2014) Ni_{24.7} Ti_{50.3} Pd_{25.0} high temperature shape memory alloy with narrow thermal hysteresis and high thermal stability, *Materials & Design*, 56 78–83.
- [3] Shabalovskaya, S. A., (1996) *Shape Memory Alloys for Biomedical Applications*. Yoneyama, T., Miyazaki, S. (Eds.), *Biocompatibility of Nitinol for biomedical applications* (6 -267), Woodhead Publishing, England.
- [4] Petrini, L., Migliavacca, F., (2011) Biomedical applications of shape memory alloys, *Journal of Metallurgy*, 1-15.
- [5] Bil, C., Massey, K., Abdullah, E.J., (2013) Wing morphing control with shape memory alloy actuators, *J. Intell. Mater. Syst. Struct.*, 24 (7) 879–898.
- [6] Pelletier, H., Muller, D., Mille, P., Grob, J., (2002) Structural and mechanical characterisation of boron and nitrogen implanted NiTi shape memory alloy. *Surface and Coatings Technology*, 158–159 309-317.

- [7] Uzun, Y., Yanıkoğlu, N., Kovacı, H., Yetim, A.F., Çelik, A., (2021) The effects of boriding on metal-ceramic bond strength of Co–Cr alloy fabricated by selective laser melting, *Journal of Adhesion Science And Technology*, 35(14) 1576–1591.
- [8] Aksöz, S., Bostan, B., Kaplan, Y., (2021) An Investigation on the Effects of Boronizing Process on Microstructure and Microhardness of NiTi Alloy Produced by P/M Technique, *Journal of Polytechnic*, 24 (2) 539-544.
- [9] Misra, S.K., Boccaccini, A.R., (2007) Tissue engineering using ceramics and polymers. Boccaccini, A.R., Gough J.E., (Eds.) (72), Woodhead Publishing Limited, England.
- [10] Boccaccini, A.R., Keim, S., Ma, R., Li, Y., Zhitomirsky, I. (2010) Electrophoretic deposition of biomaterials, *J. R. Soc. Interface* 7 581-613.
- [11] Bakhshandeh, S., & Amin Yavari, S. (2018) Electrophoretic deposition: A versatile tool against biomaterial associated infections, *Journal of Materials Chemistry B*, 6(8) 1128-1148.
- [12] Saji, V. S. (2021) Electrophoretic (EPD) coatings for magnesium alloys, *Journal of Industrial and Engineering Chemistry*, 103 358-372.
- [13] Boccaccini, A.R. and Zhitomirsky, I. (2002) Application of electrophoretic and electrolytic deposition techniques in ceramics processing, *Current Opinion in Solid State & Materials Science*, 6 251-260.
- [14] Béjar M. A., Moreno E., (2006) Abrasive wear resistance of boronized carbon and low-alloy steels, *Journal of Materials Processing Technology*, 173(3) 352-358.
- [15] Uzun, Y., Kovacı, H., Yetim, A. F., Çelik, A. (2019) Effect of boronizing on the structural, mechanical and tribological properties of CoCrW dental alloy produced by selective laser melting, *Industrial Lubrication and Tribology*, 71(3) 348–356.
- [16] Malinovschi, V., Marin, A., Negrea, D., Andrei, V., Coaca, E. Mihailescu, C. N., Lungu, C. P. (2018) Characterization of Al_2O_3/ZrO_2 composite coatings deposited on Zr-2.5Nb alloy by plasma electrolytic oxidation, *Appl. Surf. Sci.*, 451169-179.
- [17] Sourani, F., Raeissi, K., Enayati, M. H., Kharaziha, M., Hakimizad, A., Blugan, G., Salimijazi, H. R., (2022) Corrosion and tribocorrosion behavior of $ZrO_2-Al_2O_3$ composite coatings developed by plasma electrolytic oxidation for load-bearing implants, *Journal of Alloys and Compounds*, 920 165856.
- [18] Luo, Y., Wu, Y., Xiao, D., Tang, K., Huang, C., Fu, R. K. Y., Zheng, S., Chu P. K. (2019) Al_2O_3 coating for densification of SiC ceramics and sintering kinetics, *Surf. Coat. Technol.*, 374 603-609.
- [19] Zhang, B., Wang, J., Yan, F., (2018) Load-dependent tribocorrosion behaviour of nickel-aluminium bronze in artificial seawater, *Corros. Sci.*, 131 252-263.
- [20] Martini, C., Ceschini, L., Tarterini, F., Paillard, J.M., Curran, J.A., (2010). PEO layers obtained from mixed aluminate–phosphate baths on Ti–6Al–4V: Dry sliding behaviour and influence of a PTFE topcoat, *Wear*, 269 47-756.

[21] Karakaş, M. S., Günen, A., Çarboğa, C., Karaca, Y., Demir, M., Altınay, Y., Erdoğan, A., (2021) Microstructure, some mechanical properties and tribocorrosion wear behavior of boronized $Al_{0.07}Co_{1.26}Cr_{1.80}Fe_{1.42}Mn_{1.35}Ni_{1.10}$ high entropy alloy, *J. Alloy. Compd.*, 886 161222.

[22] Pina, V.G., Amigó, V., Muñoz A.I. (2016) Microstructural, electrochemical and tribo-electrochemical characterisation of titanium-copper biomedical alloys, *Corros. Sci.*, 109 115-125.

[23] Sampaio, M., Buciumeanu, M., Henriques, B., Silva, F. S., Souza, J. C. M., Gomes J. R., (2016) Comparison between PEEK and Ti6Al4V concerning micro-scale abrasion wear on dental applications, *J. Mech. Behav. Biomed. Mater.*, 60 212-219.

Investigation of the Effects of Optical Models on the Production Cross-Section Calculations of $^{22,24}\text{Na}$ Radioisotopes with some (d,x) and (α ,x) Reactions

Mert Şekerci^{1*}

¹Süleyman Demirel University, Department of Physics, 32260, Isparta, TÜRKİYE

Received: 27/09/2022, Revised: 13/12/2022, Accepted: 27/12/2022, Published: 30/12/2022

Abstract

The results of the research carried out in the field of basic sciences and the achievements obtained in these studies mediate effective and beneficial results not only for basic sciences, but also in many various fields from medicine to engineering. In this context, the theoretical investigation of the production routes of various radioisotopes, that can be used in many fields, ensures that physics and other related fields meet on a common denominator. Considering this fact as motivation, the aim of this study is to investigate how various deuteron and alpha optical models affect the cross-section calculations of $^{22,24}\text{Na}$ radioisotopes, which are known to be used in medical applications. The TALYS (v1.95) code was utilized in the calculations, which allows for the use of five different deuteron and eight different alpha optical model alternatives. The obtained results were not only visually compared to the existing experimental data in the literature, but also quantitatively by performing mean weighted deviation and relative variance analyses.

Keywords: cross-section, radioisotope, theoretical model, TALYS

Bazı (d,x) ve (α ,x) Reaksiyonlarıyla $^{22,24}\text{Na}$ Radyoizotoplarının Üretim Tesir Kesiti Hesaplamalarına Optik Modellerin Etkilerinin İncelenmesi

Öz

Temel bilimler alanında yürütülen araştırmaların sonuçları ve bu çalışmalarda elde edilen kazanımlar sadece temel bilimler için değil, aynı zamanda tıptan mühendisliğe kadar pek çok çeşitli alanda da etkili ve faydalı sonuçlara aracılık etmektedir. Bu bağlamda, birçok alanda kullanılabilecek çeşitli radyoizotopların üretim yollarının teorik olarak araştırılması, fizik ve diğer ilgili alanların ortak bir paydada buluşmasını sağlamaktadır. Motivasyon olarak bu gerçek göz önünde bulundurularak bu çalışmanın amacı, çeşitli döteron ve alfa optik modellerin tıbbi uygulamalarda kullanıldığı bilinen $^{22,24}\text{Na}$ radyoizotoplarının tesir kesiti hesaplamalarını nasıl etkilediğini araştırmak olarak belirlenmiştir. Hesaplamalarda beş farklı döteron ve sekiz farklı alfa optik model alternatifinin kullanımına olanak sağlayan TALYS (v1.95) kodu kullanılmıştır. Elde edilen sonuçlar literatürdeki mevcut deneysel verilerle sadece görsel olarak değil, ortalama ağırlıklı sapma ve bağıl varyans analizleri yapılarak nicel olarak da karşılaştırılmıştır.

Anahtar Kelimeler: tesir kesiti, radyoizotop, teorik model, TALYS

1. Introduction

Not only the results of scientific research, but also the various gains obtained during the realization of these researches provide valuable inferences that can guide both the literature and subsequent studies. Indeed, theoretical studies, particularly in natural sciences, are as significant and valuable as experimental ones. Furthermore, this circumstance motivates the development of interdisciplinary research studies oriented on common bases, which can influence and benefit one another by using the obtained results [1-3]. Theoretical studies are undoubtedly significant in physics, as they are in many other disciplines, particularly in related fields of research that might be included into nuclear physics. Many factors, which may differ depending on the investigated topic, such as technological and physical infrastructure, financial capacity, and trained manpower, are critical to the effective completion of experimental research. In the event that an experimental study, which have to be designed by combining these and many other possible factors in a functional way, cannot be realized, the way for researchers to have a foresight on the subject they are examining can be obtained from theoretical studies and computer-aided simulations [4-13]. An essential consideration here is that the involvement of a theoretical basis is required in both circumstances, whether an experimental research or computer-aided modeling study. In this context, it is evident from the studies in the previously shown literature that many models have been developed to comprehensively examine and analyze nuclear reaction mechanisms and processes. There are multiple values that can be examined in nuclear reaction processes, which are known to exist in a wide range from the formation of the universe to the applications that affect our daily lives. The cross-section quantity, which may be defined as the likelihood of a nuclear reaction take place, is one of the most remarkable among them. This value can be measured by experimental studies as well as calculated theoretically, and its presence is very important in interpreting the process and details of a nuclear reaction [14-16]. It is a known fact that nuclear models and the varied parameters of these models affect the calculation outcomes of the cross-section values, and there are also models called optical models among these models. As a consequence, investigations on the influences of optical models on the cross-section calculations will undoubtedly contribute to the literature. The cross-section calculations include complicated mathematical procedures and operations that make use of theoretical models and parameters. When the hand-made aspect comes into effect, repeating these steps several times for varying values of a parameter creates a very high chance of inaccuracy and mistake. As a response, several computer-aided calculation tools have been developed to address situations where the cross-section values are theoretically tried to be acquired. Some of these can be shown as ALICE/ASH [17], CEM95 [18, 19], PCROSS [20], and most commonly employed codes EMPIRE [21] and TALYS [22, 23].

In this study, the 1.95 version of the TALYS code, which has a high utilization rate in the literature, was chosen. The goal of this study using the TALYS code is to look at the impact of five distinct deuteron and eight different alpha optical model potentials on the production cross-section calculations of $^{22,24}\text{Na}$ radioisotopes that are known to be employed in medical applications. Even a brief review of the literature will reveal numerous clinical studies on the use of several radioisotopes in medical applications. Similarly, various theoretical

investigations on these radioisotopes can be seen in the literature. In these studies, it is generally aimed to investigate the effects of including different models and parameters in the calculations, and it is seen that they contribute to both the development of theoretical models and the research of existing and new production routes of significant radioisotopes [24-27]. The reactions investigated in this study for the production of $^{22,24}\text{Na}$ radioisotopes are some (d,x) and (α ,x) reactions on $^{\text{nat}}\text{Mg}$ which are; $^{\text{nat}}\text{Mg}(\text{d},\text{x})^{22}\text{Na}$, $^{\text{nat}}\text{Mg}(\text{d},\text{x})^{24}\text{Na}$, $^{\text{nat}}\text{Mg}(\alpha,\text{x})^{22}\text{Na}$ and $^{\text{nat}}\text{Mg}(\alpha,\text{x})^{24}\text{Na}$. For these reactions, graphical representations were presented in which the theoretical data obtained from the results of the calculations performed by using different models and the experimental data obtained from the literature are given jointly so the outcomes could be analyzed visually. In addition to the graphical representations, the mean weighted deviation [28] and relative variance analyses [28] were performed in order to analyze the outcomes quantitatively.

2. Material and Methods

The radioisotopes $^{22,24}\text{Na}$ included in this study are among the several radioisotopes that are widely used in medicinal applications. Sodium has twenty known isotopes, of which only ^{23}Na is stable, and two isomers. Half-lives of isotopes other than ^{22}Na and ^{24}Na have been reported to be less than one minute, and often less than one second [29, 30]. Sodium, an alkali metal, is the seventh most prevalent element in the earth's crust, accounting for around 2.27 % of the total, and is critical for life [31]. The half-life of ^{22}Na (decay modes: ec (electron capture) β^+ (emission of an anti-electron and a neutrino) 100 %, Q_{β^-} (energy available for β^- decay): -4781.41 ± 0.16 keV, Q_{α} (energy available for α decay): -8479.4 ± 0.5 keV, Q_{EC} (energy available for EC decay): 2843.33 ± 0.13 keV) is 2.6019 years, while the half-life of ^{24}Na (decay modes: β^- (emission of an electron and an anti-neutrino) 100 %, Q_{β^-} (energy available for β^- decay): 5515.677 ± 0.021 keV, Q_{α} (energy available for α decay): -10825.35 ± 0.03 keV, Q_{EC} (energy available for EC decay): -2466.3 ± 0.5 keV) is 14.9560 hours [32]. Given the characteristic properties of ^{22}Na , its usage for a number of applications and differ purposes, such as calibration in positron emission tomography (PET) imaging systems, has emerged [33-36]. On the other side, ^{24}Na has been demonstrated to be useful in studies on bone blood flow, postmastectomy lymphedema, intramuscular clinical trials, and noradrenaline sensitivity in hypertension [37-41]. Apart from these studies, it is possible to encounter examples of studies on the use of both radioisotopes for different purposes in the literature [42-45].

In this study, $^{22,24}\text{Na}$ isotopes were prioritized since their values could be easily realized when current and potential usage areas and the benefits they provide are considered together. In this context, production cross-section calculations were made for $^{22,24}\text{Na}$ radioisotopes in reactions with deuteron and alpha incident particles onto $^{\text{nat}}\text{Mg}$. The factor that constitutes the remarkable point of this study is directly related to how these calculations are made. In this process, different optical model potentials were imposed on the calculations and how the outcomes differ as a result of this situation was examined. As mentioned in the previous section, it is a known situation that there are many programs and tools that can be used to calculate the cross-section value. It can be easily seen from the literature that TALYS code is preferred more frequently than others among these mentioned tools. Some of the examples for this situation could be given

as follows; free and open source code distribution, there is no special training required to use the code at the beginner level, the ability to automatically or optionally adjust various parameters according to the user's level of knowledge and code mastery, diversity and choice to allow the investigations of various nuclear reaction models and the effects of many parameters on different calculations, etc. In this study, TALYS code was preferred due to its competencies and the availability of multiple optical model potentials offered to the users in order to examine the effects of deuteron and alpha optical model potentials on the calculation results.

Before describing the deuteron and alpha optical model potentials that can be utilized in the TALYS code, it will be appropriate to address the optical model expression first. This expression denotes an inherently complex interaction between a particle arriving at a nucleus with a complex mean field potential. The complex mean field potential present in the interaction causes the flux of the reaction formed to split into two parts, one for generating elastic scatterings and the other for all other channels. In the TALYS code, a subprogram called ECIS-06 [46] is used for these complex optical model calculations, and all optical model calculations are first performed for all potential outgoing particle paths and energies and recorded. In the next step, the corresponding conduction coefficients can be used in the calculations for pre-equilibrium and compound nucleus. Finally, calculations are made for each incoming energy value given by the user. The study that Koning and Rochman brought to the literature can be examined for more detailed information on this subject [47].

The models and parameters available to the users in the TALYS code version 1.95, which is the utilized version in this study, are actually used by replacing the pre-defined, or other words default-assigned, models and parameters with specific keywords. There are five different options in the TALYS code for the deuteron optical model potential examined in this study. The Normal deuteron potential is the TALYS code's standard deuteron optical model, which is generated by simplifying Watanabe's folding technique [48]. Apart from this, users can choose the deuteron optical models that have been brought to the literature as a result of the studies of Daehnick et al. [49], Bojowald et al. [50], Han et al. [51] and An and Cai's [52]. In this study, the impacts of all of these models on computations are investigated, and they will be denoted as DOMP1, DOMP2, DOMP3, DOMP4, and DOMP5 in the rest of the article, in the sequence provided above.

After mentioning the deuteron optical models, now it is the place to move on to the alpha optical models that are available in the TALYS code. The TALYS code allows users to select from eight alternative alpha optical model potentials. One of these possibilities has been adopted as the default model by TALYS for the alpha optical model potential, the one imposed by Avrigeanu et al.'s [53] study. Other than the default option, one other option is named as Normal Alpha Potential and is listed as the first option in the TALYS code [48, 54]. Even though it may appear to be a bit outdated, another model that can still be favored in certain situations, depending on the content and character of research, is presented as the second alternative, and this model is taken from McFadden and Satchler's study [55]. The TALYS code presents three possible choices for Demetriou et al.'s [56] double folding potential. The distinction among these three options is that the first two alternatives employ tables, but the third uses the

dispersion model. Another possibility is based on Nolte et al.'s work [57], which developed a set of parameters for the global optical potential of alpha particles with energy of more than 80 MeV. In another study carried out by Avrigeanu et al. [58], the definition of spherical optical potential defined for alpha particles with energies above 80 MeV was extended to lower energies. The remaining alpha optical model potential in the TALYS code, which has not been mentioned so far, is developed on the basis of this study. The abbreviations of the alpha optical models used in this study are shown with the prefix AOMP and the model names are given between AOMP1-AOMP8 since there are eight options in total.

The evaluation of the calculation results obtained for the reactions examined within the scope of the study and the analysis of their compatibility with the experimental data was made both visually and numerically. Both the computation findings and the accessible experimental data from Experimental Nuclear Reaction Data (EXFOR) [59, 60] are shown together for visual interpretation. For numerical analysis, mean weighted deviation (F) and relative variance (D) calculations were made using the equations given in Equations 1 and 2, respectively [28].

$$F = \left[\frac{1}{n} \sum_{i=1}^n [(\sigma_i^{calc} - \sigma_i^{expr}) / \Delta\sigma_i^{expr}]^2 \right]^{1/2} \quad (1)$$

$$D = \left[\frac{1}{n} \sum_{i=1}^n |\sigma_i^{calc} - \sigma_i^{expr}| / \sigma_i^{expr} \right] \quad (2)$$

As can be seen, both equations have σ_i^{calc} and σ_i^{expr} expressions. Of these, σ_i^{calc} represents the calculated values, while σ_i^{expr} is the experimental data. Apart from these, N is used to represent the number of experimental data, and $\Delta\sigma_i^{expr}$ expression is used to represent the amount of error in each experimental data. It may be questionable by some readers why two values, both F and D , are used for numerical analysis, but there is a very logical explanation for this. Of these values, D only compares the calculation results with the experimental data, while F also considers the experimental error margins as a parameter in the calculations.

3. Results and Discussion

In this section, the outcomes of the calculations obtained as a result of separately triggering five different deuteron optical models, each of which is available in the TALYS code, for the $^{nat}\text{Mg}(d,x)^{22}\text{Na}$, $^{nat}\text{Mg}(d,x)^{24}\text{Na}$, $^{nat}\text{Mg}(\alpha,x)^{22}\text{Na}$ and $^{nat}\text{Mg}(\alpha,x)^{24}\text{Na}$ reactions examined within the scope of the study are interpreted. In this context, the visual analyses of the results obtained are presented in the illustrations given in Figures 1-4, while the results of the F and D values used in the numerical analyses are given in Tables 1 and 2.

Figure 1 shows the calculation results obtained for the $^{nat}\text{Mg}(d,x)^{22}\text{Na}$ reaction and the experimental data of Hermanne et al. [61] and Vlasov et al. [62] available in the literature. As can be seen from the figure, the calculation results obtained by using the models were able to relatively form a structure similar to the distribution formed by the experimental data. However, it should be taken into account that the experimental data of Vlasov et al. [62] up to about 15 MeV are higher than the other experimental data and calculations made with all models, especially in the peak region of the hump. In the figure where it is seen that the experimental data of Hermanne et al. [61] continue up to about 50 MeV, the calculation results obtained with

the models also show a similar distribution, but especially after 40 MeV, the results were obtained with higher values than the experimental data. Considering the whole energy range, it can be seen that DOMP2, DOMP 3, DOMP 4 and DOMP5 models produce results that are more discrete than DOMP1 and closer to each other. As a result, it can be easily interpreted from the visual that DOMP1 is the model that produces the most compatible results with the experimental data in the entire energy range, and from the F and D values in Table 1, where the numerical calculation results are presented.

Table 1. The values of the statistical parameters calculated for deuteron optical model potentials

Reaction	Parameters	DOMP1	DOMP2	DOMP3	DOMP4	DOMP5
$^{nat}\text{Mg}(d,x)^{22}\text{Na}$	F	10.3703	14.2388	16.4356	14.9810	14.9040
	D	0.7313	0.7856	0.8488	0.8234	0.8120
$^{nat}\text{Mg}(d,x)^{24}\text{Na}$	F	3.5882	4.9305	5.2074	4.7788	4.8806
	D	0.2959	0.4589	0.4967	0.4280	0.4570

Table 2. The values of the statistical parameters calculated for alpha optical model potentials

Reaction	Parameters	AOMP1	AOMP2	AOMP3	AOMP4	AOMP5	AOMP6	AOMP7	AOMP8
$^{nat}\text{Mg}(\alpha,x)^{22}\text{Na}$	F	3.6999	3.9956	5.8199	3.7642	3.8376	3.5740	3.7833	3.6498
	D	0.2080	0.2332	0.3746	0.2130	0.2006	0.2021	0.2083	0.2012
$^{nat}\text{Mg}(\alpha,x)^{24}\text{Na}$	F	6.6553	6.8679	6.9307	6.6411	6.6353	6.3836	6.5399	6.5086
	D	0.3679	0.4214	0.4137	0.3662	0.3743	0.3645	0.4075	0.3738

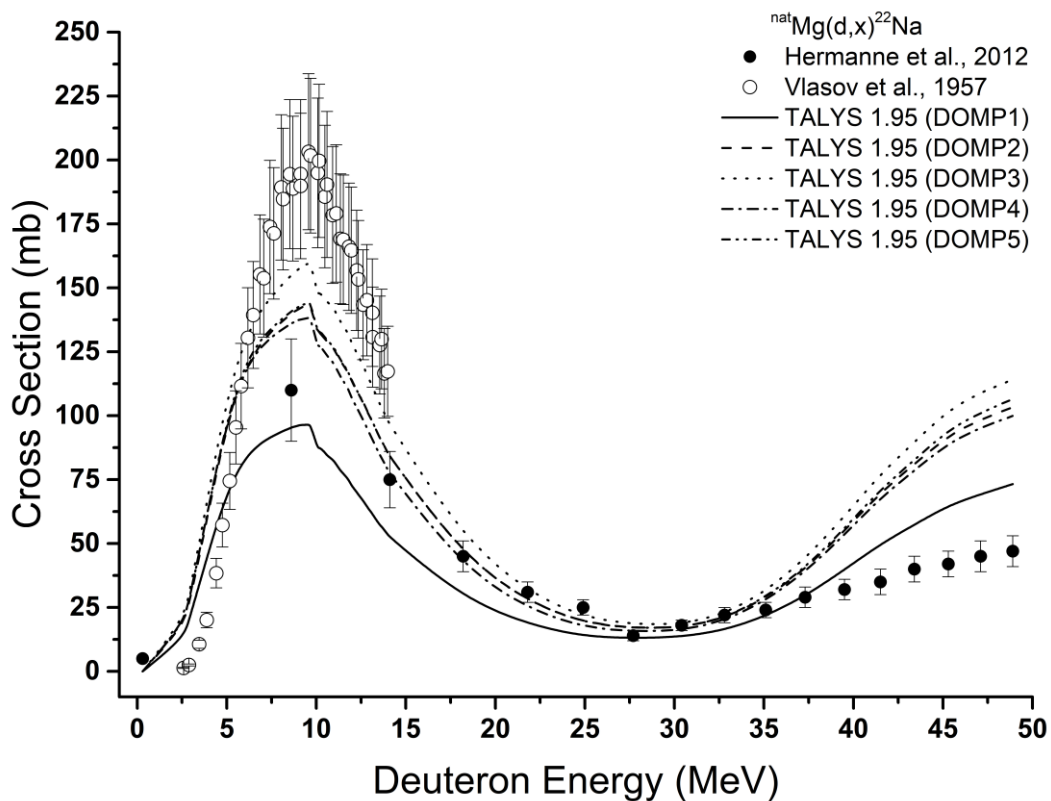


Figure 1. Calculation results and experimental data for the $^{nat}\text{Mg}(d,x)^{22}\text{Na}$ reaction

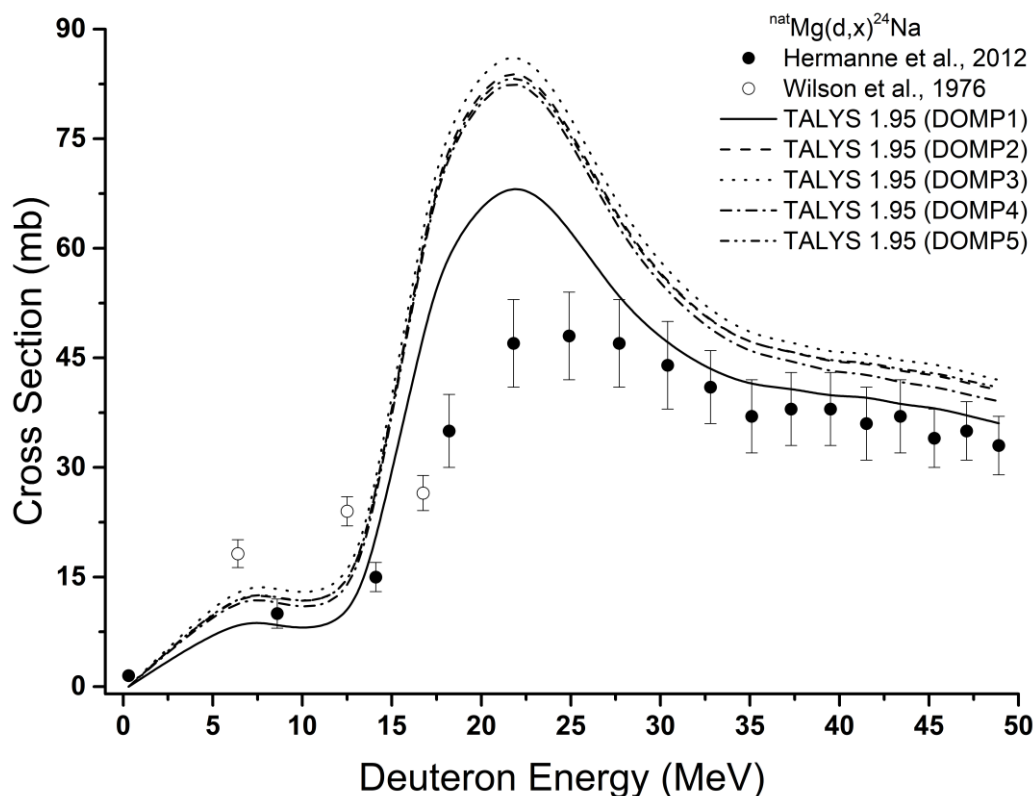


Figure 2. Calculation results and experimental data for the $^{nat}\text{Mg}(d,x)^{24}\text{Na}$ reaction

The calculation results of $^{nat}\text{Mg}(d,x)^{24}\text{Na}$, other deuteron input reaction investigated in this study, are depicted in Figure 2 together with the experimental data of Hermanne et al. [61] and Wilson et al. [63]. Although the incident particle energy shown on the x -axis is up to approximately 50 MeV in both $^{nat}\text{Mg}(d,x)^{22}\text{Na}$ and $^{nat}\text{Mg}(d,x)^{24}\text{Na}$ reactions, the difference between the order of the cross-section values shown on the y -axis is quite clear. On the other hand, similar to the $^{nat}\text{Mg}(d,x)^{22}\text{Na}$ reaction, the DOMP2, DOMP3, DOMP 4 and DOMP 5 models were very close to each other and produced different results from DOMP1 in this reaction, just as they did in $^{nat}\text{Mg}(d,x)^{22}\text{Na}$ reaction. It can also be seen from the visual that the difference between the results produced by the DOMP2, DOMP3, DOMP 4 and DOMP 5 models becomes relatively more visible with the increase in the incoming particle energy. Although it is seen that all models exhibit a distribution similar to that of the experimental data in general, it is understood from both Figure 2 and the numerical values available in Table 1 that DOMP1 produces more consistent results compared to other models when the whole energy range is considered.

In this study, the first reaction in which the effects of using different alpha optical model potentials on the calculations were examined is the $^{nat}\text{Mg}(\alpha,x)^{22}\text{Na}$ reaction. The results of the calculations obtained by triggering a total of eight different models separately are visualized in Figure 3 together. Figure 3 also shows the experimental data of this reaction that Lange et al. [64] brought to the literature with their work. It can be easily seen from Figure 3 that the model developed according to Table 1 in Demetriou et al.'s [56] study, represented by AOMP3 in this work, among the eight models employed in the calculations, provides cross-section results at

lower values than the other models in the entire examined experimental energy range. In addition, it can be said that AOMP7 around the top of the first hump and AOMP2 after the incoming particle energy region of about 75 MeV produce higher cross-section values compared to other models. Models that can be said to produce results with very close values are also noticeable in Figure 3. Since it would be more appropriate to use numerical analysis instead of visual analysis in such cases, the results of the calculations made for this purpose are presented in Table 2. As it can be understood from the presented values, the model that produces more consistent results with the experimental data for the $^{\text{nat}}\text{Mg}(\alpha,x)^{22}\text{Na}$ reaction is AOMP6 according to the F parameter, while it is AOMP5 according to the D parameter. It will be necessary to emphasize that F also takes into account the error in the experimental data, while D does not, recalling the section of this work where the difference between the F and D parameters is described.

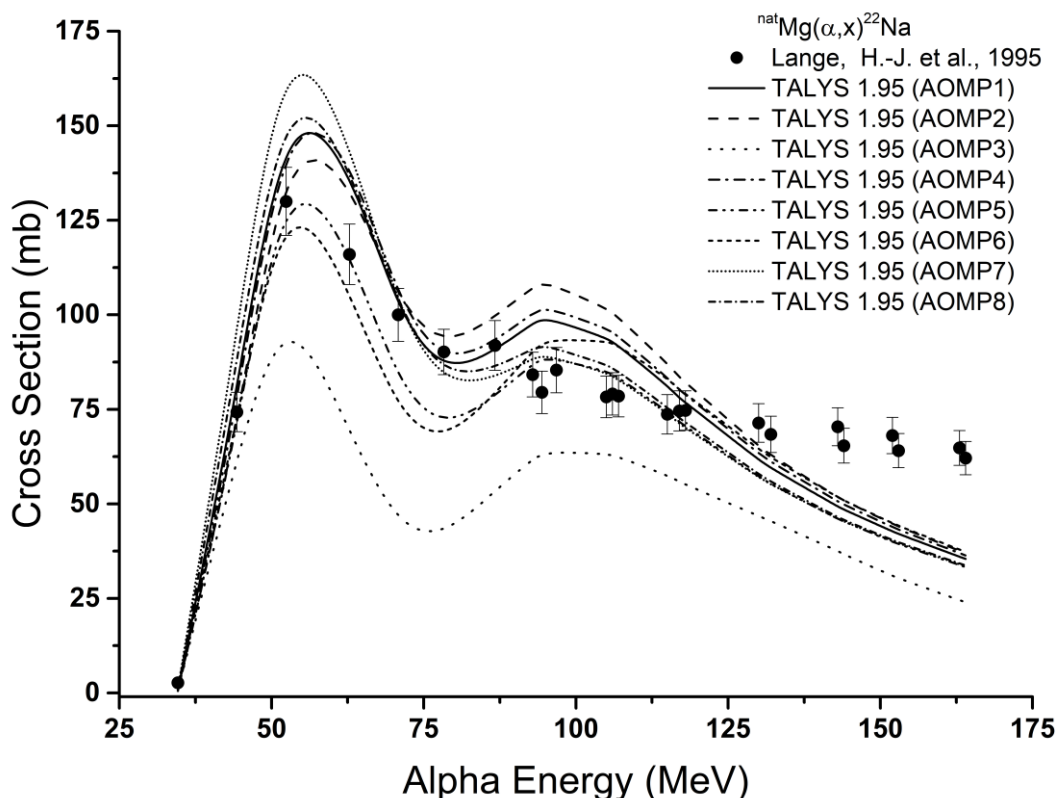


Figure 3. Calculation results and experimental data for the $^{\text{nat}}\text{Mg}(\alpha,x)^{22}\text{Na}$ reaction

The results of the $^{\text{nat}}\text{Mg}(\alpha,x)^{24}\text{Na}$ reaction, the last reaction examined within the scope of the study, are depicted together with the experimental data of Nozaki et al. [65] and Lange et al. [64] in Figure 4. In this reaction, the experimental data of Nozaki et al. [65] were limited in the region shown with the incoming particle energy range of 35-50 MeV in Figure 4, while the experimental data of Lange et al. [64] showed a distribution in a wider energy area and higher energy value. As a result of the evaluation of the experimental data as a whole, it can be easily said from Figure 4 that while the calculation results showed a relatively consistent but quite similar hump structure among themselves, this was not valid after approximately 65 MeV of the experimental data. It can be seen that in the top region of the hump structure AOMP2 produced higher cross-section values than the others from all the utilized models. On the other

hand, the model that produced the lowest cross-section value in the same area was AOMP3. The numerical results of the F and D values given in Table 2 are higher than the results obtained for $^{\text{nat}}\text{Mg}(\alpha,x)^{22}\text{Na}$ due to the fact that the calculation results are not in clear agreement with the experimental data in general. As a result of the comparisons made according to the energy range of the experimental data, the model, which managed to produce more compatible results with the experimental data in the whole energy range according to the F and D values compared to the other options, is highlighted as AOMP6 as can be seen from the numerical values available in Table 2.

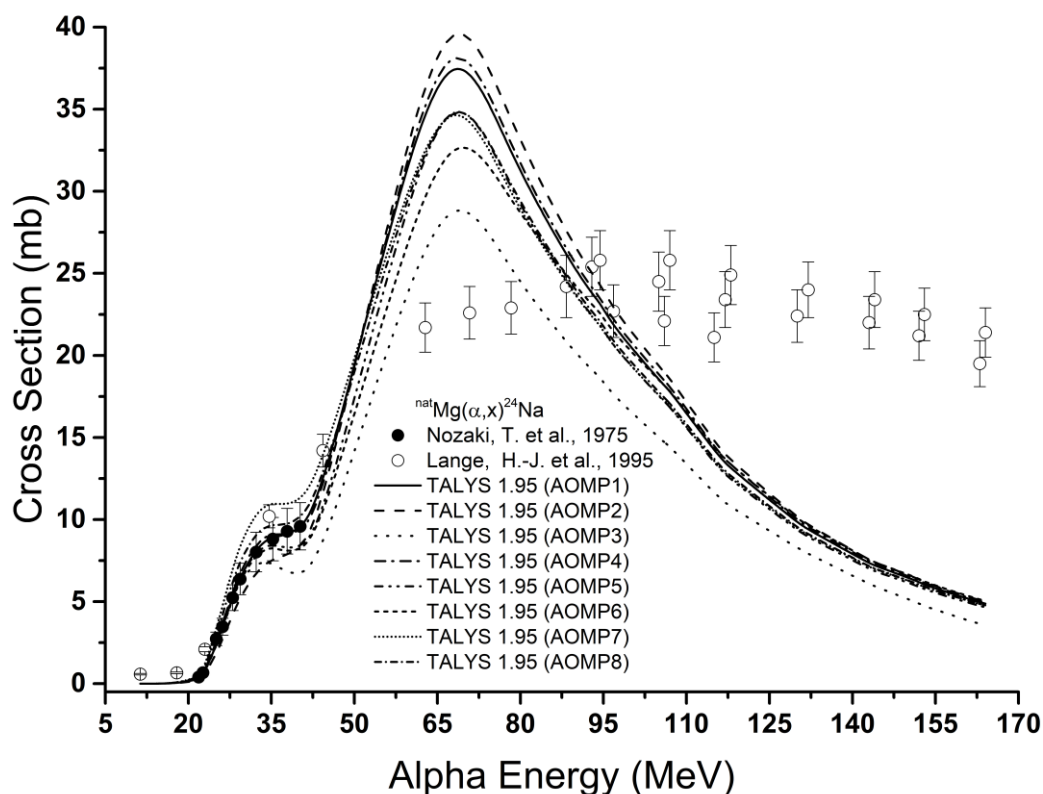


Figure 4. Calculation results and experimental data for the $^{\text{nat}}\text{Mg}(\alpha,x)^{24}\text{Na}$ reaction

4. Conclusion

This section presents a holistic evaluation of all outputs by evaluating all findings obtained in accordance with the steps taken while adhering to the motivation of this study, which is explained in the preceding sections. The first remarkable result is the differences in cross-section calculation values depending on the incoming particle type and energy, which has been observed by considering all the reactions studied. Although the incoming particle energies in the deuteron induced $^{\text{nat}}\text{Mg}(\text{d},x)^{22}\text{Na}$ and $^{\text{nat}}\text{Mg}(\text{d},x)^{24}\text{Na}$ reactions are in the range of 0-50 MeV, as can be seen from the figures, it is clearly seen that the limits of the cross-section values obtained and shown on the y-axis are different. This situation is also clearly seen in the alpha induced $^{\text{nat}}\text{Mg}(\alpha,x)^{22}\text{Na}$ and $^{\text{nat}}\text{Mg}(\alpha,x)^{24}\text{Na}$ reactions with incoming particle energies of 25-175 MeV and 0-170 MeV, respectively. Of course, the fact that the reaction processes are different by their nature is a factor in the formation of this situation, and there are different physical processes that has been experienced during the formation of the reaction routes investigated.

Another important point to be mentioned is how the use of models and parameters in theoretical calculations in which they are employed affects the results. It is clear from both the graphs and the numerical calculations performed with the calculation results obtained that the differentiation of the model or parameters used even in the same reaction can cause easily understandable differences in the results. The use of different models in the reactions examined in this study, in which deuteron and alpha optical model potentials were utilized, directly affected the cross-section results.

Among the reactions examined in this study, it can be easily seen from the figures and tables that the calculation results of both the deuteron induced $^{\text{nat}}\text{Mg}(\text{d},\text{x})^{22}\text{Na}$ and $^{\text{nat}}\text{Mg}(\text{d},\text{x})^{24}\text{Na}$ reactions exhibit harmony with the experimental data. For both reactions, both F and D values highlights the model abbreviated as DOMP1, which is the one used as the default model by TALYS, as the model that produces the most compatible results with the experimental data. In the alpha induced reactions, a harmony was observed between the experimental data and the calculation results for the $^{\text{nat}}\text{Mg}(\alpha,\text{x})^{22}\text{Na}$ reaction, while a similar agreement could not be seen in the entire energy range for the $^{\text{nat}}\text{Mg}(\alpha,\text{x})^{24}\text{Na}$ reaction, unfortunately. The F value, which includes the margins of error in the experimental data, revealed the AOMP6 model as the model that produced more compatible results with the experimental data in both $^{\text{nat}}\text{Mg}(\alpha,\text{x})^{22}\text{Na}$ and $^{\text{nat}}\text{Mg}(\alpha,\text{x})^{24}\text{Na}$ reactions. On the other hand, according to D values, AOMP5 was pointed in the $^{\text{nat}}\text{Mg}(\alpha,\text{x})^{22}\text{Na}$ reaction, while AOMP6 was highlighted in the $^{\text{nat}}\text{Mg}(\alpha,\text{x})^{24}\text{Na}$ reaction. Here, it will be useful to consider the differences between the numerical data, as well as the differences in the calculation methods of the F and D values, as explained earlier.

In the absence of experimental data, it is very important to choose the model or parameter that will provide more compatible results with the experimental data in the theoretical calculations that lead to very useful results for researchers. For this reason, with this and similar studies, a more detailed analysis of models and parameters can be made and various improvements can be achieved. From this point of view, it is necessary to contribute to the literature by conducting similar studies for different reactions too.

Ethics in Publishing

There are no ethical issues regarding the publication of this study.

Author Contributions

Mert Şekerci: Designing the study, performing the calculations, evaluating the results, writing the article.

References

[1] Özdoğan, H., Şekerci, M., Kaplan, A. (2020). An investigation on the effects of some theoretical models in the cross-section calculations of $^{50,52,53,54}\text{Cr}(\alpha,\text{x})$ reactions. *Physics of Atomic Nuclei*, 83, 820–827.

- [2] Yiğit, M., Tel, E. (2014). Theoretical study of deuteron induced reactions on $^{6,7}\text{Li}$, ^9Be and ^{19}F targets. *Kerntechnik*, 79, 63-69.
- [3] Kavun, Y., Aydın, A., Tel, E. (2020). A new formulae study for the (n,2p) reaction cross-section systematics at 14–15 MeV. *Applied Radiation and Isotopes*, 163, 109218.
- [4] Tel, E., Akca, S., Kara, A., Yiğit M., Aydın A. (2013). (p, α) reaction cross sections calculations of Fe and Ni target nuclei using new developed semi-empirical formula. *Journal of Fusion Energy*, 32, 531–535.
- [5] Artun, O. (2018). Calculation of productions of PET radioisotopes via phenomenological level density models. *Radiation Physics and Chemistry*, 149, 73-83.
- [6] Yiğit, M., Bostan, S. N. (2019). Study on cross section calculations for (n,p) nuclear reactions of cadmium isotopes. *Applied Radiation and Isotopes*, 154, 108868.
- [7] Artun, O. (2019). Calculation of productions of medical ^{201}Pb , ^{198}Au , ^{186}Re , ^{111}Ag , ^{103}Pd , ^{90}Y , ^{89}Sr , ^{77}Kr , ^{77}As , ^{67}Cu , ^{64}Cu , ^{47}Sc and ^{32}P nuclei used in cancer therapy via phenomenological and microscopic level density models. *Applied Radiation and Isotopes*, 144, 64-79.
- [8] Akkoyun, S. (2020). Estimation of fusion reaction cross-sections by artificial neural networks. *Nuclear Instruments and Methods in Physics Research Section B*, 462, 51-54.
- [9] Özdoğan, H., Üncü, Y. A., Şekerci, M., Kaplan, A. (2021). Estimations of level density parameters by using artificial neural network for phenomenological level density models. *Applied Radiation and Isotopes*, 169, 109583.
- [10] Özdoğan, H., Üncü, Y. A., Şekerci, M., Kaplan, A. (2021). A study on the estimations of (n, t) reaction cross-sections at 14.5 MeV by using artificial neural network. *Modern Physics Letters A*, 36(23), 2150168.
- [11] Özdoğan, H., Üncü, Y. A., Karaman, O., Şekerci, M., Kaplan, A. (2021). Estimations of giant dipole resonance parameters using artificial neural network. *Applied Radiation and Isotopes*, 169, 109581.
- [12] Şekerci, M., Özdoğan, H., Kaplan, A. (2022). Effects of combining some theoretical models in the cross-section calculations of some alpha-induced reactions for natSb. *Applied Radiation and Isotopes*, 186, 110255.
- [13] Özdoğan, H., Üncü, Y. A., Şekerci, M., Kaplan, A. (2022). Mass excess estimations using artificial neural networks. *Applied Radiation and Isotopes*, 184, 110162.
- [14] Aydın, A., Tel, E., Kaplan, A., Büyüksulu, H. (2010). Pre-equilibrium cross section calculations in alpha induced reactions on ^{65}Cu and ^{209}Bi , *Annals of Nuclear Energy*, 37(10), 1316-1320.

- [15] Kaplan, A., Büyükuşlu, H., Aydın, A., Tel, E., Yıldırım, G., Bölükdemir, M. H. (2010). Excitation Functions of Some Neutron Production Targets on (d,2n) Reactions, *Journal of Fusion Energy*, 29, 181-187.
- [16] Büyükuşlu, H., Kaplan, A., Tel, E., Aydın, A., Yıldırım, G. (2010). Neutron Emission Spectra of $^{104,105,106,108,110}\text{Pd}$ Isotopes for (p,xn) Reactions at 21.6 MeV Proton Incident Energy, *Journal of Fusion Energy*, 29, 41-48.
- [17] Broeders, C. H. M., Konobeyev, A. Yu., Korovin, Yu. A., Lunev, V. P., Blann, M. (2006). "ALICEIASH - Pre-compound and evaporation model code system for calculation of excitation functions, energy and angular distributions of emitted particles in nuclear reactions at intermediate energies". FZK 7183.
- [18] Gudima, K. K., Mashnik, S. G., Toneev, V. D. (1983). Cascade-exciton model of nuclear reactions, *Nuclear Physics A*, 401(2), 329–361.
- [19] Mashnik, S. G. (1995). User Manual for the Code CEM95, Joint Institute for Nuclear Research, Dubna, Moscow.
- [20] Capote, R., Lopez, R., Herrera, E., Piris, M., Osorio, V. (1991). Analysis of experimental data on neutron induced reactions and development of PCROSS code for the calculation of the differential preequilibrium spectra, INDC(NDS)-247/L, International Atomic Energy Agency (IAEA), Vienne.
- [21] Herman, M., Capote, R., Carlson, B. V., Obložinský, P., Sin, M., Trkov, A., Wienke, H., Zerkin, V. (2007). EMPIRE: Nuclear Reaction Model Code System for Data Evaluation. *Nuclear Data Sheets*, 108(12), 2655-2715.
- [22] Koning A. J., Hilaire, S., Duijvestijn, M. C. (2008). TALYS-1.0, Proceedings of the International Conference on Nuclear Data for Science and Technology, April 22-27, 2007, Nice, France, editors Bersillon, O., Gunsing, F., Bauge, E., Jacqmin, R., Leray, S., EDP Sciences, 2008, p. 211-214.
- [23] Koning, A., Hilaire, S., Goriely, S. (2019). TALYS–1.95 A Nuclear Reaction Program, User Manual, first ed. NRG, The Netherlands.
- [24] Tel, E., Aydın, E. G., Kaplan, A., Aydın, A. (2009). New Calculations of Cyclotron Production Cross Sections of Some Positron Emitting Radioisotopes in Proton Induced Reactions. *Indian Journal of Physics*, 83(2), 193-212.
- [25] Aydın, A., Tel, E., Pekdoğan, H., Kaplan, A. (2012). Nuclear Model Calculations on the Production of $^{125,123}\text{Xe}$ and $^{133,131,129,128}\text{Ba}$ Radioisotopes. *Physics of Atomic Nuclei*, 75(3), 310-314.
- [26] Tel, E., Aydın, A., Kara, A., Kaplan, A. (2012). Investigation of Ground State Features for Some Medical Radionuclides Using an effective Nuclear Force. *Kerntechnik*, 77 (1), 50-55.

- [27] Canbula, B. (2017). Bazı tellür izotoplarının nötron yakalama tesir kesiti analizi, *Celal Bayar Üniversitesi Fen Bilimleri Dergisi*, 13(2), 445-455.
- [28] Kurenkov, N. V., Lunev, V. P., Shubin, Yu. N. (1999). Evaluation of calculation methods for excitation functions for production of radioisotopes of iodine, thallium and other elements, *Applied Radiation and Isotopes*, 50(3), 541-549.
- [29] Audi, G., Bersillon, O., Blachot, J., Wapstra, A. H. (2003). The Nubase evaluation of nuclear and decay properties, *Nuclear Physics A*, 729(1), 3–128.
- [30] Haynes, W. M., Lide, D.R., Bruno, T. J. (2017). CRC Handbook of Chemistry and Physics, 97th ed., CRC Press: Boca Raton, FL.
- [31] Greenwood, N. N., Earnshaw, A. (1997). Chemistry of the Elements, 2nd Edition, Butterworth-Heinemann.
- [32] Kondev, F. G., Wang, M., Huang, W. J., Naimi, S., Audi, G. (2021). The NUBASE2020 evaluation of nuclear physics properties, *Chinese Physics C*, 45(3), 030001.
- [33] Al Faraj, A., Alotaibi, B., Pasha Shaik, A., Shamma, K., Al Jammaz, I., Gerl, J. (2015). Sodium-22-radiolabeled silica nanoparticles as new radiotracer for biomedical applications: in vivo positron emission tomography imaging, biodistribution, and biocompatibility. *International Journal of Nanomedicine*, 6293-6302.
- [34] Akamatsu, G., Yoshida, E., Mikamoto, T., Maeda, T., Wakizaka, H., Tashima, H., Wakitani, Y., Matsumoto, M., Yamaya, T. (2019). Development of sealed ^{22}Na phantoms for PET system QA/QC: uniformity and stability evaluation. 2019 IEEE Nuclear Science Symposium and Medical Imaging Conference (NSS/MIC).
- [35] Murata, T., Miwa, K., Miyaji, N., Wagatsuma, K., Hasegawa, T., Oda, K., Umeda, T., Iimori, T., Masuda, Y., Terauchi, T., Koizumi, M. (2016). Evaluation of spatial dependence of point spread function-based PET reconstruction using a traceable point-like ^{22}Na source. *EJNMMI Physics*, 3(1), 26.
- [36] Lees, M., Dombrowski, J., Botkin, C., Hubble, W., Nguyen, N., Osman, M. (2008). Utilization of ^{22}Na PET markers in radiation therapy planning: Initial experience. *Journal of Nuclear Medicine*, 49(1), 431.
- [37] Laing, P. G., Ferguson Jr, A. B. (1958). Sodium-24 as an indicator of the blood supply of bone. *Nature*, 182(4647), 1442-1443.
- [38] Scanlon, E. F., Milland, F. P., Hellman, L. (1990). Sodium-24 studies in postmastectomy lymphedema. *Journal of Surgical Oncology*, 44(1), 47-51.
- [39] Kety, S. S. (1948). Quantitative measurement of regional circulation by the clearance of radioactive sodium. *The American Journal of the Medical Sciences*, 215 (3), 352.

- [40] Moulton, R., Spencer, A. G., Willoughby, D. A. (1958). Noradrenaline sensitivity in hypertension measured with a radioactive sodium technique. *British Heart Journal*, 20(2), 224-228.
- [41] Gülümser, T., Kaplan, A. (2021). A theoretical study on the production cross-section calculations for ^{24}Na medical isotope. *Erzincan Üniversitesi Fen Bilimleri Enstitüsü Dergisi*, 14(2), 802-813.
- [42] Guo, S., Zhang, J., Shi, L., Chen, Q., Chen, W. K. (2022). Research on the application of ^{22}Na radiolocation detection technology in advanced manufacturing process control. *Kerntechnik*, 87(3), 316-322.
- [43] Yoshida, A., Kambara, T., Nakao, A., Uemoto, R., Uno, H., Nagano, A., Yamaguchi, H., Nakao, T., Kahl, D., Yanagisawa, Y., Kameda, D., Ohnishi, T., Fukuda, N., Kubo, T. (2013). Wear diagnostics of industrial material using RI beams of ^7Be and ^{22}Na . *Nuclear Instruments and Methods in Physics Research Section B*, 317, 785-788.
- [44] Pant, H. J., Sharma, V. K., Nair, A. G. C., Tomar, B. S., Nathaniel, T. N., Reddy, A. V. R., Singh, G. (2009). Application of ^{140}La and ^{24}Na as intrinsic radiotracers for investigating catalyst dynamics in FCCUs. *Applied Radiation and Isotopes*, 67(9), 1591-1599.
- [45] Epp, E. M., Griffin, H. C. (2003). Use of ^{24}Na as a γ -ray calibration source above 3MeV. *Nuclear Instruments and Methods in Physics Research Section A*, 505(1-2), 9-12.
- [46] Raynal, J. (1994). Notes on ECIS94 CEA Saclay Report No. CEA-N-2772.
- [47] Koning, A. J., Rochman, D. (2012). Modern Nuclear Data Evaluation with the TALYS Code System, *Nuclear Data Sheets*, 113(12), 2841-2934.
- [48] Watanabe, S. (1958). High energy scattering of deuterons by complex nuclei. *Nuclear Physics*, 8, 484-492.
- [49] Daehnick, W. W., Childs, J. D., Vrcelj, Z. (1980). Global optical model potential for elastic deuteron scattering from 12 to 90 MeV. *Physical Review C*, 21, 2253-2274.
- [50] Bojowald, J., Machner, H., Nann, H., Oelert, W., Rogge, M., Turek, P. (1988). Elastic deuteron scattering and optical model parameters at energies up to 100 MeV. *Physical Review C*, 38, 1153-1163.
- [51] Han, Y., Shi, Y., Shen, Q. (2006). Deuteron global optical model potential for energies up to 200 MeV. *Physical Review C*, 74, 044615.
- [52] An, H., Cai, C. (2006). Global deuteron optical model potential for the energy range up to 183 MeV. *Physical Review C*, 73, 054605.
- [53] Avrigeanu, V., Avrigeanu, M., Mănăilescu, C. (2014). Further explorations of the α -particle optical model potential at low energies for the mass range $A \approx 45-209$. *Physical Review C*, 90, 044612.

- [54] Koning, A. J., Delaroche, J. P. (2003). Local and global nucleon optical models from 1 keV to 200 MeV. *Nuclear Physics A*, 713, 231-310.
- [55] McFadden, L., Satchler, G. R. (1966). Optical-model analysis of the scattering of 24.7 MeV alpha particles. *Nuclear Physics*, 84, 177-200
- [56] Demetriou, P., Grama, C., Goriely, S. (2002). Improved global α -optical model potentials at low energies. *Nuclear Physics A*, 707, 253-276.
- [57] Nolte, M., Machner, H., Bojowald, J. (1987). Global optical potential for α particles with energies above 80 MeV. *Physical Review C*, 36, 1312-1316.
- [58] Avrigeanu, V., Hodgson, P. E., Avrigeanu, M. (1994). Global optical potentials for emitted alpha particles. *Physical Review C*, 49, 2136-2141.
- [59] Otuka, N., Dupont, E., Semkova, V., Pritychenko, B., Blokhin, A. I., Aikawa, M., Babykina, S., Bossant, M., Chen, G., Dunaeva, S., Forrest, R. A., Fukahori, T., Furutachi, N., Ganesan, S., Ge, Z., Gritzay, O. O., Herman, M., Hlavač, S., Katō, K., Lalremruata, B., Lee, Y. O., Makinaga, A., Matsumoto, K., Mikhaylyukova, M., Pikulina, G., Pronyaev, V. G., Saxena, A., Schwerer, O., Simakov, S. P., Soppera, N., Suzuki, R., Takács, S., Tao, X., Taova, S., Tárkányi, F., Varlamov, V. V., Wang, J., Yang, S. C., Zerkin, V. (2014). Towards a More Complete and Accurate Experimental Nuclear Reaction Data Library (EXFOR): International Collaboration Between Nuclear Reaction Data Centres (NRDC). *Nuclear Data Sheets*, 120, 272-276.
- [60] Zerkin, V. V., Pritychenko, B. (2018). The experimental nuclear reaction data (EXFOR): Extended computer database and Web retrieval system. *Nuclear Instruments and Methods in Physics Research Section A*, 888, 31-43.
- [61] Hermanne, A., Takács, S., Tárkányi, F., Adam-Rebeles, R., Ignatyuk, A. (2012). Excitation functions for ^7Be , $^{22,24}\text{Na}$ production in Mg and Al by deuteron irradiations up to 50MeV. *Applied Radiation and Isotopes*, 70(12), 2763-2772.
- [62] Vlasov, N. A., Kalinin, S. P., Ogloblin, A. A., Pankratov, V. M., Rudakov, V. P., Serikov, I. N., Sidorov, V. A. (1957). Excitation functions for the reactions $^{24}\text{Mg}(d,\alpha)^{22}\text{Na}$, $^{54}\text{Fe}(d,\alpha)^{52}\text{Mn}$, $^{54}\text{Fe}(d,n)^{55}\text{Co}$, $^{66}\text{Zn}(d,2n)^{66}\text{Ga}$. *Atomnaya Energiya*, 12, 169.
- [63] Wilson, R. L., Frantsvog, D. J., Kunselman, A. R., Détraz, C., Zaidins, C. S. (1976). Excitation functions of reactions induced by 1H and 2H ions on natural Mg, Al, and Si. *Physical Review C*, 13, 976 - 983.
- [64] Lange, H.-J., Hahn, T., Michel, R., Schiekel, T., Rösel, R., Herpers, U., Hofmann, H.-J., Dittrich-Hannen, B., Suter, M., Wölfli, W., Kubik, P. W. (1995). Production of residual nuclei by α -induced reactions on C, N, O, Mg, Al and Si up to 170 MeV. *Applied Radiation and Isotopes*, 46(2), 93-112.
- [65] Nozaki, T., Furukawa, M., Kume, S., Seki, R. (1975). Production of ^{28}Mg by triton and α -particle induced reactions. *Applied Radiation and Isotopes*, 26(1), 17-20.

The Effects of Cattle and Sheep Manure Applications on Soil Physical Properties and Rooting and Shoot Development of Grapevines Cuttings

Fazil HACIMUFTUOGLU¹, Muhammed KUPE^{2*}

¹Atatürk University, Faculty of Agriculture, Department of Soil Science and Plant Nutrition, 25240, Erzurum,

^{2*}Atatürk University, Faculty of Agriculture, Department of Horticulture, 254240, Erzurum, Türkiye

Received:25/10/2022, Revised: 29/11/2022, Accepted: 01/12/2022, Published: 30/12/2022

Abstract

In this study, the effects of cattle and sheep manure applications at different doses on soil physical properties, and in parallel with, the effects on rooting and shoot development of vine cuttings were investigated. In this study, 10%, 20% and 30% cattle and sheep manure was mixed into the soil as rooting medium, and the rooting and shooting performances of Karaerik and Narince grape varieties were evaluated in greenhouse conditions. During the experiment, the bud burst rates of the cuttings were recorded, and at the end of the experiment, the aggregate stability values, water permeability, bulk density, total porosity of the soil and plant parameters such as the root length, the root number, shoot length and the leaf number of the 1-year-old cuttings were determined. The highest root length values of Karaerik and Narince grape varieties were determined as 7.2 and 7.43 cm, respectively, in 20% sheep manure application. While the highest shoot length value (15.66 cm) in Karaerik grape cultivar was determined in 30% cattle manure application, the highest value (25.66 cm) in Narince grape cultivar was determined in 20% sheep manure application. As a result of the study, it was determined that sheep manure was more effective in root development and cattle manure in shoot development of Karaerik grape cultivar. It has been revealed that sheep manure gives more positive results on both root and shoot development than cattle manure in Narince grape cultivar.

Keywords: Grapevine cuttings, rooting and shooting, soil physics, farm manure

Sığır ve Koyun Gübresi Uygulamalarının Toprak Fiziksel Özellikleri ile Asma Çeliklerinin Köklenme ve Sürgün Gelişimi Üzerine Etkileri

Öz

Bu çalışmada, farklı dozlarda sığır ve koyun gübresi uygulamalarının toprağın fiziksel özelliklerine ve buna paralel olarak asma çeliklerinin köklenme ve sürgün gelişimine etkileri araştırılmıştır. Çalışmada köklendirme ortamı olarak toprağa %10, %20 ve %30 sığır ve koyun gübresi karıştırılarak Karaerik ve Narince üzüm çeşitlerinin sera koşullarında köklenme ve sürgün performansları değerlendirilmiştir. Deneme sırasında çeliklerin tomurcuk patlama oranları kaydedilmiş ve deneme sonunda toprağın agregat stabilitesi, su geçirgenliği, kütle yoğunluğu, toplam porozitesi ve bitki parametrelerinden bir yaşlı çeliklerin kök sayısı, kök uzunluğu, sürgün uzunluğu ve sürgündeki yaprak sayısı belirlenmiştir. Karaerik ve Narince üzüm çeşitlerinde en yüksek kök uzunluğu değerleri sırasıyla 7.2 ve 7.43 cm olarak 20% koyun gübresi uygulamasında tespit edilmiştir. Karaerik üzüm çeşidinde en yüksek sürgün uzunluğu değeri (15.66 cm) 30% sığır gübresi uygulamasında belirlenirken, Narince üzüm çeşidinde ise en yüksek değer (25.66 cm) 20% koyun gübresi uygulamasında tespit edilmiştir. Çalışma sonucunda Karaerik üzüm çeşidinin kök gelişiminde koyun gübresinin, sürgün gelişiminde ise sığır gübresinin daha etkili olduğu belirlenmiştir. Narince üzüm çeşidinde koyun gübresinin hem kök hem de sürgün gelişimi üzerinde sığır gübresine kıyasla daha olumlu sonuçlar verdiği ortaya konulmuştur.

Anahtar Kelimeler: Asma çeliği, köklenme ve sürme, toprak fiziği, çiftlik gübresi

1. Introduction

Sustainability in successful agriculture is inseparable with a fertile soil. Intensive agriculture and the use of various chemicals endanger the sustainability of agricultural activities. The decrease in the amount of organic matter due to increasing agricultural activities leads to the deterioration of the physico-mechanical structure of the soil after a while. Many studies have shown that organic fertilization is an effective method to increase soil organic matter content, soil fertility and organic carbon accumulation [1-9]. In agricultural production activities, the ability of the plant to develop well in the soil is related to the physical and chemical properties of the soil environment. The most used method to improve the physical properties of the soil and to ensure its sustainability is to add organic-based materials to the soil [10, 11].

Various materials such as farm manure, peat, compost are applied to keep the amount of organic matter in the soil at a certain level [12]. Soil organic matter plays a critical role in maintaining soil fertility and productivity [13, 14]. Studies in different parts of the world have shown that organic manures improve soil properties and increase the yield of crops [15]. In a 25-year study conducted by [16], farm manure was applied to the soil and it was reported that a significant increase in the amount of organic carbon and total nitrogen of the soil occurred due to this applications. [17], stated that if there is enough decomposed organic matter residues in the surface soil, it has a significant effect on the physical and chemical properties of the mineral soil. [18], reported that when a fertile soil is mentioned, it comes to mind that the soil has a high level of organic matter and biological activity, stable aggregates, an environment in which plant roots can easily move, and water can easily infiltrate from the surface. However, trying to keep organic matter in the soil at a high level is both impractical and very expensive. On the other hand, manure applications made by animal breeders on agricultural lands are an easy and low-cost way to provide organic fertilization. Farm animals provide the transport of plant nutrients from animal grazing areas to crop production areas as manure [19]. This situation increases the nutrient cycle and reduces the costs of industrial manures.

[20], stated that different types of manures of animal origin (goat, sheep, cow, poultry manure, etc.) have significant differences in macro and micronutrient content and therefore significantly affect the nutrition of the grown plant. [21] in a study investigating the effectiveness of livestock manure, found that goat manure has higher N, P and K concentrations (2.77% N, 1.78% P₂O₅ and 2.88% K₂O) compared to other animal manures. He also stated that sheep manure is a good source of K (1% K₂O). On the other hand, he stated that cow manure contains only 0.55% N, 0.10% P₂O₅ and 0.50% K₂O, while the Fe concentrations in different types of manures vary between 40 and 460 mg kg⁻¹, while the Mn and Zn contents vary between 5 and 90 mg kg⁻¹.

In the coming years, the use of organic manures to meet nutrient needs will become more common to develop sustainable agriculture. This is related to the improvement of organic manures in various yield parameters of the soil. Organic fertilization increases plant productivity by maintaining the quality of the produced crop [22] and positively affecting soil microbial biomass and activity [23]. Nutrient deficiency is one of the most important factors

affecting yield and quality in agricultural production. Animal fertilization is effective in increasing the nutrient content of the soil over the years, depending on this, in the generative and vegetative development of the plant [24]. Animal manures such as cattle, sheep and horses are used as a food source for annual and perennial crops in horticulture. The effect of animal fertilization on fruit quality and nutritional value depends on several factors, including the properties of organic matter, pedoclimatic conditions, application time and plant species. [24]. As with other plant species, organic manures are of great importance on the nutrition of the vine. [25], stated that there is a significant relationship between soil quality indices and vegetative growth of grapevines. It has been stated in many studies that soils have both direct and indirect effects on root growth, photosynthesis and shoot growth of vines; various soil types were also found to have a measurable effect on vine vigor and fruit characteristics [26-28].

Ensuring of soil fertility is one of the most important goals for sustainable viticulture [29, 30]. [23], reported in a study that organic soil management is necessary for healthy plant growth and quality product in viticulture. Internal and external factors affect rooting in cuttings. Internal factors; Genetic structure, storage materials and hormones in the plant are shown as examples, while external factors; such as irrigation, pruning, fertilization, cutting time, rooting environment, temperature and humidity can be given as examples [31,32].

Vine nutrition is also important in rooting cuttings. Related to this, there are opinions that inorganic carbon compounds can stimulate adventitious root formation in grapevine cuttings. Macro and micro nutrients are also important in adventitious root formation. Especially nitrogen, magnesium, zinc and boron affect the adventitious root formation significantly [33].

In this study, the effect of cattle and sheep manures applied to the soils in different doses, on the aggregate stability, water permeability, bulk density and total porosity values of the soils, and in parallel with this, the bud burst rate and the rooting and shooting performances of 1 year old cuttings of Karaerik and Narince grape varieties were evaluated.

2. Material and Methods

The study was carried out in Atatürk University Faculty of Agriculture application greenhouse (humidity rate: 80-85%, temperature: 27-30 °C) in 2022. Since it is known that the rooting abilities of cuttings vary greatly between species and varieties [34, 35], two different grape varieties with different rooting abilities were preferred in this study.

In the research, one-year-old cuttings belonging to Karaerik and Narince cultivars were used as plant material. In this study, coarse textured soil with high permeability was used. The study soil was sampled as degraded from a 20 cm topsoil depth of a field in the Karaçam village of Çaykara district, Trabzon province [36]. In the research, at least 1 year old burnt cattle and sheep manure taken from Atatürk University Food and Livestock Application Center farm land was used.

Physical and chemical soil analyses

For fundamental analysis and trial studies, soil samples were air-dried in laboratory conditions and sieved through 4 and 2 mm mesh.

Soil texture was determined by Bouyoucos hydrometer method [37], soil reaction (pH) by glass electrode pH meter [38], lime content by Scheibler calcimeter (Nelson, 1982), organic matter content by Smith Weldon method [39], electrical conductivity (EC) value with electrical conductivity instrument [40], aggregate stability (AS) using Yoder type wet sieving device [41], particle density by pycnometer method [42], field capacity and permanent wilting point were determined by the pressure extractor method [43]. On the other hand, Soil bulk density was determined by the cylinder method [42], and total porosity was calculated from bulk weight and particle density.

Plant phenological observations and fertilization application

In this research, one-year-old cuttings belonging to Narince and Karaerik varieties, which are important table grape varieties, were taken from 6-year-old vines grown on their own roots in the unheated greenhouses of Atatürk University Plant Production Research Directorate. Samples were taken on April 1 in the form of 10-node rods, 10-12 cm long and 1-node cuttings were prepared.

Manures were mixed into potting soils at rates of 10% - 20% and 30% on a weight basis. On the 40th day of the experiment, the shooting performances (bud burst) were recorded, and at the end of the 60th day, the study was terminated and the root lengths, root numbers, shoot lengths and the number of leaves in the shoot were determined [44].

In the study, two different manures (cattle and sheep) were applied in 4 different doses (D0: 0%, D1: 10%, D2: 20%, D3: 30%). The research carried out on two different cultivars was planned with 3 replications and a total of 48 pots (2x2x4x3) were used. Statistical analysis was performed by ANOVA, and differences between means were tested using Duncan's multiple range test [45, 46].

3. Results and Discussion

In this study, the texture class of the soils was determined as coarse textured in the sandy clay loam texture class (58% sand, 20% silt, 22% clay). Soil organic matter content (3.77%) is in the well class, pH level; It was found to be 7.5 level and neutral, the EC level of the working soils is 0.14 dS/m without salt, the CaCO₃ level was determined as 5.1% in the medium calcareous [47], class. According to the available phosphorus contents, the class of the soils was determined as medium (P₂O₅: 8 kg/da) [47], Ca⁺⁺, Mg⁺⁺, Na⁺, K⁺ contents were determined as 11.2, 5.04, 0.36, 2.17 me/100gr, respectively. Particle density were determined as 2.68 (g/cm³). Field capacity and permanent wilting point moisture content of the working soil were determined to be 25% and 13%, respectively (Table 1).

The Effects of Cattle and Sheep Manure Applications on Soil Physical Properties and Rooting and Shoot Development of Grapevines Cuttings

Table 1. Basic physical and chemical analysis results of the researched soils

Soil properties	
Sand (%)	58
Silt (%)	20
Clay (%)	22
Texture class	Sandy clay loam
Particle density (g/cm ³)	2.68
Organic matter (%)	3.77
pH	7.5
EC (dS/m)	0.14
CaCO ₃ (%)	5.1
Ca, Mg, Na, K (me/100gr)	11.2; 5.04; 0.36; 2.17
Field capacity (%)	25
Wilting point (%)	13

Soil physical properties

At the end of the 60-day plant development period of the soils applied with different doses of cattle and sheep manures; Aggregate stability, water permeability, bulk density and porosity values are given in Table 2.

Table 2. Effects of applications on the physical properties of soils

Applications	AS (%)	WP (cm/h)	BD (gr/cm ³)	Porosity (%)
D0 (Control)	46.21 ^d ± 3.35 [*]	4.6 ^d ± 0.87	1.24 ^a ± 0.02	53.4 ^c ± 0.75
M1-D1	56.48 ^{bc} ± 2.41	7.73 ^c ± 0.58	1.16 ^b ± 0.02	56.1 ^b ± 0.61
M1-D2	57.43 ^b ± 1.66	14.63 ^b ± 3.97	0.98 ^c ± 0.01	63.1 ^a ± 0.35
M1-D3	69.54 ^a ± 1.74	14.43 ^b ± 0.72	0.97 ^c ± 0.01	63.3 ^a ± 0.17
M2-D1	52.63 ^c ± 2.85	5.33 ^{cd} ± 0.15	0.99 ^c ± 0.01	62.5 ^a ± 0.23
M2-D2	59.18 ^b ± 2.84	5.43 ^{cd} ± 0.68	0.98 ^c ± 0.02	62.9 ^a ± 0.55
M2-D3	60.38 ^b ± 0.85	19.13 ^a ± 0.66	0.97 ^c ± 0.01	63.4 ^a ± 0.17

*: Standart deviation, AS: Aggregate stability, WP: Water permeability, BD: Bulk density; M1: cattle manure; M2: sheep manure; D0: 0% Control, D1: 10% dose, D2: 20% dose, D3: 30% dose

Aggregate stability, water permeability, bulk density and porosity values of the soils used in the research are given in Table 2. According to the results, it was found that different doses of cattle (M1) and sheep (M2) manure applications caused a statistical difference in all physical soil parameters examined ($p < 0.05$).

When the effects of cattle and sheep manure applications on the aggregate stability values of the soil were examined, it was determined that all doses of both manures caused a statistical difference ($p < 0.05$) in AS values compared to the control group (Table2). While the lowest value was determined to be 46.2% in the control group, it was revealed that the aggregate stability value increased linearly depending on the applications and the highest value was 69.5% in the D3 cattle manure application. When Table 2 was examined, it was determined that the different doses of sheep manure also increased the AS value, but cattle manure was more effective. When the effect of manure applications on the water permeability values of the soils

The Effects of Cattle and Sheep Manure Applications on Soil Physical Properties and Rooting and Shoot Development of Grapevines Cuttings

was examined, it was determined that there was a statistical difference in the water permeability value compared to the control group ($p < 0.05$). Considering all manure applications together, the highest water permeability value was 19.1 cm/h in the third dose application of sheep manure (M2-D3), and this value was followed by the 2nd (M1-D2) and 3rd (M1-D3) doses of cattle manure. It was determined that these applications increased the WP value by 315%, 218% and 213%, respectively (Table 2). When the bulk density values of the soils were examined, it was determined that manure applications showed a statistically significant difference ($p < 0.05$) on the BD value compared to the control group. When Table 2 was examined, it was determined that the BD value decreased due to the increase in the application dose of cattle and sheep fertilizers, and the lowest values caused a decrease of 22% in the D3 application of both manures compared to the control group. The total porosity of the applied soils was statistically different compared to the control group ($p < 0.05$). The lowest porosity value was determined to be 53.4% in the control group, while the highest value was 63.4% in the third dose application of sheep manure (M2-D3). This value was found to be 63.3% in the third dose application of cattle manure (M1-D3) and 62.9% in the second dose application of sheep manure (M2-D2) (Table 2).

The effects of the applications on the rooting and shooting performance of the cuttings

It was observed that there were differences between the bud burst rate of the cuttings of Karaerik and Narince grape varieties depending on the manure applications (Table 3). Root lengths, root numbers, shoot lengths and leaf numbers in the shoot of the cuttings used in the research are given in Tables 4 and 5. Rooting and shooting performances of Karaerik and Narince grape varieties of different manure applications are given in Figures 1 and 3. The relationship graphs between rooting and shooting performances and soil physical properties, depending on manure applications, are presented in Figures 2 and 4. According to the results, it was found that different doses of Cattle (M1) and Sheep (M2) manure applications caused a statistical difference on all rooting and shooting performances examined ($p < 0.05$). On the 40th day of the experiment, the bud burst rates of the cuttings were examined. It was determined that 100% (all cuttings on three replication) burst was achieved in the 2nd and 3rd dose applications of cattle manure in Karaerik grape cultivar and in the 1st and 3rd dose applications in Narince grape cultivar. While there was no 100% bud burst (first shooting) at the end of the 40th day in sheep manure applied in Karaerik grape cultivar, 100% burst was observed in the second dose application of Narince grape cultivar in sheep manure (Table 3).

Table 3. Bud burst rates of grapevine cuttings at the end of the 40th day

Cultivars	M1-D0 (%)	M1-D1 (%)	M1-D2 (%)	M1-D3 (%)	M2-D0 (%)	M2-D1 (%)	M2-D2 (%)	M2-D3 (%)
Karaerik	66	66	100	100	66	66	33	33
Narince	33	100	66	100	33	66	100	66

M1: cattle manure; M2: sheep manure; D0: 0% Control, D1: 10% dose, D2: 20% dose, D3: 30% dose

When the effects of manure applications at different doses on root lengths of Karaerik and Narince grape varieties were evaluated, it was revealed that all doses of cattle and sheep manures were statistically different ($p < 0.05$) compared to the control group (Table 4, 5). The most effective results on the root length of cuttings in Karaerik grape cultivar were determined

The Effects of Cattle and Sheep Manure Applications on Soil Physical Properties and Rooting and Shoot Development of Grapevines Cuttings

in the 1st (M2-D1) and 2nd dose (M2-D2) applications of sheep manure and the 3rd dose (M1-D3) applications of cattle manure, respectively (Table 4). In Narince grape cultivar, the most effective results on the root length of cuttings were determined in the second dose of sheep manure (M2-D2) and 3 doses (M2-D3), respectively, and in the second dose of cattle manure (M1-D2) (Table 5). A statistical difference was found between the applications in terms of root numbers depending on the different doses of manure applications of Karaerik and Narince grape varieties ($p < 0.05$). It was revealed that sheep manure was more effective than cattle manure on the root number of cuttings in Karaerik grape cultivar. The most effective results in terms of root numbers were determined in the first dose (M2-D1), second dose (M2-D2) and third dose (M2-D3) sheep manure applications, respectively (Table 4). It was determined that the most effective results in terms of root number of cuttings in Narince grape cultivar were in the second dose of sheep manure (M2-D2), the second dose of cattle manure (M1-D2) and the third dose of sheep manure (M2-D3) (Table 5). It was determined that manure applications at different doses caused a statistical difference ($p < 0.05$) on shoot lengths of Karaerik and Narince grape varieties (Table 4, 5). It was determined that the highest value of shoot length in Karaerik grape cultivar was in the 3rd dose (M1-D3), 2nd dose (M1-D2) and 1st dose (M1-D1) applications of cattle manure, respectively (Table 4). When the shoot length of the cuttings of Narince grape cultivar was examined, it was determined that the highest values were observed in the 2nd dose (M2-D2), 3rd dose (M2-D3) and 1st dose (M2-D1) applications of sheep manure, respectively (Table 5). It was determined that all doses of applied cattle and sheep manures caused a statistically significant difference ($p < 0.05$) on the number of leaves in the shoot. The highest number of leaves in Karaerik grape cultivar was determined in the 3rd dose application of cattle manure (M1-D3). This was followed by 2 doses (M1-D2) and 1st dose (M1-D1) applications of cattle manure, respectively (Table 4). In Narince grape cultivar, it was determined that the 2nd dose of sheep manure (M2-D2) had the highest effect, followed by the 1st (M2-D1) and 3rd (M2-D3) doses of sheep manure (Table 5).

Table 4. Rooting and shooting performances of Karaerik grape cultivar

Karaerik cultivar	Root Length (cm)	Root Numbers (item)	Shoot Length (cm)	Leaf Numbers (item)
M1-D0	1.16 ^d ± 0.28*	1.33 ^e ± 0,57	6 ^{cd} ± 1	2.33 ^d ± 0.57
M1-D1	2.33 ^c ± 0.28	7.33 ^d ± 1,52	12 ^{abc} ± 2.64	7 ^{ab} ± 1
M1-D2	5.76 ^b ± 0.68	12.33 ^c ± 1,52	13.66 ^{ab} ± 4.5	7.66 ^{ab} ± 1.52
M1-D3	6.66 ^a ± 0.87	11.33 ^c ± 0,57	15.66 ^a ± 3.51	8.33 ^a ± 1.52
M1-Mean	4.91	10.3	13.8	7.66
M2-D0	1.3 ^d ± 0.36	1.66 ^e ± 0,57	4.66 ^d ± 2.08	2 ^d ± 1
M2-D1	7.1 ^a ± 0.1	34 ^a ± 2,64	11.33 ^{abc} ± 5.03	5.66 ^{abc} ± 3.21
M2-D2	7.2 ^a ± 0.2	18 ^b ± 1	8.33 ^{bcd} ± 2.51	3.33 ^{cd} ± 1.52
M2-D3	5.26 ^b ± 0.64	14 ^c ± 2,64	9.33 ^{bcd} ± 3.05	5 ^{bcd} ± 2
M2-Mean	6.52	22	9.66	4.66

M1: cattle manure; M2: sheep manure; D0: 0% Control, D1: 10% dose, D2: 20% dose, D3: 30% dose

The Effects of Cattle and Sheep Manure Applications on Soil Physical Properties and Rooting and Shoot Development of Grapevines Cuttings

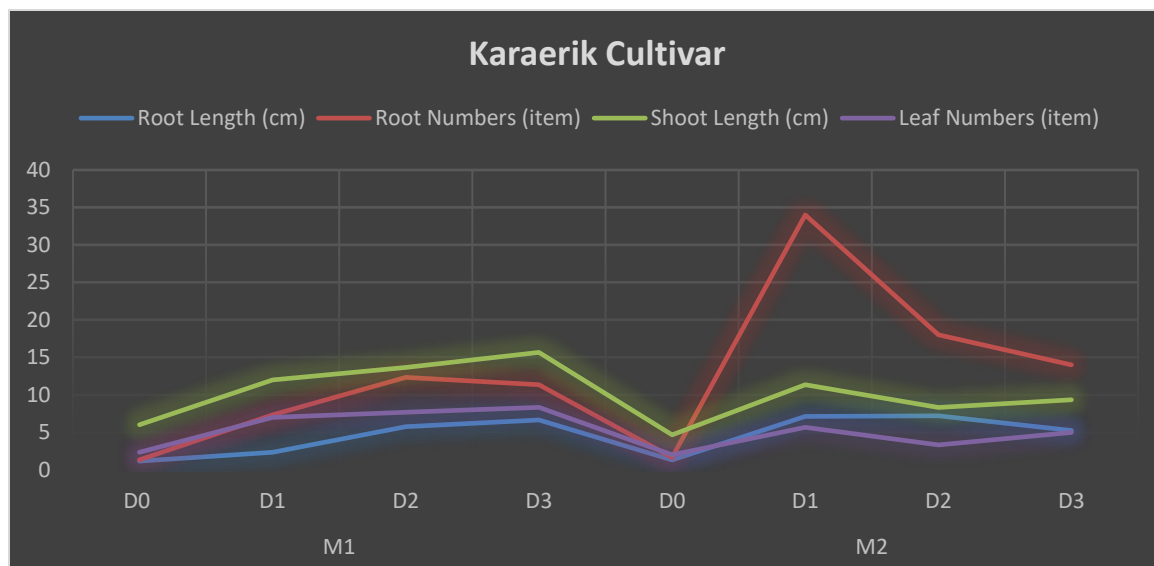


Figure 1. Rooting and shooting performance graph of cuttings of Karaerik grape cultivar

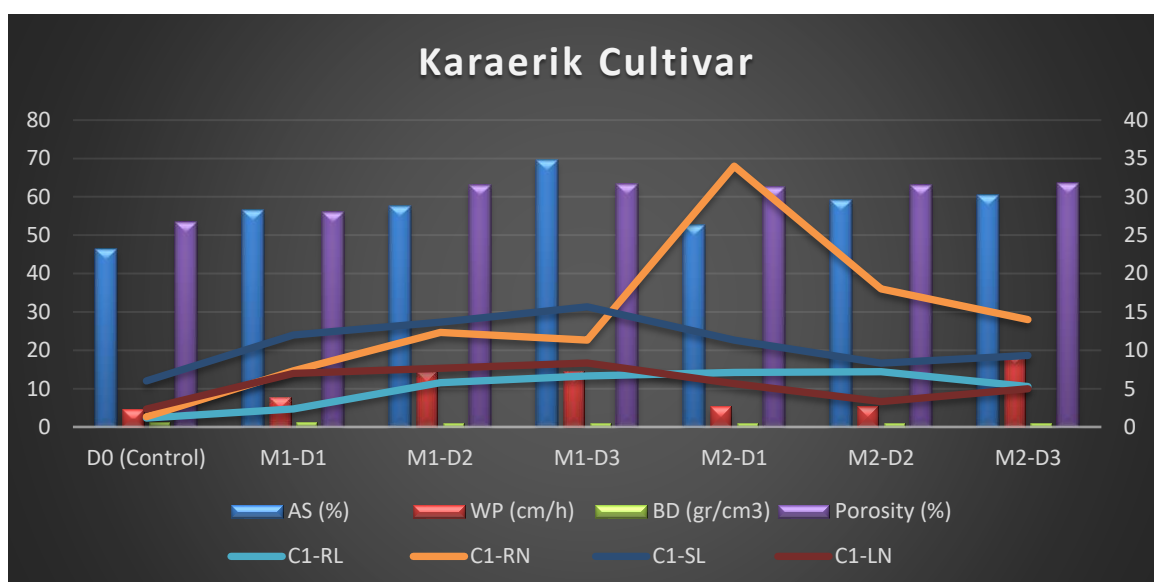


Figure 2. The relationship between rooting and shooting performances of Karaerik grape cultivar and soil physical properties.

AS: Aggregate stability, WP: Water permeability, BD: Bulk density; M1: cattle manure; M2: sheep manure; V1: Karaerik cultivar, RL: Root length, RN: Root numbers, SL: Shoot length, LN: Leaf numbers, D0: 0% Control, D1: 10% dose, D2: 20% dose, D3: 30% dose

The Effects of Cattle and Sheep Manure Applications on Soil Physical Properties and Rooting and Shoot Development of Grapevines Cuttings

Table 5. Rooting and shooting performances of Narince grape cultivar

Narince cultivar	Root Length (cm)	Root Numbers (item)	Shoot Length (cm)	Leaf Numbers (item)
M1-D0	0.76 ^e ± 0.25	2 ^c ± 1	1.66 ^d ± 0.57	1.33 ^d ± 0.57
M1-D1	1.23 ^e ± 0.25	3 ^c ± 1	6.66 ^c ± 1.52	3 ^{cd} ± 1
M1-D2	5.96 ^c ± 0.15	13.33 ^b ± 0.57	8 ^c ± 3.6	3.66 ^c ± 2.08
M1-D3	3.86 ^d ± 0.30	10 ^b ± 1	7.66 ^c ± 1.52	3 ^{cd} ± 1
M1-Mean	3.68	8.76	7.44	3.22
M2-D0	1.23 ^e ± 0.15	3 ^c ± 1	8.66 ^c ± 1.15	8.33 ^b ± 1.52
M2-D1	3.56 ^d ± 0.20	10.66 ^b ± 0.57	9.66 ^c ± 1.15	8.66 ^b ± 1.15
M2-D2	7.43 ^a ± 0.51	30.66 ^a ± 6.11	25.66 ^a ± 1.52	16.33 ^a ± 0.57
M2-D3	6.56 ^b ± 0.51	12.66 ^b ± 0.57	15.33 ^b ± 1.15	8.66 ^b ± 0.57
M2-Mean	5.85	18	16.9	11.2

M1: cattle manure; M2: sheep manure; D0: 0% Control, D1: 10% dose, D2: 20% dose, D3: 30%

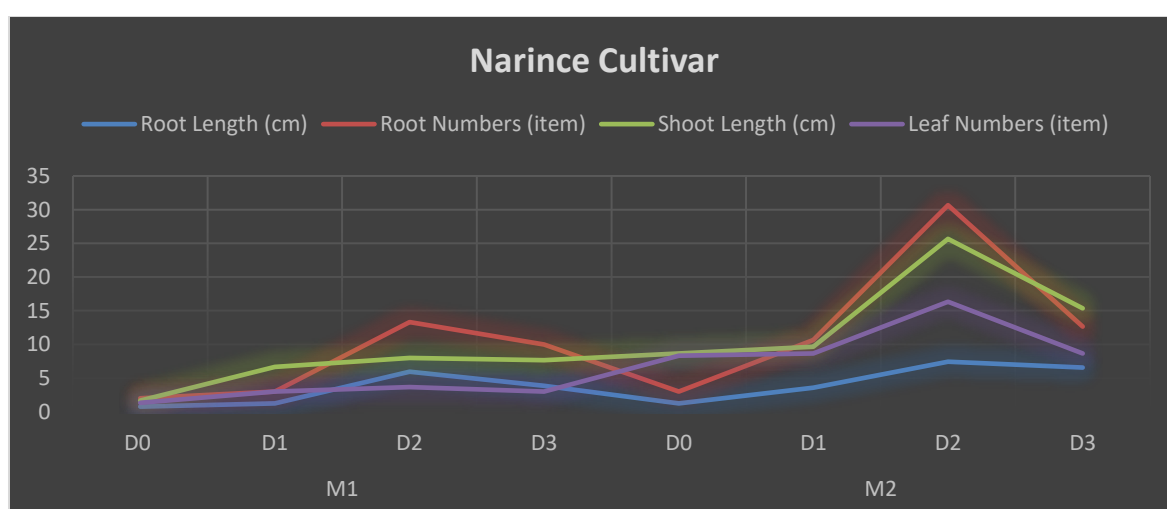


Figure 3. Rooting and shooting performance graph of cuttings of Narince grape cultivar

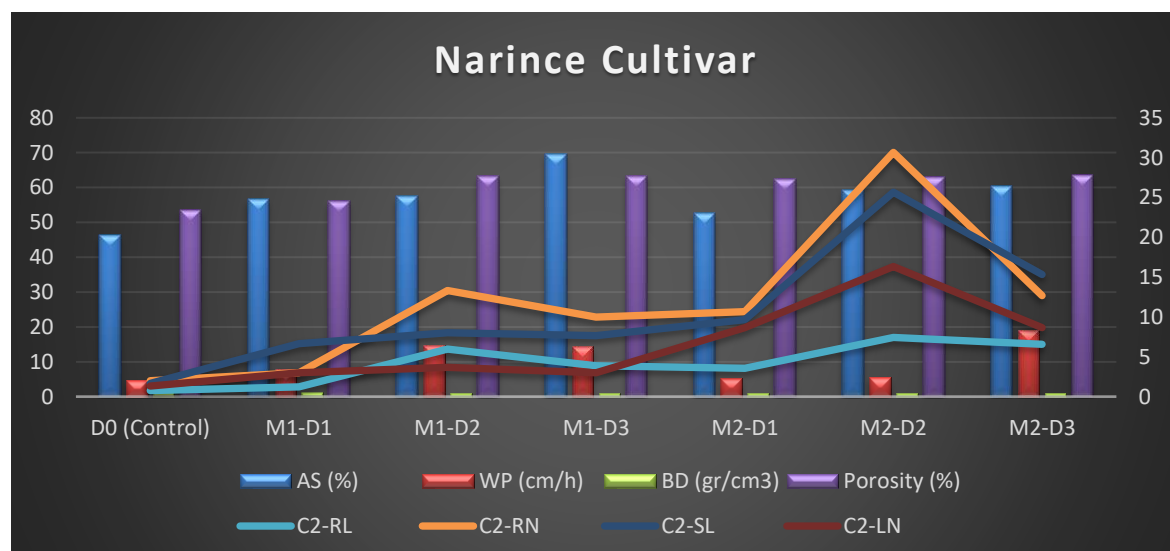


Figure 4. The relationship between rooting and shooting performances of Narince grape cultivar and soil physical properties.

AS: Aggregate stability, WP: Water permeability, BD: Bulk density; M1: cattle manure; M2: sheep manure; V2: Narince cultivar, RL: Root length, RN: Root numbers, SL: Shoot length, LN: Leaf numbers, D0: 0% Control, D1: 10% dose, D2: 20% dose, D3: 30% dose

When Figure 2 and Figure 4 are examined, it is understood that there is a relationship between the physical properties of soils and the vegetative development of plants. While manure applications improve the physical properties of the soil, they also affect the rooting and shoot performance of the plants. It was determined that there was a linear increase in AS, WP and porosity values depending on the increase in the application doses of both manures added to the soil. In parallel with the improvement in the physical properties of the soils, it was observed that the rooting and shooting performances of the cuttings also changed. While this development in soils was in direct parallel with the development of cuttings in cattle manure applied soils, it showed a partial parallelism in cuttings in sheep manure applied soils.

Fine textured heavy and impermeable soils limit root formation in plants and can cause root rot by holding excessive water. There is a significant relationship between root and shoot development in vines and soil fertility and water holding capacity [25]. The application of sheep and cattle manure to the soil increases the amount of organic matter in the soil, and accordingly, it provides a more suitable environment for plant growth by providing a positive effect on the soil's aggregate stability, water permeability, air-water balance, and uptake of plant nutrients in the soil.

For a good root formation, suitable soil air, soil water and enough oxygen must be present. It is known that organic matter affects plant vegetative and generative development positively by increasing aggregate stability, and reducing bulk density [48]. It has been revealed in many studies that there is a direct relationship between soil carbon (C) content and soil aggregation, and that organic manures added to soil improve the structural properties by increasing the aggregate stability of the soil [6, 49-55]. Parallel to the improvement in soil physical properties, the increase in the water and nutrient holding capacity of the soil has come to the fore as important factors that can affect the yield of vines [27, 56, 57]. As a matter of fact, in this study, similar to other studies, it was determined that cattle and sheep manure applications improved the physical properties of the soils, increased the water permeability and aggregate stability values, decreased the bulk density values, and in parallel increased the rooting and shooting performance of the cuttings.

[58], stated that organic materials create a more suitable environment for plants and microorganisms by increasing the aeration capacity of soils, and this situation positively affects water and nutrient availability. It is known that root and shoot development in vines is strongly affected by soil conditions, shoot development is more in places where the soil is more fertile and can hold more water [27, 56]. It is known that the level of organic matter in the soil has a significant effect on the rooting performance of grapevine cuttings [59]. In this study, it was determined that fertilizations had a positive effect on average root length and root number depending on the manure in both Karaerik and Narince grape varieties, but sheep manure was more effective than cattle manure. In addition, it was determined that different doses of cattle and sheep manure increased shoot growth in grapevine cuttings. In the study, it was found that cattle manure in Karaerik grape cultivar and sheep manure in Narince grape cultivar were more effective on average shoot growth and average leaf number. Similar to the data we obtained in this study, [60], determined that the addition of organic manures at different doses to fig

seedlings had a significant effect on the shoot length of the plants. In addition, [61], in a study investigating the effects of farm manure on the soil, emphasized that the applications provided significant increases in crop yield by promoting vegetative growth of plants. Parallel to previous similar studies, the findings obtained in this study revealed that organic farm manures have significant effects on soil and plant growth.

4. Conclusion

Since organic manures generally improve the physical, chemical and biological properties of the soil, their use in sustainable agriculture is becoming more common every day to meet the nutritional needs. For this purpose, the effects on the rooting and shooting performances of Karaerik and Narince grape varieties were evaluated by applying different doses of organic farm manures from different origins to the soil. In the study, it was revealed that there was a linear development in the root length, root number, shoot length and number of leaves on shoot of both Karaerik and Narince grape varieties, depending on the improvements in the physical properties of the soils due to different manure applications. It was determined that sheep manure was more effective than cattle manure on root length and root number in Karaerik grape cultivar, while cattle manure gave more positive results on shoot length and number of leaves in shoot. Although all doses of cattle manure applied on Narince grape cultivar had positive effects on root length, root number, shoot length and number of leaves shoot, it was determined that sheep manure was more effective than cattle manure in all parameters. As a result, it has been determined that organic farm manures have been very successful in rooting and shoot development of vine cuttings, and it has been found to cause different results in species and varieties according to the origin of the manure.

According to the findings obtained in this study, it is thought that organic farm manures can come to the fore as a successful alternative for rooting vine cuttings in terms of soil health and sustainable agriculture.

Ethics in Publishing

There are no ethical issues regarding the publication of this study.

Author Contributions

Author¹: Conceptualization, data curation, formal analysis, methodology, visualization, writing-original draft, writing-review and editing,

Author^{2*}: Conceptualization, data curation, visualization, writing-original draft, writing-review and editing

All authors have read and agreed to the published version of the manuscript.

The Effects of Cattle and Sheep Manure Applications on Soil Physical Properties and Rooting and Shoot Development of Grapevines Cuttings

References

- [1] Maillard, E., Angers, D.A., (2014) Animal manure application and soil organic carbon stocks: a meta-analysis. *Global Change Biology*, (20) 666-679.
- [2] Liang, Q., Chen, H., Gong, Y., Yang, H., Fan, M., Kuzyakov, Y., (2014) Effects of 15 years of manure and inorganic fertilizers on enzyme activities in particle-size fractions in a North China Plain soil. *European Journal of Soil Biology*, (60) 112-119.
- [3] Garcia-Orenes, F., Roldan, A., Morugan-Coronado, A., Linares, C., Cerda, A., Caravaca, F., (2016) Organic fertilization in traditional Mediterranean grapevine orchards mediates changes in soil microbial community structure and enhances soil fertility. *Land Degrad. Develop.* (27) 1622–1628.
- [4] Li, Z., Wang, M., Yang, Y., Zhao, S., Zhang, Y., Wang, X., (2017) Effect of composted manure plus chemical fertilizer application on aridity response and productivity of apple trees on the loess plateau, China. *Arid Land Research Manage.* (31) 388–403.
- [5] Ali, S., Hayat, R., Begum, F., Bohannan, B.J.M. Inebert, L., Meyer, K., (2017) Variation in soil physical, chemical and microbial parameters under different land uses in Bagrot Valley, Gilgit, Pakistan. *Journal of the Chemical Society of Pakistan*, (39) 97-107.
- [6] Wang, Y., Ge, T., Kuzyakov, Y., Hu, N., Wang, Z.L., Li, Z., Tang, Z., Chen, Wu, Y.C., Lou, Y., (2017) Soil aggregation regulates distributions of carbon, microbial community and enzyme activities after 23-year manure amendment. *Applied Soil Ecology*, (111) 65-72.
- [7] Kiczorowski, P., Kopacki, M., Kiczorowska, B., (2018) The response of Sampion trees growing on different rootstocks to applied organic mulches and mycorrhizal substrate in the orchard. *Sci. Hortic.* (241) 267–274.
- [8] Lin, Y., Ye, G., Kuzyakov, Y., Liu, D., Fan, J., Ding, W., (2019) Long-term manure application increases soil organic matter and aggregation, and alters microbial community structure and keystone taxa. *Soil Biol. Biochem.* (134) 187–196.
- [9] Ye, G., Lin, Y., Kuzyakov, Y., Liu, D., Luo, J., Lindsey, S., Wang, W., Fan, J., Ding, W., (2019) Manure over crop residues increases soil organic matter but decreases microbial necromass relative contribution in upland Ultisols: results of a 27-year field experiment. *Soil Biol. Biochem.* (134) 15–24.
- [10] Bender, D., Erdal, İ., Dengiz, O., Gürbüz, M., Tarakçıoğlu, C., (1998) Farklı Organik Materyallerin Killi Bir Toprağın Bazı Fiziksel Özellikleri Üzerine Etkileri. *International Symposium On Arid Region Soil*. 21-24 September, Menemen-İzmir-Turkey.
- [11] Das, S., Hussain, N., Gogoi, B., Buragohain, A.K., Bhattacharya, S.S., (2016) Vermicompost and farmyard manure improves food quality, antioxidant and antibacterial potential of *Cajanus cajan* (L. Mill sp.) leaves. *J. Sci. Food Agric.* (97) 956–966.
- [12] Stratton, M. L., Barker, A. V., Rehcigl, J. E. (Ed.), 1995. *Soil Amendments and Environmental Quality*. CRC Press, USA, 249-309.

The Effects of Cattle and Sheep Manure Applications on Soil Physical Properties and Rooting and Shoot Development of Grapevines Cuttings

- [13] Tiessen, H., Cuevas, E., Chacon. P., (1994) The role of soil organic-matter in sustaining soil fertility *Nature*, (371) 783-785.
- [14] Manlay, R.J., Feller, C., Swift. M.J., (2007) Historical evolution of soil organic matter concepts and their relationships with the fertility and sustainability of cropping systems. *Agriculture, Ecosystems & Environment*, (119) 217-233.
- [15] Sommerfieldt, T.G., Chang, C., (1985) Changes in Soil Properties Under Annual Applications of Feedlot Manure and Different Tillage Practices. *Soil Sci. Soc. Am. J.* (49) 983-987.
- [16] Xiyang, H., Chi, C., Greg, R. T and Fengrong, Z., (2003) Soil Carbon and Nitrogen Response to 25 Annual Cattle Manure Application. *Journal of Plant Nutrition and Soil Science*. Vol. 166 (2) 239-245.
- [17] Özbek, H., Kaya, Z., Gök, M., Kaptan, H., (1993) *Toprak Bilimi. Ç.Ü.Z.F. Genel Yayın No:73. Ders Kitapları Yayın No:16*, Adana.
- [18] Lewandowski, A, Zumwinkle, M., (1999) *Assessing the Soil System. A Review of Soil Quality Literature*. Minnessota Department of Agriculture Energy and Sustainable Agriculture Program, Boulevard
- [19] Brouwer, J., Powell, J.M., (1995) Soil aspects of nutrient cycling in a manure application experiment in Niger. In *Livestock and nutrient cycling in mixed farming systems of Sub-Saharan Africa*, J.M. Powell et al. (eds.). 1993 Addis Abeba, Ethiopia. (2) 211-226.
- [20] Chatzistathis, T., Papadakis, I.E., Papaioannou, A., Chatzissavvidis, C., Giannakoula, A., (2020) Comparative study effects between manure application and a controlled release fertilizer on the growth, nutrient uptake, photosystem II activity and photosynthetic rate of *Olea europaea* L. (cv. 'Koroneiki'). *Scientia Horticulturae*, 264 (109176).
- [21] Therios, I., (1996) *Mineral Nutrition of Plants*. Dedousi Publications, Thessaloniki In Greek. (75) 191-192.
- [22] Maheswarappa, H. P., Nanjappa, H. V., Hegde, M. R., Prabhu, S.R., (1999) Influence of planting material, plant population and organic manures on yield of East Indian galangal (*Kaempferia galanga*), soil physico-chemical and biological properties. *Indian J. Agron.* 44(3) 651–657
- [23] Meissner, G., Athmann, M.E., Fritz, J., Kauer, R., Stoll, M., Schultz, H.R., (2019) Conversion to organic and biodynamic viticultural practices: impact on soil, grapevine development and grape quality. *OENO One*, 53(4) 639-659.
- [24] Loss, A., Couto, R., Brunetto, G., Veiga M., Toselli, M., Baldi E., (2019) Animal manure as fertilizer: changes in soil attributes, productivity and food composition. *International Journal of Research –Granthaalayah*. 7(9) 307-331.
- [25] Tardaguila, J., Baluja, J., Arpon, L., (2011) Variations of soil properties affect the vegetative growth and yield components of “Tempranillo” grapevines. *Precision Agric* (12) 762–773.

The Effects of Cattle and Sheep Manure Applications on Soil Physical Properties and Rooting and Shoot Development of Grapevines Cuttings

- [26] Cortell, J.M., Halbleib, M., Gallagher, A.V., Righetti, T.L., Kennedy, J.A., (2005) Influence of vine vigor on grape (*Vitis vinifera* L. cv Pinot Noir) and wine proanthocyanidins. *Journal of Agriculture Food Chemistry*, (53) 5798–5808.
- [27] Reynolds, A.G., Senchuk, I.V., van der Reest, C., de Savigny, C., (2007) Use of GPS and GIS for elucidation of the basis for terroir, spatial variation in an Ontario Riesling vineyard. *American Journal of Enology and Viticulture*, (58) 145–162.
- [28] Andreas-de Prado, R., Yuste-Rojas, M., Sort, X., Andreas-Lacueva, C., Torres, M., Rosa, M., (2007) Effect of soil type on wines produced from *Vitis vinifera* L. cv. Grenache in commercial vineyards. *Journal of Agriculture Food Chemistry*, (55) 779–786.
- [29] Crecchio, C., Curci, M., Mininni, R., Ricciuti, P., Ruggiero, P., (2001) Short-term effects of municipal solid waste compost amendments on soil carbon and nitrogen content, some enzyme activities and genetic diversity. *Biology and Fertility of Soils*, 34(5) 311-318.
- [30] Adekiya, A.O., Ejue, W.S., Olayanju, A., (2020) Different organic manure sources and NPK fertilizer on soil chemical properties, growth, yield and quality of okra. *Sci Rep* (10) 16083.
- [31] Polat, A.A., (1990) Investigations on loquat (*Eriobotrya japonica* Lindl.) propagation by air-layering, cutting and different budding methods on various root-stocks. PhD thesis, Cukurova University, Institute of Natural Science, Adana, Turkey, 297
- [32] Hartmann, H.T., Kester, D.E., (2002) Hartmann and Kester's plant propagation: Principles and practices, 1-16, California, USA.
- [33] Smart, D.R., Kocsis, L., Andrew Walker, M., (2002) Dormant Buds and Adventitious Root Formation by *Vitis* and Other Woody Plants. *J Plant Growth Regul* (21) 296–314.
- [34] Wright, J., W., (1976) Introduction to Forest Genetics. Academic Press 463, New York, USA.
- [35] Ürgenç, S., (1982) Orman ağaçları ıslahı. İstanbul Üniversitesi Orman Fakültesi Yayın No: 293, İstanbul, Türkiye.
- [36] USDA (1999) United States Department Of Agriculture. Soil Taxonomy, A Basic System of Soil Classification for Making and Interpreting Soil Surveys. Second Edition.
- [37] Gee, G.W., Bauder, J.W., (1986) Particle-size analysis. In: Klute, A. (Ed.), Methods of soil analysis. Part 1. Physical and mineralogical methods. 2nd edition. American Society of Agronomy. 383-411. Soil Science Society of America, Madison.
- [38] McLean, E.O., (1982) Soil pH and Lime Requirement. In: Page, A. (Ed.), Methods of Soil Analysis Part 2. Chemical and Microbiological Properties. 2nd Edition. Agronomy (9) 199-224.
- [39] Nelson, D.W., Sommers, L.E., (1982) Total carbon, organic carbon, and organic matter. In: Page, A. (Ed.), Methods of soil analysis. part 2. Chemical and Microbiological Properties. Madison, 2nd edition. Agronomy (9) 539-579, 1159 Wisconsin USA.

The Effects of Cattle and Sheep Manure Applications on Soil Physical Properties and Rooting and Shoot Development of Grapevines Cuttings

- [40] Rhoades, J.D., (1982) Soluble salts. In: Page, A. (Ed.), *Methods of Soil Analysis. Part 2. Chemical and Microbiological Properties*. 2nd Edition. Agronomy (9) 167-178, 1159 Madison, Wisconsin USA.
- [41] Kemper W.D., Rosenau R.C., Aggregate stability and size distribution. *Methods of soil analysis. Physical and mineralogical methods*. 2nd edition. Agronomy, 9: 425-442, 1986.
- [42] Blake, G.R., Hartge, K.H., (1986) Bulk density. In A. Klute (ed.), *Methods of Soil Analysis. Part 1*. 2nd ed. Agronomy Monographs. 9. Soil Science Society of America, Madison, 363-382.
- [43] Cassel, D.K., Nielsen, D.R., (1986) Field capacity and available water capacity. In A. Klute (ed.), *Methods of Soil Analysis. Part 1*. 2nd ed. Agronomy Monographs. 9. Soil Science Society of America, Madison, 901-926.
- [44] Kacar, B., İnal, A., (2008) Bitki analizleri, Fen Bilimleri, Nobel Yayın No: 1241, 892.
- [45] Dowdy, S., Wearden, S., (1983) *Statistics for Res.* John Wiley & Sons, Inc. Elazar Volk, USA.
- [46] SPSS (2011) *SPSS for Windows, Version 20*, SPSS Inc., USA.
- [47] Ülgen, N., Yurtsever, N., (1995) Türkiye Gübre ve Gübreleme Rehberi (4.Baskı). Başbakanlık Köy Hizmetleri Genel Müdürlüğü Toprak ve Gübre Araştırma Enstitüsü Müdürlüğü Yayınları. Genel Yayın No: 209. Teknik Yayınlar No: T.66.s.230. Ankara.
- [48] Agbede, T.M., Adekiya, A.O., Ogeh, J.S., (2014) Response of soil properties and yam yield to *Chromolaena odorata* (Asteraceae) and *Tithonia diversifolia* (Asteraceae) mulches. *Arch. Agron. Soil Sci.* 60 (2), 209–224.
- [49] Prasad, B., Sinha, S.K., (2000) Long-Term Effects of Fertilizer and Organic Manures on Crop Yields, Nutrient Balance and Soil Properties in Rice-Wheat Cropping System in Bihar. pp: 105- 119 in *Long-Term Soil Fertility Experiments in Rice-Wheat Cropping Systems*. Rice-Wheat Consortium Paper Series 6. New Delhi, INDIA.
- [50] Conceição, P.C., (2006) *Proteção física da matéria orgânica do solo em solos do Sul do Brasil*. Porto Alegre, Universidade Federal do Rio Grande do Sul, 145p. (Tese de Doutorado)
- [51] Boeni, M., (2007) *Proteção física da matéria orgânica em Latossolo ssob sistemas com pastagens na região do Cerrado brasileiro*. Porto Alegre, Universidade Federal do Rio Grande do Sul, 136p. (Tese de Doutorado).
- [52] Salton, J.C., Mielniczuk, J., Bayer, C., Boeni, M., Conceição, P.C., Fabrício, A.C., Macedo, M.C.M., Broch, D.L., (2008) Agregação e estabilidade de agregados do solo em sistemas agropecuários em Mato Grosso do Sul. *R. Bras. Ci. Solo*, (32) 11-21.
- [53] Karami, A., Homae, M., Afzalnia, S., Ruhipour, H., Basirat, S., (2012) Organic resource management: impacts on soil aggregate stability and other soil physico-chemical properties. *Agriculture, Ecosystems Environment*,(148) 22-28.

The Effects of Cattle and Sheep Manure Applications on Soil Physical Properties and Rooting and Shoot Development of Grapevines Cuttings

- [54] Yu, H.Y., Ding, W.X., Luo, J.F., Geng, R.L., Cai, Z.C., (2012) Long term application of organic manure and mineral fertilizers on aggregation and aggregate-associated carbon in a sandy loam soil. *Soil and Tillage Research*, (124) 170–177.
- [55] Zhou, H., Peng, X., Perfect, E., Xiao, T., and Peng, G., (2013) Effects of Organic and Inorganic Fertilization on Soil Aggregation in an Ultisol as Characterized by Synchrotron Based X-ray Micro-computed Tomography. *Geoderma* (195) 23–30.
- [56] Van Leeuwen, C., Friant, P., Choné, X., Tregoat, O., Koundouras, S., Dubourdieu, D., (2004) Influence of climate soil and cultivar on terroir. *American Journal of Enology and Viticulture*, (55) 207–217.
- [57] Bodin, F., & Morlat, R., (2006) Characterization of viticultural terroirs using a simple field model based on soil depth. I Validation of the water supply regime phenology and vine vigour in the Anjou vineyard (France). *Plant and Soil*, (281) 37–54.
- [58] Karaman, M.R., Brohi, A.R., Müftüoğlu, N.M., Öztaş, T., Zengin, M., (2012) Sürdürülebilir Toprak Verimliliği. *Koyulhisar Ziraat Odası Kültür Yayınları* (3) 291-294.
- [59] Jaleta, A., Sulaiman, M., (2019) A review on the effect of rooting media on rooting and growth of cutting propagated grape (*Vitis vinifera* L). *World Journal of Agriculture and Soil Science*, 3(4) 1-8.
- [60] Ertan, B., Özen, M., (2019) Organik İncir Fidanı Yetiştiriciliğinde Farklı Ortamların Fidan Kalitesi Üzerine Etkileri. VI. Organik Tarım Sempozyumu 6th Symposium on Organic Agriculture 15-17 Mayıs, İzmir – Turkey.
- [61] Stumpe, H., Garz, J., Schliephake, W., Wittenmayer, L., Merbach, W., (2000) Effects of humus content, farmyard manuring and mineral N fertilization on yield and soil properties in a long term trial. *J. of Plant nutrition and Soil Science*, 163(6) 657- 662.

The Effects of Cattle and Sheep Manure Applications on Soil Physical Properties and Rooting and Shoot Development of Grapevines Cuttings

Fazil HACIMUFTUOGLU¹, Muhammed KUPE^{2*}

¹Atatürk University, Faculty of Agriculture, Department of Soil Science and Plant Nutrition, 25240, Erzurum,

^{2*}Atatürk University, Faculty of Agriculture, Department of Horticulture, 254240, Erzurum, Türkiye

Received:25/10/2022, Revised: 29/11/2022, Accepted: 01/12/2022, Published: 30/12/2022

Abstract

In this study, the effects of cattle and sheep manure applications at different doses on soil physical properties, and in parallel with, the effects on rooting and shoot development of vine cuttings were investigated. In this study, 10%, 20% and 30% cattle and sheep manure was mixed into the soil as rooting medium, and the rooting and shooting performances of Karaerik and Narince grape varieties were evaluated in greenhouse conditions. During the experiment, the bud burst rates of the cuttings were recorded, and at the end of the experiment, the aggregate stability values, water permeability, bulk density, total porosity of the soil and plant parameters such as the root length, the root number, shoot length and the leaf number of the 1 year old cuttings were determined. The highest root length values of Karaerik and Narince grape varieties were determined as 7.2 and 7.43 cm, respectively, in 20% sheep manure application. While the highest shoot length value (15.66 cm) in Karaerik grape cultivar was determined in 30% cattle manure application, the highest value (25.66 cm) in Narince grape cultivar was determined in 20% sheep manure application. As a result of the study, it was determined that sheep manure was more effective in root development and cattle manure in shoot development of Karaerik grape cultivar. It has been revealed that sheep manure gives more positive results on both root and shoot development than cattle manure in Narince grape cultivar.

Keywords: Grapevine cuttings, rooting and shooting, soil physics, farm manure

Sığır ve Koyun Gübresi Uygulamalarının Toprak Fiziksel Özellikleri ile Asma Çeliklerinin Köklenme ve Sürgün Gelişimi Üzerine Etkileri

Öz

Bu çalışmada, farklı dozlarda sığır ve koyun gübresi uygulamalarının toprağın fiziksel özelliklerine ve buna paralel olarak asma çeliklerinin köklenme ve sürgün gelişimine etkileri araştırılmıştır. Çalışmada köklendirme ortamı olarak toprağa %10, %20 ve %30 sığır ve koyun gübresi karıştırılarak Karaerik ve Narince üzüm çeşitlerinin sera koşullarında köklenme ve sürgün performansları değerlendirilmiştir. Deneme sırasında çeliklerin tomurcuk patlama oranları kaydedilmiş ve deneme sonunda toprağın agregat stabilitesi, su geçirgenliği, kütle yoğunluğu, toplam porozitesi ve bitki parametrelerinden bir yaşlı çeliklerin kök sayısı, kök uzunluğu, sürgün uzunluğu ve sürgündeki yaprak sayısı belirlenmiştir. Karaerik ve Narince üzüm çeşitlerinde en yüksek kök uzunluğu değerleri sırasıyla 7.2 ve 7.43 cm olarak 20% koyun gübresi uygulamasında tespit edilmiştir. Karaerik üzüm çeşidinde en yüksek sürgün uzunluğu değeri (15.66 cm) 30% sığır gübresi uygulamasında belirlenirken, Narince üzüm çeşidinde ise en yüksek değer (25.66 cm) 20% koyun gübresi uygulamasında tespit edilmiştir. Çalışma sonucunda Karaerik üzüm çeşidinin kök gelişiminde koyun gübresinin, sürgün gelişiminde ise sığır gübresinin daha etkili olduğu belirlenmiştir. Narince üzüm çeşidinde koyun gübresinin hem kök hem de sürgün gelişimi üzerinde sığır gübresine kıyasla daha olumlu sonuçlar verdiği ortaya konulmuştur.

Anahtar Kelimeler: Asma çeliği, köklenme ve sürme, toprak fiziği, çiftlik gübresi

1. Introduction

Sustainability in successful agriculture is inseparable with a fertile soil. Intensive agriculture and the use of various chemicals endanger the sustainability of agricultural activities. The decrease in the amount of organic matter due to increasing agricultural activities leads to the deterioration of the physico-mechanical structure of the soil after a while. Many studies have shown that organic fertilization is an effective method to increase soil organic matter content, soil fertility and organic carbon accumulation [1-9]. In agricultural production activities, the ability of the plant to develop well in the soil is related to the physical and chemical properties of the soil environment. The most used method to improve the physical properties of the soil and to ensure its sustainability is to add organic-based materials to the soil [10, 11].

Various materials such as farm manure, peat, compost are applied to keep the amount of organic matter in the soil at a certain level [12]. Soil organic matter plays a critical role in maintaining soil fertility and productivity [13, 14]. Studies in different parts of the world have shown that organic manures improve soil properties and increase the yield of crops [15]. In a 25-year study conducted by [16], farm manure was applied to the soil and it was reported that a significant increase in the amount of organic carbon and total nitrogen of the soil occurred due to this applications. [17], stated that if there is enough decomposed organic matter residues in the surface soil, it has a significant effect on the physical and chemical properties of the mineral soil. [18], reported that when a fertile soil is mentioned, it comes to mind that the soil has a high level of organic matter and biological activity, stable aggregates, an environment in which plant roots can easily move, and water can easily infiltrate from the surface. However, trying to keep organic matter in the soil at a high level is both impractical and very expensive. On the other hand, manure applications made by animal breeders on agricultural lands are an easy and low-cost way to provide organic fertilization. Farm animals provide the transport of plant nutrients from animal grazing areas to crop production areas as manure [19]. This situation increases the nutrient cycle and reduces the costs of industrial manures.

[20], stated that different types of manures of animal origin (goat, sheep, cow, poultry manure, etc.) have significant differences in macro and micronutrient content and therefore significantly affect the nutrition of the grown plant. [21] in a study investigating the effectiveness of livestock manure, found that goat manure has higher N, P and K concentrations (2.77% N, 1.78% P₂O₅ and 2.88% K₂O) compared to other animal manures. He also stated that sheep manure is a good source of K (1% K₂O). On the other hand, he stated that cow manure contains only 0.55% N, 0.10% P₂O₅ and 0.50% K₂O, while the Fe concentrations in different types of manures vary between 40 and 460 mg kg⁻¹, while the Mn and Zn contents vary between 5 and 90 mg kg⁻¹.

In the coming years, the use of organic manures to meet nutrient needs will become more common to develop sustainable agriculture. This is related to the improvement of organic manures in various yield parameters of the soil. Organic fertilization increases plant productivity by maintaining the quality of the produced crop [22] and positively affecting soil microbial biomass and activity [23]. Nutrient deficiency is one of the most important factors

affecting yield and quality in agricultural production. Animal fertilization is effective in increasing the nutrient content of the soil over the years, depending on this, in the generative and vegetative development of the plant [24]. Animal manures such as cattle, sheep and horses are used as a food source for annual and perennial crops in horticulture. The effect of animal fertilization on fruit quality and nutritional value depends on several factors, including the properties of organic matter, pedoclimatic conditions, application time and plant species. [24]. As with other plant species, organic manures are of great importance on the nutrition of the vine. [25], stated that there is a significant relationship between soil quality indices and vegetative growth of grapevines. It has been stated in many studies that soils have both direct and indirect effects on root growth, photosynthesis and shoot growth of vines; various soil types were also found to have a measurable effect on vine vigor and fruit characteristics [26-28].

Ensuring of soil fertility is one of the most important goals for sustainable viticulture [29, 30]. [23], reported in a study that organic soil management is necessary for healthy plant growth and quality product in viticulture. Internal and external factors affect rooting in cuttings. Internal factors; Genetic structure, storage materials and hormones in the plant are shown as examples, while external factors; such as irrigation, pruning, fertilization, cutting time, rooting environment, temperature and humidity can be given as examples [31,32].

Vine nutrition is also important in rooting cuttings. Related to this, there are opinions that inorganic carbon compounds can stimulate adventitious root formation in grapevine cuttings. Macro and micro nutrients are also important in adventitious root formation. Especially nitrogen, magnesium, zinc and boron affect the adventitious root formation significantly [33].

In this study, the effect of cattle and sheep manures applied to the soils in different doses, on the aggregate stability, water permeability, bulk density and total porosity values of the soils, and in parallel with this, the bud burst rate and the rooting and shooting performances of 1 year old cuttings of Karaerik and Narince grape varieties were evaluated.

2. Material and Methods

The study was carried out in Atatürk University Faculty of Agriculture application greenhouse (humidity rate: 80-85%, temperature: 27-30 °C) in 2022. Since it is known that the rooting abilities of cuttings vary greatly between species and varieties [34, 35], two different grape varieties with different rooting abilities were preferred in this study.

In the research, one-year-old cuttings belonging to Karaerik and Narince cultivars were used as plant material. In this study, coarse textured soil with high permeability was used. The study soil was sampled as degraded from a 20 cm topsoil depth of a field in the Karaçam village of Çaykara district, Trabzon province [36]. In the research, at least 1 year old burnt cattle and sheep manure taken from Atatürk University Food and Livestock Application Center farm land was used.

Physical and chemical soil analyses

For fundamental analysis and trial studies, soil samples were air-dried in laboratory conditions and sieved through 4 and 2 mm mesh.

Soil texture was determined by Bouyoucos hydrometer method [37], soil reaction (pH) by glass electrode pH meter [38], lime content by Scheibler calcimeter (Nelson, 1982), organic matter content by Smith Weldon method [39], electrical conductivity (EC) value with electrical conductivity instrument [40], aggregate stability (AS) using Yoder type wet sieving device [41], particle density by pycnometer method [42], field capacity and permanent wilting point were determined by the pressure extractor method [43]. On the other hand, Soil bulk density was determined by the cylinder method [42], and total porosity was calculated from bulk weight and particle density.

Plant phenological observations and fertilization application

In this research, one-year-old cuttings belonging to Narince and Karaerik varieties, which are important table grape varieties, were taken from 6-year-old vines grown on their own roots in the unheated greenhouses of Atatürk University Plant Production Research Directorate. Samples were taken on April 1 in the form of 10-node rods, 10-12 cm long and 1-node cuttings were prepared.

Manures were mixed into potting soils at rates of 10% - 20% and 30% on a weight basis. On the 40th day of the experiment, the shooting performances (bud burst) were recorded, and at the end of the 60th day, the study was terminated and the root lengths, root numbers, shoot lengths and the number of leaves in the shoot were determined [44].

In the study, two different manures (cattle and sheep) were applied in 4 different doses (D0: 0%, D1: 10%, D2: 20%, D3: 30%). The research carried out on two different cultivars was planned with 3 replications and a total of 48 pots (2x2x4x3) were used. Statistical analysis was performed by ANOVA, and differences between means were tested using Duncan's multiple range test [45, 46].

3. Results and Discussion

In this study, the texture class of the soils was determined as coarse textured in the sandy clay loam texture class (58% sand, 20% silt, 22% clay). Soil organic matter content (3.77%) is in the well class, pH level; It was found to be 7.5 level and neutral, the EC level of the working soils is 0.14 dS/m without salt, the CaCO₃ level was determined as 5.1% in the medium calcareous [47], class. According to the available phosphorus contents, the class of the soils was determined as medium (P₂O₅: 8 kg/da) [47], Ca⁺⁺, Mg⁺⁺, Na⁺, K⁺ contents were determined as 11.2, 5.04, 0.36, 2.17 me/100gr, respectively. Particle density were determined as 2.68 (g/cm³). Field capacity and permanent wilting point moisture content of the working soil were determined to be 25% and 13%, respectively (Table 1).

The Effects of Cattle and Sheep Manure Applications on Soil Physical Properties and Rooting and Shoot Development of Grapevines Cuttings

Table 1. Basic physical and chemical analysis results of the researched soils

Soil properties	
Sand (%)	58
Silt (%)	20
Clay (%)	22
Texture class	Sandy clay loam
Particle density (g/cm ³)	2.68
Organic matter (%)	3.77
pH	7.5
EC (dS/m)	0.14
CaCO ₃ (%)	5.1
Ca, Mg, Na, K (me/100gr)	11.2; 5.04; 0.36; 2.17
Field capacity (%)	25
Wilting point (%)	13

Soil physical properties

At the end of the 60-day plant development period of the soils applied with different doses of cattle and sheep manures; Aggregate stability, water permeability, bulk density and porosity values are given in Table 2.

Table 2. Effects of applications on the physical properties of soils

Applications	AS (%)	WP (cm/h)	BD (gr/cm ³)	Porosity (%)
D0 (Control)	46.21 ^d ± 3.35*	4.6 ^d ± 0.87	1.24 ^a ± 0.02	53.4 ^c ± 0.75
M1-D1	56.48 ^{bc} ± 2.41	7.73 ^c ± 0.58	1.16 ^b ± 0.02	56.1 ^b ± 0.61
M1-D2	57.43 ^b ± 1.66	14.63 ^b ± 3.97	0.98 ^c ± 0.01	63.1 ^a ± 0.35
M1-D3	69.54 ^a ± 1.74	14.43 ^b ± 0.72	0.97 ^c ± 0.01	63.3 ^a ± 0.17
M2-D1	52.63 ^c ± 2.85	5.33 ^{cd} ± 0.15	0.99 ^c ± 0.01	62.5 ^a ± 0.23
M2-D2	59.18 ^b ± 2.84	5.43 ^{cd} ± 0.68	0.98 ^c ± 0.02	62.9 ^a ± 0.55
M2-D3	60.38 ^b ± 0.85	19.13 ^a ± 0.66	0.97 ^c ± 0.01	63.4 ^a ± 0.17

*: Standart deviation, AS: Aggregate stability, WP: Water permeability, BD: Bulk density; M1: cattle manure; M2: sheep manure; D0: 0% Control, D1: 10% dose, D2: 20% dose, D3: 30% dose

Aggregate stability, water permeability, bulk density and porosity values of the soils used in the research are given in Table 2. According to the results, it was found that different doses of cattle (M1) and sheep (M2) manure applications caused a statistical difference in all physical soil parameters examined ($p < 0.05$).

When the effects of cattle and sheep manure applications on the aggregate stability values of the soil were examined, it was determined that all doses of both manures caused a statistical difference ($p < 0.05$) in AS values compared to the control group (Table2). While the lowest value was determined to be 46.2% in the control group, it was revealed that the aggregate stability value increased linearly depending on the applications and the highest value was 69.5% in the D3 cattle manure application. When Table 2 was examined, it was determined that the

The Effects of Cattle and Sheep Manure Applications on Soil Physical Properties and Rooting and Shoot Development of Grapevines Cuttings

different doses of sheep manure also increased the AS value, but cattle manure was more effective. When the effect of manure applications on the water permeability values of the soils was examined, it was determined that there was a statistical difference in the water permeability value compared to the control group ($p < 0.05$). Considering all manure applications together, the highest water permeability value was 19.1 cm/h in the third dose application of sheep manure (M2-D3), and this value was followed by the 2nd (M1-D2) and 3rd (M1-D3) doses of cattle manure. It was determined that these applications increased the WP value by 315%, 218% and 213%, respectively (Table 2). When the bulk density values of the soils were examined, it was determined that manure applications showed a statistically significant difference ($p < 0.05$) on the BD value compared to the control group. When Table 2 was examined, it was determined that the BD value decreased due to the increase in the application dose of cattle and sheep fertilizers, and the lowest values caused a decrease of 22% in the D3 application of both manures compared to the control group. The total porosity of the applied soils was statistically different compared to the control group ($p < 0.05$). The lowest porosity value was determined to be 53.4% in the control group, while the highest value was 63.4% in the third dose application of sheep manure (M2-D3). This value was found to be 63.3% in the third dose application of cattle manure (M1-D3) and 62.9% in the second dose application of sheep manure (M2-D2) (Table 2).

The effects of the applications on the rooting and shooting performance of the cuttings

It was observed that there were differences between the bud burst rate of the cuttings of Karaerik and Narince grape varieties depending on the manure applications (Table 3). Root lengths, root numbers, shoot lengths and leaf numbers in the shoot of the cuttings used in the research are given in Tables 4 and 5. Rooting and shooting performances of Karaerik and Narince grape varieties of different manure applications are given in Figures 1 and 3. The relationship graphs between rooting and shooting performances and soil physical properties, depending on manure applications, are presented in Figures 2 and 4. According to the results, it was found that different doses of Cattle (M1) and Sheep (M2) manure applications caused a statistical difference on all rooting and shooting performances examined ($p < 0.05$). On the 40th day of the experiment, the bud burst rates of the cuttings were examined. It was determined that 100% (all cuttings on three replication) burst was achieved in the 2nd and 3rd dose applications of cattle manure in Karaerik grape cultivar and in the 1st and 3rd dose applications in Narince grape cultivar. While there was no 100% bud burst (first shooting) at the end of the 40th day in sheep manure applied in Karaerik grape cultivar, 100% burst was observed in the second dose application of Narince grape cultivar in sheep manure (Table 3).

Table 3. Bud burst rates of grapevine cuttings at the end of the 40th day

Cultivars	M1-D0 (%)	M1-D1 (%)	M1-D2 (%)	M1-D3 (%)	M2-D0 (%)	M2-D1 (%)	M2-D2 (%)	M2-D3 (%)
Karaerik	66	66	100	100	66	66	33	33
Narince	33	100	66	100	33	66	100	66

The Effects of Cattle and Sheep Manure Applications on Soil Physical Properties and Rooting and Shoot Development of Grapevines Cuttings

M1: cattle manure; M2: sheep manure; D0: 0% Control, D1: 10% dose, D2: 20% dose, D3: 30% dose

When the effects of manure applications at different doses on root lengths of Karaerik and Narince grape varieties were evaluated, it was revealed that all doses of cattle and sheep manures were statistically different ($p < 0.05$) compared to the control group (Table 4, 5). The most effective results on the root length of cuttings in Karaerik grape cultivar were determined in the 1st (M2-D1) and 2nd dose (M2-D2) applications of sheep manure and the 3rd dose (M1-D3) applications of cattle manure, respectively (Table 4). In Narince grape cultivar, the most effective results on the root length of cuttings were determined in the second dose of sheep manure (M2-D2) and 3 doses (M2-D3), respectively, and in the second dose of cattle manure (M1-D2) (Table 5). A statistical difference was found between the applications in terms of root numbers depending on the different doses of manure applications of Karaerik and Narince grape varieties ($p < 0.05$). It was revealed that sheep manure was more effective than cattle manure on the root number of cuttings in Karaerik grape cultivar. The most effective results in terms of root numbers were determined in the first dose (M2-D1), second dose (M2-D2) and third dose (M2-D3) sheep manure applications, respectively (Table 4). It was determined that the most effective results in terms of root number of cuttings in Narince grape cultivar were in the second dose of sheep manure (M2-D2), the second dose of cattle manure (M1-D2) and the third dose of sheep manure (M2-D3) (Table 5). It was determined that manure applications at different doses caused a statistical difference ($p < 0.05$) on shoot lengths of Karaerik and Narince grape varieties (Table 4, 5). It was determined that the highest value of shoot length in Karaerik grape cultivar was in the 3rd dose (M1-D3), 2nd dose (M1-D2) and 1st dose (M1-D1) applications of cattle manure, respectively (Table 4). When the shoot length of the cuttings of Narince grape cultivar was examined, it was determined that the highest values were observed in the 2nd dose (M2-D2), 3rd dose (M2-D3) and 1st dose (M2-D1) applications of sheep manure, respectively (Table 5). It was determined that all doses of applied cattle and sheep manures caused a statistically significant difference ($p < 0.05$) on the number of leaves in the shoot. The highest number of leaves in Karaerik grape cultivar was determined in the 3rd dose application of cattle manure (M1-D3). This was followed by 2 doses (M1-D2) and 1st dose (M1-D1) applications of cattle manure, respectively (Table 4). In Narince grape cultivar, it was determined that the 2nd dose of sheep manure (M2-D2) had the highest effect, followed by the 1st (M2-D1) and 3rd (M2-D3) doses of sheep manure (Table 5).

Table 4. Rooting and shooting performances of Karaerik grape cultivar

Karaerik cultivar	Root Length (cm)	Root Numbers (item)	Shoot Length (cm)	Leaf Numbers (item)
M1-D0	1.16 ^d ± 0.28*	1.33 ^e ± 0,57	6 ^{cd} ± 1	2.33 ^d ± 0.57
M1-D1	2.33 ^c ± 0.28	7.33 ^d ± 1,52	12 ^{abc} ± 2.64	7 ^{ab} ± 1
M1-D2	5.76 ^b ± 0.68	12.33 ^c ± 1,52	13.66 ^{ab} ± 4.5	7.66 ^{ab} ± 1.52
M1-D3	6.66 ^a ± 0.87	11.33 ^c ± 0,57	15.66 ^a ± 3.51	8.33 ^a ± 1.52
M1-Mean	4.91	10.3	13.8	7.66
M2-D0	1.3 ^d ± 0.36	1.66 ^e ± 0,57	4.66 ^d ± 2.08	2 ^d ± 1
M2-D1	7.1 ^a ± 0.1	34 ^a ± 2,64	11.33 ^{abc} ± 5.03	5.66 ^{abc} ± 3.21
M2-D2	7.2 ^a ± 0.2	18 ^b ± 1	8.33 ^{bcd} ± 2.51	3.33 ^{cd} ± 1.52
M2-D3	5.26 ^b ± 0.64	14 ^c ± 2,64	9.33 ^{bcd} ± 3.05	5 ^{bcd} ± 2

The Effects of Cattle and Sheep Manure Applications on Soil Physical Properties and Rooting and Shoot Development of Grapevines Cuttings

M2-Mean	6.52	22	9.66	4.66
----------------	-------------	-----------	-------------	-------------

M1: cattle manure; M2: sheep manure; D0: 0% Control, D1: 10% dose, D2: 20% dose, D3: 30% dose

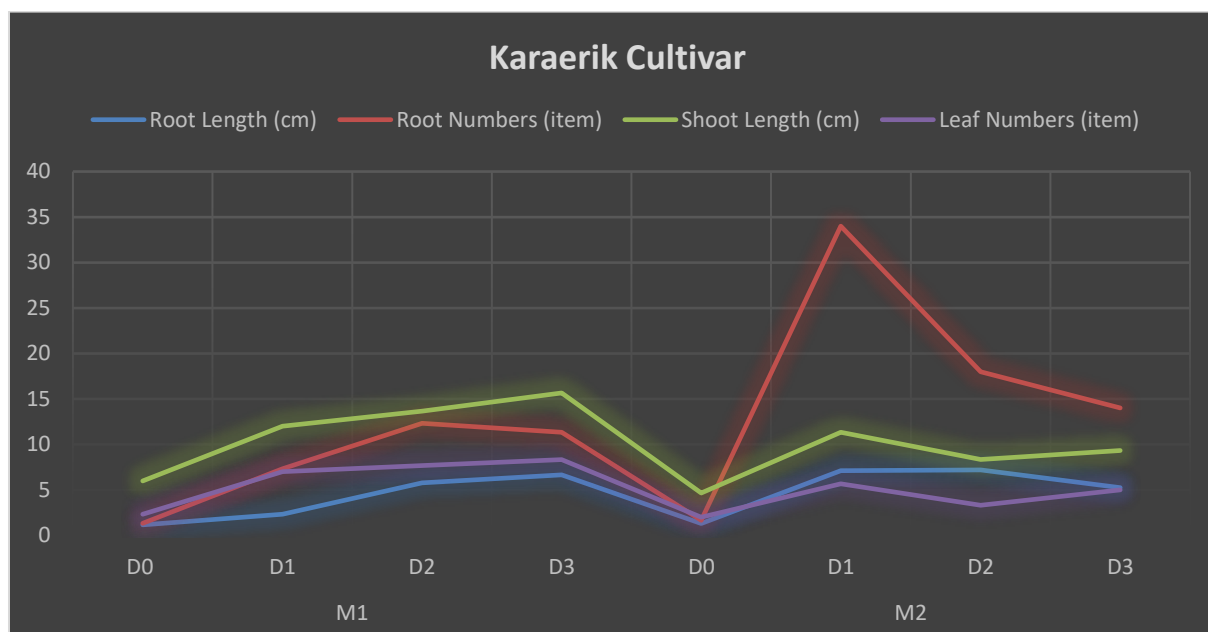


Figure 1. Rooting and shooting performance graph of cuttings of Karaerik grape cultivar

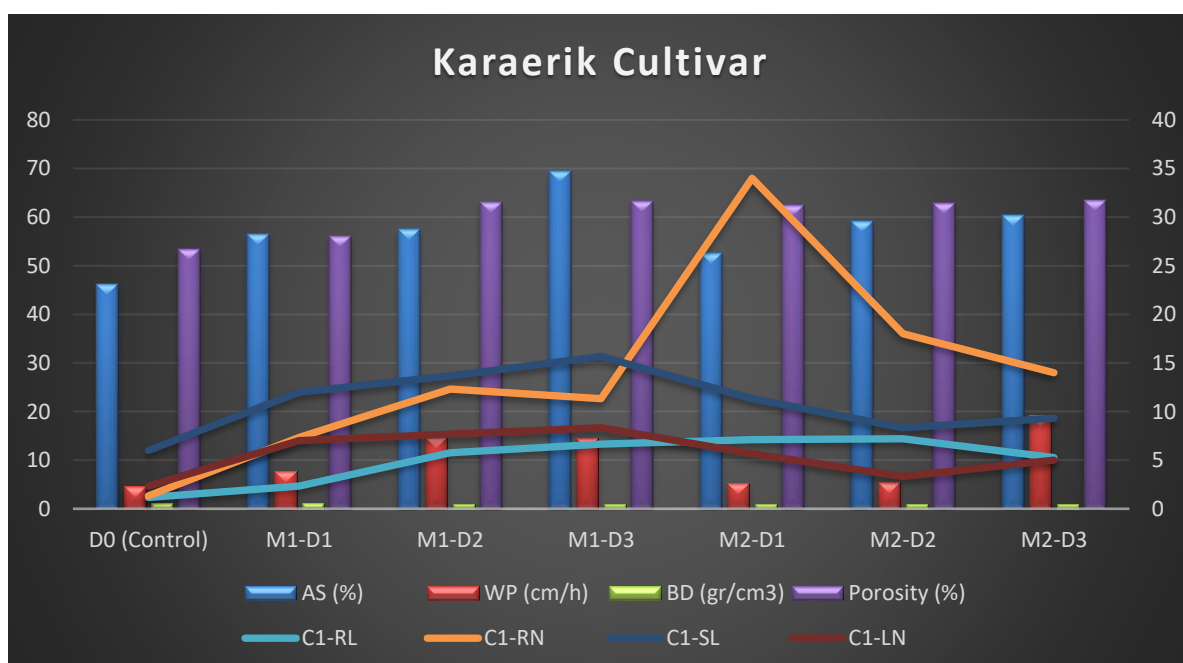


Figure 2. The relationship between rooting and shooting performances of Karaerik grape cultivar and soil physical properties.

AS: Aggregate stability, WP: Water permeability, BD: Bulk density; M1: cattle manure; M2: sheep manure; V1: Karaerik cultivar, RL: Root length, RN: Root numbers, SL: Shoot length, LN: Leaf numbers, D0: 0% Control, D1: 10% dose, D2: 20% dose, D3: 30% dose

Table 5. Rooting and shooting performances of Narince grape cultivar

Narince cultivar	Root Length (cm)	Root Numbers (item)	Shoot Length (cm)	Leaf Numbers (item)
M1-D0	0.76 ^c ± 0.25	2 ^c ± 1	1.66 ^d ± 0.57	1.33 ^d ± 0.57

The Effects of Cattle and Sheep Manure Applications on Soil Physical Properties and Rooting and Shoot Development of Grapevines Cuttings

M1-D1	1.23 ^e ± 0.25	3 ^c ± 1	6.66 ^c ± 1.52	3 ^{cd} ± 1
M1-D2	5.96 ^c ± 0.15	13.33 ^b ± 0.57	8 ^c ± 3.6	3.66 ^c ± 2.08
M1-D3	3.86 ^d ± 0.30	10 ^b ± 1	7.66 ^c ± 1.52	3 ^{cd} ± 1
M1-Mean	3.68	8.76	7.44	3.22
M2-D0	1.23 ^e ± 0.15	3 ^c ± 1	8.66 ^c ± 1.15	8.33 ^b ± 1.52
M2-D1	3.56 ^d ± 0.20	10.66 ^b ± 0.57	9.66 ^c ± 1.15	8.66 ^b ± 1.15
M2-D2	7.43 ^a ± 0.51	30.66 ^a ± 6.11	25.66 ^a ± 1.52	16.33 ^a ± 0.57
M2-D3	6.56 ^b ± 0.51	12.66 ^b ± 0.57	15.33 ^b ± 1.15	8.66 ^b ± 0.57
M2-Mean	5.85	18	16.9	11.2

M1: cattle manure; M2: sheep manure; D0: 0% Control, D1: 10% dose, D2: 20% dose, D3: 30%

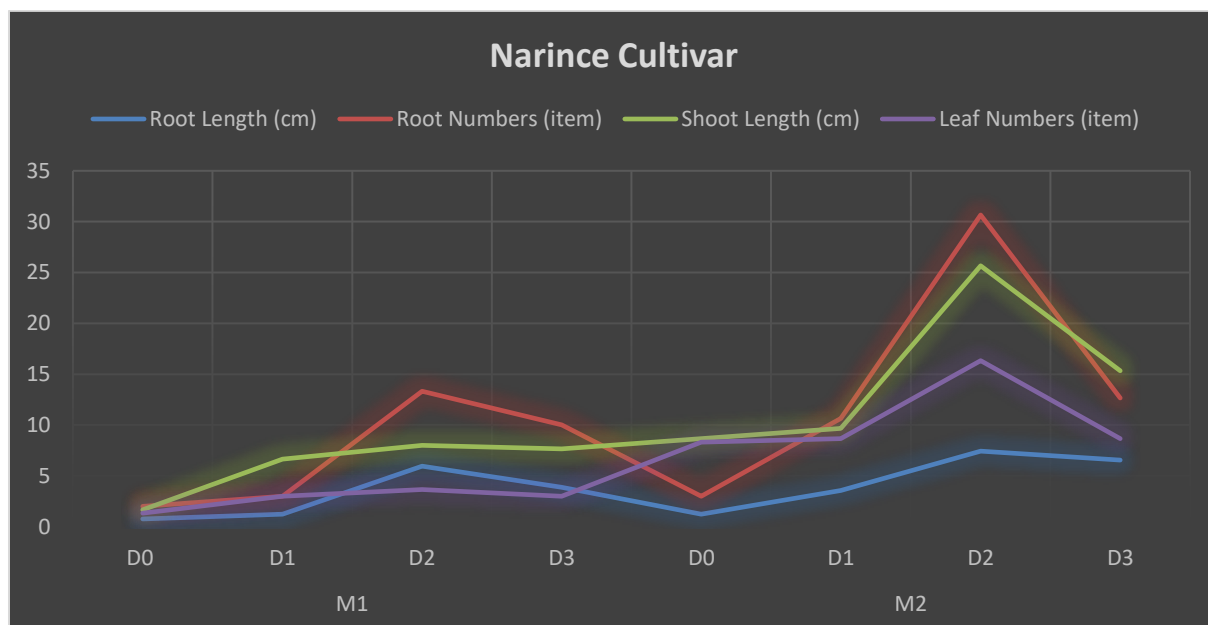


Figure 3. Rooting and shooting performance graph of cuttings of Narince grape cultivar

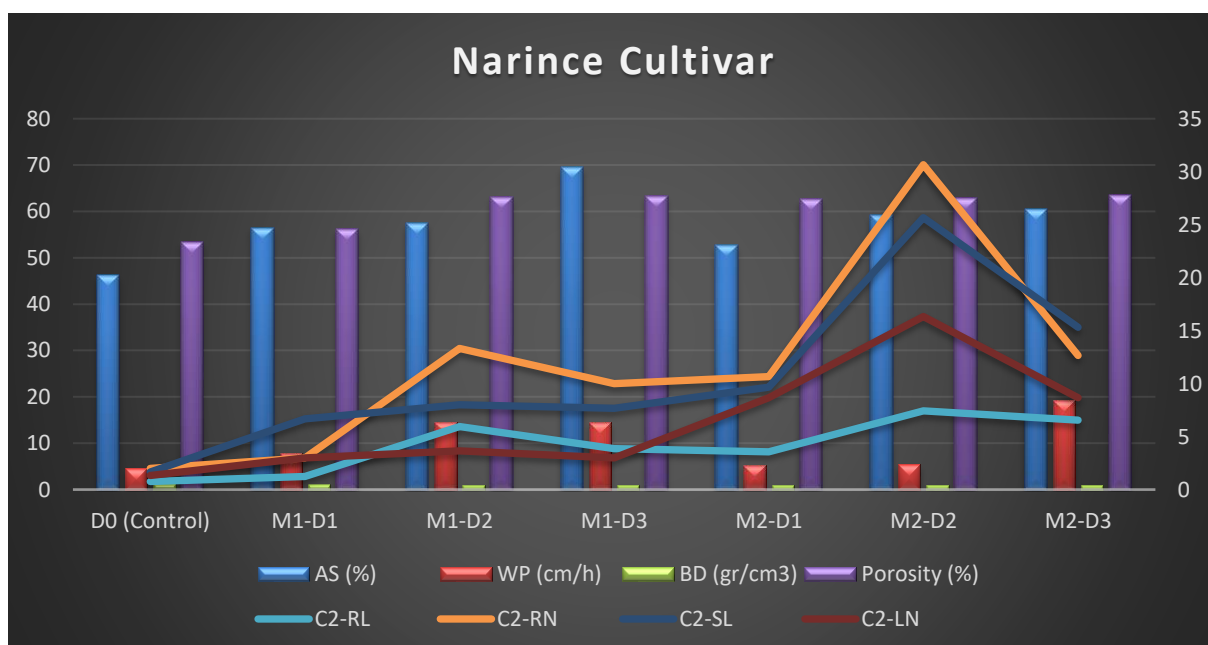


Figure 4. The relationship between rooting and shooting performances of Narince grape cultivar and soil physical properties.

The Effects of Cattle and Sheep Manure Applications on Soil Physical Properties and Rooting and Shoot Development of Grapevines Cuttings

AS: Aggregate stability, WP: Water permeability, BD: Bulk density; M1: cattle manure; M2: sheep manure; V2: Narince cultivar, RL: Root length, RN: Root numbers, SL: Shoot length, LN: Leaf numbers, D0: 0% Control, D1: 10% dose, D2: 20% dose, D3: 30% dose

When Figure 2 and Figure 4 are examined, it is understood that there is a relationship between the physical properties of soils and the vegetative development of plants. While manure applications improve the physical properties of the soil, they also affect the rooting and shoot performance of the plants. It was determined that there was a linear increase in AS, WP and porosity values depending on the increase in the application doses of both manures added to the soil. In parallel with the improvement in the physical properties of the soils, it was observed that the rooting and shooting performances of the cuttings also changed. While this development in soils was in direct parallel with the development of cuttings in cattle manure applied soils, it showed a partial parallelism in cuttings in sheep manure applied soils.

Fine textured heavy and impermeable soils limit root formation in plants and can cause root rot by holding excessive water. There is a significant relationship between root and shoot development in vines and soil fertility and water holding capacity [25]. The application of sheep and cattle manure to the soil increases the amount of organic matter in the soil, and accordingly, it provides a more suitable environment for plant growth by providing a positive effect on the soil's aggregate stability, water permeability, air-water balance, and uptake of plant nutrients in the soil.

For a good root formation, suitable soil air, soil water and enough oxygen must be present. It is known that organic matter affects plant vegetative and generative development positively by increasing aggregate stability, and reducing bulk density [48]. It has been revealed in many studies that there is a direct relationship between soil carbon (C) content and soil aggregation, and that organic manures added to soil improve the structural properties by increasing the aggregate stability of the soil [6, 49-55]. Parallel to the improvement in soil physical properties, the increase in the water and nutrient holding capacity of the soil has come to the fore as important factors that can affect the yield of vines [27, 56, 57]. As a matter of fact, in this study, similar to other studies, it was determined that cattle and sheep manure applications improved the physical properties of the soils, increased the water permeability and aggregate stability values, decreased the bulk density values, and in parallel increased the rooting and shooting performance of the cuttings.

[58], stated that organic materials create a more suitable environment for plants and microorganisms by increasing the aeration capacity of soils, and this situation positively affects water and nutrient availability. It is known that root and shoot development in vines is strongly affected by soil conditions, shoot development is more in places where the soil is more fertile and can hold more water [27, 56]. It is known that the level of organic matter in the soil has a significant effect on the rooting performance of grapevine cuttings [59]. In this study, it was determined that fertilizations had a positive effect on average root length and root number depending on the manure in both Karaerik and Narince grape varieties, but sheep manure was more effective than cattle manure. In addition, it was determined that different doses of cattle and sheep manure increased shoot growth in grapevine cuttings. In the study, it was found that cattle manure in Karaerik grape cultivar and sheep manure in Narince grape cultivar were more

effective on average shoot growth and average leaf number. Similar to the data we obtained in this study, [60], determined that the addition of organic manures at different doses to fig seedlings had a significant effect on the shoot length of the plants. In addition, [61], in a study investigating the effects of farm manure on the soil, emphasized that the applications provided significant increases in crop yield by promoting vegetative growth of plants. Parallel to previous similar studies, the findings obtained in this study revealed that organic farm manures have significant effects on soil and plant growth.

4. Conclusion

Since organic manures generally improve the physical, chemical and biological properties of the soil, their use in sustainable agriculture is becoming more common every day to meet the nutritional needs. For this purpose, the effects on the rooting and shooting performances of Karaerik and Narince grape varieties were evaluated by applying different doses of organic farm manures from different origins to the soil. In the study, it was revealed that there was a linear development in the root length, root number, shoot length and number of leaves on shoot of both Karaerik and Narince grape varieties, depending on the improvements in the physical properties of the soils due to different manure applications. It was determined that sheep manure was more effective than cattle manure on root length and root number in Karaerik grape cultivar, while cattle manure gave more positive results on shoot length and number of leaves in shoot. Although all doses of cattle manure applied on Narince grape cultivar had positive effects on root length, root number, shoot length and number of leaves shoot, it was determined that sheep manure was more effective than cattle manure in all parameters. As a result, it has been determined that organic farm manures have been very successful in rooting and shoot development of vine cuttings, and it has been found to cause different results in species and varieties according to the origin of the manure.

According to the findings obtained in this study, it is thought that organic farm manures can come to the fore as a successful alternative for rooting vine cuttings in terms of soil health and sustainable agriculture.

Ethics in Publishing

There are no ethical issues regarding the publication of this study.

Author Contributions

Author¹: Conceptualization, data curation, formal analysis, methodology, visualization, writing-original draft, writing-review and editing,

Author^{2*}: Conceptualization, data curation, visualization, writing-original draft, writing-review and editing

All authors have read and agreed to the published version of the manuscript.

The Effects of Cattle and Sheep Manure Applications on Soil Physical Properties and Rooting and Shoot Development of Grapevines Cuttings

References

- [1] Maillard, E., Angers, D.A., (2014) Animal manure application and soil organic carbon stocks: a meta-analysis. *Global Change Biology*, (20) 666-679.
- [2] Liang, Q., Chen, H., Gong, Y., Yang, H., Fan, M., Kuzyakov, Y., (2014) Effects of 15 years of manure and inorganic fertilizers on enzyme activities in particle-size fractions in a North China Plain soil. *European Journal of Soil Biology*, (60) 112-119.
- [3] Garcia-Orenes, F., Roldan, A., Morugan-Coronado, A., Linares, C., Cerda, A., Caravaca, F., (2016) Organic fertilization in traditional Mediterranean grapevine orchards mediates changes in soil microbial community structure and enhances soil fertility. *Land Degrad. Develop.* (27) 1622–1628.
- [4] Li, Z., Wang, M., Yang, Y., Zhao, S., Zhang, Y., Wang, X., (2017) Effect of composted manure plus chemical fertilizer application on aridity response and productivity of apple trees on the loess plateau, China. *Arid Land Research Manage.* (31) 388–403.
- [5] Ali, S., Hayat, R., Begum, F., Bohannan, B.J.M. Inebert, L., Meyer, K., (2017) Variation in soil physical, chemical and microbial parameters under different land uses in Bagrot Valley, Gilgit, Pakistan. *Journal of the Chemical Society of Pakistan*, (39) 97-107.
- [6] Wang, Y., Ge, T., Kuzyakov, Y., Hu, N., Wang, Z.L., Li, Z., Tang, Z., Chen, Wu, Y.C., Lou, Y., (2017) Soil aggregation regulates distributions of carbon, microbial community and enzyme activities after 23-year manure amendment. *Applied Soil Ecology*, (111) 65-72.
- [7] Kiczorowski, P., Kopacki, M., Kiczorowska, B., (2018) The response of Sampion trees growing on different rootstocks to applied organic mulches and mycorrhizal substrate in the orchard. *Sci. Hortic.* (241) 267–274.
- [8] Lin, Y., Ye, G., Kuzyakov, Y., Liu, D., Fan, J., Ding, W., (2019) Long-term manure application increases soil organic matter and aggregation, and alters microbial community structure and keystone taxa. *Soil Biol. Biochem.* (134) 187–196.
- [9] Ye, G., Lin, Y., Kuzyakov, Y., Liu, D., Luo, J., Lindsey, S., Wang, W., Fan, J., Ding, W., (2019) Manure over crop residues increases soil organic matter but decreases microbial necromass relative contribution in upland Ultisols: results of a 27-year field experiment. *Soil Biol. Biochem.* (134) 15–24.
- [10] Bender, D., Erdal, İ., Dengiz, O., Gürbüz, M., Tarakçıoğlu, C., (1998) Farklı Organik Materyallerin Killi Bir Toprağın Bazı Fiziksel Özellikleri Üzerine Etkileri. *International Symposium On Arid Region Soil*. 21-24 September, Menemen-İzmir-Turkey.
- [11] Das, S., Hussain, N., Gogoi, B., Buragohain, A.K., Bhattacharya, S.S., (2016) Vermicompost and farmyard manure improves food quality, antioxidant and antibacterial potential of *Cajanus cajan* (L. Mill sp.) leaves. *J. Sci. Food Agric.* (97) 956–966.
- [12] Stratton, M. L., Barker, A. V., Rechcigl, J. E. (Ed.), 1995. *Soil Amendments and Environmental Quality*. CRC Press, USA, 249-309.

The Effects of Cattle and Sheep Manure Applications on Soil Physical Properties and Rooting and Shoot Development of Grapevines Cuttings

- [13] Tiessen, H., Cuevas, E., Chacon. P., (1994) The role of soil organic-matter in sustaining soil fertility *Nature*, (371) 783-785.
- [14] Manlay, R.J., Feller, C., Swift. M.J., (2007) Historical evolution of soil organic matter concepts and their relationships with the fertility and sustainability of cropping systems. *Agriculture, Ecosystems & Environment*, (119) 217-233.
- [15] Sommerfieldt, T.G., Chang, C., (1985) Changes in Soil Properties Under Annual Applications of Feedlot Manure and Different Tillage Practices. *Soil Sci. Soc. Am. J.* (49) 983-987.
- [16] Xiyang, H., Chi, C., Greg, R. T and Fengrong, Z., (2003) Soil Carbon and Nitrogen Response to 25 Annual Cattle Manure Application. *Journal of Plant Nutrition and Soil Science*. Vol. 166 (2) 239-245.
- [17] Özbek, H., Kaya, Z., Gök, M., Kaptan, H., (1993) *Toprak Bilimi. Ç.Ü.Z.F. Genel Yayın No:73. Ders Kitapları Yayın No:16*, Adana.
- [18] Lewandowski, A, Zumwinkle, M., (1999) *Assessing the Soil System. A Review of Soil Quality Literature*. Minnessota Department of Agriculture Energy and Sustainable Agriculture Program, Boulevard
- [19] Brouwer, J., Powell, J.M., (1995) Soil aspects of nutrient cycling in a manure application experiment in Niger. In *Livestock and nutrient cycling in mixed farming systems of Sub-Saharan Africa*, J.M. Powell et al. (eds.). 1993 Addis Abeba, Ethiopia. (2) 211-226.
- [20] Chatzistathis, T., Papadakis, I.E., Papaioannou, A., Chatzissavvidis, C., Giannakoula, A., (2020) Comparative study effects between manure application and a controlled release fertilizer on the growth, nutrient uptake, photosystem II activity and photosynthetic rate of *Olea europaea* L. (cv. 'Koroneiki'). *Scientia Horticulturae*, 264 (109176).
- [21] Therios, I., (1996) *Mineral Nutrition of Plants*. Dedousi Publications, Thessaloniki In Greek. (75) 191-192.
- [22] Maheswarappa, H. P., Nanjappa, H. V., Hegde, M. R., Prabhu, S.R., (1999) Influence of planting material, plant population and organic manures on yield of East Indian galangal (*Kaempferia galanga*), soil physico-chemical and biological properties. *Indian J. Agron.* 44(3) 651–657
- [23] Meissner, G., Athmann, M.E., Fritz, J., Kauer, R., Stoll, M., Schultz, H.R., (2019) Conversion to organic and biodynamic viticultural practices: impact on soil, grapevine development and grape quality. *OENO One*, 53(4) 639-659.
- [24] Loss, A., Couto, R., Brunetto, G., Veiga M., Toselli, M., Baldi E., (2019) Animal manure as fertilizer: changes in soil attributes, productivity and food composition. *International Journal of Research –Granthaalayah*. 7(9) 307-331.
- [25] Tardaguila, J., Baluja, J., Arpon, L., (2011) Variations of soil properties affect the vegetative growth and yield components of “Tempranillo” grapevines. *Precision Agric* (12) 762–773.

The Effects of Cattle and Sheep Manure Applications on Soil Physical Properties and Rooting and Shoot Development of Grapevines Cuttings

- [26] Cortell, J.M., Halbleib, M., Gallagher, A.V., Righetti, T.L., Kennedy, J.A., (2005) Influence of vine vigor on grape (*Vitis vinifera* L. cv Pinot Noir) and wine proanthocyanidins. *Journal of Agriculture Food Chemistry*, (53) 5798–5808.
- [27] Reynolds, A.G., Senchuk, I.V., van der Reest, C., de Savigny, C., (2007) Use of GPS and GIS for elucidation of the basis for terroir, spatial variation in an Ontario Riesling vineyard. *American Journal of Enology and Viticulture*, (58) 145–162.
- [28] Andreas-de Prado, R., Yuste-Rojas, M., Sort, X., Andreas-Lacueva, C., Torres, M., Rosa, M., (2007) Effect of soil type on wines produced from *Vitis vinifera* L. cv. Grenache in commercial vineyards. *Journal of Agriculture Food Chemistry*, (55) 779–786.
- [29] Crecchio, C., Curci, M., Mininni, R., Ricciuti, P., Ruggiero, P., (2001) Short-term effects of municipal solid waste compost amendments on soil carbon and nitrogen content, some enzyme activities and genetic diversity. *Biology and Fertility of Soils*, 34(5) 311-318.
- [30] Adekiya, A.O., Ejue, W.S., Olayanju, A., (2020) Different organic manure sources and NPK fertilizer on soil chemical properties, growth, yield and quality of okra. *Sci Rep* (10) 16083.
- [31] Polat, A.A., (1990) Investigations on loquat (*Eriobotrya japonica* Lindl.) propagation by air-layering, cutting and different budding methods on various root-stocks. PhD thesis, Cukurova University, Institute of Natural Science, Adana, Turkey, 297
- [32] Hartmann, H.T., Kester, D.E., (2002) Hartmann and Kester's plant propagation: Principles and practices, 1-16, California, USA.
- [33] Smart, D.R., Kocsis, L., Andrew Walker, M., (2002) Dormant Buds and Adventitious Root Formation by *Vitis* and Other Woody Plants . *J Plant Growth Regul* (21) 296–314.
- [34] Wright, J.W., (1976) Introduction to Forest Genetics. Academic Press 463, New York, USA.
- [35] Ürgenç, S., (1982) Orman ağaçları ıslahı. İstanbul Üniversitesi Orman Fakültesi Yayın No: 293, İstanbul, Türkiye.
- [36] USDA (1999) United States Department Of Agriculture. Soil Taxonomy, A Basic System of Soil Classification for Making and Interpreting Soil Surveys. Second Edition.
- [37] Gee, G.W., Bauder, J.W., (1986) Particle-size analysis. In: Klute, A. (Ed.), Methods of soil analysis. Part 1. Physical and mineralogical methods. 2nd edition. American Society of Agronomy. 383-411. Soil Science Society of America, Madison.
- [38] McLean, E.O., (1982) Soil pH and Lime Requirement. In: Page, A. (Ed.), Methods of Soil Analysis Part 2. Chemical and Microbiological Properties. 2nd Edition. Agronomy (9) 199-224.
- [39] Nelson, D.W., Sommers, L.E., (1982) Total carbon, organic carbon, and organic matter. In: Page, A. (Ed.), Methods of soil analysis. part 2. Chemical and Microbiological Properties. Madison, 2nd edition. Agronomy (9) 539-579, 1159 Wisconsin USA.

The Effects of Cattle and Sheep Manure Applications on Soil Physical Properties and Rooting and Shoot Development of Grapevines Cuttings

- [40] Rhoades, J.D., (1982) Soluble salts. In: Page, A. (Ed.), *Methods of Soil Analysis. Part 2. Chemical and Microbiological Properties*. 2nd Edition. Agronomy (9) 167-178, 1159 Madison, Wisconsin USA.
- [41] Kemper W.D., Rosenau R.C., Aggregate stability and size distribution. *Methods of soil analysis. Physical and mineralogical methods*. 2nd edition. Agronomy, 9: 425-442, 1986.
- [42] Blake, G.R., Hartge, K.H., (1986) Bulk density. In A. Klute (ed.), *Methods of Soil Analysis. Part 1*. 2nd ed. Agronomy Monographs. 9. Soil Science Society of America, Madison, 363-382.
- [43] Cassel, D.K., Nielsen, D.R., (1986) Field capacity and available water capacity. In A. Klute (ed.), *Methods of Soil Analysis. Part 1*. 2nd ed. Agronomy Monographs. 9. Soil Science Society of America, Madison, 901-926.
- [44] Kacar, B., İnal, A., (2008) Bitki analizleri, Fen Bilimleri, Nobel Yayın No: 1241, 892.
- [45] Dowdy, S., Wearden, S., (1983) *Statistics for Res.* John Wiley & Sons, Inc. Elazar Volk, USA.
- [46] SPSS (2011) *SPSS for Windows, Version 20*, SPSS Inc., USA.
- [47] Ülgen, N., Yurtsever, N., (1995) Türkiye Gübre ve Gübreleme Rehberi (4.Baskı).Başbakanlık Köy Hizmetleri Genel Müdürlüğü Toprak ve Gübre Araştırma Enstitüsü Müdürlüğü Yayınları. Genel Yayın No: 209. Teknik Yayınlar No:T.66.s.230. Ankara.
- [48] Agbede, T.M., Adekiya, A.O., Ogeh, J.S., (2014) Response of soil properties and yam yield to *Chromolaena odorata* (Asteraceae) and *Tithonia diversifolia* (Asteraceae) mulches. *Arch. Agron. Soil Sci.* 60 (2), 209–224.
- [49] Prasad, B., Sinha, S.K., (2000) Long-Term Effects of Fertilizer and Organic Manures on Crop Yields, Nutrient Balance and Soil Properties in Rice-Wheat Cropping System in Bihar. pp: 105- 119 in *Long-Term Soil Fertility Experiments in Rice-Wheat Cropping Systems*. Rice-Wheat Consortium Paper Series 6. New Delhi, INDIA.
- [50] Conceição, P.C., (2006) *Proteção física da matéria orgânica do solo em solos do Sul do Brasil*. Porto Alegre, Universidade Federal do Rio Grande do Sul,. 145p. (Tese de Doutorado)
- [51] Boeni, M., (2007) *Proteção física da matéria orgânica em Latossolo ssob sistemas com pastagens na região do Cerrado brasileiro*. Porto Alegre, Universidade Federal do Rio Grande do Sul, 136p. (Tese de Doutorado).
- [52] Salton, J.C., Mielniczuk, J., Bayer, C., Boeni, M., Conceição, P.C., Fabrício, A.C., Macedo, M.C.M., Broch, D.L., (2008) Agregação e estabilidade de agregados do solo em sistemas agropecuários em Mato Grosso do Sul. *R. Bras. Ci. Solo*, (32) 11-21.
- [53] Karami, A., Homae, M., Afzalnia, S., Ruhipour, H., Basirat, S., (2012) Organic resource management: impacts on soil aggregate stability and other soil physico-chemical properties. *Agriculture, Ecosystems Environment*,(148) 22-28.

The Effects of Cattle and Sheep Manure Applications on Soil Physical Properties and Rooting and Shoot Development of Grapevines Cuttings

- [54] Yu, H.Y., Ding, W.X., Luo, J.F., Geng, R.L., Cai, Z.C., (2012) Long term application of organic manure and mineral fertilizers on aggregation and aggregate-associated carbon in a sandy loam soil. *Soil and Tillage Research*, (124) 170–177.
- [55] Zhou, H., Peng, X., Perfect, E., Xiao, T., and Peng, G., (2013) Effects of Organic and Inorganic Fertilization on Soil Aggregation in an Ultisol as Characterized by Synchrotron Based X-ray Micro-computed Tomography. *Geoderma* (195) 23–30.
- [56] Van Leeuwen, C., Friant, P., Choné, X., Tregoat, O., Koundouras, S., Dubourdieu, D., (2004) Influence of climate soil and cultivar on terroir. *American Journal of Enology and Viticulture*, (55) 207–217.
- [57] Bodin, F., & Morlat, R., (2006) Characterization of viticultural terroirs using a simple field model based on soil depth. I Validation of the water supply regime phenology and vine vigour in the Anjou vineyard (France). *Plant and Soil*, (281) 37–54.
- [58] Karaman, M.R., Brohi, A.R., Müftüoğlu, N.M., Öztaş, T., Zengin, M., (2012) Sürdürülebilir Toprak Verimliliği. *Koyulhisar Ziraat Odası Kültür Yayınları* (3) 291-294.
- [59] Jaleta, A., Sulaiman, M., (2019) A review on the effect of rooting media on rooting and growth of cutting propagated grape (*Vitis vinifera* L). *World Journal of Agriculture and Soil Science*, 3(4) 1-8.
- [60] Ertan, B., Özen, M., (2019) Organik İncir Fidanı Yetiştiriciliğinde Farklı Ortamların Fidan Kalitesi Üzerine Etkileri. VI. Organik Tarım Sempozyumu 6th Symposium on Organic Agriculture 15-17 Mayıs, İzmir – Turkey.
- [61] Stumpe, H., Garz, J., Schliephake, W., Wittenmayer, L., Merbach, W., (2000) Effects of humus content, farmyard manuring and mineral N fertilization on yield and soil properties in a long term trial. *J. of Plant nutrition and Soil Science*, 163(6) 657- 662.

The Effects of Light Produced in Different Ways on *Triticum aestivum* L. (Wheat) and *Hordeum vulgare* L. (Barley)

Mustafa ŞAHİN^{1*}, Elçin KILIÇ², Etem OSMA³

¹Hamidiye Vocational School of Health Services, University of Health Sciences, İstanbul, Turkey

² Department of Electrical & Electronics Engineering, Graduate School of Natural and Applied Science, Erzincan University, Erzincan, Turkey

³Department of Biology, Faculty of Science and Arts, Erzincan Binali Yıldırım University, Erzincan, Turkey

Received:25/03/2022, Revised: 20/06/2022, Accepted: 27/07/2022, Published: 30/12/2022

Abstract

It produces lights of different qualities with different lighting elements used in agricultural practice. This situation creates different effects on living things. In this study, the effect of incandescence, electric discharge and electroluminescence light, which is the most used light production method in lighting applications, on *Triticum aestivum* L. (Wheat) and *Hordeum vulgare* L. (Barley) was investigated. For this purpose, different lighting environments where sources of light with LED, incandescence, sodium vapor, mercury vapor and metal halide discharge were used were created, and all variables except for the sources of light were kept the same. Wheat and barley plants were grown in these environments, and harvested after 15 days. After the harvesting processes had been completed, wet weight, height, amounts of electrolyte leakage, chlorophyll and carotene amounts, SOD (superoxide dismutase) and (CAT) Catalase enzyme activities were determined. Differences between the plants grown under the light parameters were determined by evaluating the data with SPSS. There were statistically significant differences between the data obtained from wheat and barley grown under different lamps.

Keywords: Artificial light sources, agriculture, *Triticum aestivum* L., *Hordeum vulgare* L.

Farklı Şekillerde Üretilen Işığın *Triticum aestivum* L. (Buğday) ve *Hordeum vulgare* L. (Arpa) Üzerindeki Etkileri

Öz

Tarımsal uygulamada kullanılan farklı aydınlatma elemanları ile farklı niteliklerde ışıklar üretmektedir. Bu durum canlılar üzerinde farklı etkiler oluşturmaktadır. Bu çalışmada, aydınlatma uygulamalarında ışık üretim yöntemlerinden en fazla kullanılan termik, deşarja dayanan ve elektrolüminesans yol ile üretilen ışığın *Triticum aestivum* L. (Buğday) ve *Hordeum vulgare* L. (Arpa) üzerindeki etkisi incelenmiştir. Bu amaçla, LED, enkandesan, sodyum buharlı, civa buharlı ve metal halojenli deşarj ışık kaynaklarının kullanıldığı farklı aydınlatma ortamları oluşturulmuş ve ışık kaynağı haricinde diğer tüm değişkenlerin aynı olması sağlanmıştır. Sonrasında bu ortamlarda buğday ve arpa bitkileri yetiştirilmiş ve 15 gün sonunda hasat edilmiştir. Hasat işlemleri tamamlandıktan sonra bitkilerin yaş ağırlıkları, boyları, elektrolit sızıntı, klorofil ile karoten miktarları, Süperoksit dismutaz (SOD) ve Katalaz (CAT) enzim aktiviteleri belirlenmiştir. Elde edilen veriler SPSS İstatistik Paket Programı'nda değerlendirilerek çalışılan ışık parametreleri altında yetiştirilen bitkiler arasındaki farklılıklar belirlenmiştir. Farklı lambalar altında yetiştirilen buğday ve arpalarda elde edilen veriler arasında istatistiksel olarak anlamlı farklılıklar olduğu gözlenmiştir.

Anahtar Kelimeler: Yapay ışık kaynakları, tarım, *Triticum aestivum* L., *Hordeum vulgare* L..

1. Introduction

Light has been an irreplaceable source of energy since the existence of humanity, and the need for light increases daily. In order to provide sustainable light sources when the sun was not enough for lighting, people invented artificial sources of light [1]. Artificial light sources are used for many purposes. Venue design, environmental luminance, plant growth rooms, among others are examples of intended uses with different purposes and functions [2]. Artificial light is generally produced via three different light production methods. These are produced via incandescence, an electrical discharge [3] and electroluminescence [4]. The foundation for light production methods is based on the principle of conversion of electric energy to light. Since each of these light production methods differs from one another, each source of light has different physical and structural properties [5].

Producing light via the incandescence method is the oldest known method. Electrical current is conducted through a metal wire in the lamp and light is obtained when the metal wire becomes incandescent in this method of production [6]. The first incandescent lamp was researched by H. Goebel in 1854, and T. Edison invented lightbulbs in 1879, which have been technologically improved until the present day [7].

In the method based on electrical discharge, the gas between the two plates in the lamp starts to ionise by interacting, and light is produced. Radiation for this production method occurs in two ways: in the visible wavelength zone or in the ultraviolet radiation zone. Discharge lamps are described as low-pressure lamps or high-pressure lamps in accordance with the pressure of the gas in the tube. Discharge lamps need auxiliary sources during operation. Therefore, they are operated with ballast and ignitor [8]. The purpose of the ballasts used in discharge lamps is to prevent the current from short-circuiting by limiting ionization, in other words, discharge current [9]. It is quite important for a discharge lamp to be suitable for the ballast and it is preferred for ballasts to be electronic and electromagnetic [10]. If the current provided by the ballast is less than it should be, it causes inefficient current to be conveyed to the lamp. This leads the lamp to illuminate inefficient luminous flux and causes it not to reach the necessary brightness [11]. Therefore, it is important to pay attention to the compatibility of lamps and ballast. These blasters, called starters or ignitors, are electronic devices, which provide suitable voltage and energy to start and maintain luminescence discharge [12].

Light production with the electroluminescence method was developed in recent years as solid-state semiconductor-based devices. This method is where electric energy is converted into direct luminous energy [13]. LEDs, which produce light through this method, are small and durable. LED, which means light-emitting diode, is a semiconductor-based lighting equipment

consisting of semiconductor equipment, called n-types or p-types, which have undergone some processes. The property that distinguishes LEDs from other diodes is that they emit light through photons in p-n joint parts [14].

In addition to other environmental parameters, plants need substantial amounts of light. Light affects the physiological development of plants as well as the formation of blooming and floral organs and the morphology of organs. Briefly stated, plants need light for growth, development and various metabolic purposes. Applying insufficient light has some negative impacts on plants as does having excess light [15]. The sources of light that are needed for plant development can be the sun or artificial lights [16].

The beams emitted by the sun to the earth have various wavelengths. The light spectrum contains a wide range of wavelengths including infrared, visible light and ultraviolet [17]. The range that plants use for photosynthesis includes the 390–760 nm wavelengths [18]. Besides being a source of energy for plants used for photosynthesis, light is a factor that affects various developmental processes [19]. Photosynthesis, a photochemical process, is a function of wavelength of the light source. The speed of photosynthesis depends on both wavelengths and the addition of light sources with different wavelengths can cause photosynthesis speed to increase. Consequently, this situation is an important aspect when it comes to artificial lighting [20].

The lives of all living creatures depend on green plants that photosynthesise. Therefore, plants form the basic level of most food chains. Leaves are the main organ of plants that have an effective part in photosynthesis [21]. The most important pigment of plants that is used in photosynthesis is chlorophyll [22]. Chlorophyll generates the carbohydrates, which have the most significant role in the growth and development of plants using sunlight [23]. There are eight different chlorophylls in plants, and the most important ones are chlorophyll a and chlorophyll b. Light is a basic need for these coloured pigments to function. Chlorophylls absorb photons at certain wavelengths of 430 nm (blue) and 662 nm (red) while the green color is reflected strongly [24].

In this study, the effects of the placement of artificial sources of light and light production methods on agricultural production and the effects of light on plants were analysed. The lengths, wet weights, electrolyte leakage, chlorophyll and the activities of CAT and SOD enzyme plants were investigated and analysed.

2. Material and Methods

Fertile soil mixed with manure from the fields where agriculture activities have been performed and seeds of wheat (*T. aestivum* L.) and barley (*H. vulgare* L.) that can be easily grown in a laboratory environment were used in the study. Soil, consisting of 25% of perlite, and 25% of manure, was prepared. Then 750 g of this mixture was put into 1kg plastic pots. Three pots each were prepared with seeds of barley and wheat for each source of light application. After the seeds to be planted had been weighed, 7 g of wheat or 5 g of barley were planted in each pot. Next, the seeds were covered with 100 g of soil. The pots were placed under incandescent lamps, LEDs, metal halide discharge lamps, sodium vapour lamps or mercury vapour discharge lamps (Table 1). Since wheat and barley are long-day plants, they were subjected to 13–14 hours of light exposure [25]. After germination, the plants were grown and harvested, barley after 11 days and wheat after 15 days, by being cut at the soil surface. The lengths of the plants, which had been grown under five different lighting mechanisms, were determined and their wet weight values were measured. Then, samples were collected from harvested plants, and amounts of electrolyte leakage, chlorophyll, carotene, CAT and SOD enzyme activities values were determined.

Table 1. Lamp Parameters

Lamp Types	Lamp Power (W)	Color correlated temperature - CCT (°K)	Illumination level (Lux)
Sodium Vapor	70	2003	1548
Incandescent	42	2759	279
Metal Halogen	400	5767	6082
LED	18	6729	475
Mercury Vapor	125	3985	3076

Determination of Electrolyte Leakage

First, each of the 12 test tubes received 0.1 g of fresh plant material taken from plant leaves. The tubes were then filled with 4 mL of distilled water and stored at 4 °C for 1 day. An electrical conductivity meter was then used to quantify the levels of ions in distilled water from the samples collected to determine cell damage [26].

Determination of Chlorophyll and Carotenoid

First, 0.5 g of harvested leaves was placed in a porcelain mortar and ground in the porcelain mortar to homogenize in 20 mL of 80% acetone. The mixture was filtered through filter paper

and placed in a centrifuge tube that was filled up to 10 mL. The solution was then centrifuged for 10 minutes. Finally, the absorbance values of the resulting combination at 663, 646, and 440 nm were determined individually using a spectrophotometer.

The following formulas were used to calculate the amount of chlorophyll:

$$\text{Chl}_a = 12.25 A_{663} - 2.55 A_{646}$$

$$\text{Chl}_b = 20.31 A_{646} - 4.91 A_{663}$$

$$\text{Chl}_a + \text{Chl}_b = 17.76 A_{646} + 7.34 A_{663}$$

$$\text{Carotenoid (Car)} = 4.69 A_{440} - 0.267 \text{Chl}_{a+b}$$

The results were obtained as mg mL^{-1} [27, 28].

Antioxidant Activity

After weighing 0.5 g of tissue and placing it in the porcelain mortar, 5 mL of cold homogenate buffer (0.1 M KH_2PO_4 at pH 7.0 with 1% PVP and 1 mM EDTA) was added. The mixture was transferred to a centrifuge tube and centrifuged for 15 minutes at 15000 g and 4 °C. The supernatant antioxidant produced from centrifugation was employed as a source for enzyme activity deaths [29]. Whether the plants were under stress physiologically was assessed by measuring antioxidant enzyme (superoxide dismutase, catalase, and peroxidase) activities in response to increases in reactive oxygen species during watering and soil stress conditions. Each antioxidant enzyme had its own set of substances and methodologies [30].

Catalase Enzyme Activity

The method was used to determine the activity of Catalase (CAT). This method of measuring activity is based on the premise of seeing a drop in absorbance in a CAT activity measurement setting when H_2O_2 is transformed into O_2 and H_2O at 240 nm [31]. A 5 mM H_2O_2 solution was used to assess catalase activity in the extraction solution derived from plant samples. Following the addition of 103.5 mM of KH_2PO_4 buffer and 40 mM of H_2O_2 substrate solution to 3 mL quartz vials, 20 L of enzyme extract from leaves and 50 L of enzyme extract from roots were added. The absorbance of the vial against a blank was observed at 240 nm for 3 minutes at 1 minute intervals after it was placed in the spectrophotometer. The absorbance per minute was estimated from the point where the absorbance dropped linearly. A standard curve was used to convert these average absorbance values into mol H_2O_2 . One enzyme unit was identified as the amount of enzyme that reduced absorbance by 1 mol at 25 °C in 1 minute, and the results are provided as enzyme units per gram of tissue (EU g^{-1} tissue) [31, 32].

Superoxide Dismutase Enzyme Activity

The inhibition of the photochemical reduction of nitro blue tetrazolium (NBT) by superoxide dismutase (SOD) activity was determined spectrophotometrically [33]. 3.84 mL

spectrophotometer vials were filled with a reduction mixture containing 50 mM of KH_2PO_4 (pH 7.8), 13 mM of methionine, 75 M of NBT, 2 M of riboflavin, and 0.1 mM of EDTA or 2.84 mL of a comparable reduction mixture that did not contain riboflavin. The mixture was then pipetted with 100 mL of enzyme extract. After pipetting and mixing 60 mL of 100 mL of riboflavin solution into the tube, the reaction was begun by placing the tube under a white light source. The color fading density of NBT was measured in 15 minutes against a blank at 560 nm. The blank was an enzyme-free sample that went through the same procedure. The amount of enzyme producing 50% inhibition of NBT reduction detected at 560 nm was recognized as one enzyme unit in this analysis, and values were determined as EU g^{-1} tissue [32].

Statistical evaluations were then performed using data obtained from this study. Average values of data and standard errors were calculated using SPSS 22 at a 95% confidence interval.

3. Result and Discussion

Significant data was obtained for wheat and barley are grown under five different lighting mechanisms. When the data were evaluated, the average weight measurement was 13.5–19 g in barley, and 13–18 g in wheat. The weight was at its lowest under the metal halide lamp for both of the plants (Fig. 1). When length data was evaluated, it was 12.2–13.7 cm in barley, and 13–18 cm in wheat (Fig. 1). Plant length was also at its shortest under the metal halide lamp for both of the plants. Electrolyte leakage from barley was $63.63 \pm 6.5 \mu\text{S cm}^{-1}$ to $115 \pm 7.7 \mu\text{S cm}^{-1}$. This value was $53.33 \pm 3.1 \mu\text{S cm}^{-1}$ to $82.27 \pm 3.65 \mu\text{S cm}^{-1}$ in wheat (Fig. 1).

Chlorophyll a values of barley were $7.68 \pm 0.21 \text{ mg mL}^{-1}$ to $13.54 \pm 0.06 \text{ mg mL}^{-1}$, and the values of wheat were $9.73 \pm 0.24 \text{ mg mL}^{-1}$ to $14.49 \pm 0.4 \text{ mg mL}^{-1}$ (Fig. 2). Chlorophyll b values of barley were $4.56 \pm 0.44 \text{ mg mL}^{-1}$ to $6.28 \pm 0.12 \text{ mg mL}^{-1}$, and the values for wheat were $4.41 \pm 0.13 \text{ mg mL}^{-1}$ to $6.41 \pm 0.26 \text{ mg mL}^{-1}$ (Fig. 2). When chlorophyll a + b values were evaluated, these values were $12.25 \pm 0.64 \text{ mg mL}^{-1}$ to $19.83 \pm 0.18 \text{ mg mL}^{-1}$ for barley and $14.06 \pm 0.50 \text{ mg mL}^{-1}$ to $20.75 \pm 0.86 \text{ mg mL}^{-1}$ for wheat (Fig. 2). Regarding carotene values, they were $8.40 \pm 0.99 \text{ mg mL}^{-1}$ to $19.8 \pm 0.45 \text{ mg mL}^{-1}$ for barley and $10.12 \pm 0.87 \text{ mg mL}^{-1}$ and $20.22 \pm 0.82 \text{ mg mL}^{-1}$ for wheat (Fig. 3).

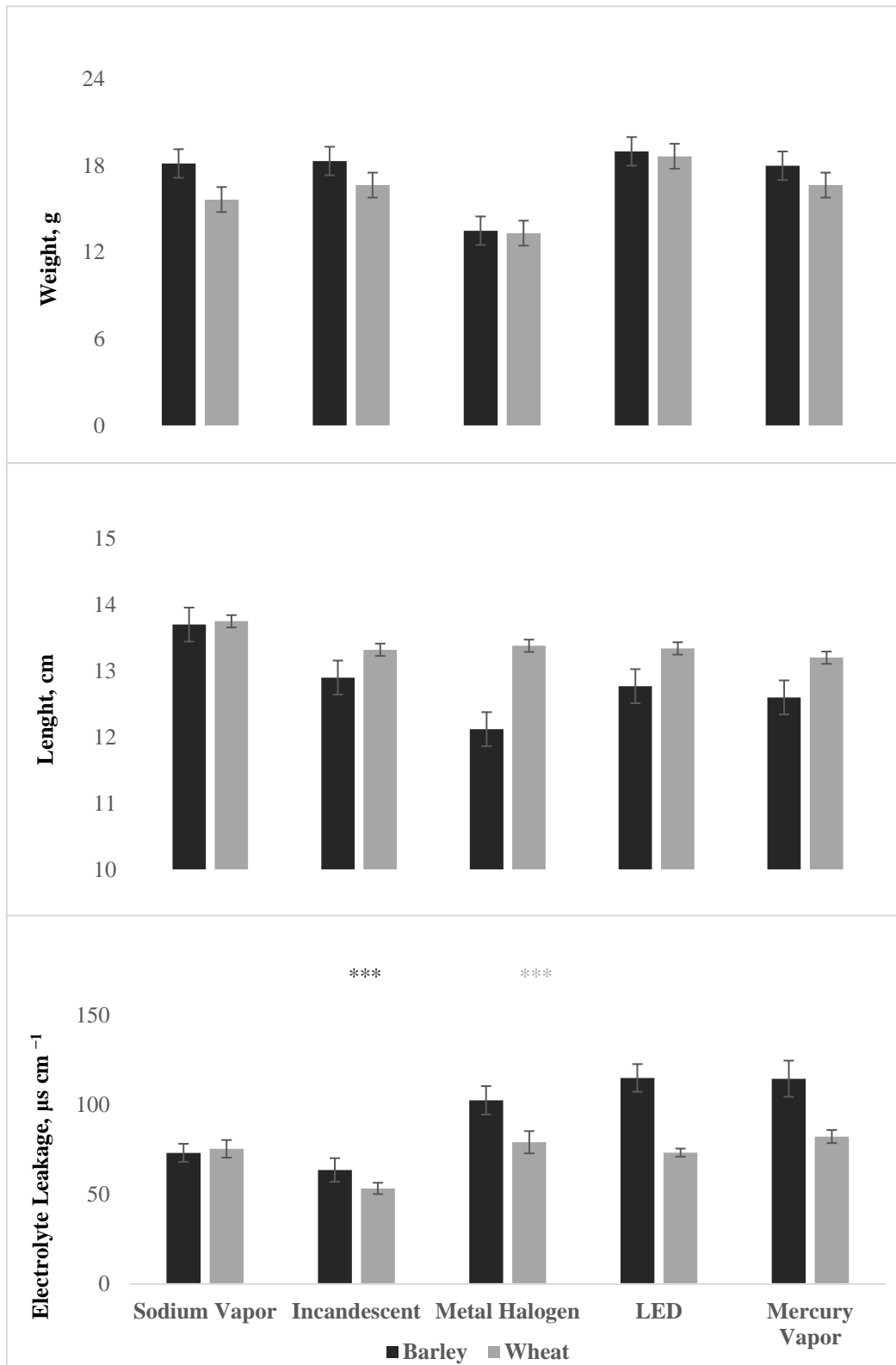


Figure 1. Weights, length and amount of electrolyte leakage barley and wheat plants grown under different light sources (* $p < 0,05$; ** $p < 0,01$; *** $p < 0,001$ significant).

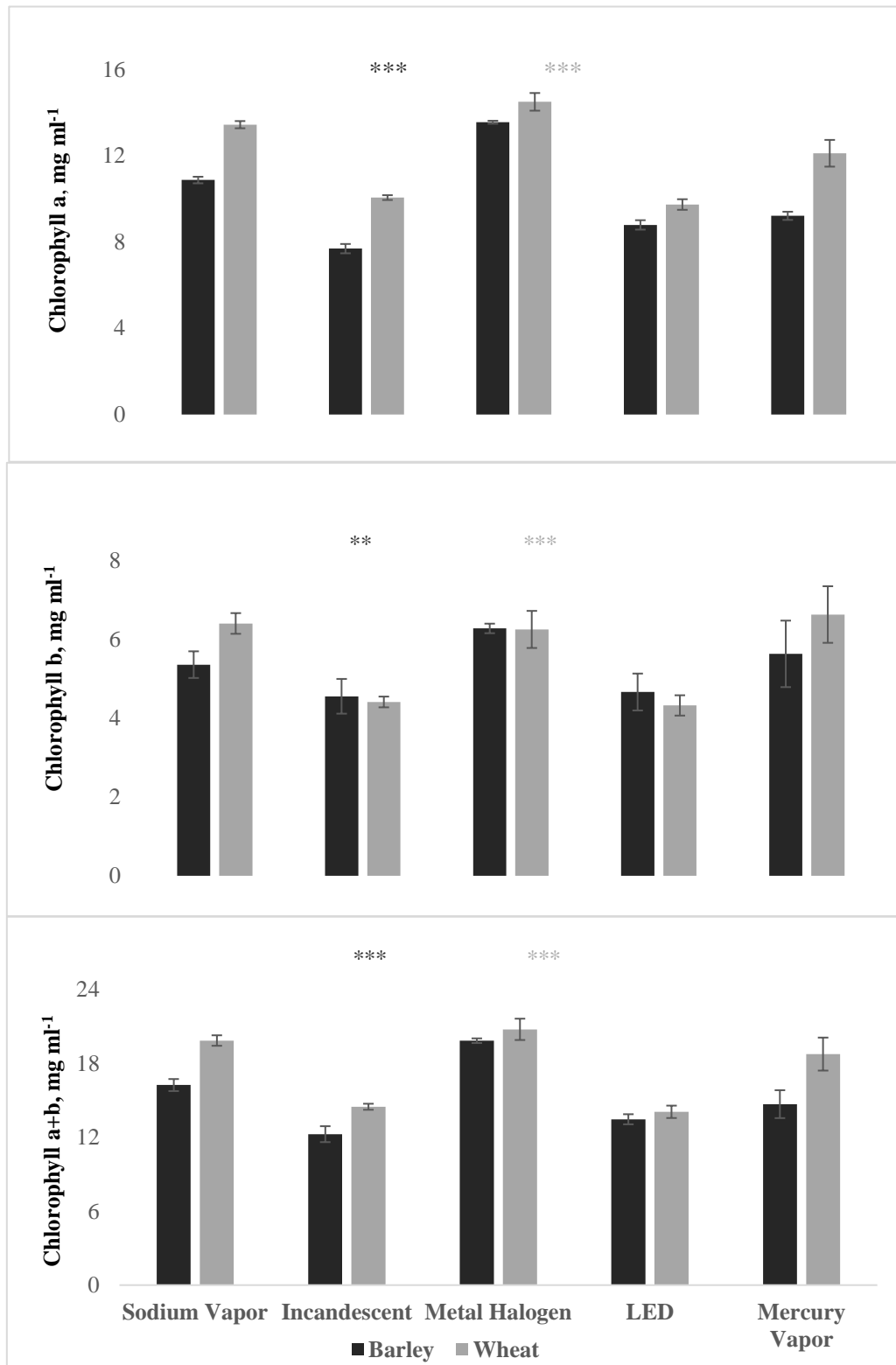


Figure 2. Chlorophyll a, chlorophyll b, chlorophyll a + b amounts of barley and wheat plants grown under different light sources (* $p < 0,05$; ** $p < 0,01$; *** $p < 0,001$ significant).

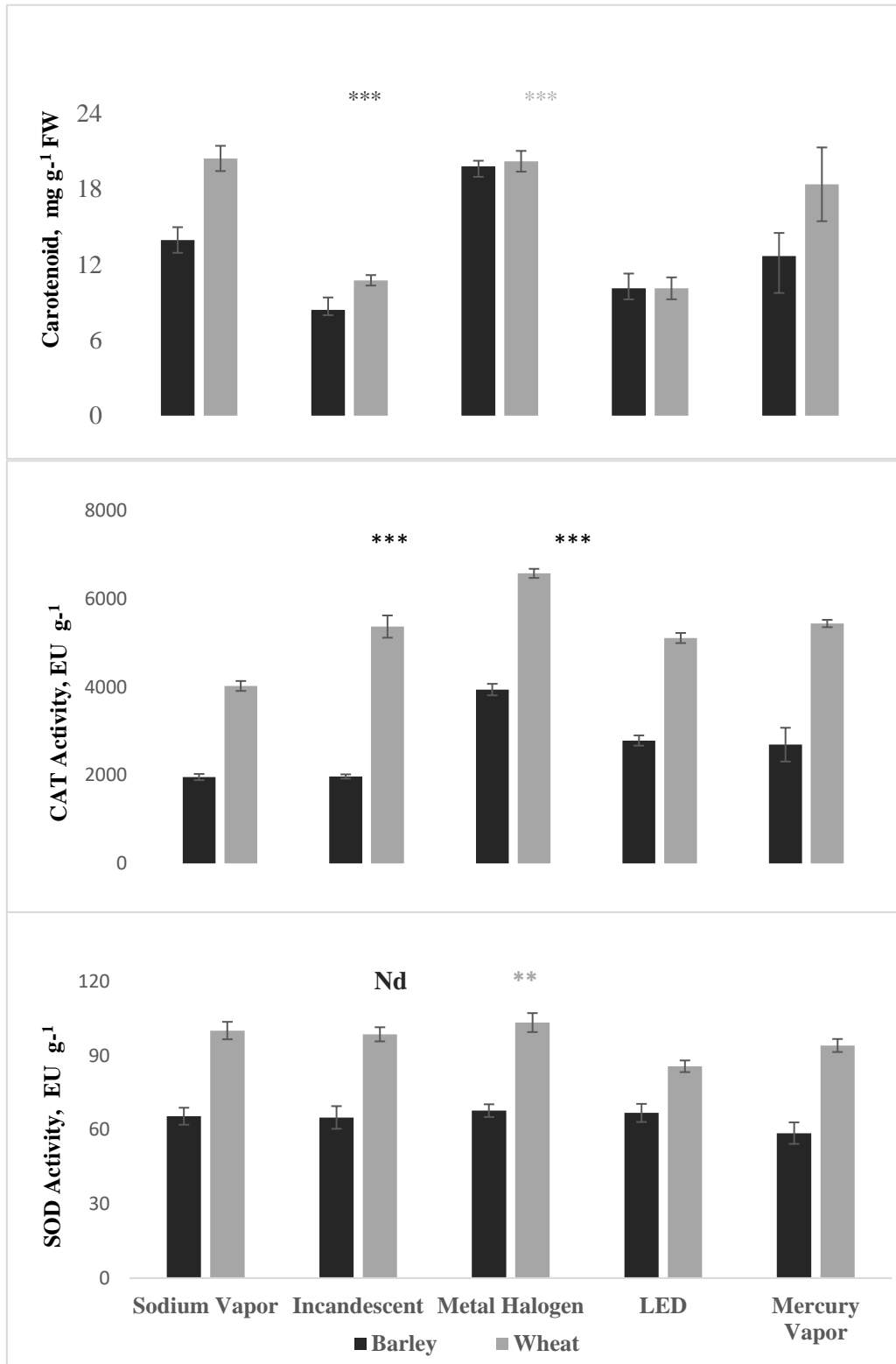


Figure 3. Carotenoid, CAT and SOD enzyme activity of barley and wheat plants grown under different light sources (* $p < 0,05$; ** $p < 0,01$; *** $p < 0,001$ significant).

Catalase data for the barley was 1960–3945 EU g⁻¹ and 4028–6583 EU g⁻¹ for wheat. SOD enzyme activity for the barley was 58.62–67.73 EU g⁻¹, and for wheat 85.6675–103.3397 EU

g⁻¹ for wheat (Fig. 3). When the length and weight data of the plants grown under the lamps were compared, the values for plants grown under metal halide lamps were lower than those of plants grown under other light sources. The amounts of chlorophyll a and b and carotene were at their highest under metal halide lamps and they were at their lowest under incandescent lamps.

The amount of electrolyte leakage was lower under incandescent lamps compared to other sources of light. CAT and SOD enzyme activities were higher in barley and wheat that were grown under metal halide lamps. In conclusion, since the light intensity of metal halide lamps was higher, the amount of chlorophyll in plants was also higher. In addition, the increase in the temperature of the environment due to the intensity of the light caused negative impacts on the development of plants. Therefore, it is necessary to consider the distance of lighting while using artificial lights for growing plants.

Unlike other studies in the literature that were based on different production methods of light, this study has examined the effects of the light produced by various methods, on barley and wheat. Aydınşakir (2005) [34] analysed the development of goldenrod under incandescent and sodium vapour lamps and determined that the use of sodium vapour lamps led to the best results in yield, length of the stalk and bunch, stem diameter, flower offshoot and wet weight values of the plants. Demirsoy et al. (2016) [35] analysed proportional leaf weight, proportional stem weight, proportional root weight, leaf zone, leaf thickness, specific leaf zone and proportional leaf zone parameters of eggplant (*Solanum melongena* L.) seedlings during two different periods (autumn and spring) with three different sources of light (high-pressure sodium vapour lamp (HPS), incandescence lamp (IL) and light-emitting diode (LED)). They determined that artificial lighting applications increased the proportional stem weights and proportional leaf weights of eggplant seedlings. When lengths of eggplant seedlings were compared, those grown under incandescent lamps had the shortest length for both periods. Uzun (1996) [36] stated that change in eggplant plant length increased linearly with heat and curvilinearly with light. Kandemir (2005) [37] confirmed that when the intensity of the light increased, the plants became shorter and stem diameter increased, and they determined that the formation of plants with thin stems occurred in low light. Islam et al. (2012) [38] compared LED and traditional high-pressure sodium vapour lamps while growing *Euphorbia pulcherrima*. Plants grown both in greenhouses and in plant growth rooms were compared in terms of both high-pressure sodium vapour lamp and LEDs; plants grown under LEDs were 20–34% shorter. Mitchell et al. (2015) [39] analysed a number of characteristics and effects related to incandescence lamps, metal halide lamps, fluorescent lamps, high-pressure sodium vapour discharge lamps and LED

sources of light that are commonly used on garden plants, on plants under separate titles in his collection. They concluded that high-pressure sodium vapour lamp increased the yield and quality of tomatoes and increased the numbers and zones of leaves per seedling of tomatoes, pepper, cucumber and eggplant. Sumarni et al. (2022) [40] investigated the effects of red-blue LED and white fluorescent lamps on the growth and yield of aroponic potato seeds grown in the highlands. Artificial lighting was applied to on the plant at 110 cm, 120 cm and 130 cm distances. As a result of the experiments, it was observed that the red-blue LED lamp combination with a height of 110 cm had the highest efficiency. Yeh and Chung (2009) [41] mentioned that fluorescent, high-pressure sodium vapor, metal halogen lamps and incandescent lamps have long been used in tissue culture and growth chambers. And with that, they examined the potential of LEDs in indoor plant growing. As a result, they suggested that LEDs, which provide higher energy efficiency, are the primary light source. Köksal (2013) [42] used artificial lighting with red-orange LED light and determined that there were statistical differences in terms of plant height, biomass weight, number of flowers and leaves.

With the help of technology currently under development, the technological progress in artificial lights has enabled more opportunities for studies in the field of plant biology. Applying lower light intensity to plants has a limiting impact on photosynthesis as does apply applying high amounts of light above critical value. A suitable lighting source should be provided through artificial lighting for plant growth. In this way, the technical properties of light sources are quite important. In order to utilise productivity in agricultural production ideally, studies need to be continued to understand the interaction of the quality of light and other environmental parameters.

4. Conclusion

In this study, the effects of three commonly used sources of light on wheat and barley were analysed, and the data obtained corresponded with previous literature. The following results can be withdrawn from this study:

The effect of lower intensity light on plants has a limiting impact on photosynthesis as does apply high amounts of light above a critical light intensity value. Suitable lighting source should be provided through artificial lighting methods for improved growth in wheat and barley plants. For the maximum weight and length of wheat and barley plants, sodium vapour, incandescent lamps and LEDs perform better than those of other sources of lighting, respectively. Carotenoid levels and SOD activity in both plants are mainly improved with sodium vapour lamps whereas CAT activity was dominantly influenced by metal halogen lights especially effective on wheat

plant. Chlorophyll levels (i.e. a, b and a+b) improve mainly with sodium vapour and metal halogen lamps irrespective of the type of plant.

Ethics in Publishing

There are no ethical issues regarding the publication of this study.

References

- [1] Şahin M., Oguz Y., Buyuktumturk F., (2015). Approximate and Three-Dimensional Modeling of Brightness Levels in Interior Spaces by Using Artificial Neural Networks, *Journal of Electrical Engineering and Technology*, 10, 1822-1829.
- [2] Nikoudel, F., Mahdavinejad, M., Vazifehdan, J., (2018). Nocturnal architecture of buildings: interaction of exterior lighting and visual beauty, *Light & Engineering*, 26(1).
- [3] Lister, G. 2018. Gas discharge lamps—a requiem.
- [4] Karlicek, R., Sun, C. C., Zissis, G., Ma, R. (Eds.), (2017). *Handbook of advanced lighting technology*, Springer.
- [5] Craver, J. K., Boldt, J. K., Lopez, R. G., (2019). Comparison of supplemental lighting provided by high-pressure sodium lamps or light-emitting diodes for the propagation and finishing of bedding plants in a commercial greenhouse, *Hortscience*, 54(1), 52–59.
- [6] Cole, L., Hoggatt, L. R., Sterrenberg, J. A., Suttmiller, D. R., Penney, W. R., Clausen, E. C., (2018). A Transient experiment to determine the heat transfer characteristics of a 100 W incandescent light bulb, operating at 48 W. *Fluid Mechanics and Heat Transfer: Inexpensive Demonstrations and Laboratory Exercises*, 179.
- [7] Habich, N., Homeyer, I. K., (2018). *Untersuchung zur vermeidung der blaulichtanteile bei der hintergrundbeleuchtung von displays unter einatz von LED-Clustern mit steuerbarem farbspektrum (Doctoral dissertation, Universität Hildesheim)*.
- [8] Ponce-Silva, M., Aqwi, J. A., Osorio, R., & Lozoya-Ponce, R. E., (2018). Starting circuit adapted to stabilize hid lamps and reducing the acoustic resonances, *IEEE Transactions on Power Electronics*.
- [9] Gavrilov, S. A., Gavrish, S. V., Puchnina, S. V., (2019). Investigation of processes in glass-ceramic solders of sapphire-niobium seals in gas-discharge lamps, *Glass and Ceramics*, 1-5.
- [10] Shahzad K., Čuček, L., Sagir, M., Ali, N., Rashid, M.I., Nazir, R., Nizami, A.S., Al-Turaif, H.A., Ismail, I.M.I., (2018). An ecological feasibility study for developing sustainable street lighting system, *Journal of Cleaner Production*, 175, 683-695.

- [11] Pena-Garcia, A., & Sędziwy, A., (2019). Optimizing lighting of rural roads and protected areas with white light: a compromise among light pollution, energy savings, and visibility, *Leukos*, 1-10.
- [12] Kwok, K.F., Cheng, K.W.E., Ping, D., (2006). General study for design the HID ballasts, 2nd International Conference on Power Electronics Systems and Applications, 182-184.
- [13] Cox, G., (2019). *Fundamentals of fluorescence imaging*, Pan Stanford.
- [14] Dupuis, R. D., Krames, M. R., (2008). History, development, and applications of high-brightness visible light-emitting diodes. *Journal of Lightwave Technology*, 26(9), 1154-1171.
- [15] Vialet-Chabrand, S., Matthews, J.S.A., Simkin, A.J., Raines, C.A., Lawson, T., (2017). Importance of fluctuations in light on plant photosynthetic acclimation, *Plant Physiology*, 173(4), 2163-2179.
- [16] Ohasi-Kaneko K., Takase M., Kon N., Fujiwara K., Kurata K., (2007). Effect of light quality on growth and vegetable quality in leaf lettuce, spinach and komatsuna, *Environmental Control in Biology*, 45, 189-198.
- [17] McCree, K.J., (1973). A Rational approach to light measurements in plant ecology. *Current Advances in Plant Science*, 3(4), 39-43.
- [18] Zhu, XG., Long, S.P., Ort, D.R., (2008). What is the maximum efficiency with which photosynthesis can convert solar energy into biomass?, *Current Opinion in Biotechnology*, 19(2), 153-159.
- [19] Galvao, V. C., Fankhauser, C., (2015). Sensing the light environment in plants: photoreceptors and early signaling steps, *Current Opinion in Neurobiology*, 34, 46-53.
- [20] Van Iersel, M.W. Weaver, G. Martin, M.T. Ferrarezi, R.S. Mattos, E. Haidekker, M., (2016). A chlorophyll fluorescence-based biofeedback system to control photosynthetic lighting in controlled environment agriculture, *Journal of the American Society for Horticultural Science*, 141, 169–176.
- [21] Taiz, L., Zeiger, E., (2008). *Plant Physiology*, Palme Yayıncılık, Ankara.
- [22] Çetin, M., (2016). Changes in the amount of chlorophyll in some plants of landscape studies, *Kastamonu Univ. Journal of Forestry Faculty*, 16(1), 239-245.
- [23] Tanaka, Y., Sasaki, N. and Ohmiya, A. (2008) Biosynthesis of Plant Pigments: Anthocyanins, Betalains and Carotenoids, *Plant Journal*, 54, 733-749.
- [24] Demirtaş, M.N., Kırnak H., (2009). Effects of different irrigation systems and intervals on physiological parameters in apricot, *Yuzuncu Yıl University Journal of Agricultural Sciences*, 19(2), 79-83.

- [25] Keddy, P. A., (2017). Plant ecology, Cambridge University Press.
- [26] Griffith M., Ala P., Yang DS., Hon WC., Moffatt BA., (1992). Antifreeze protein produced endogenously in winter rye leaves, *Plant Physiology*, 100(2), 593-596.
- [27] Porra, R.J., Thompson W.A., Kriedemann P.E., (1989). Determination of accurate extinction coefficients and simultaneous equations for assaying chlorophylls a and b extracted with four different solvents: verification of the concentration of chlorophyll standards by atomic absorption spectroscopy, *Biochimica et Biophysica Acta (BBA)-Bioenergetics*, 975(3), 384-394.
- [28] Osma, E., İlhan, V., Yalçın, İ.E., (2014). Heavy metals accumulation causes toxicological effects in aquatic *Typha domingensis* Pers, *Brazilian Journal of Botany*, 37, 461–467
- [29] Angelini, R., Federico, R., (1989). Histochemical evidence of polyamine oxidation and generation of hydrogen peroxide in the cell wall. *Journal of Plant Physiology*, 135, 212-217.
- [30] Osma, E., Cigir, Y., Karnjanapiboonwong, A., Anderson, TA., (2018). Evaluation of selected pharmaceuticals on plant stress markers in wheat, *International Journal of Environmental Research*, 12, 179–188.
- [31] Havir, E. A., & McHale, N. A., (1987). Biochemical and developmental characterization of multiple forms of catalase in tobacco leaves, *Plant Physiology*, 84(2), 450-455.
- [32] Osma, E., Cigir, Y., Karnjanapiboonwong, A., Anderson, TA. 2018. Evaluation of selected pharmaceuticals on plant stress markers in wheat, *International Journal of Environmental Research*, 12, 179–188.
- [33] Agarwal, S., Pandey, V., (2004). Antioxidant enzyme responses to NaCl stress in *Cassia angustifolia*. *Biologia Plantarum*, 48(4), 555-560.
- [34] Aydınşakir, K., Özkan, H., Karagüzel, Ö., Kaya, A., (2005). The effects of different artificial light sources on yield and quality characteristics of goldenrod (*Solidago x hybrida* ‘tara’), *Akdeniz University Journal of the Faculty of Agriculture*, 18(3), 377-384.
- [35] Demirsoy, M., Balkaya, A., Uzun, S., (2016). The Effect of different light sources and artificial colour treatments on eggplant (*Solanum melongena* L.) seedling growth parameters, *Selcuk. Journal of Agricultural Sciences*, 3(2), 238-247.
- [36] Uzun, S., (1996). The quantitative effects of temperature and light environment on the growth, development and yield of tomato and aubergine. PhD Thesis, The University of Reading (Unpublished), England.
- [37] Kandemir, D., (2005). The quantitative effects of temperature and light environment on the growth, development and yield of pepper (*Capsicum annuum* L.) grown in

- greenhouses. PhD Thesis, Ondokuz Mayıs University, Institute of Science and Technology, Samsun.
- [38] Islam, M. A., Kuwar, G., Clarke, J. L., Blystad, D. R., Gislerød, H. R., Olsen, J. E., & Torre, S., (2012). Artificial light from light emitting diodes (LEDs) with a high portion of blue light results in shorter poinsettias compared to high pressure sodium (HPS) lamps, *Scientia Horticulturae*, 147, 136-143
- [39] Mitchell, C. A., Dzakovich, M. P., Gomez, C., Lopez, R., Burr, J. F., Hernández, R., Bourget, C. M., (2015). Light-emitting diodes in horticulture, *Horticultural Reviews*, 43, 1-87.
- [40] Sumarni, E., Soesanto, L., Purnomo, W.H., Priswanto., (2022). The effect of light distance on aeroponic potato seed production in tropical high land, *Jurnal Teknik Pertanian Lampung*, 11(1), 99-109.
- [41] Yeh, N., Chung, J., (2009). High-brightness LEDs energy efficient lighting sources and their potential in indoor plant cultivation, *Renewable and Sustainable Energy Reviews*, 13(8), 2175-2180.
- [42] Köksal, N., İncesu, M., Teke A., (2013). Effects of LED Lighting on Plant Development of Tomato, *Research Journal of Agricultural Sciences*, 6(2), 71-75.

Structural, Surface and Optical Characterization of ZnO Thin Films Deposited by SILAR and Spin-Coating Methods

Melih Özden^{1*} and Çağlar Duman²

^{1*}Department of Electrical and Electronics Engineering, Erzincan Binali Yıldırım University, Erzincan, Turkey

²Department of Electrical and Electronics Engineering, Erzurum Technical University, Erzurum, Turkey

Received: 11/04/2022, Revised: 07/07/2022, Accepted: 17/07/2022, Published: 30/12/2022

Abstract

In this study, ZnO thin films were deposited on (1 1 1) oriented n-type and (1 0 0) oriented p-type Si substrates using SILAR and spin-coating methods, respectively. The XRD, SEM, and PL measurements of the samples were performed. The XRD results showed the presence of ZnO peaks. The SEM results showed that the surfaces were homogeneous in both methods. The PL results showed that the samples emitted light at different wavelengths. The PL results under different powers were interpreted from the samples, and it was determined that this sample reached a higher emission intensity with increasing excitation power.

Keywords: ZnO, SILAR, spin-coating, thin-film

SILAR ve Dönel Kaplama Yöntemleri Kullanılarak Büyütülen ZnO İnce Filmlerin Yapısal, Yüzeysel ve Optik Karakterizasyonu

Öz

Bu çalışmada, ZnO ince filmler sırasıyla (1 1 1) yönelimli n-tipi ve (1 0 0) yönelimli p-tipi Si altlıklar üzerine SILAR ve dönel kaplama (spin-coating) yöntemleri kullanılarak büyütülmüştür. Numunelerin XRD, SEM ve PL ölçümleri alınmıştır. XRD sonuçları, ZnO piklerinin varlığını göstermiştir. SEM sonuçları, yüzeylerin her iki yöntemde de homojen olduğunu göstermiştir. PL sonuçları, numunelerin farklı dalga boylarında ışık yaydığını göstermiştir. Örneklerden farklı güçler altında PL ölçümleri alınmış ve yorumlanmış ve bir örneğin artan uyartım gücü ile daha yüksek bir emisyon yoğunluğuna ulaştığı tespit edilmiştir.

Anahtar Kelimeler: ZnO, SILAR, dönel kaplama, ince film

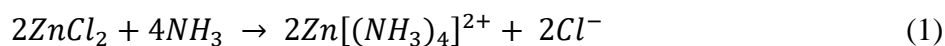
1. Introduction

Zinc oxide (ZnO) is a II-VI group compound and is a direct band semiconductor with high electrical conductivity and a bandgap of approximately 3.2-3.3 eV at room temperature [1-2]. One of the most significant advantages of ZnO is its high exciton binding energy (60 meV) [3]. In addition, it is a significant advantage that it is a material resistant to particle radiation damage [4]. Owing to these properties, ZnO has been used in solar cells, transparent conductive films, chemical sensors, varistors, LEDs, ultraviolet photodetectors, laser diodes, and gas sensors [5]. Various methods have been developed such as chemical vapor deposition (CVD) [6], RF magnetron sputtering [7], pulsed laser deposition [8], spray pyrolysis [9], metal oxide chemical vapor deposition (MOCVD) [10], electrochemical deposition [11], chemical bath deposition (CBD) [12], spin-coating [13-15] and successive ionic layer adsorption and reaction (SILAR) [16-18]. In this study, the spin-coating and SILAR methods were preferred for the deposition of ZnO thin films because these methods are simple, economical and more easily accessible than other methods. The remainder of this paper is organized as follows. In Section 2, the stages of the SILAR and spin-coating methods are described in detail. The structural, surface and optical characterizations and obtained results are discussed in Section 3. Finally, Section 4 concludes the paper.

2. Materials and Methods

2.1 Deposition of ZnO thin films

In this study, ZnO thin films were deposited using SILAR and spin-coating methods. In the SILAR method, 682 mg of zinc chloride (ZnCl₂) was added to 50 ml of deionized water to obtain a 0.1 M precursor cationic solution. The pH of the solution was adjusted to 10 by adding 6 ml ammonia (NH₃). The resulting solution was mixed for 5 min and then transferred to a beaker. A SILAR round was completed by keeping the substrates in a zinc chloride solution for 30 s, in air for 15 s and deionized water at 90°C for 10 s. This process was repeated for 100 cycles. Figure 1 shows a schematic of the SILAR cycle used to produce ZnO thin films. The chemical reactions that occur during the deposition of ZnO structures using the SILAR method are shown in Equation 1 to Equation 4 [17].



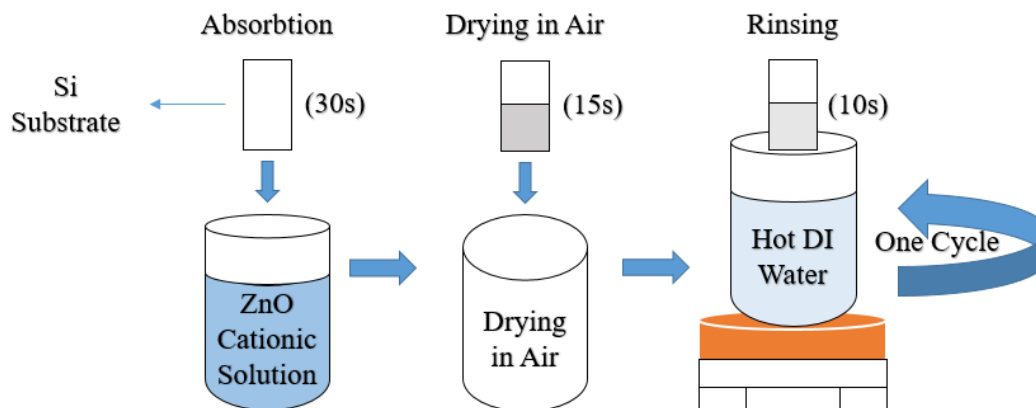


Figure 1. Schematic diagram of SILAR method.

The spin coating method starts with preparation of a 0.5M precursor solution. It was obtained by adding 5.48775g of zinc acetate dihydrate ($\text{Zn}(\text{CH}_3\text{COO})_2 \cdot 2\text{H}_2\text{O}$) to 50ml of 2-methoxy ethanol ($\text{C}_3\text{H}_8\text{O}_2$). To obtain a 0.5M secondary solution, 1.512ml of monoethanolamine ($\text{C}_2\text{H}_7\text{NO}$) was mixed with 50ml of 2-methoxy ethanol ($\text{C}_3\text{H}_8\text{O}_2$). A homogeneous solution was formed by combining the two solutions in a beaker and mixing at 60°C for 2 h. The prepared solution was dripped onto a silicon substrate, and the substrate was spun at 3000 rpm for 30 s. The samples were then baked at 250°C for 10 min. These processes were repeated ten times, and the samples were annealed at 450°C for 30 min as the final step. Figure 2 shows the stages of the spin-coating method.

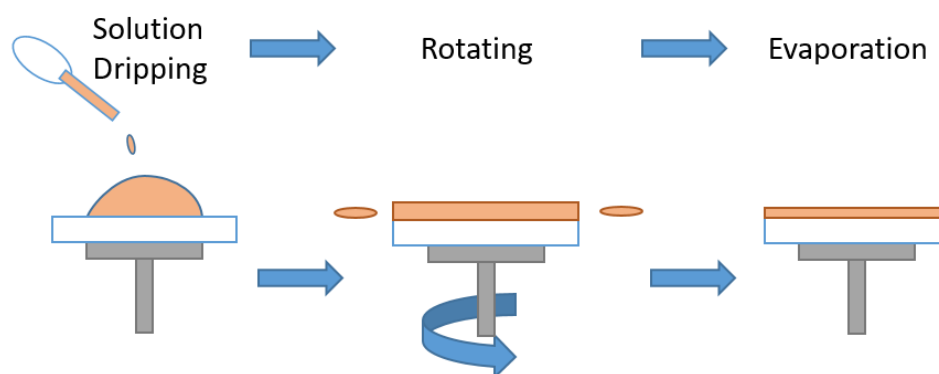


Figure 2. Schematic diagram of spin-coating method.

2.2 Characterization

A Laurell WS-650MZ-23NPPB0 spinner was used for film deposition via the spin-coating method. XRD, SEM, and PL were used for the structural, surface, and optical characterization of the ZnO thin films. For structural analysis, a GNR-Explorer X-ray diffractometer with $\text{Cu K}\alpha$ ($k=1.5405 \text{ \AA}$) radiation for 2h at $10\text{--}60^\circ$ was used. The surface morphology was studied using a Quanta FEG 250 SEM model. For the PL measurements, the ‘MAPLE-II low-temperature macro photoluminescence system was used with laser excitation at 650 nm.

3. Results and discussion

Figure 3 shows the XRD measurement results of samples deposited on (1 1 1) oriented n-type and (1 0 0) oriented p-type Si by SILAR and spin-coating methods, respectively. When the figures are examined, it is understood that the marked peaks are compatible with the ZnO peaks reported in the literature [19], and the ZnO thin films grow in wurtzite structure.

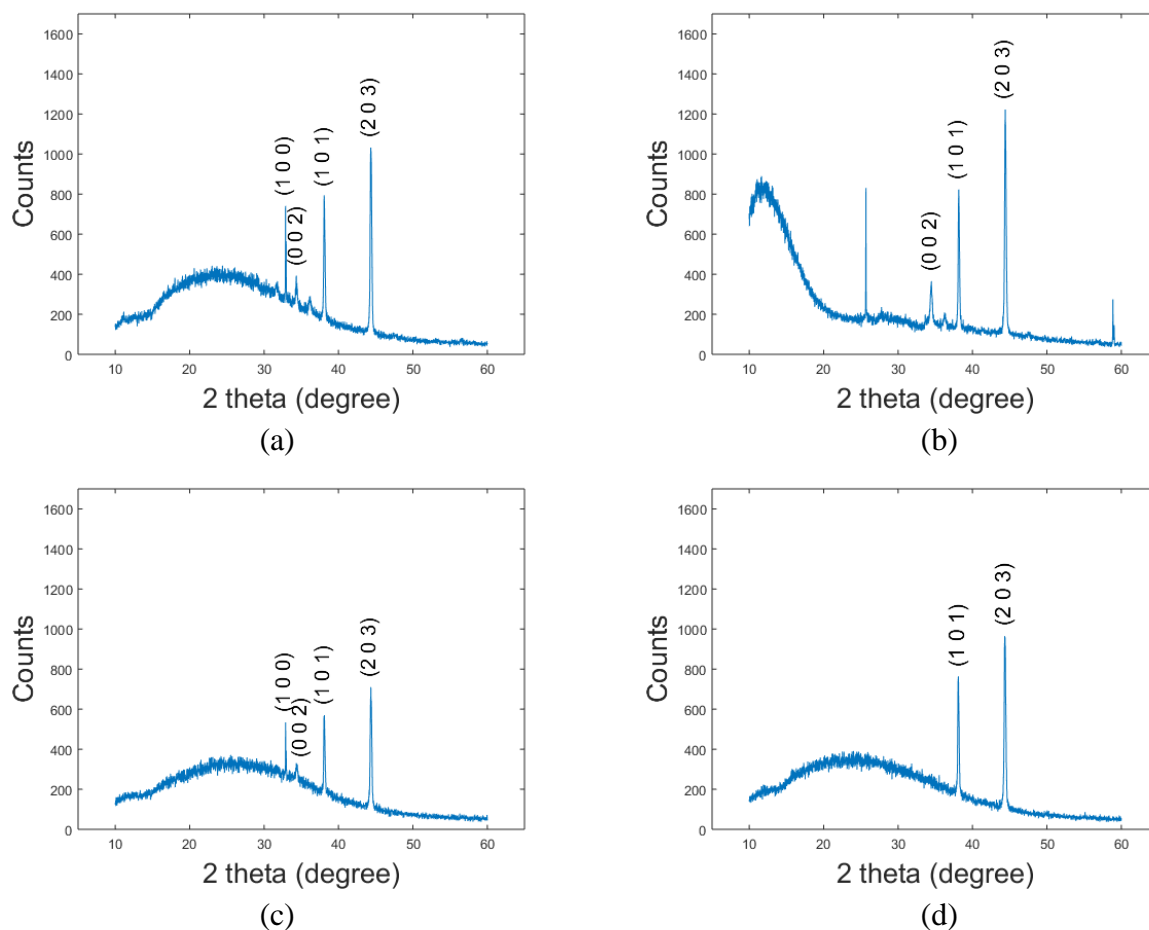


Figure 3. XRD measurement results of ZnO deposited by (a) SILAR method on n-type, (b) SILAR method on p-type Si, (c) spin coating method on n-type Si, (d) spin coating method on p-type Si.

Table 1 shows the micro strain values (ϵ), dislocation density (δ) datas, and crystal sizes (D) obtained from the XRD data.

Table 1. Crystal size calculation results from XRD results

	Miller indices	2 θ (°)	FWHM (°)	ϵ (lin-m ⁴)x10 ⁻⁴	δ (lin/m ²)*10 ¹⁴	D (nm)
SILAR on n-type Si	100	32,88574	0,03440	1,439600	0,157860	251,69023
	002	34,34439	0,30026	12,51728	11,93454	28,946580
	101	38,10436	0,20674	8,526590	5,537790	42,494390
	203	44,36986	0,24618	9,946430	7,535630	36,428400
	002	34,45766	0,34117	14,21839	15,39879	25,483362

SILAR on p-type Si	101	38,16712	0,20866	8,604151	5,638995	42,111347
	203	44,42552	0,24520	9,904867	7,472793	36,581249
Spin coating on n-type Si	100	32,89336	0,03465	1,450030	0,160155	249,87918
	002	34,37999	0,26614	11,09382	9,374487	32,660756
	101	38,16711	0,20832	8,590132	5,620634	42,180076
Spin coating on p-type Si	203	44,42561	0,24836	10,03251	7,666640	36,115820
	101	38,10701	0,20490	8,450639	5,439572	42,876330
	203	44,37243	0,25862	10,44894	8,316306	34,676461

As can be seen from Table 1, similar micro strain values, dislocation densities and crystal sizes were obtained for the dominant (1 0 1) and (2 0 3) peaks for all samples. Figure 4 shows SEM images of the samples coated by using the SILAR method on (1 1 1) oriented n-type and (1 0 0) oriented p-type Si, respectively. When SEM images are examined, it is seen that the surfaces are completely covered with ZnO.

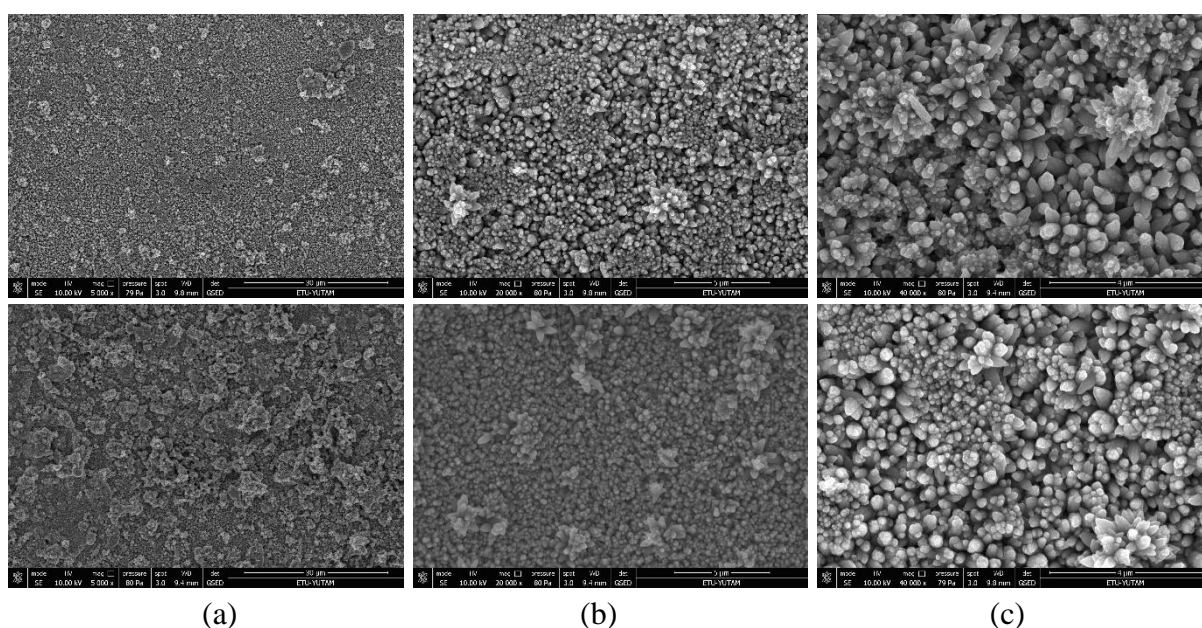


Figure 4. SEM images of deposited by SILAR method on n-type and p-type Si with (a) 5000x, (b) 20000x, (c) 40000x magnification ratios.

Figure 5 shows SEM images of the samples coated by using the spin coating method on (1 1 1) oriented n-type and (1 0 0) oriented p-type Si, respectively. When the SEM images of the samples are examined, it is seen that the homogeneity of the samples deposited with spin coating is better than the samples deposited with SILAR method. However, difference of the SEM images for SILAR and spin coating deposited samples cannot be explained with XRD data since sizes of the formed crystals are very small compared to the resolution of the obtained SEM images.

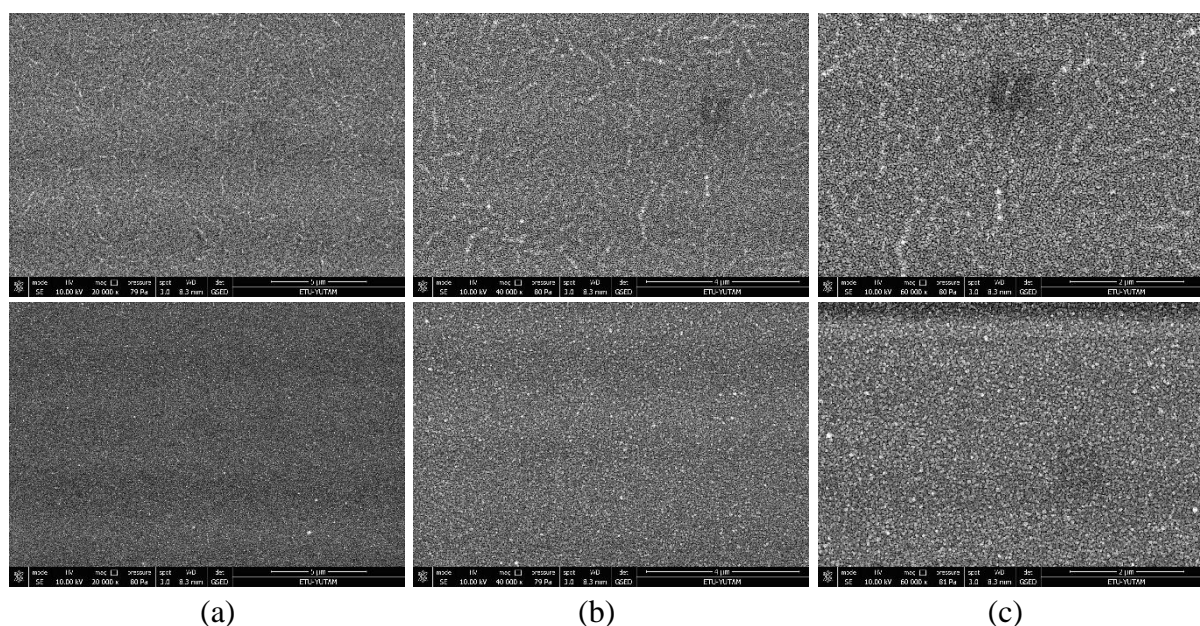


Figure 5. SEM photos of deposited by spin-coating method on n-type and p-type Si with (a) 20000x, (b) 40000x, (c) 60000x magnification ratios.

Figure 6 shows Tauc plots used to determine band gap of the ZnO thin films deposited by SILAR and spin coating methods. As can be seen from Figure 6, the band gap of the sample deposited by the SILAR method is 3.98 eV and the band gap of the sample deposited by spin coating is 3.88 eV.

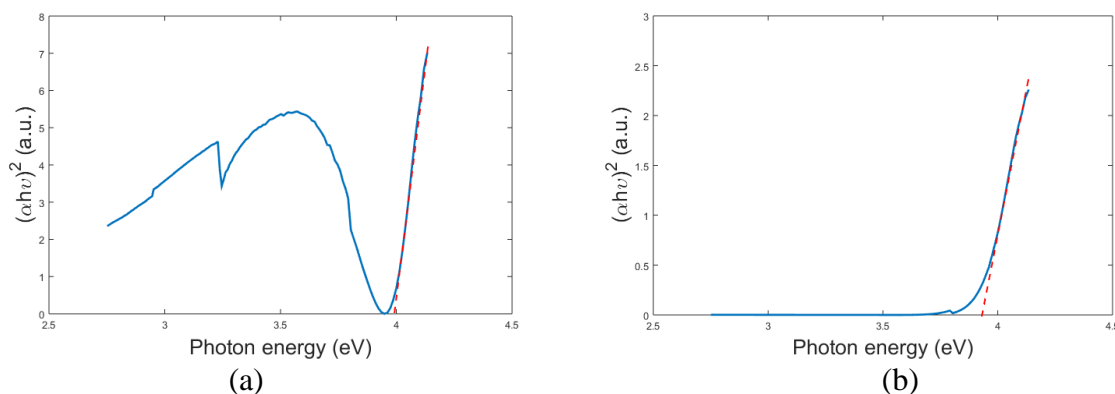


Figure 6. Tauc plots of the ZnO thin films deposited by (a) SILAR, (b) spin coating method on the n-type Si substrates

Figure 7, 8 and 9 show the photoluminescence spectra graphs under different laser excitation intensities of the samples deposited on n-type, p-type Si by the SILAR method and on n-type Si by the spin-coating method, respectively. The PL system used in the measurements gives at what percent of the maximum power of the excitation laser is operated with, instead of giving exact output power of the laser. Considering that the stimulated emission is dominant due to the nature of the laser and output of the laser is linear in this situation, it is thought that this will not pose any problem in the evaluation of the PL spectrum.

All spectra exhibited similar PL features. Upon examination of the graphs, it was observed that the PL density increased. ZnO thin films luminesce in the visible and UV regions [20]. The emission in the visible region is due to the intrinsic defects of ZnO, and the emission in the UV region is due to excitonic recombination. The peak at approximately 750 nm is more controversial. Some scientists attribute this to defects in the ZnO structure, whereas others have argued that such emission is a quadratic feature of UV emission [21]. In addition, the regions with maximum PL intensity (especially between 500-670 nm) in the graphs draw attention. This was due to the saturation of the detector in the PL system.

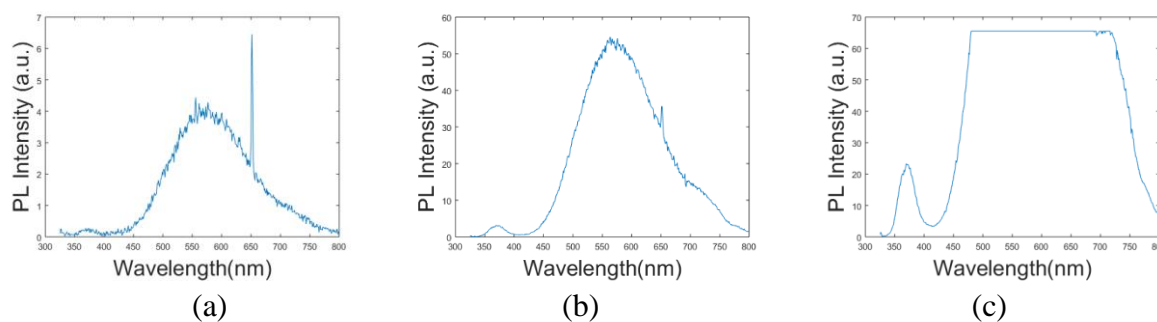


Figure 7. PL densities of deposited by SILAR method on n-type Si at the laser powers of (a) 0.5%, (b) 1.5%, (c) 7%.

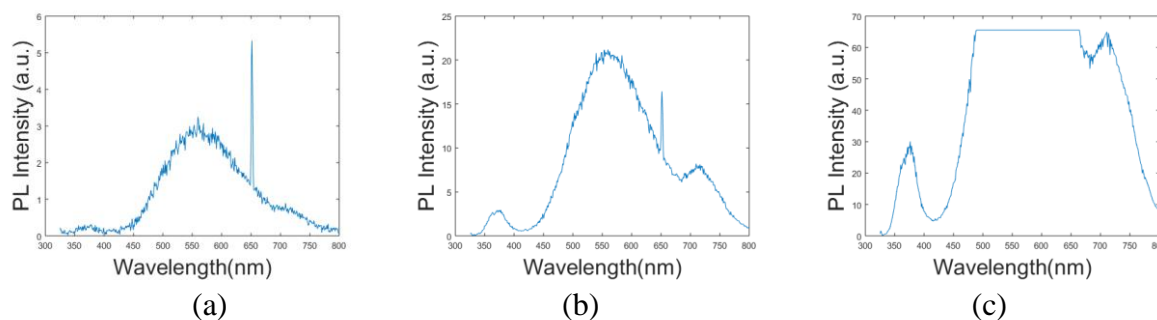


Figure 8. PL densities of deposited by SILAR method on p-type Si at the laser powers of (a) 0.5%, (b) 1.5%, (c) 7%.

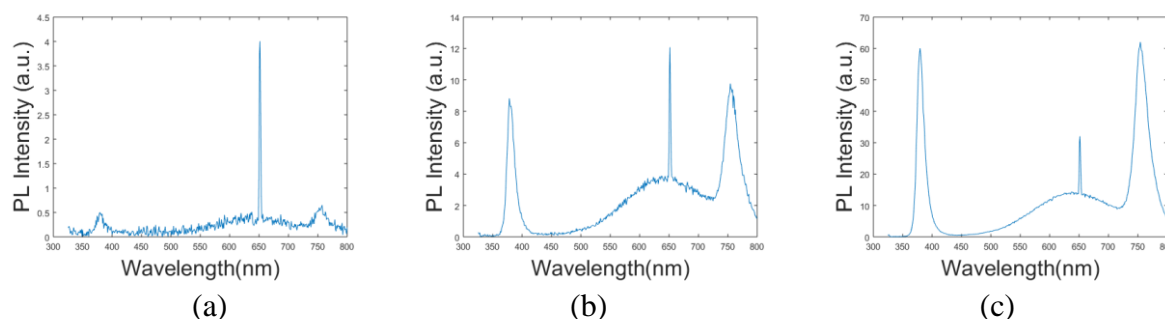


Figure 9. PL densities of deposited by spin-coating method on n-type Si at the laser powers of (a) 0.5%, (b) 1.5%, (c) 7%.

Figure 10 shows the photoluminescence spectra graphs under different laser excitation intensities of the samples deposited on n-type Si coated by the spincoating method. Notably as the laser intensity increased, the emission intensity in the UV and visible regions also increased.

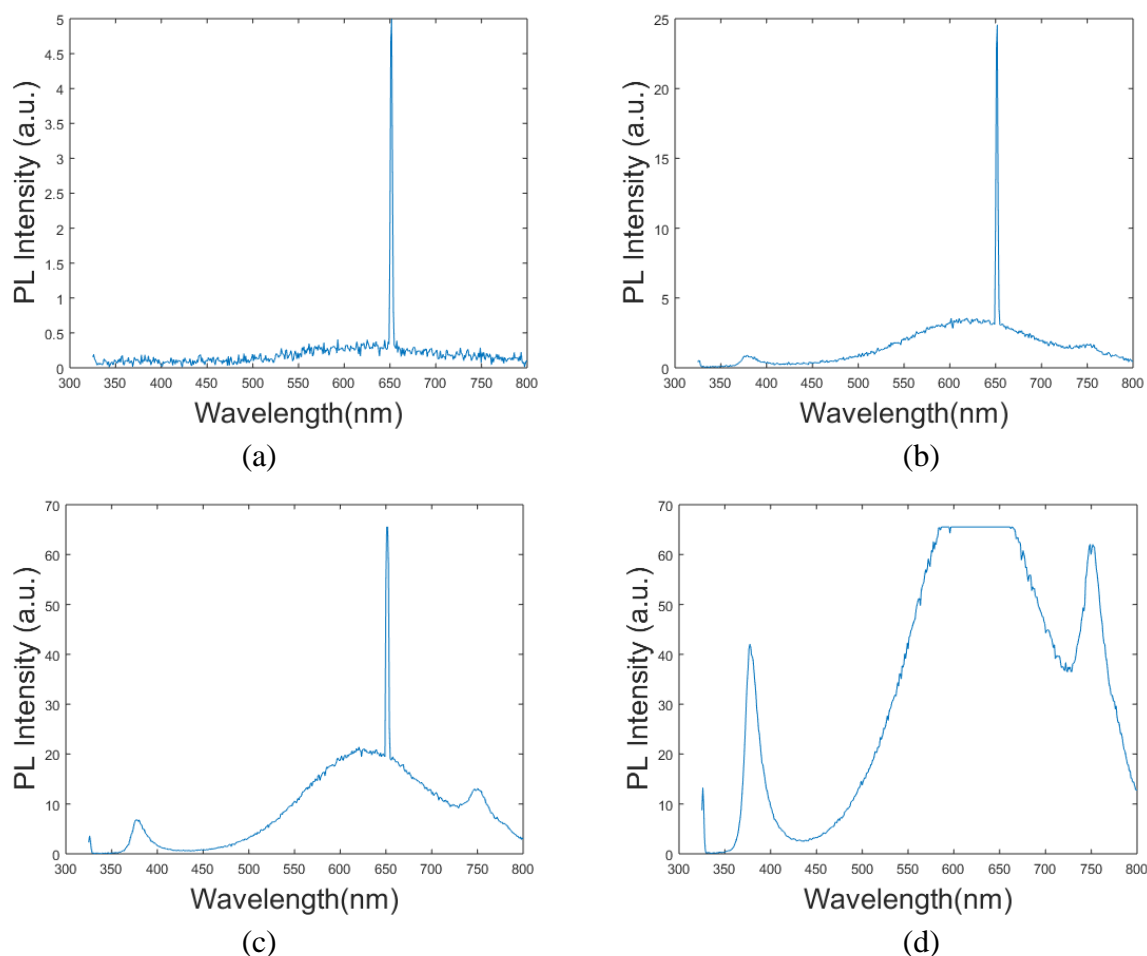


Figure 10. PL densities of deposited by spin-coating method on p-type Si at the laser powers of (a) 0.5%, (b) 1.5%, (c) 7%, (d)15%.

When focusing on PL emissions around 380 nm, it is seen that the samples have the potential for random lasing, given the increased PL emissions due to the increasing excitation intensity. Figure 11 shows the photoluminescence for laser powers of 0.5%, 1.5%, 7% and 15% at 377.25 nm. As mentioned before, higher-power measurements could not be obtained because of the measurement system.

In these measurements, despite the saturation of the detector used in the PL system, an increase in photoluminescence at 377.25 nm was observed. In addition, in the PL figures, the FWHM of the peaks at 377.25 nm decreased with increasing excitation power. These results indicate the well-known random lasing phenomena in ZnO thin films. The direct bandgap nature of ZnO and the random nature of ZnO thin films enable these films to generate high optical gain and high levels of scattering [22]. Owing to these properties, ZnO thin films can exhibit random lasing.

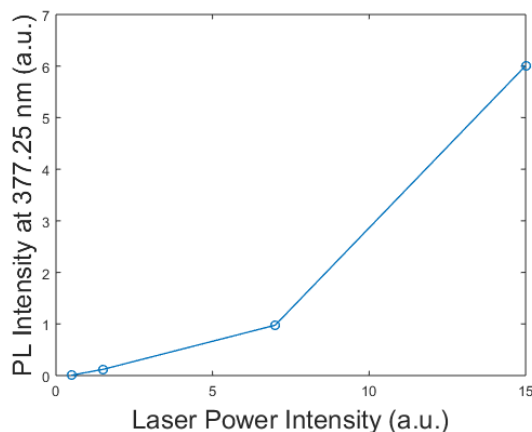


Figure 11. PL densities at 377.25 nm

4. Conclusion

In summary, SILAR and spin-coating methods were used to synthesize ZnO thin films on Si substrates at room temperature. The structural, morphological, and optical properties of the ZnO thin films were investigated. The XRD measurements showed that the ZnO thin films had a polycrystalline structure. The SEM images showed that the surfaces were homogeneously coated. PL measurements showed that the samples gave light output in the UV region, visible region and around 750 nm. When all the measurement results were examined, it was determined that the samples coated using the spin-coating method gave better results than the samples coated using the SILAR method. During the PL measurements, the power could not be increased as desired because the detector in the system was saturated. Despite this problem, PL measurements were performed at four different power levels, and an increase in photoluminescence at 377.25 nm was observed. Moreover, the FWHM of the peaks at 377.25 nm decreased with increasing excitation power. This can indicate well-known random lasing phenomena.

Acknowledgements

This paper is supported by Erzurum Technical University BAP Program (Project No: ETÜ BAP 2017/24).

Ethics in publishing

There are no ethical issues regarding the publication of this study.

Author Contributions

These authors contributed equally to this work.

References

- [1] Gupta, T. K. (1990). Application of Zinc Oxide Varistors. *Journal of the American Ceramic Society*, 73(7), 1817–1840.
- [2] Raoufi, D. & Raoufi, T. (2009). The effect of heat treatment on the physical properties of sol-gel derived ZnO thin films. *Applied Surface Science*, 255(11), 5812–5817.
- [3] Liang, W. Y. & Yoffe, A. D. (1968). Transmission Spectra of ZnO Single Crystals. *Physical Review Letters*, 20(2), 59–62.
- [4] Look, D. C. (2001). Recent advances in ZnO materials and devices. *Materials Science and Engineering: B*, 80(1–3), 383–387.
- [5] Wan, Q., Li, Q. H., Chen, Y. J., Wang, T. H., He, X. L., Li, J. P. & Lin, C. L. (2004). Fabrication and ethanol sensing characteristics of ZnO nanowire gas sensors. *Applied Physics Letters*, 84(18), 3654.
- [6] Barnes, T. M., Leaf, J., Fry, C. & Wolden, C. A. (2005). Room temperature chemical vapor deposition of c-axis ZnO. *Journal of Crystal Growth*, 274(3–4), 412–417.
- [7] Water, W. & Chu, S. Y. (2002). Physical and structural properties of ZnO sputtered films. *Materials Letters*, 55(1–2), 67–72.
- [8] King, S. L., Gardeniers, J. G. E. & Boyd, I. W. (1996). Pulsed-laser deposited ZnO for device applications. *Applied Surface Science*, 96(98), 811–818.
- [9] Ashour, A., Kaid, M. A., El-Sayed, N. Z. & Ibrahim, A. A. (2006). Physical properties of ZnO thin films deposited by spray pyrolysis technique. *Applied Surface Science*, 252(22), 7844–7848.
- [10] Liu, Y., Gorla, C. R., Liang, S., Emanetoglu, N., Lu, Y., Shen, H. & Wraback, M. (2000). Ultraviolet detectors based on epitaxial ZnO films grown by MOCVD. *Journal of Electronic Materials*, 29(1), 69–74.
- [11] Weng, J., Zhang, Y., Han, G., Zhang, Y., Xu, L., Xu, J., ... & Chen, K. (2005). Electrochemical deposition and characterization of wide band semiconductor ZnO thin film. *Thin Solid Films*, 478(1-2), 25-29.
- [12] Yi, S.-H., Choi, S.-K., Jang, J.-M., Kim, J.-A. & Jung, W. G. (2007). Low-temperature growth of ZnO nanorods by chemical bath deposition. *Journal of Colloid and Interface Science*, 313(2), 705–710.
- [13] Kaviyarasu, K., Magdalane, C. M., Kanimozhi, K., Kennedy, J., Siddhardha, B., Reddy, E. S., ... & Maaza, M. (2017). Elucidation of photocatalysis, photoluminescence and antibacterial studies of ZnO thin films by spin coating method. *Journal of Photochemistry and Photobiology B: Biology*, 173, 466-475.
- [14] Lanjewar, M. & Gohel, J. V. (2017). Enhanced performance of Ag-doped ZnO and pure ZnO thin films DSSCs prepared by sol-gel spin coating. *Inorganic and Nano-Metal Chemistry*, 47(7), 1090–1096.
- [15] Youl Bae, H. & Man Choi, G. (1999). Electrical and reducing gas sensing properties of ZnO and ZnO–CuO thin films fabricated by spin coating method. *Sensors and Actuators B: Chemical*, 55(1), 47–54.
- [16] Kumar, P. S., Raj, A. D., Mangalaraj, D. & Nataraj, D. (2010). Hydrophobic ZnO nanostructured thin films on glass substrate by simple successive ionic layer absorption and reaction (SILAR) method. *Thin Solid Films, Symposium on Functional Ceramic*

- Materials, Oxide Thin Films and Heterostructures (ICMAT 2009)*, 518(24, Supplement), e183–e186.
- [17] Pathan, H. M. & Lokhande, C. D. (2004). Deposition of metal chalcogenide thin films by successive ionic layer adsorption and reaction (SILAR) method. *Bulletin of Materials Science*, 27(2), 85–111.
- [18] Shei, S. C. & Lee, P. Y. (2013). Influence of rinsing temperature on properties of ZnO thin films prepared by SILAR method with propylene glycol. *Journal of Alloys and Compounds*, 546, 165–170.
- [19] Gür, E., Asıl, H., Coşkun, C., Tüzemen, S., Meral, K., Onganer, Y. & Şerifoğlu, K. (2008). Optical and structural properties of ZnO thin films; effects of high energy electron irradiation and annealing. *Nuclear Instruments and Methods in Physics Research Section B: Beam Interactions with Materials and Atoms*. 266(9), 2021–2026.
- [20] Rauwel, P., Salumaa, M., Aasna, A., Galeckas, A. & Rauwel, E. (2016). A Review of the Synthesis and Photoluminescence Properties of Hybrid ZnO and Carbon Nanomaterials. *Journal of Nanomaterials*, 2016, e5320625.
- [21] Guidelli, E. J., Baffa, O. & Clarke, D. R. (2015). Enhanced UV Emission From Silver/ZnO And Gold/ZnO Core-Shell Nanoparticles: Photoluminescence, Radioluminescence, And Optically Stimulated Luminescence. *Scientific Reports*. 5(1), 14004.
- [22] Fallert, J., Dietz, R. J. B., Hauser, M., Stelzl, F., Klingshirn, C. & Kalt, H. (2009). Random lasing in ZnO nanocrystals. *Journal of Luminescence, Special Issue based on The 15th International Conference on Luminescence and Optical Spectroscopy of Condensed Matter (ICL '08)*, 129(12), 1685–1688.

Determination of Genetic Diversity in Some Pumpkin Genotypes Using SSR Marker Technique

Ömer Faruk COŞKUN¹*

¹Hatay Mustafa Kemal University, Faculty of Agriculture, Department of Horticulture, Hatay, Turkey

Received:07/05/2022, **Revised:** 16/08/2022, **Accepted:** 21/09/2022, **Published:** 30/12/2022

Abstract

Pumpkin (*Cucurbita pepo* L.) is one of the important vegetables in the *Cucurbita* genus of the *Cucurbitaceae* family. DNA markers can be used in the selection studies carried out on vegetables. Microsatellite DNA sequences, which are a very good source of polymorphisms for eukaryotic genomes, are used in the investigation of genetic diversity, the creation of genetic maps and variety determination. In this study, molecular genetic characterization determined by using 16 SSR markers in 47 pumpkin genotypes. A similarity coefficient between 0.68-1.0 was determined between genotypes. It was determined that three genotypes clustered separately from the others. It was concluded that SSR (Simple Sequence Repeats) markers are a good choice for assessment of genetic diversity and differentiation between genotypes. As a result of this study genetic structures of the pumpkin genotypes, and important data were obtained that can shorten the duration of breeding studies.

Keywords: *Cucurbita pepo*, SSR, Molecular characterization

Bazı Kabak Genotiplerinde Genetik Çeşitliliğin SSR Markör Tekniği Kullanılarak Belirlenmesi

Öz

Kabak (*Cucurbita pepo* L.), *Cucurbitaceae* familyasının *Cucurbita* cinsi içerisinde yer alan önemli sebzelerden biridir. Sebzelerde gerçekleştirilen seleksiyon çalışmalarında DNA markörlerinden yararlanılabilmektedir. Ökaryotik genomlar için çok iyi bir polimorfizm kaynağı olan mikrosatellit DNA dizileri, genetik çeşitliliğin araştırılmasında, genetik haritaların oluşturulmasında ve çeşit tayininde kullanılmaktadır. Bu çalışmada 47 kabak genotipinde 16 SSR markörü kullanılarak genetik karakterizasyon belirlenmiştir. Genotipler arasında 0.68-1.0 arasında benzerlik katsayısı tespit edilmiştir. Üç genotipin diğerlerinden ayrı olarak kümelendiği belirlenmiştir. SSR markörlerinin (Basit Dizi Tekrarları) genetik çeşitlilik ve genotipler arası varyasyonun değerlendirilmesi için iyi bir seçim aracı olduğu sonucuna varılmıştır. Bu çalışma sonucunda bazı kabak genotiplerinin genetik yapıları belirlenerek ıslah çalışmalarının süresini kısaltabilecek önemli veriler elde edilmiştir.

Anahtar Kelimeler: *Cucurbita pepo*, SSR, Moleküler karakterizasyon

1. Introduction

There are about 30 species in humans that provide the majority of food sources [1]. On the other hand, thousands of species that are potential food sources are not used. This situation has revealed the necessity of determining the characteristics of other plant species and their consumption in different ways. The *Cucurbitaceae* family includes 118 genera and 825 species [2]. *Cucurbita* genus constitutes the plant group with the highest morphological variation in the plant kingdom [3]. In this genus, there are three species (*Cucurbita pepo* L., *Cucurbita maxima* Duchesne and *Cucurbita moschata* Duchesne) that are cultivated economically [4]. *C. pepo* is a type of vegetable that is highly cultivated and whose fruits, seeds and flowers can be consumed. In Turkey, both edible and snack pumpkin belonging to the *C. pepo* type are grown. In the world, 27.962.742 tons of pumpkin is produced on an area of 2.019.564 hectares. While China ranks first in world pumpkin production with 7.433.743 tons, this order is followed by India (5.113.692 tons), Ukraine (1.268.270), Russia (1.143.127) and America (1.050.713 tons). Due to its favorable conditions, Turkey ranks seventh in the world with 698.051 tons of pumpkin production value in terms of pumpkin cultivation [5]. The production of pumpkin for snacks in Turkey was realized as 64.861 ton in 2021 [6].

Unripe and ripe fruits of pumpkin are used in human nutrition because they contain important bioactive components (polysaccharides, proteins, peptides, vitamins and sterols) [7,8]. Consumption of these fruits provides relief from constipation, cleanses the blood and is good for digestion [9]. Pumpkin seeds are also evaluated in the food and pharmaceutical industry [10] and are used in many cultures of the world as a snack in raw or roasted form due to their high nutritional value. In addition, these seeds are used as flavor enhancer in meals or in minced meat formulations [11]. Pumpkin seeds are beneficial for health due to important nutrients (phenolic compounds, phytosterol, polyunsaturated fatty acid) contained in them [12]. Pumpkin seeds are rich in unsaturated fatty acids, oleic and linoleic acids, and contain squalene, which has a cholesterol-lowering effect [13]. At the same time, pumpkin seeds are also important in terms of the high amount of essential amino acids [14]. For these reasons, it can be considered that pumpkin seeds are beneficial for human health.

Pumpkin is one of the most polymorphic species in terms of fruit characters. Studies on the genetic characterization of pumpkin species and genotypes with high morphological differences are scarce. The most important biomarkers used for genetic characterization are DNA markers. Genetic studies in horticultural crops have been successfully carried out with many DNA marker techniques developed [15-20]. Different marker techniques such as SSR, RAPD, SRAP, ISSR and AFLP were used to determine genetic diversity among *Cucurbita* species [17,21-24]. One of the molecular markers, SSR (Simple Sequence Repeat), is called "microsatellite" and has been widely used in genetic characterization studies in recent years. SSR is an important marker technique that can be used in genetic analyzes due to its codominant, easy use, high polymorphism, and ubiquitous advantages in the eukaryotic genome [25]. The use of molecular data in the identification of pumpkin lines can play an active role in revealing true genetic relationships. In this study, it was aimed to determine the genetic diversity among different pumpkin genotypes by using the SSR marker technique.

2. Material and Methods

In the study, a total of 47 pumpkin genotypes selected from Kayseri and Nevşehir province (in Turkey) were used as plant material, considering their plant and fruit characteristics (Table 1). In the study, CTAB total DNA extraction protocol was applied and 30 mg of plant tissue was used for each genotype. After isolation, the DNA concentration was adjusted to 10 ng/1 by measuring with a 1% agarose gel. For SSR analysis, Danin -Poleg, [26], Watchawongpoiboon and Chungwongse, [27] and Jarret et al., [28] developed 16 of the SSR primers were used. In this study, the best optimized primer pairs determined by Coskun et al., [29] were used. Polymerase chain reaction optimized 15 µL reactions contained 50 ng template DNA, 10 nmol dNTPs, 10 nmol SSR primers, 5 U Taq DNA polymerase, 1.5 mL of 10X polymerase chain reaction (PCR) buffer (50 mM KCl, 10 mM Tris-HCl, 2.5 mM MgCl₂, pH 8.3). Typical amplification parameters were used and PCR products (5 mL) were resolved on 6.5% polyacrylamide gels at 50 W for 2.5 h.

For PCR, DNA samples were denaturated for 5 minutes at 95 °C, and then kept for 45 cycles at 95 °C for 1 minute, at 55 °C for 30 seconds, and at 72 °C for 1 minute. Finally, the marker was amplified by keeping the PCR mixture at 72 °C for 6 minutes. PCR products were visualized by running on acrylamide gel. For this purpose, M13 forward and reverse primers were added to synthetically prepared SSR primers. In this way, PCR products labeled at 700 or 800 nm wavelengths could be observed in the Li-Cor gel system.

Genotypes were scored as 1, 0 and 9 (for missing data). These data were analyzed using NTSYS (Numerical Taxonomy Multivariate Analysis System, NTSYS-pc version 2.1, Exeter Software, Setauket, N.Y., USA) package program [30]. Similarity indexes between individuals were determined. A dendrogram was created using the UPGMA method by using similarity indices. With the analyzes made, the variation and similarity levels between the pumpkin genotypes used in the study were determined and the characteristics of the genetic structure were revealed.

Table 1. The test materials of *Cucurbita pepo* (*C. pepo*) (n=47).

No	Origin	Pumpkin taxon	No	Origin	Pumpkin taxon	No	Origin	Pumpkin taxon
1	Kayseri-Tomarza	<i>C. pepo</i>	17	Kayseri-Develi	<i>C. pepo</i>	33	Kayseri-Develi	<i>C. pepo</i>
2	Kayseri-Tomarza	<i>C. pepo</i>	18	Kayseri-Develi	<i>C. pepo</i>	34	Kayseri-Develi	<i>C. pepo</i>
3	Kayseri-Tomarza	<i>C. pepo</i>	19	Kayseri-Develi	<i>C. pepo</i>	35	Kayseri-Develi	<i>C. pepo</i>
4	Kayseri-Tomarza	<i>C. pepo</i>	20	Kayseri-Develi	<i>C. pepo</i>	36	Kayseri-Develi	<i>C. pepo</i>
5	Kayseri-Tomarza	<i>C. pepo</i>	21	Kayseri-Develi	<i>C. pepo</i>	37	Kayseri-Yeşilhisar	<i>C. pepo</i>
6	Kayseri-Tomarza	<i>C. pepo</i>	22	Kayseri-Develi	<i>C. pepo</i>	38	Kayseri-Yeşilhisar	<i>C. pepo</i>
7	Kayseri-Tomarza	<i>C. pepo</i>	23	Kayseri-Develi	<i>C. pepo</i>	39	Kayseri-Yeşilhisar	<i>C. pepo</i>
8	Kayseri-Tomarza	<i>C. pepo</i>	24	Kayseri-Develi	<i>C. pepo</i>	40	Kayseri-Yeşilhisar	<i>C. pepo</i>
9	Kayseri-Tomarza	<i>C. pepo</i>	25	Kayseri-Develi	<i>C. pepo</i>	41	Nevşehir-Ürgüp	<i>C. pepo</i>
10	Kayseri-Tomarza	<i>C. pepo</i>	26	Kayseri-Develi	<i>C. pepo</i>	42	Nevşehir-Ürgüp	<i>C. pepo</i>
11	Kayseri-Develi	<i>C. pepo</i>	27	Kayseri-Develi	<i>C. pepo</i>	43	Nevşehir-Ürgüp	<i>C. pepo</i>
12	Kayseri-Develi	<i>C. pepo</i>	28	Kayseri-Develi	<i>C. pepo</i>	44	Nevşehir-Acıgöl	<i>C. pepo</i>

13	Kayseri-Develi	<i>C. pepo</i>	29	Kayseri-Develi	<i>C. pepo</i>	45	Nevşehir-Kozaklı	<i>C. pepo</i>
14	Kayseri-Develi	<i>C. pepo</i>	30	Kayseri-Develi	<i>C. pepo</i>	46	Nevşehir-Kozaklı	<i>C. pepo</i>
15	Kayseri-Develi	<i>C. pepo</i>	31	Kayseri-Develi	<i>C. pepo</i>	47	Nevşehir-Kozaklı	<i>C. pepo</i>
16	Kayseri-Develi	<i>C. pepo</i>	32	Kayseri-Develi	<i>C. pepo</i>			

3. Results and Discussion

Within the scope of this study, the genetic analysis of 47 different pumpkin genotypes was investigated using the SSR marker technique. In some studies, it was stated that SSR was successful in detecting polymorphism in species belonging to the genus *Cucurbita* [31,32]. Katzir et al., [33] also determined in their study that the SSR technique was much better in revealing the kinship relationships of *C. pepo*. They determined that SSR primers developed in different cucurbit species could yield successful results in *C. pepo* genotypes.

In this study, PCR studies were carried out on 47 pumpkin genotypes selected with a total of 16 SSR primers (Table 2). Twenty-nine of the 49 bands obtained were determined as polymorphic. The total number of alleles per primer ranged from 2 to 5 (mean 4.7). The number of polymorphic alleles is again between 2 and 7 (mean 3.1). In terms of the total number of alleles obtained, CSTCC813 loci produced the most alleles (5). Paris et al., [32] identified 2-5 alleles in 45 *C. pepo* genotypes. In the study conducted by Paris et al., [34], 16-30 scoreable bands and 15-23 polymorphic bands were obtained from 6 SSR primer pairs. Stift et al., [25] determined an average of 4.4 alleles per locus using 22 primer pairs on 48 genotypes. In a study, a total of 56 bands were obtained by using 10 SSR markers among *C. pepo* genotypes [35]. In another study, a total of 43 bands varying between 123 bp and 285 bp were obtained with nine primers [36]. Kayak et al., [37] determined the number of bands per primer to be 3.9 using SSR markers in the pumpkin genotypes in their study. Meru et al., [38] obtained an average of 3.92 alleles per locus in their study with SSR primer on 29 pumpkin genotypes. In a study on *C. pepo* genotypes, an average of 4.12 bands was obtained from SSR primers [39]. In the genetic diversity study among genotypes including 47 *C. pepo* and 1 *C. foetidissima*, 85 (mean 3.2) of 271 primers were polymorphic [40]. Findings from these studies are consistent with this study (mean number of bands 4.7). Aslan et al., [17] obtained 52 scoreable bands with 18 SSR primers in their study. In this study, more scoreable bands and more bands per primer were obtained. It is expected that the number of alleles at similar rates will be detected in different studies with similar sample groups. Small differences may be due to the use of natural populations in this study or to the large number of repetitions of different primers used.

The total polymorphism rate obtained from primer pairs was found to be 59% (Table 2). In the study, the rate of polymorphism was found 59% in the pumpkin collection, which includes genotypes with geographical origins in and around Kayseri. Paris et al., [34] tried to determine the genetic relationships of 45 *C. pepo* genotypes and it was determined that 280 (63%) of a total of 448 easily scored bands were polymorphic. Mujaju et al., [36] obtained an average of 67.86% polymorphism in watermelon genotypes using the SSR technique. Kayak et al., [37] determined the polymorphism rate as 87.7% and the mean dissimilarity value as 0.28 by using SSR markers in the pumpkin genotypes in their study. The results from the present study are

consistent with results from previous molecular studies. Martins et al., [41] used SSR markers to determine genetic diversity using 54 *C. pepo*, 32 *C. maxima* and 21 *C. moschata* populations, and it was stated that a 100% polymorphism was observed. The obtained polymorphism value is higher than this study findings. This may be due to the presence of genotypes of different species in the gene pool. The polymorphism values obtained from this study revealed that SSR markers can be used successfully in determining genetic relationships in pumpkin.

Table 2. Informations of primer sequence, total number of alleles (TNA), number of polymorphic alleles (PAN) and polymorphism rate (PR-%).

Primer	Primer Sequence	References	TNA	NPA	PR
CSTCC813	F:GTTGTGCTCCCAATAGTTG R:CACCACTTCTTCCACCGAA	[26]	5	5	100
CSJCT14	F:TTCCACGTTACATTGGACGA R:AGAATTCATGGCCTGCAGAT	[27]	4	4	100
CSCCT571	F: CCTTTCTGCTGTTTCTTCTTC R: CCTTTCTGCTGTTTCTTCTTC	[26]	2	2	100
CSJCT 191	F:ACAATGGCAGGTCAATTAGC R:CCTTGGGTTGTATCGAAGAC	[27]	2	0	0
CSTA050	F: GAATTATGCAGATGGGTCTT R:CAAGAAGATCAAATGATAGC	[26]	4	2	50
CSJCT 216	F:CAGTAGGAGGAAGTGGGTTC R: CTTACTCCAACCAACCCAAC	[27]	2	0	0
CMCTT144	F:CAAAAGGTTTCGATTGGTGGG R:AAATGGTGGGGTTGAATAGG	[26]	2	0	0
CMTC51	F: ATTGGGGTTTCTTTGAGGTGA R:CCATGTCTAAAACTCATGTGG	[26]	4	2	50
CSJCT 71	F:AATTCATGGACATCCAGCCGAG R:CAGTGAAAGGCACTAAAGCGGAG	[27]	2	2	100
CSJCT 252	F:GATGGTGGAGATGGAATTGGGAT R: TTAGAGCTGGA ACTCTCCGCAAC	[27]	4	2	50
CI.1-06	F: CACCCTCTCCAGTTGTCATTTCG R: AAGGTCAGCAAAGCGGCATAGG	[28]	4	2	50
CI.1-120	F: CGCGCGTGAGGACCCTATA R: AGCAATTGATTGAGGCGGTCT	[28]	2	0	0
CSJCT 656	F: TCCTACA ACTCAAAGGGCCAAC R: GAAGTGGAGTGGAGTGGAGTGA	[27]	2	2	100
CI.2-23	F: GAGGCGGAGGAGTTGAGAG R: ACAAACAACGAAACCCATAGC	[28]	2	0	0
CSJCT 662	F: ACGTCGTAAAACCATCGGAGTC R: GCTTCCAAGCGTCAAAGGTATC	[27]	4	2	50

CSJCT 664	F: AAGTGGGCTCGATTGGAAGA R: CCGTCGCCTTTCTCAAGTTC	[27]	4	4	100
Total			49	29	

According to the UPGMA dendrogram obtained using the scoring data, the similarity index between the pumpkin genotypes varied between 0.68 and 1.00. Barzegar et al., [42] used 14 SSR primer pairs to detect genetic diversity among 26 local cultivars of *C. pepo*. The percentage of polymorphic loci estimated using the genetic diversity index and the information index revealed moderate or high genetic diversity. Yunli et al., [39] determined the similarity coefficient in pumpkin genotypes between 0.73 and 1.0 in their study using SSR primers. The results from the present study are consistent with results from previous molecular studies. The similarity coefficient values (0.68-1.0) obtained in this study were found to be in a similar range (0.64-0.93) with the values determined by Aslan et al., [17]. Inan et al., [24] with the aim of determining genetic relationships between *C. pepo* samples, the genetic similarity coefficients were found between 0.07 and 0.96 in ISSR analysis. The wider variation may be due to the wider frequency of genotypes or the use of different marker techniques. Meru et al., [38] determined the genetic distance in pumpkin genotypes between 0.08 and 0.76 in their study. A wider variation was detected in this study. This may be due to the use of different pumpkin subspecies as genetic resources. In this study, genetic diversity among *C. pepo* populations was found to be narrower than in some studies [24,38]. This may be because these populations congregate from a narrow location. This is probably on a small scale to show high genetic diversity. It may also be due to material ingestion or gene flow from a single *Cucurbita* species.

Among some of the pumpkin genotypes (2 and 26; 3, 4, 6, 8, 16, 27 and 39; 10, 12, 13, 15, 17, 38, 18, 32 and 21; 19 and 20; 5, 11, 22 and 28; 9, 36, 39, 37, 29 and 30; 24 and 25) no genetic variation was detected. In this case, it was determined that a total of 35 genotypes could be collected in 8 different groups among themselves, the other 12 genotypes were determined with different genetic structures, and as a result, it was determined that 47 different genotypes could show 20 different genetic structures. According to the UPGMA dendrogram, it was determined that the pumpkin genotypes formed 6 different clusters. No polymorphism was determined among genotypes 45, 46 and 47 in the first cluster, and these three genotypes were clustered separately from other genotypes. There is one genotype (43) in the second cluster, two genotypes (23 and 41) in the third cluster, three genotypes (2, 26 and 34) in the fifth cluster, one genotype (1) in the sixth cluster, and the remaining 37 genotypes in the fourth cluster has received (Fig 1). The similarity between the thirty-seven genotypes in the fourth cluster is high. In the dendrogram obtained by Kayak et al., [37] using SSR markers in the pumpkin genotypes, the majority of the genotypes were clustered together, similar to this study findings. The pumpkin plant has a monoic plant structure and is open to foreign pollination. This may have caused some genotypes to be located outside of the clusters.

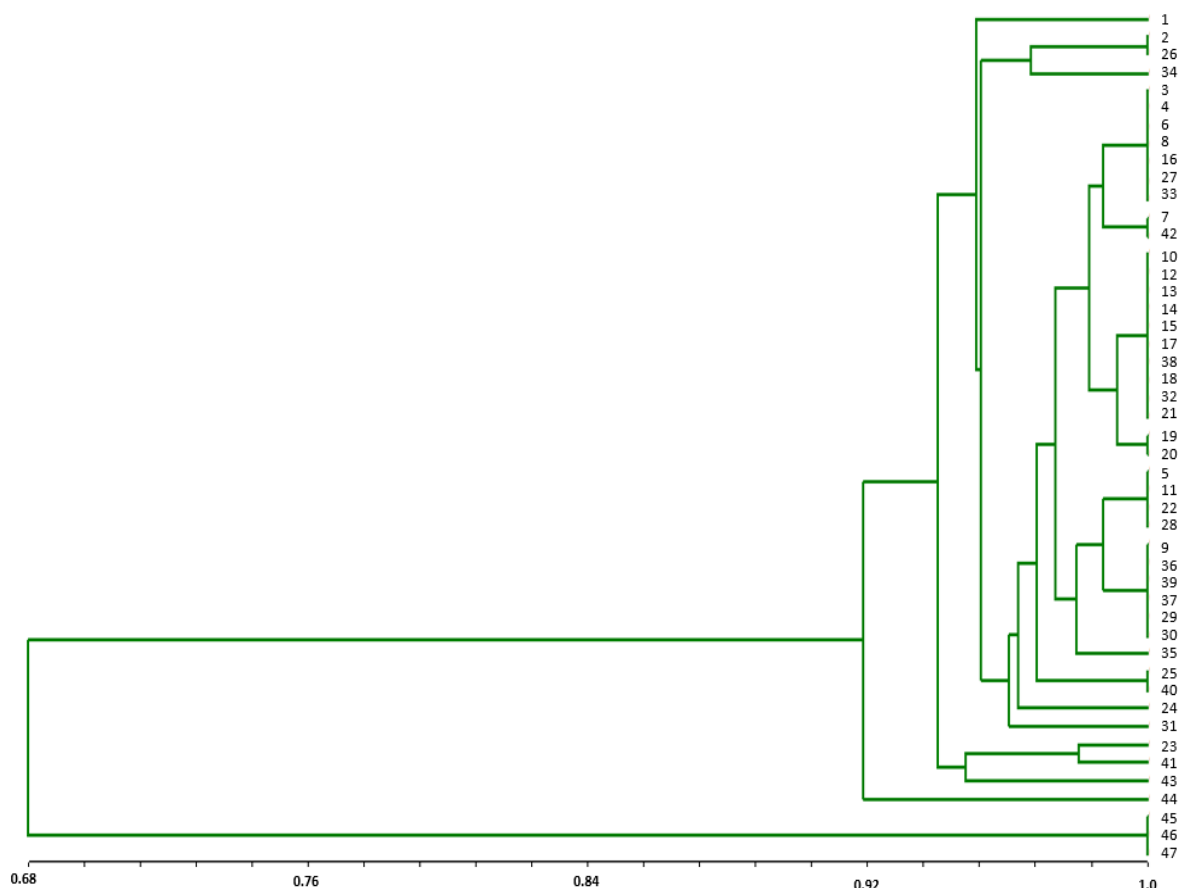


Figure 1. Dendrogram of resulting from a UPGMA cluster analysis based on SSR markers. The accessions correspond with the designations listed in Table 2.

Conclusion

Turkey is rich in genetic material, but the number of developed varieties is not high. Since market demands cannot be met, foreign varieties enter the country. This situation may cause a risky situation such as the extinction of native varieties. Although it is an important sector in Turkey, molecular studies have been carried out in a limited number of pumpkin. It is important to focus on variety development studies and to carry out genetic characterization studies for this purpose. It has been determined that SSR primers are suitable for pumpkin research. Successful primer pairs can be used in association mapping, purity testing and new marker development studies. Successful primers can be recommended for use in breeding programs. This study provided genetic information about *C. pepo* genotypes. These genotypes are an important source of diversity that can be used in breeding programs in the future. Determining the genetic diversity among Cucurbita species in Turkey, which is rich in plant diversity, may be useful in selecting and developing the most suitable genotype for use in genetic studies and breeding programs.

Ethics in Publishing

There are no ethical issues regarding the publication of this study.

References

- [1] FAO, (2010) Second report on the state of the world's plant genetic resources for food and agriculture; UK Distributor, Stationery Office; FAO, Viale delle Terme di Caracalla: Rome, Italy, ISBN 925-106-5-349.
- [2] Jeffrey, C., (1990) Systematics of the Cucurbitaceae: An overview. In biology and utilization of the Cucurbitaceae; Bates, D. M., Robinson, R.W., Eds.; Cornell University Press: Ithaca, NY, USA, 3–9.
- [3] Aruah, C. B., Uguru, M. I., Oyiga, B. C., (2010) Variations among some Nigerian Cucurbita landraces. African Journal of Plant Science, 4, 374–386.
- [4] Maynard, D. N., Elmstrom, G. W., Talcott, S. T., Carle, R. B., (2002) El dorado'and'La estrella: Compact plant tropical pumpkin hybrids. American Society for Horticultural Science, 37, 831–833. doi: 10.21273/HORTSCI.37.5.831
- [5] FAO, (2020) World pumpkin production list. <http://www.fao.org/faostat/en/#data/QC>. Access date: 13.02.2022
- [6] TUIK, (2021) Bitkisel üretim istatistikleri. <https://biruni.tuik.gov.tr/medas/?kn=92&locale=tr>, Access date: 13.02.2022
- [7] Dar, A. H., Sofi, S. A., Rafiq, S., (2017) Pumpkin the Functional and therapeutic ingredient: A review, International Journal of Food Science and Nutrition, 168–173.
- [8] Dotto, J. M., Chach, J. S., (2020) The potential of pumpkin seeds as a functional food ingredient: A review, Scientific African, 10, e00575. doi:10.1016/j.sciaf. 2020.e00575
- [9] Bisognin, D. A., (2002) Origin and evolution of cultivated cucurbits. Ciencia Rural, 32, 715-723.
- [10] Robinson, R. W., Decker-Walters, D. S., (1997) Cucurbits. In: Crop production department of horticultural science. Cornell Univ. and D.S. Decker-Walters, The Cucurbit Network U.S.A.
- [11] El-Adawy, T. A., Taha, K. M., (2001) Characteristics and composition of watermelon pumpkin, paprika seed oils and flours. Journal of Agriculture and Food Chemistry, 49, 1253-1259. doi: 10.1021/jf001117+
- [12] Fu, C. L., Shi, H., Li, Q. H., (2006) A review on pharmacological activities and utilization technologies of pumpkin. Plant Foods for Human Nutrition, 61, 73-80. doi: 10.1007/s11130-006-0016-6
- [13] Ermis, S., (2010) The effect of ecology on seed production and snack quality of pumpkin (*Cucurbita pepo* L.) in Turkey. PhD, Ankara University, Graduate School of Natural and Applied Sciences, Ankara, Turkey.

- [14] Glew, R. H., Glew, R. S., Chuang, L. T., Huang, Y. S., Millson, M., Constans, D., Vanderjagt, D. J., (2006) Amino acid, mineral and fatty acid content of pumpkin seeds (*Cucurbita* spp) and *Cyperus esculentus* nuts in the Republic of Niger. *Plant Food for Human Nutrition* 61, 49–54. doi: 10.1007/s11130-006-0010-z
- [15] Karaman, K., Dalda-Şekerci, A., Yetişir, H., Gülşen, O., Coskun, O. F., (2018) Molecular, morphological and biochemical characterization of some Turkish bitter melon (*Momordica charantia* L.) genotypes. *Industrial Crops and Products*, 123, 93–99. doi: 10.1016/j.indcrop.2018.06.036
- [16] Uzun, A., Cil, A., Yaman, M., Coskun, O. F., (2020) Genetic diversity and some fruit characteristics of quince genotypes collected from Kayseri region. *Turkish Journal of Agriculture - Food Science and Technology*, 8 (2), 318–323. doi: 10.24925/turjaf.v8i2.318-323.3012
- [17] Aslan, N., Coskun, O. F., Dalda-Sekerci, A., Gulsen, O., (2021) Estimation of purity levels of pumpkin genotypes (*Cucurbita pepo* L.) using molecular marker. *Mustafa Kemal University Journal of Agricultural Sciences*, 26 (3), 759-769. doi: 10.37908/mkutbd.995779
- [18] Morilipinar, E. O., Dalda-Sekerci, A., Coskun, O. F., Gulsen, O., (2021) Genetic analysis of local pumpkin populations. *International Journal of Agricultural and Natural Sciences*, 14 (3), 264-272.
- [19] Kırac, H., Dalda-Sekerci, A., Coskun, O. F., Gulsen, O., (2022) Morphological and molecular characterization of garlic (*Allium sativum* L.) genotypes sampled from Turkey. *Genetic Resources and Crop Evolution*, 1-9. doi: 10.1007/s10722-022-01343-4
- [20] Kamasak, S., Coskun, O. F., Sekerci, A. D., Gulsen, O., (2022) Microsatellite analysis in some watermelon (*Citrullus lanatus*) genotypes. *International Journal of Agriculture, Environment and Food Sciences*, 6 (1), 58-64. doi: 10.31015/jaefs.2022.1.10
- [21] Ferriol, M., Pico, B., Nuez, F., (2003) Genetic diversity of a germplasm collection of *Cucurbita pepo* using SRAP and AFLP markers. *Theoretical and Applied Genetics*, 107, 271-282. doi: 10.1007/s00122-003-1242-z
- [22] Gong, L., Stift, G., Kofler, R., Pachner, M., Lelley, T., (2008) Microsatellites for the genus *Cucurbita* and an SSR-based genetic linkage map of *Cucurbita pepo*. *Theoretical and Applied Genetics*, 117, 37-48. doi: 10.1007/s00122-008-0750-2
- [23] Tsivelikas, A. L., Koutita, O., Anastasiadou, A., Skaracis, G. N., Traka-Mavrona, E., Koutsika-Sotiriou, M., (2009) Description and analysis of genetic diversity among squash accessions. *Brazilian Archives of Biology and Technology*, 52 (2), 32-38. doi: 10.1590/S1516-89132009000200003

- [24] Inan, N., Yildiz, M., Sensoy, S., Kafkas, S., Abak, K., (2012) Efficacy of ISSR and SRAP techniques for molecular characterization of some *Cucurbita* genotypes including naked (hull-less) seed pumpkin. *The Journal of Animal & Plant Sciences*, 22 (1), 126-136.
- [25] Stift, G., Zraid, A., Lelley, T., (2004) Development and characterization of microsatellite markers (SSR) in *Cucurbita* species. *Cucurbit Genetics Cooperative Report*, 27, 61-65.
- [26] Danin-Poleg, Y., Reis, N., Tzuri, G., Katzir, N., (2001) Development and characterization of microsatellite markers in *Cucumis*. *Theoretical and Applied Genetics*, 102, 61—72. doi: 10.1007/s001220051618
- [27] Watcharawongpaibon, N., Chunwongse, J., (2008) Development and characterization of microsatellite markers from an enriched genomic library of cucumber (*Cucumis sativus*). *Plant Breeding*, 127, 74—81. doi: 10.1111/j.1439-0523.2007.01425.x
- [28] Jarret, R. L., Merrick, L. C., Holms, T., Evans, J., Aradhya, M. K., (1997) Simple sequence repeats in watermelon (*Citrullus lanatus* (Thunb.) Matsum. & Nakai). *Genome*, 40(4), 433-441.
- [29] Coskun, O. F., Gulsen, O., Dalda-Sekerci, A., Yetisir, H., Pinar, H., (2017) SSR marker analysis at some seed pumpkin lines. *Akademik Ziraat Dergisi*, 6, 151-156.
- [30] Rohlf, F. J., (2010) NTSYSpc: Numerical taxonomy and multivariate analysis system. Version 2.21j. Exeter Software, Setauket, New York.
- [31] Gong, L., Paris, H. S., Nee, M. H., Stift, G., Pachner, M., Vollmann, J., Lelley, T., (2012) Genetic relationships and evolution in *Cucurbita pepo* (pumpkin, squash, gourd) as revealed by simple sequence repeat polymorphisms. *Theoretical and Applied Genetics*, 124, 875–891. doi: 10.1007/s00122-011-1752-z
- [32] Paris, H. S., Yonah, N., Portnoy, V., Mozes-Daube, N., Tzuri, N., Katzir, N., (2003) Assessment of genetic relationships in *Cucurbita pepo* (Cucurbitaceae) using DNA markers. *Theoretical and Applied Genetics*, 106, 971-978. doi: 10.1007/s00122-002-1157-0
- [33] Katzir, N., Tadmor, Y., Tzuri, G., Leshzashen, E., Mozes-Daube, N., Danin-Poleg, Y., Paris, H. S., (2000) Further ISSR and preliminary SSR analysis of relationships among accessions of *Cucurbita pepo*. In: Katzir, N., Paris, H.S. (Eds.), *Proc Cucurbitaceae 2000*, Acta. Hort. 510. Israel, pp. 433–439.
- [34] Paris, H. S., Portnoy, V., Mozes-Daube, N., Tzuri, G., Katzir, N., Yonash, N., (2004) AFLP, ISSR, and SSR polymorphisms are in accordance with botanical and cultivated plant taxonomies of the highly polymorphic *Cucurbita pepo*. *Acta Horticulturae*, 634, 167-173. doi: 10.17660/ActaHortic.2004.634.20

- [35] Ntuli, N. R., Tongoona, P. B., Zobolo, A. M., (2015) Genetic diversity in *Cucurbita pepo* landraces revealed by RAPD and SSR markers. *Scientia Horticulturae*, 189, 192–200. doi: 10.1016/j.scienta.2015.03.020
- [36] Mujaju, C., Sehic, J., Werlemark, G., Garkava-Gustavsson, L., Fatih, M., Nybom, H., (2010) Genetic diversity in watermelon (*Citrullus lanatus*) landraces from Zimbabwe revealed by RAPD and SSR markers. *Hereditas* 147, 142–153. doi: 10.1111/j.1601-5223.2010.02165.x
- [37] Kayak, N., Türkmen, Ö., Uncu, A. T., Dal, Y., (2018) Characterization of edible seed pumpkin (*Cucurbita pepo* L.) lines by SSR (simple sequence repeat) markers. *Manas Journal of Agriculture Veterinary and Life Sciences*, 8 (2), 17-24.
- [38] Meru, G., Leyva, D., Michael, V., Mainviel, R., Dorval, M., Fu, Y., (2019) Genetic variation among *Cucurbita pepo* accessions varying in seed nutrition and seed size. *American Journal of Plant Sciences*, 10, 9. doi: 10.4236/ajps.2019.109109
- [39] Yunli, W., Yangyang, W., Wenlong, X., Chaojie, W., (2020) Genetic diversity of pumpkin based on morphological and SSR markers. *Pakistan Journal of Botany*, 52 (2), 477-487. doi: 10.30848/PJB2020-2(6).
- [40] Wang, W., Shi, Y., Liu, Y., Xiang, C., Sun, T., Zhang, M., Shu, Q., Qiu, X., Bo, K., Duan, Y., Wang, C., (2021) Genetic relationships among *Cucurbita pepo* ornamental gourds based on EST-SSR markers. *Czech Journal of Genetics and Plant Breeding*, 57, 125–139. doi: 10.17221/27/2021-CJGPB
- [41] Martins, S., Pinto, O., Carlos, C., Carvalho, de R., Carnide, V., (2015) Assessing genetic diversity in landraces of *Cucurbita* spp. using a morphological and molecular approach. *Procedia Environmental Sciences*, 29, 68-69. doi: 10.1016/j.proenv.2015.07.162
- [42] Barzegar, R., Peyvast, G., Ahadi, A. M., Rabiei, B., Ebadi, A. A., Babagolzadeh, A., (2013) Biochemical systematic, population structure and genetic variability studies among Iranian *Cucurbita* (*Cucurbita pepo* L.) accessions, using genomic SSRs and implications for their breeding potential. *Biochemical Systematics and Ecology*, 50, 187-198. doi: 10.1016/J.BSE.2013.03.048

Exploring Genetic Diversity and Population Structure of Turkish Black Sea Region Maize (*Zea mays* L.) Germplasm using SSR Markers

Nurettin BARAN^{1*}, Muhammad Azhar NADEEM², Abdurrahim YILMAZ³,
Mehtap ANDIRMAN⁴, Fırat KURT¹, Mefhar Gültekin TEMİZ⁵,
Faheem Shehzad BALOCH²

¹Mus Alpaslan University, Faculty of Applied Sciences, Department of Plant Production and Technologies, Mus, Turkey

²Sivas University of Science and Technology, Faculty of Agricultural Sciences and Technologies, Sivas, Turkey

³Bolu Abant İzzet Baysal University, Faculty of Agriculture, Department of Field Crops, Bolu, Turkey

⁴Batman University Sason Vocational School, Department of Plant and Animal Production. Organic Agriculture Program Batman, Turkey

⁵Dicle University, Faculty of Agriculture, Department of Field Crops, Diyarbakır, Türkiye

Received: 10/06/2022, **Revised:** 20/07/2022, **Accepted:** 27/07/2022, **Published:** 30/12/2022

Abstract

This study aimed to investigate the genetic diversity and population structure of 32 local maize genotypes collected from the Black Sea Region of Turkey using SSR markers. 14 most polymorphic primers yielded a total of 42 bands. An average of 3 alleles per SSR primer was detected, and the number of alleles varied from 1 (ϕ 022) to 6 (umc1571). The unweighted pair-group method with arithmetic means (UPGMA) clustering divided maize accessions into three main populations. According to Nei's genetic distances, DZ-M-145 (Corum) and DZ-M-20 (Trabzon) genotypes were the closest (0.03) genetically related populations, while DZ-M-68 (Artvin) and DZ-M-55 (Rize) were the most genetically distant (0.63) populations. The study identified molecular genetic diversity not mentioned for maize plants from the Black Sea.

Keywords: SSR, maize, genetic, local maize populations, molecular characterization

Türkiye Karadeniz Bölgesi Mısır (*Zea mays* L.) Germplazmının Genetik Çeşitliliğinin ve Popülasyon Yapısının SSR Markörleri Kullanılarak Araştırılması

Öz

Bu çalışma, Türkiye'nin Karadeniz Bölgesi'nden toplanan 32 yerel mısır genotipinin SSR belirteçleri kullanılarak genetik çeşitliliğini ve popülasyon yapısını araştırmayı amaçlamıştır. Moleküler karakterizasyon çalışmasında toplamda 42 bant veren en polimorfik 14 primer kullanılmış, SSR primeri başına ortalama 3 alel saptanmış ve alel sayısı 1 (ϕ 022) ile 6 (umc1571) arasında değişim göstermiştir. UPGMA (Unweighted Pair Group Method with Arithmetic Mean) yöntemi, mısır aksesyonlarını üç ana popülasyona bölmüştür. Nei'nin genetik mesafelerine göre, DZ-M-145 (Çorum) ve DZ-M-20 (Trabzon) genotipleri genetik olarak en yakın (0.03) popülasyonlar iken, DZ-M-68 (Artvin) ve DZ-M-55 (Rize) genetik olarak en uzak (0.63) popülasyonlar olarak tespit edilmiştir. Çalışma, Karadeniz'deki mısır bitkileri için daha önce bahsedilmeyen moleküler genetik çeşitliliği tanımlamıştır.

Anahtar Kelimeler: SSR, mısır, genetik, yerel mısır popülasyonları, moleküler karakterizasyon

*Corresponding Author: n.baran@alparslan.edu.tr

953

Nurettin BARAN, <https://orcid.org/0000-0003-2212-3274>

Muhammad Azhar NADEEM, <https://orcid.org/0000-0002-0637-9619>

Abdurrahim YILMAZ, <https://orcid.org/0000-0001-9991-1792>

Mehtap ANDIRMAN, <https://orcid.org/0000-0001-8566-3388>

Fırat KURT, <https://orcid.org/0000-0003-0172-1953>

Mefhar Gültekin TEMİZ, <https://orcid.org/0000-0001-6479-6050>

Faheem Shehzad BALOCH, <https://orcid.org/0000-0002-7470-0080>

1. Introduction

Maize (*Zea mays* L.) is the most important crop in the cereals after wheat and rice. According to genetic data, the maize plant was domesticated from its wild relative, Balsas teosinte (*Zea mays subspecies parviglumis*), in Mexico [1]. Annual production of maize exceeds 1 billion tons worldwide [2] and increases day by day. Maize is used as food and feed. It is estimated to be the most produced grain crop in the world by 2025. Its current demand is expected to be double by 2050 [3-4].

Landraces are very important as there is a vast amount of genetic material utilized in crop improvement and development methods [5]. Landraces of maize plants, which are frequently used in breeding programs, are essential genetic resources [6]. To understand the genetic structure of maize, researching genetic diversity is very important. Future breeding programs need parental genotypes with desired characteristics [7]. Therefore, the crop gene pool should be evaluated according to the degree of genetic diversity [8] and the diverse genotypes must be utilized in different breeding programs.

Molecular markers, which offer an effective way of combining genotypic and phenotypic variation, have recently been used in the agricultural sector to determine genetic diversity [9]. Molecular markers play crucial roles in the in-depth detection of genetic diversity modeling in maize and in determining gene flow from the center of origin to migration pathways [10-11-12-13-14-8]. SSR technique or microsatellite polymorphism, which is one of the PCR-based techniques, can be defined as PCR amplification of tandemly repeated sequences [15-16]. In this co-dominant and multi-allelic technique, the number of repeating units determines the polymorphism for fragment lengths, while heterozygous can be distinguished for different fragments in diploid genomes [17]. In the SSR technique, which contains locus-specific side primers that produce a high level of polymorphic banding, genetic variation is quite good due to the differences in the number of consecutively repeated SSR units in a locus. SSR or microsatellites are preferred for genetic analysis because they are very strong, polymorphic, and common in plant genomes [16].

Detecting genetic diversity is a crucial step in plant breeding programs that helps in the development of more productive and desired varieties. This study aimed to investigate the molecular diversity of 32 local maize genotypes collected from the Black Sea region of Turkey with SSR markers.

2. Material and Methods

2.1. Plant materials and DNA Extraction

In this study, 32 local maize genotypes collected from 26 Turkish provinces in the Black Sea region were used as plant material (Supp Table 1, Fig. 1). From the young leaves of the plants representing each genotype, 0.8 grams of sample was taken and crushed in liquid nitrogen with the help of mortar and pestle. The crushed samples in powdered form were kept at -80°C until

the DNA isolation started. Genomic DNA was extracted from the stored samples according to the CTAB protocol [18] with slight modifications [19].



Fig. 1. Locations of 32 maize genotypes used in the study.

2.2. SSR Analysis

A total of 22 SSR markers were tested with 8 randomly isolated DNA samples. Band images of 14 SSR markers were selected as they showed a polymorphic feature. The names, sequences, and annealing temperatures of these markers are shown in Table 1. The electrophoresis procedure was performed by capillary electrophoresis method using ABI 3130xl automatic genetic analyzer device. Amplification of SSR was performed with 12.5 μ l reaction mixture containing 10-20 ng DNA, 2.0 mM MgCl₂, 20 mM (NH₄)₂ SO₄, 75 mM Tris-HCl, %0.01 Tween 20, 200M dNTP, 20 nM 5' M13 universal primer (average base: 40), 200 nM reverse primer (average base: 20), M13 universal primer marked with 200 nM PET, NED, VIC or FAM and 0.7 units Taq DNA polymerase.

Reactions consisted of 5 min pre-denaturation at 94 °C, 45 seconds of 28 denaturation cycles at 94 °C, 45 seconds of annealing temperature at 50-54 °C, 1.5 min of extension step at 72 °C, and denaturation stage (45 seconds at 94°C, 45 seconds at 52°C, 1.5 min at 72°C) in 8 cycles, and 5 min final extension at 72°C in one cycle.

PCR products were run on 1.8% (w/v) agarose gel using 0.5 X TBE (Tris-Boric Acid-EDTA) buffer for 2 hours. Gel taken from the electrophoresis system was visualized in UV Imager Gel Doc XR + system (Bio-Rad, USA) after immersion in ethidium bromide solution. A 100 bp ladder was used for observing the DNA polymorphism of maize genotypes.

Table 1. SSR primer names, sequences, and annealing temperatures used in this study

Primer name	Sequence	Annealing temp (°C)
Umc1675	ATCGCGACGAGTTAATTCAAACAT	52
Phi022	GTTCTTCCTCTTCCCCATCAGTCT	52
Umc2084	ACGAGCGAGTGGAGAATAGG	52
bnlg1839	AGCAGACGGAGGAAACAAGA	52
umc1743	TGGACTTCGAAAATTCTCTTCAGC	52
umc1993	CTTTTCTGCTACTCCTGCCTGC	52
phi 032	CTCCAGCAAGTGATGCTGGAC	52
umc1571	GCACTTCATAACCTCTCTGCAGGT	52
umc1450	ACAGCTCTTCTTGGCATCGT	52
umc1893	TCCAGTGCCACCCCTAGATAGTAA	54
umc1432	GGCCATGATACAGCAAGAAATGAT	54
umc1279	CAATCCAATCCGTTGCAGGTC	50
umc1129	GAGAGTATGCTACTCGCCGC	50
umc2016	AGAGACGACATGTCTATCCTTGCC	50

2.3. Data Analysis

SSRs were scored as either present or absent according to the presence of bands as 1 and absence as 0, respectively. A matrix was created by determining genetic distances, according to [20]. PIC (Polymorphism Information Content) was determined, according to [21]. At the same time, the effective number of alleles, gene diversity, Shannon's information index, and unbiased heterozygosity were calculated in PopGene ver 1.32 [2]. Analysis of molecular variance (AMOVA) and UPGMA (Cluster analysis) was performed using R software [20]. STRUCTURE software was used for the Bayesian clustering model. The cluster numbers (K) were detected by the protocol of [23].

3. Results and Discussion

3.1. SSR Genetic Diversity

Bands were detected and selected in 14 of 22 SSR primers obtained from the website MaizeGDB.org and 42 alleles were obtained from these bands. All primers used were 100% polymorphic. An average of 3 alleles per SSR primer was determined (Table 2). Most alleles were detected at the umc1571 locus (6), and the least alleles were seen at the phi022 (1) locus. The PIC value varied between 0.43-0.95, and the mean PIC value was 0.65 (Table 2).

Table 2. Primer names, allele numbers, PIC values and Polymorphism rates obtained from this study.

Primer Names	DNA sequences (5' - 3')	Allele Numbers	PIC Values	Polymorphism (%)
umc1675	F-ATCGCGACGAGTTAATTCAAACAT R-TACGATGTCTTCAGTGTGACACCA	2	0.43	100
phi022	F-GTTCTTCCTCTTCCCCATCAGTCT R-ATAGCTGCGCGTAAAGCAACC	1	0.53	100
umc1526	F-ACGAGCGAGTGGAGAATAGG R-AGCCCAGTACGTGGGGTC	3	0.61	100
bnlg1839	F-AGCAGACGGAGGAAACAAGA R-TCTCCCTCTCCCTCTTGACA	2	0.51	100
umc1743	F-TGGACTTCGAAAATTCTTTCAGC R-GAGAGGAGGAGCTTCACGAGC	4	0.67	100
umc1993	F-CTTTTCTGCTACTCCTGCCTGC R-CTAGCTGATGGAGGCTGTAGCG	2	0.59	100
phi032	F-CTCCAGCAAGTGATGCTGGAC R-GACACCCGGATCAATGATGGAAC	2	0.44	100
umc1571	F-GCACTTCATAACCTCTCTGCAGGT R-CACCGAGGAGCACGACAGTATTAT	6	0.81	100
umc1450	F-ACAGCTCTTCTTGGCATCGT R-GACTTTGCTGGTCAGCTGGT	4	0.95	100
umc1893	F-TCCAGTGCCACCCCTAGATAGTAA R-ACCCAGAGTATCTCATCACCCCTT	3	0.62	100
umc1432	F-GGCCATGATACAGCAAGAAATGAT R-TACTAGATGATGACTGACCCAGCG	5	0.79	100
umc1279	F-CAATCCAATCCGTTGCAGGTC R-GATGAGCTTGACGACGCCTG	2	0.69	100
umc1129	F-GAGAGTATGCTACTCGCCGC R-GACGAGTTTGGAGTGCCATT	3	0.74	100
umc2016	F-AGAGACGACATGTCTATCCTTGCC R-ATTGCATTGCATTACAGCTGTTGT	3	0.65	100
Mean		3	0.65	100

PIC. Polymorphism information content

The lowest Shannon's information index, genetic diversity, and unbiased heterozygosity were detected in Izmit province. The lowest effective alleles number (N_e) was detected in Corum province. The highest gene diversity parameters were seen in the Trabzon province (Table 3). The value of polymorphic alleles number was found higher than [8] and [24]. The PIC value determines the effectiveness of the discriminant power between polymorphic loci [25] and genotypes [26] mean PIC value of 0.65 was calculated during this study and was found higher than [27-7-28-29-8] and [24]. The mean number of effective alleles was 1.25 during is the investigation and in agreement with [17]. The mean gene diversity (H_e) value was 0.18 and was found lower than [31] and [28]. Obtaining higher values for various diversity indices during the current investigation proposed the presence of higher genetic diversity in the studied maize germplasm.

Table 3. Genetic diversity indices computed among 32 maize genotypes using 14 SSR primers.

Provinces	Ne	I	He	uHe
Amasya	1.314	0.250	0.173	0.207
Artvin	1.369	0.338	0.221	0.235
Corum	1.01	0.15	0.12	0.13
Duzce	1.12	0.17	0.14	0.12
Izmit	1.09	0.13	0.11	0.09
Karabuk	1.15	0.18	0.19	0.14
Rize	1.371	0.335	0.221	0.245
Sakarya	1.264	0.244	0.161	0.194
Trabzon	1.442	0.380	0.257	0.293
Zonguldak	1.321	0.285	0.190	0.211
Mean	1.245	0.246	0.178	0.187

NE: Effective alleles number, **He:** Gene diversity, **I:** Shannon's information index, **uHe:** Unbiased heterozygosity

The mean genetic distance between all genotypes was 0.28. The lowest genetic distance (0.03) was present between DZM-68 (Artvin) and DZM-55 (Rize). The highest genetic distance (0.63) was observed between DZM-145 (Corum) and DZM-20 (Trabzon) (Supp Fig. 1). Identification of genetically diverse genotypes is critical in breeding programs and can be observed with distant genetic distances between genotypes. With this determination, the possibility of heterosis or heterobeltiosis increases in crosses. Therefore, it can be said that DZM-20 and DZM-145 genotypes are the most distant genotypes and can be recommended as parents for maize breeding activities.

Analysis of molecular variance (AMOVA) reflected major variation within population (96%) as compared to among populations (4%) (Table 4). The presence of higher variation within the population as compared to among the population may be due to gene flow, genetic drift, foreign pollination, ecotype variation, adaptation [32], human activities, and environmental transformation [33].

Table 4. Analysis of molecular variance to determine the genetic diversity of 32 Maize genotypes.

Source	Df	SS	MS	Est. Var.	%
Among Pops	9	10.727	2.145	0.069	4%
Within Pops	22	40.298	1.832	1.832	96%
Total	31	51.025		1.901	100%

Est. Var: Estimated variance, **MS:** Mean square, **SS:** Sum of squares, **Df:** Degrees of freedom

The Unweighted Pair Group Method with Arithmetic Mean (UPGMA) method separated the 32 maize genotypes into three main groups as A, B, and C (Supp Fig. 2). Maize genotypes observing a higher level of genetic similarity were clustered very close to each other and vice versa. Group A comprised of 15 genotypes and was divided into two subgroups as A1 and A2. Group B clustered 14 genotypes and was divided into two subgroups as B1 and B2. Group C revealed 3 genotypes and was divided into two subgroups as C1 and C2.

The principal component analysis divided 32 maize genotypes into three populations (Fig. 2). The results obtained were compatible with UPGMA.

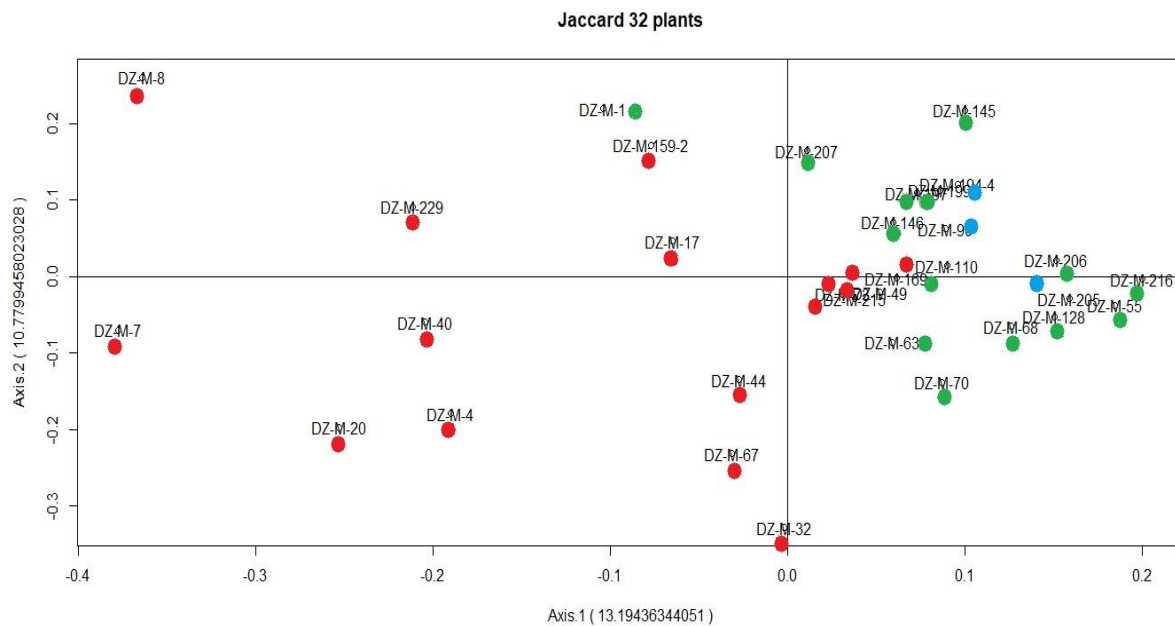


Fig. 2. Principle component analysis of 32 maize genotypes.

The number of groups (K) ranged from 1 to 10, according to STRUCTURE analyses. The most suitable goodness of fit was observed at the value of K = 3 (Fig. 3). The Bayesian clustering model constructed in STRUCTURE software separated the 32 maize genotypes into three clusters observing consistency with the UPGMA and principal component analyses (Supp Fig. 3). As a result, it can be said that the obtained genetic diversity findings contain beneficial information for maize breeders.

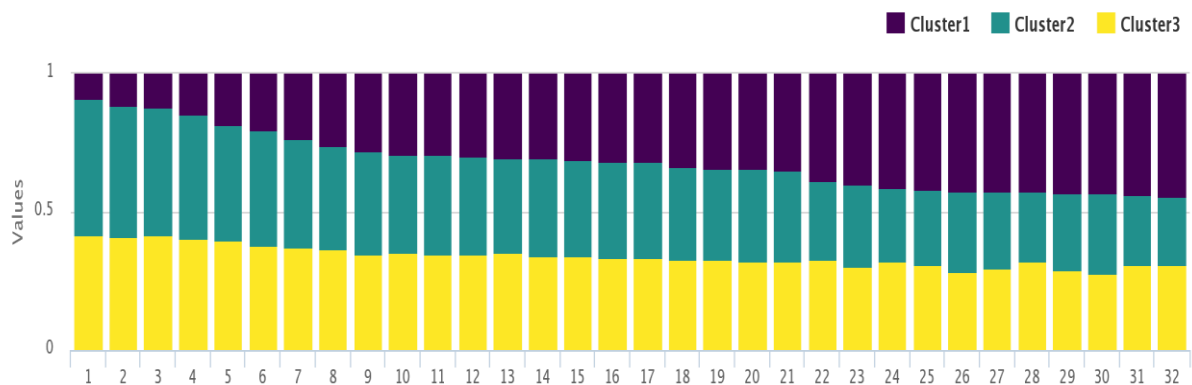


Fig. 3. Structure-based clustering of 32 maize genotypes using 14 SSR markers.

4. Conclusion

A sufficient amount of genetic diversity at the molecular level was reported among the studied 32 maize genotypes. The average of 3 alleles per SSR primer was detected, and the number of alleles varied from 1 (phi022) to 6 (umc1571). Clustering algorithms i.e., Bayesian-based clustering, UPGMA, and PCA separated the 32 maize genotypes into three groups. Analysis of molecular variance (AMOVA) reflected major variation within the population (96%) as compared to among populations (4%). Nei's genetic distances resulted in DZ-M-68 (Artvin) and DZ-M-55 (Rize) as the most genetically distant genotypes and can be implemented in future maize breeding programs.

Ethics in Publishing

There are no ethical issues regarding the publication of this study

Author Contributions

NB and FK contributed equally to this paper, and all authors made substantial contributions. NB and AY conceived and designed the study. All authors participated in the analysis of the results obtained from data and interpretation of the data. NB, MAN, AY, MA, FK, MGT, FSB wrote the manuscript. All authors reviewed and edited the manuscript and approved the final version before submission.

Acknowledgements

Dicle University Scientific Research Project Coordination supported this research with the project code ZIRAAT.16.006.

References

- [1] Van Heerwaarden, J., Doebley, J., Briggs, W. H., Glaubitz, J. C., Goodman, M. M., Gonzalez, J. D. J. S., Ross-Ibarra, J., (2011). Genetic signals of origin, spread, and introgression in a large sample of maize landraces. *Proceedings of the National Academy of Sciences*, 108(3), 1088-1092.
- [2] Yang, F., Liao, D., Wu, X., Gao, R., Fan, Y., Raza, M. A., Wang, X., Yong, T., Liu, W., Liu, J., Du, J., Shu, K., Yang, W., (2017). Effect of aboveground and belowground interactions on the intercrop yields in maize-soybean relay intercropping systems. *Field Crops Research*, 203, 16-23.
- [3] Avramova, V., Abdelgawad, H., Zhang, Z., Fotschki, B., Casadevall, R., Vergauwen, L., & Beemster, G. T., (2015). Drought induces distinct growth response, protection, and recovery mechanisms in the maize leaf growth zone. *Plant physiology*, 169(2), 1382-1396.
- [4] Saiyad, M. M., Kumar, S., (2018). Evaluation of maize genotypes for fodder quality traits and SSR diversity. *Journal of Plant Biochemistry and Biotechnology*, 27(1), 78-89.

- [5] Pachauri, A., Sarawgi, A. K., Bhandarkar, S., Ojha, G. C., (2017). Genetic variability and association study for yield contributing traits of promising core rice germplasm accessions (*Oryza sativa* L.). *Research on Crops*, 18(1), 133-138.
- [6] Omere, E. A., Nwaoguala, C. N., Emede, T. O., (2019). Microsatellite DNA Marker For Molecular Characterization of African Maize (*Zea mays* L.) Landraces. *Journal of Microbiology, Biotechnology and Food Sciences*, 976-978.
- [7] Al-Badeiry, N. A. H., Al-Saadi, A. H., Merza, T. K., (2014). Analysis of Genetic Diversity in Maize (*Zea mays* L.) Varieties Using SimpleSequence Repeat (SSR) Markers. *J. Babylon Uni. Pure Appl. Sci.* 22(6):1768-1776.
- [8] Kumari, A., Sinha, S., Rashmi, K., Mandal, S. S., Sahay, S., (2018). Genetic diversity analysis in maize (*Zea mays* L.) using SSR markers. *Journal of Pharmacognosy and Phytochemistry*, 1, 1116-1120.
- [9] Garrido-Cardenas, J. A., Mesa-Valle, C., Manzano-Agugliaro, F., (2018). Trends in plant research using molecular markers. *Planta*, 247(3), 543-557.
- [10] Vigouroux, Y., Glaubitz, J.C., Matsuoka, Y., Goodman, M.M., Sánchez, J., Doebley, J., (2008). Population structure and genetic diversity of New World maize races assessed by DNA microsatellites. *Amer. J. Bot.* 95: 1240-1253.
- [11] Sharma, L., Prasanna, B.M., Ramesh, B., (2010). Analysis of phenotypic and microsatellite-based diversity of maizelandraces in India, especially from the Northeast Himalayanregion. *Genetica* 138: 619-631.
- [12] Warburton, M.L., Wilkes, G., Taba, S., Charcosset, A., Mir, C., Dumas, F., Madur, D., Dreisigacker, S., Bedoya, C., Prasanna, B.M., Xie C.X., (2011). Gene flow among different teosinte taxa and intothe domesticated maize gene pool. *Genet. Res. Crop. Evol.*58: 1243-1261.
- [13] Lenka, D., Tripathy, S.K., Kumar, R., Behera, M., Ranjan, R., (2015). Assessment of genetic diversity in quality protein maize (QPM) inbreds using ISSR markers. *J. Environ. Biol.* 36:985-992
- [14] Kashiani, P., Saleh, G., Panandam, J.M., Abdullah, N.A.P., Selamat, A., (2012). Molecular characterization of tropical sweet corn inbredlines using microsatellite markers. *Maydica* 57 : 154-163.
- [15] Morgante, M., Olivieri, A. M., (1993). PCR-amplified microsatellites as markers in plant genetics. *The plant journal*, 3(1), 175-182.
- [16] Shukla, N., Kuntal, H., Shanker, A., Sharma, S. N., (2018). Mining and analysis of simple sequence repeats in the chloroplast genomes of genus *Vigna*. *Biotechnology Research and Innovation*, 2(1), 9-18.

- [17] Boopathi, N.M., (2013). Genetic mapping and marker assisted selection: basics, practice and benefits. Springer, New Delhi.
- [18] Doyle, J.J., Doyle, J.L., (1990). Isolation of plant DNA from fresh tissue, *Focus* 12:13-15.
- [19] Baloch, F.S., Alsaleh, A., Andeden, E.E., Hatipoglu, R., Nachit, M., Ozkan, H., (2016). High levels of segregation distortion in the Molecular linkage map of bread wheat representing West Asia and NorthAfrica region. *Turk J Agric For.* 40:352–364.
- [20] Nei, M., (1978). Estimation of average heterozygosity and genetic distance from a small number of individuals. *Genetics*, 89(3), 583-590.
- [21] Baloch, F.S., Alsaleh, A., de Miera, L.E.S., Hatipoglu, R., Ciftci, V., Karakoy, T., Yıldız, M., Ozkan, H., (2015). DNA based iPBS-retrotransposon markers for investigating the population structure of pea (*Pisumsativum*) germplasm from Turkey. *Biochem Syst Ecol* 61:244–252
- [22] Schliep, K. P., (2011). Phangorn: phylogenetic analysis in R. *Bioinformatics*, 27(4), 592-593.
- [23] Evanno, G., Regnaut, S., Goudet, J., (2005). Detecting the number of clusters of individuals using the software STRUCTURE: a simulation study. *Molecular Ecology*, 14(8), 2611-2620.
- [24] Joshi, B. K., Rawat, J., Adhikari, B., Pokhrel, R., (2020). SSR Markers Based Genetic Diversity in Nepalese Maize Landraces. *SAARC Journal of Agriculture*, 18(1), 23-37.
- [25] Gedik, A., Duygu, A.T.E.S., Erdogmus, S., Comertpay, G., Tanyolac, M.B., Ozkan, H., (2017). Genetic diversity of *Crocus sativus* and its close relative species analyzed by iPBS-retrotransposons. *Turk. J. Agric. For.* 22, 243–252.
- [26] Nemli, S., Kianoosh, T., Tanyolac, M.B., (2015). Genetic diversity and population structure of common bean (*Phaseolus vulgaris* L.) accessions through retrotransposon-based inter primer binding sites (iPBSs) markers. *Turk. J.Agric. For.* 39, 940–948.
- [27] Aci, M. M., Lupini, A., Mauceri, A., Morsli, A., Khelifi, L., Sunseri, F., (2018). Genetic variation and structure of maize populations from Saoura and Gourara oasis in Algerian Sahara. *BMC genetics*, 19(1), 51.
- [28] Belalia, N., Lupini, A., Djemel, A., Morsli, A., Mauceri, A., Lotti, C., ... & Sunseri, F., (2019). Analysis of genetic diversity and population structure in Saharan maize (*Zea mays* L.) populations using phenotypic traits and SSR markers. *Genetic Resources and Crop Evolution*, 66(1), 243-257.
- [29] Nyaligwa, L., (2016). Genetic diversity analysis of elite maize inbred lines of diverse sources using SSR markers. *Maydica*, 60(3), 1-8.

- [30] Sharma, T., Kumar, A., Dwivedi, S. C., Vyas, R. P., (2018). Molecular characterization and genetic diversity analysis of selected maize inbreds using SSR markers. *Journal of Environmental Biology*, 39(2), 228-236.
- [31] Barcaccia, G., Lucchin, M., Parrini, P., (2003). Characterization of a flint maize (*Zea mays* var. *indurata*) Italian landrace, II. Genetic diversity and relatedness assessed by SSR and Inter-SSR molecular markers. *Genetic Resources and Crop Evolution*, 50(3), 253-271.
- [32] Pour, A. H., Karahan, F., Ilhan, E., İlçim, A., Haliloglu, K., (2019). Genetic structure and diversity of *Adonis* L. (Ranunculaceae) populations collected from Turkey by inter-primer binding site (iPBS) retrotransposon markers. *Turk. J. Bot.* 43, 585–596.
- [33] Solouki, M.; Mehdikhani, H.; Zeinali, H.; Emamjomeh, A.A., (2018). Study of genetic diversity in Chamomile (*Matricaria chamomilla*) based on morphological traits and molecular markers. *Sci. Hortic.* 117, 281–287.

Fuzzy Entropy Based COPRAS Method in Determining the Investment Priorities of Logistics Centers in Survey and Planning Stage in Turkey

Ümran ŞENGÜL^{1*}, Ahmet Bilal ŞENGÜL²

¹Department of Business Administration, Faculty of Political Sciences, Çanakkale Onsekiz Mart University, 17100, Çanakkale/Turkey.

²Department of Mechanical Engineering, Faculty of Engineering, Yalova University, 77100 Yalova/Turkey.

Received: 16/08/2022, **Revised:** 07/10/2022, **Accepted:** 12/10/2022, **Published:** 30/12/2022

Abstract

The logistics center is a logistics region that is connected to all kinds of transportation networks, have low-cost, fast, and safe transfer equipment between different transportation modes, and have a direct impact on the country's economy and operational efficiency. Since Turkey is geographically located on logistics routes, the establishment of logistics centers are important in terms of economic development. However, the establishment of logistics centers requires serious costs, and the return of costs takes a long time. In this respect, it is necessary to determine the investment priority of the regions that are candidates for establishing a logistics center. Considering the costs of establishing a logistics center, it is significant to research which logistics center investment priority will be given. In this study, the fuzzy entropy-based COPRAS method was used to determine the order of investment priority, considering 5 logistics centers in the survey and planning stage of Turkish State Railways, and 17 criteria. According to the results, the first four most important criteria in logistics center investment priority are proximity to the port, foreign trade potential, number of transport modes, and proximity to the railway. The investment priority order of logistics centers in Istanbul/Yeşilbayır, İzmir/Çandarlı, Mardin, Zonguldak/Filyos, and Şırnak/Habur.

Keywords: Logistic center, fuzzy entropy, COPRAS, investment priorities, sensitivity analysis

Türkiye’de Etüt ve Planlama Aşamasındaki Lojistik Merkezlerin Yatırım Önceliklerinin Belirlenmesinde Bulanık Entropi Temelli COPRAS yöntemi

Öz

Lojistik merkez, her türlü ulaşım ağına bağlı, farklı ulaşım modları arasında düşük maliyetli, hızlı ve güvenli transfer ekipmanlarına sahip, ülke ekonomisine ve operasyonel verimliliğe doğrudan etki eden lojistik bölgelerdir. Türkiye coğrafik olarak lojistik güzergahlar üzerinde yer aldığından lojistik merkezlerin kurulması ekonomik kalkınma açısından önemlidir. Ancak lojistik merkezlerin kurulması ciddi maliyetler gerektirmekte ve maliyetlerin geri dönüşü uzun zaman almaktadır. Bu doğrultuda lojistik merkez kurmaya aday bölgelerin yatırım önceliğinin belirlenmesi gerekmektedir. Lojistik merkez kurmanın maliyetleri düşünüldüğünde hangi lojistik merkeze yatırım önceliğinin verileceğinin araştırılması önemlidir. Bu çalışmada, Türkiye Cumhuriyeti Devlet Demiryolları'nın etüt ve planlama aşamasında yer alan 5 lojistik merkez ve 17 kriter dikkate alınarak yatırım öncelik sırasının belirlenmesi için bulanık entropi tabanlı COPRAS yöntemi kullanılmıştır. Elde edilen sonuçlara göre, lojistik merkez yatırım önceliğinde en önemli ilk dört kriter limana yakınlık, dış ticaret potansiyeli, taşıma modlarının sayısı ve demiryoluna yakınlıktır. Lojistik merkezlerin yatırım öncelik sıralaması İstanbul/Yeşilbayır, İzmir/Çandarlı, Mardin, Zonguldak/Filyos ve Şırnak/Habur'dur.

Anahtar Kelimeler: Lojistik merkez, bulanık entropi, COPRAS, yatırım öncelikleri, duyarlılık analizi

1. Introduction

The increase in the level of international trade throughout the world, the globalization of production, the timely delivery of products to the user, and the requirements for good management of transportation, storage, and distribution centers have increased the interest in the logistics sector. Providing goods to reach all over the world with globalization has led to an increase in logistics movements and the emergence of fields such as intermodal transportation, combined transportation, multi-type transportation, warehouse, and stock management, 3PL logistics enterprises, customs, and insurance management. It has revealed that all these services should be provided with quality, fast, integrated, and at the least cost by making use of economies of scale. All these logistics activities and service areas that have emerged to realize this led to the emergence of logistics centers [1].

A logistics center is an area where all activities related to national and international transportation, logistics, and distribution of goods are carried out by various operators. These are the centers where many integrated logistics activities such as transportation, distribution, warehousing, handling, consolidation, separation, customs clearance, export, import and transit operations, infrastructure services, insurance and banking, consultancy, and production, have effective connections to all modes of transportation, are carried out by businesses in a certain area on a commercial basis [1-2]. Logistics centers make a significant contribution to the country's economy by enabling transportation modes to be used more efficiently and by ensuring that the transportation modes are used at the points where they are most economical. By increasing the interaction between logistics centers, highways, and railways, the use of the railway for long-distance transport and the use of the railway for short-distance transportation, and by intensifying the traffic on the railways, reduce noise and environmental pollution and providing relief in terms of freight traffic on the highways. Thus, logistics centers provide an effective competitive advantage in the growth of the region where they are established, increase business volume, reduce carbon emissions, etc. [3-5].

The concept of a logistics center is very popular today and its definitions in some countries are as follows; FreightVillage (England), Transport Center (Denmark), Kombiterminal (Hungary), Interporto (Italy), Terminal Multimodal (Portugal), Güterverkehrszentrum (Germany), Platesforme Logistique, Centres Logistiques de FRET, (France), Inland port, Disicenters, Global Freight Villages (United States), Rail Service Center (RSC) and Tradesports (Netherlands), Dry port (Northern European countries), CentroIntegrado de Mercancias, Zona Actividades Logistica (Spain). In Turkey, the concepts of a logistics village, logistics center, logistics base, freight village, and logistics specialized organized industrial zone are preferred [6], [7]. In this study, the nomenclature "Logistics center" was used.

Logistics centers first came to the fore in Europe as a "freight village" phenomenon in the late 1960s. Turkish State Railways (TSR) "Logistics Centers" project was initiated in line with the

understanding of the importance of railway transportation in freight transportation in the transportation system and the plan to gradually shift the weight from highways to railroads [8]. Later, a logistics center was established by the private sector. The total project amount of the logistics centers built by TSR between 2007 and 2023 is 1 785 038 Turkish liras [9]. Logistics centers were established primarily in İstanbul (Halkalı), İzmit (Köseköy), Eskişehir (Hasanbey), Balıkesir (Gökköy), Samsun (Gelemen), Denizli (Kaklık), Mersin (Yenice), Erzurum (Palandöken), Uşak, Konya (Kayacık), Kahramanmaraş (Türkoğlu) ve Kars', where the load carrying potential is intense, in connection with the organized industrial zones. There are 3 ongoing constructions in Sivas, Rize (Iyidere), and İzmir (Kemelpasa); there are logistics centers with 3 completed projects in Bilecik (Bozüyük), Kayseri (Boğazköprü) and Tekirdağ (Çerkezköy). Five surveys and logistics centers with ongoing planning stages have been planned in İstanbul (Yeşilbayır), İzmir (Çandarlı), Zonguldak (Filyos), Mardin, Şırnak (Habur). In this case, it is aimed to reach a total of 23 logistics centers.

There are many different criteria in the selection of the logistics center locations that are functional, environmentally friendly, and in compliance with the legislation. The main factors when choosing the location of the logistics center are the intense logistics flow in the region and the proximity of the region to a wide variety of dense transportation networks. In addition, the suitability of the land and infrastructure, the suitability of its geographical location, the natural structure and current use of the land, its geological structure, the availability of quality transportation, intermodal transportation opportunities, social structure, cultural, historical, and natural assets, current urbanization situation and prospective planning, the economic development of the immediate environment, the annual development of the population, the diversity and number of industries in the region, and demographic factors [10].

The selection of logistics center locations is a decision-making problem that includes many criteria. By using Multi-Criteria Decision-Making Methods (MCDM), the investment priorities of logistics centers can be determined for which the location of the logistics center and the location of the organization are determined. The purpose of using MCDM methods is to keep the decision-making mechanism under control and to obtain the decision result as easily and quickly as possible in case of many situations and alternatives containing both qualitative and quantitative criteria.

The establishment of logistics center locations in Turkey is carried out by both the public and private sectors. Good planning of the logistics centers established in Turkey (functional, size, location, etc.), the establishment of some of them as logistics centers and the establishment of some of them at the scale of the transfer terminal, and the establishment of them without considering the current and future potential needs of the region cause inefficient investments [11]. Considering the input costs of logistics centers, it is seen that they consist of expropriation, excavation, coating, infrastructure, road construction, environment and security area, and superstructure costs. These costs are approximately 181 257 657 US\$ for a logistics center of 1

500 000 m² [12]. Due to the high input costs, it is important to determine the investment priority of the places determined for the logistics center establishment. In addition, since logistics centers are long-term investments, it is not attractive to invest in the private sector in this area in the first place [7]. In this respect, the decision to establish a logistics center is mostly made by using public capital. When using public capital, it is necessary to decide in which region this capital will be allocated for the logistics center first. In the study, in Turkey, the survey and planning stage are ongoing in Istanbul/Yeşilbayır, İzmir/Çandarlı, Zonguldak/Filyos, Mardin, and Şırnak/Habur logistics centers were evaluated with the fuzzy entropy based COPRAS (COMplex PROportional ASsessment) method to determine investment priorities under 17 criteria.

Most of the studies for Turkey are on the logistics center installation location selection. This study, it is aimed to determine the investment priority ranking of the logistics centers whose establishment locations have been determined by TSR and which are in the survey and planning stage. The COPRAS method, which has never been used in the literature, was used for the first time in this study in order the alternatives to determine the investment priority. In the following parts of the study, some of the literature review, the explanation of the method, the application, and the conclusion are included.

2. Literature Review

Ballis and Mavrotas (2007) used the PROMETHEE method, which is one of the MCDM methods, to determine the order of preference for three alternative locations nominated for a logistics center to be established in the Thrasio region near Athens [13]. Wang and Lui (2007) used fuzzy AHP and TOPSIS methods to determine the most suitable logistic center using fuzzy triangle numbers [14]. Baohua and Shiwei (2009), focus on the logistics center location and allocation problem under an uncertain environment. To solve the problem in the study, a genetic algorithm has been developed for the stochastic optimization model [15]. Kayıkçı (2010) developed a conceptual model from the combination of AHP and artificial neural networks (ANN) methods to determine the most appropriate logistics center location [16]. Turskis and Zavadskas (2010) developed the ARAS-F method for the selection of the logistics center location [17]. Boile et al., (2011) used a different methodology in the valuation of logistics centers by making use of the Delphi method, which includes both qualitative and quantitative evaluations [18]. Karadeniz and Akpınar (2011) determined the position of Trabzon in national and international transportation, and a new proposal was developed for the establishment of a logistics center in Trabzon [19]. Hong and Xiaohua (2011) used AHP, one of the MCDM methods, to select the logistics center location and conducted a simulation study in Matlab to measure the effectiveness of the model [20]. Notteboom (2011) used MCA (multi-criteria analysis) method for the select three container hub port locations in South Africa [21]. Elgün and Elitaş (2011) applied the model used by Boile et al (2010) to determine the establishment locations of logistics centers in Turkey. Candidates and potential candidates in Turkey's North-

South logistics line were compared with the model they proposed. Ranking of places to be nominated; Mersin, Konya, Bilecik, and Eskişehir [22]. Erkayman et al (2011), using the Fuzzy TOPSIS method, selected the logistics center location of Erzurum, Diyarbakır, and Malatya provinces. Erzurum, Diyarbakır, and Malatya came out as the most suitable ranking [23]. Bayraktutan and Özbilgin (2014), with classical and fuzzy logic methods, evaluated the basis of foreign trade volume, transportation infrastructure, and freight traffic parameters of provinces in Turkey and compared the results [24]. Tomić et al., (2014) used the Greedy Heuristics Algorithm and AHP, one of the MCDM methods, for the selection of the most suitable logistics center located in the Balkan Peninsula [25]. Hamzaçebi et al., (2016) used the MOORA method, one of the MCDM methods, for the selection of the most suitable logistics center located in the Black Sea region [26]. Aydın (2016) compared the performance of three logistic center locations by applying negative fuzzy numbers to the AHP method [11]. Elgün and Aşıkoğlu (2016) used TOPSIS, one of the MCDM methods, to determine the suitability of candidate places to establish logistics centers. They aimed to determine the most suitable center or centers to become a logistics center in Turkey. As the most suitable places to establish logistics centers in Turkey; are found in Mersin, Konya, and Bilecik (Bozüyük) [10]. Karaşan (2016) used the intuitive fuzzy DEMATEL, fuzzy ANP, and fuzzy TOPSIS methods in his study and chose the most suitable logistics center location for Istanbul. He found that the most suitable location was the Pendik-Orhanlı location [27]. Pham et al., (2017) used Fuzzy Delphi TOPSIS to locate a logistics center to be established in Vietnam [28]. Yazdani et al., (2020) used Data Envelopment Analysis (DEA), FUCOM, and CoCoSo methods to determine the priority order of five candidate locations for the logistics center in Spain [29]. Özdemir et al., (2020) evaluated 6 logistics center locations determined by the Turkish state railways with AHP and TOPSIS methods from MCDM methods in line with the criteria determined in the Logistics Master Plan [9]. Shahparvari et al., (2020), to determine the location of a logistics center to be established in the Northwest region of Iran, firstly used GIS to identify potential regions and applied VIKOR and PROMETHEE methods to prioritize these potential regions [30]. Demirkıran and Öztürkoğlu (2020) used the PROMETHEE II method, one of the MCDM methods, in terms of establishing Logistics Centers for 26 regions in Turkey in NUTS-Level 2. Istanbul has emerged as the most suitable region for the logistics center located in all scenarios [31]. Dumlu and Wolff (2021) used the MOORA method, one of the MCDM methods, to determine the efficiency of 11 logistics centers whose construction was completed by the Turkish state railways [32]. Çakmak et al., (2021) proposed a method by combining the Binary Particle Swarm Optimization algorithm and GIS to determine the location of a logistics center to be established in Istanbul [33]. Nong (2021) used ANP and TOPSIS methods to determine the most suitable logistics center located in Dong Nai, Vietnam [34]. Türkmen (2021), using AHP and TOPSIS, tried to determine which of the provinces of İzmir, Samsun, Kocaeli, İstanbul, and Balıkesir would be the most appropriate logistics center. Respectively, İstanbul, Kocaeli, Samsun, Izmir, and Balıkesir came out [35]. Tumenbatur (2021), using AHP and Center Gravity Method, aimed to evaluate which railway line to carry to Europe over Turkey

in freight transportation by the Baku-Tbilisi-Kars railway line and to determine a logistics center location to be created on the line. Erzincan and Osmaniye were determined as the most suitable location for the logistics center [36].

Most of the studies for Turkey are on the logistics center installation location selection. This study, it is aimed to determine the investment priority ranking of the logistics centers whose establishment locations have been determined by TSR and which are in the survey and planning stage. The intensity of the input costs of logistics centers; expropriation, excavation, coating, infrastructure, road construction, environmental and safety belt, superstructure, etc. It is predicted that for a logistics center of 1,500,000 m², including costs, it will be approximately 181 257 657 US\$ [12]. Since the Turkish economy has the status of a developing country, it is not possible to establish all the logistics village centers that are in the survey and planning stage at the same time. In this respect, the main subject of this study is which center should be given investment priority. When the 2nd Revised investment plan of TSR for 2022 is examined, the project amount of 2,662,295,127 TL should be used from 2007 to 2025 under the title of “establishment of logistics and load centers”. It is seen that 205.012.000 TL of this amount is distributed in different amounts to 9 cities (Kars, Sivas, Istanbul, Mardin, Kayseri, Bilecik, Erzurum, Kahramanmaraş, Niğde) [37]. As can be seen in the 2022 investment plan, it has not been possible to allocate a budget to all the logistics centers planned to be built. In this respect, it is important to determine the investment priorities of logistics centers, whose survey and planning work has been completed, to use the limited budget most efficiently.

In studies conducted in this area, the criteria to be considered in determining the investment priority of logistics centers are also important. When the studies in this field are examined, it has been observed that the criteria have been chosen by considering the expert opinion or the criteria used in previous studies. However, in this study, the criteria obtained by Pekkaya and Keleş (2021) [38] by conducting qualitative research were used to determine the criteria considered in the selection of logistics locations, since they were more inclusive and were found because of research. Expert opinion is needed to determine the weights of the criteria discussed. Expert opinions are usually expressed verbally. In the study, Fuzzy Logic was used for the analysis of verbal expressions. The COPRAS method, which has never been used in the literature, was used for the first time in this study in order the alternatives to determine the investment priority. The reasons for the use of the COPRAS method in this study are that it was used first in this field, it is easy to apply and understand compared to other MCDM techniques, and it can evaluate both minimize and maximize criteria. It also compares the decision options with each other and gives a percentage of how good or bad it is from other alternatives [39].

As given in the literature review above, it has been observed that 8 studies are using MCDM techniques related to the determination of logistics center locations in Turkey. These articles are summarized in Table 1.

Table 1. MCDM techniques related to the determination of logistics center locations in Turkey

Author/year	MCDM method	The purpose of the article	Findings
Erkayman et al (2011),[23]	Fuzzy TOPSIS	Erzurum, Diyarbakir, and Malatya provinces are ranked for logistics village location selection.	According to the authors, the logistics center establishment location is Erzurum, Diyarbakir, and Malatya, respectively.
Elgün and Elitaş (2011), [22]	Model proposal	Candidates and potential candidates in Turkey's North-South logistics line were compared with their proposed model.	According to the authors, the most suitable places for the logistics center are Mersin, Konya, Bilecik, and Eskişehir.
Karaşan (2016), [27]	Intuitionistic fuzzy DEMATEL, Fuzzy ANP, and Fuzzy TOPSIS	The most suitable logistics center location in Istanbul has been determined.	According to the author, the most suitable location for the logistics center is the Pendik-Orhanlı location.
Elgün and Aşıkoğlu (2016), [10]	TOPSIS	Determining the most suitable center or centers to be a logistics center in Turkey	According to the authors, the most suitable places for the logistics center are Mersin, Konya, and Bilecik (Bozüyük).
Özdemir et al (2020), [9]	AHS and TOPSIS	Six logistics center investments were evaluated.	According to the authors, the most suitable logistics center locations for investments were Istanbul (Yeşilbayır), Bilecik (Bozüyük), Kayseri (Boğazköprü), Karaman, Mardin, Bitlis (Tatvan).
Demirkıran and Öztürkoğlu (2020), [30]	Promethee II	NUTS 2 levels in Turkey 26 regions were compared for logistics center location selection.	According to the authors, Istanbul was the most suitable region for the logistics center located in all scenarios.
Türkmen (2021), [34]	AHP and TOPSIS	It has been tried to determine which of the provinces of Izmir, Samsun, Kocaeli, Istanbul, and Balıkesir can be the most suitable logistics center.	According to the authors, the most suitable places for the logistics center are İstanbul, Kocaeli, Samsun, İzmir, and Balıkesir.
Tümenbatur (2021), [35]	AHP and Centre Gravity Method	With the Baku-Tbilisi-Kars railway line, freight transport to Europe via Turkey It was evaluated which railway line would be good to transport. In addition, it is aimed to determine a logistics center to be created on the line.	Erzincan and Osmaniye were determined as the most suitable location for the logistics center.

3. Methodology

Multi-Criteria Decision Methods began to be used in the 1960s to help solve decision-making problems. More than one criterion is considered when making a decision. In multi-criteria decision-making, the criteria are primarily weighted, and the priority order of the alternatives is determined according to the weighted criteria. Many methods have been developed in the literature to solve multi-criteria decision-making problems. In this study, COMplex PROportional ASsessment (COPRAS) method, which was developed in 1996, will be used to determine the investment priority of logistics centers. In the COPRAS method, no method is

given to determine the criterion weights. In the study, the fuzzy entropy method was used to determine the criterion weights. The COPRAS method has been used in the literature in the performance ranking of construction companies using financial ratios, in the performance evaluation of Turkish Coal enterprises between 2008-2012, in the performance ranking of the Mechanical Chemistry Institute between 2008-2012, in the evaluation of different learning management systems, in material selection problems, in hotels' performance rankings and in many areas such as evaluating the environmental sustainability of construction projects [39].

3.1. Fuzzy Shanon's entropy based on alpha-level sets

Zadeh (1965) developed the theory of fuzzy sets to be able to express linguistic terms in the decision-making process and eliminate the uncertainty and subjectivity in human decisions and be precise. In the concept of a fuzzy set, membership degrees ranging from 0 to 1 are mentioned. In a fuzzy set, the number 0 indicates that the relevant object is not a member of the set, the number 1 indicates that the relevant object is a full member of the set, and any number between these two values indicates the degree of membership or partial membership of the related object to the set [40-43].

The fuzzy number is expressed as a fuzzy set describing a fuzzy range in the real number R. The range is also a fuzzy set because the boundaries of this range are indefinite. Among the various fuzzy numbers, the most popular is the triangular fuzzy numbers (TFNs) [44]. Generally, the triangular fuzzy number A is the number with the starting point l , the ending point u , and the vertex m and is shown as $[l, m, u]$ [41].

$$\mu_{\tilde{A}}(x) = \begin{cases} \frac{x-l}{m-l} & a \leq x \leq b \\ \frac{u-x}{u-m} & b \leq x \leq c \\ 0 & \text{other} \end{cases} \quad (1)$$

For the fuzzy number equivalent of linguistic expressions, the values given in Table 2 will be used.

Table 2. Linguistic expressions and triangle fuzzy number value [45]

Linguistic Expressions	Triangle Fuzzy number value
very little important	(0.0,0.1,0.3)
less important	(0.1,0.3,0.5)
moderately important	(0.3,0.5,0.7)
too important	(0.5,0.7,0.9)
too much important	(0.7,0.9,1)

The entropy concept, which was firstly proposed by Shanon in 1948 [46], was developed by Wang and Lee as a weighting method in 2009. For α cut sets covering interval data, Lotfi and

Fallahnejad (2010) extended Shannon's application of entropy. The solution of Shannon's fuzzy Entropy based on α -level clusters is calculated with the following steps [47].

Step 1) Fuzzy data \tilde{x}_{ij} comprising the decision matrix which is shown as Equation (2) is transformed into interval data according to different α -level sets.

$$\tilde{D} = \begin{bmatrix} \tilde{x}_{11} & \tilde{x}_{12} & \dots & \tilde{x}_{1n} \\ \tilde{x}_{21} & \tilde{x}_{22} & \dots & \tilde{x}_{2n} \\ \vdots & \vdots & \ddots & \vdots \\ \tilde{x}_{m1} & \tilde{x}_{m2} & \dots & \tilde{x}_{mn} \end{bmatrix}_{m \times n} \quad (2)$$

The α -level set of fuzzy variables \tilde{x}_{ij} can be expressed in the following interval form:

$$[(\tilde{x}_{ij})_{\alpha}^L, (\tilde{x}_{ij})_{\alpha}^R] = \left[\min_{x_{ij}} \{x_{ij} \in R \mid \mu_{\tilde{x}_{ij}}(x_{ij}) \geq \alpha\}, \max_{x_{ij}} \{x_{ij} \in R \mid \mu_{\tilde{x}_{ij}}(x_{ij}) \geq \alpha\} \right], \quad 0 < \alpha < 1 \quad (3)$$

Fuzzy data are transformed into different α -level sets by setting different levels of confidence, namely $1-\alpha$. Then the matrix composed of interval data is obtained as follows:

$$\tilde{B} = \begin{bmatrix} [x_{11}^L, x_{11}^R] & [x_{12}^L, x_{12}^R] & \dots & [x_{1n}^L, x_{1n}^R] \\ [x_{21}^L, x_{21}^R] & [x_{22}^L, x_{22}^R] & \dots & [x_{2n}^L, x_{2n}^R] \\ \vdots & \vdots & \ddots & \vdots \\ [x_{m1}^L, x_{m1}^R] & [x_{m2}^L, x_{m2}^R] & \dots & [x_{mn}^L, x_{mn}^R] \end{bmatrix}_{m \times n} \quad (4)$$

Step 2) The normalized values p_{ij}^L and p_{ij}^R are calculated as follows:

$$p_{ij}^L = \frac{x_{ij}^L}{\sum_{j=1}^m x_{ij}^R} \quad j = 1, 2, \dots, m, \quad i = 1, 2, \dots, n \quad (5)$$

$$p_{ij}^R = \frac{x_{ij}^R}{\sum_{j=1}^m x_{ij}^L} \quad j = 1, 2, \dots, m, \quad i = 1, 2, \dots, n \quad (6)$$

Step 3) The lower bound e_i^L and upper bound e_i^R of interval entropy are calculated as follows:

$$e_i^L = \min \left\{ -e_0 \sum_{j=1}^m p_{ij}^L \ln p_{ij}^L - e_0 \sum_{j=1}^m p_{ij}^R \ln p_{ij}^R \right\}, \quad i = 1, 2, \dots, n \quad (7)$$

$$e_i^R = \max \left\{ -e_0 \sum_{j=1}^m p_{ij}^L \ln p_{ij}^L - e_0 \sum_{j=1}^m p_{ij}^R \ln p_{ij}^R \right\}, \quad i = 1, 2, \dots, n \quad (8)$$

Where e_0 is equal to $(\ln m)^{-1}$ and $p_{ij}^L \cdot \ln p_{ij}^L$ or $p_{ij}^R \cdot \ln p_{ij}^R$ is equal to 0 if $p_{ij}^L = 0$ or $p_{ij}^R = 0$.

Step 4) The lower bound d_i^L and upper bound d_i^R of interval diversification are computed as follows:

$$d_i^L = 1 - e_i^R \quad i = 1, 2, \dots, n \quad (9)$$

$$d_i^R = 1 - e_i^L \quad i = 1, 2, \dots, n \quad (10)$$

Step 5) The lower bound w_i^L and upper bound w_i^R of interval weight of criterion i are calculated as follows:

$$w_i^L = \frac{d_i^L}{\sum_{s=1}^n d_s^L} \quad i = 1, 2, \dots, n \quad (11)$$

$$w_i^R = \frac{d_i^R}{\sum_{s=1}^n d_s^R} \quad i = 1, 2, \dots, n \quad (12)$$

Step 6) To calculate the average criterion weight, the arithmetic mean of the lower and upper values is taken.

3.2. COPRAS (COmplex PROportional ASsessment) Method

The ‘‘Complex Proportional Assessment’’ or COPRAS method was introduced by Zavadskas and Kaklauskas. This method can be applied to maximize or minimize criteria in an assessment where more than one criterion should be considered. The steps of the COPRAS method are as follows [48].

Step 1) Decision matrix $F = [x_{ij}]_{m \times n}$ is normalized using Eq. (13).

The normalized decision matrix is denoted by $G = [g_{ij}]_{m \times n}$. The purpose of normalization is to obtain different dimensionless values to compare all criteria.

$$g_{ij} = \frac{x_{ij}}{\sum_{i=1}^m x_{ij}} \quad i = 1, 2, \dots, m; \quad j = 1, 2, \dots, n \quad (13)$$

Step 2) The weighted normalized decision matrix $Y = [y_{ij}]_{n \times m}$ was determined using Eq. (14).

$$y_{ij} = w_j g_{ij} \quad i = 1, 2, \dots, m; \quad j = 1, 2, \dots, n \quad (14)$$

Where g_{ij} is the normalized value of i th alternative according to j th criterion.

Step 3) The sums of the weighted normalized values were calculated for both the beneficial and non-beneficial criteria. These sums were calculated using Eq. (15) and (16).

$$K_{+i} = \sum_{j=1}^n y_{+ij} \quad (15)$$

$$K_{-i} = \sum_{j=1}^n y_{-ij} \quad (16)$$

where y_{+ij} and y_{-ij} are the weighted normalised values of the beneficial and non-beneficial criteria, respectively. The larger the K_{+j} value and the lower the K_{-j} value, the better the alternative. The values of K_{+j} and K_{-j} indicate the degree of goals reached by each alternative.

Step 4) The significance of the alternatives is determined by defining the characteristics of the positive alternatives K_{+j} and negative alternatives K_{-j} .

Step 5) The relative significance or priorities of the alternatives were determined. The relative significance value of the j th alternative, C_j , was calculated using Eq. (17).

$$C_j = K_{+i} \left(\left(K_{-min} \sum_{i=1}^m K_{-i} \right) / \left(K_{-i} \sum_{i=1}^m (K_{-min}/K_{-i}) \right) \right) \quad i = 1, 2, \dots, m \quad (17)$$

where K_{-min} is the minimum value of K_{-i} . C_j is ordered from largest to smallest. The higher the C_i , the greater its relative importance.

Step 6) The degree of utility of an alternative, determining the rank of the alternative, is determined by comparing the priorities of all alternatives for efficiency. It is calculated using Eq. (18).

$$U_i = \left[\frac{C_i}{C_{max}} \right] \times 100 \quad (18)$$

where C_{max} is the maximum relative significance value.

4. Application and Findings

In the study, 5 logistics centers in the survey and planning stage of TSR; İstanbul/Yeşilbayır, İzmir/Çandarlı, Zonguldak/Filyos, Mardin, Şırnak/Habur are discussed. These five logistics centers were taken as alternatives and the criteria considered to determine the investment priority of these alternatives were taken from the criteria determined by the benchmarking approach, to be used in the selection of logistics center locations, discussed by Pekkaya and Keleş (2021) [38]. These criteria are shown in Table 3.

Table 3. Criteria considered in determining the investment priority of the logistics center location

Short name	Criteria name	Description	
C1	Foreign trade potential	Total import and export amount in the province (thousand \$)	max
C2	Number of companies operating	Number of corporate taxpayers in the province	max
C3	Number of transport modes	Number of transport modes used in the province (Modes: Road, sea, air, rail, oil pipeline)	max
C4	Proximity to the port	Average proximity of the place to the port (km)	min
C5	Proximity to the airway	Average proximity of the place to the port (km)	min
C6	Proximity to the railway	Average proximity of the location to the railway (km)	min
C7	The possibility of expansion of the land	Expansion status of the land in the future (valued from 1 to 5 and weighted for this criterion)	max
C8	Land cost	Land prices per square meter in the province/region (₺/m ²)	min
C9	Rivalry	Distance to the nearest logistics village (km)	max
C10	Government incentive	Provincial incentive level	max
C11	Traffic	Traffic density of the province (number of cars/thousand people)	min
C12	Solid waste disposal	The ratio of municipality population to total municipal population (%)	max
C13	Education	Enrollment rate at the secondary level of the province (%)	max
C14	Population density	Number of people per square kilometer in the province	max
C15	Business climate	The unemployment rate in the province (%)	min
C17	Life Quality	GDP per capita (\$)	max
C17	Presence of experienced workers	Labor force participation rate (%)	max

Fuzzy entropy was used to determine criterion weights. For the data to be considered in determining the criterion weights with Fuzzy Entropy, 5 experts working in private and public, who are experts in the field of logistics, were consulted. The scale given in Table 1 was used to

evaluate the opinions of the experts. In Table 4, the triangular fuzzy number equivalent of expert (Expert, Exp.) opinions are given.

Table 4. Fuzzy evaluation matrix

	Exp1	Exp2	Exp3	Exp4	Exp5
C1	(0.7,0.9,1)	(0.7,0.9,1)	(0.7,0.9,1)	(0.7,0.9,1)	(0.7,0.9,1)
C2	(0,0.1,0.3)	(0.1,0.3,0.5)	(0,0.1,0.3)	(0.5,0.7,0.9)	(0.3,0.5,0.7)
C3	(0.7,0.9,1)	(0.5,0.7,0.9)	(0.7,0.9,1)	(0.5,0.7,0.9)	(0.7,0.9,1)
C4	(0.7,0.9,1)	(0.7,0.9,1)	(0.7,0.9,1)	(0.7,0.9,1)	(0.7,0.9,1)
C5	(0.1,0.3,0.5)	(0.3,0.5,0.7)	(0.5,0.7,0.9)	(0.3,0.5,0.7)	(0.3,0.5,0.7)
C6	(0.7,0.9,1)	(0.7,0.9,1)	(0.3,0.5,0.7)	(0.7,0.9,1)	(0.7,0.9,1)
C7	(0.7,0.9,1)	(0.7,0.9,1)	(0.5,0.7,0.9)	(0.1,0.3,0.5)	(0.3,0.5,0.7)
C8	(0.3,0.5,0.7)	(0.7,0.9,1)	(0.5,0.7,0.9)	(0.5,0.7,0.9)	(0.3,0.5,0.7)
C9	(0.5,0.7,0.9)	(0.5,0.7,0.9)	(0.1,0.3,0.5)	(0,0.1,0.3)	(0,0.1,0.3)
C10	(0.5,0.7,0.9)	(0.5,0.7,0.9)	(0,0.1,0.3)	(0.7,0.9,1)	(0,0.1,0.3)
C11	(0.1,0.3,0.5)	(0.7,0.9,1)	(0.1,0.3,0.5)	(0.5,0.7,0.9)	(0.1,0.3,0.5)
C12	(0.1,0.3,0.5)	(0.1,0.3,0.5)	(0,0.1,0.3)	(0.3,0.5,0.7)	(0.1,0.3,0.5)
C13	(0,0.1,0.3)	(0.3,0.5,0.7)	(0.3,0.5,0.7)	(0.1,0.3,0.5)	(0.3,0.5,0.7)
C14	(0,0.1,0.3)	(0.5,0.7,0.9)	(0.3,0.5,0.7)	(0,0.1,0.3)	(0.3,0.5,0.7)
C15	(0.3,0.5,0.7)	(0.5,0.7,0.9)	(0.3,0.5,0.7)	(0.3,0.5,0.7)	(0.1,0.3,0.5)
C16	(0.1,0.3,0.5)	(0.7,0.9,1)	(0.3,0.5,0.7)	(0.1,0.3,0.5)	(0.1,0.3,0.5)
C17	(0.5,0.7,0.9)	(0.3,0.5,0.7)	(0.3,0.5,0.7)	(0.1,0.3,0.5)	(0.7,0.9,1)

After the fuzzy decision matrix was created, the normalized interval decision matrix given in Table 4 was obtained by using Equations (3), (4), and (5). The segment set α , A_α , consists of members whose memberships are not less than α . α is an arbitrary value and is expressed by Equation (19).

$$A_\alpha = \{x \in E | \mu_A(x) \geq \alpha\} \tag{19}$$

α is a probability value, for example, if $\alpha=0.3$, it means a set containing 0.3 and higher probability values [49]. In the order of the criteria, the value of α takes a value between 0-1. In studies conducted in the literature, $\alpha = 0.5$ was generally taken. In the study, the α cutoff value for weighting the criteria/alternatives was handled at three different levels ($\alpha=0.1;0.5;0.9$) and sensitivity analysis was performed. The lower and upper bound of interval entropy (e_i^L and e_i^R) and interval diversification (d_i^L and d_i^R) values are computed and shown in Table 5.

Table 5. The values e_i^L, e_i^R, d_i^L and d_i^R

	$\alpha=0,1$		$\alpha=0,5$		$\alpha=0,9$	
	e_i^L, e_i^R	d_i^L, d_i^R	e_i^L, e_i^R	d_i^L, d_i^R	e_i^L, e_i^R	d_i^L, d_i^R
C1	[0.871,1.00]	[0.078,0.17]	[0.932,1.00]	[0.00,0.068]	[0.987,1.00]	[0.00,0.013]
C2	[0.475,0.938]	[0.042,0.16]	[0.655,0.910]	[0.090,0.345]	[0.813,0.870]	[0.13,0.187]
C3	[0.836,0.999]	[0.074,0.17]	[0.911,1.00]	[0.00,0.089]	[0.979,1.00]	[0.00,0.021]
C4	[0.871,1.00]	[0.078,0.17]	[0.932,1.00]	[0.00,0.068]	[0.987,1.00]	[0.00,0.013]
C5	[0.666,0.989]	[0.059,0.17]	[0.812,0.990]	[0.010,0.187]	[0.948,0.980]	[0.020,0.052]
C6	[0.833,0.994]	[0.074,0.17]	[0.906,0.990]	[0.010,0.094]	[0.971,0.990]	[0.010,0.029]
C7	[0.737,0.980]	[0.066,0.17]	[0.842,0.970]	[0.030,0.158]	[0.936,0.960]	[0.040,0.064]
C8	[0.762,0.993]	[0.068,0.17]	[0.866,0.990]	[0.010,0.134]	[0.962,0.990]	[0.010,0.038]
C9	[0.497,0.926]	[0.044,0.16]	[0.660,0.90]	[0.10,0.340]	[0.800,0.850]	[0.150,0.200]
C10	[0.589,0.922]	[0.052,0.16]	[0.708,0.890]	[0.110,0.292]	[0.809,0.850]	[0.150,0.191]
C11	[0.647,0.900]	[0.058,0.16]	[0.881,0.880]	[0.120,0.119]	[0.918,0.920]	[0.080,0.082]
C12	[0.460,0.978]	[0.041,0.17]	[0.687,0.970]	[0.030,0.314]	[0.894,0.950]	[0.050,0.106]
C13	[0.558,0.972]	[0.050,0.17]	[0.735,0.960]	[0.040,0.265]	[0.896,0.940]	[0.060,0.104]
C14	[0.527,0.939]	[0.047,0.16]	[0.629,0.940]	[0.060,0.371]	[0.715,0.940]	[0.060,0.285]
C15	[0.666,0.989]	[0.059,0.17]	[0.813,0.990]	[0.010,0.187]	[0.948,0.990]	[0.020,0.052]
C16	[0.541,0.948]	[0.048,0.16]	[0.703,0.930]	[0.070,0.298]	[0.843,0.890]	[0.110,0.157]
C17	[0.70,0.982]	[0.062,0.17]	[0.824,0.970]	[0.030,0.176]	[0.936,0.960]	[0.040,0.064]

In the last stage, the arithmetic average of the lower and upper entropy values was taken to determine the criterion weights and it is shown in Table 6.

Table 6. Weights of criteria

	Weights				
	$\alpha=0,1$		$\alpha=0,5$		$\alpha=0,9$
Proximity to the port	0.7997	Foreign trade potential	0.6520	Foreign trade potential	0.5267
Foreign trade potential	0.7997	Proximity to the port	0.6510	Proximity to the port	0.5267
Number of transport modes	0.7726	Number of transport modes	0.6420	Number of transport modes	0.5265
Proximity to the railway	0.7702	Proximity to the railway	0.6420	Proximity to the airway	0.5258
Land cost	0.7104	Traffic	0.6360	Business climate	0.5258
The possibility of expansion of the land	0.6934	Land cost	0.6190	Proximity to the railway	0.5213
Presence of experienced workers	0.6599	The possibility of expansion of the land	0.6040	Land cost	0.5210
Proximity to the airway	0.6340	Presence of experienced workers	0.5910	The possibility of expansion of the land	0.5156
Business climate	0.6340	Proximity to the airway	0.5880	Presence of experienced workers	0.5156
Traffic	0.6163	Business climate	0.5600	Traffic	0.5102
Government incentive	0.5692	Education	0.5500	Education	0.5097
Education	0.5462	Government incentive	0.5240	Solid waste disposal	0.5095
Life Quality	0.5305	Life Quality	0.5220	Life Quality	0.4784
Population density	0.5180	Solid waste disposal	0.5200	Population density	0.4732
Rivalry	0.4959	Population density	0.5150	Number of companies operating	0.4678
Number of companies operating	0.4756	Number of companies operating	0.5000	Rivalry	0.4625
Solid waste disposal	0.4623	Rivalry	0.5000	Government incentive	0.4578

In the study, the weights of criteria according to three different cut-off levels, at $\alpha=0.1$, were the first four most important criteria, proximity to the port, foreign trade potential, number of transport modes, and proximity to the railway. The first four most important criteria at $\alpha=0.5$ were foreign trade potential, proximity to the port, number of transport modes, and proximity to the railway. At $\alpha=0.9$, the first four most important criteria were foreign trade potential, proximity to the port, number of transport modes, and proximity to the railway. The first four criteria at all three alpha cut levels were proximity to the port, foreign trade potential, number of transport modes, and proximity to the railway. When we look at the literature, Pekaya, and Keleş (2021) [38], in their study to determine the criteria weights in determining the logistics center location, according to the opinion of 46 experts, "foreign trade potential", "proximity to the port", "market opportunities" and "proximity to the" railway" was found to be the most important criteria. Therefore, it has been seen that the criterion importance order determined in the study is in harmony with the literature. When looking at the distribution of import-export values in Turkey in 2021 by transport modes, the values in Figure 1 are observed.

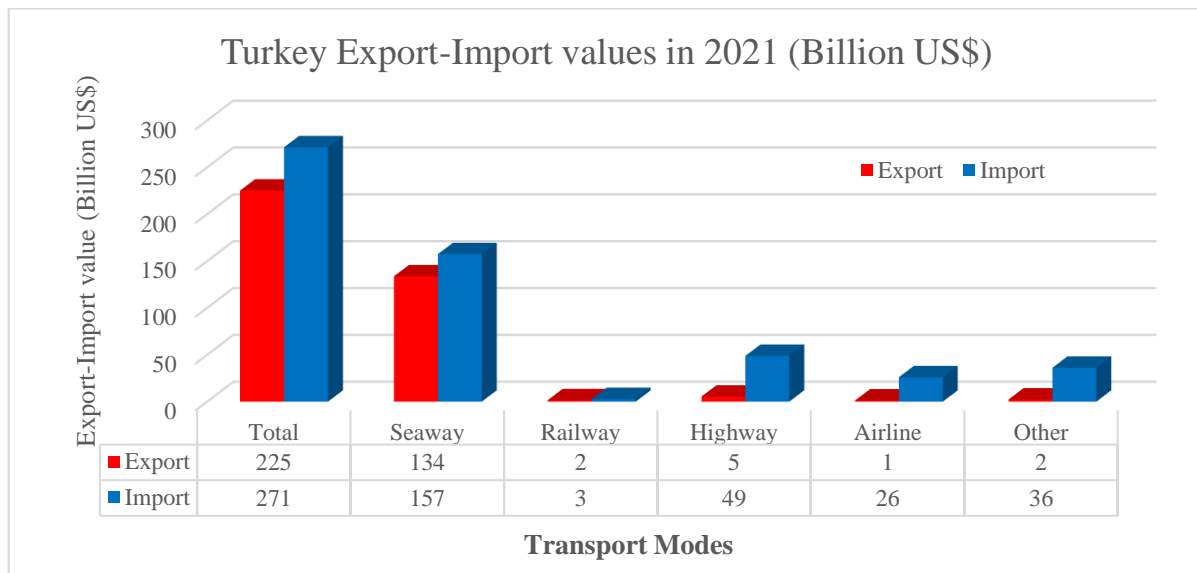


Figure 1. Column chart of Turkey's import-export values in 2021 according to transport modes [50]

As can be seen in Figure 1, Turkey's import and export values are made by using the seaway, which is one of the transportation modes most frequently. In this case, proximity to the port of the logistics center will increase its efficiency. Logistics centers are places where intermodal transportation is carried out intensively. In Turkey, which is surrounded by seas on four sides, intermodal transportation by using the maritime route and the railroad in the terrestrial part will reduce costs and increase the efficiency of logistics centers. When looking at the importance level of the criteria, the proximity of the logistics center to be established to the sea and railway is important. When looking at the weights of the criteria, the first criterion is the proximity to the port, the second is the foreign trade potential, and then the number of transport modes and

proximity to the railway. The criteria in order of weight are different α cutting levels, with little change in the rankings; land cost, the possibility of expansion of the land, presence of experienced workers, proximity to the airway, business climate, traffic, government incentive, education, life quality, population density, rivalry, number of companies operating and solid waste disposal. After determining the criteria weights, the values of 17 criteria for logistics center locations were determined (a decision matrix was created) and given in Table 7, to determine the investment priority of logistics center locations.

Table 7. Values of logistics center locations according to criteria

Criteria Shortname	Criteria	İstanbul/Yeşilbayır (A1)	Zonguldak/Filyos (A2)	İzmir /Çandarlı (A3)	Şırnak/Habur (A4)	Mardin (A5)
C1	Foreign trade	236.185.264	2.708.000	22.183.510	764.845	1.608.477
C2	potential Number of companies operating	950.836	13.564	208.471	7.597	16.581
C3	Number of transport modes	4	4	4	3	4
C4	Proximity to the port	20	5	50	670	480
C5	Proximity to the airway	27	10	100	50	15
C6	Proximity to the railway	20	5	50	180	10
C7	The possibility of expansion of the land	1	1	2	5	5
C8	Land cost	450	1.000	130	50	50
C9	Rivalry	30	280	100	610	420
C10	Government incentive	1	3	1	6	6
C11	Traffic	200	168	195	10	28
C12	Solid waste disposal	100	100	100	97	91
C13	Education	91,26	94,20	91,53	72,52	75,23
C14	Population density	3.048,67	178,48	368,45	76,42	97,97
C15	Business climate	14,70	9,30	17,10	33,50	33,50
C17	Life Quality	15.285	Quality	10.663	5.083	4.804
C17	Presence of experienced workers	52,60	47,20	51,70	39,10	39,10

The data in Table 6 are taken from the websites of TSI (Turkish Statistical Institute), BOTAŞ, TSR, and National Consultancy.

A normalized decision matrix was created by using the created decision matrix Eq. 13. The normalized decision matrix is given in Table 8.

Table 8. The normalized decision matrix

	C1	C2	C3	C4	C5	C6	C7	C8	C9	C10	C11	C12	C13	C14	C15	C16	C17
A1	0,897	0,794	0,211	0,016	0,134	0,075	0,071	0,268	0,021	0,059	0,333	0,205	0,215	0,809	0,136	0,361	0,229
A2	0,010	0,011	0,211	0,004	0,050	0,019	0,071	0,595	0,194	0,176	0,280	0,205	0,222	0,047	0,086	0,153	0,205
A3	0,084	0,174	0,211	0,041	0,495	0,189	0,143	0,077	0,069	0,059	0,324	0,205	0,215	0,098	0,158	0,252	0,225
A4	0,003	0,006	0,158	0,547	0,248	0,679	0,357	0,030	0,424	0,353	0,017	0,199	0,171	0,020	0,310	0,120	0,170
A5	0,006	0,014	0,211	0,392	0,074	0,038	0,357	0,030	0,292	0,353	0,047	0,186	0,177	0,026	0,310	0,114	0,170

According to equation 14, the weighted normalized decision matrix is obtained for $\alpha=0.1$, $\alpha=0.5$, and $\alpha=0.9$ levels. It is given in Table 9.

Table 9. The weighted normalized decision matrix

$\alpha=0,1$																	
	MAX	MAX	MAX	MİN	MİN	MİN	MAX	MİN	MAX	MİN	MİN	MAX	MAX	MAX	MİN	MAX	MAX
	C1	C2	C3	C4	C5	C6	C7	C8	C9	C10	C11	C12	C13	C14	C15	C17	C17
A1	0,7169	0,3777	0,1626	0,0131	0,0847	0,0581	0,0495	0,1903	0,0103	0,0335	0,2051	0,0947	0,1174	0,4189	0,0862	0,1917	0,1511
A2	0,0082	0,0054	0,1626	0,0033	0,0314	0,0145	0,0495	0,4229	0,0964	0,1004	0,1723	0,0947	0,1211	0,0245	0,0545	0,0810	0,1356
A3	0,0673	0,0828	0,1626	0,0326	0,3139	0,1453	0,0991	0,0550	0,0344	0,0335	0,2000	0,0947	0,1177	0,0506	0,1003	0,1337	0,1485
A4	0,0023	0,0030	0,1220	0,4374	0,1569	0,5232	0,2477	0,0211	0,2101	0,2009	0,0103	0,0919	0,0933	0,0105	0,1965	0,0637	0,1123
A5	0,0049	0,0066	0,1626	0,3134	0,0471	0,0291	0,2477	0,0211	0,1446	0,2009	0,0287	0,0862	0,0967	0,0135	0,1965	0,0602	0,1123
$\alpha=0,5$																	
A1	0,5846	0,3969	0,1351	0,0106	0,0786	0,0484	0,0431	0,1659	0,0104	0,0308	0,2117	0,1066	0,1181	0,4167	0,0762	0,1887	0,1351
A2	0,0067	0,0057	0,1351	0,0027	0,0291	0,0121	0,0431	0,3687	0,0972	0,0925	0,1778	0,1066	0,1219	0,0244	0,0482	0,0798	0,1212
A3	0,0549	0,0870	0,1351	0,0266	0,2911	0,1211	0,0862	0,0479	0,0347	0,0308	0,2064	0,1066	0,1185	0,0504	0,0887	0,1317	0,1328
A4	0,0019	0,0032	0,1014	0,3559	0,1455	0,4360	0,2156	0,0184	0,2117	0,1850	0,0106	0,1034	0,0939	0,0104	0,1737	0,0628	0,1004
A5	0,0040	0,0069	0,1351	0,2550	0,0437	0,0242	0,2156	0,0184	0,1457	0,1850	0,0296	0,0970	0,0974	0,0134	0,1737	0,0593	0,1004
$\alpha=0,9$																	
A1	0,4722	0,3715	0,1108	0,0086	0,0703	0,0393	0,0368	0,1396	0,0096	0,0269	0,1698	0,1044	0,1095	0,3827	0,0715	0,1729	0,1181
A2	0,0054	0,0053	0,1108	0,0021	0,0260	0,0098	0,0368	0,3101	0,0899	0,0808	0,1426	0,1044	0,1130	0,0224	0,0452	0,0731	0,1059
A3	0,0444	0,0815	0,1108	0,0215	0,2603	0,0984	0,0737	0,0403	0,0321	0,0269	0,1655	0,1044	0,1098	0,0462	0,0832	0,1206	0,1161
A4	0,0015	0,0030	0,0831	0,2881	0,1302	0,3541	0,1841	0,0155	0,1959	0,1616	0,0085	0,1013	0,0870	0,0096	0,1630	0,0575	0,0878
A5	0,0032	0,0065	0,1108	0,2064	0,0390	0,0197	0,1841	0,0155	0,1349	0,1616	0,0238	0,0950	0,0903	0,0123	0,1630	0,0543	0,0878

Using equations 15, 16, and 17, the performance levels of the alternatives (logistics centers) were determined for the three alpha levels.

Table 10. Performance values of alternatives

	$\alpha=0,1$							
	K-min/K-i					Ci	Ui	1
	K+i	K-i	K-min	K-i-Sum	K-min/K-i Sum			
İstanbul/Yeşilbayır	2.291	0.671	0.671	4.734	1.000	3.837	3.525	1.000

Fuzzy Entropy Based COPRAS Method in Determining the Investment Priorities of Logistics Centers in Survey and Planning Stage in Turkey

Zonguldak/Filyos	0.779	0.799			0.839		1.815	0.515	4
İzmir /Çandarlı	0.992	0.881			0.762		1.932	0.548	2
Şırnak/Habur	0.957	1.546			0.434		1.492	0.423	5
Mardin	0.935	0.837			0.802		1.925	0.546	3
	$\alpha=0.5$								
İstanbul/Yeşilbayır	2.372	0.622	0.622	4.221	1.000	3.940	3.443	1.000	1
Zonguldak/Filyos	0.986	0.731			0.851		1.898	0.551	4
İzmir /Çandarlı	1.175	0.813			0.766		1.995	0.580	2
Şırnak/Habur	1.092	1.325			0.470		1.595	0.463	5
Mardin	1.070	0.730			0.853		1.983	0.576	3
	$\alpha=0.9$								
İstanbul/Yeşilbayır	2.108	0.526	0.526	3.589	1.000	3.914	3.024	1.000	1
Zonguldak/Filyos	0.893	0.617			0.853		1.675	0.554	4
İzmir /Çandarlı	1.059	0.696			0.756		1.752	0.579	2
Şırnak/Habur	0.985	1.121			0.469		1.415	0.468	5
Mardin	0.960	0.629			0.836		1.727	0.571	3

The order of investment priority for the 5 logistics center locations, which are in the survey and planning stage, is the same at all three α levels (Table 10). According to the results, the order of investment priority for logistics center locations was İstanbul/Yeşilbayır, İzmir/Çandarlı, Mardin, Zonguldak/Filyos, and Şırnak/Habur. İstanbul/Yeşilbayır logistics center, which is one of these logistics centers in the survey and planning stage, is planned to have an area of 1 million m² and a carrying capacity of 6 million tons. The logistics center to be built in Zonguldak/Filyos is planned to be established with a capacity of 1 million tons of cargo and 25 million tons of cargo [7]. Information about the capacities of the logistics centers to be established in İzmir/Çandarlı and Şırnak/Habur could not be obtained from the literature.

5. Results and Discussion

Turkey is a bridge between Asia and Europe, the Black Sea, and the Mediterranean, and is at the intersection of three continents. Turkey is the distribution and collection (transfer) center for European, Balkans, Black Sea, Caucasus, Caspian, Central Asian, Middle Eastern, and North African countries. Turkey established the first public-owned Samsun/Gelemen logistics center in 2006 to gain the advantage of being on the logistics routes. In addition, logistics centers are planned to be built in 25 different places, and when all of them are opened, it is aimed to gain 12.8 million m² open area, stock area, container stock, and handling area with 35.6 million tons of additional transportation [7]. The establishment of these logistics centers is a necessity for Turkey's economic development in the short, medium, and long term. While determining the priority order of establishment from the logistics centers to be established, it is important to obtain the targeted benefit as soon as possible. The establishment of logistics centers requires serious costs and investment costs are expected to return in a short time. Because, in a feasibility report prepared for the establishment of a logistics center, the payback period of the investment was calculated as 18 years, considering the economic life of 55 years [12]. On the other hand, when the gross domestic product in Turkey is evaluated according to

the economic activity codes (A21) at current prices, as the transport and storage logistics sector data, the share of the logistics sector in GDP is 7.9% for 2020. The logistics sector constitutes 10%-12% of the GDP in developed countries [51]. In this respect, a value of 7.9% is a low value for a country that aims to be a logistics epicenter. The establishment of effective logistics centers that will recycle the investment costs in a short time is important for the production and commercial development of the country. According to the research on the subject of logistics, no matter what the job is, logistics costs constitute 10% of the cost of that job [52]. International competition is increasing in the logistics sector as well as in all areas.

In this study, investment priority rankings were determined under 17 criteria determined from the literature in 5 logistics centers that are in the survey and planning stage. The problem of determining the investment priority of the Logistics Center location is in the structure of the decision problem. Such problems with criteria and alternatives can be solved by multi-criteria decision analysis methods. In the study, fuzzy entropy was used to determine the criterion weights, namely the order of importance, and the COPRAS method was used for the investment priority ranking of the alternatives, namely the logistics center locations.

Considering the priority order of 17 criteria, when expert opinions are analyzed according to the fuzzy entropy method, the first four criteria for three alpha levels ($\alpha=0.1; 0.5; 0.9$) are proximity to the port, foreign trade potential, number of transport modes, proximity to the railway. It is important to establish logistics centers in places close to railways, where foreign trade potential is high, close to the port, where all types of transportation modes are available and accessible, and since railways are more economical than other land transportation modes in terms of transportation costs. Turkey's import and export values are made by using the most common maritime transport modes. In this case, the proximity of the logistics center to the port will increase its efficiency. Logistics centers are places where intermodal transportation is carried out intensively. The realization of intermodal transportation by using the maritime route and the railroad on the land side in Turkey, which is surrounded by seas on all four sides, will provide development in a way that reduces costs and increases the efficiency of logistics centers. When we look at the importance level of the criteria, the proximity of the logistics center to be established to the sea and railway is important. In the ranking of the criteria, the first criterion was the proximity to the port, the second was the foreign trade potential, and then the number of transport modes and proximity to the railway. According to the criteria weights, the criteria in the last four of the 17 criteria are population density, rivalry, number of companies operating, solid waste disposal, and government incentive. When these criteria are examined, it is noteworthy that there are criteria that are mostly related to the environment.

6. Conclusion

It is important to establish logistics centers in places close to railways, where foreign trade potential is high, close to the port, where all types of transportation modes are available and

accessible, and since railways are more economical than other land transportation modes in terms of transportation costs. In the ranking of the criteria, the first criterion was the proximity to the port, the second was the foreign trade potential, and then the number of transport modes and proximity to the railway. According to the criteria weights, the criteria in the last four of the 17 criteria are population density, rivalry, number of companies operating, solid waste disposal, and government incentive. When these criteria are examined, it is noteworthy that there are criteria that are mostly related to the environment.

In the selection of the logistics center location, the variables that have a direct relationship with the logistics activities came to the fore, and the weight of the variables that had an indirect relationship was relatively low. When the criteria weights are used to rank the investment priorities of the logistics center locations according to the COPRAS method, in the performance ranking of the three alpha levels of the five logistics centers that have been studied and planned, Istanbul/Yeşilbayır is in the first place, followed by İzmir/Çandarlı, Mardin, Zonguldak/Filyos, Şırnak/Habur. Considering the weights of the criteria, foreign trade potential took place in the first place. According to the result of this evaluation under 17 criteria, Istanbul/Yeşilbayır and İzmir/Çandarlı, which have a considerably higher foreign trade potential compared to other regions and yet are close to the port, took the first two places. Although the main objective is to make all these 5 logistics center locations, whose survey and planning stages have been completed, operational as soon as possible, this is not possible. According to the results of the study in 2023 investment planning of TSR, it is recommended to focus on logistics center locations in Istanbul/Yeşilbayır and İzmir/Çandarlı regions.

The result obtained in the study is a recommendation. The weights of the criteria were determined by taking the opinions of 5 experts in the study. Expert opinions are personal judgments. Suggestions can be developed by increasing the number of expert opinions, consulting different experts, considering different criteria, and using different MCDM methods.

Ethics in Publishing

There are no ethical issues regarding the publication of this study.

Author Contributions

In the study carried out, Ümran ŞENGÜL contributed to the determination of the analysis method of the data, the analysis, the literature review, and the evaluation of the results. Ahmet Bilal ŞENGÜL contributed to the creation of the idea, obtaining the data, evaluating the data and the results, and literature review studies.

References

- [1] Aydın, G.T. and Öğüt, K.S. (2008). Lojistik köy nedir?. 2. Uluslararası Demiryolu Sempozyumu, Demiryolu Fuarı Bildiriler Kitabı, İstanbul, 1439-1448.

- [2] Erdumlu, R. M. (2006). Kentsel lojistik ve lojistik köy uygulaması, (Yayınlanmamış Yüksek Lisans tezi), İstanbul: İstanbul Teknik Üniversitesi, Endüstri ve Endüstri Mühendisliği.
- [3] Bodaubayeva, G. (2015). Formation of industrial and logistic parks in Kazakhstan, 4th International Conference on Advanced Logistics and Transport (ICALT), Kazakhstan, 41-46.
- [4] Yang, C., Taudes, A. and Dong, G. (2017). Efficiency analysis of European freight villages: Three peers for benchmarking. *Central European Journal of Operations Research*, 25(1), 91-122. doi: 10.1007/s10100-015-0424-5.
- [5] Çalış, A. and Gencer, C. (2014). Historical development of worldwide freight villages and freight villages in Turkey. Paper presented in CIE44 & IMSS'14 Proceedings, Istanbul, 1351.
- [6] Demir, F. (2016). Türkiye'nin konumu açısından lojistik köylerin önemi: Kars lojistik köy örneği (Yayınlanmamış Yüksek Lisans Tezi). Kilis: Klis 7 Aralık Üniversitesi, İşletme Ana Bilim Dalı.
- [7] Genç, E. and Coşmuş, Ş. (2021). Logistics villages management features and logistics villages in Turkey. *International Journal of Social, Humanities and Administrative Sciences*, 7(35), 68-79. doi:10.31589/JOSHAS.511.
- [8] Aksoy, O. (2012). Lojistik köy yerlerinin belirlenmesi için bir tam sayılı programlama modeli: TCDD için bir uygulama (Yayınlanmamış Yüksek Lisans Tezi). Ankara: Gazi Üniversitesi, Endüstri Mühendisliği.
- [9] Özdemir, S., Keskin, B., Eren, T. and Özcan, E. (2020). Multi-criteria for the evaluation of logistics centers in Turkey investment priority decision model proposal. *Demiryolu Mühendisliği*, 12, 83-94. doi:10.47072/demiryolu.722626.
- [10] Elgün, M.N. and Aşıkoğlu, N.O. (2016). Lojistik köy kuruluş yeri seçiminde TOPSIS yöntemiyle merkezlerin değerlendirilmesi. *AKÜ ÜÜBF Dergisi*, 18 (1), 161-170. doi: 10.5578/jeas.27638.
- [11] Aydın, S. (2016). Lojistik merkez değerlendirmesi için karar verme modeli ve uygulama. 5. Ulusal ve Tedarik Zinciri Kongresi, Mersin, 137.
- [12] Yılmaz, R., Kubaş, A., Erbay, E.R. and Bengi, S.B., (2014). Çorlu Lojistik Köt Fizibilite Raporu, lojistik_koy_fizibilite_raporu_Çorlu.pdf.
- [13] Ballis, A. and Mavrotas, G. (2007). Freight Village Design Using the Multicriteria Method PROMETHEE. *Operational Research*, 7(2), 213–231. doi:10.1007/BF02942388.
- [14] Wang, S. and Liu, P. (2007). The Evaluation study on location selection of logistics center based on fuzzy AHP and TOPSIS. *International Conference on Wireless Communications, Networking and Mobile Computing*, 3779-3782.
- [15] Baohua, W. and Shiwei, H.E. (2009). Robust optimization model and algorithm for logistics center location and allocation under uncertain environment. *Journal of*

- Transportation Systems Engineering and Information Technology, 9(2), 69-74. doi: 10.1016/S1570-6672(08)60056-2.
- [16] Kayıkçı, Y. (2010). A conceptual model for intermodal freight logistics center location decisions. *Procedia-Social and Behavioral Sciences*, 2(3),6297-6311. doi: 10.1016/j.sbspro.2010.04.039.
- [17] Turskis, Z. and Zavadskas, E. K. (2010). A new fuzzy additive ratio assessment method (ARAS-F) Case study: The analysis of fuzzy multiple criteria to select the logistic center's location. *Transport*, 25(4), 423-432. doi: 10.3846/transport.2010.52
- [18] Boile, M., Theofanis, S. and Ozbay, K. (2011). Feasibility of freight villages in the NYMTC region. Center for Advanced Infrastructure and Transportation Freight and Maritime Program Rutgers, The State University of New Jersey, 1-24. <https://rosap.ntl.bts.gov/view/dot/23252>.
- [19] Karadeniz, V. and Akpınar, E. (2011). Logistic village applications in Turkey and proposal of a new kind of logistic village. *Marmara Coğrafya Dergisi*, 23, 49-71.
- [20] Hong, L. and Xiaohua, Z. (2011). Study on location selection of multi-objective emergency logistics center based on AHP. *Procedia Engineering*, 15, 2128-2132. doi: 10.1016/j.proeng.2011.08.398.
- [21] Notteboom, T. (2011). An application of multi-criteria analysis to the location of a container hub port in South Africa. *Maritime Policy Management*, 38(1), 51-79. doi: 10.1080/03088839.2010.533710.
- [22] Elgün, M. N. and Elitaş, C. (2011). Yerel, ulusal ve uluslararası taşıma ve ticaret açısından lojistik köy merkezlerinin seçiminde bir model önerisi. *Manisa Celal Bayar Üniversitesi Sosyal Bilimler Dergisi*, 9 (2) , 630-645
- [23] Erkeyman, B., Gundogar, E., Akkaya, G. and Ipek, M. (2011). A Fuzzy TOPSIS approach for logistics center location selection. *Journal of Business Case Studies*, 7(3), 49–54. doi: 10.19030/jbcs.v7i3.4263.
- [24] Bayraktutan, Y. and Özbilgin, M. (2014). Tüskiye'de illerin lojistik Merkez yatırım düzeylerinin bulanık mantık yöntemiyle belirlenmesi. *Erciyes Üniversitesi İktisadi ve İdari Bilimler Fakültesi Dergisi*, 43, 1-36. doi: 10.18070/euiibfd.67041.
- [25] Tomić, V., Marinković, D. and Marković, D. (2014). The selection of logistic centers location using multi-criteria comparison: a case study of the Balkan Peninsula. *Acta Polytechnica Hungarica*, 11(10), 97-113.
- [26] Hamzaçebi, C., İmamoğlu, G. and Alçı, A. (2016). Selection of logistics center location with MOORA method for black sea region of Turkey. *Journal of Economics Bibliography*, 3(15), 74-82. doi: 10.1453/jeb.v3i1S.785.
- [27] Karaşan, A. (2016). Lojistik köy ter seçiminde sezgisel bulanık bütünleşik bir çok ölçütlü yöntem önerisi (Yayınlanmamış Yüksek Lisans Tezi), İstanbul: İstanbul Teknik Üniversitesi, Fen Bilimleri Enstitüsü.

- [28] Pham, T.Y., Ma, H.M. and Yeo, G.T. (2017). Application of fuzzy Delphi TOPSIS to locate logistics centers in Vietnam: The Logisticians' Perspective. *The Asian Journal of Shipping and Logistics*, 33(4), 211-219. doi: 10.1016/j.ajsl.2017.12.004.
- [29] Yazdani, M., Chatterjee, P., Pamucar, D. and Chakraborty, S. (2020). Development of an integrated decision-making model for location selection of logistics centers in the Spanish autonomous communities. *Expert Systems with Applications*, 148. doi: 10.1016/j.eswa.2020.113208.
- [30] Shahparvari, S., Nasirian, A., Mohammadi, A., Noori, S. and Chhetri, P. (2020). A GIS-LP integrated approach for the logistics hub location problem. *Computers & Industrial Engineering*, 146, 1-17. doi: 10.1016/j.cie.2020.106488.
- [31] Demirkıran, Y. and Öztürkoğlu, Y. (2020). Türkiye'deki bölgelerin lojistik köy kurulması açısından potansiyelinin PROMETHEE II yöntemi ile incelenmesi. *Journal of Yasar University*, 15/58, 347-367.
- [32] Dumlu, H. and Wolff, A. (2021). Türkiye'deki lojistik köylerin potansiyel etkinliklerine göre değerlendirilmesi: MOORA yöntemi ile bir uygulama . *Kafkad Üniversitesi İktisadi ve İdari Bilimler Fakültesi Dergisi*, 12(24), 1000-1026. doi: 10.36543/kauibfd.2021.041.
- [33] Çakmak, E., Onden, I., Acar, A.Z. and Eldemir, F. (2021). Analyzing the location of city logistics centers in Istanbul by integrating geographic information systems with binary particle swarm optimization algorithm. *Case Studies on Transport Policy*, 9 (1), 59–67. doi: 10.1016/j.cstp.2020.07.004.
- [34] Nong, T.N-M. (2022). A hybrid model for distribution center location selection. *The Asian Journal of Shipping and Logistics*, 38(1), 40-49. doi: 10.1016/j.ajsl.2021.10.003.
- [35] Türkmen, B. (2021). Lojistik Köyü Yer Seçimi ve Türkiye'de Örnek Bir Uygulama (Yayınlanmamış yüksek lisans tezi), Konya: Necmettin Erbakan Üniversitesi, Fen Bilimleri Enstitüsü Endüstri Mühendisliği Anabilim Dalı.
- [36] Tümenbatur, A. (2021). Orta koridor üzerindeki demir ipekyolu güzergahı ve lojistik merkez yer seçimi. *Çukurova Üniversitesi Sosyal Bilimler Enstitüsü Dergisi*, Adana'nın Kurtuluşunun 100. Yılına Özel Sayı, 102-110. Doi: 10.35379/cusosbil.977922.
- [37] TSR, "Lojistik Merkezler," [Online]. Available: <http://www.tcdd.gov.tr/content/33>. [Accessed: 10.02.2022].
- [38] Pekkaya, M. and Keleş, N. (2021). Determining criteria interaction and criteria priorities in the freight village location selection process: the experts perspective in Turkey. *Asia Pacific Journal of Marketing and Logistics*, 34(7), 1348-1367. doi: 10.1108/APJML-05-2021-0338
- [39] Özbek, A. (2019). Çok kriterli karar verme yöntemleri ve Excel ile problem çözümü. 2. Baskı, Ankara: Seçkin Yayınevi
- [40] Chen, G. and Pham, T.T. (2001). Introduction to fuzzy sets, fuzzy logic, and fuzzy control systems. *Appl. Mech. Rev.* Nov 2001, 54(6): B102-B103.
- [41] Zadeh, L.A. (1965). Fuzzy Sets. *Information and Control*, 8(3), 338-353.

- [42] Tsaur, S.H., Chang T.Y. and Yen, C.H. (2002). The evaluation of airline service quality by fuzzy MCDM. *Tourism Management*, 23(2), 107-115. doi: 10.1016/S0261-5177(01)00050-4
- [43] Ertugrul, I. and Tuş, A. (2007). Interactive fuzzy linear programming and an application sample at a textile firm. *Fuzzy Optimization and Decision Making*, 6(1), 29-49. doi: 10.1007/s10700-006-0023-y
- [44] Lee, HS. (2005). “A Fuzzy Multi-Criteria Decision-Making Model for the Selection of the Distribution Center”. In: Wang L., Chen K., Ong Y.S. (eds) *Advances in Natural Computation. ICNC 2005. Lecture Notes in Computer Science, Vol 3612*. Springer, Berlin, Heidelberg.
- [45] Klir, G. J. and Yuan, Bo. (1995). *Fuzzy Sets and Fuzzy Logic: Theory and Applications, 1st ed.*, Pearson College Div.
- [46] Shannon, C. E. (1948). A Mathematical theory of communication. *Bell System Technical Journal*, 27, 379–423.
- [47] Hosseinzadeh, L. F. and Fallahnejad, R. (2010). Imprecise Shannon’s entropy and multi-attribute decision making. *Entropy*, 12, 53–62. doi: 10.3390/e12010053.
- [48] Zavadskas, A. and Kaklauskas, E.K. (1996). Determination of an efficient contractor by using the new method of multicriteria assessment, *International Symposium for “The Organization and Management of Construction”, Shaping Theory and Practice*, 94-104.
- [49] Baykal, N. and Beyan, T. (2004). *Bulanık Mantık İlke ve Temelleri*. Ankara: Bıçaklar Kitapevi.
- [50] www.tuik.gov.tr, [Accessed]: 01.07.2022.
- [51] Yurdakul, E. M. (2020). Türkiye’de lojistik sektörü ve ekonomik büyüme arasındaki ilişkinin VAR analizi ile incelenmesi. *Sosyal Ekonomik Araştırmalar Dergisi*, 20 (40), 174-185. doi: 10.30976/susead.707425.
- [52] Tanyaş, M. and Paksoy, T. (2012). *TR52 Konya – Karaman Bölgesi Lojistik Strateji Planı Ön hazırlık Raporu*, MÜSİAD Konya Şubesi.

Investigation of the Effects of Distress on Health Practices in Pregnant Women

Demet Kışlak¹, Sevinç Köse Tuncer^{2*}

¹Erzincan Binalı Yıldırım University Health Sciences Institute, Department of Nursing, Erzincan, Turkey.

²Erzincan Binalı Yıldırım University, Faculty of Health Sciences, Department of Nursing, Erzincan, Turkey.

Received:09/11/2022, **Revised:** 01/12/2022, **Accepted:** 19/12/2022, **Published:** 30/12/2022

Abstract

This study was conducted to examine the effect of distress on health practices in pregnant women at 12 weeks and over of pregnancy. The universe of this descriptive study consisted of women at 12 weeks and over of pregnancy who were admitted to the Obstetrics and Gynecology Department of a City Hospital. To calculate the minimum sample size to be included in the study, the sample selection formula was used in cases where the number of elements in the universe was unknown, and it was completed with 353 pregnant women. The data of the study were collected between November 2016 and April 2017, using the "Pregnancy Info Form", "Tilburg Pregnancy Distress Scale (TPDS)" and "Health Practices in Pregnancy Questionnaire" (HPPQ). In evaluating the data, the following were used: percentage distributions, averaging, t-test, Kruskal Wallis Variance Analysis, Mann-Whitney U-test, and Correlation Analysis. There is a statistically significant, negative, and low-level correlation between the total HPPQ score, the Spousal Involvement sub-dimension, and the total TPDS score ($p < 0.05$). It was found that increased distress of pregnant women decreases health practices. It is required to identify pregnant women under distress and reduce or eliminate the distress, contributing to mother-child health by increasing health practices accordingly.

Keywords: Pregnancy, health practices, distress

Gebelerdeki Distresin Sağlık Uygulamaları Üzerine Etkisinin İncelenmesi

Öz

Bu araştırma 12 hafta ve üzeri gebelerde distresin gebelikteki sağlık uygulamaları üzerine etkisinin incelenmesi amacı ile yapılmıştır. Tanımlayıcı türde olan bu araştırmanın evrenini bir Şehir Hastanesine bağlı doğum ve kadın hastalıkları polikliniğe başvuran 12 hafta üzeri gebelerden oluşmuştur. Çalışmaya alınması gereken minimum örneklem büyüklüğünü hesaplamak için evrendeki eleman sayısının bilinmediği durumlarda örneklem seçme formülü kullanılmış ve 353 gebe ile tamamlanmıştır. Araştırmanın verileri Kasım 2016-Nisan 2017 arasında, "Gebe Bilgi Formu", "Tilburg Gebelikte Distres Ölçeği (TGDÖ)" ve "Gebelikte Sağlık Uygulamaları Ölçeği"(GSUÖ) ile toplanmıştır. Verilerin değerlendirilmesinde; yüzdeler dağılımlar, ortalama, t testi, Kruskal Wallis Varyans analizi, Mann-Whitney U testi ve Korelasyon Analizi kullanılmıştır. GSUÖ toplam puanı ile Eş Katılımı alt boyutu ve TGDÖ toplam puanı arasında istatistiksel olarak anlamlı, negatif yönlü ve düşük düzeyli ilişki vardır ($p < 0.05$). Gebelerin distresin artması sağlık uygulamalarını azalttığı bulunmuştur. Distres altında olan gebeler tespit edilerek distresi azaltmak veya ortadan kaldırmak ve buna bağlı sağlık uygulamalarını artırarak ana çocuk sağlığına katkıda bulunulmalıdır.

Anahtar Kelimeler: Gebelik, sağlık uygulamaları, distres

*Corresponding Author: svnckose1024@hotmail.com

Demet Kışlak, <https://orcid.org/0000-0002-5531-8089>

Sevinç Köse Tuncer, <https://orcid.org/0000-0002-2598-6182>

1.Introduction

Pregnancy is a natural event that lasts 280 days starting from the first day of the last menstruation [1]. In addition to its joy and excitement, the physiological burden of pregnancy also brings along negative emotions such as an intense sense of responsibility and anxious anticipation [2]. This period can be considered as a crisis period that requires changes in women's lives and adaptation to new roles [3].

Pregnancy can be considered as a stress period in women's lives and is often concomitant with stress and depression [4]. In pregnant women, occasions such as delivering a stillborn baby, difficult birth, birth pain, fear of death, fear of not being a good mother, the mother having to leave her job or take a break after birth, and finally the family being under an economic burden can cause anxiety and stress [5]. Health practices during pregnancy include pregnant, fetus, and newborn health, and affect the course of pregnancy and its outcome [6]. As a result of stress, depression and anxiety experienced in pregnant women, norepinephrine and cortisol levels increase and blood flow to this uterus decreases. In this case, serious obstetric and neonatal consequences occur on both the fetus and the mother [7]. Diego et al. in their study found that women having depression had 13% preterm birth, 15% low birth weight babies, compared to the non-depressed women, and those with a diagnosis of pregnancy depression had a smaller fetus for their current week of gestation and a slower fetal growth rate and finally, the rate of low birth weight babies was higher [8]. The distress experienced during pregnancy is nausea-vomiting, fear of childbirth, cesarean delivery rate, bacterial vaginosis incidence and birth greater need for epidural anesthesia is indicated [9]. It has been reported that the increase in anxiety and depression levels of pregnant women is associated with obstetric complications, preterm labor, and increased need for analgesics during delivery [10]. In the study conducted by Çiçek and Mete, stress, anxiety and depression during pregnancy are shown among the causes of fear of childbirth [11]. We can say that this situation causes anxiety birth smell. In the study conducted by Öznas in 2019, the rate of cesarean section preference was found to be high in those who lived through birth protection [12]. In addition, the intense stress experienced during pregnancy causes an increase in the usual discomforts (nausea, vomiting, bacterial vaginosis, etc.) [13]. Depressed pregnant women receive less care from the healthcare personnel and care less for their own self-care, and as a result of this inadequate care, pregnant women experience more discomfort. In pregnant women with depression, nausea and vomiting, stomach pain, respiratory problems, GI complaints, heart palpitations and dizziness are more common than in pregnant women without depression [4]. In addition to the biological effects of increased stress during pregnancy, unhealthy behaviors such as not going to prenatal controls may occur in mothers [5]. There are studies showing that as a result of distress during pregnancy, changes in sleep, loss of appetite, deterioration in nutrition, decrease in energy, decrease in self-confidence, increase in alcohol and cigarette use, and lack of self-care lead to negative health behaviors [3,14]. In addition, it is stated that the intense stress experienced during pregnancy causes an increase in the usual discomforts (such as nausea, vomiting, gastrointestinal complaints, heartburn, reflux, constipation) [13].

Prevention of problems caused by distress during pregnancy is very crucial for the health of women and children. The occasion of distress in pregnant in Turkey and its preventability make the health practices during pregnancy and the factors influencing them significant. Nurses' awareness of distress should be elevated. Also, it is an important factor in terms of mother and child health for nurses to identify pregnant women at risk of distress and reduce it, facilitating physical and psychological adaptation to these periods.

This study was conducted to determine the effect of distress in pregnant women on health practices.

Research Questions

- Does distress in pregnant women affect health practices?

2. Materials and Methods

Research Type, Place-Time and Universe-Sample

This descriptive study was conducted with pregnant women who were admitted to the Gynecology and Obstetrics Department of the Gynecology and Pediatrics Supplementary Service Building affiliated to a City Hospital between November 2016 and April 2017.

The universe of the study consisted of pregnant of 12 weeks and more who applied to the hospital clinic within the specified time frame. To calculate the sample size, the number of participants was calculated as 384 people using the sample formula used in cases where the number of elements in the universe is unknown, but when the research data reached 353 people, the power of the study was calculated as 0.99. Sampling criteria: Pregnancy of over 12 weeks, availability to communication and cooperation, being primiparous or multiparous, not having a risky pregnancy, and having no diagnosed psychiatric disorder.

Data Collection: The data of the research were collected using face to face interview method. Filling out the forms took an average of 20-25 minutes.

Data Collection Tools: Pregnant Info Form, Tilburg Distress Scale (TPDS) and Pregnancy Health Practices Scale were used.

Pregnant Info Form

This form, prepared in line with the literature [15], consists of questions that can determine the socio-demographic characteristics of pregnant women.

Pregnancy Health Practices Scale

The Health Practices in Pregnancy Scale (GSSS) was developed by Lindgren in 2005 and adapted into Turkish by Er in 2006.

There are 34 items in the original form of the questionnaire. However, since one item was removed in the adaptation study, the Turkey form consists of 33 items. Items 1 to 16 in the questionnaire include 5-point Likert-type responses ranging from “always” to “never”. Never option starts from 1 point. However, items 6, 7, 21, 22, 23, 24, 25, 26, 32 and 33 of the scale

are reverse coded starting from 5 points towards 1. A minimum of 33 and a maximum of 165 points are obtained from the scale, and an increase in the score indicates an increase in health practices. [16]. The internal consistency coefficient of the study was 0.66.

Tilburg Pregnancy Distress Scale (TPDS)

This scale was developed by Pop et al. It was developed by Capık in 2011 and its Turkish adaptation was made by Çapık in 2013[17]. The scale is in 4-point Likert type, and the "very often" option starts with zero (0) points and the "never" option ends with three (3) points. However, items 3, 5, 6, 7, 9, 10, 11, 12, 13, 14 and 16 are reverse scored. t is the cut-off point of the total score that can be obtained from the scale, and a cut-off point of 28 and above determines the pregnant women at risk for distress. The cut-off points for the sub-dimensions are 10 and more for the spousal involvement sub-dimension, and 22 and more for the negative affect sub-dimension. In the validity and reliability study conducted by Çapık (2013), the internal consistency coefficient was found to be 0.83, and in this study, the internal consistency coefficient was found to be 0.70 for the TPDS, 0.78 for the negative affect sub-dimension, and 0.76 for the spousal involvement sub-dimension.

Negative Affect Sub-Dimension: It consists of 11 items and includes items 3,5,6,7,9,10,11,12,13,14 and 16. The minimum 0 maximum score that can be obtained from the sub-dimension is 33.

Spouse Participation Sub-Dimension: Consists of 5 items and includes items 1,2,4,8 and 15. The minimum 0 maximum score that can be obtained from the sub-dimension is 15.

A minimum of 0 and a maximum of 48 points are taken from the total of the scale.

Analysis of Data: The data were analyzed in the SPSS information package, and percentages, numbers, spearman correlation analysis, mean and standard deviations were used in the analysis.

3. Results and Discussion

Table 1. Distribution of Demographic Characteristics of the Pregnants (N=353)

Demographic Characteristics		n	%
Education Level	Illiterate	3	0.8
	Literate	6	1.7
	Primary Education	231	65.4
	High School	85	24.1
	University	28	7.9
Place of Residence	Province	44	12.5
	District	257	72.8
	Village-Town	52	14.7
Employment Status	Yes	26	7.4
	No	327	92.6
Health Insurance	Existent	305	86.4
	Nonexistent	48	13.6
Family Type	Nuclear	241	68.3

Investigation of the Effects of Distress on Health Practices in Pregnant Women

	Extended	112	31.7		
Income status	Low	13	3.7		
	Moderate	281	79.6		
	High	59	16.7		
Spouse Education Level	Illiterate	2	0.6		
	Literate	2	0.6		
	Primary Education	163	46.2		
	High School	140	39.7		
	University	46	13.0		
Spouse's Employment Status	Employed	332	94.1		
	Unemployed	21	5.9		
	n	Min.	Max.	Avg.	SS.
Age	353	17	40	26.19	4.96
Spouse's Age	353	19	57	31.17	5.61

As seen in Table 1, the mean age of the pregnant women was 26.19±4.96, and the mean age of the spouses was 31.17±5.61. 65.4% of the pregnant women were primary school graduates, 72.8% lived in the district, 92.6% did not use to work, and 86.4% had health insurance. 68.3% of the pregnant lived in a nuclear family, 79.6% of them had a moderate income. The spouses of 46.2% of the pregnant women were primary school graduates, and the spouses of 94.1% were actively working.

Table 2. Distribution of Pregnant Women's Scores from PHPS and TPDS Sub-dimensions (N=353)

SCALES	n	Min.	Max.	Avg.	SS.
Negative Affect Sub-dimension	353	0	23	5.12	4.42
Spousal Involvement Sub-dimension	353	0	13	5.25	2.59
TPDS	353	0	36	10.37	4.91
HPPQ	353	94	146	121.04	10.32
TPDS Based on Cutoff Points	Distress Yes		Distress No		
		N	%	N	%
Spousal Involvement Subdimension		16	4.5	337	95.5
Negative Affect Sub-dimension		1	0.3	352	99.7
TPDS		2	0.6	351	99.4

As seen in Table 2, pregnant women scored 5.12±4.42 from the Negative Affect sub-dimension, 5.25±2.59 from the Spousal Involvement sub-dimension, and 10.37±4.91 from the total of TPDS. 0.3% of the pregnant women scored from the Negative Affect sub-dimension

above the cutoff points, and 4.5% from the Spousal Involvement sub-dimension and 0.6% from the total TPDS did so. Pregnant women had 121.04 ± 10.32 points from the total of PHPS.

Table 3 The Correlation Between Total HPPQ Scores and TPDS and its Sub-dimensions (N = 353)

SCALES		HPPQ Total Score
Negative Affect	r	0.082
	p	0.126
Spousal Involvement	r	-0.377
	p	0.000
TPDS Total Score	r	-0.138
	p	0.009

As seen in Table 3, there is no statistically significant correlation between the total HPPQ scores and Negative Affect sub-dimension scores of the pregnant ($p > 0.05$). There is a statistically significant, negative, and low-level correlation between the total HPPQ score, the Spousal Involvement sub-dimension, and the total TPDS score ($p < 0.05$). As the HPPQ total score increases, the spousal involvement sub-dimension and the TPDS total score decrease. It was found that increasing distress in pregnant women decreases health practices during pregnancy.

In this study, the research conducted with the aim of examining the effects of distress on health practices in pregnant women has been discussed according to the literature.

In this study, the pregnant women scored above the cutoff point from the total TPDS, and 0.6% were found to be distressed. In the study conducted by Bacacı et al. in 2018, it was found that 13.1% of the pregnant women were distressed [18], in the study by Çapık, this rate was 11.9% [19], and in the study by Çiltaş and Köse, 33% were found to be at risk of distress [20]. In the study by Pottinger et al., they determined the rate of depressive disorder during the whole pregnancy as 25% [21]. In the study by Dağlar et al. (2015), it was determined that 50.7% of the pregnant women were at risk of depression [22]. Other studies have also found distress in pregnant women, and we can state that the risk of depression is too high to be underestimated. According to the results of the research, pregnant women with depression and distress risk should be diagnosed early and the risk should be reduced, thus contributing to the improvement of mother-child health.

In the study, no statistically significant correlation was found between HPPQ total score and the TPDS negative affect sub-dimension score, while a statistically significant, negative, and low-level correlation was found between the HPPQ total score, the TPDS spousal involvement sub-dimension, and TPDS total score. As the HPPQ total score increases, the spousal involvement sub-dimension and the TPDS total score decrease. Increasing distress in pregnant women decreases health practices during pregnancy (Table 3). Bacacı et al. (2018) found that as pregnant women felt inadequate in physically and in terms of health, the level of distress increased [18]. In the study conducted by Goodwin in the USA between 2005 and 2014, the smoking in pregnant women with depression was found to be four times higher than in the non-depressed [23]. In a study conducted by Smedberg among European countries, a strong relationship was found between depression and continuation of smoking during pregnancy, and

low education level and inability to attend birth preparation courses were identified as risk factors [24]. De Jesus Silva et al. (2016) found that depression during pregnancy was associated with the number of births, the number of children, the number of pregnancies, family support, the number of cigarettes smoked per day, alcohol consumption, daily drug use, a history of mental disorders, and the presence of remarkable events and the risk was higher for the pregnant women in the depression group [25]. Habashneh et al. found a significant relationship between health practices and receiving dental care during pregnancy, and it was found that pregnant women with higher health practices had a higher rate of dental care [26]. Miyake et al. (2015), in their study in Japan, vitamin D intake and depressive symptoms during pregnancy were investigated and vitamin D intake was associated with a lower prevalence of depressive symptoms during pregnancy [27]. Ormsby et al. (2018), In their study with 8 depressed pregnant women in Sydney, Australia who wanted to get acupuncture treatment, they found that acupuncture allowed them to adapt better to the changes brought by pregnancy [28]. Our study is in parallel with other study findings, and it can be concluded that there is a relationship between distress and health practices, and as the level of distress in pregnant women increases, health practices during pregnancy decrease.

4. Conclusion

According to the results of the research, as the distress increases in pregnant women, health practices during pregnancy decrease. In line with this result, prenatal education programs should be made widespread, reducing the stress of pregnant women and spouses and preparing them for the role of parenting. In addition, it is recommended to increase the health practices during pregnancy by determining the factors that may play a role in women experiencing distress during pregnancy and thus to contribute to the overall health of the mother and child.

Ethics in Publishing

Ethics approval (No:2016/40229) from the Ethics Committee of a university and written permission from the Provincial Health Directorate of the province where the research was conducted were obtained in order to conduct the research. To protect the rights of pregnant women within the scope of the research, before starting to collect the research data, the aim and duration of the research were explained to the pregnant women, and care was taken to comply with the principle of "Autonomy" and the principle of "Confidentiality and Protection of Confidentiality". In general, the ethical principles of 'Do No Harm/Beneficence' have been fulfilled.

Author Contributions

DK: Conceptualization, Methodology, Software, Investigation, Formal analysis, Writing - Review & Editing, Data curation, Resources

SKT: Conceptualization, Methodology, Software, Investigation, Formal analysis, Writing - Review & Editing, Data curation, Resources

Acknowledgements

* This study was presented as an oral presentation at the 7th International Congress on Woman and Child Health and Education. 24-25 May 2021 Istanbul; Turkey

** Produced from Master's thesis.

*** This work has not received funding.

References

- [1] Aydemir, H., & Uyar Hazar, H. (2014). Low-Risk, Risky, High-Risk Pregnancy and the Role of the Midwife. *Gumushane University Journal of Health Sciences*, 3(2), 815–833.
- [2] Kumcagız, H. (2017). The development of a Self-perception of Pregnants Scale and its Psychometric Features. *Journal of Psychiatric Nursing*.
- [3] Dağlar, G., Nur, N., Bilgiç, D., & Kadioğlu M. (2015). Affective Disorder in Pregnancy. *Kashed*, 2(1), 27–40.
- [4] Yeşilçiçek Çalık, K., & Aktaş, S. (2011). Depression in Pregnancy: Frequency, Risk Factors and Treatment. *Current Approaches in Psychiatry*, 3(1), 142–162.
- [5] Atasever, İ., & Sis Çelik, A. (2018). The Effect of Prenatal Stress on Mother-Child Health. *Anatolian Journal of Nursing and Health Sciences*, 21(1), 60–68.
- [6] Lindgren, K. (2005). Testing the Health Practices in Pregnancy Questionnaire–II. *Journal of Obstetric, Gynecologic & Neonatal Nursing*, 34(4), 465–472.
- [7] Akmeşe, ZB, and B. Karaca Saydam. 2020. *Doğum Öncesi Bakım*. edited by N. Soğukpınar and B. Saydam Karaca. Ayrıntı Basımevi.
- [8] Diego, M. A., Field, T., Hernandez-Reif, M., Schanberg, S., Kuhn, C., & Gonzalez-Quintero, V. H. (2009). Prenatal depression restricts fetal growth. *Early Human Development*, 85(1), 65–70.
- [9] Atasever İ, Sis Çelik A.2018. The Validity and Reliability of The Antenatal Perceived Stress Inventory Turkish Version: A Methodological Study. *Health Care for Women International*, 39(10):1140-57.
- [10] Alder, J., Fink, N., Bitzer, J., Hösl, I., Holzgreve, W., 2007. Depression and anxiety during pregnancy: a risk factor for obstetric, fetal and neonatal outcome? A critical review of the literature. *The Journal of Maternal Fetal Neonatal Medicine* 20, 189-209
- [11] Çiçek, Ö. ve Mete, S. (2015). A common problem: fear of childbirth. *Journal of Dokuz Eylül University Faculty of Nursing*, 8 (4), 263-268.
- [12] Öznas S, Türkçapar AF. (2019) Investigation of Cognitive Factors Affecting Fear of Birth in Pregnants, Hasan Kalyoncu University, Institute of Social Sciences, Department of Psychology, M.Sc. Thesis, page: 1-75.
- [13] Can, R., Yılmaz Dereli, S., Çankaya, S., Kodoz, N. (2019). Problems Experienced During Pregnancy and Their Associations With Quality Of Life. *Sağlık ve Toplum*, 2, 58–64.
- [14] Savrun M. (2008). Pregnancy and Depression. *Journal of Clinical Development*, 21(1):164-166.
- [15] Coşkun, A., Kızılay Beji, N., Hotun Şahin, N., Yeşiltepe Oskay, Ü., Küçük-Dikencik, B., & Yıldırım, G. (2008). *Women's Health and Diseases Learning Guide for Nurses and Midwives*. pages: 15-50.

- [16] Er, S. (2006). Gebelikte Sağlık Uygulamaları Ölçeği Türkçe Formunun Geçerlik ve Güvenirlik Çalışması. Ege Üniversitesi.
- [17] Capık, A. (2013). Validity and Reliability Study of the Tilburg Pregnancy Distress Scale. Ataturk University. Institute of Health Sciences, Department of Obstetrics and Gynecology Nursing.
- [18] Bacacı, H., & Ejder Apay, S. (2018). The Relationship Between Body Image Perception and Distress in Pregnant Women. *Duzce University Journal of Health Sciences Institute*, 8(2), 76–82.
- [19] Çapık, A., Apay, E. ., & Sakar, T. (2015). Determination of Distress Level in Pregnant Women. *Anatolian Journal of Nursing and Health Sciences*, 18(3), 196–203.
- [20] Yıldız Çiltaş, N., & Tuncer Köse, S. (2019). Distressin Defining in Pregnancy: Erzincan Case. *Mehmet Akif Ersoy Üniversitesi Sağlık Bilimleri Enstitüsü Dergisi*, 7(1), 15–24.
- [21] Pottinger, A., & Trotman Edwards, H, Younger, N. (2009). Detecting Depression During Pregnancy And Associated Lifestyle Practices And Concerns Among Women İn A Hospital-Based Obstetric Clinic İn Jamaica. *General Hospital Psychiatry*, 31, 254–261.
- [22] Dağlar, G., & Nur, N. (2014). Anxiety and Stress Coping Styles of Pregnant Women Relationship with Depression Level. *Cumhuriyet Medical Journal*, 36, 426–441.
- [23] Goodwin, R. D., Cheslack-Postava, K., Nelson, D. B., Smith, P. H., Wall, M. M., Hasin, D. S., Nomura, Y., et al. (2017). Smoking during pregnancy in the United States, 2005–2014: The role of depression. *Drug and Alcohol Dependence*, 179, 159–166.
- [24] Smedberg, J., Lupattelli, A., Mårdby, A.-C., Øverland, S., & Nordeng, H. (2015). The relationship between maternal depression and smoking cessation during pregnancy—a cross-sectional study of pregnant women from 15 European countries. *Archives of Women’s Mental Health*, 18(1), 73–84.
- [25] Silva, M. M. de J., Leite, E. P. R. C., Nogueira, D. A., & Clapis, M. J. (2016). Depression in pregnancy. Prevalence and associated factors. *Investigación y Educación en Enfermería*, 34(2).
- [26] Al Habashneh, R., Guthmiller, J. M., Levy, S., Johnson, G. K., Squier, C., Dawson, D. V., & Fang, Q. (2005). Factors related to utilization of dental services during pregnancy. *Journal of Clinical Periodontology*, 32(7), 815–821.
- [27] Miyake, Y., Tanaka, K., Okubo, H., Sasaki, S., & Arakawa, M. (2015). Dietary vitamin D intake and prevalence of depressive symptoms during pregnancy in Japan. *Nutrition*, 31(1), 160–165.
- [28] Ormsby, S. M., Dahlen, H. G., & Smith, C. A. (2018). Women’s experiences of having depression during pregnancy and receiving acupuncture treatment—A qualitative study. *Women and Birth*, 31(6), 469–478.

Some Properties of r -Small Submodules

Celil NEBİYEY^{1*}, Hasan Hüseyin ÖKTEN²

¹Department of Mathematics, Ondokuz Mayıs University, 55270 Kurupelit-Atakum/Samsun/TÜRKİYE

²Technical Sciences Vocational School, Amasya University, Amasya/TÜRKİYE

Received:26/09/2022, **Revised:** 26/11/2022, **Accepted:** 09/12/2022, **Published:** 30/12/2022

Abstract

In this work, some properties of r -small submodules are investigated. It is proved that the finite sum of r -small submodules is r -small. It is also proved that every homomorphic image of an r -small submodule is r -small. Let M be an R -module and $N, K \leq M$. If $K \ll_r M$ and $(N+K)/K \ll_r M/K$, then $N \ll_r M$. Let $f: M \rightarrow N$ be an R -module epimorphism and $\text{Ker}f \ll_r M$. If $T \ll_r N$, then $f^{-1}(T) \ll_r M$. Let M be an R -module. Then $\text{Rad}(\text{Rad}M) = \sum_{L \ll_r M} L$.

Keywords: Small Submodules, Maximal Submodules, Radical, Supplemented Modules.

r -Küçük Alt Modüllerinin Bazı Özellikleri

Öz

Bu çalışmada r -küçük alt modüllerle ilgili birtakım özellikler incelendi. r -küçük alt modüllerin sonlu toplamlarının r -küçük olduğu gösterildi. Ayrıca r -küçük alt modüllerin homomorfik görüntülerinin de r -küçük olduğu gösterildi. M bir R -modül ve $N, K \leq M$ olsun. Eğer $K \ll_r M$ ve $(N+K)/K \ll_r M/K$ ise $N \ll_r M$ olur. $f: M \rightarrow N$ bir R -modül epimorfizması ve $\text{Ker}f \ll_r M$ olsun. Eğer $T \ll_r N$ ise bu durumda $f^{-1}(T) \ll_r M$ olur. M bir R -modül olsun. Bu durumda $\text{Rad}(\text{Rad}M) = \sum_{L \ll_r M} L$ olur.

Anahtar Kelimeler: Küçük Alt Modüller, Maksimal Alt Modüller, Radikal, Tümlenmiş Modüller.

1. Introduction

Throughout this paper all rings are associative with identity and all modules are unital left modules.

Let R be a ring and M be an R -module. We denote a submodule N of M by $N \leq M$. Let M be an R -module and $N \leq M$. If $L = M$ for every submodule L of M such that $M = N + L$, then N is called a *small* (or *superfluous*) submodule of M and denoted by $N \ll M$. Let M be an R -module and $U, V \leq M$. If $M = U + V$ and V is minimal with respect to this property, or equivalently, $M = U + V$ and $U \cap V \ll V$, then V is called a *supplement* of U in M . M is said to be *supplemented* if every submodule of M has a supplement in M . The intersection of maximal submodules of an R -module M is called the *radical* of M and denoted by $RadM$. If M have no maximal submodules, then we denote $RadM = M$. Let M be an R -module and $U, V \leq M$. If $M = U + V$ and $U \cap V \leq RadV$, then V is called a *generalized (Radical) supplement* (briefly, *Rad-supplement*) of U in M . M is said to be *generalized (Radical) supplemented* (briefly, *Rad-supplemented*) if every submodule of M has a Rad-supplement in M . Let M be an R -module and $K \leq V \leq M$. We say V *lies above* K in M if $V/K \ll M/K$.

More details about supplemented modules are in Clark et al. (2006), Nebiyev and Pancar (2013), Wisbauer (1991) and (Zöschinger, 1974). More details about generalized (Radical) supplemented modules are in Xue (1996) and (Wang and Ding, 2006).

2. Preliminaries

Lemma 2.1. Let M be an R -module. The following assertions are hold.

- (1) If $K \leq L \leq M$, then $L \ll M$ if and only if $K \ll M$ and $L/K \ll M/K$.
- (2) Let N be an R -module and $f: M \rightarrow N$ be an R -module homomorphism. If $K \ll M$, then $f(K) \ll N$. The converse is true if f is an R -module epimorphism and $Kerf \ll M$.
- (3) If $L \leq M$ and $K \ll L$, then $K \ll M$.
- (4) If $K_1, K_2, \dots, K_n \ll M$, then $K_1 + K_2 + \dots + K_n \ll M$.
- (5) Let $K_1, K_2, \dots, K_n, L_1, L_2, \dots, L_n \leq M$. If $K_i \ll L_i$ for every $i = 1, 2, \dots, n$, then $K_1 + K_2 + \dots + K_n \ll L_1 + L_2 + \dots + L_n$.

Proof. See Clark et al. (2006), 2.2 and (Wisbauer, 1991, 19.3).

Lemma 2.2. Let M be an R -module. The following assertions are hold.

- (1) $RadM = \sum_{L \ll M} L$.
- (2) Let N be an R -module and $f: M \rightarrow N$ be an R -module homomorphism. Then $f(RadM) \leq RadN$. If $Kerf \leq RadM$, then $f(RadM) = Radf(M)$.
- (3) If $N \leq M$, then $RadN \leq RadM$.
- (4) For $K, L \leq M$, $RadK + RadL \leq Rad(K + L)$.
- (5) $Rx \ll M$ for every $x \in RadM$.

Proof. See (Wisbauer, 1991, 21.5 and 21.6).

3- Theorems and Proofs

r -Small Submodules

Definition 3.1. Let M be an R -module and $N \leq M$. If $N \ll \text{Rad}M$, then N is called a *radical small* (or briefly *r -small*) submodule of M and denoted by $N \ll_r M$ (See (Nebiyev and Ökten, 2020)).

Clearly we can see that if M is a radical module ($\text{Rad}M = M$) and $N \leq M$, then $N \ll_r M$ if and only if $N \ll M$.

Proposition 3.2. Let M be an R -module and $N \leq M$. If $N \ll_r M$, then $N \ll M$.

Proof. Since $N \ll_r M$, $N \ll \text{Rad}M$. Then by Lemma 2.1(3), $N \ll M$.

Lemma 3.3. Let $N \leq M$. If $N \ll M$ and $\text{Rad}M$ is a supplement submodule in M , then $N \ll_r M$.

Proof. Since $N \ll M$ and $\text{Rad}M$ is a supplement submodule in M , by Wisbauer (1991) 41.1(5), $N = N \cap \text{Rad}M \ll \text{Rad}M$. Hence $N \ll_r M$, as desired.

Corollary 3.4. Let $N \leq M$. If $N \ll M$ and $\text{Rad}M$ is a direct summand of M , then $N \ll_r M$.

Proof. Clear from Lemma 3.3.

Corollary 3.5. Let M be an R -module and $\text{Rad}M$ be a supplement submodule in M . Then $Rx \ll_r M$ for every $x \in \text{Rad}M$.

Proof. Let $x \in \text{Rad}M$. Then by Lemma 2.2(5), $Rx \ll M$. Since $\text{Rad}M$ is a supplement submodule in M , by Lemma 3.3, $Rx \ll_r M$.

Corollary 3.6. Let M be an R -module and $\text{Rad}M$ be a direct summand of M . Then $Rx \ll_r M$ for every $x \in \text{Rad}M$.

Proof. Clear from Corollary 3.5.

Lemma 3.7. Let M be an R -module with $\text{Rad}(\text{Rad}M) = \text{Rad}M$. If $Rx \ll M$ for $x \in M$, then $Rx \ll_r M$.

Proof. Since $Rx \ll M$, by Lemma 1.2(1), $Rx \leq \text{Rad}M$ and $x \in \text{Rad}M = \text{Rad}(\text{Rad}M)$. Then by Lemma 2.2(5), $Rx \ll \text{Rad}M$ and $Rx \ll_r M$.

Corollary 3.8. Let M be an R -module and $\text{Rad}M$ be a Rad-supplement submodule in M . If $Rx \ll M$ for $x \in M$, then $Rx \ll_r M$.

Proof. Clear from Lemma 3.7, since $\text{Rad}(\text{Rad}M) = \text{Rad}M$.

Corollary 3.9. Let M be an R -module with $\text{Rad}(\text{Rad}M) = \text{Rad}M$. Then $Rx \ll_r M$ for every $x \in \text{Rad}M$.

Proof. Let $x \in \text{Rad}M$. By Lemma 2.2(5), $Rx \ll M$. Then by Lemma 3.7, $Rx \ll_r M$.

Corollary 3.10. Let M be an R -module and $\text{Rad}M$ be a Rad-supplement submodule in M . Then $Rx \ll_r M$ for every $x \in \text{Rad}M$.

Proof. Clear from Corollary 3.9, since $\text{Rad}(\text{Rad}M) = \text{Rad}M$.

Proposition 3.11. If $N \ll_r M$, then $N \ll K$ for every maximal submodule K of M .

Proof. Since $N \ll_r M$, $N \ll \text{Rad}M$ and since $\text{Rad}M \leq K$ for every maximal submodule K of M , by Lemma 2.1(3), $N \ll K$.

Let M be an R -module. It is defined the relation β^* on the set of submodules of an R -module M by $X\beta^*Y$ if and only if $Y+K=M$ for every $K \leq M$ such that $X+K=M$ and $X+T=M$ for every $T \leq M$ such that $Y+T=M$ (See (Birkenmeier et al., 2010)).

Lemma 3.12. Let $N \ll_r M$ and $L \leq \text{Rad}M$. If $N\beta^*L$ in $\text{Rad}M$, then $L \ll_r M$.

Proof. Clear from Birkenmeier et al. (2010) Theorem 2.6(i).

Corollary 3.13. Let $N \ll_r M$ and $L \leq \text{Rad}M$. If L lies above N in $\text{Rad}M$, then $L \ll_r M$.

Proof. Since L lies above N in $\text{Rad}M$, $N\beta^*L$ in $\text{Rad}M$. Then by Lemma 3.12, $L \ll_r M$ holds.

Lemma 3.14. Let M be an R -module and $N \leq K \leq M$. If $N \ll_r K$, then $N \ll_r M$.

Proof. Since $N \ll_r K$, $N \ll \text{Rad}K$. By Lemma 2.2(3), $\text{Rad}K \leq \text{Rad}M$. Then by Lemma 2.1(3), $N \ll \text{Rad}M$ and $N \ll_r M$.

Lemma 3.15. Let M be an R -module and $N \leq K \leq M$. If $K \ll_r M$, then $N \ll_r M$.

Proof. Since $K \ll_r M$, $K \ll \text{Rad}M$. Then by Lemma 2.1(1), $N \ll \text{Rad}M$. Hence $N \ll_r M$, as desired.

Lemma 3.16. Let M be an R -module and $N, K \leq M$. If $N \ll_r M$, then $(N+K)/K \ll_r M/K$.

Proof. Since $N \ll_r M$, $N \ll \text{Rad}M$. By Lemma 2.1, $(N+K)/K \ll (\text{Rad}M+K)/K$. By Lemma 2.2, $(\text{Rad}M+K)/K \leq \text{Rad}(M/K)$. Then by Lemma 2.1(3), $(N+K)/K \ll \text{Rad}(M/K)$. Hence $(N+K)/K \ll_r M/K$, as desired.

Lemma 3.17. Let M be an R -module and $N, K \leq M$. If $K \ll_r M$ and $(N+K)/K \ll_r M/K$, then $N \ll_r M$.

Proof. Since $K \leq \text{Rad}M$, $\text{Rad}(M/K) = (\text{Rad}M)/K$. Since $(N+K)/K \leq \text{Rad}(M/K) = (\text{Rad}M)/K$, $N \leq \text{Rad}M$. Let $N+T = \text{Rad}M$ for $T \leq \text{Rad}M$. Then $(N+K)/K + (T+K)/K = (N+T)/K = (\text{Rad}M)/K$ and since $(N+K)/K \ll \text{Rad}(M/K) = (\text{Rad}M)/K$, $(T+K)/K = (\text{Rad}M)/K$ and $T+K = \text{Rad}M$. Since $K \ll \text{Rad}M$, $T = \text{Rad}M$. Hence $N \ll \text{Rad}M$ and $N \ll_r M$, as required.

Corollary 3.18. Let M be an R -module, $N \leq M$ and $K \ll_r M$. Then $N \ll_r M$ if and only if $(N+K)/K \ll_r M/K$.

Proof. Clear from Lemma 3.16 and Lemma 3.17.

Lemma 3.19. Let $f: M \rightarrow N$ be an R -module homomorphism. If $K \ll_r M$, then $f(K) \ll_r f(M)$.

Proof. Since $K \ll_r M$, $K \ll \text{Rad}M$. By Lemma 2.1(2) and Lemma 2.2(2), $f(K) \ll f(\text{Rad}M) \leq \text{Rad}f(M)$. Hence $f(K) \ll_r f(M)$, as desired.

Corollary 3.20. Let $f: M \rightarrow N$ be an R -module homomorphism. If $K \ll_r M$, then $f(K) \ll_r N$.

Proof. Clear from Lemma 3.19 and Lemma 3.14.

Lemma 3.21. Let $f: M \rightarrow N$ be an R -module epimorphism and $\text{Ker}f \ll_r M$. If $T \ll_r N$, then $f^{-1}(T) \ll_r M$.

Proof. By Lemma 1.2(2), $f(\text{Rad}M) = \text{Rad}f(M) = \text{Rad}N$. Let $x \in f^{-1}(T)$. Then $f(x) \in T \leq \text{Rad}N = f(\text{Rad}M)$. Since $f(x) \in f(\text{Rad}M)$, there exists $a \in \text{Rad}M$ with $f(x) = f(a)$. Since $f(x) = f(a)$, $f(x-a) = 0$ and $x-a \in \text{Ker}f \leq \text{Rad}M$. Then $x = x-a+a \in \text{Rad}M$ and $f^{-1}(T) \leq \text{Rad}M$. Let $f^{-1}(T) + K = \text{Rad}M$ with $K \leq \text{Rad}M$. Then $T + f(K) = f(\text{Rad}M) = \text{Rad}N$ and since $T \ll_r N$, $f(K) = \text{Rad}N$. Since $f(K) = \text{Rad}N$, we can see that $K + \text{Ker}f = \text{Rad}M$ and since $\text{Ker}f \ll_r M$, $K = \text{Rad}M$. Hence $f^{-1}(T) \ll_r M$, as required.

Corollary 3.22. Let $f: M \rightarrow N$ be an R -module homomorphism and $\text{Ker}f \ll_r M$. If $T \ll_r f(M)$, then $f^{-1}(T) \ll_r M$.

Proof. Clear from Lemma 3.21.

Corollary 3.23. Let $f: M \rightarrow N$ be an R -module homomorphism and $K \leq \text{Rad}M$. If $\text{Ker}f \ll_r M$ and $f(K) \ll_r f(M)$, then $K \ll_r M$.

Proof. By Corollary 3.22, $K + \text{Ker}f = f^{-1}(f(K)) \ll_r M$. Then by Lemma 3.15, $K \ll_r M$, as desired.

Corollary 3.24. Let $f: M \rightarrow N$ be an R -module epimorphism and $K \leq \text{Rad}M$. If $\text{Ker}f \ll_r M$ and $f(K) \ll_r N$, then $K \ll_r M$.

Proof. Clear from Corollary 3.23.

Corollary 3.25. Let $f: M \rightarrow N$ be an R -module epimorphism and $K \leq \text{Rad}M$. If $\text{Ker}f \ll_r M$, then $K \ll_r M$ if and only if $f(K) \ll_r N$.

Proof. Clear from Lemma 3.19 and Corollary 3.24.

Lemma 3.26. Let M be an R -module and $K, L \leq M$. If $N \ll_r K$ and $T \ll_r L$, then $N+T \ll_r K+L$.

Proof. Since $N \ll_r K$ and $T \ll_r L$, $N \ll_r \text{Rad}K$ and $T \ll_r \text{Rad}L$. By Lemma 2.1(5) and Lemma 2.2(4), $T+N \ll_r \text{Rad}K + \text{Rad}L \leq \text{Rad}(K+L)$. Hence $N+T \ll_r K+L$, as desired.

Corollary 3.27. Let $M_1, M_2, \dots, M_k \leq M$. If $N_1 \ll_r M_1$, $N_2 \ll_r M_2$, ..., $N_k \ll_r M_k$, then $N_1 + N_2 + \dots + N_k \ll_r M_1 + M_2 + \dots + M_k$.

Proof. Clear from Lemma 3.26.

Corollary 3.28. Let M be an R -module and $K_i \ll_r M$ for $i=1, 2, \dots, n$. Then $K_1 + K_2 + \dots + K_n \ll_r M$.

Proof. Clear from Corollary 3.27.

Corollary 3.29. Let M be an R -module. Then $\text{Rad}(\text{Rad}M) = \sum_{L \ll_r M} L$.

Proof. Clear from Lemma 2.2(1).

Remark 3.30. The converse of the Proposition 3.2 is not true in general. Consider an R -module M with $0 \neq \text{Rad}M \ll_r M$. Since $\text{Rad}M$ is not small in $\text{Rad}M$, $\text{Rad}M$ is not r -small in M .

Example 3.31. Consider the Z -module Z_8 . Here $\text{Rad}Z_8=2Z_8\ll Z_8$. But $2Z_8$ is not r-small in Z_8 . Here also $\text{Rad}(\text{Rad}Z_8)=4Z_8\neq\text{Rad}Z_8$.

Ethics in Publishing

There are no ethical issues regarding the publication of this study.

References

Birkenmeier, G. F., Mutlu, F. T., Nebiyev, C., Sokmez, N., Tercan, A. 2010. "Goldie*-Supplemented Modules", *Glasgow Mathematical Journal*, 52A, 41-52.

Clark, J., Lomp, C., Vanaja, N., Wisbauer, R. (2006). "Lifting Modules Supplements and Projectivity In Module Theory", *Frontiers in Mathematics*, Birkhauser, Basel.

Nebiyev, C., Ökten, H. H. 2020. "r-Small Submodules", *3rd International E-Conference on Mathematical Advances and Applications (ICOMAA-2020)*, Yıldız Technical University, Istanbul-Turkey.

Nebiyev, C., Pancar, A. 2013. "On Supplement Submodules", *Ukrainian Mathematical Journal*, 65(7), 1071-1078.

Xue, W. 1996. "Characterizations of Semiperfect and Perfect Rings", *Publications Mathematiques*, 40, 115-125.

Wang, Y., Ding, N. 2006. "Generalized Supplemented Modules", *Taiwanese Journal of Mathematics*, 10(6), 1589-1601.

Wisbauer, R. 1991. "Foundations of Module and Ring Theory", *Gordon and Breach*, Philadelphia.

Zöschinger, H. 1974. "Komplementierte Moduln Über Dedekindringen", *Journal of Algebra*, 29, 42-56.